

1993

Static and dynamic responses of prestressed concrete beams with openings.

Hany Ahmed Aly. Abdalla
University of Windsor

Follow this and additional works at: <http://scholar.uwindsor.ca/etd>

Recommended Citation

Abdalla, Hany Ahmed Aly., "Static and dynamic responses of prestressed concrete beams with openings." (1993). *Electronic Theses and Dissertations*. Paper 3577.

This online database contains the full-text of PhD dissertations and Masters' theses of University of Windsor students from 1954 forward. These documents are made available for personal study and research purposes only, in accordance with the Canadian Copyright Act and the Creative Commons license—CC BY-NC-ND (Attribution, Non-Commercial, No Derivative Works). Under this license, works must always be attributed to the copyright holder (original author), cannot be used for any commercial purposes, and may not be altered. Any other use would require the permission of the copyright holder. Students may inquire about withdrawing their dissertation and/or thesis from this database. For additional inquiries, please contact the repository administrator via email (scholarship@uwindsor.ca) or by telephone at 519-253-3000ext. 3208.



National Library
of Canada

Acquisitions and
Bibliographic Services Branch

395 Wellington Street
Ottawa, Ontario
K1A 0N4

Bibliothèque nationale
du Canada

Direction des acquisitions et
des services bibliographiques

395, rue Wellington
Ottawa (Ontario)
K1A 0N4

Your file - Votre référence

Our file - Notre référence

NOTICE

The quality of this microform is heavily dependent upon the quality of the original thesis submitted for microfilming. Every effort has been made to ensure the highest quality of reproduction possible.

If pages are missing, contact the university which granted the degree.

Some pages may have indistinct print especially if the original pages were typed with a poor typewriter ribbon or if the university sent us an inferior photocopy.

Reproduction in full or in part of this microform is governed by the Canadian Copyright Act, R.S.C. 1970, c. C-30, and subsequent amendments.

AVIS

La qualité de cette microforme dépend grandement de la qualité de la thèse soumise au microfilmage. Nous avons tout fait pour assurer une qualité supérieure de reproduction.

S'il manque des pages, veuillez communiquer avec l'université qui a conféré le grade.

La qualité d'impression de certaines pages peut laisser à désirer, surtout si les pages originales ont été dactylographiées à l'aide d'un ruban usé ou si l'université nous a fait parvenir une photocopie de qualité inférieure.

La reproduction, même partielle, de cette microforme est soumise à la Loi canadienne sur le droit d'auteur, SRC 1970, c. C-30, et ses amendements subséquents.

**STATIC AND DYNAMIC RESPONSES OF
PRESTRESSED CONCRETE BEAMS
WITH OPENINGS**

by

Hany Ahmed Aly Abdalla

**A Dissertation
submitted to the Faculty of Graduate Studies and Research through
the Department of Civil and Environmental Engineering
in Partial Fulfilment of the Requirements for the
degree of Doctor of Philosophy at the
University of Windsor**

**Windsor, Ontario, Canada
1993**



National Library
of Canada

Acquisitions and
Bibliographic Services Branch

395 Wellington Street
Ottawa, Ontario
K1A 0N4

Bibliothèque nationale
du Canada

Direction des acquisitions et
des services bibliographiques

395, rue Wellington
Ottawa (Ontario)
K1A 0N4

Your file - *Votre référence*

Our file - *Notre référence*

The author has granted an irrevocable non-exclusive licence allowing the National Library of Canada to reproduce, loan, distribute or sell copies of his/her thesis by any means and in any form or format, making this thesis available to interested persons.

The author retains ownership of the copyright in his/her thesis. Neither the thesis nor substantial extracts from it may be printed or otherwise reproduced without his/her permission.

L'auteur a accordé une licence irrévocable et non exclusive permettant à la Bibliothèque nationale du Canada de reproduire, prêter, distribuer ou vendre des copies de sa thèse de quelque manière et sous quelque forme que ce soit pour mettre des exemplaires de cette thèse à la disposition des personnes intéressées.

L'auteur conserve la propriété du droit d'auteur qui protège sa thèse. Ni la thèse ni des extraits substantiels de celle-ci ne doivent être imprimés ou autrement reproduits sans son autorisation.

ISBN 0-315-83019-0

Canada

Name _____

Dissertation Abstracts International is arranged by broad, general subject categories. Please select the one subject which most nearly describes the content of your dissertation. Enter the corresponding four-digit code in the spaces provided.

	5	4	3
--	---	---	---

U·M·I

SUBJECT TERM

SUBJECT CODE

Subject Categories

THE HUMANITIES AND SOCIAL SCIENCES

COMMUNICATIONS AND THE ARTS

Architecture	0729
Art History	0377
Cinema	0900
Dance	0378
Fine Arts	0357
Information Science	0723
Journalism	0391
Library Science	0399
Mass Communications	0708
Music	0413
Speech Communication	0459
Theater	0465

EDUCATION

General	0515
Administration	0514
Adult and Continuing	0516
Agricultural	0517
Art	0273
Bilingual and Multicultural	0282
Business	0688
Community College	0275
Curriculum and Instruction	0727
Early Childhood	0518
Elementary	0524
Finance	0277
Guidance and Counseling	0519
Health	0680
Higher	0745
History of	0520
Home Economics	0278
Industrial	0521
Language and Literature	0279
Mathematics	0280
Music	0522
Philosophy of	0998
Physical	0523

Psychology	0525
Reading	0535
Religious	0527
Sciences	0714
Secondary	0533
Social Sciences	0534
Sociology of	0340
Special	0529
Teacher Training	0530
Technology	0710
Tests and Measurements	0288
Vocational	0747

LANGUAGE, LITERATURE AND LINGUISTICS

Language	
General	0679
Ancient	0289
Linguistics	0290
Modern	0291
Literature	
General	0401
Classical	02: 1
Comparative	0295
Medieval	0297
Modern	0298
African	0316
American	0591
Asian	0305
Canadian (English)	0352
Canadian (French)	0355
English	0593
Germanic	0311
Latin American	0312
Middle Eastern	0315
Romance	0313
Slavic and East European	0314

PHILOSOPHY, RELIGION AND THEOLOGY

Philosophy	0422
Religion	
General	0318
Biblical Studies	0321
Clergy	0319
History of	0320
Philosophy of	0322
Theology	0469

SOCIAL SCIENCES

American Studies	0323
Anthropology	
Archaeology	0324
Cultural	0326
Physical	0327
Business Administration	
General	0310
Accounting	0272
Banking	0770
Management	0454
Marketing	0338
Canadian Studies	0385
Economics	
General	0501
Agricultural	0503
Commerce-Business	0505
Finance	0508
History	0509
Labor	0510
Theory	0511
Folklore	0358
Geography	0366
Gerontology	0351
History	
General	0578

Ancient	0579
Medieval	0581
Modern	0582
Black	0328
African	0331
Asia, Australia and Oceania	0332
Canadian	0334
European	0335
Latin American	0336
Middle Eastern	0333
United States	0337
History of Science	0585
Law	0398
Political Science	
General	0615
International Law and Relations	0616
Public Administration	0617
Recreation	0814
Social Work	0452
Sociology	
General	0626
Criminology and Penology	0627
Demography	0938
Ethnic and Racial Studies	0631
Individual and Family Studies	0628
Industrial and Labor Relations	0629
Public and Social Welfare	0630
Social Structure and Development	0700
Theory and Methods	0344
Transportation	0709
Urban and Regional Planning	0999
Women's Studies	0453

THE SCIENCES AND ENGINEERING

BIOLOGICAL SCIENCES

Agriculture	
General	0473
Agronomy	0285
Animal Culture and Nutrition	0475
Animal Pathology	0476
Food Science and Technology	0359
Forestry and Wildlife	0478
Plant Culture	0479
Plant Pathology	0480
Plant Physiology	0817
Range Management	0777
Wood Technology	0746
Biology	
General	0306
Anatomy	0287
Biostatistics	0308
Botany	0309
Cell	0379
Ecology	0329
Entomology	0353
Genetics	0369
Limnology	0793
Microbiology	0410
Molecular	0307
Neuroscience	0317
Oceanography	0416
Physiology	0433
Radiation	0821
Veterinary Science	0778
Zoology	0472
Biophysics	
General	0786
Medical	0760

Geodesy	0370
Geology	0372
Geophysics	0373
Hydrology	0388
Mineralogy	0411
Paleobotany	0345
Paleoecology	0426
Paleontology	0418
Paleozoology	0985
Palynology	0427
Physical Geography	0368
Physical Oceanography	0415

HEALTH AND ENVIRONMENTAL SCIENCES

Environmental Sciences	0768
Health Sciences	
General	0566
Audiology	0300
Chemotherapy	0992
Dentistry	0567
Education	0350
Hospital Management	0769
Human Development	0758
Immunology	0982
Medicine and Surgery	0564
Mental Health	0347
Nursing	0569
Nutrition	0570
Obstetrics and Gynecology	0380
Occupational Health and Therapy	0354
Ophthalmology	0381
Pathology	0571
Pharmacology	0419
Pharmacy	0572
Physical Therapy	0382
Public Health	0573
Radiology	0574
Recreation	0575

Speech Pathology	0460
Toxicology	0383
Home Economics	0386

PHYSICAL SCIENCES

Pure Sciences	
Chemistry	
General	0485
Agricultural	0749
Analytical	0486
Biochemistry	0487
Inorganic	0488
Nuclear	0738
Organic	0490
Pharmaceutical	0491
Physical	0494
Polymer	0495
Radiation	0754
Mathematics	0405
Physics	
General	0605
Acoustics	0986
Astronomy and Astrophysics	0606
Atmospheric Science	0608
Atomic	0748
Electronics and Electricity	0607
Elementary Particles and High Energy	0798
Fluid and Plasma	0759
Molecular	0609
Nuclear	0610
Optics	0752
Radiation	0756
Solid State	0611
Statistics	0463
Applied Sciences	
Applied Mechanics	0346
Computer Science	0984

Engineering	
General	0537
Aerospace	0538
Agricultural	0539
Automotive	0540
Biomedical	0541
Chemical	0542
Civil	0543
Electronics and Electrical	0544
Heat and Thermodynamics	0348
Hydraulic	0545
Industrial	0546
Marine	0547
Materials Science	0794
Mechanical	0548
Metallurgy	0743
Mining	0551
Nuclear	0552
Packaging	0549
Petroleum	0765
Sanitary and Municipal	0554
System Science	0790
Geotechnology	0428
Operations Research	0796
Plastics Technology	0795
Textile Technology	0994

PSYCHOLOGY

General	0621
Behavioral	0384
Clinical	0622
Developmental	0620
Experimental	0623
Industrial	0624
Personality	0625
Physiological	0989
Psychobiology	0349
Psychometrics	0632
Social	0451



Hany Ahmed Aly Abdalla

©

1993

All Rights Reserved

I hereby declare that I am the sole author of this document.

I authorize the University of Windsor to lend this document to other institutions or individuals for the purpose of scholarly research.

Hany Ahmed Aly Abdalla

I further authorize the University of Windsor to reproduce the document by photocopying or by other means, in total or in part, at the request of other institutions or individuals for the purpose of scholarly research.

Hany Ahmed Aly Abdalla

THE UNIVERSITY OF WINDSOR requires the signatures of all persons using or photocopying this document.

Please sign below, and give address and date.

ABSTRACT

Web openings in beams occur quite often in practice to provide convenient passage of environmental services. As a result, storey heights in buildings can be reduced resulting in major cost savings. Some openings generally give rise to excessive deflections and stresses which have to be taken into consideration. In this research, a theoretical and experimental study is carried out to determine the influence of openings on the static and dynamic responses of prestressed concrete beams. The effect of openings on the behaviour of such beams at different stages of loading - transfer stage, working stage, and ultimate stage - as well as under excitation of dynamic load, is presented. The influence of opening dimensions, horizontal and vertical locations, type of cross section on the static behaviour is investigated from the stand point of deformations, stresses, cracking, and ultimate strength capacity. Also the effect of these parameters as well as the number and dimensions of continuous spans on the natural frequencies, mode shapes, stresses, and deformations is presented. The results from a

non-linear finite element static analysis are substantiated by static test results from thirteen post-tensioned prestressed concrete beams, six of which were rectangular in section, five were T- , and two were of I- section. Also the results from a finite element dynamic analysis are substantiated by dynamic test results in the literature. Good agreement is shown between the theoretical and experimental results. Furthermore, an extensive parametric study is performed on prestressed beams with openings to: develop a design procedure against cracking of the opening chords; estimate the beam maximum deflection; find the distributing ratio of the shear force between the opening chords; obtain the ultimate capacity of prestressed beams with openings; and determine the natural frequencies, and hence the dynamic response of simply supported and continuous prestressed beams with openings.

TO MY FAMILY

ACKNOWLEDGEMENTS

The author wishes to express his sincere gratitude to his advisor Dr. J. B. Kennedy, Distinguished Professor, for his guidance, effort and patient encouragement during the development of this research. Dr. Kennedy devoted his time and effort to make this study a success. His most helpful supervision is greatly appreciated.

Thanks are due to Dr. G. Abdel-Sayed and Dr. M. K. S. Madugula for their willingness to lend support at all times. The author would also like to thank the faculty and staff of the Department of Civil and Environmental Engineering as well as the computer consultants of the Computing Services at the University of Windsor for their assistance. Special thanks are also due to Mr. Frank Kiss, the laboratory technician. His assistance during the preparation and testing of the beams is very much acknowledged. The author is also thankful to Mr. L. Collavino, Prestressed Systems Incorporated for supplying the form of the I-Beam tested in this study. The author would also like to thank his friend Alaa Aly for his help during casting and testing the beams used in the experimental study.

The author wishes to acknowledge the financial support provided by the Natural Sciences and Engineering Research Council of Canada.

Last but not least the author wishes to thank his wife Eman for her great support throughout the course of this study and for assisting in drafting the figures in this dissertation. Also without her understanding, encouragement and patience the completion of this work would not have been possible.

TABLE OF CONTENTS

ABSTRACT	vi
ACKNOWLEDGEMENTS	ix
List of Tables	xiv
List of Figures	xv
Nomenclature	xxxii
CHAPTER	
I- INTRODUCTION	1
1.1 General	1
1.2 Objectives and Scope	2
II- LITERATURE REVIEW	6
2.1 General	6
2.2 Steel Beams with Openings	7
2.3 Reinforced Concrete Beams with Openings	14
2.4 Prestressed Concrete Beams with Openings	22
2.5 Concrete Beams with Openings Subjected to Dynamic Loading	29
III- THEORETICAL ANALYSIS	33
3.1 General	33
3.2 Finite Element Static Analysis	34
3.3 The 'ABAQUS' Computer Program	36
3.4 Finite Element Model	37
3.5 Reinforced Concrete Modelling	38
3.6 Prestressing Modelling	39
3.7 Non-Linearity Control	40
3.8 Dynamic Analysis	42
3.8.1 Natural Frequency and Mode Shapes Extraction	42
3.8.2 Dynamic Analysis by the Modal Methods	42

3.9	Non-Linear Static Analysis of Prestressed Beams with Openings	43
3.10	Dynamic Analysis of Prestressed Beams with Openings	44
3.10.1	Natural Frequencies and Associated Mode Shapes	45
3.10.2	Dynamic Response of Simply Supported Beams with Openings	46
3.11	Parametric Study	48
IV-	EXPERIMENTAL INVESTIGATION	50
4.1	General	50
4.2	Materials	54
4.2.1	Concrete	54
4.2.1.1	Cement	54
4.2.1.2	Coarse Aggregates	54
4.2.1.3	Fine Aggregates	54
4.2.1.4	Mixing Water	55
4.2.2	Steel	55
4.2.3	Auxiliary Materials	56
4.3	Experimental Equipment	57
4.3.1	Equipment for Post-tensioning	57
4.3.2	Equipment for Loading	57
4.4	Preparation of the Test Beams	58
4.5	Experimental Test Procedure	62
V-	STATIC ANALYSIS AND DISCUSSION OF RESULTS	64
5.1	General	64
5.2	Deflection	65
5.2.1	Rectangular Beams	65
5.2.2	T-Beams	76
5.2.3	I-Beams	86
5.3	Strain and Stress Distribution	89
5.3.1	Horizontal Strain and Stress Distribution	89
5.3.1.1	Rectangular Beams	89
5.3.1.2	T-Beams	97
5.3.1.3	I-Beams	103
5.3.2	Vertical Strain and Stress Distribution	106
5.3.2.1	Rectangular Beams	106
5.3.2.2	T-Beams	115
5.3.2.3	I-Beams	121
5.3.3	Shear Strain and Stress Distribution	123
5.3.3.1	Rectangular Beams	123
5.3.3.2	T-Beams	131
5.3.3.3	I-Beams	136

5.4	Cracking and Mechanism of Failure	139
5.4.1	Rectangular Beams	139
5.4.2	T-Beams	147
5.4.3	I-Beams	154
VI-	DYNAMIC ANALYSIS AND DISCUSSION OF RESULTS	157
6.1	General	157
6.2	Natural Frequency of Simply Supported Prestressed Beams with Openings	158
6.3	Natural Frequency of Continuous Beams with Openings	161
6.4	Dynamic Response of Simply Supported Beams with Openings	165
6.4.1	Deflection	166
6.4.2	Horizontal Stress	168
6.4.2.1	Mid-Span Stress	168
6.4.2.2	Stresses at the Opening Chords	170
6.4.3	Splitting Stress at the Opening Corners	173
VII-	DESIGN METHODS AND PARAMETRIC STUDY	175
7.1	General	175
7.2	Distribution of Shear between Top and Bottom Chords of Opening	177
7.3	Design Procedure Against Cracking of the Opening Chords	180
7.4	Vertical Tensile Stress at the Opening due to Prestressing Force and the Externally Applied Load	184
7.4.a	Vertical Tensile Stress at the Opening due to Prestressing Force	184
7.4.b	Vertical Tensile Stress at the Opening due to Vertical Load	187
7.4.c	Parametric Study for Determining the Vertical Tensile Stress at the Opening due to Vertical Load	190
7.5	Illustrative Design Example (Prestressed Beam with Opening under Static Loading)	193
7.6	Deflection Due to Vierendeel Action	197
7.7	Ultimate Capacity of Prestressed Beams with Openings	200
7.7.1	Strut Failure of Prestressed Beams with Openings	201
7.7.2	Illustrative Design Example (Ultimate Failure of Prestressed Beam with Opening)	204
7.7.3	Formation of a Plastic Hinge at the Opening Ends	206
7.7.4	Shear Failure in the Opening Chords	212
7.8	Dynamic Analysis of Simply Supported Prestressed Beams with Openings	215
7.8.1	Mid-Span Deflection	216

7.8.2	Bending Moment at Mid-Span and at Mid-Opening .	217
7.8.3	Shear Force at Support and at Mid-Opening	218
7.8.4	Secondary Moment at the Opening Edges	219
7.8.5	Splitting Stress at Opening Corners	219
7.8.6	Illustrative Design Example	
	Dynamic Response of Simply Supported Beam	
	with Shear Opening	221
VIII-	SUMMARY AND CONCLUSIONS	227
8.1	Summary	227
8.2	Conclusions	228
8.3	Recommendations for Future Research	233
TABLES	240
FIGURES	241
Appendix A.1	'ABAQUS' INPUT DATA	597
Appendix A.2	CONCRETE MIX DESIGN	613
Appendix A.3	CALLIBRATION OF LOAD CELLS AND	
	STRAIN GAUGE ARRANGEMENT	617
REFERENCES	630
VITA AUCTORIS	638

LIST OF TABLES

<u>Table</u>		<u>Page</u>
3.1	Characteristics of Rectangular Beams Used in the Non-Linear Analysis	234
3.2	Characteristics of T- and I- Beams Used in the Non-Linear Analysis	235
3.3	Characteristics of Rectangular Beams (Parametric Study for Shear Distribution)	236
3.4	Characteristics of T- and I- Beams (Parametric Study for Shear Distribution)	237
4.1	Characteristics of the Tested Rectangular Beams	238
4.2	Characteristics of the Tested T- and I- Beams	239
6.1	Percentage Change in First Three Natural Frequencies as Compared to Those of Solid Beam	240

LIST OF FIGURES

<u>Figure</u>	<u>Page</u>
1.1 Static Analysis Layout (Theoretical Analysis)	241
1.2 Static Analysis Layout (Experimental Study)	242
1.3 Dynamic Analysis Layout (Natural Frequencies)	243
1.4 Dynamic Analysis Layout (Dynamic Response)	244
3.1 Newton's Method	245
3.2 Plane Stress Element CPS4	246
3.3 Shell Element S4R	247
3.4 Uniaxial Behaviour of Plain Concrete	248
3.5 Yield and Failure Surfaces of Concrete in Plane Stress	249
3.6 Tension Stiffening of Concrete	250
3.7 Typical Rectangular Beam Layout	251
3.8 Typical T-Beam Layout	252
3.9 Typical I-Beam Layout	253
3.10 Definition of the Beams Used in the Non-Linear Analysis	254
3.11 Typical Finite Element Mesh for a Rectangular Beam	255
3.12 Typical Finite Element Mesh for a T-Beam	256
3.13 Typical Finite Element Mesh for an I-Beam	257

3.14	Simply Supported Beams Used in the Dynamic Analysis	258
3.15	Typical Finite Element Mesh for a Simply Supported Beam (a) with Opening in High Shear Region; (b) with Opening in High Moment Region	259
3.16	Opening Locations in the Analyzed Continuous Beams	260
3.17	Typical Finite Element Mesh for a Continuous Beam	261
3.18	Typical Layout of Simply Supported Beams Used in the Parametric Study	262
3.19	Typical Finite Element Mesh for Simply Supported Beam	263
4.1.a	Test Arrangement to Study the Effect of Continuity	264
4.1.b	Actual Test Arrangement to Simulate (a) above	264
4.2	Test Set-up for a Rectangular Beam	265
4.3	Test Set-up for a T-Beam	266
4.4	Test Set-up for an I-Beam	267
4.5	Reinforcement Details for Beam BIIA	268
4.6	Reinforcement Details for Beam BIII A	269
4.7	Reinforcement Details for Beam BIII1A	270
4.8.a	Unjacked End of the First Type of Prestressing Wires	271
4.8.b	Jacked End of the First Type of Prestressing Wires	272
4.9.a	Unjacked End of the Second Type of Prestressing Wires	273
4.8.b	Jacked End of the Second Type of Prestressing Wires	274
4.10	Typical Stress-Strain Curve for the Prestressing Steel (Type 1)	275
4.11	Non-Prestressing Reinforcement of a T-beam	276
4.12	End-Plate for an I-beam	277

4.13	Anchorage Units and Load Cell Used in Prestressing	278
4.14	The Prestressing Hydraulic Jack	279
4.15	Electric Strain Gauges on a Rectangular Beam	280
4.16	Electric Strain Gauges on a T-Beam	281
4.17	Electric Strain Gauges on an I-Beam	282
4.18	The Automatic Strain Indicator	283
5.1	Load-Deflection Relationship for BI1A	284
5.2	Load-Deflection Relationship for BI1B	285
5.3	Load-Deflection Relationship for BI1, BI1A, BI1B& BI1C	286
5.4	Opening Deflection for BI1A (Experimental)	287
5.5	Opening Deflection for BI1B (Experimental)	288
5.6	Deflected Shape for BI1, BI1A, BI1B& BI1C	289
5.7	Deflected Shape for BI1, BI1A, BI1B& BI1C (P=0 & P=2 kip)	290
5.8	Load-Deflection Relationship for BI2A	291
5.9	Load-Deflection Relationship for BI2B	292
5.10	Load-Deflection Relationship for BI2C	293
5.11	Load-Deflection Relationship for BI2, BI2A, BI2B& BI2C	294
5.12	Opening Deflection for BI2A (Experimental)	295
5.13	Opening Deflection for BI2B (Experimental)	296
5.14	Opening Deflection for BI2C (Experimental)	297
5.15	Deflected Shape for BI2, BI2A, BI2B& BI2C (P=0 & P=2 kip)	298
5.16	Deflected Shape for BI2, BI2A, BI2B& BI2C (Due to P=2 kip)	299

5.17	Load-Deflection Relationship for BI3C	300
5.18	Load-Deflection Relationship for BI3, BI3A, BI3B& BI3C	301
5.19	Opening Deflection for BI3C (Experimental)	302
5.20	Deflected Shape for BI3, BI3A, BI3B& BI3C (P=0& P=2 kip)	303
5.21	Load-Deflection Relationship for BI4, BI4A, BI4B& BI4C	304
5.22	Deflected Shape for BI4, BI4A, BI4B& BI4C (P=0 & P=2 kip)	305
5.23	Deflected Shape for BI4, BI4A, BI4B& BI4C (P=2 kip)	306
5.24	Load-Deflection Relationship for BII1A	307
5.25	Load-Deflection Relationship for BII1B	308
5.26	Load-Deflection Relationship for BII1C	309
5.27	Load-Deflection Relationship for BII1, BII1A, BII1B& BII1C	310
5.28	Opening Deflection for BII1A (Experimental)	311
5.29	Opening Deflection for BII1B (Experimental)	312
5.30	Opening Deflection for BII1C (Experimental)	313
5.31	Deflected Shape for BII1, BII1A, BII1B& BII1C (P=0, P=2.5& P=5 kip)	314
5.32	Load-Deflection Relationship for BII2B	315
5.33	Load-Deflection Relationship for BII2, BII2A, BII2B& BII2C	316
5.34	Opening Deflection for BII2B (Experimental)	317
5.35	Deflected Shape for BII2, BII2A, BII2B& BII2C (P=0 & P=2.5& P=5 kip)	318
5.36	Deflected Shape for BII2, BII2A, BII2B& BII2C (Due to P=2.5& P=5 kip)	319
5.37	Load-Deflection Relationship for BII3, BII3A, BII3B& BII3C	320
5.38	Deflected Shape for BII3, BII3A, BII3B& BII3C (P=0, P=2.5& P=5 kip)	321

5.39	Load-Deflection Relationship for BII4C	322
5.40	Load-Deflection Relationship for BII4, BII4A, BII4B& BII4C	323
5.41	Opening Deflection for BII4C (Experimental)	324
5.42	Deflected Shape for BII4, BII4A, BII4B& BII4C (P=0 & P=2.5& P=5 kip)	325
5.43	Load-Deflection Relationship for BIII1A	326
5.44	Load-Deflection Relationship for BIII1C	327
5.45	Load-Deflection Relationship for BIII1, BIII1A, BIII1B& BIII1C	328
5.46	Opening Deflection for BIII1A (Experimental)	329
5.47	Opening Deflection for BIII1C (Experimental)	330
5.48	Deflected Shape for BIII1, BIII1A, BIII1B& BIII1C (P=0, P=4& P=8 kip)	331
5.49	Horizontal Stress Distribution for Beam BI1A	332
5.50	Horizontal Stress Distribution for Beams BI1B& BI3A	333
5.51	Horizontal Stress Distribution for Beam BI1C	334
5.52	Horizontal Stress Distribution for Beam BI2A	335
5.53	Horizontal Stress Distribution for Beam BI2B	336
5.54	Horizontal Stress Distribution for Beam BI2C	337
5.55	Horizontal Stress Distribution at Mid-Opening for Group BI2 (P=2 kip)	338
5.56	Horizontal Stress Distribution for Beams BI3B& BI4A	339
5.57	Horizontal Stress Distribution for Beam BI3C	340
5.58	Horizontal Stress Distribution for Beam BI4B	341
5.59	Horizontal Stress Distribution for Beam BI4C	342
5.60	Horizontal Stress Distribution for Beam BII1A	343

5.61	Horizontal Stress Distribution for Beams BII1B, BII2A, BII3B& BII4B	344
5.62	Horizontal Stress Distribution for Beam BII1C	345
5.63	Horizontal Stress Distribution for Beam BII2B	346
5.64	Horizontal Stress Distribution for Beam BII2C	347
5.65	Horizontal Stress Distribution for Beam BII3A	348
5.66	Horizontal Stress Distribution for Beam BII3C	349
5.67	Horizontal Stress Distribution for Beam BII4A	350
5.68	Horizontal Stress Distribution for Beam BII4C	351
5.69	Horizontal Stress Distribution for Beam BIII1A	352
5.70	Horizontal Stress Distribution for Beam BIII1B	353
5.71	Horizontal Stress Distribution for Beam BIII1C	354
5.72	Vertical Stress Distribution for Beam BI1A	355
5.73	Vertical Stress Distribution for Beams BI1B& BI3A	356
5.74	Vertical Stress Distribution for Beam BI1C	357
5.75	Vertical Stress Distribution at the Opening for Beam BI1A	358
5.76	Vertical Stress Distribution at the Opening for Beam BI1B	359
5.77	Vertical Stress Distribution at the Opening for Beam BI1C	360
5.78	Vertical Stress Distribution for Beam BI2A	361
5.79	Vertical Stress Distribution for Beam BI2B	362
5.80	Vertical Stress Distribution for Beam BI2C	363
5.81	Vertical Stress Distribution at the Opening for Beam BI2A	464
5.82	Vertical Stress Distribution at the Opening for Beam BI2B	365

5.83	Vertical Stress Distribution at the Opening for Beam BI2C	366
5.84	Vertical Stress Distribution at the Opening for Group BI2 (P=2 kip)	367
5.85	Vertical Stress Distribution for Beam BI3B	368
5.86	Vertical Stress Distribution for Beam BI3C	369
5.87	Vertical Stress Distribution at the Opening for Beam BI3A	370
5.88	Vertical Stress Distribution at the Opening for Beam BI3B	371
5.89	Vertical Stress Distribution at the Opening for Beam BI3C	372
5.90	Vertical Stress Distribution at the Opening for Group BI3 (P=0)	373
5.91	Vertical Stress Distribution at the Opening for Group BI3 (P=2 kip)	374
5.92	Vertical Stress Distribution at the Opening for Group BI3 (P=4 kip)	375
5.93	Vertical Stress Distribution for Beam BI4A	376
5.94	Vertical Stress Distribution for Beam BI4B	377
5.95	Vertical Stress Distribution for Beam BI4C	378
5.96	Vertical Stress Distribution at the Opening for Beam BI4A	379
5.97	Vertical Stress Distribution at the Opening for Beam BI4B	380
5.98	Vertical Stress Distribution at the Opening for Beam BI4C	381
5.99	Vertical Stress Distribution at the Opening for Group BI4 (P=0)	382
5.100	Vertical Stress Distribution at the Opening for Group BI4 (P=2 kip)	383
5.101	Vertical Stress Distribution at the Opening for Group BI4 (P=3.5 kip)	384
5.102	Vertical Stress Distribution for Beam BII1A	385
5.103	Vertical Stress Distribution for Beams BII1B, BII2A, BII3B& BII4B	386
5.104	Vertical Stress Distribution for Beam BII1C	387

5.105	Vertical Stress Distribution at the Opening for Beam BII1A	388
5.106	Vertical Stress Distribution at the Opening for Beam BII1B	389
5.107	Vertical Stress Distribution at the Opening for Beam BII1C	390
5.108	Vertical Stress Distribution for Beam BII2B	391
5.109	Vertical Stress Distribution for Beam BII2C	392
5.110	Vertical Stress Distribution at the Opening Edges for Group BII2 (P=2.5 kip)	393
5.111	Vertical Stress Distribution at the Opening for Beam BII2A	394
5.112	Vertical Stress Distribution at the Opening for Beam BII2B	395
5.113	Vertical Stress Distribution at the Opening for Beam BII2C	396
5.114	Vertical Stress Distribution for Beam BII3A	397
5.115	Vertical Stress Distribution for Beam BII3C	398
5.116	Vertical Stress Distribution at the Opening for Beam BII3A	399
5.117	Vertical Stress Distribution at the Opening for Beam BII3B	400
5.118	Vertical Stress Distribution at the Opening for Beam BII3C	401
5.119	Vertical Stress Distribution for Beam BII4A	402
5.120	Vertical Stress Distribution for Beam BII4C	403
5.121	Vertical Stress Distribution at the Opening for Beam BII4A	404
5.122	Vertical Stress Distribution at the Opening for Beam BII4B	405
5.123	Vertical Stress Distribution at the Opening for Beam BII4C	406
5.124	Vertical Stress Distribution for Beam BIII1A	407
5.125	Vertical Stress Distribution for Beam BIII1B	408
5.126	Vertical Stress Distribution for Beam BIII1C	409

5.127	Vertical Stress Distribution at the Opening for Beam BIII1A	410
5.128	Vertical Stress Distribution at the Opening for Beam BIII1B	411
5.129	Vertical Stress Distribution at the Opening for Beam BIII1C	412
5.130	Shear Stress Distribution for Beam BI1A	413
5.131	Shear Stress Distribution for Beams BI1B& BI3A	414
5.132	Shear Stress Distribution for Beam BI1C	415
5.133	Distribution of Shear Force between Top and Bottom Chords for Group BI1	416
5.134	Shear Stress Distribution for Beam BI2A	417
5.135	Shear Stress Distribution for Beam BI2B	418
5.136	Shear Stress Distribution for Beam BI2C	419
5.137	Distribution of Shear Force between Top and Bottom Chords for Group BI2	420
5.138	Shear Stress Distribution for Beam BI3B	421
5.139	Shear Stress Distribution for Beam BI3C	422
5.140	Distribution of Shear Force between Top and Bottom Chords for Group BI3	423
5.141	Shear Stress Distribution for Beam BI4A	424
5.142	Shear Stress Distribution for Beam BI4B	425
5.143	Shear Stress Distribution for Beam BI4C	426
5.144	Distribution of Shear Force between Top and Bottom Chords for Group BI4	427
5.145	Shear Stress Distribution for Beam BII1A	428
5.146	Shear Stress Distribution for Beams BII1B, BII2A, BII3B& BII4B	429

5.147	Shear Stress Distribution for Beam BII1C	430
5.148	Distribution of Shear Force between Top and Bottom Chords for Group BII1	431
5.149	Shear Stress Distribution for Beam BII2B	432
5.150	Shear Stress Distribution for Beam BII2C	433
5.151	Distribution of Shear Force between Top and Bottom Chords for Group BII2	434
5.152	Shear Stress Distribution for Beam BII3A	435
5.153	Shear Stress Distribution for Beam BII3C	436
5.154	Distribution of Shear Force between Top and Bottom Chords for Group BII3	437
5.155	Shear Stress Distribution for Beam BII4A	438
5.156	Shear Stress Distribution for Beam BII4C	439
5.157	Distribution of Shear Force between Top and Bottom Chords for Group BII4	440
5.158	Shear Stress Distribution for Beam BIII1A	441
5.159	Shear Stress Distribution for Beam BIII1B	442
5.160	Shear Stress Distribution for Beam BIII1C	443
5.161	Distribution of Shear Force between Top and Bottom Chords for Group BIII1	444
5.162	Crack Pattern for Beam BI1A	445
5.163	Failure Mode for Beam BI1A	446
5.164	Crack Pattern for Beam BI1B	448
5.165	Failure Mode for Beam BI1B	449
5.166	Theoretical Crack Pattern for Beam BI1A	452

5.167	Theoretical Crack Pattern for Beam BI1B	453
5.168	Theoretical Crack Pattern for Beam BI1C	454
5.169	Crack Pattern and Failure Mode for Beam BI2A	455
5.170	Crack Pattern for Beam BI2B	457
5.171	Failure Mode for Beam BI2B	458
5.172	Crack Pattern for Beam BI2C	460
5.173	Failure Mode for Beam BI2C	462
5.174	Theoretical Crack Pattern for Beam BI2A	464
5.175	Theoretical Crack Pattern for Beam BI2B	465
5.176	Theoretical Crack Pattern for Beam BI2C	466
5.177	Crack Pattern for Beam BI3C	467
5.178	Failure Mode for Beam BI3C	469
5.179	Theoretical Crack Pattern for Beam BI3C	470
5.180	Theoretical Crack Pattern for Beam BI4A	471
5.181	Theoretical Crack Pattern for Beam BI4B	472
5.182	Theoretical Crack Pattern for Beam BI4C	473
5.183	Crack Pattern for Beam BII1A	474
5.184	Failure Mode for Beam BII1A	477
5.185	Crack Pattern for Beam BII1B	479
5.186	Failure Mode for Beam BII1B	482
5.187	Crack Pattern for Beam BII1C	486
5.188	Failure Mode for Beam BII1C	488

5.189	Theoretical Crack Pattern for Beam BII1A	491
5.190	Theoretical Crack Pattern for Beam BII1B	492
5.191	Theoretical Crack Pattern for Beam BII1C	493
5.192	Crack Pattern for Beam BII2B	494
5.193	Failure Mode for Beam BII2B	497
5.194	Theoretical Crack Pattern for Beam BII2B	498
5.195	Theoretical Crack Pattern for Beam BII2C	499
5.196	Theoretical Crack Pattern for Beam BII3A	500
5.197	Theoretical Crack Pattern for Beam BII3C	501
5.198	Crack Pattern for Beam BII4C	502
5.199	Failure Mode for Beam BII4C	506
5.200	Theoretical Crack Pattern for Beam BII4A	508
5.201	Theoretical Crack Pattern for Beam BII4C	509
5.202	Crack Pattern for Beam BIII1A	510
5.203	Failure Mode for Beam BIII1A	513
5.204	Crack Pattern for Beam BIII1C	517
5.205	Failure Mode for Beam BIII1C	519
5.206	Theoretical Crack Pattern for Beam BIII1A	520
5.207	Theoretical Crack Pattern for Beam BIII1B	522
5.208	Theoretical Crack Pattern for Beam BIII1C	524
6.1	Simply Supported Prestressed Beams Considered in the Dynamic Analysis	526
6.2	Geometries of Simply Supported Beams Considered	

	in the Parametric Study	527
6.3	Fundamental Frequency for Beam with Shear Opening	528
6.4	Fundamental Frequency for Beam with Bending Opening	529
6.5	First Three Mode Shapes of Simply Supported Beam with Shear Opening	530
6.6	First Three Mode Shapes of Simply Supported Beam with Bending Opening	531
6.7	Natural Frequencies for Solid Beam, Beam with Shear Opening & Beam with Bending Opening	532
6.8	Frequency Spectrum Response (Steady State Analysis)	533
6.9	Natural Frequencies for Continuous Beams with Two Equal-Spans	534
6.10	Natural Frequencies for Continuous Beams with Two Unequal-Spans	535
6.11	Relationship between Opening Width and Fundamental Frequency for Continuous Beams with Two-Equal Spans	536
6.12	Relationship between Opening Depth and Fundamental Frequency for Continuous Beams with Two-Equal Spans	537
6.13	Relationship between Opening Width and Fundamental Frequency for Continuous Beams with Two-Unequal Spans	538
6.14	Relationship between Opening Depth and Fundamental Frequency for Continuous Beams with Two-Unequal Spans	539
6.15	First Three Mode Shapes of Two Equal-Spans Continuous Beam with No Openings	540
6.16	First Three Mode Shapes of Two Equal-Spans Continuous Beam with Opening Close to the Exterior Support	541
6.17	First Three Mode Shapes of Two Equal-Spans Continuous Beam with Opening at Mid-Span	542
6.18	First Three Mode Shapes of Two Equal-Spans Continuous Beam with Opening Close to the Interior Support	543

6.19	First Three Mode Shapes of Two Unequal-Spans Continuous Beam with Opening Close to the Interior Support	544
6.20.a	First Mode Shape of Two Equal-Spans Continuous T-Beam with Opening	545
6.20.b	Second Mode Shape of Two Equal-Spans Continuous T-Beam with Opening	546
6.20.c	Third Mode Shape of Two Equal-Spans Continuous T-Beam with Opening	547
6.20.d	Fourth Mode Shape of Two Equal-Spans Continuous T-Beam with Opening	548
6.21.a	Sinusoidal Forcing Function for the Applied Load ($\Omega=10$ Hz, $P_0=0.5$ kip)	549
6.21.b	Sinusoidal Forcing Function for the Applied Load ($\Omega=30$ Hz, $P_0=0.5$ kip)	550
6.22	Sinusoidal Forcing Function for the Applied Load ($\Omega=10$ Hz, $P_0=0.2$ kip, $P_1=0.3$ kip)	551
6.23.a	Mid-Span Deflection ($\Omega=10$ Hz, $P_0=0.5$ kip)	552
6.23.b	Mid-Span Deflection ($\Omega=30$ Hz, $P_0=0.5$ kip)	553
6.24.a	Mid-Span Deflection ($\Omega=10$ Hz, $P_0=0.5$ kip)	554
6.24.b	Mid-Span Deflection ($\Omega=30$ Hz, $P_0=0.5$ kip)	555
6.25	Variation of Amplitude Ratio with Frequency Ratio	556
6.26.a	Beam Deflected Shape ($\Omega=10$ Hz, $P_0=0.5$ kip)	557
6.26.b	Beam Deflected Shape ($\Omega=30$ Hz, $P_0=0.5$ kip)	558
6.27	Mid-Span Deflection ($\Omega=10$ Hz, $P_0=0.2$ kip, $P_1=0.3$ kip)	559
6.28.a	Maximum Horizontal Stress at Mid-span ($\Omega=10$ Hz, $P_0=0.5$ kip)	560
6.28.b	Maximum Horizontal Stress at Mid-span ($\Omega=30$ Hz, $P_0=0.5$ kip)	561

6.29	Maximum Horizontal Stress at Mid-span (Steady State Analysis)	562
6.30	Maximum Horizontal Stress at Mid-span ($\Omega=10$ Hz, $P_0=0.2$ kip, $P_1=0.3$ kip)	563
6.31.a	Horizontal Stress at the Opening Lower Right Corner ($\Omega=10$ Hz, $P_0=0.5$ kip) Shear Opening	564
6.31.b	Horizontal Stress at the Opening Lower Left Corner ($\Omega=10$ Hz, $P_0=0.5$ kip) Shear Opening	565
6.32.a	Horizontal Stress at the Opening Lower Right Corner ($\Omega=10$ Hz, $P_0=0.5$ kip) Bending Opening	566
6.32.b	Horizontal Stress at the Opening Lower Left Corner ($\Omega=10$ Hz, $P_0=0.5$ kip) Bending Opening	567
6.33.a	Horizontal Stress at the Opening Lower Right Corner ($\Omega=30$ Hz, $P_0=0.5$ kip) Shear Opening	568
6.33.b	Horizontal Stress at the Opening Lower Left Corner ($\Omega=30$ Hz, $P_0=0.5$ kip) Shear Opening	569
6.34.a	Horizontal Stress at the Opening Lower Right Corner ($\Omega=30$ Hz, $P_0=0.5$ kip) Bending Opening	570
6.34.b	Horizontal Stress at the Opening Lower Left Corner ($\Omega=30$ Hz, $P_0=0.5$ kip) Bending Opening	571
6.35.a	Horizontal Stress at the Opening Lower Left Corner ($\Omega=10$ Hz, $P_0=0.2$ kip, $P_1=0.3$ kip) Shear Opening	572
6.35.b	Horizontal Stress at the Opening Lower Right Corner ($\Omega=10$ Hz, $P_0=0.2$ kip, $P_1=0.3$ kip) Shear Opening	573

6.36.a	Horizontal Stress at the Opening Lower Left Corner ($\Omega=10$ Hz, $P_0=0.2$ kip, $P_1=0.3$ kip) Bending Opening	574
6.36.b	Horizontal Stress at the Opening Lower Right Corner ($\Omega=10$ Hz, $P_0=0.2$ kip, $P_1=0.3$ kip) Bending Opening	575
6.37	Splitting Stress at the Corners of Opening ($\Omega=10$ Hz, $P_0=0.5$ kip)	576
6.38	Splitting Stress at the Corners of Opening ($\Omega=30$ Hz, $P_0=0.5$ kip)	577
6.39.a	Splitting Stress at the Corner of a Shear Opening (Steady State Analysis)	578
6.39.b	Splitting Stress at the Corner of a Bending Opening (Steady State Analysis)	579
6.40	Splitting Stress at the Corners of Opening ($\Omega=10$ Hz, $P_0=0.2$ kip, $P_1=0.3$ kip)	580
7.1	Shear Force Carried by the Bottom Chord (Rectangular Section)	581
7.2	Shear Force Carried by the Bottom Chord (T-Section)	582
7.3	Shear Force Carried by the Bottom Chord (T-Section)	583
7.4	Free-Body Diagram for a Prestressed I-Beam with Opening	584
7.5	Development of Vertical Tensile Force at an Opening	585
7.6	Vertical Tensile and Compressive Stresses at the Opening due to Vertical Load Only	586
7.7	Framing Action Around the Opening	587
7.8	Splitting Stress at the Opening due to Prestressing	588
7.9	Cross-Section of Prestressed I-Beam in Illustrated Design Example	589
7.10	Relative Displacement between the End ; of Opening due to Vierendeel Action	590

7.11	Factor α for Estimating the Local Deflection at the Opening	591
7.12	Free-Body diagram at Beam Opening	592
7.13	Prestressed Beam in Illustrated Design Example (a) Beam Geometry; (b) Dimensions of Bottom Chord	593
7.14	Plastic Analysis of Prestressed Beams with Openings	594
7.15	Geometry of Reinforced and Prestressed Concrete Sections	595
7.16	Effect of Prestressing on the Natural Frequencies	596

NOMENCLATURE

A_b, A_t	cross-sectional areas of bottom and top chords, respectively.
A_{pr}	area of prestressed reinforcement.
B	width of beam's flange(s).
b	width of beam's web.
C	distance from centre of the opening to the bottom (top) of the simply supported (continuous) beam.
d	depth of reinforced concrete section.
d_c, d_t	lengths of compression and tension fields, respectively.
e	eccentricity of force, F , from centroidal axis of section.
F	prestressing force.
F_v	component of prestressing force causing vertical tensile stress at opening.
f'_c	compressive strength of concrete.
f_t	allowable tensile stress of concrete.
f_t	splitting tensile stress.
f_{tc}	splitting tensile stress at the opening corner.
f_{tr}	splitting tensile stress due to prestressing force.
f_{tv}	splitting tensile stress due to vertical load.
f_y	yield stress of steel.
H	total depth of cross section of beam.
h	depth of opening.

h_b, h_t	depth of bottom and top chords of opening, respectively.
I	moment of inertia of beam cross-section.
I_b, I_t	moments of inertia of bottom and top chords, about their centroidal axes, respectively.
L	length of the beam.
l	distance between the support and the edge of the opening.
M_{cr}	moment causing flexural cracks at section considered.
M_m	moment at mid-width of the opening.
M_{tb}, M_{tt}	secondary moment at the bottom and top chords, respectively.
N	normal force in the opening chords.
P	externally applied load.
T_t	vertical tensile force near opening due to prestressing force.
T_v	vertical tensile force near opening due to vertical load.
t	thickness of beam's flange(s).
V	total shear force.
V_b, V_t	shear force carried by bottom and top chords, respectively.
W	width of opening.
Z	distance between the plastic centroids of the chords of opening.
Δ_b	deflection of beam.
Δ_{bg}	deflection of beam with opening in high moment region.
Δ_v	deflection of opening chords due to the Vierendeel action.
Δ_{vt}	deflection of opening chords due to the Vierendeel action considering fixed-fixed ends.

ξ	damping ratio.
Ω	frequency of the exciting load.
ω_{bg}	natural frequency of beam with opening in high moment region.
ω_o	natural frequency of solid beam.
ω_{sh}	natural frequency of beam with opening in high shear region.

CHAPTER I

INTRODUCTION

1.1 General

There is a growing trend in recent years in constructing high-rise buildings where the extra space above false ceilings is eliminated by passing service ducts through openings in the floor beams. Such an arrangement in building services minimizes the dead space and thus leads to economy. However, introducing an opening in the web of reinforced and prestressed concrete beams reduces the beam stiffness and leads to more complicated behaviour. Therefore, the effect of openings on the strength, serviceability, and dynamic response of beams containing such openings must be considered in the design process.

It should be pointed out that the design of prestressed concrete beams with openings is more involved than the design of their counterparts in reinforced concrete construction. The openings in the latter are usually located in the zone below the neutral axis where the concrete is assumed cracked and therefore flexurally inactive. On the

other hand, in prestressed concrete construction, the whole cross-section is fully utilized and hence, the presence of an opening will reduce the strength of such beams.

In the past, many researches had been carried out on reinforced concrete and steel beams with openings. Comparatively little attention had been directed toward the behaviour of post-tensioned prestressed beams with openings. Moreover a very limited number of investigations had been conducted to predict the dynamic response of such beams.

In this dissertation, the prediction of non-linear static behaviour of continuous prestressed concrete rectangular, T- , and I- beams is presented. Also the dynamic response of simply supported and continuous beams with equal and unequal spans is investigated. Simple design methods to predict such behaviours are given.

1.2 Objectives and Scope

This study is an attempt to examine the behaviour of prestressed concrete beams with openings: in the transfer stage, where the beam is subjected to prestressing force only; in the working stage where the beam is subjected to a transverse load and its behaviour is elastic, and, in the non-linear stage where the transverse load has caused excessive cracking in the critical sections of the beam, leading to collapse. In this respect, experimental and analytical efforts were carried out to examine the effect of openings on such behaviour.

The primary objectives of this investigation may be summarized as follows (see Figs. 1.1 to 1.4):

1- To examine theoretically and experimentally, the behaviour of prestressed beams with openings during the previously mentioned stages of loading from the stand point of (i) the stress distribution in the vicinity of the opening, (ii) the crack propagation pattern, and (iii) the global deflection of the beam and the local deflection of the opening chords.

2- To find a rational method of distributing the shear force between the top and bottom chords of the opening. This ratio plays an important role in determining the cracking as well as ultimate capacities of beams with openings.

3- To develop a design method against cracking of the opening chords, and to determine the cracking load of such beams.

4- To determine the effect of the vertical load on the splitting tensile stress at the opening edges caused by prestressing force.

5- To estimate the deflection of simply supported and continuous prestressed concrete beams with openings.

6- To develop a method for estimating the ultimate capacity of the prestressed beams with openings due to different failure modes.

7- To investigate the effect of the presence of rectangular openings on the natural frequencies and mode shapes of prestressed concrete beams with openings, and to find an approximate method to determine these frequencies.

8- To examine the effect of openings on the dynamic response of prestressed

concrete beams from the stand point of displacements, horizontal and vertical stresses at mid-spans of simple beams and at the critical sections in the vicinity of the opening.

9- To develop a simple design method to determine the displacements and stresses mentioned in (8) under the excitation of dynamic loads.

The contributions of this candidate to the advancement of knowledge of this field of engineering are that all the above objectives were achieved.

The experimental program consisted of testing a total of thirteen prestressed concrete beams with openings, six with rectangular cross-sections, five with T-sections, and two with I-sections. Also the results from six prestressed concrete beams with openings under dynamic loading and conducted by Chami (1987), were used for comparison with the finite element dynamic analysis. Non-linear finite element analyses were carried out to determine the effect of different parameters on the static behaviour of prestressed concrete beams with openings. The following design parameters were considered: (i) horizontal and vertical location of the opening, (ii) opening width and depth, (iii) type of cross-section, and (iv) continuity of prestressed beams with openings. An extensive parametric study was carried out to achieve the objectives mentioned above.

The contents of this dissertation are as follows:

~~Chapter~~ **Chapter III** contains a review of the theoretical and experimental study of the behaviour of prestressed, reinforced, and steel beams with openings under static loading, and concrete beams with openings under dynamic loading.

Chapter III focuses on the finite element formulation and gives a brief description for the parts of the 'ABAQUS' computer code (Hibbitt et al., 1989) which were used in the analysis. Also a description of the methods dealing with concrete non-linearity and of the methods of dynamic analysis are presented.

Chapter IV deals with the experimental program with a full description of the prestressed beams tested in the laboratory, the prestressing procedure, the equipment and material used to accomplish the experimental program.

Chapter V presents the discussion of results from the experimental and theoretical analyses and the effect of different parameters on the static behaviour of prestressed beams with openings.

Chapter VI presents the discussion of results from the theoretical dynamic analysis and the effect of different design parameters on the natural frequencies, mode shapes, and dynamic response of prestressed beams with openings.

Chapter VII deals with developing design methods for analysis of prestressed concrete beams with openings under the effect of static and dynamic loading.

Chapter VIII contains the summary and conclusions of the study as well as recommendations for future research.

CHAPTER II

LITERATURE REVIEW

2-1 General

Design of prestressed concrete beams with openings is more complicated than that of reinforced concrete beams. Openings in reinforced concrete beams are normally provided in the bending zone below the neutral axis where the concrete is cracked and assumed to be inactive. On the other hand, the problem is different in prestressed concrete beams where the whole cross section is fully utilized and assumed to be free from cracks. Accordingly, the presence of an opening in prestressed concrete beams reduces the strength of such beams.

Many researchers have studied the behaviour of reinforced concrete and steel beams with openings. However, only a limited number of investigations has been carried out on the behaviour of prestressed concrete beams with rectangular openings.

The literature survey conducted is presented as follows:

- 1- Steel beams with openings.
- 2- Reinforced concrete beams with openings.
- 3- Prestressed concrete beams with openings.
- 4- Concrete beams with openings subjected to dynamic loading.

2-2 Steel Beams with Openings

Senger (1964) presented a method for determining the amount of, as well as the necessity for, reinforcement around large rectangular openings in the webs of wide-flange beams subjected to varying combinations of bending moment and shear. His method was based on a Vierendeel Truss analogy. During the course of his research, the entire project was limited to I-shaped beams with rectangular openings centred on the neutral axis of the members. According to his approach, the flexural stress at any end section of the opening was the algebraic sum of the stress produced by the applied bending moment, M , at the centre of the opening and the shear bending moment $VW/4$ where V is the shear at the centre of the opening and W is the opening width. In other words, he assumed the vertical shear to be equally distributed to the remaining material above and below the opening. According to his study, no appreciable difference was found in the ultimate moment of the reinforced section as compared to the ultimate moment of the gross section. From his test results, he found that the analysis based on Vierendeel Truss analogy was appropriate.

Bower (1966) investigated the elastic stress around elliptic and circular holes in

wide-flange simply supported beams under uniform load. He computed the stresses in the beam with no hole and the stresses as a result of forces applied to the boundary of the hole. These latter forces were applied in such a manner that the resulting perturbed stresses and the basic stresses satisfied the required boundary condition at the hole. The applicability of this analysis depends on the size of the web hole and on the magnitude of the moment-shear ratio at the hole.

Redwood and McCutcheon (1968) made some tests to failure on steel wide flange beams containing one or two unreinforced openings of various shapes under different ratios of shear to moment. By measuring the plastic moment at the opening when failure occurred, they concluded that under pure bending, the moment capacity of the beams with one or two openings can be calculated based on the plastic modulus of the net section through the opening and that the presence of shear reduces the moment capacity of the beam at the opening below that for pure bending. They also found that the presence of an identical adjacent opening produces a very small reduction in strength when it is spaced a distance equal to the opening depth from the more heavily loaded opening. When the spacing was half the opening depth there was a significant decrease in strength at the higher shear/moment ratios resulting from buckling or tearing, or both, of the web between the openings.

A plastic analysis based on perfect plasticity was used for the analysis of beams with reinforced holes by Congdon and Redwood (1970). They presented a method for

predicting, somewhat conservatively, the loads above which deflection would increase rapidly. In 1971 suggested changes and additions to AISC specification of steel beams with web holes were made by the ASCE Task Subcommittee on Beams with Web Openings. Guides were given for both allowable-stress design (elastic design) and maximum-strength design (plastic design); some new formulas were suggested for use in design. A considerable amount of research was performed to investigate also stresses in steel beams with web holes, ultimate strength, stability of the web, deflection and the ability of such beams to carry concentrated loads near the hole. The results were documented and presented by Bower et al. (1971), Aglan and Redwood (1973), and Redwood and Uenoya (1979).

Douglas and Gambrell (1974) investigated the validity of a generalized Vierendeel truss analysis to wide-flange beams having off-centre unreinforced rectangular openings in their webs. Using photo-elastic models of wide flange beams for comparison with results predicted by the generalized Vierendeel truss analysis, they found that it accurately predicts the behaviour of these beams except in the areas of large stress concentration. Applying von Mises yield theory and the Vierendeel truss analysis, design curves were obtained for a large number of different beam sizes.

Elastic tests were conducted by Knostman, Cooper, and Snell (1977) on five full size steel beams with eccentric web holes. All the test specimens were simply supported and subjected to a concentrated load at mid-span. By varying the span of the beams, the

ratio of the moment at the centre line of the opening to the shearing force at the opening was changed. They used a numerical integration procedure to obtain the distribution ratio of the shearing force between the top and bottom chords, from normal stresses at the high and low moment section of the opening. This ratio was also determined from the shearing stresses obtained from the finite element method. They found that the distribution of the shearing force at the web opening was independent of the moment-shear ratio at the opening. The finite element procedure used in this investigation overestimated the normal stresses at the opening, but when these normal stresses were used in the numerical integration program, the resulting values of the shear ratio were in good agreement with the experimental results.

Redwood and Shrivastava (1980) gave concise design recommendations related to the design of W-shaped beams, followed by a commentary describing the background to each of the recommendations. Redwood and Poubouras (1983) also published some test results on composite beams comprised of a concrete slab supported on a steel deck and a steel wide-flange beam containing large web openings. Special attention was directed to the amount of shear connection between the slab and steel section in the region of the web hole and on the effect of the construction loads acting on the steel section prior to composite action becoming effective. Comparing the test results with the analysis, they concluded that the omission of shear connectors within the length of the hole produces a significant reduction in the ultimate strength of the beam in the region of the hole. They suggested an approximate method of analysis which takes into account

the effect of limited shear connection in the hole region . Based on their reported test results, it was concluded that construction loads acting on the unshored non-composite steel shape do not significantly affect the ultimate load of the composite section when the non-composite beam in the region of the hole is subjected to 60% of its predicted ultimate strength.

Buckland and Barlett (1988) introduced solutions for the design of reinforcement for a wide range of holes in steel webs. Five methods of dealing with multiple holes in a web panel were presented, each appropriate for different circumstances: elastic analysis, Vierendeel action, plastic summation, the use of stiffeners for "trussing", and the "checkerboard" technique. The research was carried out on 350 holes in the webs of an offshore oil structure. It was concluded that the rule of thumb of maintaining constant cross section through the centre of a hole by adding doubler plates is non-conservative, especially for rectangular holes.

Donahey and Darwin (1988) conducted experimental work on fifteen full-scale composite beams with web openings. The beams had ribbed slabs with formed steel decks. They studied the effects of moment-shear ratio, quantity and placement of shear connectors, deck orientation, deck thickness, opening shape and its eccentricity. The beams were first cycled elastically and then loaded monotonically to failure. Generally the failure of the beams was ductile and the peak loads were preceded by major cracking in the concrete deck, yielding of steel and large deflections. Concrete strains remained

low until well after the steel began to yield. The study confirmed that the behaviour of composite beams with web openings is largely controlled by the moment-shear ratio at the opening. Some of the conclusions drawn were:

1- The concrete in composite beams significantly contributes to both the flexural and shear strength of the beams at web openings.

2- As the ratio of moment to shear at the opening decreases, the deflection across the opening increases and transverse cracking occurs at a lower load.

3- The peak loads attained by composite beams with ribbed slabs at web openings are governed by the failure of the concrete slab.

4- As the capacity of the shear connectors above the opening and between the opening and the support increases, the capacity of the opening increases.

5- The interaction between moment and shear capacity at a web opening is relatively weak; i.e, shear capacity is largely unaffected by moment until the moment approaches the peak strength of the section.

Based on the previous experimental work, Darwin and Donahey (1988) presented design procedures for composite beams with unreinforced web openings. The procedures applied to beams with either solid or ribbed slabs. They discussed the appropriate resistance factors for use in load and resistance factor design (LRFD). The design procedures included rational solutions for the pure moment and pure shear strengths at the openings, as well as a direct solution for member capacity at an opening subjected to both bending and shear.

Fahmy (1988) presented a method for the analysis of steel-concrete composite beams with unreinforced rectangular web opening. The method was based on the ultimate strength analysis. The steel was represented in the analysis as an elastic-plastic material with no strain hardening and yielding follows the von Mises yield criterion. He studied the effect of the eccentricity of web opening on the strength of the beam. Buckling and instability failures of the composite beam were not considered in his analysis. The analysis showed that the strength of the composite beam decreases with increase of depth and width of opening. The increase of positive opening eccentricity (towards the slab) increases the strength up to a certain moment-shear ratio after which the strength decreases with increase in the positive eccentricity. It is shown that negative opening eccentricity has an opposite effect to that of positive eccentricity.

In 1991 Ito et al. investigated the elastic-plastic behaviour and ultimate strength of built-up simply supported beams with U-shaped holes. The test results were compared with analytical results based on the finite element method, the beam theory, and the ultimate strength method taking account of Vierendeel action. They found that the bending stress distribution in a beam with U-shaped holes can be accounted for by beam theory, and that the elastic and ultimate strength analyses taking into account the Vierendeel action were effective for these beams.

2-3 Reinforced Concrete Beams with Openings:

In 1962 Lorentsen reported a design method for reinforced concrete beams with web openings. He considered the lower chord of an opening in a simply supported beam to be cracked and unable to resist any moment. He recommended to consider the beam as a rigid frame with a tension rod. To check if the theoretical analysis was practical, he tested four beams under different loading conditions. Lorentsen found that the tests confirmed in general the behaviour pattern predicted by the elastic theory presented. He recommended that for statically loaded structures, satisfactory structural capacity may be achieved if the sections near the edge of the holes are assigned to carry the normal and bending forces obtained from his theory and by proportioning through the ultimate stress procedure of the German Concrete Code, DIN 4227. With dynamic loadings, he mentioned that care should be taken to prevent high tensile stresses in the concrete in order to safeguard against fatigue failure.

K.T.Burton (1965) published an experimental work of two wide- shallow T-beams subjected to uniform load over an 18 ft. (5.5 m) span with a negative restraint moment at one end. The two beams were identical in all respects except that one of them had ten $7 \times 1\frac{3}{8}$ in. (178 x 35 mm) ducts spaced at 12-in. (305 mm) centres embedded in the 7-in. (178 mm) T-beam flange. The purpose of the work reported in this paper was to evaluate the effects on the strength of T-beams when introducing a number of closely spaced ducts into a floor system. The test loading was such that a constant ratio of the field moment to the negative restraint moment was maintained until these moments corresponded to the

ultimate moment computed according to the ACI Building Code (ACI 318-63). When this stage was reached, the moment at the support (negative moment) was held constant and loading was increased in the beam span until failure. This method of loading was to insure failure in the beam span where all the service ducts were located. The ducts were positioned so that three of them were in the region of negative bending moment and seven were in the area of positive bending moment. Spacing was such that one duct was placed near the point of maximum positive bending moment in the beam span, and one was located at a distance from the cantilever support approximately equal to d , the effective depth of the member. The major difference in the behaviour of the two beams was that higher stresses developed in the compression steel in the beam span of the specimen containing the ducts. Burton concluded that provided that sound detailing practices are observed and that the reinforcement and the ducts are accurately positioned before casting the member, it appears that embedment of the ducts will not influence beam strength significantly.

In 1967 Nasser, Acavolos and Daniel presented a theoretical approach for the behaviour of rectangular reinforced concrete beams with large openings. They also compared the results of pilot, full-size beam tests with the behaviour of an identical beam having no openings. The following assumptions were envisaged necessary to start their research program:

1-The top and bottom cross members of the opening are assumed to behave similar to the chords of a Vierendeel panel.

2-The cross members of the openings, when they are not subjected to transverse loads, have contraflexure points at their mid-span.

3-The cross members, when they have adequate stirrups, carry the external shear in proportion to their cross-sectional areas.

4-There is a diagonal force concentration at the corners induced by the chord shear, and its value is twice the simple shear force.

The tests were used to examine the validity of the above assumptions. The investigation was also concerned with the reinforcement of the corners of the opening. Comparing the results of the beams containing large openings with an identical solid beam without any openings, they concluded that their outlined design procedure was satisfactory for the tested members. Furthermore, the presumed assumptions concerning contraflexure points, shear distribution and shear concentration factor were found to be valid for rectangular beams and that adequately reinforced large openings in rectangular beams do not reduce the ultimate capacity of the beam but reduce its stiffness i.e, increase its deflection.

Hanson (1969) investigated the effect on strength and behaviour of square web openings in continuous light weight-aggregate concrete joist floors. The aim of his study was to develop design information for web openings located in regions of high shear near supports of reinforced concrete joists. The principal variables were size, location, and reinforcement of the opening. The applied loading represented the conditions in the

negative moment region of a continuous joist. The main findings of his research were:

1- An unreinforced web containing a square opening of one-quarter the depth of the web did not reduce the strength of the test specimens. An unreinforced opening of three-quarters the depth of the web reduced the strength of the test specimen by about 67%.

2- Near the mid-length of the compressive strut, the compressive force could be considered to be concentrated at the centroid of the strut.

3- Prior to cracking, the distribution of shear between the regions above and below the opening was approximately in proportion to the cross-sectional area of the struts. After cracking, the compressive strut tended to carry all of the shear.

In 1984, Mansur, Tan and Lee developed a method to predict the ultimate strength of a reinforced concrete beam that contains a large rectangular opening and is subjected to a concentrated load. According to their method, collapse of the structure occurs if it is possible to find a distribution of internal actions such that the conditions of equilibrium, yielding and a mechanism are satisfied simultaneously. The analytical model predictions were compared by available tests conducted by Nasser et al. (1967). The results showed that the ratio of shear force taken by the top chord to the total shear force (V_t / V) decreases with an increase in opening size (either width or depth). In case of small opening almost the entire shear is carried by the top chord. But for large opening, the bottom chord carries a significant part of the total shear. In contrast, V_t / V increases with an increase in opening eccentricity since more concrete area becomes available for the

compression (top) chord to resist the shear.

Again in 1985 Mansur, Tan, and Lee proposed a design method for reinforced concrete beams with large openings. Twelve beams designed by the proposed method were tested under a concentrated load and varying: width, depth, eccentricity and location of openings, and the amount and arrangement of corner reinforcement. They used the Vierendeel analogy in their analysis considering that the amount of shear carried by each chord depends not only on their section properties but also on the size and location of the openings. Collapse of the beam occurred due to the formation of a mechanism with four hinges, with one at each corner of the opening. Some of the conclusions drawn were:

1- Both the maximum crack width and maximum beam deflection increase with an increase in opening length, opening depth, or moment-shear ratio at the centre of the opening.

2- The effect of opening eccentricity is insignificant for the small eccentricities used in the test program.

3- Diagonal bars for corner reinforcement are more effective in controlling cracking and reducing beam deflection.

4- For a symmetrical arrangement of chord member reinforcement, the position of contraflexure point occurs approximately at mid-span of the chord members.

It was mentioned that the proposed design method has been found to be safe and satisfactory but is applicable to beams when the chord members are not directly loaded.

Also the slenderness ratio for the compression chord should be limited to 22 as suggested by the ACI Building code (318-83) for unbraced compression members.

Cook and Mitchell (1988) studied the disturbed regions caused by changes in cross-sectional dimensions or by concentrated loads which result in disturbance in the stress flow around the discontinuities. They used a simple strut and tie model to analyze and design disturbed regions such as beams with openings, corbels, dapped end beams, and deep beams. Strength predictions of a corbel and a dapped end beam using strut and tie models were compared with test results while complete response predictions using a non-linear finite element computer program were used to verify the strut and tie models. They found that the presence of the opening in a uniformly loaded beam interrupts the uniform field of diagonal compression causing higher shear stresses in the section beneath the opening and requiring an increase in the amount of stirrup reinforcement in this region. They found also that to make use of the full depth of the section beyond the opening, a vertical tension tie has to be provided to lift the shear force to the top of the beam. This vertical tie enables the force to flow into the support reaction area by means of direct compressive strut. It was mentioned that the simple strut and tie models provide conservative estimates of the ultimate capacities of the disturbed regions investigated, and that the finite element analysis provides a means of predicting the complete response of reinforced concrete members containing disturbed regions.

Mansur (1988) presented a method to design reinforced concrete beams with large

openings using design charts. He assumed that the collapse occurred due to a mechanism which consisted of four hinges in the chord members, with one at each corner of the opening. The chord members were assumed to be adequately reinforced in shear and linearized interaction relationships between bending and axial forces were considered as the required yield conditions. He presented design steps to calculate the collapse load based on these assumptions. He presented also a method to construct a graph for estimating the ultimate axial load in the opening struts.

In 1991, Mansur et al. conducted an experimental work on eight reinforced concrete continuous beams, each containing a large opening. The beams were rectangular in cross section and all contained the same amount and arrangement of longitudinal reinforcement. Three of these beams were of two spans, while the other five were of three spans. The major variables investigated included the horizontal location and the size of the opening. All the tested beams exhibited remarkably similar behaviour as far as the deflections were concerned. The authors divided the behaviour of the beams into four distinctly different stages. Stage (1) corresponded to the uncracked state of the beam which was terminated by the occurrence of the first crack; stage (2) was marked by the initiation of cracks and it continued up to the point where the first plastic hinge developed; stage (3) was termed as a hinge development stage where some of the existing cracks at critical sections kept growing excessively wide and only very few additional cracks were formed; and stage (4) where theoretically the beam should continue to deform at exactly the same load until the rotation capacities of plastic hinges were exhausted and

crushing of the concrete occurred. In their observations, they mentioned that all the beams showed reversal of curvature with the contraflexure point located approximately at the opening mid-span which confirmed the existence of a Vierendeel action in beams containing a large rectangular opening. They also described the sequence of hinge formation and the mode of collapse for each beam. They identified the formation of a hinge on a basis of visual observation of the extent of cracking, measured steel strains and the load-curvature relationships obtained from the critical sections. They concluded that the final failure of a continuous beam occurs by the formation of a mechanism and that the two opening ends represent the most vulnerable locations for the development of plastic hinges. They found also that an increase in either the length or depth of opening leads to early cracking of a beam, produces large deflections, gives more pronounced Vierendeel action, and decreases the collapse load. According to their observations, the location of opening along the span had very little effect on the cracking load but when openings were located in a relatively high-moment region, larger deflections and smaller collapse loads had taken place.

Again Mansur et al. (1991) proposed a method to predict the load-deflection response of reinforced concrete beams containing large openings. According to their method, an elastic analysis of the beam is carried out to find the load level at which the first plastic hinge forms. The forces and moments throughout the beam and the load at this stage are recorded and deflections are calculated. This load and corresponding deflections represent the coordinates of a point on the load deflection curve. A hinge is

then inserted at the position indicated and an elastic analysis is carried out on the modified structure. From this second analysis the location of the next plastic hinge is found. The load at which the second hinge forms together with the corresponding deflection gives another point on the load deflection curve. This process is continued until the final hinge forms giving rise to a mechanism of failure. In their calculations of deflections at each successive plastic hinge formation, they considered the total deflection to be the summation of the two deflection components; one due to flexural action of the whole beam and is obtained from the bending moment diagram given by the successive elastic analyses using the conjugate analogy, and the other component due to Vierendeel action resulting from the transfer of shear through the opening segment of the beam. They compared test results conducted by Mansur et al. (1985, 1991) with the theoretical predictions. They found that the theory gave good predictions for the load-deflection relationship and for the mode of collapse for all the tested beams.

2.4 Prestressed Concrete Beams with Openings:

Regan and Warwaruk (1967) published an experimental study on prestressed concrete T-beams with large web openings. A testing program involving four model beams and two full size beams was decided upon with all model beams being subjected to a two-point symmetrical loading arrangement while the loading of full size beams was approximately uniform. The results showed that the failure moment was two to three times that at which cracking was first observed. The mode of failure of all the model beams with openings was through formation of mechanisms. The loading used for these

beams produced a shear condition much more severe than that which would be produced by the uniform load. They concluded that sizable web openings could be accommodated without sacrificing strength and that deflections of beams with openings are not significantly greater than those for beams without openings.

Sauve (1970) conducted experimental work on prestressed concrete T-beams with large web openings. He studied the effect of reinforcing the opening on the behaviour of such beams. Some of the conclusions drawn were:

1- Any additional shear reinforcement provided served to increase the load carrying capacity of a beam containing large web openings by an amount ranging from 15% to 22%.

2- A considerable increase in supplementary longitudinal reinforcement did not significantly increase the shear capacity of the beams.

3- An extra amount of vertical reinforcement placed in the posts between openings gave these posts the capacity required to localize the failure in the lower chord if this chord had no vertical reinforcement. However a minimum amount of inclined shear reinforcement placed in the lower chord caused the failure to be localized in the post.

4- The reinforcing of both the posts and the lower chord resulted in a redistribution of stresses in the shear span such that all sections were more equally stressed in diagonal tension.

In 1977 Barney, Corley, Hanson and Parmelee established an analytical procedure

for the design of pre-tensioned prestressed concrete beams with large web openings. This procedure was based on the findings of tests on 18 full-size prestressed, pre-tensioned concrete T-beams. The variables investigated were size and location of opening along the span, type and amount of shear reinforcement, and amount of primary flexural reinforcement. The test specimens with adequate strength at the openings reached their capacity in flexure while for those having openings in the high shear regions, the capacity was limited by an unrestrained shear crack extending from the low moment side of an opening toward the support. Such cracks normally propagated along the prestressing strands. In some beams the cracks extended into the region required for strand embedment causing the strand to slip. Of the variables considered in their investigation, those having the greatest effect on beam strength and behaviour were the location of web openings along the span and the amount of web shear reinforcement. According to the recorded strain data, the behaviour of the test beams was similar to that of a Vierendeel truss. As cracking was observed to have a significant effect on the shear distribution in the struts, they proposed an iterative method to determine the shear forces in each strut according to the cracking condition. When no cracking has occurred in the struts, shear is carried in proportion to the uncracked moments of inertia. A simplified procedure for estimating shear forces in the struts for design purposes was suggested. They also recommended that adjacent web openings be separated by web elements (posts) having overall width-to-depth ratios of at least 2.0 where the width of the of the posts is the distance between adjacent stirrups. In conclusion, they mentioned that large web openings can be placed in prestressed concrete beams without sacrificing strength or

serviceability. However, openings must be located outside the required strand embedment length and that adequate shear reinforcement must be provided adjacent to openings.

In 1978 El-Laithy conducted a theoretical and experimental investigation on rectangular prestressed concrete beams. He studied the effect of openings on rectangular post-tensioned prestressed concrete beams from the stand point of deformations, stresses, cracking and ultimate strength capacity. From the theoretical and experimental studies, some of the conclusions drawn were:

1- The presence of an opening in a rectangular prestressed concrete beam increases the deflection of such a beam. The increase in deflection depends mainly on the depth and width of the opening.

2- There is a difference between the vertical deflection of the top and bottom chords of the opening, the deflection of the top chord being larger than the bottom one; however, the deflection of the bottom chord is larger than the top chord when the load acts at the middle of the beam.

3- In both cases of loading (at the middle of the beam and at the middle of the opening), the deflection lines of the top and bottom chords of the opening have a point of contraflexure approximately at the middle of the opening.

4- The top and bottom chords of the opening do not act together as one section and the assumption of plane sections (composed of top and bottom chords) remaining plane after deformations is not valid.

Abdus Salam and Harrop (1979) studied the effect of the presence of circular holes on the design of prestressed concrete beams. Consideration was given to the prediction of beam strength and to the different methods of reinforcing around the holes; the methods investigated were steel liners to the holes, bonded ring reinforcement in the concrete around the holes, and vertical stirrups on both sides of each hole. It was concluded that the presence of many holes reduces the peak stresses below the single-hole values. Also compensation for the presence of the holes is best provided by vertical stirrups by the sides of the holes. This reinforcement takes care of the horizontal splitting due to prestress and diagonal tensile stress at working load. They mentioned also that a perforated beam can be as strong as a similar solid beam provided the holes do not protrude into the ultimate rectangular stress block required for flexure failure.

Kennedy and El-Laithy (1982) investigated theoretically and experimentally the behaviour of prestressed concrete beams with rectangular openings at the transfer stage. A plane stress rectangular element with two degrees of freedom at each corner was used in the finite element analysis while eighteen post-tensioned concrete beams were utilized for the experimental analysis. The main parameters studied were the depth of the opening and its horizontal and vertical location. The results indicated that the depth and the vertical location of the opening were the two parameters that significantly affect the various stresses around the opening; whereas the horizontal location of the opening did not have an appreciable influence on the stresses at the transfer stage. The analysis also revealed that the maximum vertical tensile stress occurs at or near the mid depth of the

opening and this stress increases linearly with the increase in the prestressing load until the formation of a horizontal crack; furthermore, the presence of the opening also gives rise to significant shear stresses near the four corners of the opening. They also studied the influence of transverse reinforcement on the cracking load. It was found that reinforcing against the vertical tension force was effective in increasing the cracking load by approximately 30% for both rectangular and T-beams. Based on the results from the finite element solution, substantiated by the experimental tests, a simple method was developed to estimate the vertical tensile force around the openings due to the prestressing force. From the results of their investigation, the following main conclusions were drawn:

1- The presence of an opening gives rise to a potentially splitting-tension field, followed by a compression field, whose distances are functions of the depth and vertical location of the opening.

2- The assumption of plane sections remaining plane does not apply in the vicinity of the opening.

3- The presence of an opening increases the deflection only slightly at the transfer stage.

Dinakaran and Sastry (1984) presented the results of analytical and experimental investigation on the behaviour of simply supported prestressed T-beams with web openings. The variables considered were the size of openings, location of openings and type of reinforcement around openings. The openings were positioned both in the shear

span as well as in flexure span. The results showed that the first crack appeared from the side of the opening closer to the support for the beams having openings in the shear span due to the shear concentration of the corners of the openings. This shear crack propagated towards the support. Beams having openings in the constant moment zone did not exhibit crack propagation from the corner of the opening. The test results revealed also that the location of the opening has the greatest effect on the strength and the behaviour of the beams. It was concluded that post-tensioned prestressed concrete T-beams with large openings behave similarly to a Vierendeel panel. Also, beams with openings in the high moment region behave better than those having openings in shear span. The ultimate moment capacity of the former is also larger. They found also that vertical stirrups and hooks provided adjacent to openings control cracking. They mentioned that compressive struts and tensile struts carry external shear in proportion to their cross-sectional areas and that the influence of openings on deflection is minor in properly reinforced beams.

Alves and Scanlon (1984) determined analytically the load-deflection response of prestressed concrete beams with web openings. They used a truss model that included the effects of progressive cracking. According to their procedure, it is assumed initially that the beam is uncracked and a linear elastic analysis is made for loading due to prestress, dead load, and live load. Forces in the truss members are then used to calculate the net axial force and bending moment at the centre of each panel of the truss. By comparing the bending moment at sections along the beam with the cracking moment, it

is possible to scale the applied load to the value at which cracking first occurs. The analysis can then be repeated at selected load levels to trace the load-deflection response as affected by progressive cracking. The numerical results showed good agreement when compared to tests on three prestressed beams with openings.

2.5 Concrete Beams with Openings Subjected to Dynamic Loading

In 1986, Pool and Lopes published a theoretical and experimental work on reinforced concrete beams with web openings subjected to cyclic load. The aim of their investigation was to determine an optimum shape of opening through photo-elastic and finite element studies and to obtain results from a physical test program on reinforced concrete beams with openings under cyclic load. In the first part of their work, a photo-elastic study was made on clear polyester beam models with web openings under a mid-span concentrated load. Rectangular-, square-, diamond-, circular-, and elliptical- shaped openings were tested to find the shape of the opening least prone to stress concentration. This study also focused on the effect of the position of the opening with respect to its horizontal distance from a support point. In the second part, two optimum shapes of openings were selected based upon results from the first part, and six full-sized reinforced concrete beams were tested under cyclic loads of increasing magnitude until ultimate failure was achieved. The study of the optimum shape of web openings revealed that an elliptical shape is least prone to stress concentrations around the opening. A circular shape was shown to be second best. Rectangular openings with sharp corners had a stress concentration twice that of the elliptical openings. The results obtained from the photo-

elastic study were confirmed by finite element analysis. Based upon these results, a testing sequence was devised for full scale beams with elliptical and circular openings, as well as for beams without any openings. Five of the tested beams were subjected to cyclic loads and one to static loads. The loads chosen for the cyclic tests were applied in the form of a sine-wave. They concluded that cyclically loaded reinforced concrete beams with openings can maintain the strength of similarly loaded beams without openings if special welded circumferential reinforcement was provided around the opening. Without such special reinforcement, the ultimate load capacity could be reduced by as much as 33% and the number of cycles of loading was correspondingly reduced. They recommended not to use openings unless they are specially reinforced.

Kennedy, Chami, and Grace (1990) examined the dynamic and fatigue behaviours of prestressed concrete girders with openings. In their analytical study, the influence of several design parameters was examined, such as the size and location of the opening, one versus two openings, and different cross sections. The aim of the experimental work was to determine the natural frequencies and the associated mode shapes, damping characteristics, and the deformation of the upper and lower chords of the opening. The fatigue response was also examined by subjecting these beams to repeated loads. The following tests were carried out on six simply supported post-tensioned concrete beams with openings: (i) the impact-hammer test; (ii) the sine-wave sweep test; (iii) the normal mode test; (iv) the log-decrement test; and (v) fatigue test. The theoretical parametric study was conducted using the finite element computer program 'STRUDL-DYNAL'.

The results from the hammer test as well as from the finite element analysis revealed that changes in the opening width and its eccentricity did not significantly alter the fundamental frequency when the opening was in the shear span. However, for an opening in mid-span, the fundamental frequency increased somewhat by approximately 9%. They found also that varying the opening width and (or) its location did not influence the first mode shape of the prestressed beams. The width of the opening was found to have a measurable influence on the amplitude of displacements of the opening chords and at mid-span at the first natural frequency. Moving the opening vertically upward from the longitudinal centre line did not appear to have much effect on the displacements. The free-vibration transient decay test at the first natural frequency was repeated twice for every beam and the two results were averaged. The amount of viscous damping in the tested beams was determined by the logarithmic decrement method. It was observed that neither the presence of an opening nor its size and (or) location influenced the amount of viscous damping in such structural members. The damping ratio for the tested beams varied from 1.9% to 2.1%. The parametric study revealed that for beams with relatively wide openings, local modes of vibration existed resulting in a sudden drop of 30% in the third natural frequency. Furthermore, a gradual decrease in the fourth natural frequency of approximately 30% was also noted. No significant difference was found between the natural frequencies of prestressed concrete beams provided with one or two openings in the shear span. They concluded that the value of the first natural frequency of prestressed beams with openings is not significantly affected by repeated cycles of loading; however, a considerable reduction in the vibration amplitudes in the mode shape can be expected.

The Vierendeel local bending action was quite evident under the influence of repeated cyclic loading for beams with openings in the shear span but not for beams with openings at mid-span. They found also that beam failure due to cyclic loading occurred away from the opening region in prestressed beams with openings in the shear span.

CHAPTER III

THEORETICAL ANALYSES

3.1 General

The finite element method has become a reliable tool to determine the response of a structure during the linear and nonlinear stages of loading. A description of the finite element technique used in this study is presented in this chapter. The theoretical modelling of the concrete, steel, and prestressing wires in the linear and non-linear static analyses as well as in the dynamic analysis is explained. A general description of the finite element program 'ABAQUS' (Hibbitt et al. 1989) which was used throughout this analysis is presented.

The objectives of the theoretical analyses were to predict (i) the stress distribution in the vicinity of the opening, (ii) the deformations of prestressed beams with openings due to the prestressing alone as well as to combined prestressing and vertical load, (iii) the crack propagation pattern at the critical sections along the beam, (iv) the natural frequencies and the associated mode shapes of simply supported and continuous prestressed beams with openings, and (v) the dynamic response of simply supported

prestressed beams with openings. Also the finite element analysis was used to carry out a parametric study on prestressed concrete beams with openings in order to develop simple analytical methods for design purposes.

3.2 Finite Element Static Analysis

The finite element method is a technique that first discretizes the structure into a set of elements with same physical assumptions. Each finite element is associated with a displacement function and is interconnected with the adjacent elements by nodal points. Acting at each nodal point are nodal forces and the node is subjected to displacements referred to as degrees of freedom. Thus for each element a standard set of simultaneous equations can be formulated to relate the degrees of freedom. The result is a large set of these equations which are suited for solution by a computer. Upon implementing the loading and boundary conditions for the structural problem, the assembled set of equations can be solved and the unknown parameters found. Substituting these values back to each element formulation provides the distributions of displacement and stress everywhere within each element.

In the finite element method, the matrix equation relating the global displacements and loads may be expressed as:

$$K U = P \quad (3.1)$$

in which K = the structure stiffness matrix, U = displacement vector at the nodes, and P

= vector of the applied loads at the nodes. The structure stiffness matrix K is the assemblage of the element stiffness matrices k_e for each element, where

$$k_e = \int B^T E B dV \quad (3.2)$$

in which the integration in Eq.(3.2) is performed over the element volume V , B = strain displacement matrix, and E = elasticity matrix.

In the non-linear analysis the load is applied gradually in small increments. The definition of these increments is given automatically by the 'ABAQUS' computer code as will be discussed later in this section. This automatic scheme is based on the convergence of the iteration process at each increment. 'ABAQUS' generally uses the Newton's method as a numerical technique for solving the non-linear equilibrium equations. The method starts from

$$\psi(U) = K(U) \cdot U - P \quad (3.3)$$

where $\psi(U)$ = non-linear discrete equation operator and $K(U)$ is the stiffness matrix at displacement U . If an approximate solution $U=U^n$ is reached for Eq.(3.3), an improved solution using a curtailed Taylor expression can be written as:

$$\begin{aligned} \psi(U^{n+1}) &= \psi(U^n) + \left(\frac{d\psi}{dU}\right)_n \Delta U^n \\ \psi(U^{n+1}) &= 0 \end{aligned} \quad (3.4)$$

with $U^{(n+1)} = U^n + \Delta U^n$. In the above $\frac{d\psi}{dU} \equiv K_T(U)$ represents a tangential matrix.

The improved value of U^{n+1} can be obtained by computing:

$$\begin{aligned}\Delta U^n &= -(K_T^n)^{-1} \psi^n \\ &= -(K_T^n)^{-1} [K^n U^n - P]\end{aligned}\tag{3.5}$$

The process is illustrated in Fig. 3.1, and it should be noted that at every iteration, a new set of linearized equations has to be solved for ΔU^n .

Increments must be kept small to assure correct modelling of history-dependent effects, but most commonly the choice of increment size is a matter of computational efficiency - if the increments are too large, more iterations will be required. Newton's method has a finite radius of convergence, which means that too large an increment can prevent any solution from being obtained because the initial state is too far away from the equilibrium state that is being sought.

3.3 The 'ABAQUS' Computer Program

The finite element program used in the analysis, 'ABAQUS' (Hibbitt et al. 1989), is a batch program. Therefore, a data deck which describes the problem has to be provided to 'ABAQUS'. A data deck for the program contains model data and history data. Model data define the finite element model: the elements, nodes, element properties, material definitions and boundary conditions. History data define what

happens to the model, the sequence of loading for which the model's response is sought. In 'ABAQUS' this history is divided, by the user, into a sequence of steps. Each step is a period of response of a particular type such as static loading or dynamic response. The definition of a step includes the procedure type, the control parameters for the non-linear solution procedures, the loading, and the output request. All data definitions in 'ABAQUS' are accomplished with option blocks - sets of data describing a part of the problem definition. Each option is introduced by a keyword card. If the option requires data cards, they follow the keyword.

3.4 Finite Element Model

The finite element mesh is usually chosen based on pilot runs and is a compromise between economy and accuracy. Several element types from the element library in 'ABAQUS' were tested in the pilot runs. The number of elements used in the static and dynamic analysis was varied as well. A rectangular plane stress element named CPS4 in 'ABAQUS' with two degrees of freedom (U_1, U_2) at each node was used to analyze beams of rectangular cross-sections. For beams of T- and I- sections, the same rectangular plane stress element was used to model the web while a four node plate element, named S4R in 'ABAQUS' with six degrees of freedom ($U_1, U_2, U_3, \phi_1, \phi_2, \phi_3$) at each node was used to represent the flange(s). Figures 3.2 and 3.3 show the characteristics of the plane stress and the plate bending finite elements used in the analysis respectively.

3.5 Reinforced Concrete Modelling

The concrete model in 'ABAQUS' is designed to provide a general capability for modelling plain and reinforced concrete. 'ABAQUS' provides a REBAR option to model the reinforcing. Rebars are one-dimensional strain theory elements which are used with standard metal plasticity models to describe the behaviour of the rebar material, and are superposed on a mesh of standard elements types used to model plain concrete. Effects associated with the rebar/concrete interface, such as bond slip and dowel action is modelled by introducing some "tension stiffening" to simulate load transfer across cracks through the rebar.

Cracking in the concrete model is assumed to occur when the stress reaches the failure surface represented by a simple Coulomb line in terms of the equivalent pressure stress, p , and the Mises equivalent deviatoric stress, q . The model is a smeared crack model, in the sense that it does not track individual "macro" cracks: rather, constitutive calculations are performed independently at each integration point of the finite element model, and the presence of cracks enters into these calculations by the way in which the cracks effect the stress and material stiffness associated with the integration point.

As the concrete cracks its shear stiffness is diminished. This effect is defined in 'ABAQUS' by specifying the reduction in the shear modulus as a function of the opening strain across the crack. Also the program provides a definition for the reduced shear modulus for closed cracks, so that, after a crack has been formed, even when the normal

stress across the crack becomes compressive, the shear stiffness will have been degraded by the presence of the crack.

When the principal stress components are dominantly compressive the response of the concrete is modelled by elastic-plastic theory, using a simple form of yield surface written in terms of the equivalent pressure stress and the Mises equivalent deviatoric stress. The cracking and compressive response of concrete that are incorporated in the model are illustrated by the uniaxial response of a specimen shown in Fig. 3.4. When the concrete is located in compression it initially exhibits elastic response. As the stress is increased some non-recoverable straining occurs, and the response of the material softens. When a uniaxial concrete specimen is loaded in tension it responds elastically until, at a stress that is typically 7% - 10% of the ultimate compressive stress, cracks form so quickly that, it is very difficult to observe the actual behaviour. 'ABAQUS' models the cracking as strain softening, the softening rate being dependent on the size of the finite elements in the cracked region. In multiaxial stress states the previous observations are generalized through the concept of surfaces of failure. The surfaces used are shown in Fig. 3.5. Figure 3.6 shows the response of the concrete in tension where the influence of tension stiffening is illustrated.

3.6 Prestressing Modelling

'ABAQUS' introduces an option for post-tensioning of the rebar contained in the finite element mesh through the PRESTRESS HOLD card. Prestress in the rebar is

defined by using INITIAL CONDITIONS option where the structure is brought to a state of equilibrium before it is actively loaded. This is accomplished by an initial STATIC analysis step with no external loads applied. During this step the prestress in the rebar may be allowed to change according to the straining of the structure as the self-equilibrating stress state establishes itself. Alternatively, by using the PRESTRESS HOLD option, the stress in the rebar may be kept constant during this initial equilibrium solution, as though the rebar were sliding through the concrete. This is the case in post-tensioning simulation.

3.7 Non-Linearity Control

When the problem is non-linear it may not be possible, or even desirable, to obtain the solution immediately: the load must be applied gradually. Non-linear static analysis requires the solution of non-linear equilibrium equations, and 'ABAQUS' uses Newton's method for this purpose. The solution is obtained as a series of increments, with iteration within each increment to obtain equilibrium. Increments must sometimes be kept small to assure correct modelling, but most commonly the choice of increment size is a matter of computational efficiency- if the increments are too large, more iteration will be required. 'ABAQUS' introduces an automatic incrementation scheme which selects the increment sizes based on these considerations.

The program provides a force tolerance, PTOL, and a moment tolerance, MTOL. These tolerances define the accuracy with which equilibrium must be satisfied at each

node. Very tight tolerances will require more iterations in the non-linear solution scheme, while loose tolerances will give incorrect answers, because the structure will not be in equilibrium.

During the loading STEP, the user assigns a time scale to the analysis. This is necessary to determine the variation of loads and other externally prescribed parameters through the step. During the step, 'ABAQUS' prints out a "load proportionality factor" at each increment. This defines the current local magnitudes according to:

$$P_{total} = P_0 + \lambda(P_{ref} - P_0) \quad (3.6)$$
$$0 < \lambda < 1$$

where P_{total} is the current magnitude for the load component; P_0 is the magnitude of this load component at the start of the step; P_{ref} is the magnitude of this load component as defined in the data for the step; and λ is the "load proportionality factor" that is printed. In the non-linear solution 'ABAQUS' uses RIKS parameter which depends on choosing increments based on controlling the path length along the load-displacement response curve. This means that the load magnitude is determined by the solution which means that the user has no control on this magnitude. This causes a control problem- the user must specify when the step will be completed. This is accomplished by defining maximum value of the load proportionality factor or by specifying a displacement value beyond which the solution is not of interest. If neither of the finishing conditions described above is specified, the analysis will continue for the number of increments defined at the beginning of the step.

3.8 Dynamic Analysis

3.8.1 Natural Frequency and Mode Shapes Extraction

The natural frequencies and the corresponding mode shapes of the structure are extracted in 'ABAQUS' by eigenvalue techniques. The stiffness determined at the end of the previous step is used as the basis for the extraction, so that vibrations of a preloaded structure, prestressed beams in this research, can be modelled. The FREQUENCY option in the program when used with NLGEOM parameter results in including the initial stress and displacements effects. The number of eigenvalues to be extracted has to be defined by the user.

3.8.2 Dynamic Analysis by the Modal Methods

'ABAQUS' includes response spectrum analysis, time history analysis, steady-state harmonic response analysis, and random response analysis procedures, to analyze linear dynamic problems using modal superposition. All these procedures are based on using a subset of eigenmodes of the system, which must first be extracted in a FREQUENCY step. The number of modes extracted must be sufficient to model the dynamic response of the system adequately: this is a matter of judgment on the part of the user.

Time history analysis gives the response of the model as a function of time, based on a given time-dependent loading. This response is obtained by using the MODAL DYNAMIC procedure in which the modal amplitudes are integrated through time and the response synthesized from these modal responses. This procedure can be used only with

a linear system. In this research, prestressed concrete was considered a linear material as high stresses are not recommended in beams under dynamic loading. The MODAL DAMPING option is used with this analysis to describe the damping of the system.

The steady-state harmonic response, which was used also in this research, provides the response of the system when it is excited by harmonic loading at a given frequency. Such analysis is performed as a frequency sweep, by applying the loading at a series of different frequencies and recording the response. The input for the STEADY STATE DYNAMICS procedure allows for such sweeping, with a bias function option that allows the sampling points on the frequency axis to be closer together at the resonant frequencies of the system, thus allowing detailed definition of the response close to resonance.

3.9 Non-Linear Static Analysis of Prestressed Beams with Openings

In the static analysis the following design parameters were considered: (i) horizontal and vertical locations of the opening; (ii) opening width and depth; (iii) type of cross section. The effect of these parameters on the behaviour of prestressed concrete continuous beams was investigated. Only the part of the continuous beam where maximum moment and maximum shear occur together was considered. Therefore, the analysis was carried out on a cantilever beam fixed at one end and loaded with a concentrated load at the other end.

Three types of cross sections were considered, namely; rectangular section, T-

section, and I-section. The analyzed beams were divided into three sets; BI, BII, BIII respectively according to the type of the cross-sections mentioned above. Each set was divided into groups where each group is concerned with one parameter. The parameters: horizontal location, vertical location, opening width, and opening depth were assigned the numbers 1,2,3, and 4 respectively. This means that for example group BIII3 is for T-beams where the changing parameter is the opening width.

Typical layouts of the rectangular, T-, and I-beams are given in Figs. 3.7, 3.8, and 3.9 respectively. Table 3.1 shows the dimensions and prestressing force used for each of the analyzed rectangular beams while Table 3.2 shows the same thing for the T- and I-beams. Figure 3.10 shows the definition of all the non-linear analyzed beams. It should be noted that in that figure, the horizontal location of the opening is referred to by the non-dimensional moment-shear ratio, M/VH , where M , and V are the moment and the shear at the centre of the opening, and H is the beam depth. Most of these beams in Fig. 3.10 were tested also in the laboratory as will be shown in detail in Chapter IV. Figures 3.11, 3.12, 3.13 show a typical finite element mesh for rectangular, T-, and I-beams respectively which were used in the non-linear finite element analysis. A data deck for non-linear static analysis of I-beam BIII1A is given in Appendix A.1 showing the description of the finite element mesh and the different loading steps.

3.10 Dynamic Analysis of Prestressed Beams with Openings

The objective of this analysis is to determine the natural frequencies and the

associated mode shapes of simply supported prestressed beams with openings and to predict the dynamic response including the beam maximum deflection, deflection of the opening chords, and horizontal and vertical stresses at mid-span and at the vicinity of the opening.

3.10.1 Natural Frequencies and Associated Mode Shapes

In this analysis the following design parameters were considered: (i) opening width and depth, (ii) horizontal and vertical locations of the opening, (iii) type of cross section. This was applied for simple beams, continuous beams with equal spans, and continuous beams with unequal spans. For simply supported beams, two locations for an opening were selected, one being in the high shear region and the other in the high moment region. Figure 3.14 shows the dimensions of these two types of beams, respectively. Typical finite element mesh for each of these two beams is given in Fig. 3.15. A solid beam with the same dimensions was also analyzed for comparison purposes.

With an opening in the shear span, nine cases were studied varying the width of the opening, W , from 5 in. (127 mm) to 45 in. (1143 mm) and having a constant depth $h=2$ in. (51 mm). The same nine cases for the opening width were then repeated for $h=3.2$ in. (81 mm), 4 in. (102 mm), 4.8 in. (122 mm), and 6 in. (152 mm). The same forty five cases were then repeated for T-, and I-beams. The description of these beams along with their natural frequencies will be given in Chapter VI.

For the dynamic analysis of two span continuous beams, three opening locations were considered: in the shear span, in the middle of one span, and in the maximum moment-maximum shear zone. Figure 3.16 shows these three different locations. Ten cases were studied for each location, varying the width of opening from 6 in. (152 mm) to 36 in. (914 mm), the depth of opening from 2 in. (51 mm) to 6 in. (152 mm), and vertical eccentricity of the opening from zero to 2 in. (51 mm). The above analysis was applied to continuous beams having two unequal spans of 120 in. (3.05 m) and 60 in. (1.52 m). For comparison, two solid beams were also studied. The above analysis was applied to rectangular, T- and I-sections. Furthermore, the dynamic analysis of two equal span continuous beams with two openings in one span and with one opening in each span were compared; the openings were located close to the interior support in both cases. Figure 3.17 shows a typical finite element mesh for the continuous beam with (a) two equal spans and (b) two unequal spans. The description of these continuous beams as well as their natural frequencies will be given in Chapter VI.

3.10.2 Dynamic Response of Simply Supported Beams with Openings

The objective of this analysis, besides the prediction of the dynamic response of simply supported prestressed beams with openings, was to find a simple method to estimate the critical deflections and stresses for such beams when they are excited by a dynamic load. Two types of dynamic procedures using the 'ABAQUS' computer program were carried out on simply supported beams with opening at high shear and at high moment regions. These procedures were modal analysis and steady state analysis.

The modal analysis procedure is a time history which was utilized to determine the deflections and stresses due to a specified dynamic load with a certain frequency. The equation of the exciting load was given to the program in the form:

$$P = P_0 \sin \Omega t \quad (3.7)$$

where P is the exciting load, P_0 is the load amplitude, Ω is the frequency of the exciting load, and t is the time. The analysis was carried out for Ω equal to 10 Hz and 30 Hz which are almost one-half and twice the fundamental frequency of the analyzed beams. The analysis was then repeated for the first frequency when the exciting load had the form:

$$P = P_1 + P_0 \sin \Omega t \quad (3.8)$$

where P_1 is a constant load which is active for all t . In the second procedure, the steady state analysis, the same two beams mentioned above were excited by a harmonic load at a series of different frequencies. The applied frequencies varied from zero to about 10 times the fundamental frequency of the analyzed beams. The deflections and stresses were determined in the margin of frequencies for the simply supported prestressed beams for an opening in the high shear and moment regions. A data deck for each of the previously mentioned procedures is given in Appendix A.1 showing the description of the finite element mesh and the different dynamic steps.

3.11 Parametric Study

In addition to the parametric work carried out on the previously mentioned beams under static and dynamic loads, the 'ABAQUS' computer program was used to conduct a parametric study, varying a number of factors which could influence the static and dynamic responses of simply-supported and continuous prestressed concrete beams. Such factors were: (i) variation in the size and location of the opening; (ii) presence of more than one opening; (iii) use of different cross-sections; and (iv) continuity. The goals of the parametric study were:

1- To find the distribution ratio of the shear force between the top and bottom chords of the opening.

2- To investigate the influence of different parameters on the cracking load of prestressed beams with openings and to find a simple method for determining this load.

3- To investigate the influence of different parameters on the vertical tensile stress at the opening due to prestressing force and due to the combined prestressing force and the vertically applied load, as well as to estimate this stress.

4- To find a simple method to predict the relative deflection between the edges of the opening due to the Vierendeel action.

5- To estimate the natural frequencies of prestressed beams with openings.

6- To find a simple procedure for predicting the dynamic response of prestressed concrete beams with openings.

Figure 3.18 shows the layout for the simply-supported prestressed beam used for the parametric study to achieve the first three goals mentioned above, while Fig. 3.19 shows the finite element mesh used for the same purpose. Tables 3.3 and 3.4 show the description of the beams used in this study. The same two beams used for the dynamic analysis, Fig. 3.15, were used to achieve the last three goals of the parametric study.

CHAPTER IV

EXPERIMENTAL INVESTIGATION

4.1 General

This chapter is concerned with the experimental research program. The construction of the tested beams and the test set-up are presented. The objectives of the experimental investigation were to determine (i) the strain distribution in the vicinity of the opening; (ii) the crack propagation pattern; (iii) the deflection due to prestressing and the externally applied vertical load; and, (iv) the ultimate strength of the prestressed concrete two-span beams with openings located near the interior support.

Tests were carried out on thirteen post-tensioned prestressed concrete beams, six of which were rectangular in section, five were of T-section and the remaining two were of I-section. Typical overall beam layouts for the rectangular, T-, and I-beam were shown in Figs. 3.7, 3.8, 3.9, respectively. Each test beam was symmetric about a centre line representing an interior support.

The beams were tested in an inverted position as shown in Fig. 4.1.b rather than

the normal position for continuous beams shown in Fig. 4.1a. This means that in the theoretical analysis, the beams were analyzed as continuous beams, while in the laboratory, they were tested as simply supported beams. Figures 4.2, 4.3, and 4.4 illustrate the test set-up for a rectangular, T- and I- beams. Figures 4.5, 4.6, and 4.7 show typical reinforcement details for each type of these sections.

The beams with rectangular section were classified into three groups B11, B12, and B13. The first group - included B11A, B11B, and B11C - was prepared to study the effect of the horizontal location of the opening represented by the moment-shear ratio M/VH on the response of the prestressed concrete beams with openings. This ratio was 4.5 for B11A and 4.0 for B11B. The third ratio of 3.5, was studied theoretically only using the finite element method. The opening was located at mid-depth of the beam and the opening width was 12 in. (305 mm) for this group.

The second group which included beams B12A, B12B, and B12C was prepared to investigate the effect of the eccentricity of opening, C . Three vertical locations for the opening were considered. For beam B12B, the opening was centrally located at mid-depth. In beams B12A and B12C, the centre line of the opening was one inch (25.4 mm) above and below, respectively, the mid-depth of the beam. The moment-shear ratio M/VH was considered equal to 4 for these beams.

The third group contained beams B13A, B13B, and B13C. The moment-shear ratio,

M/VH , was kept constant and equal to 4 for all the members of this group. The openings were located centrally at mid-depth. This group was considered to study the effect of the width of opening, W . The width of opening was 12 in. (305 mm), 16 in. (406 mm), and 20 in. (508 mm) for BI3A, BI3B, and BI3C, respectively.

The beams with T-sections were divided into three groups BII1, BII2, and BII4. The moment-shear ratio, M/VH , was varied in group BII1. This ratio was 3.5, 3.0, 2.5 in beams BII1A, BII1B, and BII1C, respectively. The centre line of opening was located at 6.5 in. (165 mm) from the top fibre of the beam and the depth of opening was 4 in. (102 mm) for all members of this group.

The eccentricity of the opening along the depth of the beam was investigated in group BII2. The opening centre line was located at 6.5 in. (165 mm) and 5 in. (127 mm) from the top fibre (the tension fibre) in BII2A and BII2B, respectively. BII2C with C, the opening eccentricity, equal to 3.5 in. (89 mm) was studied using the finite element method.

In the third group, BII4, the vertical location of opening was the same as for group BII1. The moment-shear ratio M/VH was equal to 3 but the opening depth was 4 in. (102 mm) for BII4A, 5 in. (127 mm) for BII4B, and 6 in. (152 mm) for BII4C. The latter beam, BII4C, was studied theoretically using the finite element method.

Two beams with I-section were studied. The first one, BIII1A, had a moment-shear ratio M/VH of 2.6 while the second one BIII1B had an M/VH ratio of 1.9. The opening was located centrally at the beam mid-depth, with a depth of opening of 5 in. (127 mm) for both beams.

4.2 Materials

Local materials were used to prepare the tested beams.

4.2.1 Concrete

4.2.1.1 Cement

Type 30, CSA High Early Strength cement was used in the concrete mix of the tested beams. This type of portland cement accelerates the hydration process resulting in rapid hardening and development of strength. This made it possible to test the beams shortly after casting.

4.2.1.2 Coarse Aggregates

The coarse aggregates consisted of crushed durable stone of maximum size of 0.5 inch (13 mm) in diameter. The maximum size of coarse aggregate did not exceed $b/5$ where b is the beam cross-section width nor $3/4$ the clear spacing between the steel bars according to ACI code.

4.2.1.3 Fine Aggregate

Coarse sand from lake Erie was used in the concrete mix. This sand available in the laboratory was assumed to be free of chemicals, coating of clay, or other fine materials that may affect hydration and bond of the cement paste.

4.2.1.4 Mixing Water

Natural tap water having no impurities was used in the concrete mix. Water cement ratio of about 0.4 was selected to achieve the required concrete strength of 6000 psi (41 MPa). A concrete mixer of five cubic feet (0.14 m³) charging capacity was used for mixing the required concrete. Three standard cylinders were cast for each beam. Such cylinders were tested on the day of beam testing to determine the concrete compressive strength. Appendix A.2 contains the concrete mix design.

4.2.2 Steel

The following types of steel were used:

1- High tensile strength prestressing wires which have a diameter of 0.276 in., exactly 7 mm., available in the structural laboratory, were used in the tested beams. The ultimate strength of these wires was given by the manufacturer as 255,000 psi (1760 MPa). The above values were checked in the laboratory. Two types of these wires were used, the first type had one of its ends deformed and came in lengths of 19.7 ft (6 m). Figures 4.8.a and 4.8.b show the unjacked end (deformed end) and the jacked end of these wires respectively. The second type, used after the first type was used up completely, had the same properties but it came in coils, and it was cut to the desired length. The two ends of this type of wires are shown in Fig. 4.9. Figure 4.10 shows the stress-strain relationship for the first type of the prestressing wires used in the experimental work. The second type of these wires showed almost the same stress-strain relationship.

2- Mild steel wires of 1/4 inch (6.3 mm) in diameter were used as longitudinal non-prestressing steel and 3/16 inch (4.8 mm) mild steel wires were used as stirrups. Figure 4.11 shows the mild steel for one of the T- beams.

3- Two end steel bearing plates, 3/8 inch (9.5 mm) thick were used to distribute the prestressing force at the beam ends. The dimensions of these bearing plates were 4x10 inch (102x254 mm) for beams with rectangular sections, 4x12 inch (102x305 mm) for the T-beams, and 4x14 inch (102x356 mm) for the I-beams. Figure 4.12 shows the end plate for an I-beam.

4.2.3 Auxiliary Materials

The following items were used during the construction of the beams:

- 1- Forms consisting of 3/4 in. (19.1 mm) thick plywood.
- 2- Plastic tubes having 7/16 inch (11.1 mm) outer diameter and 5/16 in. (7.9 mm) inner diameter, were properly greased with oil and used to house the prestressing wires during casting of the concrete.
- 3- Thin steel wire was used to tie the stirrups to the non-prestressing longitudinal steel.
- 4- Styrofoam pieces having the same dimensions as those of the openings were placed inside the form at the selected location of the opening and then removed after removing the forms.

4.3 Experimental Equipment

4.3.1 Equipment for Post-tensioning

1- The prestressing hydraulic jack with a capacity of 20 kip (89 kN) was used in post-tensioning the wires. This jack shown in Fig. 4.14 can stress only one tendon at a time and it has a pressure indicator to give a guide as to the value of the prestressing force in the wires.

2- Anchorage units consisting of washers and open-type grips consisting of an exterior cylinder and a split conical interior wedge. These units are shown in Fig. 4.13.

3- Cylindrical load cells were used to monitor the prestressing force in the tendons during and after prestressing. These cells are shown in Fig. 4.9b as well as Fig. 4.13. Figure A.3.1, in Appendix A.3 shows the calibration of the seven load cells used in measuring the prestressing force.

4- A strain indicator was used to read the strain and consequently the force in each load cell.

4.3.2 Equipment for Loading

1- Two supports, each consisting of a steel base and a steel roller, were used at the ends of a tested beam to represent the roller and hinged supports of the prestressed beams. These supports are shown in Figs. 4.2, 4.3, and 4.4.

2- A hydraulic jack was used to apply the vertical load at mid-span of the tested beams. This jack is shown in Figs. 4.2, 4.3, and 4.4. Also shown in those figures is the universal Flat Load Cell, model FL 500(C)-25 GKT, attached to the vertical jack. This

load cell, having a capacity of 50 kips (222.6 kN) was used to monitor the vertically-applied load. The calibration of this load cell is given in Fig. A.3.2, Appendix A.3.

3- Electric strain gauges type N11-FA-30-120-11 of 1.2 in. (30 mm) length, 119.7 Ω resistance, and 2.12 \pm 1% gauge factor were used to measure the horizontal and vertical strains while 45° electric strain gauge rosettes, type N31-FA-10-120-11 of 0.4 in. (10 mm) length, 120.0 \pm 0.3% Ω resistance and 2.08 \pm 1% gauge factor were used to calculate the shear strain on the surface of the beams. Figures 4.15, 4.16, and 4.17 show these types of electric strain gauges mounted on the concrete surface.

4- Mechanical dial gauges with travel sensitivity of 0.001 in. (0.025 mm) were used to measure the camber and deflection profile of the beam during prestressing and during the application of the external loading.

5- The automatic strain indicator manufactured by Vishay Intertechnology was used in recording the strains during prestressing and during the application of the vertical loading. The strain indicator shown in Fig. 4.18 consists of mainly four devices: the V1E-21 switch balance, eight digital strain indicator V1E-20, the V1E-25 scan controller, and the automatic printer V1E-22. Each strain indicator V1E-20 was able to record ten readings with an overall capacity of eighty strain gauges for the system.

4.4 Preparation of the Test Beams

1- For beams with rectangular and T-sections, the sides and base of the forms were cut into the required dimensions from a plywood 3/4 in. (19.1) thick. The form for the beams with I-sections was prepared by Prestressed Systems Incorporated (PSI

company). Four holes for the rectangular, five holes for the T- and seven holes for the I-sections were drilled in position to pass through the plastic tubes housing the prestressing wires. After applying two coats of oil to the inside face of the plywood to avoid undesirable bond with the concrete and leaving it to dry, the ends were nailed to the base and the side. Two styrofoam pieces with the required opening dimensions were glued to the inside face of the form-side by a styrofoam glue.

The required number of stirrups were prepared from 3/16 in. (4.8 mm) diameter steel bars. They were distributed along the beam length according to the pre-designed distribution shown in Figs. 4.5, 4.6, and 4.7. These stirrups were tied to the longitudinal non-prestressing steel and thus forming a steel cage which was placed inside the form.

3- Mild steel bars of 1/4 in. (6.4 mm) were inserted in the plastic tubes. The outside surface of these tubes was well greased with oil and placed in position through the drilled holes in the form. The tubes were kept in position using small steel bars placed across the form and tied to the stirrups. The remaining side of the form was screwed and thin wires were stretched across the form at the level of the tendons along different positions of the beam length to make sure that the tubes are horizontally levelled and no movement would occur during the concrete casting.

4- Three intermediate U-shaped steel clamps were used in the beams with rectangular section to maintain the two sides of the form parallel to each other. In the

case of T- and I-sections, stiffeners were used along the sides to keep them in position during the casting operation. The form was then placed on the casting bed and care was taken to keep it in position by clips and stiffeners.

5- The required weights of concrete ingredients were prepared for each batch. First, the gravel, sand, and cement were mixed in the concrete mixer for few minutes, then the water was added in stages. During the casting operation, three standard cylinders were prepared. Care was taken to make sure that the concrete filled the space under the styrofoam, especially for wide openings. Appropriate compaction by vibrating the bed and by steel rods was applied with special care to the beam ends and the opening region. After casting the beam and the cylinders, all surfaces were given a smooth final finish by hand trowelling.

6- Few hours after casting, wet burlap sheets were placed on the concrete surface. Curing continued for two or three days until the concrete surface seemed sufficiently wet. The three concrete cylinders were taken out of the aluminum moulds one day after casting and placed in a sink full of water in the curing room.

7- After leaving the beam air-cured for about one day, the plastic tubes were pulled out and the form removed. The styrofoam was taken off using an air hose and a special valve. Then the beam was sprayed by water and left for another three days to gain its full strength. A crane was then used to move the beam to its final place.

8- The strain gauge locations on the concrete surface were first smoothed using fine sand paper and all dust was removed using compressed air and then the surface was cleaned using acetone. A ratio of 60% of RTC Epoxy Resin A and of 40% RTC Epoxy Activator B were mixed together and used for installing the strain gauges. After the surfaces got dried, they were smoothed again with fine silicon carbide paper and then the gauges were mounted using the epoxy mix. The gauges were left for one day to make sure that the epoxy was fully hardened and then the wires were soldered to the strain gauges. Then the strain gauges were coated using Gagekote #3 and cured for one day under room temperature. The wires were then connected to the automatic strain indicator, balanced to zero and made ready for testing. Figures A.3.3a to A.3.3m in Appendix A.3 show the locations of the strain gauges on the tested beams.

9- The two end bearing plates were placed in position and the prestressing wires were passed through them. At the unjacked end, anchorage was provided by the deformed ends of the prestressing wires, Fig. 4.8a, or by anchorage wedges and cylinders shown in Fig. 4.9a. At the jacked end, cylindrical load cells were placed on the tendons followed by washers, anchorage wedges, and cylinders as shown in Figs. 4.8b and 4.9b. The load cells were connected to a strain indicator and balanced to zero.

10- The mechanical dial gauges were placed in position under the central concentrated load and at opening region, to measure the camber during the prestressing process and the deflection during the loading process.

4.5 Experimental Test Procedure

The testing procedure was carried out to investigate the static behaviour of the prestressed concrete beams with openings. Experimental measurements were directed to determine:

(i) the beam displacement and the deflection line of the opening chords during prestressing and during application of loading.

(ii) the horizontal strain distribution just under the vertical central load, the horizontal and vertical strain distribution at the edges of opening, and the horizontal and shear strain in the chords of opening.

(iii) the cracking load, the propagation of cracks with the increase of load, and the crack pattern before failure.

(iv) the ultimate capacity of the tested beams.

The beam testing program was carried out in the following steps:

1- Each wire was pulled out to attain a certain prestressing force to obtain the required total force and eccentricity. Proper sequencing was followed in prestressing the wires in order to guard against premature lateral failure. After pulling out all the wires, the prestressing force in each wire was again recorded to measure the force after losses due to anchorage deformation. The camber of the beam due to prestressing was recorded and the strains were printed using the Automatic Strain Indicator Printer.

2- The central vertical load was transmitted through the jack, the flat load cell, one

inch (25.4 mm) thick steel circular plate, one inch (25.4 mm) thick rectangular aluminum plate resting on a piece of rubber placed on the top surface of the beam as shown in Fig. 4.3.

3- The load was applied at constant rate in increments of 0.5 kip (2.2 kN). After each increment the load was maintained constant during recording the deflections, printing the strains, and marking the cracks. At about 90% of the ultimate load, the dial gauges were removed and the load was increased until failure. After recording the failure load and corresponding strains, the load was released slowly.

CHAPTER V

STATIC ANALYSIS AND DISCUSSION OF RESULTS

5.1 General

In this chapter, the results from the non-linear static finite element solution and from the tests conducted on prestressed concrete beams with openings, are presented. Tests were conducted on thirteen post-tensioned unbonded prestressed concrete beams with openings. Six of which were rectangular in section, five were T-, and the remaining two were of I-section. The details of the test program for such beams were given in Chapter IV, and a typical finite element mesh for each type of cross-section was given in Chapter III. The tests were carried out on these beams in an inverted position to represent a continuous beam behaviour as was shown in Fig. 4.1.

In the static analysis, the following design parameters were considered: (i) horizontal and vertical locations of the opening; (ii) width and depth of opening; and (iii) type of cross section. The objectives of this study were to determine: (i) the maximum

deflection of the beam as well as of the opening chords; (ii) the horizontal and vertical stress distribution at the critical sections of the beam; (iii) the shear stress distribution in the vicinity of the opening, (iv) the crack propagation pattern, and (v) the ultimate failure mode. The loading stages were divided into: (i) transfer stage, where the beam is subjected only to the prestressing force; (ii) working stage, where the vertically applied load is below the cracking load; (iii) ultimate stage, where the beam is about to collapse.

In addition to the experimentally and theoretically analyzed beams with openings, one solid beam with the same dimensions for each group of beams was analyzed theoretically for comparison purposes. The results from both the experimental and theoretical analyses are discussed below.

5.2 Deflection

The objective of this section is to study the effect of the presence of the opening, and the associated parameters on the deflection of prestressed beams. It should be noted that the experimental results were plotted using the cubic spline fitting. This means that these results pass by all the recorded points.

5.2.1 Rectangular Beams

(i) Group BI1

For beams with rectangular sections, group BI1 was used to study the effect of the horizontal location of the opening on the behaviour of such beams. Beams BI1A, BI1B,

and BIIC had a moment-shear ratio, M/VH where H is the beam depth, of 4.5, 4.0, and 3.5 respectively. The first two beams were examined experimentally and theoretically while the third one and an equivalent solid beam, denoted by BII, were examined theoretically only.

Figures 5.1, and 5.2 show the experimental and theoretical load versus maximum deflection curves for beams BIIA and BIIB, respectively. It should be noted that by the maximum deflection, it is meant the deflection at the free ends of the continuous beam shown in Fig. 4.1a or the deflection at the mid-span of the simply supported beam shown in Fig. 4.1b. The load-deflection relationship of the solid beam, BII, is presented in Figs. 5.1 and 5.2 for comparison. The results show that there is good agreement between the experimental and the theoretical results. Figure 5.3 shows the load-deflection relationship for all the beams of group BII which includes the solid beam and the three beams with an opening whose horizontal location is varied. It can be observed that all the beams of this group exhibited remarkably similar behaviour as far as the maximum deflection is concerned.

From these results, it can be observed that the relationship between the load and the maximum deflection consists of a linear part which describes the behaviour of the beam before cracking followed by a curved part, with decreasing slope, representing the non-linear stage. In this stage new cracks were formed at the critical sections and the crack width and length were increasing leading to final collapse. It can be also noted

from Fig. 5.3 that the horizontal location of the opening has a minor effect on the maximum beam deflection and that as the moment-shear ratio increases, the maximum deflection slightly increases. Comparing the results for the solid beam with the other results in Fig. 5.3, shows that the presence of the opening increases the maximum deflection by about 10% at the end of the working stage and that this ratio increases to 18% before failure.

Figures 5.4 and 5.5 show the experimental load-deflection relationship at the opening for beams BIIA and BIIB respectively. The maximum experimental deflection results were also plotted for comparison. It is interesting to notice in the first curve that the deflection of the opening edge close to the fixed support decreases with increase in the vertical load after cracking has occurred. This may be explained as follows: The total deflection at the opening region is divided into two parts: one due to bending and the other due to the Vierendeel action; and, in the case of the left edge of the opening of BIIA, the deflection due to the Vierendeel action exceeds the one due to bending since this edge is closer to the fixed support.

Figure 5.6 shows the theoretical deflected shape for the beams of group BII at load of 2 kip (8.9 kN) where no cracks had occurred yet. The difference between the deflected shape for solid beam and that for beams with opening can be observed. The Vierendeel action is also seen in the results for beams with openings. It can be noted that the deflection due to the shear in the opening chords increases as the moment-shear ratio

decreases. When the beams of this group were subjected to prestressing force only, i.e. at the transfer stage, the deflected shape was almost the same for all of them. Figure 5.7 shows the deflected shapes for one half of the span for the beams in this group at transfer and at working load stages. It can be noted that at the working load stage, the deflection line of the opening has a point of contraflexure approximately at the middle of the opening.

Summary of Findings:

The presence of an opening has the effect of increasing the maximum beam deflection. This increase becomes quite significant in the non-linear stage of loading following cracking of the opening chords. At this stage, the maximum deflection at the free end greatly increases as the opening moves towards the fixed support.

(ii) Group BI2

Group BI2 was considered to study the effect of the vertical location of the opening along the beam depth on the behaviour of such beams. This group contained beams BI2A, BI2B, and BI2C with the centre line of opening located 6 in. (152 mm), 5 in. (127 mm), and 4 in. (102 mm) respectively from the top fibre (the tension fibre). It contained also a solid beam BI2 for comparison purposes. All the three beams with opening were analyzed theoretically and experimentally while the solid beam was analyzed theoretically only.

In Figs. 5.8, 5.9, and 5.10, the experimental and theoretical load-deflection relationships for beams BI2A, BI2B, and BI2C are illustrated. The theoretical load-deflection relationship for the solid beam BI2 is also plotted for comparison purposes. Good agreement between the experimental and the theoretical results in the pre-cracking stage can be observed. Some discrepancy can be noted in the non-linear stage due to assuming the same concrete properties for all the beams in the finite element analysis. These properties differed from one beam to another in the laboratory. The concrete properties were assumed to be the same to make the comparison possible.

In Fig. 5.11 the theoretical deflection for beams BI2, BI2A, BI2B, and BI2C are presented. It can be seen from this figure that all the beams with opening of this group exhibited almost the same maximum deflection at the pre-cracking stage, i.e. the linear stage. After cracking, beam BI2C having the most shallow tensile chord had the least maximum deflection. This may be attributed to that, having a shallow tensile chord controls the depth of the cracks to be within that chord, while for shallow compression chord, the secondary moment may cause some additional cracks in that chord. This reduces the stiffness of beam with shallow compression chord (BI2A) more than that of beam with shallow tension chord (BI2C).

Figures 5.12, 5.13, and 5.14 show the experimental load-deflection relationship at the opening for beams BI2A, BI2B, and BI2C, respectively. The beam maximum deflection was also plotted for comparison purposes. Comparing the deflections at the

opening region for the three beams before failure, it can be seen that as the depth of the compression chord (the bottom one in this case) increases, the deflection decreases. This may be attributed to an increase in the moment of inertia of the opening section with increase in the depth of the compression chord since the tension chord is mostly cracked and does not contribute to the moment of inertia.

In Fig. 5.14 experimental deflections were not recorded after the applied load reached 3.75 kip (16.7 kN); the dial gauges were removed since it was observed that the beam was about to collapse.

The deflections of beams of group BI2 are presented in Fig. 5.15. The upper curves show the deflections after prestressing, while the lower curves show the deflections for an applied load of 2 kip (8.9 kN). It can be seen from the upper group of curves that beam BI2A exhibited the least camber due to the prestressing even less than the solid beam. Beam BI2B exhibited a little more camber than the solid beam BI2, while beam BI2C showed maximum camber in this group. The reason for beam BI2A having less camber than the solid beam may be explained as follows: in beam BI2A since the opening was moved downward, the centre of gravity of the section at the opening moved upward close to the resultant of the prestressing force. This reduced the bending moment resulting from the prestressing. The effect of this decrease in the bending moment exceeded the loss in the moment of inertia of this beam, and hence the smaller camber.

The reason for beam BI2C to have greater camber than beams BI2B and BI2A can be explained by referring also to Figs. 5.52, 5.53, and 5.54; for beam BI2A the resultant of the prestressing force at the opening region is located in the top chord where the centre of gravity is also located, while for beam BI2C, the resultant is located in the bottom chord, thus creating additional moment leading to greater camber.

In the lower part of Fig. 5.15 the deflections of beams of group BI2 corresponding to a vertical load of 2 kip (8.9 kN) are shown. In this figure, using the horizontal position before prestressing as the datum, one cannot estimate the actual displacement of each beam due to the vertical load. Thus Fig. 5.16 is presented with a datum being the position after prestressing. From this figure, it can be seen that in the linear stage (before cracking), all the beams with openings of this group exhibited almost the same deflection due to applying the vertical load. This may be attributed to the presence of the openings in the same horizontal location for these beams, which resulted in almost the same deflections due to the Vierendeel action. This action will be presented in Chapter VII.

Summary of Findings:

The vertical location of an opening greatly affects the beam maximum deflection at the transfer stage. As the opening moves upward close to the line of action of the prestressing force, the beam camber increases. At the working load stage, the vertical location of an opening has a minor effect on the beam deflection. At the ultimate load stage, the beam maximum deflection increases as the depth of the compression chord

decreases.

--

(iii) Group BI3

In group BI3 the effect of the width of opening, W , on the behaviour of prestressed beams was investigated. A moment-shear ratio of 4 was fixed for all beams of this group. Three beams, namely, BI3A, BI3B, and BI3C with opening widths of 12 in. (305 mm), 16 in. (406 mm), and 20 in. (508 mm), respectively, were considered in this group.

Beam BI3A with an opening width of 12 in. (305 mm) and beam BI3B with an opening width of 16 in. (406 mm) were introduced before as beams BI1B and BI2B, respectively. The load-deflection relationships for these two beams can be found in Figs. 5.2, and 5.9, respectively. Figure 5.17 shows the experimental and theoretical load-deflection relationships of beam BI3C. Before cracking, the experimental results coincided with the theoretical ones, while in the non-linear stage, the experimental deflections were slightly greater than the theoretical ones.

Figure 5.18 presents the load-deflection relationship for the beams with openings of this group as well as the results of the solid beam with no opening. It can be seen from these results that as the opening width increases, the maximum deflection increases. It can be observed also that the increase in deflection when the opening width increased from 16 in. (406 mm) to 20 in. (508 mm) is more than the increase in deflection when

the opening width increased from 12 in. (305 mm) to 16 in. (406 mm). At a vertical applied load of 2 kip (8.9 kN) the maximum deflections of beams with openings were compared to the maximum deflection of the solid beam: it was found that the deflections of the former increased by ratios of 6%, 11%, and 19%, respectively, due to the presence of openings. In the non-linear stage at a load of 3.5 kip (15.6 kN), these ratios were 9%, 14%, and 40%, respectively.

The experimental deflections at the edges and at centre of the opening were plotted with the maximum deflection at mid-span of the beam in Fig. 5.19. The difference between the deflection of the opening right edge and of the opening centre is the same as the difference between the deflection of the opening left edge and of the opening centre as a result of the Vierendeel action.

In Fig. 5.20 two sets of results are plotted for the deflected shape of the beams of group BI3. The upper curves show the deflected shape, i.e the camber due to prestressing while the lower curves show the deflected shape due to the vertical applied load of 2 kip (8.9 kN) as well as the prestressing force. It can be seen from this figure that the opening width has almost no effect on the camber of the beams with openings. Due to the vertical applied load, however, the opening width has an effect of increasing the deflection of beams with openings as can be seen from the lower set of curves in Fig. 5.20. As the opening width increases the effect of the Vierendeel action on the deflected shape becomes more pronounced.

Summary of Findings:

The increase in the width of opening greatly increases the maximum deflection of beams with openings, in the working and ultimate load stages, while it has insignificant effect on the camber due to prestressing force.

(iv) Group BI4

Group BI4 was considered to study the effect of the opening depth, h , on the behaviour of prestressed concrete beams with openings. The horizontal and vertical locations of the opening were fixed for all beams of this group. Three beams, viz., BI4A, BI4B, and BI4C with opening depths of 3 in. (76 mm), 4 in. (102 mm), and 5 in. (127 mm), respectively, were considered. The first beam BI4A, was tested experimentally while the other two were investigated theoretically only.

Figure 5.21 shows the load-deflection relationship for the three beams with openings of this group as well as for a solid beam BI4. It can be seen from these results that the maximum deflection of the beam increases as the opening depth increases. Comparing the maximum deflection of the beams with openings with that of the solid beam at a vertical applied load of 2 kip (8.9 kN), it was found that this deflection increases by 11%, 18%, and 32% due to the presence of openings of depth 3 in. (76 mm), 4 in. (102 mm), and 5 in. (127 mm), respectively. In the non-linear stage at a load of 3 kip (13.35 kN), these ratios were 16%, 44%, and 73%, respectively. The reason for the last beam to have this excessive increase in deflection at the ultimate load stage is that

the opening depth of 50% of the beam depth caused significant cracking and hence more reduction in the beam stiffness.

In Fig. 5.22, the deflection results due to prestressing are plotted for all beams of group BI4 in the upper part while the deflection results at a vertical load of 2 kip (8.9 kN) are shown in the lower part. It can be seen from the upper set of curves that the maximum camber of the beam, at the free edge, increases with increase in the opening depth. Comparing the maximum camber for beams with openings to that of the solid beam, it is found that the maximum camber increases by 1%, 3%, and 6% when the opening depth is 3 in. (76 mm), 4 in. (102 mm), and 5 in. (127 mm), respectively. It can be observed that in the opening region - from distance 9 in. (229 mm) to 25 in. (635 mm), the beams with openings have less camber than the solid beam. This can be explained as follows: the prestressing force has two effects, one as a normal force and the other producing bending moment, the latter causes the beam to deflect upward while the former has the effect of deflecting the two chords of the opening away from the beam longitudinal centre line. This means that the upper chord deflects upward while the lower chord deflects downward. This means that the lower chord has two components of deflection, one downward due to the prestressing force and the other upward due to the moment resulting from the eccentricity of the prestressing force. In this case, the downward deflection exceeds the upward one. The deflection of the bottom chord is the one plotted in Fig. 5.22 representing the opening region as the experimental measurements were taken for that chord.

Figures 5.22 and 5.23 show the deflections due to a vertical load of 2 kip (8.9 kN) for the beams of that group. In the opening region, the effect of the Vierendeel action is quite obvious. The existence of a contraflexural point in the mid-width of the opening can be observed especially in beam BI4C where the opening depth is the largest. From these results, it can be concluded that the opening depth has a significant effect on the deflected shape and the value of the maximum deflection of prestressed beams with openings.

Summary of Findings:

The increase in the depth of opening significantly increases the deflections of beams with openings in the working and ultimate load stages. Also in the transfer stage, this increase in the opening depth increases the camber of these beams.

In all the above groups of beams, the deflection at the opening centre is almost the average of the deflections at the two edges of the opening. This indicates that the point of inflection lies very close to the middle of the opening chords.

5.2.2 T-Beams

(i) Group BII1

For beams with T-section, group BII1 was considered to study the effect of the horizontal location of the opening on the behaviour of such beams. This group contains, in addition to a solid beam BII1, three other beams with openings namely; BII1A, BII1B,

and BII1C, where the moment-shear ratio was 3.5, 3.0, and 2.5, respectively. All the three beams with openings of this group were tested experimentally while the reference solid beam BII1 was investigated theoretically only.

Figures 5.24, 5.25, and 5.26 show the experimental and theoretical load versus maximum deflection relationships for beams BII1A, BII1B, and BII1C, respectively. In addition, the load-deflection relationship for the solid beam BII1 is plotted for comparison purposes. From these results, it can be shown that for beams with T-sections, the presence of an opening has the effect of increasing the maximum deflection of the beam. This increase becomes quite significant in the non-linear stage of loading after cracking occurred.

Good agreement can be observed between the experimental and the theoretical results. Some difference is seen in the linear part for beam BII1C. This may be attributed to the fact that all the beams were given the same concrete properties in the finite element analysis for comparison reasons. However, in the laboratory beam BII1C had slightly higher concrete compressive strength than the other two beams.

In Fig. 5.27, the load-deflection relationships for all the beams of group BII1 are presented. It can be seen from this figure that beam BII1A which has the opening closest to the continuous support, i.e. 6 in. (152 mm) between the support and the left edge of the opening, experiences the highest maximum deflection in this group. The solid beam

BII1 has the lowest maximum deflection among the beams of this group, while beams BII1B and BII1C have almost the same load-deflection relationships. Figures 5.28, 5.29, and 5.30 show the experimental load-deflection relationships at the opening for beams BII1A, BII1B, and BII1C, respectively. The beam maximum deflection curve was also plotted for comparison purposes. It can be seen from these figures that the deflection at the centre of the opening is almost the average of the deflections at the opening edges. This supports the Vierendeel action theory where the contraflexural point lies almost at the middle of the opening chords.

Figure 5.31 shows the deflection results for the beams of group BII1 due to the prestressing force, due to a vertical load of 2.5 kip (11.1 kN), and due to a vertical load of 5 kip (22.25 kN). It can be seen from these results that the beams with opening exhibit more camber than the solid beam. Also the horizontal location of the opening has almost no effect on the deflections of the beams due to prestressing. At a vertical load of 2.5 kip (11.1 kN), it can be observed that the three beams with openings - BII1A, BII1B, and BII1C - have almost the same deflected shape along the portion to right of the opening. In the opening region, beam BII1A exhibited the maximum deflection followed by beam BII1B and BII1C, respectively. This means that as the opening moves toward the continuous support, the deflection of the opening chords increases. At a load of 5 kip (22.25 kN), the beams with openings were heavily cracked and about to collapse. As can be observed from Fig. 5.31, beam BII1A undergoes greater deflection than the other beams of this group, both in the opening region and at the end of the beam.

Summary of Findings:

Moving the opening towards the fixed support, has the effect of increasing the deflection of the opening chords and hence the overall beam deflection at the ultimate load stage. Also having an opening very close to the continuous support (at a distance smaller than one depth of the beam), leads to excessive deflections in that beam at the ultimate load stage.

(ii) Group BII2

Group BII2 was considered to study the effect of the vertical location of the opening on the behaviour of prestressed concrete T-beams. The distance, C , between the centre of opening and the top fibres of the beam was 6.5 in (165 mm), 5 in. (127 mm), and 3.5 in. (89 mm) for beams BII1A, BII1B, and BII1C, respectively. Beam BII2A is the same beam BII1B which was analyzed before. Beam BII2B was tested experimentally and theoretically while beam BII2C was analyzed theoretically only.

Figure 5.32 shows the results for load versus beam maximum deflection for beam BII2B. The theoretical relationship for the solid beam BII2 is presented for comparison. Good agreement is shown between the experimental and the theoretical results. In Fig. 5.33, a comparison between the load-deflection relationships of all the beams of group BII2 is presented. It can be seen from this figure that there is no significant difference between the maximum deflection of the beams with openings of this group, especially in the linear stage, before cracking.

In Fig. 5.34 the experimental load-deflection relationships for the edges as well as for the centre of the opening are presented. The experimental maximum deflection of the beam is also plotted for comparison. The deflection results for the opening centre lie almost at the middle between the two results for the opening edges during all the stages of loading. This supports the Vierendeel behaviour in beams with openings.

The deflection results of the whole beam were studied at three different stages of loading, viz., at transfer where the beam is subjected to the prestressing force only, at working load where the beam is subjected to a vertical load of 2.5 kip (11.1 kN) in addition to the prestressing force, and at ultimate load where the vertical load was increased to 5 kip (22.25 kN). The results of this study are presented in Fig. 5.35 where the beam deflected shapes at each stage of loading are shown. The very upper group of curves show the deflected shapes for the three beams with openings of group BII2 as well as for the solid beam due to the prestressing force only. As was previously explained in group BI2 for rectangular beams, the presence of the opening affects the location of the centre of gravity of the sections in the opening region, resulting in changing the moment due to the prestressing eccentricity. This along with the change in the beam moment of inertia due to the presence of the opening, cause the change in camber for the beams in this group.

The other two groups of curves in Fig. 5.35, give the deflected shapes of the beams at the working and ultimate load stages. Using the horizontal position before

prestressing as the datum for these two groups of curves, one cannot estimate the actual displacement of each beam due to the vertical load from this figure. Thus, Fig. 5.36 is presented with a datum being the position after prestressing. It can be observed from this figure that in the elastic stage, no significant difference is observed in the deflected shape of the beams of group BII2. Near the ultimate stage before collapse, the crack pattern which affects the inertia of the beams causes some difference in the deflected shapes of the beams of this group. As the opening moves down toward the flange, the deflection of the beam increases at the ultimate stage. Thus the Vierendeel action can be observed in the beams with openings of this group.

Summary of Findings:

The vertical location of an opening has a minor effect on the deflection of beams with openings when they are subjected to vertical load. At the prestress transfer stage, this vertical location greatly affects the beam camber.

(iii) Group BII3

In group BII3 the effect of the opening width, W , on the behaviour of prestressed T-beams with openings was studied. Beam BII3B with opening width equal to 18 in (457 mm) denoted earlier as BII1B, was investigated theoretically and experimentally. Beams BII3A and BII3C with opening widths 12 in. (305 mm) and 24 in. (610 mm) respectively, were studied theoretically only. Figure 5.37 shows the load-deflection relationships for the beams in this group. It can be seen from this figure that beam BII3C experiences

significant deflections especially in the non-linear stage when compared to beams BII3A and BII3B. At a load of 2.5 kip (11.1 kN), the maximum deflection for beams with openings increased compared to that of the solid beam by about 10%, 25%, and 65% for BII3A, BII3B, and BII3C, respectively.

The deflection results for the three beams with openings as well as the solid beam of group BII3 are shown in Fig. 5.38 at the transfer stage, working stage, and ultimate stage.

At the transfer stage where the beam is subjected to prestressing only, the opening width has minor effect on the deflection results of the beam. This can be seen from the top four curves for the solid beam and the three beams with openings in this group. Compared to the solid beam, the beam maximum camber increased by 7%, 9%, and 11% in beams BII3A, BII3B, and BII3C, respectively.

At the working stage, where the beams are subjected to a vertical load of 2.5 kip (11.1 kN), the Vierendeel action which is affected by the geometries of the opening chords causes a significant difference between the deflection results of the beams in this group. Due to the load of 2.5 kip (11.1 kN), the maximum deflection of beams when compared to that of the solid beam, increased by 10%, 25%, and 65% as mentioned earlier.

At the ultimate stage, the Vierendeel action as well as the cracking of the opening chords play a significant role in the deflection results of the beams in this group. It can be seen from Fig. 5.38 that the deflection of the opening region significantly affects the deflection of the whole beam. The difference between the deflection of BII3A and the solid beam is very small compared to the difference between the deflection of BII3C and the solid beam. This may be attributed to the fact that the width of opening of beam BII3C is almost double the width of opening of beam BII3A. This increases the deflection resulting from the Vierendeel action. Furthermore, the increase in the opening width causes more cracks resulting in a significant loss of stiffness and greater deflections.

Summary of Findings:

The increase in the opening width greatly increases the maximum deflection of beams with openings, in the working and ultimate load stages, while it has insignificant effect on the camber due to prestressing force. Also in the non-linear stage when the tension chord is shallow, the cracking of that chord may cause significant reduction in the beam stiffness resulting in higher deflections.

(iv) Group BII4

The last group in the T-beams is group BII4, which was considered to investigate the effect of opening depth, h , on the behaviour of such beams. The depth of opening was 3 in. (76 mm), 4 in. (102 mm), and 5 in. (127 mm) in beams BII4A, BII4B, and

BII4C, respectively. The first beam was studied theoretically only, while the other two were studied theoretically and experimentally. Results of beam BII4B were discussed before under beam BII1B since these two beams are the same.

Figure 5.39 shows a comparison between the theoretical and the experimental load-deflection relationship for beam BII4C. The deflection of an identical solid beam is also presented in this figure. It can be seen from the results that the presence of the opening with this depth, i.e., about 40% of the beam depth, increases the deflection by about 40% at a load of 2.5 kip (11.1 kN) and double that deflection at a load of 5 kip (22.25 kN). This shows that at the ultimate stage, the cracks which develop at the opening region, remarkably decrease the beam stiffness, resulting in higher deflections.

Figure 5.40 shows a comparison between the deflections of the four beams of this group. It can be seen from the results that the difference between the deflections of beams BII4A and BII4B is less than the difference between BII4B and BII4C especially in the non-linear stage.

The experimental deflections of the opening edges and at the opening centre for beam BII4B are presented in Fig. 5.29, since beams BII4B and BII1B are identical. Figure 5.41 shows the experimental deflections of the opening edges and its centre for beam BII4C. The maximum deflection for the same beam is also shown for comparison purposes. It can be observed from these results that the deflection at the centre of the

opening intermediates the deflections of the opening edges which means that the point of inflection exists at the opening centre.

The deflections of the beams in group BII4 were investigated at three stages of loading namely; at transfer, at working, and at ultimate stage. Figure 5.42 shows the deflection profile of each beam in this group at the different stages of loading. Comparing the maximum camber for these beams due to prestressing, it is found that compared to the solid beam, the maximum camber increased by 6%, 9%, and 14% in beams BII4A, BII4B, and BII4C, respectively. Measuring the deflection from the prestressing position, the maximum deflection increased by 18%, 26%, and 38% compared to the solid beam for beams BII4A, BII4B, and BII4C, respectively, at a vertical load of 2.5 kip (11.1 kN). At the ultimate stage, beam BII4C with an opening depth of 5 in. (127 mm) exhibited larger deflections when compared to the other beams in this group. This is due to the excessive cracking in the opening region of this beam. Compared to the deflection of the solid beam, and measuring the deflection from the prestressing position, the maximum deflection increased by 9%, 30%, and 100% for beams BII4A, BII4B, and BII4C, respectively.

Summary of Findings:

Increasing the opening depth reduces the beam stiffness which leads to an increase in the beam deflection at the transfer and working load stages. At the ultimate load stage, this increase in the opening depth creates more cracks in the opening chords resulting in

more pronounced increase in deflection.

5.2.3 I-Beams

Group BIII1 was considered to study the behaviour of prestressed concrete I-beams with openings. Three different horizontal locations were studied in this group. Beams BIII1A, BIII1B, and BIII1C with the opening left edge located at distances of 12 in. (305 mm), 16 in. (406 mm), and 21 in. (533 mm) from the support were studied in this group. The first and third beams were investigated theoretically and experimentally, while the second one was studied theoretically only. A solid beam with the same dimensions was analyzed theoretically for comparison purposes.

Figures 5.43 and 5.44 show the experimental and theoretical load-deflection relationships for beams BIII1A and BIII1C, respectively. The theoretical deflection for the solid beam BIII1 is also presented. It is observed from these figures that the behaviour of the solid beam continued to be linearly elastic while the beams with openings behaved non-linearly approaching collapse. Also good agreement can be found between the experimental and the theoretical results especially in the elastic stage.

Figure 5.45 shows a comparison between the theoretical results for the four beams of group BIII1. From this figure, it can be noticed that moving the opening towards the high moment region has the effect of increasing the beam maximum deflection in the non-linear stage of loading. No significant difference can be observed in the elastic stage

between the deflections of the three beams with openings in this group.

The experimental deflections of the opening edges and centre for beam BIII1A and BIII1C, are presented in Figs. 5.46 and 5.47. It is noted that, the deflection at the opening left edge is very small. This is expected since that edge is very close to the support. It can also be observed that the deflection results at the opening centre lie almost in middle between the results for the left and the right edges. This indicates that the contraflexure point lies almost at the mid-length of the opening chords.

The beam deflected shape for group BIII1 was investigated at three stages of loading, viz., at transfer, at working, and at ultimate stage. Figure 5.48 shows the position of each beam of this group at the different stages of loading. Due to the prestressing force only, all the beams of this group including the solid beam exhibited almost the same deflected shape. This means that the presence of the opening or its horizontal location has no effect on camber of the prestressed I-beams. At the working stage, within a vertical load of 4 kip (17.8 kN), it can be seen from the middle set of curves in Fig. 5.48 that the opening has only a local effect on the deflected shape of each beam. In the opening region, as the opening moves toward the continuous support, the deflection of the opening chords increases. At a vertical load of 8 kip (35.6 kN), the three beams with openings of this group had different deflected shapes. The deflection increased as the opening moved toward the continuous support. At this load stage, a remarkable difference between the deflection profile of the solid beam and that of the

beams with openings, can be observed.

Summary of Findings:

The presence of an opening in a prestressed I-beam significantly increases the deflections of such beams especially at the ultimate load stage. Moving the opening horizontally toward the high moment region has the effect of increasing the beam maximum deflection in the non-linear stage of loading. There is no significant difference in deflections at the transfer or working load stages for beams with openings of this group.

5.3 Strain and Stress Distribution

The objective of this section is to investigate the effect of different parameters on the horizontal, vertical, and shear stresses in prestressed concrete beams with openings. Three different stages of loading were studied, namely; transfer stage, working stage, and ultimate stage. The first stage is where the beam is subjected to the prestressing force only. The second stage is where the beam behaves elastically under the effect of a vertical load. The results of this stage were considered when the vertical load was equal to 2 kip (8.9 kN) for rectangular beams, 2.5 kip (11.1 kN) for T-beams, and 4 kip (17.8 kN) for I-beams, since these loads are below the cracking loads of such sections. The third stage is where the beam was heavily cracked and was about to collapse. The results of this stage were considered when the vertical load was 4 kip (17.8 kN) for rectangular beams, 5 kip (22.25 kN) for T-beams, and 8 kip (35.6 kN) for I-beams. Results from the non-linear finite element analysis are compared when applicable to those from tests on the prestressed concrete beams. The solid lines in all the figures of this section represent the theoretical results while the dashed lines represent the experimental results.

5.3.1 Horizontal Strain and Stress Distribution

5.3.1.1 Rectangular Beams

(i) Group BII

The horizontal stress distributions for beams with openings in group BII, to study the effect of the horizontal location of the opening, are shown in Figs. 5.49, 5.50, and 5.51 for beams BIIA, BII B, and BII C, respectively. The experimental and the theoretical

normal stresses in the vicinity of the opening as well as at section above the continuous support are shown. At the transfer stage, it can be seen that the horizontal location of the opening has little effect on the normal stresses around the opening, while the stresses at the continuous support increased in beam B11A due to the fact that the opening left edge was very close to the support. This also changed the stress distribution to a non-linear one. At this load stage, it is observed that the maximum horizontal stress above the support for beam B11A was more than that for beams B11B and B11C. This may be attributed to that the opening in beam B11A was one time the beam depth away from the support.

Considering the working load stage, with the vertical load equal to 2 kip (8.9 kN), it was found that the horizontal stress distribution at the continuous support was still linear except for beam B11A where the opening is very close to the support; this disturbed the distribution as shown in Figs. 5.49b, 5.50b, and 5.51b. It is observed from these three figures that the maximum compressive stress in the vicinity of the opening increased as the opening moved toward the support.

At the ultimate stage of loading, cracks were developing rapidly and the crack width increased. The maximum compressive stress occurred at the upper right corner of the bottom chord for all beams with openings in this group. The maximum tensile stress occurred at the upper left corner of the top chord. At a load of 4 kip (17.8 kN), this corner was already cracked and thus carried no tension in beams B11A and B11B, while

for beam BI1C, the concrete elements in that corner were still carrying some tension since the opening was away from the support. For beam BI1A, the presence of the opening close to the support disturbed the horizontal stress distribution at the support section resulting in less compressive stress than that in beams BI1B and BI1C.

Summary of Findings:

The horizontal location of the opening has little effect on the horizontal stresses around the opening at the transfer stage. At the working and ultimate stages, these stresses increase as the opening moves closer to the continuous support. The presence of the opening within one beam depth from the continuous support increases the maximum horizontal stress in the beam above this support.

(ii) Group BI2

In group BI2, the varying parameter was the vertical location of the opening. Figures 5.52, 5.53, and 5.54 show the experimental and theoretical horizontal stress distributions for beams BI2A, BI2B, and BI2C, respectively. Although the experimental prestressing force in beam BI2B was higher than in beams BI2A and BI2C, for comparison purposes, it was assumed to be the same in the theoretical analysis for all beams in this group.

Comparing the horizontal stress distribution for the three beams at the transfer stage, it can be observed that the vertical location of the opening greatly influences the

stress in the opening region. As the depth of the top chord decreases, the stress distribution in that chord acquires a rectangular shape, which means that the stresses at the top and bottom fibres of this chord become almost equal. Also with the increase of the bottom chord depth, the stress in that chord acquires a triangular shape.

Comparing the stress distribution at the opening edges with that at the middle of the opening for the three beams at the transfer stage, it can be seen that there is some stress concentration at the opening edges. Such concentration is not evident at the middle of the opening. At the section above the continuous support, the stress distribution is the same for the three beams at the transfer stage.

Figures 5.52b, 5.53b, and 5.54b, illustrate the horizontal stress distribution at the working load stage. These stresses are the sum of stresses due to prestressing and due to a vertically applied load of 2 kip (8.9 kN). To study the effect of the vertical load only, Fig. 5.55 presents the stresses at the middle of the opening. In this figure, the stresses at the transfer stage were subtracted from the total stresses at the working stage. The stresses from beam theory were also plotted shown dashed lines for comparison. The maximum difference between the stresses from the beam theory and those from the finite element analysis for the beams in this group is about 15%. In Fig. 5.55, it can be noticed that for BI2B, the stresses in the top chord were less than those in the bottom chord since the top chord contained more reinforcement than the bottom chord; this resulted in shifting the neutral axis toward the top chord and causing the difference in the stresses.

At the ultimate stage, at a load of 4 kip (17.8 kN), the compressive stresses in the middle of the bottom chord increased with the decrease of its depth. In beam BI2A where the depth of the bottom chord was minimum, the stresses in that chord were all compressive while in the other two beams, some tension developed in the compression chord. In the same beam, it can be noticed that the left bottom corner of the top chord experienced the maximum compressive stress among the three beams. This may be attributed to the high secondary moment resulting from the high shear carried by that chord due to its large depth. It was expected that the bottom chord in beam BI2C would also reveal maximum horizontal stress but since this chord was not cracked, its full inertia was effective unlike the top chord of beam BI2A which was cracked at this stage. The solid section above the support in beam BI2B was subjected to the highest compressive stresses among the three beams. Theoretically and experimentally, this section experienced the longest crack among the three beams.

Summary of Findings:

The vertical location of the opening influences the horizontal stress distribution in the vicinity of the opening at all stages of loading. As the depth of the top chord decreases, the horizontal stress distribution acquires a rectangular shape. Also with increase in depth of the bottom chord, the horizontal stress in that chord acquires a triangular shape.

(iii) Group BI3

Group BI3 was considered to study the effect of the width of the opening on the response of prestressed beams with openings. Since beam BI3A is the same beam denoted earlier as BI1B, the horizontal stress distribution for that beam can be seen in Fig. 5.50. Figures 5.56, and 5.57 show the experimental and theoretical horizontal stress distributions for beams BI3B, and BI3C, respectively. The three beams in this group were subjected to the same prestressing force in the finite element analysis. In the laboratory, the prestressing force was slightly different from one beam to another which accounts for the little difference between the experimental and the theoretical results. At transfer stage, the above results show that as the opening width, W , increases, the stress concentration at the opening upper and lower edges decreases. Since the prestressing force is constant, the stresses at the upper and lower fibres of the beam in the opening region, increase with increase in the opening width; this is due to the decrease in the stress concentration around the opening. Comparing the stresses at the solid section above the continuous support, it can be observed that in beam BI3C with an opening width of 20 in. (508 mm), the stress distribution becomes non-linear with the highest stresses at the beam edges. The stresses in the same beam at the centre of the opening, are very close to those calculated from the simple beam theory since the stress concentration is very small and can be ignored. In beam BI3A, where the opening is just 12 in. (305 mm) wide, the stress distribution at the upper chord due to the prestress is almost rectangular in shape instead of trapezoidal. This is due to the stress concentration at the opening upper edge which increases the stress at the bottom of the top chord to be

equal to that at the top of the same chord.

At the working stage, with a vertical load of 2 kip (8.9 kN), the stresses at the solid section above the continuous support increase with increase in the opening width as shown in Figs. 5.50b, 5.56b, and 5.57b. It can be seen also from these figures that as the opening width increases, the stresses at the upper right and the lower left corners of the opening chords increase while the stresses at the other four corners decrease. This is due to the secondary moment, resulting from the Vierendeel action which increases with the opening width.

Beam BI3C collapsed in the laboratory at a cantilever load of just less than 3.5 kip (15.6 kN); its stress distribution at the ultimate stage was plotted for a load of 3 kip (13.4 kN) instead of 4 kip (17.8 kN) which was used for all other beams. At this loading the presence of cracks causes the stress distribution to be non-linear in most sections of the beam. The maximum compressive stresses at the opening region occur at the upper right and the lower left corners of the bottom chord as shown in Figs. 5.50c, 5.56c, and 5.57c.

Summary of Findings:

Increasing the opening width decreases the stress concentration at the upper and lower edges of the opening at the transfer stage. At the working and ultimate stages, the horizontal stresses at the opening edges increase with increase in the opening width.

(iv) Group BI4

In group BI4, the effect of the opening depth on the behaviour of prestressed concrete beams with openings was studied. Figures 5.56, 5.58, and 5.59 show the horizontal stress distributions for beams BI4A, BI4B, and BI4C, respectively. At the transfer stage, the horizontal stress distribution at the solid section above the support is the same for all the beams in this group as can be seen from Figs. 5.56a, 5.58a, and 5.59a. The maximum horizontal stress at the opening region is at the upper right corner of the top chord for all the three beams. Increasing the opening depth from 3 in. (76 mm) to 4 in. (102 mm), has the effect of increasing that stress by about 10%, while increasing the opening depth from 3 in. (76 mm) to 5 in. (127 mm), results in increasing the stress by about 25%. It can be seen also from these figures that increasing the opening depth increases all the stresses around the opening at the transfer stage.

Applying a vertical load of 2 kip (8.9 kN) has the effect of increasing the compressive stresses at the bottom fibres of the solid section above the support and decreasing them at the top fibres of the same section, as shown in Figs. 5.56b, 5.58b, and 5.59b. The opening depth in this group has no effect on the horizontal stresses at the solid section above the support. The maximum horizontal stress at the opening region is at in the upper right corner of the bottom chord. Increasing the opening depth from 3 in. (76 mm) to 4 in. (102 mm) and from 3 in. (76 mm) to 5 in. (127 mm), has the effect of increasing this stress by 20% and 48%, respectively.

Since beam BI4C failed at a load of about 3.7 kip (16.5 kN), the stresses at the ultimate stage were chosen to be plotted at a load of 3.5 kip (15.6 kN) for this particular beam. The maximum compressive stress around the opening at a load of 4 kip (17.8 kN) increased by about 26% when the opening depth was increased from 3 in. (76 mm) to 4 in. (102 mm). The stresses around the opening were higher in beam BI4C than the other two beams of this group, although the stresses were plotted at a load of only 3.5 kip (15.6 kN) for beam BI4C.

Summary of Findings:

The opening depth has a significant effect on increasing the horizontal stresses around the opening at all stages of loading of prestressed concrete beams with openings. As long as the opening is at least one beam depth away from the continuous support, the opening depth does not affect much the horizontal stresses in the beam above this support at the transfer and working load stages. At the ultimate stage, the severe cracking does influence these stresses.

5.3.1.2 T-Beams

(i) Group BII1

Group BII1 was considered to study the effect of the horizontal location of the opening on the behaviour of prestressed concrete T-beams with openings. The experimental and horizontal stress distributions for beams BII1A, BII1B, and BII1C, are shown in Figs. 5.60, 5.61, and 5.62, respectively.

It can be observed from Fig. 5.60, that the horizontal stress distribution at the solid section above the support is non-linear in all the loading stages, because of the closeness of the opening to the support.

At the transfer stage, it can be seen that the stresses in the vicinity of the opening are about the same in beams BIII1B and BIII1C. Minor difference is noticed between the maximum horizontal stress at the section above the support for these two beams. It can be concluded from this that as long as the opening edge is far enough from the support, about one depth of the beam, the horizontal location of the opening does not affect the horizontal stresses at the transfer stage.

Considering the working load stage, with a vertical load of 2.5 kip (11.1 kN) it can be seen that the moment due to this load almost balances the moment resulting from the eccentricity of the prestressing, creating a rectangular stress distribution above the support, as shown in Figs. 5.60b, 5.61b, and 5.62b. At the vicinity of the opening where the Vierendeel action is observed, the maximum compressive stresses occur at the upper left and the lower right corners of the opening for the three beams in this group.

At a vertical load of 5 kip (22.25 kN) when the beams are near collapse, the horizontal stress distribution at the vicinity of the opening as well as above the support are shown in Figs. 5.60c, 5.61c, and 5.62c. The crack pattern for the beams play an important role in the stress distribution above the support. This crack pattern will be

discussed later in this chapter. The maximum horizontal compressive stresses which occur at the upper left and the lower right corners of the opening are found to increase as the opening gets closer to the support.

(ii) Group BII2

In group BII2, the effect of the vertical location of the opening on the behaviour of prestressed concrete T-beams was investigated. The horizontal stress distributions for beams BII2A, BII2B, and BII2C are shown in Figs. 5.61, 5.63 and 5.64, respectively.

At transfer stage, the stress distribution above the support is almost the same in the three beams with openings in this group. As the opening moves upward closer to the line of the resultant prestressing force higher stresses develop in the opening region. This is expected, since moving the opening up increases the distance between the line of action of the prestressing force and the centroid of the beam, leading to more bending stresses.

Applying a vertical load of 2.5 kip (11.1 kN), causes the stress above the support to have almost a rectangular shape in the three beams of this group. The opening vertical location has a minor effect on this stress, above the support. At the opening region, the stresses generally increase as the opening moves away from the flange. This can be observed from Figs. 5.61b, 5.63b, and 5.64b where the stresses at the opening horizontal edges increase as the opening moves up.

At the ultimate stage, the crack pattern significantly controls the distribution of the horizontal stresses in beams with openings. The horizontal stress distribution above the support, shown in Figs. 5.61c, 5.63c, and 5.64c, is almost the same for the three beams of this group at a load of 5 kip (22.25 kN). In beam BII2C with the top chord is significantly cracked, all the tensile force is carried by the steel in the top chord, while the compressive force is carried by the bottom chord. This is shown at the opening mid-section in Fig. 5.64c. At the edges of the opening, in the same figure, the secondary moment resulting from the Vierendeel action is inducing compressive and tensile stresses in both the top and bottom chords.

From Figs. 5.61, 5.63, and 5.64, it can be seen that the opening vertical location affects the horizontal stress distribution at the opening region. This is due to the change in the section characteristics and the prestress distribution. Prediction of the horizontal stress will be discussed later and simple methods for estimating these stresses will be presented.

(iii) Group BII3

Group BII3 was considered to study the effect of opening width on the behaviour of prestressed T-beams with openings. Beam BII3B is the same beam denoted earlier as BII1B and its horizontal stress distribution was presented in Fig. 5.61. Figures 5.65 and 5.66 show that distribution for beams BII3A and BII3C.

At the transfer stage, the stress above the support is slightly affected by the opening width. Comparing the stress distribution at the middle of the opening for the three beams with that calculated from the beam theory, it is found that beam BII3C with the maximum opening width is the closest one to the beam theory. In beam BII3A where the opening has the minimum width, the stresses at the upper and lower opening edges are the highest among the three beams. This is due to the stress concentration which has its maximum value at the opening corners, with not much change at the middle of the opening since the opening width is small.

At the working stage, the effect of the Vierendeel action causes the edges of the opening chords to be subjected to a secondary moment; this moment is largest in BII3C since the chords have the maximum span. The maximum compressive stress occurs at the lower left corner of the upper chord in all the beams of this group. Beam BII3C has the maximum compressive stress among the beams of this group. The results are shown in Figs. 5.65b, 5.61b, and 5.66b.

At the ultimate stage, where the beams are subjected to a load of 5 kip (22.25 kN), beam BII3C suffers the highest stresses either at the opening region or at the section above the support. In beam BII3C where the opening edge is close to the support, the stress distribution at the solid section above the support is interrupted in the distance between the opening top and bottom edges.

It can be noticed from Figs. 5.65c, 5.61c, and 5.66c that the maximum compressive stresses in beams BII3A, and BII3B occur at the upper right corner of the lower chord rather than the lower left corner of the upper chord as in BII3C. This is due to the fact that the left edge of the top chord is more cracked in beam BII3C than in the other two beams. This reduces the moment of inertia of that section resulting in higher stresses.

(iv) Group BII4

The horizontal stress distribution for group BII4 is discussed in this section. This group was considered to study the effect of the opening depth on the behaviour of prestressed concrete T-beams. Beam BII4B is the same beam denoted earlier as BII1B and its results were presented in Fig. 5.61. Figures 5.67 and 5.68 show the horizontal stress distributions for beams BII4A and BII4C, respectively. At the transfer stage, Figs. 5.67a, 5.61a, and 5.68a show the stress at the solid section above the support is not much affected by the opening depth. At the opening region, the stresses in general decrease as the opening depth decreases.

At the working stage, the stresses above the support are still not affected by the opening depth. At this stage, the maximum compressive stress occurs at the upper left corner of the opening. Compared to beam BII4A, this stress increased by 14% due to the 1 in. (25.4 mm) increase of the opening depth and by about 36% due to the 2 in (51 mm) increase in the opening depth. At this stage no tensile stresses occurred in beam BII4A

while in beams BII4B and BII4C, small tension developed in the upper left and the lower right corners of the bottom chord, as shown in Figs. 5.67b, 5.61b, and 5.68b.

At the ultimate stage, where a load of 5 kip (22.25 kN) was applied on the three beams of this group, it can be seen from Figs. 5.67c, 5.61c, and 5.68c, that higher stresses developed as the opening depth increased. At this stage, all the beams were cracked above the support and in the top chord. Beam BII4C with an opening depth of 5 in. (127 mm) suffered more cracks than the other two beams. The maximum compressive stress occurred in the lower right corner of the opening in beams BII4A and BII4B and in the upper left corner of the opening for beam BII4C.

Summary of Findings:

The same findings for the effect of different parameters on the horizontal stresses of rectangular beams with openings can be applied to the horizontal stresses in T-beams with openings.

5.3.1.3 I-Beams

Group BIII1 was considered to study the effect of the presence of an opening on the behaviour of prestressed concrete I-beams. Three stages of loading, viz., at transfer stage, at working stage, and at ultimate stage were considered. Figures 5.69, 5.70, and 5.71 show the horizontal stress distribution for beams BIII1A, BIII1B, and BIII1C, respectively. At the transfer stage it can be seen from Figs. 5.69a, 5.70a, and 5.71a that

the horizontal location of the opening has almost no effect on the horizontal stress distribution. The stress distribution at the opening region is rectangular for the top chord and triangular for the bottom chord, with some stress concentrations at the four corners of the opening.

At the working stage, Figs. 5.69b, 5.70b, and 5.71b show that the stress at the solid section, above the support, is not significantly affected by the horizontal location of the opening. At the opening region, the secondary moment plays an important role in changing the shape of the horizontal stress distribution at the edges of the opening. The effect of the secondary moment is almost the same in the three beams of this group since the shear force is the same at the middle of the opening for the three beams. The primary moment is the reason why the three beams have different stress distributions at the opening region.

At the ultimate stage, the three beams have the same shape for the horizontal stress distribution; the observed difference in the values is due to the primary moment caused by the external load. Furthermore, the crack pattern affects the distribution of that stress. In the three beams of this group, the maximum compressive stresses occur at the lower right corner and upper left corner of the opening.

The stress at the solid section above the continuous support is not significantly affected by the change in the horizontal location of the opening. This section was

already cracked in the three beams of this group at this stage of loading.

Summary of Findings:

The presence of an opening in an I-beam results in a rectangular horizontal stress distribution at the top chord of the opening and a triangular horizontal stress distribution at the bottom chord, at the transfer stage. At the working stage, the shear forces at the opening chords cause secondary moments at the edges of these chords. These moments result in cracking of the corners of the opening chords. The effect of the horizontal location of the opening on the horizontal stresses in I-beams is almost the same as that in rectangular and T-beams.

5.3.2 Vertical Strain and Stress Distributions

The vertical stress distribution for beams with openings is discussed in this section. The stresses at the opening edges were plotted at three different stages of loading, namely, transfer stage, working stage, and ultimate stage.

5.3.2.1 Rectangular Beams

(i) Group BI1

Figures 5.72, 5.73, and 5.74 illustrate the vertical stress distributions for beams BI1A, BI1B, and BI1C, respectively, where the horizontal location of the opening (moment-shear ratio) is the varying parameter. It can be seen from these results that at the transfer stage, the stress distribution is almost symmetric about the opening horizontal axis with the maximum vertical splitting stress near the middle of the opening, despite the fact that the prestressing force is eccentric.

Applying a vertical load (working load stage) results in shifting the maximum splitting tensile stress away from the opening centre line toward the upper corner for the right edge of the opening, and toward the lower corner for the left edge of the opening. This is accompanied by some vertical compression stresses developing at this stage.

Increasing the applied load results in cracking of the upper right and the lower left corners of the opening, and creating a field of vertical compressive stress at the other two corners of the opening. In Figs. 5.72c, 5.73c, and 5.74c, the vertical stress distribution

at the vicinity of the opening was plotted discontinuous at certain locations. These locations are where the concrete is cracked and carries almost no tensile stresses. It can be observed from these results that the horizontal location of the opening has almost no effect on the maximum splitting stress at the opening edges for the beams of group BI1.

Figures 5.75, 5.76, and 5.77, present the vertical stress distribution along a horizontal line from the centre of the opening vertical edges, for beams BI1A, BI1B, and BI1C, respectively. It can be seen from these figures that the values of the vertical stress at the centre of the opening edges are almost the same for the transfer stage and the working stage before cracking. This means that the vertical load creates almost no vertical stresses at the middle of the opening edges.

When the vertical load was increased to 4 kip (17.8 kN), the splitting tensile stress at the centre of the opening edges decreased as a result of cracking around the edges. This cracking reduced the tensile capacity of the cracked elements.

Summary of Findings:

The prestressing force creates vertical splitting tensile stresses at the opening edges. The maximum value of these stresses occurs at mid-depth of the opening. The vertical load creates vertical tensile stresses at the upper right and lower left corners of the opening. It also creates vertical compressive stress at the other two corners of the opening. The horizontal location of the opening has a minor effect on these stresses.

(ii) Group BI2

In group BI2, which was considered to investigate the influence of the vertical location of the opening, three different beams with openings were tested, namely; BI2A, BI2B, and BI2C. Figures 5.78, 5.79, and 5.80 show the vertical stress distribution at the opening edges for beams BI2A, BI2B, and BI2C, respectively at the transfer stage, working stage, and the ultimate stage.

At the transfer stage it can be observed from Figs. 5.78a, 5.79a, and 5.80a that the maximum vertical stress occurs at the centre of the opening regardless of its vertical location. Furthermore, the results show that as the opening moves toward the resultant of the prestressing force, (from beam BI2A to beam BI2C), the value of the vertical stress increases significantly. Comparing the values of the vertical stresses for the three beams, it is found that moving the opening from the centre line of the beam by 1 in. (25.4 mm) towards the line of action of the prestressing force increases the vertical splitting stress at the centre of the opening edges by about 20%. This stress decreases by the same ratio when the opening moves down the same distance away from the line of the prestressing force.

Applying the vertical load has the effect of moving the peak of the splitting stress upward at the right edge of the opening and downward at the left edge of the opening, as shown in Figs. 5.78b, 5.79b, and 5.80b. It can be noticed also in the case of beams BI2A and BI2C that the maximum tensile stress occurs at the corner corresponding to the

deeper chord. In beam BI2A, the maximum occurs at the upper right corner since the top chord is deeper than the bottom chord, while in beam BI2C the maximum splitting stress occurs at the lower left corner where the bottom chord is deeper than the top chord. In beam BI2B, where the two chords have the same depth, the difference between the splitting stresses at the upper right corner and at the lower left corner is very small. Comparing the peaks of the splitting stresses at the working stage with those at the transfer stage for the three beams with openings in this group, it can be seen that applying a vertical load of 2 kip (8.9 kN) to these beams almost doubles the splitting stress in case of beam BI2A, and increases that stress by 50% and 35% in the case of beams BI2B and BI2C, respectively.

When the vertically applied load reaches 4 kip (17.8 kN), and the beams had excessively cracked and about to collapse, the upper right and the lower left corners of the opening become heavily cracked while the other two corners of the opening exhibit high vertical compressive stresses. These latter stresses increase as the depth of the chord corresponding to that corner increases, e.g. in beam BI2A, the vertical compressive stresses were 16% higher than in beam BI2B.

Figures 5.81, 5.82, and 5.83 show the vertical stress distributions on a horizontal line passing by the centre of the opening edges for beams BI2A, BI2B, and BI2C, respectively. Comparing the results for $P=0$, and $P=2$ kip (8.9 kN) in the three figures, it can be seen that in beam BI2A, where the opening is away from the line of action of

the prestressing force, the maximum tensile stress at the middle of the opening edge is less when $P=0$ than when $P=2$ kip (8.9 kN). In beam BI2B where the opening is located at the centre of the beam depth, the two results are almost identical. In beam BI2C, where the opening is very close to the line of prestressing force, the maximum vertical stress at the middle of the opening edge when $P=0$ exceeds that when $P=2$ kip (8.9 kN).

Figure 5.84 shows the vertical stress distribution at the opening edge due to the vertically applied load only. It can be seen from this figure that for beam BI2B where the top and bottom chords have the same depth, the splitting stress due to the vertical load is almost zero at the middle of opening depth with equal vertical tensile and compressive stresses above and below the mid-depth of the opening. In the other two beams, it can be seen that the absolute value for the vertical stress is maximum at the deeper chord. It was found that there is a relation between this vertical stress and the secondary moments in the opening chords. This will be explained in Chapter VII, where a method to determine that vertical stress will be given.

At the ultimate stage where the beam is near collapse, the distribution of the vertical stress changes since many elements around the opening are already cracked and have much less capability to carry tensile stresses.

Summary of Findings:

The vertical location of the opening significantly affects the vertical stresses at the opening region. At the transfer stage, as the opening moves toward the horizontal line

of action of the prestressing force, the maximum vertical splitting stress increases. At the working stage, the maximum splitting stress occurs at the opening corner corresponding to the deeper chord. At the ultimate stage, the upper right and the lower left corners of the opening become heavily cracked.

(iii) Group BI3

In Figs. 5.73, 5.85, and 5.86, the vertical stress distributions for beams BI3A, BI3B, and BI3C, respectively, are shown. At transfer stage, it can be noted that the opening width has a minor effect on the maximum value of the splitting tensile stress at the middle of the opening vertical edges.

Applying a vertical load of 2 kip (8.9 kN) on each of the three beams of group BI3 results in moving the maximum tensile stress upward at the right edge of the opening and downward at the left edge of the opening as shown in Figs. 5.73b, 5.85b, 5.86b. The maximum vertical tensile stress at the opening edges increases by about 25%, 35%, and 50% for beams BI3A, BI3B, and BI3C, respectively.

At the ultimate stage, the upper right and the lower left corners of the opening are already cracked leading to discontinuous stress distribution at the opening edges. The other two corners are subjected to vertical compression stresses, which increase with increase in the load as shown in Figs. 5.73c, 5.85c, and 5.86c.

Figures 5.87, 5.88, and 5.89 show the vertical stress distributions for beams BI3A, BI3B, and BI3C, respectively. It can be seen from these results that the stress at mid-depth of the opening edges changes only slightly with increase in the vertical load up to cracking. As was shown earlier, the maximum vertical tensile stress at the opening edges increases with increase in the applied load and the peak of this stress moves toward the upper right and the lower left corners of the opening.

Figures 5.90, 5.91, and 5.92 show the same stress distributions for the three beams of group BI3 at the transfer stage, working stage, and ultimate stage, respectively. It can be noted that the splitting stress at the mid-depth of the opening edges is not affected by the opening width before cracking. After cracking, the distribution takes on an irregular shape depending on the crack propagation pattern.

Summary of Findings:

The splitting stresses at the mid-depth of the opening are not affected by the width of opening, at the transfer stage. At the working stage, increasing the width of opening, increases the secondary moment at the opening edges, hence increasing the vertical splitting stress at the opening corners. After cracking, the vertical stress distribution at the opening edges takes on an irregular shape.

(iv) Group BI4

The vertical stress distributions at the opening edges for the beams of group BI4,

where the opening depth was the varying parameter, are shown in Figs. 5.93, 5.94, and 5.95. Due to the prestressing force, a splitting tensile stress develops at the opening edges with the maximum stress at the mid-depth of the opening. Increasing the opening depth from 3 in. (76 mm) to 4 in. (102 mm) and from 3 in. (76 mm) to 5 in. (127 mm) causes the maximum splitting stress to increase by about 25% and 50% respectively, as shown in Figs. 5.93a, 5.94a, and 5.95a.

At a vertical load of 2 kip (8.9 kN) it was found that the upper right and the lower left corners of the opening in beams BI4B and BI4C were already cracked. Therefore, for a more meaningful representation the results were re-plotted for a load of 1 kip. (4.45 kN) where no cracking had taken place. Figures 5.93b, 5.94b and 5.95b present the vertical stress distribution due to a load of 1 kip (4.45 kN) for beams BI4A, BI4B, and BI4C, respectively. From these results, it can be seen that the maximum splitting tensile stress moves upward at the right edge and downward at the left edge of the opening as a result of applying the vertical load. Applying 1 kip (4.45 kN) as a vertical load has the effect of increasing the maximum splitting tensile stress due to prestressing by about 5% in all the three beams with openings of group BI4.

Increasing the vertical applied load beyond the working stage causes the vertical stress at the opening edges to be compressive at the upper left and the lower right corners of the opening. This vertical compressive stress increases with increase in the opening depth. The other two corners of the opening were already cracked at this stage with the

elements carrying less tensile stress as a result of the tension stiffening criterion.

Figures 5.96, 5.97, and 5.98 show the vertical stress distribution on a horizontal plane passing by the mid-depth of the opening edges for beams BI4A, BI4B, and BI4C, respectively. From these results, it can be seen that the vertical stress at mid-depth of the opening, created due to the prestressing force, almost does not change when the vertical load is applied until cracking occurs. This is due to the fact that the maximum value of this stress moves downward at the left edge of the opening and upward at the right edge of the opening. As the vertical load increases, the concrete elements around the opening edges become cracked and the vertical stress takes an irregular distribution as shown in Figs. 5.96, 5.97, and 5.98.

In Fig. 5.99, the stress concentration at the opening mid-depth due to the prestressing force only is plotted for the three beams with openings in this group. It can be seen from the results that the maximum splitting stress due to the prestressing force increases with increase in the opening depth.

Figures 5.100, and 5.101 show the stress concentration around the opening for the three beams of this group at the working stage and at the ultimate stage, respectively. As previously mentioned the stress distribution at the ultimate stage is an irregular one as shown in Fig. 5.101.

Summary of Findings:

Increasing the depth of opening significantly increases the maximum splitting stress at mid-depth of the opening at the transfer stage. Also, increasing the depth of opening increases the vertical splitting stress at the upper right and the lower left corners of the opening at the working and ultimate load stages.

5.3.2.2 T-Beams

(i) Group BII1

For beams in group BII1 where the effect of the horizontal location of the opening on the behaviour of prestressed concrete T-beams with openings is investigated, the vertical stress distributions at the opening edges are presented in Figs. 5.102, 5.103, and 5.104. It can be seen from the distribution at the transfer stage that the maximum vertical splitting stress occurs at the mid-depth of the opening and that this stress has almost the same value in the three beams with openings of this group.

Figures 5.102b, 5.103b, and 5.104b present the splitting stresses due to applying a vertical load of 2.5 kip (11.1 kN) for beams BII1A, BII1B, and BII1C, respectively. It can be seen from these results that applying a vertical load has the effect of moving the maximum vertical splitting stress upward at the right edge of the opening as in the case of rectangular beams. When the vertically applied load reaches 5 kip (22.25 kN), the beams were already cracked at the upper right and the lower left corners of the opening; therefore the tensile capacities of the concrete elements are reduced at these locations.

The other two corners exhibit vertical compressive stress. The compressive stress increases as the opening moves closer to the continuous support. This may be attributed to that moving the opening closer to the support, i.e toward heavier cracked regions, reduces the stiffness of the sections at the opening edges. Thus, higher stresses take place.

In Figs. 5.105, 5.106, and 5.107 the splitting stresses on a section passing through the mid-depth of the opening edges are plotted for beams BIII A, BIII B, and BIII C, respectively. It can be seen from these results that at the working stage the splitting stress at mid-depth of the opening is slightly less than its value at the transfer stage. It should be noted here that the maximum splitting stress at this stage is below the mid-depth of the left edge and above the mid-depth of the right edge of the opening. When the load is just below the ultimate load (taken 5 kip (22.25 kN)) the concrete elements at the opening mid-depth had already cracked carrying very small tensile stresses.

(ii) Group BII2

Figures 5.103, 5.108, and 5.109 show the vertical stress distributions for beams BII2A, BII2B, BII2C, respectively. At the transfer stage, results in Figs. 5.103a, 5.108a, and 5.109a show that the opening vertical location significantly influences the maximum splitting stress at the opening edges. It can be seen from these results that the maximum tensile vertical stresses occur at mid-depth of the opening regardless of its vertical position. As the opening moves toward the prestressing line of action, the maximum

splitting stress increases significantly. Moving the opening 1.5 in. (38 mm) up towards the prestressing force increases the maximum splitting stress by about 35% and moving the opening up by 3.0 in. (76 mm) increases this stress by about 70%.

At the working load stage, the peak of the splitting stress distribution moves, as usual, to the upper right and the lower left corners of the opening as shown in Figs. 5.103b, 5.108b, and 5.109b. It can be seen from these results that at the right edge of the opening the vertical tensile stress is less at the working stage than at the transfer stage. To understand this, the vertical stresses due to the vertically applied load only (without the prestressing) were plotted in Fig. 5.110 for the three beams in this group. It can be observed from the results that stresses have almost the same negative and positive values for beam BII2A, where the upper chord carries a shear force (and consequently secondary moment) almost equal to that carried by the bottom chord. For beam BII2B, the bottom chord carries more shear and hence greater secondary moment than the top chord. This secondary moment is transmitted to the right edge of the opening by the framing action between the chords and a specific width from the solid part of the beam. The moment at the right edge creates compression at the opening lower right corner and creates tension at the opening upper right corner. In beam BII2C the top chord carries almost no shear, and hence the secondary moment is almost zero at the top of the right edge and maximum at the bottom of the right edge of the opening. This creates a field of vertical compression stress along the depth of the beam. When this compression stress is added to the stresses due to the prestressing force, the tensile stresses are reduced as shown in

Fig. 5.109b. A method to determine this stress will be presented in Chapter VII.

At the ultimate stage, the tensile stresses at the upper right and the lower left corners of the opening cause the concrete elements to crack at these locations except for beam BII2C; in the latter beam the upper right corner of the opening exhibit very small tensile stresses due to the effect of the compression field resulting from applying the vertical load. In the same beam, BII2C, high vertical compressive stresses can be observed in the lower right corner of the opening. See Figs. 5.103c, 5.108c, and 5.109c.

In Figs. 5.111, 5.112, and 5.113, the vertical stress distributions on a horizontal section passing by the mid-depth of the opening is shown for beams BII2A, BII2B, and BII2C, respectively. It can be seen from these results that higher stresses are developed as the opening moves towards the prestressing force.

(iii) Group BII3

The vertical stress distributions for beams BII3A, BII3B, and BII3C are shown in Figs. 5.114, 5.103, and 5.115, respectively. It can be seen from Figs. 5.114c, 5.103c, and 5.115c that at the transfer stage, the opening width (W) has a minor effect on the vertical splitting tensile stress at the opening edges. During the working stage, the opening width begins to have an effect on the value of the splitting stress. This is due to the fact that the splitting stress resulting from the vertical load is related to the secondary moment developed at the edges of the opening chords. This splitting stress

increases with increase in the opening width.

At the ultimate stage, the two corners which were subjected to vertical tensile stress at the working stage are now heavily cracked. The other two corners are subjected to vertical compressive stresses which increase with increase in the opening width. See Figs. 5.114c, 5.103c, and 5.115c.

Figures 5.116, 5.117, and 5.118 show the vertical stress distributions at the opening mid-depth for beams BII3A, BII3B, and BII3C, respectively. It can be seen from these results that at the opening mid-depth, the vertical splitting stress is less at the working stage than at the transfer stage. At the ultimate stage, the concrete elements at mid-depth of the opening edges become heavily cracked carrying very small amount or no vertical tensile stresses. Therefore, the vertical stress distribution at this stage become an irregular one depending on the crack pattern distribution.

(iv) Group BII4

Group BII4 was considered to study the effect of the opening depth (h) on the behaviour of prestressed concrete T-beams with openings. Beam BII4B with opening depth 4 in. (102 mm) was presented before and denoted as beam BII1B. Results of the other two beams of this group namely BII4A and BII4C are discussed in this section.

Figures 5.119, 5.103, and 5.120 show the vertical stress distributions for beams

BII4A, BII4B, and BII4C respectively. It can be seen from Figs. 5.119a, 5.103a, and 5.120a that the opening depth has a significant effect on the vertical splitting tensile stress due to prestressing force. An increase of opening depth by 1 in. (25 mm) and by 2 in. (51 mm) has the effect of increasing the vertical splitting tensile stress by 21% and 44%, respectively.

At the working stage where the beam is subjected to a vertical load of 2.5 kip (11.1 kN) the maximum vertical tensile stress moves downward at the left edge of the opening and upward at the right edge of the opening. The maximum vertical stress at this stage increases by 18% and 38% due to an increase of the opening depth by 1 in. (25 mm) and 2 in. (51 mm) respectively. Refer to Figs. 5.119b, 5.103b, and 5.120b.

At the ultimate stage, the lower left and the upper right corners of the opening are heavily cracked. At the other two corners, high vertical compressive stresses are developed. These compressive stresses increase with opening depth.

The vertical splitting tensile stress on a horizontal section passing by the middle of the opening edges is studied for the three stages of loading. Figures 5.121, 5.122, and 5.123 show the distribution of this stress for beams BII4A, BII4B, and BII4C. It can be seen from these results that at the middle of the opening depth, the maximum tensile stress occurs due to the prestressing force only. At the ultimate stage, the stress takes an irregular shape due to the presence of cracked elements.

Summary of Findings:

The same findings for the effect of different parameters on the vertical stress distribution of rectangular beams with openings can be applied to those for T-beams with openings. It is observed from the results that although the top and bottom chords are different in shape in T-beams, the maximum vertical stress occurs at the middle of the opening at the transfer stage. At the working stage, the maximum vertical tensile stress at the upper right corner of the opening is different from that at the lower left corner of the opening, since the top and bottom chords have different geometries.

5.3.2.3 I-Beams

The vertical stress distributions for beams BIII1A, BIII1B, and BIII1C are shown in Figs. 5.124, 5.125, and 5.126, respectively. At the transfer stage the maximum vertical tensile stress occurs at the mid-depth of the opening and the distribution of the vertical stress is symmetrical about the centre of gravity of the beam since the opening is located at the beam horizontal centre line. As the opening moves towards the point of application of the prestressing force, the splitting stress slightly increases.

Applying a vertical load of 4 kip (17.8 kN) on the three beams of this group has the effect of moving the maximum vertical tensile stress upwards at the right edge of the opening and downwards at the left edge of the opening. This is due to the development of a secondary moment on the opening chords. This moment is transmitted to the solid section at the right and left edges of the opening, creating a vertical tensile stress at the

upper right and lower left corners of the opening, and a vertical compressive stress at the lower right and upper left corners of the opening. This will be explained further in methods of design in Chapter VII where a method for evaluating this stress will be given.

At the ultimate stage where the beam is subjected to a vertical load of 8 kip (35.6 kN), the upper right and lower left corners of the opening become heavily cracked carrying no or very small amount of tensile stress. The crack pattern at this stage affects the value of the vertical compressive stress at the other two corners of the opening.

Figures 5.127, 5.128, and 5.129 show the vertical tensile stress at the mid-depth of the opening for beams BIII1A, BIII1B, and BIII1C, respectively. It can be observed from these results that the vertical load has absolutely no effect on the vertical stress at the opening mid-depth; this means that due to the vertical load only, the vertical stress is tensile above the mid-depth and compressive below the mid-depth at the right edge of the opening. The reverse occurs at the left edge of the opening.

At the ultimate stage, the cracking of the opening edges causes this stress to have irregular shape as shown in Figs. 5.127, 5.128, and 5.129.

Summary of Findings:

Results indicate similarities between rectangular and I-beams as far as the vertical stress distribution and the effect of the different parameters studied.

5.3.3 Shear Stress Distribution

In this section the shear stress distribution in the vicinity of the opening and its effect on developing cracks around the opening are discussed. Using the finite element results, the shear stresses at the opening edges were plotted at the transfer stage, working stage, and ultimate stage for all the tested beams. The effect of increasing the vertical load on the ratio of the shear force carried by each of the opening chords is also discussed. The calculated shear forces were compared to the experimental results using strain gauges.

5.3.3.1 Rectangular Beams

(i) Group BI1

Figures 5.130, 5.131, and 5.132 show the shear stress distributions at the opening edges for beams BI1A, BI1B, and BI1C. It can be observed from these results that at transfer stage, the maximum shear stress occurs at the opening corners with different signs.

Applying the vertical load causes a vertical tensile stress which causes cracking at the upper right and the lower left corners of the opening. This causes the shear stresses carried by the concrete elements at these two corners to decrease. As a result, the other two corners, which are subjected to vertical compressive stresses, will carry more shear stresses, as shown in Figs. 5.130c, 5.131c, and 5.132c.

It may be seen from these results that the horizontal location of the opening does not influence the value of the shear stress around the opening at the transfer or working stages of loading. Prior to the beam's collapse, i.e. close to the ultimate stage, the maximum shear stress at the left edge of the opening increases and the maximum shear stress at the right edge of the opening decreases as the opening moves toward the load, i.e. when ratio M/VH decreases.

The shear stress distribution at the middle of the top and bottom chords is zero at the transfer stage since there is no vertical load. At the working stage, the top and bottom chords have almost the same shear stresses.

With a vertical load of 4 kip (17.8 kN), incurring considerable cracks, the bottom chord in compression carries more shear force than the top chord which is in tension. It can be observed also that the difference between the shear force in the top and bottom chords is very small in case of beam BIIC since the top chord had not cracked yet at this load level.

Figure 5.133 shows the percent shear force taken by each chord for beams BI1A, BI1B, and BI1C. It can be seen that the top chord carries 50% of the total shear force until the chord starts to crack. After cracking, the chord in compression carries more shear force than the tension chord. It can be observed also from the same figure that for beam BI1C, the top and bottom chords carry the same shear until the vertical load had

reached 4 kip (17.8 kN). This is because the opening is away from the maximum bending zone which postpones the cracking of the top chord.

Summary of Findings:

The prestressing force creates shear stresses at the opening corners, while the vertical load creates shear stresses at the opening chords as well as at the opening edges. The horizontal location of the opening has almost no effect on these stresses before cracking. After cracking, the tension chord loses some of its shear carrying capacity, hence the compression chord carries more shear. The horizontal location of the opening affects the level of cracking of the tension chord and therefore affects its shear carrying capacity.

(ii) Group BI2

The vertical location of the opening is one of the main factors affecting the shear stresses in the opening region. The dimensions of the top and bottom chords control the distribution of the shear force between the two chords. Group BI2 was considered to study this effect. In Figs. 5.134, 5.135, and 5.136 the shear stress distributions at the edges of the opening as well as at the middle of the opening are plotted for beams BI2A, BI2B, and BI2C. At the transfer stage, where the beam is subjected to the prestressing force only, the maximum shear stresses occur at opening corners. As the opening moves vertically toward the line of action of the prestressing force, the shear stress increases. This can be observed from Figs. 5.134a, 5.135a, and 5.136a. It can be noted here that

as the opening moves closer to the line of action of the prestressing force, the shear stress as well as the vertical tensile stress at the opening corners increase. In other words, beam BI2C in this group is the most critical beam for corner cracking at the transfer stage. In the middle of the opening chords, the shear stress due to the prestressing force is almost zero.

Applying a vertical load of 2 kip (8.9 kN) has the effect of changing the shear stress distribution at the opening edges. It also creates a shear stress in the middle of the chords as a result of the distribution of the total applied load as shears in the two chords.

At the stage where the applied load is 2 kip (8.9 kN), the maximum shear stress occurs at the upper left and the lower right corners of the opening. The corner attached to the deeper chord exhibits higher shear stresses as in the case of the upper left corner of the opening in BI2A and the lower left corner of BI2C. In beam BI2B, the two corners are subjected to the same shear. It can be observed also that the shear stress distribution at the middle of the chords is a parabolic distribution as predicted by simple beam theory.

As the load increases, the upper chord begins to crack which results in transferring some of the shear force from the top chord to the bottom chord. This can be observed in Fig. 5.135c, where the two chords have the same depth but the stresses in the bottom chord exceed those in the top chord.

In beam BI2A when the load reaches 4 kip (17.8 kN), the shear stresses in the top chord (in tension) are greater than the ones in the bottom chord, since the top chord is not cracked because of its large depth. As the upper right and the lower left corners of the opening become cracked, their concrete elements carry only a small amount of shear.

In Fig. 5.137, the percentage shear force carried by each chord is plotted for beams BI2A, BI2B, and BI2C. At the beginning, each of the top and bottom chords of beam BI2B carries about 50% of the load since they have almost the same cross-section. The top chord has a little more reinforcing steel than the bottom chord; therefore this would slightly increase the shear force taken by the former chord.

At a load of just above 2 kip (8.9 kN), the proportion of shear carried by top chord increased until a load of about 2.75 kip (12.24 kN) was reached. Such an increase may be attributed to the fact that in the finite element analysis the lower left corner of the opening attached to the bottom chord cracks before the upper right corner attached to the top chord. This time lag in cracking for the two corners was not observed during the tests.

For the load exceeding 2.75 kip (12.24 kN), the top chord exhibits some vertical bending cracks which decrease the shear force carried by that chord. At a load of 3.5 kip (15.58 kN) where the number of cracks as well as their width increase, the part of shear carried by the top chord decreases significantly. The same description can be applied for

beams BI2A and BI2C except that the preliminary shear force carried by the top and bottom chords was 20% and 80%, respectively, for BI2A and 80% and 20% for BI2C. The limits for the decrease and the increase in the ratio of the shear taken by each chord is also different from one beam to another.

Summary of Findings:

The vertical location of the opening is the main factor controlling the shear force carried by each chord of the opening. As the depth of an opening chord increases, the shear force carried by that chord increases. At the transfer stage, as the opening moves toward the line of action of the prestressing force, the shear stresses at the opening corner increase.

(iii) Group BI3

Group BI3 was considered to study the effect of the opening width, W , on the behaviour of prestressed concrete beams with openings. Figures 5.131, 5.138, and 5.139 show the shear stress distribution for beams BI3A, BI3B, and BI3C, respectively. From Figs. 5.131a, 5.138a, and 5.139a, it can be seen that the shear stresses at the opening corners due to prestressing only, decrease slightly with increase in the opening width. These shear stresses vanish at the opening centre. When applying a vertical load of 2 kip (8.9 kN) shear stresses are created at the upper and lower chords of the opening. Before cracking, the shear stresses in the upper chord are almost the same as those in the lower chord, since they both have almost the same area and moment of inertia. At this stage,

the maximum shear stresses at the opening corners increase with increase in the opening width.

Increasing the load above the cracking load leads to increasing the part of the shear force carried by the compression chord and decreasing the part carried by the tension chord. Also as the upper right and the lower left corners of the opening crack, the other two corners carry higher shear stresses. These shear stresses increase with increase in the opening width. It should be noted that in Fig. 5.139c, the stresses shown are due to a vertical load of 3 kip (13.35 kN), and not 4 kip (17.8 kN) as for the two other beams, because the beam failed at a load below 4 kip (17.8 kN).

Figure 5.140 shows the percentage shear force carried by each chord as the applied load increases. As before, when the top and bottom chords have almost the same dimensions, each of them carries 50% of the total shear until cracking. At that time the top (tension) chord carries less shear and the bottom (compression) chord carries more shear.

Summary of Findings:

The width of opening affects the shear stresses at the opening region only at the ultimate stage of loading. As the opening width increases, more cracks develop and hence higher shear stresses are created.

(iv) Group BI4

In group BI4, the effect of the opening depth, h , on the behaviour of the prestressed beams with openings is studied. Figures 5.141, 5.142, and 5.143 show the shear stress distribution for beams BI4A, BI4B, and BI4C, respectively, with opening depths of 3 in. (76 mm), 4 in. (102 mm), and 5 in. (127 mm), respectively. Due to the prestressing force only, no shear stress exists at the middle of the opening. At the edges, high shear stresses develop at the opening corners with the upper right and the lower left corners having the same shear sign and the other two corners having the opposite sign. This shear stress increases with increase in the opening depth as noted in Figs. 5.141a, 5.142a, and 5.143a. This increase was about 20% at the upper corners of the opening close to the resultant prestressing force for each 1 in. (25 mm) increase in the opening depth, while this increase was only about 8% at the lower corners of the opening, the corners away from the resultant prestressing force.

Applying a vertical load of 1 kip (4.45 kN) results in increasing the maximum shear stress at the opening edges. As the opening depth increases, the maximum value of the shear stress at the opening edges also increases. Observing the shear stress at the middle of the opening chords, it can be seen that the maximum shear stress increases as the opening depth increases in the same ratio as the decrease in the area of the opening chords. This means that the shear force in the top chord, for instance, is the same in all the three beams.

As the vertical load reaches a value just below the collapse load, the shear stress at the opening edges increases significantly, especially with increase in the opening depth. The shear stress in the top chord becomes smaller than that in the bottom chord since more elements become cracked in the former chord.

In Fig. 5.144, the ratio of the shear force carried by each chord is shown. It can be seen from these results that, as the opening depth increases, the top chord begins to lose some of its capacity to carry shear at a lower load.

Summary of Findings:

The shear stresses at the opening corners due to the prestressing force increase with increase in the opening depth. Also, increasing the opening depth reduces the areas and moments of inertia of the opening chords resulting in higher shear stresses in these chords.

5.3.3.2 T-Beams

(i) Group BIII

Group BIII was considered to study the effect of the horizontal location of the opening on the behaviour of the prestressed concrete T-beams with openings. The shear stress distribution is plotted for the three beams with openings of this group in Figs. 5.145, 5.146, and 5.147. The shear stress in the flange of the T-section was neglected in plotting these figures. At the transfer stage, the shear stress distribution at the opening

edges is similar to that for beams with rectangular sections. The value of this shear is almost the same in beams BIII A, BIII B, and BIII C. No shear stress is present at the middle of opening due to prestressing.

Applying a vertical load has the effect of developing shear stresses at the middle of the opening chords. The ratio of the shear force taken by each chord will be discussed later in Chapter VII. As can be seen from Figs. 5.146b, 5.147b, and 5.148b, the horizontal location of the opening has almost no effect on the ratio of the shear force carried by each chord. At this stage the maximum shear stresses occur at the upper left and the lower right corners of the opening and these stresses increase slightly as the moment-shear ratio decreases.

As the vertical load increases further, the shear stresses at the middle of the chords and at the opening edges increase. When this load is beyond the cracking load and the upper right and the lower left corners of the opening are cracked, the shear capacity of the concrete elements at these two locations remarkably decreases. This increases the shear stress at the other two corners of the opening. Such an increase becomes larger as the opening moves away from the load, toward the high moment region. Refer to Figs. 5.145c, 5.146c, and 5.147c. At a load of 5 kip (22.25 kN), the shear stress at the middle of the top chord was reduced only in beam BIII A where the opening was very close to the support.

In Fig. 5.148, the shear force carried by each chord in the three beams with opening of group BII1 is illustrated. In all the three beams, the top chord begins to carry about 53% of the total shear force while the bottom chord carries about 47% of the shear. These ratios are maintained until cracking occurs in the beams. Beam BII1A, which suffered maximum cracking in the tensile chord, failed with the tension chord carrying only about 27% of the total shear; this means that this chord lost about half its shear carrying capacity to the bottom chord. As the opening moves away from the highly cracked region, the ratio of the shear force transferred from the tension chord to the compression chord decreases.

(ii) Group BII2

In group BII2, the effect of the vertical location of the opening on the behaviour of prestressed concrete T-beams with openings is investigated. Figures 5.146, 5.149, and 5.150 show the shear stress distribution at the opening region for beams BII2A, BII2B, and BII2C, respectively. It can be seen from Figs. 5.146a, 5.149a, and 5.150a that at transfer stage, the shear stresses at the opening corners increase with decrease in C , i.e. the distance between the beam top fibre and the mid-depth of the opening.

Applying a vertical load of 2.5 kip (11.1 kN), creates shear stresses in the chords of the opening according to their geometric characteristics, i.e. their areas and moments of inertia. This will be discussed later in Chapter VII under design methods. The maximum shear stress at the opening edges increases at this stage compared to the stress

at the transfer stage.

At the ultimate stage, where a load of 5 kip (22.25 kN) is applied, the cracking of the upper right and the lower left corners of the opening causes the shear stress carried by the concrete elements at these locations to decrease. The shear force carried by the top chords of the beams in group BII2 decreases with increase in the vertical load as shown in Fig. 5.151. This is because the cracks in these top chords propagate faster than in the bottom chords. In Fig. 5.150c although the shear force is very small in the top chord at the ultimate stage, the resulting shear stress is still higher than that at the working stage. This is because the cracking of the top chord leaves only a very small concrete area to carry this shear.

(iii) Group BII3

The shear stress distribution in the opening region for beams BII3A, BII3B, and BII3C where the opening width is the varying parameter is shown in Figs. 5.152, 5.146, and 5.153, respectively. It can be seen from these results that at the transfer stage, the shear stress at the opening corners decreases slightly as the opening width increases as shown in the above figures.

At the working stage the shear stress distribution at the middle of the opening is almost the same in the three beams of this group; this means that the opening width has no effect on the shear force in the opening chords. Due to the vertical load, the shear

stress at the opening corners increases as the opening width increases, as shown in Figs. 5.152b, 5.146b, and 5.153b for beams BII3A, BII3B, and BII3C, respectively.

At the ultimate stage, the shear stress at the middle of the upper chord decreases with increase in the opening width. This is due to the fact that this chord suffers extensive cracking with increase in the opening width. This is also supported by Fig. 5.154 where the top chord in beam BII3C begins to lose some of its shear capacity earlier than the other two beams of this group. Also at failure that chord carries the least shear force among the upper chords of beams of group BII3. From Figs. 5.152c, 5.146c, and 5.153c, it can be seen that the shear stress at the opening corners increases further at this stage of loading with increase in the opening width.

(iv) Group BII4

Group BII4 was considered to study the effect of the opening depth, h , on the behaviour of prestressed concrete T-beams with openings. Figures 5.155, 5.146, and 5.156 show the shear stress distribution for beams BII4A, BII4B, and BII4C, respectively. At the transfer stage, the shear stresses at the opening corners slightly increase with increase in the opening depth as can be seen from Figs. 5.155a, 5.146a, and 5.156a. No shear stresses develop in the opening chords at this stage.

At the working stage, the stresses at the opening edges increase by about 11% and 22%, respectively, due to increase in the opening depth by 1 in. (25 mm) and 2 in. (51

mm), respectively. At the middle of the opening chords, the shear stress increases with increase in the opening depth as the depth of the chord decreases. This is shown in Figs. 5.155b, 5.146b, and 5.156b.

At the ultimate stage, the lower left and the upper right corners of the opening are heavily cracked and therefore carry almost no shear stresses. The other two corners carry shear stress which increases with increase in the opening depth. At the middle of the opening, the shear stress increases also with increase in the opening depth. Figure 5.157 shows the shear force carried by each chord as the vertical load is increased. From the results, it can be seen that the amount of the shear force carried by the tensile top chord decreases with increase in the applied load after cracking. The cracking stage started first in beam BII4C followed by beams BII4B and BII4A.

Summary of Findings:

The effect of different parameters on the shear stress distribution at the opening region in T-beams is similar to that in rectangular beams. The ratio of the shear force carried by each chord is different in T-beams from that in rectangular beams as will be discussed later in Chapter VII.

5.3.3.3 I-Beams

Group BIII1 was considered to study the behaviour of prestressed concrete I-beams with openings. Figures 5.158, 5.159, 5.160 show the shear stress distribution for beams

BIII1A, BIII1B, and BIII1C, respectively, at the three stages of loading, namely, at the transfer, at the working stage, and at the ultimate stage.

At the transfer stage, the shear stress is concentrated at the corners of the opening as shown in Figs. 5.158a, 5.159a, and 5.160a. The distributions are similar to those for beams with rectangular and T-sections. The opening chords carry almost no shear stresses due to prestressing. Furthermore, the horizontal location of the opening has minor effect on the shear stresses at the opening corners.

Applying a vertical load of 4 kip (17.8 kN) has the effect of creating shear stresses in the opening chords and increasing the shear stresses at the opening edges. This load gives rise to negative shear stress at all the opening corners as shown in Figs. 5.158b, 5.159b, and 5.160b.

At the ultimate stage, the upper right and the lower left corners of the opening were already cracked and therefore carry a small amount of shear stress; this leads to a significant increase in the stress at the other two corners. The value of the shear stress at the opening edges depends, to a great extent, on the crack pattern of the opening region. At a load of 8 kip (35.6 kN), the difference between the shear force carried by the top and bottom chords of the opening was small compared to the rectangular and T-beams. This can also be observed from Fig. 5.161 where the difference between the shear force carried by each chord is not significant. This is due to the fact that most of the

cracks in the top chord occurred in the flange which carried a negligible shear force before cracking.

Summary of Findings:

Results show similarities between the shear stress distribution in rectangular and I-beams with openings. The presence of the flange in the top chord of the opening reduces the loss in the shear carrying capacity of that chord after cracking. This results in small difference between the shear forces carried by the top and bottom chords of the opening if these chords have the same dimensions.

5.4 Cracking and Mechanism of Failure

The aims of this section are to discuss the experimental crack pattern of all the tested beams; to compare these patterns with the theoretical ones from the finite element analysis; and, to discuss the failure mechanism of the beams based on the experimental observations and the theoretical expectations. It should be noted that the loads written on the tested beams in the photos are the total loads which have to be divided by 2 to be analogous to the cantilever load used in the theoretical analysis.

5.4.1 Rectangular Beams

(i) Group BI1

Figure 5.162 shows the experimental crack pattern for beam BI1A of group BI1. It can be observed from this figure that cracks first appeared at the upper left and the lower right corners of the right opening and at the upper right and the lower left corners of the left opening. Just after the appearance of these cracks, another crack started at the bottom fibre of the high moment end of the bottom tension chord. These main cracks propagated until the bottom fibres at the mid-span, exactly under the load, started to crack. These cracks continued to propagate until the failure occurred.

The failure of beam BI1A occurred at an experimental load of 10.5 kip (46.8 kN) resulting from the collapse of the compression chord (strut failure) as a result of high principal stresses. These principal stresses were formed due to high compressive load and shear stresses in that chord. The failure can be observed in Fig. 5.163. This failure was

accompanied by an exploding sound and buckling of the mild steel at the top chord.

In Fig. 5.164, the crack pattern of beam BI1B is illustrated. The cracks in this case developed first at the same corners as in beam BI1A at an experimental load of 6 kip (26.7 kN). At almost the same load, two other locations started to crack. One was at the bottom fibres of the tension chord close to the high moment end, and the other one at mid-span under the applied load. These cracks continued to propagate up to a load of 8 kip (35.6 kN) when another crack at the middle of the bottom tension chord was observed. All these cracks stopped to propagate at a load of 9 kip (40 kN) except the one at mid-span which continued to propagate until failure occurred at about a load of 11 kip (49 kN).

The failure of this beam was due to crushing of the concrete at the top fibres just below the applied load, after the crack at mid-span had propagated for about 8 in. (203 mm) as shown in Fig. 5.165.

Figures 5.166, 5.167, and 5.168 show the theoretical crack patterns for beams BI1A, BI1B, and BI1C. It is observed that in the solid part between the support and the opening of beam BI1A, the crack depth was not as deep as in the other two beams. This is because the opening region was subjected to high principal stresses which lead to strut failure in the compression chord of the opening. On the other hand in beams BI1B and BI1C, these cracks extended and the failure occurred in the solid section and not in the

opening region.

It can be noticed also from Fig. 5.166, that the top tension chord was heavily cracked which reduced the shear capacity of this chord. This increased the shear force carried by the bottom chord. This shear force along with the high compression force in the bottom chord caused its collapse. The upper right and the lower left corners of the opening were cracked in all the three beams as a result of the vertical tensile stresses at these locations.

(ii) Group BI2

Figure 5.169 shows the crack pattern and the mechanism of failure for beam BI2A of group BI2 which was considered to study the effect of the vertical location of the opening on the behaviour of prestressed beams. In this beam, cracks started early at the upper left and the lower right corners of the opening at a load of 3 kip (13.35 kN) as shown in Fig. 5.169.

These cracks continued to propagate up to a load of 5 kip (22.25 kN), when another crack at the lower right corner of the bottom chord was observed, as shown in Fig. 5.169b. This crack was due to the secondary moment at the opening edges. At a load of 7 kip (31.15 kN), the bottom fibres under the applied load was observed to have a crack of about 4 in. (102 mm).

At a total load of 8.5 kip (37.8 kN), the compression chord failed. The failure, which was accompanied by an exploding sound, was due to the high principal stresses resulted from the compressive and shear stresses in that chord. The buckling of the mild steel at the failed corner was also observed.

In beam BI2B where the top and bottom chords had the same depth, and the experimental prestressing was a little higher than in beams BI2A and BI2C, the cracks started at the upper left and the lower right corners of the right opening at a load of 4.5 kip (20 kN) as shown in Fig. 5.170. These cracks continued to propagate up to a load of 8 kip (35.6 kN). At a load of 5.5 kip (24.5 kN), two other cracks started at the bottom fibres under the applied load and at the bottom fibres of the bottom chord.

Figure 5.171a shows a crack at the upper left corner of the top chord. This crack developed at a load of 10 kip (44.5 kN) and was due to the tensile stresses resulted from the secondary moment at this location.

Trying to increase the vertical load above 10.5 kip (44.5 kN) caused the beam to collapse. The collapse mode was the same as in beam BI2A due to high compressive and shear stresses in the top chord. Removing the load caused the beam to have the deflected shape shown in Fig. 5.171. This was due to the fact that the bottom chord could not resist all the prestressing force since the top chord had already failed. This was not observed in beam BI2A since the bottom chord had greater depth.

Figure 5.172 shows the crack pattern for beam BI2C where the bottom tension chord had smaller depth than the top chord. It can be observed that the three usual cracks, namely; at the opening critical corners, at the bottom fibres of the bottom chord, and at the centre of the beam under the applied load, started at the same load of 5 kip (22.25 kN). The first two cracks continued to propagate up to a load of 6 kip (26.7 kN) while the third one stopped at a load of 7.5 kip (23.4 kN). At a load of 7 kip (31.2 kN), the bottom chord had a crack along its full depth. This crack was observed only in this beam since the depth of the bottom chord could not resist the tensile force. At the same load of 7 kip (31.2 kN), a bending crack was observed at the upper right corner of the bottom chord. This crack is due to the secondary moment resulting from the Vierendeel action.

At a load of 8.5 kip (37.8 kN), the crack width at the section under the load significantly increased. Also the top fibres crushed, and the beam was not able to carry any more load, as shown in Fig. 5.173.

Figures 5.174, 5.175, and 5.176 show the theoretical crack patterns for beams BI2A, BI2B, and BI2C, respectively. It can be observed from these figures that the critical sections for cracking are as follows: the solid section above the support, the top fibres of the tension chord, and the lower left and the upper right corners of the opening. The intensity of the cracks at these sections was different from one beam to another. It can be seen from these figures also that, in beam BI2C where the tension chord had the

smallest depth, the crack at the left edge of the top chord propagated to about 80% of its depth, while in beam BI2B, this ratio was about 70%. In beam BI2A where the tension chord had the greatest depth, the crack propagated to about 55% only of its depth. The cracks at the opening corners propagated in beam BI2B more than in the other two beams.

(iii) Group BI3

Group BI3 was considered to study the effect of the opening width, W , on the behaviour of the prestressed beams with openings. The crack patterns and mechanisms of failure of beams BI3A and BI3B were described earlier in beams BI1B and BI2B, respectively.

Figure 5.177a shows that the cracks started in beam BI3C at the upper right and the lower left corners of the opening at a load of 3.5 kip (15.6 kN). At a load of 4.5 kip (20 kN), the lower right corner of the bottom chord had a 2 in. (51 mm) crack. At a load of 6 kip (26.7 kN) another crack was observed at the upper right corner of the top chord as shown in Fig. 5.177b. This crack supports the Vierendeel action theory where a secondary moment exists at the edges of the top chord and bottom chords. Before a load of 7 kip (31.2 kN) was reached, an exploding sound was heard and the top chord (in compression) collapsed with crushing of the concrete as shown in Fig. 5.178.

Figure 5.179 shows the theoretical crack pattern for beam BI3C. It can be seen

from this figure that the compression chord had the same crack in its bottom fibres which was observed in the test. This verifies the Vierendeel action behaviour since this crack was resulted from the secondary moment. The previous discussion showed that not only the tension chord is subjected to cracking but also the compression chord may crack when the opening is wide. This shows the importance of the secondary reinforcement placed in the compression fibres.

(iii) Group BI4

Figures 5.180, 5.181, and 5.182 show the theoretical crack pattern for beams BI4A, BI4B, and BI4C. In the three beams, the cracks started at the lower left and the upper right corners of the opening and at the upper left corner of the top chord. These cracks propagated with increase in the load. The solid section above the support was the third location to crack followed by the lower right corner of the bottom chord. The crushed elements due to compressive stresses are also shown in these figures. These crushed elements are present at the upper right corner of the bottom chord and at the lower left corner of the top chord. In Fig. 5.180 for beam BI4A, another location for compression failure is shown at the solid section just above the support.

The ultimate theoretical loads for the three beams of group BI4 were 5.35 kip (23.8 kN), 4.9 kip (21.8 kN), and 3.68 kip (16.4 kN), respectively. This means that increasing the opening depth from 3 in. (76 mm) to 4 in. (102 mm), reduces the maximum load by about 8% while increasing the opening depth from 3 in (76 mm) to 5

in. (127 mm), decreases the maximum load by 31%. The splitting tensile stresses at the opening edges cause the two edges of the opening to be cracked at the maximum load. Figures 5.170 and 5.171 show the experimental crack pattern and mechanism of failure for beam BI4A which is the same beam denoted earlier as BI2B.

Summary of Findings:

The critical locations for cracking of prestressed beams with openings are as follows: at the upper right and the lower left corners of the opening due to the framing action between the opening chords and the adjacent solid parts close to the opening edges, as will be discussed later in Chapter VII; at the locations where the secondary moments cause tensile stresses; at the tension chord due to axial tensile force; and at the continuous support due to the primary moment.

The failure of rectangular prestressed beams with openings may occur due to: strut failure in the compression chord; shear failure in the opening chords; tension failure through the developing of wide cracks in the tension chord; and high stresses in the beam over the continuous support.

The horizontal location of the opening does not have a significant effect on the cracking of the opening region as long as the opening is far enough from the continuous support. If the opening is close to the continuous support, strut failure is most likely to occur.

The vertical location of the opening greatly affects the crack pattern and the modes of failure of beams with openings. If the compression chord is shallow, strut failure may be expected, while if the tension chord is shallow, tension failure in that chord may occur.

The width of opening controls the crack pattern at the opening region, especially the cracks resulting from the secondary moment. Wide openings may fail by strut failure or through the formation of a mechanism at the opening corners.

The depth of opening is the most important parameter affecting the crack pattern and the ultimate load capacity of beams with openings. Increasing the depth of opening significantly reduces the cracking load and the ultimate load capacities.

5.4.2 T-Beams

(i) Group BII1

In group BII1, the effect of the horizontal location of the opening on the behaviour of the prestressed concrete T-beams with openings is investigated. The three beams with openings of this group were tested experimentally and verified using the finite element method.

Figure 5.183 shows the experimental crack pattern for beam BII1A. At a load of 5 kip (22.25 kN), the upper right and the lower left corners of the left opening started to

crack. These cracks propagated up to a load of 8 kip (35.6 kN) when another crack was observed at the lower right corner of the left opening. All these web cracks continued to propagate as shown in Fig. 5.183b up to a load of 12 kip (53.4 kN). At a load of 14 kip (62.3 kN) the flange exhibited transverse cracks in the solid part between the openings and the point of load application as shown in Fig. 5.183c.

Trying to increase the load above 14 kip (62.3 kN) caused the beam to collapse with diagonal crack passing by the top and bottom chords of the opening as shown in Fig. 5.184a. In Fig. 5.184b the concrete cover was split as a result of the increase in the vertical load, and a plastic joint was developed in the bottom fibres of the lower chord causing the opening to have a significant deflection.

In beam BIII B, the opening was moved 6 in. (152 mm) away from the vertical load compared to beam BIII A. The same two corners of the opening as in BIII A, started to crack at a load of 6 kip (26.7 kN) delaying 1 kip (4.45 kN) after BIII A which started to crack at a load of 5 kip (22.25 kN). These cracks were followed by cracking of the bottom fibres of the high moment ends of the bottom chords as shown in Fig. 5.185a. These cracks continued to propagate until the section under the load had a 7.5 in. (191 mm) crack as shown in Fig. 5.185b.

At a load of 13 kip (57.9 kN), a wide crack, propagating in the direction between the load and the support was observed in the two openings. This crack is shown Figs.

5.185c and 5.186a. Increasing the load above 13 kip (57.9 kN) caused the beam to have the mechanism of failure shown in Fig. 5.186b where four plastic hinges can be seen in the four corners of the opening. Removing the vertical load caused the beam to buckle under the effect of the prestressing force since the opening sections were already collapsed and unable to resist this force. This buckling failure mode is shown in Figs. 5.186c and 5.186d.

Beam BIII C where the opening was moved another 6 in. (152 mm) away from the vertical load compared to beam BIII B, exhibited the same cracking as beam BIII B as shown in Figs. 5.187a and 5.187b. The cracks at the opening corners continued to propagate up to a load of 12 kip (53.4 kN). Trying to increase the load above 12 kip (53.4 kN) caused the beam to have a major diagonal crack passing by both chords of the opening as shown in Fig. 5.188a. Increasing the load further caused the concrete to completely split between the bottom chord and the support as shown in Fig. 5.188b. Removing the load at this stage did not lead to buckling as in the case of beam BIII B. Figure 5.188c shows the beam after removing the load.

Figures 5.189, 5.190, and 5.191 show the theoretical crack pattern for beams BIII A, BIII B, and BIII C, respectively. The agreement between the theoretical and experimental crack patterns is quite good. In beam BIII A, the top fibres of the flange were cracked in the region between the left edge of the opening and the support. Another crack in the lower right corner of the bottom chord was observed in the three beams,

especially in beam BII1A. This crack is due to the tensile stresses resulting from the secondary moment. At the upper right corner of the bottom chord a compression failure was observed in few concrete elements. This failure resulted also from the secondary moments at the edges of the chords.

Beam BII1A exhibited the greatest number of cracked elements in the top chord among the three beams of this group. This is attributed to the closeness of the opening to the maximum moment section.

(ii) Group BII2

Group BII2 was considered to study the effect of the vertical location of the opening on the behaviour of prestressed concrete T-beams. Beam BII2A is the same beam denoted earlier as BII1B. Beam BII2B was tested experimentally while beam BII2C was analyzed theoretically.

Figure 5.192 shows the crack pattern for beam BII2B. The cracks first appeared at the upper left corner of the right opening at a load of 6 kip (26.7 kN). At a load of 8 kip (35.6 kN), two cracks were observed, one at the lower right corner of the right opening and the other at the lower left corner of the bottom chord of the same opening. These cracks continued to propagate up to a load of 12 kip (53.4 kN) when a long crack was observed at the middle of the beam just below the load. When the vertical load reached 14 kip (62.3 kN), the bottom chord had a vertical crack through its full depth as

shown in Fig. 5.192b.

Trying to increase the load above 15 kip (66.75 kN) caused a wide diagonal crack at the top chord as shown in Fig. 5.192c. The width of this crack increased with increase in the load leading to the failure of the beam. At a load of 17 kip (75.65 kN), this diagonal crack penetrated the bottom chord as shown in Fig. 5.193. After the collapse of the opening chords, two plastic hinges developed at the upper and the lower left corners of the opening as shown in the same figure.

Figure 5.194 shows the theoretical crack pattern for beam BII2B. The agreement between the experimental and the theoretical crack patterns can be observed. In Fig. 5.195, the theoretical crack pattern for beam BII2C is shown. It can be seen from this figure that the top chord was fully cracked at failure. The bottom chord had a small vertical crack due to the secondary moment. The upper right and the lower left corners of the opening were also cracked. At the support, a deep crack can be observed.

(iii) Group BII3

Group BII3 was considered to study the effect of the opening width on the behaviour of prestressed concrete T-beams with openings. The experimental and theoretical results of beam BII3B were discussed earlier in beam BII1B. Beams BII3A and BII3C were analyzed theoretically only. The crack patterns for these two beams are presented in Fig. 5.196 and 5.197. Comparing the crack pattern for the three beams of

this group shown in Fig. 5.196, 5.196, and 5.197, respectively, it can be seen that the opening width has a great effect on the cracking of the opening region. In beam BII3C, the crack at the lower right corner of the opening penetrated the flange for a long distance. This is due to the high secondary moment at this location.

(iv) Group BII4

Group BII4 was used to study the effect of the opening depth on the behaviour of prestressed beams. The theoretical and experimental results of beam BII4B were discussed earlier in beam BII1B. Beam BII4A with opening depth of 3 in. (76 mm) was analyzed theoretically only.

Figure 5.198 shows the crack propagation pattern for beam BII4C with opening depth of 5 in. (127 mm). The cracks started at the upper right and the lower left corners of the left opening and at the upper left and the lower right corners of the right opening at a load of 5 kip (22.25 kN). The two cracks close to the middle of the beam continued to propagate until they hit the beam flange. At a load of 8 kip (36 kN) another crack was observed at the bottom fibres of the lower chord. This crack is due to the secondary moment at the bottom chord. Figure 5.198b shows a shear crack in the top chord developed at a load of 11 kip (49 kN). At a load of 12 kip (53 kN), the upper fibres of the top chord had a crack which is also due to the secondary moment as shown in Fig. 5.198c and 5.198d.

The shear crack in the top chord was the sign for the failure of the beam. The width of this crack was increasing with increase in the vertical load as shown in Fig. 5.199a. In Fig. 5.199b, the mechanism of failure is shown for beam BII4C where the shear crack penetrated both the top and bottom chords of the opening. This crack was also trying to separate the flange from the web.

Figures 5.200 and 5.201 show the theoretical crack patterns for beams BII4A and BII4C. The cracks started at the upper right and the lower left corners of the opening followed by cracking of the top tension chord. The depth of the crack at the solid section above the support was greater in beam BII4A than in beam BII4C since the former beam failed at a higher load. The right edge of the bottom chord had a crack in beam BII4C and not in beam BII4A since the latter beam had a deeper bottom chord.

Summary of Findings:

The same findings for the effect of different parameters on cracking and modes of failure of rectangular beams are applicable to T-beams. Since the prestressing forces in T-beams are greater than those in rectangular beams, the failure of the compression chord may be followed by buckling of the whole beam due to the prestressing force. Also the cracks at the opening corners may cause splitting between the flange and the web. This should be resisted by adequately reinforcing the connection between the flange and the web.

The presence of secondary moments at the opening edges may cause cracking of the flange even if it is under compression. Thus adequate non-prestressing reinforcement should be provided to resist this moment. Having the flange in the compression chord decreases the possibility of strut failure. This can be observed from the failure modes of the tested beams which were mostly due to shear failure or mechanism failure.

5.4.3 I-Beams

The behaviour of the prestressed I-beams with openings was investigated by testing two beams in the laboratory, namely; BIII1A and BIII1C in group BIII1. This group contains in addition to these two beams, beam BIII1B which was analyzed theoretically only.

Figure 5.202 shows the first cracks for beam BIII1A where the opening edge is just 12 in. (305 mm) away from the vertical load. These cracks started at the upper right and the lower left corners of the left opening at a load of 12 kip (53.4 kN). At the same load a hair crack was observed at the top fibres of the bottom chord flange at the left edge of the opening. Figure 5.202b shows the propagation of the cracks at the corners of the opening with increase in the applied load. When the load reached 18 kip (80.1 kN), a crack was observed at the bottom fibres of the lower chord just at the left edge of the opening shown in Fig. 5.202b. This crack is due to the tensile stresses resulted from the primary and the secondary moments. Increasing the load above that level developed a crack at the top fibres of the flange at the left edge of the opening shown in Fig.

5.202c. The cracks at the corners of the openings continued to propagate up to a load of 24 kip (106.8 kN). Increasing the load above 24 kip (106.8 kN) caused a wide crack at the bottom chord. This crack extended to the upper right corner as shown in Figs. 5.203a and 5.203b. Trying to increase the load at this stage caused crushing of the concrete from the upper right corner of the opening towards the point of application of the load and from the lower left corner of the opening about 2 ft. (607 mm) towards the support as shown in Fig. 5.203c. Figure 5.203d shows also this crushing just under the load.

The crack pattern for beam BIII1C was similar to that of beam BIII1A except that the cracking loads were smaller than those in beam BIII1A. This may be attributed to that the concrete used in beam BIII1C was weaker than that used in beam BIII1A. In beam BIII1C, the cracks started at the critical corners of the opening at a load of 10 kip (44.5 kN) as shown in Fig. 5.204a. Some other cracks were observed at the locations where the secondary moment was creating tensile stresses as shown in Fig. 5.204b. At a load of just above 18 kip (80.1 kN) these cracks became very wide and propagated rapidly from both sides of the opening as shown in Fig. 5.205. The cracks also penetrated the flanges of the top and bottom chords leading to the failure of the beam.

Figures 5.206, 5.207, and 5.208 show the theoretical crack patterns of beams BIII1A, BIII1B, and BIII1C, respectively. From these figures, it can be observed that all the three beams had almost the same crack pattern. The cracked regions were those at the upper right and the lower left corners of the opening and at the locations where the

secondary moment was causing tensile stresses at the opening region.

The theoretical maximum load carried by the beam increased as the opening moved away from the continuous support. Beam BIII1C had more cracked elements than the other two beams since its theoretical failure load was higher than that of the other two beams.

Summary of Findings:

The same findings for rectangular and T-beams are applicable to I-beams. The cracking of both flanges of an I-beam may occur due to the secondary moment at the compression flange or due to both the secondary and the primary moments at the tension flange. The presence of the flange in the tension chord reduces the possibility of having a fully cracked tensile chord. In I-beams, cracking of the opening corners is more critical than the other types of cracking.

CHAPTER VI

DYNAMIC ANALYSIS AND DISCUSSION OF RESULTS

6.1 General

The 'ABAQUS' computer program was used to conduct a parametric study, varying a number of factors that could influence the dynamic response of prestressed concrete beams with openings. Such factors included: (i) variations in the width and depth of the opening; (ii) variations in the horizontal and vertical locations of the opening, (iii) presence of more than one opening, and (iv) use of different cross sections. Some of the analytical results were compared to the experimental study carried out by Chami (1987) and by Kennedy et al. (1992).

In this chapter the effects of the presence of opening and of the associated parameters for simple and continuous beams are presented. The dynamic responses

involving the maximum beam deflection, the horizontal and vertical stresses and the shear distribution are analyzed for two kinds of openings in simple beams, namely; shear openings, and bending openings.

6.2 Natural frequency of Simply Supported Prestressed Beams with Openings

The objective of the parametric study was to examine the influence of the opening width and location on the natural frequencies and mode shapes of vibrations of prestressed concrete beams with openings. For the simply supported beams, two locations for the opening were selected, one being in the high shear region, 10 in. (254 mm) from the left support, and the second being in the high moment region, 10 in. (254 mm) from mid-span. A solid beam with the same dimensions was also analyzed for comparison purposes.

Figure 6.1 shows the dimensions of a simply supported beam with a shear opening and a simply supported beam with a bending opening. The finite element meshes for these two beams were presented in Fig. 3.15. Regarding the opening in the shear span, nine cases were studied varying the width of the opening, W , from 5 in. (127 mm) to 45 in. (1143 mm), with a constant opening depth, $h = 2$ in. (51 mm). The same nine cases were then repeated for $h = 3.2$ in. (81 mm), 4 in. (102 mm), 4.8 in (122 mm), and 6 in. (152 mm). These forty five cases were then repeated for beams with a bending opening. The geometries of the simply supported beams with shear openings and bending openings are shown in Fig. 6.2. The results from the parametric study for the fundamental

frequency are shown in Fig. 6.3 for beams with shear openings and in Fig. 6.4 for beams with bending openings. The width and depth of the opening were presented in dimensionless form as W/L and h/H , respectively, where L is the beam span and H is the beam depth. The fundamental frequency for beam with opening, ω , was also presented in dimensionless as ω/ω_0 where ω_0 is the fundamental frequency of a similar solid beam.

It can be seen from Fig. 6.3 that increasing the opening width or depth has the effect of decreasing the first natural frequency of beams with shear opening. This indicates that when an opening is located at the shear span, the loss in stiffness has a greater influence on the first natural frequency than the loss in mass. As the opening width increases, the rate of decrease in the first natural frequency increases. This rate also increases with increase in the opening depth.

For the bending opening, the results in Fig. 6.4 show that as the opening width increases the first natural frequency increases up to a certain limit and then it decreases with increase of the opening width. It can be noticed that the ratio ω/ω_0 increases very slowly as long as the width of the opening is less than 0.15 of the beam span and the depth of the opening is less than 0.6 of the beam's depth.

Figure 6.5 shows the first three mode shapes for beams with shear openings; it can be noted that the presence of opening does not affect the number of sine waves for each mode. In the third mode some local effect can be seen at the opening region. This local

effect increases at the higher mode shapes leading to significant reductions in the fourth and fifth natural frequencies. This can be observed in Fig. 6.7 where comparisons between the first five natural frequencies for a solid beam, a beam with a shear opening, and a beam with a bending opening, are plotted.

In Fig. 6.6, the first three mode shapes for a beam with a bending opening are shown. It can be seen from the results that the local effect of the opening becomes significant at the second mode causing the second natural frequency for the beam with the bending opening to be smaller than that for the solid beam; the reverse occurred for the first natural frequency as shown in Fig. 6.7. Such decrease in the second and higher natural frequencies can be attributed to the opening being located in the area surrounding a point of inflection where a node of zero displacement exists. The opening region around such a node is subjected to excessive changes in strains causing serious degradation in the stiffness and hence the noted reductions in the natural frequencies. In Fig. 6.7, it can be seen that for the solid beam $\omega_n \approx n^2 \omega_1$ where ω_n is the natural frequency at the n th mode and ω_1 is the first natural frequency. This is not the case for beams with openings due to the local effect of the opening.

A steady state analysis was carried out to determine the natural frequencies of three beams: a solid beam, a beam with a shear opening, and a beam with a bending opening. The results of this study are shown in Fig. 6.8 where the first, third, and fifth natural frequencies can be determined from the peaks of each curve.

6.3 Natural Frequency of Continuous Beams with Openings

For the dynamic analysis of 2-span continuous beams, three opening locations were considered: In the shear span 10 in. (254 mm) from the exterior support; in the middle of the one span; and, in the high moment-high shear zone, 10 in. (254 mm) from the interior support. These three different locations of the opening were shown in Fig. 3.16. Ten cases were studied for each location, varying: width of opening from 6 in. (152 mm) to 36 in. (914 mm); depth of opening from 2 in. (51 mm) to 6 in. (152 mm); and vertical eccentricity of the opening from zero to 2 in. (51 mm). The above analysis was applied to continuous beams having equal spans of 120 in. (3.05 m) each as well as to continuous beams with two unequal spans of 120 in. (3.05 m) and 60 in. (1.52 m). For comparison two solid beams were also studied. The above analysis was applied to beams with rectangular, T- and I-sections. Also the dynamics of two-equal span continuous beams with two openings in one span and with one opening in each span were compared; the opening was located close to the interior support in both cases.

The parametric results revealed some significant differences in the natural frequencies of two-span continuous beams due to the presence of an opening in the shear span, at mid-span and near the interior support when compared to solid beams. Table 6.1 presents these percentage differences and Figs. 6.9 and 6.10 show the values of these natural frequencies for beams with rectangular section for equal spans and unequal spans, respectively. The results show that the presence of an opening significantly influences the natural frequencies when the opening is located near the interior support, which is a

region of high moment and high shear. This influence becomes even greater for a continuous beam with unequal spans.

An opening at mid-span effects a significant change in the second natural frequency for beams with unequal spans, and in the third natural frequency for beams with equal spans. In both cases it is noted that the centre of the opening is in close proximity to a point of zero displacement; in this region the continuous beam is subjected to steep strain gradients which cause serious degradation in stiffness, hence the reduction in the frequency. The results in Table 6.1 and Figs. 6.9 and 6.10 show that an opening in the shear span has the least influence on the natural frequencies.

Figure 6.11 shows the relationship between opening width and fundamental frequency while Fig. 6.12 shows the relationship between opening depth and fundamental frequency for continuous rectangular beams with equal spans. Figures 6.13 and 6.14 show the same relations for continuous beams with unequal spans. The results reveal that increasing the width and depth of an opening has an insignificant effect on the fundamental frequency for the three critical locations of an opening in the two-equal span continuous beam. This indicates that the loss in mass and in stiffness, due to the presence of an opening, have almost the same effect on the frequency. This is unlike the case of a continuous beam with two unequal spans where variations in both the width and depth of an opening have a significant effect on the fundamental frequency as shown in Figs. 6.13 and 6.14 as well as in Table 6.1. Comparison of the fundamental frequencies for

continuous beams with openings in different vertical locations reveals that the vertical eccentricity of an opening has no significant influence on the fundamental frequency of beams with openings.

The dynamics of two equal-span continuous beams with two openings in one span and with one opening in each span were compared; the openings were located close to the interior support in both cases. It was found that the effect of the opening was to decrease the first and second natural frequencies by 14% and 37%, respectively, in the case of one opening in each span, compared to 5% and 19%, respectively, in the case of two openings in the same span. In the latter case, the third natural frequency decreased by 32% due to the presence of a local mode shape in the opening region. The corresponding change in the former case was negligible.

The mode shapes corresponding to the first three natural frequencies were determined for all the continuous beams studied. Figures 6.15, 6.16, 6.17, and 6.18 show the first three mode shapes for two equal-span continuous beams with no opening, with an opening close to the exterior support, at mid-span, and close to the interior support, respectively. From the results it was found that the maximum displacement occurs at the opening region irrespective of its location along the span.

Figure 6.19 shows the first three mode shapes for a continuous beam with two unequal spans and the opening in the long span close to the interior support. It can be

seen from these results that the first mode of vibration nullifies almost all displacements in the short span, Fig. 6.19a. This induces larger moments at the opening which can be critical in design. Furthermore, the above opening location forces the third mode shape to three half-waves in the long span instead of two, thus resembling the third mode shape of a simple-span beam. In other words, this opening location influences the continuity at the interior support. The above phenomena were not observed when the opening was in the shear span or at mid-span. Locating an opening in the middle of the short span incurred reductions of 7% and 17% in the first and third natural frequencies; however the second natural frequency was not affected.

Figure 6.20 shows the first three mode shapes for a two equal-span continuous beam with T-section with an opening close to the interior support. No differences were observed between the mode shapes for the continuous beams with T- and rectangular sections.

6.4 Dynamic Response of Simply Supported Beams with Openings

In this section the dynamic response of simply supported beams with openings is investigated. The effect of the presence of an opening near the support (in the shear span), or close to the mid-span (in the bending span) on (i) deflection, (ii) axial stresses, and (iii) splitting vertical stresses, is studied. Sinusoidal concentrated load was applied at mid-span to excite the three types of beams analyzed, namely; solid beam, beam with shear opening, and beam with bending opening. Figure 6.1 shows the geometries of the beams with openings considered in this study. The equation of the applied load is given by:

$$P = P_o \sin \Omega t \quad (6.1)$$

where P is the exciting load, P_o is the amplitude of the exciting load, Ω is the frequency of the exciting load, and t is the time. Since the first natural frequency of the analyzed solid beam was about 17 Hz, the frequency of the exciting load was taken as 10 Hz and 30 Hz to avoid the occurrence of resonance.

Each of the three types of beams was investigated under the excitation of these two frequencies and with a load amplitude of 0.5 kip (2.2 kN) which is less than the cracking load of the analyzed beams. The same analysis was then carried out under the effect of an applied load given by:

$$P = P_1 + P_o \sin \Omega t \quad (6.2)$$

where P_1 is a constant load taken as 0.3 kip (1.3 kN), and P_o was taken as 0.2 kip (0.9

kN). Figures 6.21 and 6.22 show the types of loading used in this analysis. A viscous damping of 2% was assumed in the analysis of the three beams. This value was determined experimentally by Kennedy et al. (1990).

6.4.1 Deflection

The applied load causes the beams to undergo sustained vibrations. Such vibrations have two components: a transient component and a steady-state component. The transient component is present at the start of the vibration, while the steady-state component lasts as long as the exciting force. After the transient component has died, only the steady-state component remains. Figure 6.23 shows the mid-span deflection for the three analyzed beams in the first 0.5 sec., while Fig. 6.24 shows the same deflection after the transient component had died and the system exhibiting a steady state component only. Figures 6.23a and 6.24a present the results for the case when the frequency of the exciting load is 10 Hz, while Figs. 6.23b and 6.24b are for the case when that frequency is equal to 30 Hz.

It can be observed from Fig. 6.24b that the deflection of a beam with a bending opening exceeds that for the solid beam, while the deflection of the beam with a shear opening is less than the deflection of the solid beam. This can be explained as follows: The fundamental frequency ω_b for a beam with a shear opening is less than that for the solid beam, ω_s , which is less than the fundamental frequency of the beam with a bending opening, ω_g in the beams analyzed in this study. This means that the frequency ratio,

$\beta = \Omega/\omega$ is maximum for the beam with a shear opening followed by the solid beam, then for the beam with a bending opening, i.e. $\beta_{sh} > \beta_s > \beta_{bg}$. From Fig. 6.25 after "Humar, J.L." (1991) when $\beta > 1$ and the damping ratio, ξ , is close to zero, the increase in β has the effect of decreasing the amplitude of the response. This explains why $\rho_{sh} < \rho_s < \rho_{bg}$ in Fig. 7.24b, where ρ is the amplitude of the deflection.

For a frequency ratio, β , less than one, an increase in β has the effect of increasing the deflection amplitude as shown in Fig. 6.25. In Fig. 6.24a, where $\beta < 1$ and $\beta_{sh} > \beta_s > \beta_{bg}$ the deflection of a beam with a shear opening is more than that for the solid beam which is supposed to be more than the deflection for a beam with a bending opening. In that figure, the deflection for a beam with a bending opening exceeded that for the solid beam. This is due to the local effect resulting from the presence of the opening close to mid-span. This local effect will be examined in Chapter VII.

The beam deflected shape for the three analyzed cases is shown in Figs. 6.26a and 6.26b where Ω is equal to 10 Hz and 30 Hz, respectively. In the first figure, the local effect resulting from the presence of the opening close to mid-span causes the beam with a bending opening to have a mid-span deflection greater than that for the solid beam.

In Fig. 6.27, the three analyzed beams were subjected to an exciting force $P = 0.3 + 0.2 \sin(10 t)$ kip ($1.3 + 0.9 \sin(10 t)$ kN). It can be seen from the results that the mid-span deflection fluctuates around an average value. This value is the deflection resulting

from the prestressing and the constant part of the load of 0.3 kip (1.3 kN).

It can be observed from Fig. 6.27 that the amplitude of the mid-span deflection for the beam with a shear opening exceeds that for the beam with a bending opening as well as for the solid beam. This is the same sequence which was noticed earlier when the three beams were subjected to a load $-0.5 < P < 0.5$ kip ($-2.2 < P < 2.2$ kN) discussed earlier.

6.4.2 Horizontal Stress

The horizontal stress was determined at the critical locations for the beams with shear openings and those with bending openings. This stress was also determined at mid-span for the solid beam for comparison purposes. The stress response was determined for the two frequencies of 10 Hz and 30 Hz.

6.4.2.1 Mid-Span Stress

Figure 6.28 shows the mid-span maximum stress for the solid beam, beam with a shear opening, and beam with a bending opening when (a) $\Omega = 10$ Hz and (b) $\Omega = 30$ Hz. It can be seen that in the former case, the horizontal stress in the beam with a shear opening is maximum, followed by the solid beam, and then by the beam with a bending opening. This is because $\omega_{sb} < \omega_s < \omega_{bg}$ as explained earlier. When $\Omega = 30$ Hz, the results are opposite, where the beam with a bending opening gives the maximum stress response, followed by the solid beam, and then by the beam with a shear opening.

In both cases, it is noticed that the average stress is about 625 psi (4.31 MPa), which is the value resulting from prestressing the section. Comparing the amplitude of stress for both cases of forcing frequencies, it can be observed that the amplitude of stress in the case of $\Omega = 10$ Hz is greater than that in case of $\Omega = 30$ Hz. This does not mean that increasing the load frequency causes the response to increase. Actually this is the case when the frequency ratio (β) is less than one. When β is more than one, the opposite occurs as previously shown in Fig. 6.25.

Figure 6.29 shows the steady-state analysis for the horizontal stress at mid-span for the three analyzed beams. It is noted from the results that the response when $\Omega = 10$ Hz is greater than that when $\Omega = 30$ Hz. It can be seen also from the results that only the first and third natural frequencies affect the mid-span horizontal stress. The second natural frequency does not affect the horizontal stress response since the load is applied at mid-span.

Figure 6.30 shows the horizontal stresses at mid-span for the solid beam, the beam with a shear opening, and the beam with a bending opening when the exciting load has the form of $P = P_1 + P_0 \sin \Omega t$. The earlier discussion for the load of $P = P_0 \sin \Omega t$ is applied in this case. It can be observed from Fig. 6.30 that the horizontal stresses at mid-span fluctuate around a certain value resulting from the prestressing force and the constant part of the load (P_1).

6.4.2.2 Stresses at the Opening Chords

The horizontal stresses at the opening chords due to the exciting dynamic force were determined. These stresses were compared to the mid-span stress for design purposes. Figure 6.31 shows the horizontal stress at (a) the right edge of the lower chord and (b) the left edge of the lower chord of the beam with a shear opening. It is noted that stresses fluctuate around a certain compressive stress which is due to prestressing. At the opening, the stress due to prestressing is greater than that at mid-span due to the reduction in the section area and stiffness at the opening region. Since the prestressing force was applied at mid-depth of the beam, the compressive stress at the top of the lower chord is slightly greater than that at the bottom of the same chord. This difference is denoted as stress concentration at the opening edge.

Examining the dynamic stresses at the right and left edges of the opening bottom chord, it was found that these stresses consist of two parts: one part due to the primary moment resulting directly from the exciting load, and the other part due to the secondary moment resulting from the shear force in the opening chords. Figure 6.31a shows the horizontal stresses at the opening right edge as well as at mid-span. It is observed from the results that the stress amplitude at location (4) is greater than that at location (5) although the opening is located in the low moment region. This may be attributed to the effect of the secondary moment which causes high horizontal stress at location (4). At location (3), it can be observed that the horizontal stress has an opposite sign to the horizontal stress at mid-span (180° out of phase with the mid-span horizontal stress).

This is because the secondary moment has a greater effect than the primary moment at this location; this secondary moment causes a horizontal stress with an opposite sign to that at mid-span. It can be observed also from Fig. 6.31a that although the stress amplitude at location (4) is greater than that at location (5), the tensile stress at the former location is smaller than the tensile stress at the latter location. This is due to the effect of the prestressing force which causes higher compressive stress at location (4) than at location (5).

In Fig. 6.31b, the stresses at locations (1) and (2) are plotted. It is seen from the results that the stresses at these locations are almost similar to the stresses at locations (3) and (4), respectively. From Figs. 6.31a and 6.31b, it can be concluded that the maximum compressive stress at the opening chords is higher than that at mid-span, while the maximum tensile stress at mid-span is higher than that at the opening chords.

The previous discussion was for a beam with a shear opening, where the effect of the secondary moment significantly exceeds the effect of the primary moment. When the opening is located close to mid-span, the horizontal stresses at the opening region resulting from the secondary moment become almost equal to those resulting from the primary moment. This can be observed in Fig. 6.32b where at location (1), the horizontal stress resulting from the secondary moment balances the horizontal stress resulting from the primary moment leading to almost a zero stress amplitude at this location.

In Fig. 6.32a it can be observed that at location (4), the secondary moment causes a horizontal stress with the same sign as that produced by the primary moment. This leads to a horizontal stress with a greater amplitude than that of the stress at location (5). Since the compressive stress due to the prestressing force at location (4) is greater than that at location (5), the maximum tensile stress at both locations are almost equal.

The above discussion is also applied in Figs. 6.33 and 6.34 where the frequency of the exciting load is increased from 10 Hz to 30 Hz. It can be observed from Fig. 6.34 that all the horizontal stresses at the bottom chord have the same sign as the horizontal stress at location (5). This is because the effect of the primary moment exceeds that of the secondary moment in this case. A simple method for determining the horizontal stresses at the opening chords will be presented in Chapter VII.

Figures 6.35 and 6.36 show the horizontal stresses at the opening region for the beam with a shear opening and the beam with a bending opening, respectively, when the load has the form of $P = P_1 + P_o \sin \Omega t$. The earlier discussion for $P = P_o \sin \Omega t$ applies also in this case.

6.4.3 Splitting Stress at the Opening Corners

In the static analysis, it was mentioned that the prestressing force creates a splitting tensile stress with a maximum value at the mid-depth of the opening. When the vertical load was applied, it was found that for a simple beam with opening located to the left of the applied load, the maximum splitting tensile stress moves upward at the right edge of the opening and downward at the left edge of the opening.

In the dynamic analysis, as the exciting load changes its direction after the half cycle, the four corners of the opening are exposed to high tensile stresses with the lower left and the upper right corners of the opening exhibiting high tensile stresses, simultaneously. Simultaneously, the other two corners are subjected to high vertical compressive stresses. When the exciting load changes its direction, the opposite occurs.

Figure 6.37 shows the change in the splitting stress with change in time for the forcing frequency equal to 10 Hz. It is seen from the results that the vertical stress fluctuates around an average tensile stress developed due to the prestressing force. Figure 6.38 shows this splitting stress at the opening corners when the frequency of the exciting load is equal to 30 Hz. It can be seen from the results in these figures that the amplitude of the splitting stress in the beam with a shear opening is larger than that in the beam with a bending opening. Also the amplitude when the forcing frequency is equal to 10 Hz is greater than that when the forcing frequency is equal to 30 Hz.

The steady state analysis for the splitting stress at the opening corners was carried out when the opening was located at the maximum shear field and when it was in the maximum moment field. The results of this analysis are shown in Fig. 6.39a for the shear opening and in Fig. 6.39b for the bending opening. It can be observed that at the second natural frequency, some splitting stresses are developed. This can be attributed to the fact that in the second mode shape, the zero node is slightly displaced from mid-span due to the presence of the opening. This results in a non-symmetric mode shape, hence creating some tensile stresses. Also it can be noticed that the peak at the second natural frequency is greater in the beam with a bending opening than in the beam with a shear opening. This is due to the higher displacement which occurs at mid-span in the second mode when the opening is located at the maximum moment field.

Figure 6.40 shows the splitting tensile stress at the corners of a shear opening and a bending opening when the exciting load has the form $P = P_1 + P_0 \sin \Omega t$. It can be seen from the results that the amplitude of the splitting stress in the case of a shear opening is greater than that in the case of a bending opening. This is the same behaviour that was noticed when the exciting load had the form $P = P_0 \sin \Omega t$. This can be attributed to the fact that the shearing force at the opening chords is larger in the case of a shear opening than in case of a bending opening, since the shear force distribution along the span takes the shape of a cosine function. A larger shear force in the opening chords causes larger secondary moment which causes higher splitting stresses as will be discussed in Chapter VII. An analytical method as well as an approximate method for determining the splitting stresses at the opening corners due to a vertical load will be given in Chapter VII.

CHAPTER VII

DESIGN METHODS AND PARAMETRIC STUDY

7.1 General

The finite element method was used to conduct an extensive parametric study on the static and dynamic responses of simply supported and continuous prestressed beams with openings. The objective of this study was to develop simple procedures to predict the response of such beams. The available experimental results from this research, from El-Laithy (1978), and Chami (1987), were compared to the finite element results as well as to the developed analytical and design procedures. Good agreement was observed.

This chapter includes the following:

(i) An equation is deduced for the shear force carried by each chord of the opening;

(2) From the theoretical and experimental observations, a design procedure is

developed against cracking of the opening chords;

(iii) From the parametric study, a method is developed to determine the vertical tensile stress at the opening edges due to the prestressing force and due to the vertically applied load;

(iv) From the parametric study, a simple procedure is formulated to determine the relative deflections between the opening edges;

(v) From the non-linear finite element analysis, substantiated by the test results, a method is proposed to determine the ultimate capacity of prestressed concrete beams with openings.

(vi) From the dynamic analysis of prestressed beams with openings, a simple procedure is presented to predict the fundamental frequency of such beams; furthermore, a design method is developed to determine the dynamic response of the prestressed concrete beams with openings when they are excited by a harmonic load.

7.2 Distribution of Shear between Top and Bottom Chords of Opening

It is important to predict accurately the distribution of shear between the top and bottom chords of the opening. Some researchers (Dinakaran and Sastry, 1984) have suggested that the amount of the transverse shear carried by the chords should be distributed according to their respective cross-sectional areas, while others (Barney et al., 1977) have proposed that the total shear force be proportioned according to the moments of inertia of the chords if these are uncracked; once a chord(s) has cracked, then the distribution of shear will depend on the extent of cracking. In the present investigation, a parametric study was undertaken to determine the ratio of the shear force carried by each chord of the opening. Using the 'ABAQUS' computer program (Hibbitt et al., 1989), theoretical analyses were carried out on 18 rectangular, five T- and four I-beams with rectangular openings. The width and depth of the opening as well as its horizontal and vertical locations were varied. Tables 3.3 and 3.4 show the dimensions of these beams

The area ratio and the inertia ratio were compared to the results of the finite element analysis. It was found that the results lie in between the area and the inertia ratio which means that the shear force carried by each chord depends on both the area and the inertia of this chord. Applying statistical methods to the finite element results of the investigated beams, the shear force carried by each chord of the opening was determined. Figures 7.1, 7.2, and 7.3 show the shear force carried by the bottom chord of an opening in rectangular-, T- and I-section beams, respectively, using the area ratio, the inertia ratio, and a root ratio given by:

$$\frac{V_b}{V} = \frac{\sqrt{A_b I_b}}{\sqrt{A_t I_t} + \sqrt{A_b I_b}} \quad (7.2.1)$$

in which V_b = shear force carried by the bottom chord; V = total shear force at the opening; A_b and A_t = cross sectional areas of bottom and top chords, respectively; and I_b , I_t = moments of inertia of bottom and top chords, about their centroidal axes, respectively. Also shown in Figs. 7.1, 7.2, and 7.3 is the ratio from the finite element computer solution. One can observe that the results based on the proposed root ratio given by Eq. (7.2.1) are very close to those from the computer solution in rectangular- and I- section beams. However, for T-beams with openings, it was found that the inertia ratio is the most suitable one to determine the proportion of shear carried by each chord; this is illustrated in Fig. 7.2. This may be attributed to the fact that the shear force carried by the flange is negligible. Therefore including the area of that flange in the root ratio does not represent the actual shear distribution between the opening chords.

The results from the parametric study indicated that the width of the opening has a negligible effect on the root ratio for design purposes. The shear stress at the middle of each chord was determined experimentally, and assuming a second degree parabola for the shear stress distribution in each chord, the shear force was calculated experimentally and compared to the finite element results. Rosette strain gauges were used for this purpose as previously mentioned in Chapter IV.

The root ratio given by Eq. (7.2.1) can be applied as long as the tension chord is

not cracked. Once it cracks, the moment of inertia of the cracked chord should be used to determine the shear force in each chord. Once the shear force carried by each chord is determined, the cracking load for the chords can be estimated using the Vierendeel panel method proposed below. However, in order to estimate reliably and conservatively the ultimate load of the beam, it is recommended that the total shear force be assumed to be carried by the compression chord only.

7.3 Design Procedure Against Cracking of the Opening Chords

Based on the theoretical study, substantiated by test results, a simple design procedure is presented below to estimate the cracking load of the opening chords for prestressed concrete beams subjected to external transverse load.

Figure 7.4 illustrates the forces acting on a simply supported prestressed beam with an opening. Transverse loads on the beam produce bending moment, M and shear force, V at the centre of the opening. The bending moment M is assumed to be resisted by two internal forces, namely C_c acting at the c.g. of the top chord, and T acting at the c.g. of the bottom chord. Thus

$$C_c = T = \frac{M}{(H - \bar{y}_t - \bar{y}_b)} \quad (7.3.1)$$

in which H = depth of the section; and, $y_t(y_b)$ = distance of c.g. of top (bottom) chord from top (bottom) of the section. For a transverse load applied outside the opening, the shear force V is assumed to be constant over the width of the opening, W . This shear is distributed to the top chord as V_t and to the bottom chord as V_b according to Eq. (7.2.1). The shear forces V_t and V_b produce secondary moments at the top and bottom chords equal to:

$$M_s = (V) \frac{W}{2} \quad (7.3.2)$$

and

$$M_{ab} = (V_b) \frac{W}{2} \quad (7.3.3)$$

The prestressing force F is assumed to be resisted by internal forces F_t and F_b in the top and bottom chords respectively. Results from the parametric study substantiated by the test results have shown that the forces F_t and F_b can be assumed to have triangular and rectangular distributions, respectively, as shown in Fig. 7.4. To find the magnitude and location of the force F_t for a T- or an I- section, it is assumed that the max. stress at the middle of the opening width due to prestressing is S . Then the component forces, F_1 , F_2 , and F_3 acting on the top chord become:

$$F_1 = \frac{B t^2 S}{2 h_t} \quad (7.3.4)$$

$$F_2 = \frac{t b}{h_t} (h_t - t) S \quad (7.3.5)$$

$$F_3 = \frac{b}{2} (h_t - t) \left(S - \frac{t S}{h_t} \right) \quad (7.3.6)$$

in which B , b , t , h_t are section geometries defined in Fig. 7.4. Taking moments about F_b , Fig. 7.4, yields:

$$\begin{aligned} F_1 \left(H - \frac{2}{3} t - \bar{y}_b \right) + F_2 \left(H - \bar{y}_b - \frac{h_t + t}{2} \right) + F_3 \left(H - \bar{y}_b - \frac{2h_t + t}{3} \right) \\ = F(\bar{y} - e - \bar{y}_b) \end{aligned} \quad (7.3.7)$$

in which y and e are dimensions shown in Fig. 7.4. Substituting Eqs. (7.3.4) to (7.3.6)

into Eq. (7.3.7), one finds the value of S, and hence the values of F_1 , F_2 , and F_3 from Eqs. (7.3.4) to (7.3.6). Thus,

$$F_b = F - (F_1 + F_2 + F_3) \quad (7.3.8)$$

With F_b known, the tensile stress f_t at the bottom chord is given by:

$$f_t = -\frac{F_b}{A_b} + \frac{T}{A_b} + \frac{M_{zb} \bar{y}_b}{I_b} \quad (7.3.9)$$

Equating f_t to the allowable flexural tensile stress of $7.5 \sqrt{f'_c}$ psi ("Building" 1989), one can estimate the external transverse load P causing cracking.

For a rectangular section, the force F_b can be readily shown to be:

$$F_b = \left(\frac{\frac{d}{2} + e - \frac{2}{3}h_t}{h + \frac{h_b}{2} + \frac{h_t}{3}} \right) F \quad (7.3.10)$$

and,

$$F_t = F - F_b \quad (7.3.11)$$

The resulting tensile stress f_t at the bottom chord can be readily calculated as:

$$f_t = -\frac{F_b}{A_b} + \frac{T}{A_b} + \frac{1}{2} h_b \frac{M_{zb}}{I_b} \quad (7.3.12)$$

in which h_b is the depth of the bottom chord of the opening.

Limitations

The above proposed design procedure is subject to the following limitations: (1) procedure is applicable to beams with prestressing force producing zero or near-zero stress at the top fibre of the beam; (2) openings should be located in the web at least one depth of the web away from the end zone or from continuous support; (3) the depth of the compression chord of the opening should be more than or at least equal to that of the tension chord; (4) for beams with more than one opening, the distance between two openings should be at least twice the length of the tension field d_t which will be presented in the next section.

7.4 Vertical Tensile Stress at the Opening due to Prestressing Force and the Externally Applied Load

Kennedy and El-Laithy (1982) examined the relationship between the prestressing force and the vertical splitting tensile stress at the opening. A practical design method was developed to estimate and then design for the resulting tensile stress at the opening due to prestressing. This method was modified later by Kennedy et al. (1992) to accommodate beams with T- and I-sections.

In this investigation the effect of the external load on such tensile stresses is presented. An approximate method is established to calculate the splitting stress at the critical corners of the opening due to both the prestressing and the vertically applied load. The method for calculating the splitting stress due to the prestressing force only, established by Kennedy and El-Laithy (1982) and Kennedy et al. (1992), will be presented first since it is the starting point for the method developed here.

7.4.a Vertical Tensile Stress at the Opening due to Prestressing Force

Figure 7.5 shows the free-body diagram for an I-beam with a rectangular opening and subjected to applied prestressing forces, F_1 , F_2 , and F_3 . The component of the prestressing force causing the vertical tensile force at the opening, F_v , is composed of three parts: one is the prestressing force F_3 , applied directly to the web; the second and third parts are the fractions of F_1 and F_2 , whose diffusions into the web are interrupted by the presence of the web opening. Thus it can be shown that:

$$F_s = F_1 \left(\frac{A_w}{A - A_{f_2}} \right) + F_2 \left(\frac{A_w}{A - A_{f_1}} \right) + F_3 \quad (7.4.1)$$

in which A_w , A_{f_1} , A_{f_2} , and A are the areas of the web, bottom flange, top flange, and total cross section, respectively. The eccentricity of F_s from the centre of gravity of the cross-section, e , is:

$$e = [F_1 \left(\frac{A_w}{A - A_{f_2}} \right) e_1 + F_3 e_3 - F_2 \left(\frac{A_w}{A - A_{f_1}} \right) e_2] / F_s \quad (7.4.2)$$

For a T-section,

$$F_s = F_2 \left(\frac{A_w}{A} \right) + F_3 \quad (7.4.3)$$

For a rectangular section,

$$F_s = F_1 + F_2 + F_3 \quad (7.4.4)$$

It is assumed that the force F_s is resisted by internal forces F_t and F_b in the top and bottom chords of the opening and that the diffusion of the force F_s is through the skeletal truss ABC as shown in Fig. 7.5. It can be shown (El-Laithy 1978, and Kennedy and El-Laithy 1982) that the vertical tensile force, T , can be estimated as:

$$T = \frac{\alpha (\gamma - \alpha)}{\beta \gamma} F_p \quad (7.4.5)$$

where

$$\alpha = \bar{y} - e - \frac{h_b}{2} \quad (7.4.6)$$

$$\gamma = h + \frac{h_t}{3} + \frac{h_b}{2} \quad (7.4.7)$$

$$\beta = d_t + d_c \quad (7.4.8)$$

$$d_t = \frac{H^2}{2 h C} \quad (7.4.9)$$

$$d_c = \frac{2 H C}{3 h} \quad (7.4.10)$$

in which h = depth of the opening; h_t and h_b = depths of the top and bottom chords, respectively; H = depth of the beam; C = distance from the centre of the opening to the bottom edge of the beam; the coefficient 2 in d_t is a dimensional constant in inches.

Since the vertical tensile stress distribution was assumed to have a triangular shape the maximum vertical tensile stress due to the prestressing force is given by:

$$f_t = \frac{2 T}{d_t b} \quad (7.4.11)$$

7.4.b Vertical Tensile Stress at the Opening due to Vertical Load

Based on the finite element analysis substantiated by the test results, it was found that due to the application of the vertical load, the maximum splitting tensile stress shifts upward at the right edge of the opening and shifts downward at the left edge of the opening. This means that the maximum vertical tensile stress due to the vertical load as well as the prestressing force occurs at locations (1) and (3) in Fig. 7.6a rather than at mid-depth of the opening as in the case for the prestressing force. Furthermore, this stress was found to have a distribution, on a horizontal plane passing by corner (3), similar to that shown in Fig. 7.6b. Taking a horizontal plane passing by corner (2), it was found that the vertical stress distribution takes the shape shown in Fig. 7.6c with a maximum vertical compression stress at corner (2), and changing to tensile stress after almost the same distance d_t . The same states of stress at corners (2) and (3) occur at corners (4) and (1), respectively.

From these stress distributions, it can be assumed that there is a segment of the beam at each edge of the opening, forming a framing action to the opening chords. These two segments of the beam along with the opening chords create a frame ABCD similar to the one shown in Fig. 7.7b.

The width of these beam segments is assumed to be equal to $(d_t + d_c)$ as shown in Figs. 7.6b and 7.7a. From the parametric study, it was found that d_t and d_c are almost the same as those previously given in Eqs. (7.4.9) and (7.4.10). It can be assumed also

that at corner (3) for instance, the moment transferred to segment CB is resisted by two forces T_v and C_v shown in Fig. 7.6b, where T_v can be assumed to act at $d/3$ from corner (3) and C_v to act at the middle of the distance d_c . Thus, the tensile force T_v due to the vertical load can now be calculated from:

$$T_v = \frac{M_x}{\left(\frac{2}{3} d_t + \frac{d_c}{2}\right)} \quad (7.4.12)$$

in which M_x is the secondary moment at the top chord of the opening. Assuming a triangular distribution for the vertical splitting stress, the maximum tensile stress can be calculated as:

$$f_{sv} = \frac{2 T_v}{d_t b} \quad (7.4.13)$$

This stress is due to the vertical load only. The vertical stresses due to prestressing at the corners should be added to this stress to yield the total vertical splitting stress at the opening corner due to prestressing force and the vertically applied load.

The maximum value of the tensile stress at the four corners of the opening due to the prestressing force only can be found from Fig. 7.8 as:

$$f_{st} = \left(\frac{h_b - t_f}{C - t_f}\right) f_i \quad (7.4.14)$$

Therefore, the maximum tensile force at the four corners of the opening due to the prestressing force can be estimated from:

$$T_f = \left(\frac{d_t b}{2}\right) f_{vf} \quad (7.4.15)$$

The total tensile stress at the critical corners of the opening (corners (1) and (3)) due to the prestressing force as well as the vertically applied load can then be estimated from:

$$f_{tc} = f_{tv} + f_{tf} \quad (7.4.16)$$

where f_{tv} and f_{tf} are found from Eqs. (7.4.13) and (7.4.14), respectively. Equating f_{tc} to the allowable flexural tensile stress of $7.5 \sqrt{f'_c}$ psi ("Building" 1989), one can estimate the external vertical load causing corner cracking.

The required area of vertical reinforcement must accommodate the tensile force at mid-depth of the opening due to prestressing, given by Eq. (7.4.5). Also this reinforcement must accommodate the combined stress field, namely the vertical tensile force resulting from the sum of T_v and T_f given by Eqs. (7.4.12) and (7.4.15), respectively, and the shear stresses resulting from the external loads on the beam. It should be noted that since the vertical tensile stress has a steep gradient, it is recommended that the design stress for the steel reinforcing be taken as one-half the allowable stress as was proposed before (Kennedy and Abdalla, 1992).

7.4.c Parametric Study for Determining the Vertical Tensile Stress at the Opening due to Vertical Load

Using the 'ABAQUS' computer program (Hibbitt et al., 1989), theoretical analyses were carried out on 15 simply supported rectangular beams with the opening located in the shear span close to the support and on 15 beams with the opening located in the bending span close to the vertical load which was located at mid-span in all cases.

The objective of this study was to determine the vertical tensile stress at the opening corners due to vertical load, to find an approximate formula to determine this stress directly, and to compare this stress with that presented in section (7.4.b). The width and depth of the opening were varied while the vertical location of the opening was considered to be at mid-depth of the beam in this study. Although the study was done on concentric openings, located at mid-depth of the beam, the proposed approximate method can still be applicable to beams with eccentric opening as it will be shown later in this section.

The ratio of the opening depth to the beam depth was taken as 0.4, 0.5, and 0.6. For each of these ratios, the opening width was taken as 5, 15, 25, 35, and 45 in. (127, 381, 635, 889, and 1143 mm) in a rectangular beam with cross section 3x8 in. (76x203 mm) and span of 180 in. (4.57 m). This analysis was carried out for an opening located 10 in. (254 mm) from the support, and for an opening 10 in. (254 mm) from mid-span.

The vertical splitting tensile stress resulting from the finite element solution at the opening corners was compared to that at the bottom fibres of the section at mid-span.

It was found from the parametric study that:

$$f_{iv} = \Phi \left(\frac{h}{H}\right) \left(\frac{W}{L}\right) f_{ms} \quad (7.4.17)$$

where f_{iv} is the vertical splitting stress at the opening corners due to the effect of the vertical load only, f_{ms} is the tensile stress at the bottom fibres of the section at mid-span, and Φ is a dimensionless factor given by the following equations:

$$\Phi_{bg} = 7 + 1.6 \left(\frac{h}{H}\right)^2 - 8.5 \sqrt{\frac{W}{L}} \quad (7.4.18)$$

$$\Phi_{sh} = 6.5 + 0.8 \left(\frac{h}{H}\right) - 5 \left(\frac{W}{L}\right)^{0.2} \quad (7.4.19)$$

where Φ_{bg} is the factor Φ in the case of a beam with a bending opening, and Φ_{sh} is the factor Φ in the case of a beam with a shear opening.

These results from the finite element analysis were compared to the analytical method given in section (7.4.b). Good agreement was observed between the two methods.

The results from Eq. (7.4.17) do not account for the eccentricity of the opening. The opening is considered to be at the mid-depth of the beam. For an eccentric opening,

the maximum vertical tensile stress occurs at the corner corresponding to the deeper chord. This tensile stress results from the secondary moment at that corner. Since this secondary moment is related to the shear force at the opening chord, then to take the opening eccentricity into consideration, Eq. (7.4.17) is modified using Eq. (7.2.1) as follows:

$$f_{iv} = 2 \Phi \left(\frac{h}{H} \right) \left(\frac{W}{L} \right) f_{ms} \left(\frac{\sqrt{A I}}{\sqrt{A_t I_t} + \sqrt{A_b I_b}} \right) \quad (7.4.20)$$

in which A_b and A_t = cross sectional areas of bottom and top chords, respectively; I_b and I_t = moments of inertia of bottom and top chords, about their centroidal axes, respectively; and A and I are the cross sectional area and the moment of inertia of the deeper chord of the opening, respectively.

7.5 Illustrative Design Example (Prestressed Beam with Opening under Static Loading):

A 36-ft (11 m) simply supported post-tensioned prestressed concrete I-beam has been designed to resist a total moment of 320 kip.ft (434 kN.m) due to a load P at mid span and due to its own weight, $w_D = 0.25$ kip/ft (3.65 kN/m). Six 0.6 inch (15 mm) steel strands with an ultimate tensile strength of 250 ksi (1722 MPa) concrete. The effective prestressing force was 186 kip (828 kN). One 10-inch (254 mm) depth by 36-inch (914 mm) width web opening, shown in Fig. 7.9, was required for the passage of electrical services. The centre of the opening was to be located 10 ft (3.05 m) from the support. (i) Check whether the beam can accommodate such an opening without cracking the opening chords; (ii) Check on the shear reinforcing in the opening chords; (iii) Design reinforcement for the vertical tensile forces at the opening due to prestressing.

- (i) Defining A_w , A_{t1} , A_{t2} , and A as the areas of the web, bottom and top flanges, and of the total cross-section, respectively, then from Fig. 7.9, $A_w = 112$ in² (72×10^3 mm²); $A_{t1} = A_{t2} = 68$ in² (44×10^3 mm²), and $A = 248$ in² (160×10^3 mm²). The areas and moments of inertia of the top and bottom chords of the opening are: $A_t = 116$ in² (75×10^3 mm²), $I_t = 2467$ in⁴ (0.25×10^9 mm⁴), $\sqrt{A_b I_b} = 236.2$ in³ (3.9×10^6 mm³). The shear force at the centre of the opening, $V = P/2 + 0.25 (18 \cdot 10) = P/2 + 2.0$. From Eq. (7.2.1), $V_b = 0.153 P + 0.612$. The moment at the centre of the opening, $M = 5 P + 32.5$. From Eq. (7.3.1), $T = 2.19 P + 14.24$; from Eq. (7.3.3), $M_{tb} = 2.75 P + 11.02$. From Eqs. (7.3.4) to (7.3.6), $F_1 = 8.5 S$, $F_2 = 12 S$, $F_3 = 18 S$. From Eq. (7.3.7), $S = 1.1178$ ksi (8.12 MPa). Hence, F_1

= 10.0 kip (44.5 kN); $F_2 = 14.1$ kip (62.7 kN); $F_3 = 21.2$ kip (94.3 kN). From Eq. (7.3.8), $F_b = 140.7$ kip (626 kN). Using Eq. (7.3.9) and Equating f_t to the allowable tensile stress, $f_r = 7.5 \sqrt{f'_c} = 503$ psi (3466 kPa) ("Building" 1989), yield $P = 46.9$ kip (208.7 kN). Applying the stress equation for combined bending and axial force,

$$f_c = -\frac{F}{A} + \frac{M}{I} \left(\frac{H}{2} \right), \text{ at mid-span, yields the load causing cracking at mid-span,}$$

$W = 38.3$ kip (170.4 kN) which is less than $P = 46.9$ kip (208.7 kN). Therefore, the section at mid-span will crack before the bottom chord of the opening. Using the design moment of 320 kip.ft. (434 kN.m) the concentrated load P at mid-span

$$\text{is obtained from: } 320 = \frac{(P)(36)}{4} + \frac{(0.25)(36)^2}{8}, \text{ or } P = 31.1 \text{ kip (138.4}$$

kN). Thus the beam will carry the required moment without cracking. ACI Committee 318 ("Building" 1989) limits the slenderness ratio for the top compression chord to 22. The moment of inertia of the top chord about its weak axis = 1702 in.⁴ (97.3 mm). Thus, the slenderness ratio = $36/3.83 = 9.4 < 22$ which is acceptable.

- (ii) For $P = 31.1$ kip (138.4 kN), $w_D = 0.25$ kip/ft (3.65 kN/m) and using load factors of 1.7 and 1.4, respectively, the shears carried by the top and bottom chords of the opening become, $V_t = 20.4$ kip (90.8 kN) and $V_b = 9.0$ kip (40.1 kN). The shear capacity of the bottom chord, using ACI notation, is given by ("Building" 1989):

$$V_{ci} = 0.6 \sqrt{f'_c} b_w d + \frac{V_i M_{cr}}{M_{max}} \quad (7.5.1)$$

in which b_w = minimum width of tensile chord; d = distance from the extreme compression fibre to the centroid of prestressed steel but not less than $0.8 h_b$; M_{max} = maximum moment in tensile chord = $V_b (W/2)$; V_i = shear force in tensile chord = V_b ; M_{cr} = moment causing flexural cracks at section considered =

$$\frac{I_b}{y_b} \left[6 \sqrt{f'_c} + f_{pe} - \frac{M}{y A_b} \right], \text{ where } f_{pe} = \text{compressive stress in bottom chord}$$

due to prestressing; y = distance between the centres of gravity of the top and bottom chords. Thus

$$M_{cr} = \frac{606}{3.3} \left\{ 6 \sqrt{6000} + \frac{(140.7)(10)^3}{92} - \frac{[(2.19)(31.1)(1.7)(14.24)(1.4)]}{92} \right\} = 97.2 \times 10^3 \text{ lb. inch}$$

$$= 11.0 \times 10^3 \text{ N.m.} \quad \text{Also} \quad \frac{V_i}{M_{max}} = \frac{V_b}{V_b \left(\frac{W}{2}\right)} = \frac{1}{18}$$

$$\text{Hence, } V_{ci} = 0.6 \sqrt{6000} (4)(8) + \frac{97.2 \times 10^3}{18} = 6.9 \text{ kip (30.7 kN)}$$

which is smaller than $V_b = 9.0$ kip (40.1 kN). Since $V_b > V_{ci}$, shear reinforcement of tensile chord is required. Design for shear force = $9.0 - (0.85)(6.9) = 3.1$ kip (13.8 kN). Use #3 U stirrups; area = 0.22 in^2 (141 mm^2); spacing of stirrups = $(0.22)(50)(8)/(3.1) = 28 \text{ in. (710 mm)}$ which is greater than the minimum spacing of $0.75 h = 7.5 \text{ inch (190 mm)}$. Therefore, use 6#3 U stirrups, spaced 7 inch (178

mm).

- (iii) The vertical tensile force at the opening due to prestressing and due to the vertical loads can be estimated using the procedure outlined in section 7.4. Figure 7.5 shows the component F_v of the prestressing force causing the vertical tensile force. Using the effective prestressing force of 186 kip (828 kN) and the geometries of the I-beam in Eq. (7.4.1), it can be shown that $P_v = 139.2$ kip (619 kN). Hence, from Eq. (7.4.5), $T = 10.4$ kip (46.3 kN). Due to $P = 31.1$ kip (138.4 kN), the shear force in the top chord $V_t = 12.2$ kip (54.2 kN). From Eq. (7.3.3), $M_{tt} = 219.2$ kip.in (24.8 kN.m). Hence, from Eq. (7.4.12), $T_v = 10.5$ kip (46.7 kN) and from Eq. (7.4.15), $T_r = 7.3$ kip (32.5 kN). Hence the maximum tensile force at the opening corners, $T = 17.8$ kip (79.3 kN). Results reported in this research have shown that the force T gives rise to stress distribution which can be assumed to be triangular with a maximum vertical tensile stress, f_t , at the opening as shown in Fig. 7.5. Since this stress has a steep gradient, it is recommended that the design stress for the steel reinforcing be taken one-half the allowable stress. Thus, using a 20 ksi (138 MPa) steel, the area of steel required is
- $$A_s = \frac{17.8}{(0.5)(20)} = 1.78 \text{ in}^2 (1148 \text{ mm}^2).$$
- On each side of the opening, #4 U-shaped stirrups should be provided; these stirrups should be well anchored into the top compression flange with the first stirrup placed at 1 inch (25.4 mm) from the side of the opening and the other four spaced at 1.5 inch (38 mm).

7.6 Deflection Due to the Vierendeel Action

The shear force in the opening chords, determined in section (7.2) gives rise to local deflection in these chords. To determine the relative displacement between the two edges of the opening, a parametric study was done using the finite element technique. The same set of beams used to carry out the parametric study on the splitting stress at the opening corners, is used here to determine the deflection of the opening chords due to the Vierendeel action.

Considering the opening chords to be fixed to the solid parts around the opening, and referring to Fig. 7.10, the Vierendeel deflection at the opening, Δ_v , can be shown using the slope deflection method to be:

$$\Delta_v = \frac{V W^3}{12 E (I_t + I_b)} \quad (7.6.1)$$

in which Δ_v is the Vierendeel deflection if the chords are fixed to the solid parts, V is the sum of the shear forces in the opening chords, W is the opening width, E is the modulus of elasticity, and I_t , I_b are the moment of inertia of the top and bottom chords, about their own centroidal axes, respectively.

Comparing the results from Eq. (7.6.1) to the finite element results, significant differences were observed for many of the analyzed beams. When Δ_v obtained from the finite element was substituted in the equation, the term $(I_t + I_b)$ was calculated and found that in some beams this term was less than the actual $(I_t + I_b)$. This meant that the factor

12 in Eq. (7.6.1) should be less than 12 since the chords are not completely fixed to the solid parts. Furthermore, the moment of inertia used in that equation should have a value between the moment of inertia of the section at the opening and $(I_t + I_b)$.

Taking the above into consideration, it was assumed that the relative deflection between the opening ends due to the Vierendeel action can be expressed as:

$$\Delta_v = \frac{V W^3}{\alpha E (I_t + I_b)} \quad (7.6.2)$$

where α is a factor given in Fig. 7.11 and which was developed from the parametric study. It should be noted that α might exceed 12; this will compensate when the moment of inertia used in Eq. (7.6.1) exceeds $(I_t + I_b)$.

It is recommended that for a beam with a bending opening half the deflection due to the Vierendeel action is added to the deflection of the beam Δ_b when calculating the deflection at the right edge of the opening or at mid-span, Fig. 7.10b; or,

$$\Delta_{bg} = \Delta_b + \frac{\Delta_v}{2} \quad (7.6.3)$$

where Δ_{bg} is the deflection of the beam with a bending opening, Δ_b is the beam deflection taking into consideration the reduction in stiffness due to the presence of the opening, and Δ_v is the relative deflection due to the Vierendeel action given by Eq. (7.6.2).

In the case of a beam with a shear opening, half Δ_v is to be added when calculating the deflection at the right edge of the opening; while, for the deflection at mid-span, this Vierendeel deflection can be ignored as shown in Fig. 7.10c.

In the case of a continuous or cantilever beam, it is recommended that Δ_v be added to the beam deflection as shown in Fig. 7.10d. This gives:

$$\Delta_c = \Delta_b + \Delta_v \quad (7.6.4)$$

where Δ_c is the deflection at the free end of a cantilever beam or at the edge far from the interior support for a continuous beam.

7.7 Ultimate Capacity of Prestressed Beams with Openings

The ultimate capacity of prestressed concrete beams with openings is discussed in this section. The beams may collapse with different modes of failure according to the dimensions and location of the opening, and according to the reinforcement of the opening chords. The failure may be;

(a) strut failure due to high compressive stresses or buckling of the compression chord.

(b) mechanism failure due to the formation of plastic hinges at the ends of the opening.

(c) shear failure in the opening chords.

(d) tension failure from the development of wide cracks in the tensile chord which may cause corrosion of the prestressing cables.

Simple methods of analyses for these failures will be given below; the ultimate load for design will be the smallest value derived from the above failure modes.

7.7.1 Strut Failure of Prestressed Beams with Openings

Prestressed beams may collapse due to a strut failure when the compression chord fails due to the compression force caused by the primary moment, and due to the effect of the secondary moment at the edges of that chord. To estimate the ultimate load P_u carried by the beam, it is assumed that the compression chord bends in double curvature and the contraflexure point occurs at the middle of its length. It is assumed also that this chord has a symmetric reinforcement. The free body diagram at the beam opening is shown in Fig. 7.12b.

Initially the shear force is distributed between the top and bottom chords according to Eq. (7.2.1). After the first crack appears in the tension chord, the shear force in that chord is assumed to be constant and will not increase with increase in the vertical load P . Thus an increase in the load P increases the shear force carried by the compression chord. When the tension chord is fully cracked, the whole shear is assumed to be carried by the compression chord only.

For each increment of loading, the moment at mid-opening M_m is calculated and the normal axial force in each chord is calculated as:

$$N = \frac{M_m}{Z} \quad (7.7.1)$$

where Z is the distance between the plastic centroids of the two chords and M_m is the applied moment at mid-opening.

The secondary moment at the opening edges is determined from:

$$M_x = V_t \cdot \frac{W}{2} \quad (7.3.2)$$

The normal force N and the moment M_x , can be replaced by a force N acting at an eccentricity e , where

$$e = \frac{M_x}{N} \quad (7.7.2)$$

The ultimate compressive force N_u can be calculated assuming that this e is the same when M_x and N lie on the yield surface of the interaction diagram. Whitney's formula (1942) for the interaction diagram which assumes that the yield surface is a straight line, will be used here for simplicity. According to that formula, the compression force N_u is given by:

$$N_u = A_g \left[\frac{f'_c}{\left(\frac{3}{\xi^2}\right) \left(\frac{e}{H}\right) + 1.18} + \frac{\rho_g f_y}{\left(\frac{2}{\gamma}\right) \left(\frac{e}{H}\right) + 1} \right] \quad (7.7.3)$$

In which:

$$A_g = b H, \quad \rho_g = \frac{2 A_s}{A_g}, \quad \gamma = \frac{d - d'}{H}, \quad \xi = \frac{d}{H}$$

With the normal force N_u and knowing e from Eq. (7.7.2), the moment at the middle of the opening causing a strut failure can be calculated, and hence the load at mid-span P_u . This load is compared to the assumed one, which is equal to $(P_{cr} + \text{load}$

increment); if there is a significant difference between them, another iteration is carried out until the assumed load and the load resulting from the yield surface are close to each other.

For long compression chords, the effect of the slenderness ratio should also be taken into consideration. According to the ACI code (Building 1989), the length effect can be ignored if:

$$\frac{K l_u}{r} \leq 22 \quad (7.7.4)$$

where l_u is the unbraced length and K is the effective length factor, and $r = \sqrt{I/A_c}$. In the case of an opening chord, l_u is equal to W and K is equal to unity.

If $Kl_u / r > 22$, the moment M_{st} , should be magnified by a factor δ given by the ACI code (Building 1989) as:

$$\delta = \frac{C_m}{1 - \frac{N}{\Phi \frac{\pi^2 E I_t}{W^2}}} \quad (7.7.5)$$

in which $C_m = 1$ for unbraced members, and $\Phi = 0.7$. Hence Eq. (7.3.2) is modified as:

$$M_{st} = \delta \cdot V_t \cdot \frac{W}{2} \quad (7.7.6)$$

and the rest of the procedure will remain the same.

7.7.2 Illustrative Design Example (Ultimate Failure Load of Prestressed Beam with Opening)

Cantilever Beam BI2B which was tested in the laboratory had the following data: cantilever span 60 in. (1.5 m); beam cross-section 4x10 in. (101x254 mm); opening width, $W = 16$ in. (406 mm); opening depth, $h = 3$ in. (76 mm); the distance between the concentrated load, P , and the centre of the opening right edge, $l = 32$ in. (813 mm); the opening was centred at the mid-depth of the beam; the prestressing force, F , was measured in the lab to be 31.78 kip (141.4 kN) with eccentricity, $e = 1.888$ in. (48 mm); the concrete compressive strength, $f'_c = 6200$ psi (42.7 MPa); the compression chord was reinforced by 4-3/16 in. (4.8 mm) steel bars, the concrete cover for the steel bars, $d' = 0.75$ in. (19 mm). Figure 7.13 shows the dimensions of the beam and the cross-section of the bottom chord. It is required to determine the ultimate load due to strut failure of this beam.

Referring to section 7.7.1, the following section properties for the bottom chord (the compression chord) can be estimated, $A_g = 14$ in² (9×10^3 mm²), $\rho_g = 0.008$, $\gamma = 0.57$, and $\xi = 0.786$. Applying Eqs. (7.3.4) to (7.3.8), the prestressing force in the top chord $F_t = 24.46$ kip (108.8 kN). From Eq. (7.3.9), the vertical load causing cracking in the top chord, $P_{cr} = 2.45$ kip (10.9 kN). This procedure to determine the cracking load was presented in detail in the illustrative example in section 7.5. Since the top and bottom chords have the same dimensions, the shear force at the opening is equally distributed between them. Hence, $V_t = 1.225$ kip (5.45 kN) at cracking. Adding an increment of 1 kip (4.45 kN) to the cracking

load, the initially assumed ultimate load becomes: $P_u = 2.45 + 1 = 3.45$ kip (15.35 kN); the shear force in the bottom chord, $V_b = 3.45 - 1.225 = 2.225$ kip (9.9 kN); the secondary moment in the bottom chord, $M_{bb} = 2.225 \times 8 = 17.8$ kip.in (2 kN.m); the primary moment at the centre of the opening, $M_m = 3.45 \times 40 = 138$ kip.in (15.6 kN.m); the normal force in the compression chord, $N = 138/6.5 = 21.23$ kip (94.5 kN); the eccentricity of this normal force, $e = M_{bb}/N = 17.8/21.23 = 0.838$ in. (21.3 mm). Applying Eq. (7.7.3), the ultimate normal force in the bottom chord, $N_u = 40.06$ kip (178.3 kN). This leads to $M_m = 40.06 \times 6.5 = 260.4$ kip.in (29.4 kN.m), and $P_u = 260.4/40 = 6.5$ kip (29 kN). For the second trial take $P_u = 6.5$ kip (29 kN). Hence $V_b = 6.5 - 1.225 = 5.275$ kip (23.5 kN), $M_{bb} = 5.275 \times 8 = 42.2$ kip.in (4.8 kN.m), $M_m = 6.5 \times 40 = 260$ kip.in (29.4 kN.m), $N = 260/6.5 = 40$ kip (178 kN), $e = 40/42.2 = 0.95$ in. (24.1 mm). From Eq. (7.7.3), $N_u = 37.5$ kip (166.9 kN). Hence, $M_m = 37.5 \times 6.5 = 244.3$ kip.in (27.6 kN.m), $P_u = 6.1$ kip (27.1 kN). For the third trial, $P_u = 6.1$ kip (27.1 kN). Hence, $V_b = 6.1 - 1.225 = 4.88$ kip (21.7 kN), $M_{bb} = 4.88 \times 8 = 39.06$ kip.in (4.4 kN.m), $M_m = 6.1 \times 40 = 244$ kip.in (27.6 kN.m), $N = 244/6.5 = 37.5$ kip (166.9 kN), $e = 39.06/37.5 = 1.04$ in. (26.4 mm). From Eq. (7.7.3), $N_u = 35.8$ kip (159.3 kN). Hence, $M_m = 35.8 \times 6.5 = 232.7$ kip.in (26.3 kN.m), and $P_u = 5.8$ kip (25.8 kN). One more trial will lead to $P_u = 5.86$ kip (26.1 kN) which means that for the design purpose, the ultimate load can be considered to be $P_u = 5.8$ kip (25.8 kN). It should be noted that this beam was failed in the laboratory at a load between 5.25 kip (23.4 kN) and 5.5 kip (24.5 kN).

7.7.3 Formation of a Plastic Hinge at the Opening Ends

This method was given by Mansur et al. (1992) for reinforced concrete beams with openings. In this thesis the method is modified to be suitable for the behaviour of prestressed beams. It is assumed that under the applied load, the top and bottom chords of the opening deflect in double curvature with contraflexure points occurring at their mid-span. The free body diagram at a beam opening is presented in Fig. 7.12b.

The axial force in the opening chords is given by Eq. (7.7.1). The edges of the top chord are subjected to a compressive force, N , resulting from the applied moment at the opening. This force acts at the centroid of the top chord. The edges of the top chord are subjected also to a secondary moment M_{t1} and to a shear force V_t . The edges of the bottom chord are subjected to an axial tensile force, N , a secondary moment M_{b1} , and to a shear force V_b . Furthermore, the top and bottom chords are also subjected to a prestressing force F_t , F_b , respectively. At ultimate load such prestressing forces do not affect the ultimate strength of the section.

The compression chord is subjected to a positive (sagging) moment at the right edge and from the experimental observations, the collapse of that chord is usually a compression type failure. It is also recommended that the reinforcement of that chord be symmetric. Therefore, the yield surface of that chord can be represented by surface AB shown in Fig. 7.14a, and expressed as:

$$M = \left(\frac{N_o - N}{N_o - N_{ba}} \right) M_{ba} \quad (7.7.2.a)$$

When the moment is negative, surface AB' can be expressed as:

$$M = \left(\frac{N_o - N}{N_o - N'_{ba}} \right) M'_{ba} \quad (7.7.2.b)$$

where M, N = the bending moment and normal force on the yield surface, respectively; N_o = the ultimate strength of section in axial compression; M_{ba}, M'_{ba} = moments of balanced failure under positive and negative moments, respectively; and N_{ba}, N'_{ba} = axial compressive force corresponding to M_{ba}, M'_{ba} , respectively.

The tension chord which usually contains the prestressing cables is subjected to a normal tensile force and to positive and negative bending moments, the yield surfaces in this case are given, respectively, by:

$$M = \left(\frac{N'_o - N}{N'_o} \right) M_o \quad (7.7.3.a)$$

$$M = \left(\frac{N'_o - N}{N'_o} \right) M'_o \quad (7.7.3.b)$$

where M_o, M'_o = ultimate moments of a section in positive and negative bending, respectively; N_o, N'_o = ultimate capacity of a section in axial compression and tension, respectively.

The plastic moment capacity of a section at the right and left edges of the opening, respectively, can be represented as:

$$M_{pr} = \left(\frac{N_o - N}{N_o - N_{ba}} \right) M_{ba} + \left(\frac{N'_o - N}{N'_o} \right) M'_o + N.Z \quad (7.7.4)$$

$$M_{pl} = - \left(\frac{N_o - N}{N_o - N'_{ba}} \right) M'_{ba} - \left(\frac{N'_o - N}{N'_o} \right) M'_o + N.Z \quad (7.7.5)$$

Replacing N in Eq. (7.7.4) and in (7.7.5) by M_m and using Eq. (7.7.1) lead to:

$$M_{pr} = \left(\frac{N_o - \frac{M_m}{Z}}{N_o - N_{ba}} \right) M_{ba} + \left(\frac{N'_o - \frac{M_m}{Z}}{N'_o} \right) M'_o + M_m \quad (7.7.6)$$

and

$$M_{pl} = - \left(\frac{N_o - \frac{M_m}{Z}}{N_o - N'_{ba}} \right) M'_{ba} - \left(\frac{N'_o - \frac{M_m}{Z}}{N'_o} \right) M'_o + M_m \quad (7.7.7)$$

Equations (7.7.6) and (7.7.7), are the plastic moment capacities at the edges of the opening expressed as a function of M_m , the applied bending moment at the centre of the opening. Since the value of M_m varies with increase in the applied load, the plastic moment at the plastic hinges will not remain constant, but will change during subsequent loading. Hence, the plastic moment at the opening edges is adjusted for each increment of loading.

If the plastic hinge occurs at the edge of the opening as shown in Fig. 7.14b, then:

$$M_p (\theta_1 + \theta_2) = P \cdot y \quad (7.7.8)$$

From geometry:

$$\begin{aligned} y &= \frac{L}{2} \cdot \theta_1 \\ \theta_2 &= \frac{L - l'}{l'} \cdot \theta_1 \end{aligned} \quad (7.7.9)$$

Substituting for y and θ_1 in Eq. (7.7.8) yields:

$$P = \frac{2 M_p}{l'} \quad (7.7.10)$$

Hence, P can be written as :

$$P = \frac{2 M_{pr}}{\left(l + \frac{W}{2}\right)} \quad (7.7.11)$$

or

$$P = \frac{2 M_{pl}}{\left(l - \frac{W}{2}\right)} \quad (7.7.12)$$

and the smaller of the two values will yield the maximum collapse load.

The moments and normal forces for the balanced section can be calculated for the compression chord using the ACI code ("Building" 1989) and considering symmetric reinforcement as follows:

$$N_{ba} = N'_{ba} = 0.85 f'_c a b - 0.85 A_s f'_c \quad (7.7.13)$$

$$M_{ba} = M'_{ba} = \frac{1}{2} (0.85 f'_c a b) (d - a + d') + A_s f_y d - 0.85 A_s f'_c \left(\frac{d}{2}\right) \quad (7.7.14)$$

In which

$$a = \beta_1 \left(\frac{87000 d}{f_y + 87000} \right) \quad (7.7.15)$$

$$\beta_1 = 0.85 - 0.05 \left(\frac{f'_c - 4000}{1000} \right) \geq 0.65 \quad (7.7.16)$$

for f'_c greater than 4000 psi (27.6 MPa)

and b, d, and d' are dimensions defined in Fig. 7.15a

Also for the compression chord, N_o is given by:

$$N_o = 0.85 f'_c b H + 2 f_y A_s \quad (7.7.17)$$

For the tension chord which usually contains prestressing cables, the ultimate moment capacity M_o and M'_o depend on the location of the cables in the section.

Referring to Fig. 7.15b one can write:

$$T = T_s + T_p - C_s \quad (7.7.18.a)$$

Taking moments about T_s , yields

$$g = \left(\frac{T_p (d'' - d') - C_s d}{T} \right) + d' \quad (7.7.18.b)$$

$$M_o = T \cdot Z \quad (7.7.18.c)$$

In which :

$$T_s = A_s f_y, \quad T_p = A_{ps} f_{ps}, \quad C_s = A'_s f_y \quad (7.7.19.a)$$

and according to the ACI code (Building 1989):

$$f_{ps} = f_{se} + 10,000 + \frac{f'_c}{100 \rho_p} \leq f_{py} \quad (7.7.19.b)$$

$$\leq f_{se} + 60,000$$

$$\rho_p = \frac{A_{ps}}{b (H - d'')} \quad (7.7.20)$$

$$Z = H - \frac{a}{2} - d'' \quad (7.7.21)$$

where (a) can be calculated from

$$C = T \quad (7.7.22)$$

$$a = \frac{T}{0.85 f'_c b}$$

7.7.4 Shear Failure in the Opening Chords

The failure of the opening chords may occur due to high shear stresses in these chords. The effect of the axial forces whether compression or tension has to be taken into consideration. Before cracking, the shear force is distributed between the top and bottom chords according to the root ratio given by Eq. (7.2.1).

After cracking, a simplified conservative procedure for estimating shear forces in the opening chords was presented earlier. If the crack in the bottom chord extends the full depth of the tension chord, it was recommended earlier that the compression chord carry the total shear. Thus when

$$T \geq 7.5 A_b \sqrt{f'_c} \quad (7.7.23)$$

it is recommended that

$$\begin{aligned} V_t &= V \\ V_b &= 0 \end{aligned} \quad (7.7.24)$$

If Eq. (7.7.23) is not fulfilled, i.e;

$$T < 7.5 A_b \sqrt{f'_c} \quad (7.7.25)$$

the shear force in the tensile chord is calculated at cracking, i.e. V_{bcr} , with the

compression chord carrying the remaining shear, i.e;

$$V_t = V - V_{bcr} \quad (7.7.26)$$

where V_t is the shear force in the top chord (compression chord), V is the total shear force, and V_{bcr} is the shear force carried by the bottom chord just at cracking. The shear force carried by the bottom chord for purpose of design, if Eq. (7.7.25) is applicable, is:

$$V_b = V \frac{\sqrt{A_b I_b}}{\sqrt{A_b I_b} + \sqrt{A_t I_t}} \quad (7.7.27)$$

The use of this simplified method for determining the shear forces in the opening chords results in a conservative design against shear failure in the opening chords.

The shear force in the top and bottom chords of the opening resulting from Eqs. (7.7.26) and (7.7.27) are then compared to the ultimate shear capacity of the concrete section subjected also to a normal force. Thus, according to the ACI code (Building 1989), the shear force taken by the compression chord is given by:

$$V_c = 2 \left(1 + \frac{N_u}{2000 A_g} \right) \sqrt{f'_c} b d \quad (7.7.28)$$

and

$$V_c \leq 3.5 \sqrt{f'_c} b d \sqrt{1 + \frac{N_u}{500 A_g}} \quad (7.7.29)$$

When the net force in the bottom chord is tension, the shear force capacity of the tensile chord is given by the ACI code (Building 1989) as:

$$V_c = 2 \left(1 + \frac{N_u}{500 A_g} \right) \sqrt{f'_c} b_w d \quad (7.7.30)$$

In the above equations it should be noted that N is considered negative for tension and that N_u/A_g is in psi.

7.8 Dynamic Analysis of Simply Supported Prestressed Beams with Openings:

The natural frequencies and mode shapes of prestressed concrete beams with openings were discussed in Chapter VI. A parametric study using the 'ABAQUS' computer code (Hibbitt et al. 1989), was carried out to determine the fundamental frequency of simple beams with shear opening and with bending opening. The finite element results were compared to the experimental results given by Chami (1987). Good agreement between the theoretical and the experimental results was observed. A method for determining the natural frequencies for simply supported prestressed beams was given in Chapter VI.

In this section, the method of modal analysis is used to determine the dynamic response of simply supported prestressed beams with openings. The results from the modal analysis method given in this section and from the finite element method are compared in the illustrative example given at the end of this section.

The method for estimating the dynamic response starts with the fundamental frequency of a solid beam with the same dimensions as the beam with an opening for which the dynamic response is required. The natural frequencies of a solid simply supported beam is given by (Humar 1990):

$$\omega_n = n^2 \Pi^2 \sqrt{\frac{E I}{m L^4}} \quad (\text{rad/sec.}) \quad (7.8.1)$$

in which ω_n = the natural frequency at mode n , E = Young's modulus for concrete, I =

beam moment of inertia, m = mass per unit length of the beam, and L = the span of the beam. The presence of prestressing has the effect of decreasing the natural frequency of the beam. This is because the prestressing force increases the vibration amplitude. This means reduction in the beam stiffness, hence reduction in the natural frequency. Figure 7.16, after Blevins (1979), shows the effect of the axial load on the natural frequency of a simply supported beam. It can be noticed from results that the effect of the axial load is significant only in the first mode. Furthermore, a tensile axial force increases the frequency while a compressive axial force decreases the frequency. It can be shown (Blevins 1979) that:

$$\omega_{n(F \neq 0)} = \omega_{n(F = 0)} \sqrt{1 + \frac{F}{n^2 |F_b|}} \quad (7.8.2)$$

where F is the prestressing load (negative since it is a compression force), F_b is the axial force required to buckle the beam. For a pinned-pinned beam, F_b is given by:

$$F_b = \frac{\Pi^2 E I}{L^2} \quad (7.8.3)$$

Knowing the dimensions of the opening as well as its location, the natural frequencies for a beam with a shear opening or with a bending opening can be determined using Figs. 6.3 and 6.4, respectively.

7.8.1 Mid-Span Deflection

For a simply supported beam loaded at mid-span with an exciting load of the form

$P = P_o \sin \Omega t$, the deflection along the span resulting from the modal analysis is given by (Ferties 1984):

$$y(t,x) = \frac{2}{m L} \sum^n \frac{P_o \sin \frac{n \pi}{2}}{\omega_n^2 [1 - \beta_n^2]} \sin \Omega t \sin \frac{n \pi x}{L} \quad (7.8.4)$$

in which $y(t,x)$ = the deflection at any time t and distance x from the beam support, and ω_n = the natural frequency in the n th mode for a simply supported beam with an opening, and $\beta_n = \Omega/\omega_n$.

At mid-span where $x = L/2$, the deflection is given by:

$$y(t, \frac{L}{2}) = \frac{2}{m L} \sum^n \frac{P_o \sin \frac{n \pi}{2}}{\omega_n^2 [1 - \beta_n^2]} \sin \Omega t \sin \frac{n \pi}{2} \quad (7.8.5)$$

7.8.2 Bending Moment at Mid-Span and at Mid-Opening:

It is well known that the relationship between bending moment and deflection is given by:

$$M = E I \frac{d^2 y}{d x^2} \quad (7.8.6)$$

Differentiating Eq. (7.8.4) twice with respect to x and substituting in Eq. (7.8.6), yields

the bending moment at any distance x from the support as:

$$M(t, x) = \frac{\Pi^2 E I}{L^2} \sum^n n^2 y_n(t, x) \quad (7.8.7)$$

and the moment at mid span is then given by:

$$M(t, \frac{L}{2}) = \frac{\Pi^2 E I}{L^2} \sum^n n^2 y_n(t, \frac{L}{2}) \quad (7.8.8)$$

The bending moment at mid-opening where $x = l$ is given by:

$$M(t, l) = \frac{\Pi^2 E I}{L^2} \sum^n n^2 y_n(t, l) \quad (7.8.9)$$

7.8.3 Shear Force at Support and at Mid-Opening

It is well known that the shear force at any location along the beam is given by:

$$V = \frac{dM}{dx} = EI \frac{d^3 y}{dx^3} \quad (7.8.10)$$

Differentiating Eq. (7.8.4) three times and substituting in Eq. (7.8.10), yields the shear force at any x along the span as:

$$V(t, x) = \frac{2 E I \Pi^3}{m L^4} \sum^n n^3 \frac{P_o \sin \frac{n\Pi}{2}}{\omega_n^2 [1 - \beta_n^2]} \sin \Omega t \cos \frac{n \Pi x}{L} \quad (7.8.11)$$

At the support where $x = 0$, the reaction will be equal to:

$$R = V(t, 0) = \frac{2 E I \Pi^3}{m L^4} \sum^n n^3 \frac{P_o \sin \frac{n \Pi}{2}}{\omega_n^2 [1 - \beta_n^2]} \sin \Omega t \quad (7.8.12)$$

At the centre of the opening where $x = l$, the shear force is given by:

$$V_o = V(t, l) = \frac{2 E I \Pi^3}{m L^4} \sum^n n^3 \frac{P_o \sin \frac{n \Pi}{2}}{\omega_n^2 [1 - \beta_n^2]} \sin \Omega t \cos \frac{n \Pi l}{L} \quad (7.8.13)$$

7.8.4 Secondary Moment at the Opening Edges

Having determined the shear force at mid-opening, the secondary moment at the opening edges can be determined. The same procedure used in the static analysis was applied in the modal analysis. The shear force at mid-opening was distributed between the top and bottom chords according to Eq. (7.2.1). Once the shear force in the opening chords is determined, the secondary moment can be calculated from Eqs. (7.3.2) and (7.3.3).

7.8.5 Splitting Stress at Opening Corners

From the parametric study, it was found that the splitting stress at the opening

corners due to the exciting load can be determined by Eqs. (7.4.17), (7.4.18), and (7.4.19) for beams with a shear opening and with a bending opening.

Knowing the moments and shear forces at the critical location in the vicinity of the opening due to the exciting load, the total response can be determined by adding the stresses due to the prestressing. The total stresses have to be less than the allowable cracking tensile stress as well as the allowable compression stress to ensure that the beam is safe under the working load condition.

An illustrative example is given below, to determine the maximum deflection and the critical stresses in the vicinity of the opening and at mid-span for a beam under dynamic load. The results are also compared to the results from the finite element analysis. This comparison shows that the modal analysis method presented herein is accurate for engineering design purposes.

7.8.5 Illustrative Design Example (Dynamic Response of Simply Supported Beam with Shear Opening)

A simply supported beam with span 180 in. (4.6 m), and cross section 3x8 in. (76x203 mm), is subjected to a harmonic load with an amplitude of 0.5 kip (2.22 kN) and a forcing frequency of 10 Hz. One 4 in. (102 mm) deep by 30 in. (762 mm) width web opening, was required to be located at a distance of 10 in. (254 mm) from the left support. The resultant of the prestressing force was equal to 15 kip (66.8 kN). At time $t = 2$ sec., (i) determine the beam max. deflection at the mid-span, (ii) estimate the horizontal stresses at the mid span and at the vicinity of the opening, (iii) determine the splitting stress at the opening corners due to the vertical exciting load. Compare the results with those of the finite element analysis.

The natural frequencies of a solid beam with the same dimensions has to be determined first. Assuming that the concrete density is 150 lb/ft³ (2400 kg/m³), the mass of the beam per unit length will be $m = 0.00054$ lb.sec/in² (37.2 kg/m). The modulus of elasticity of the concrete is assumed to be 4.7×10^6 psi (32.4x10³ MPa) for concrete compressive strength f'_c of 6800 psi (46.65 MPa). The moment of inertia of the beam section, $I = 128$ in⁴ (53x10⁶ mm⁴). The fundamental frequency of the solid beam can now be determined from Eq. (7.8.1), $\omega_1 (F=0) = 16.87$ Hz, $\omega_3 (F=0) = 151.83$ Hz, and $\omega_5 (F=0) = 421.75$ Hz. To take the effect of prestressing into consideration, the beam buckling load has to be determined using

Eq. (7.8.3) as follows: $F_b = \frac{\Pi^2 (4.7 \times 10^6) (128)}{(180)^2} = 184.4$ kip (820.6 kN).

Using Fig. 7.16 with $F/F_b = 15/184.4 = 0.08$, leads to a reduction in the first natural frequency by about 3%. Hence, $\omega_1 (F+\omega) = 0.97 \times 16.87 = 16.36$ Hz. The effect of prestressing can be neglected in the third and fifth natural frequencies as shown in Fig. 7.16. Using Fig. 6.3, with $h/H = 0.5$, $W/L = 0.167$, the fundamental frequency of the beam with shear opening, $\omega_1 = 0.925 \times 16.36 = 15.15$ Hz. Using Fig. 6.7, the third and fifth natural frequencies of the beam with shear opening can be approximately determined; $\omega_3 = 0.97 \times 151.83 = 148$ Hz, $\omega_5 = 0.7 \times 421.75 = 286$ Hz.

(i) Mid-Span Deflection:

Applying Eq. (7.8.5), the contribution of the first mode in the mid-span deflection:

$$y_1 = \frac{2}{(0.0054)(180)} \times \frac{500 \sin \frac{\pi}{2}}{(95.2)^2 [1 - (0.66)^2]} \times [\sin (62.8)(2)] \quad (1) = -0.19107 \text{ inch (4.85 mm)}$$

Applying the same Equation for the third and fifth modes, it can be found that $y_3 = -0.00126$ in. (0.03 mm), and $y_5 = -0.000356$ in. (0.009 mm). Hence, the total deflection $y = y_1 + y_3 + y_5 = -0.19268$ in. (4.9 mm). The value for this deflection from the finite element analysis was 0.1873 in. (4.75 mm).

(ii) Horizontal Stresses:

- Mid-Span Moment:

Applying Eq. (7.8.8), the contribution of the first mode in the bending moment at

mid-span can be estimated as follows:

$$M_1 = \frac{\Pi^2 (4.7 \times 10^6) (128)}{(180)^2} (1)^2 (-0.19107)$$

$$= -35.23 \text{ kip.inch (3.98 kN.m)}$$

Applying the same Equation for the third and fifth mode, it can be found that $M_3 = -2.0911 \text{ kip.in (0.236 kN.m)}$, and $M_5 = -1.641 \text{ kip.in (0.185 kN.m)}$. Hence, the total moment at mid span, $M = M_1 + M_3 + M_5 = -38.96 \text{ kip.in (4.4 kN.m)}$.

- Horizontal Stress at Mid-Span:

Applying the beam theory equation, $f = M.y/I$, the stress at mid-span due to the vertical load $= (38.96 \times 10^3)(4)/128 = \pm 1217.5 \text{ psi (8.4 MPa)}$. The stress due to the prestressing force $= F/A = 15 \times 10^3/24 = -625 \text{ psi (4.3 MPa)}$. Hence the total stress at mid-span, $f = -625 \pm 1217.5 = -1842.5 \text{ psi (12.7 MPa)}$, or $+592.5 \text{ psi (4.1 MPa)}$. These values were determined from the finite element analysis to be $-1772.8 \text{ psi (12.2 MPa)}$, and $+523 \text{ psi (3.6 MPa)}$, respectively. It should be noted that the stresses from the proposed method are on the conservative side when compared to the finite element results.

Mid-Opening Moment:

At the mid-opening section, $X/L = 25/180 = 0.139$. Hence, the bending moment at this section, $M_o = M \sin (n \Pi X/L) / \sin (n \Pi/2)$, where M is the moment at mid-span. The contribution of the first mode to the moment at the mid-opening,

$M_{o1} = (-35.23) \sin(\pi) (0.139) / (1) = -14.89 \text{ kip.in (1.68 kN.m)}$. Also $M_{o3} = 2.637 \text{ kip.in (0.3 kN.m)}$, and $M_{o5} = -1.344 \text{ kip.in (0.15 kN.m)}$. The total moment at the mid-opening, $M_o = M_{o1} + M_{o3} + M_{o5} = -13.6 \text{ kip.in (1.54 kN.m)}$.

- Mid-Opening Shear:

The shear force at the mid-opening can be calculated by substituting $X/L = 0.139$ in Eq. (7.8.11) to determine the contribution of each mode. Adding the shear force from the first, third, and fifth modes as before, gives the shear force at the middle of the opening $V_o = 0.447 \text{ kip (2 kN)}$.

- Horizontal Stress at the Opening Chords:

The shear force at the mid-opening section is distributed equally between the top and bottom chords, since they both have the same dimensions. $V_t = V_b = 0.447/2 = 0.224 \text{ kip (1 kN)}$. The secondary moment at the ends of the opening chords, $M_s = V_t W / 2 = (0.224) (30) / 2 = 3.36 \text{ kip.in (0.38 kN.m)}$. The primary moment at the mid-opening, M causes two normal forces, one is compression in the bottom chord and the other is tension in the top chord, and given by $N = M / (H - h/2 - h/2) = 13.6 / 6 = 2.27 \text{ kip (10.1 kN)}$. This force results in creating a compressive stress in the bottom chord equal to $2.27 \times 10^3 / (2 \times 3) = 378 \text{ psi (2.6 MPa)}$. In the same chord, the secondary moment causes horizontal stress,

$$f_s = \frac{M_s \times \frac{h_b}{2}}{I_b} = \frac{3.36 \times 1}{2} = 1.680 \text{ ksi (11.6 MPa)}. \text{ Hence the stress}$$

at the bottom chord due to the vertical load is now equal to $-1680 - 378 = -2058$ psi (14.18 MPa) at the bottom fibre and $+1680 - 378 = +1302$ psi (8.97 MPa) at the top fibre. The prestressing force causes compressive stresses in both chords equal to $15 \times 10^3 / (2 \times 3 \times 2) = -1250$ psi (8.61 MPa). The total stress at the bottom chord can now be determined by adding the stress due to the prestressing force to that due to the vertical load. This leads to a compressive stress at the bottom fibre of the bottom chord equals to $-2058 - 1250 = -3308$ psi (22.8 MPa) and to a tensile stress at the top fibre of the bottom chord equals to $1302 - 1250 = 52$ psi (0.36 MPa). These stresses are compared to -3003 psi (20.7 MPa) and to -166 (1.14 MPa), respectively, from the finite element analysis. It should be noted that the prestressing force results in higher stresses in the top fibre of the bottom chord than in the bottom fibre of the same chord due to the stress concentration which is neglected in the present calculations. This is the reason why there is a small tensile stress in the top fibre of the bottom chord in the present analysis, which is not the case from the finite element analysis.

(iii) Max. Splitting Stress due to the Vertical Load at the Opening Corners:

From Eq. (7.4.9), the length of the tension field, $d_t = (H^2)/2hC = (8^2)/(2 \times 4 \times 4) = 2$ in. (51 mm), from Eq. (7.4.10), the length of the compression field, $d_c = 2HC/3h = (2 \times 8 \times 4)/(3 \times 4) = 5.33$ in. (135.4 mm). The shear force and the secondary moment were determined to be $V_t = V_b = 0.224$ kip (1.0 kN), and $M_s = 3.36$ kip.in (0.38 kN.m). From Eq. (7.4.12), the tensile force due to the vertical load

can be determined;

$$T_v = \frac{(3.36)}{\left(\frac{2}{3} \times 2\right) + \left(\frac{5.33}{2}\right)} = 0.84 \text{ kip } (3.74 \text{ kN}). \text{ Hence, the splitting}$$

stress can be determined using Eq. (7.4.13),

$$f_{tv} = \frac{2 \times 0.84}{2 \times 3} \times 1000 = 280 \text{ psi } (1.93 \text{ MPa}). \text{ This compared to 285 psi}$$

(1.96 MPa) from the finite element analysis.

CHAPTER VIII

SUMMARY AND CONCLUSIONS

8.1 Summary

In this investigation the static and dynamic behaviour of prestressed concrete beams with openings was studied. Extensive experimental and theoretical analyses were carried out to determine the influence of openings on the response of such beams. A detailed literature review was conducted to establish the foundation for this study.

The finite element method was used to predict the behaviour at the transfer stage (due to the prestressing force only), at the working stage (before cracking), and at the ultimate stage, where the beams are near collapse. Tests on thirteen continuous prestressed rectangular, T- and I-beams were conducted to verify and substantiate the theoretical study. Furthermore, the finite element method was used to carry out a parametric study to develop simple and reliable procedures for the analysis and design of these beams.

An extensive parametric study was also conducted to determine the natural frequencies and mode shapes of simply supported and continuous prestressed beams with different cross-sections. The results from this study were compared to the dynamic experimental test results reported in the literature. Good comparison between the analytical and experimental results was noted.

The finite element technique was also used to predict the dynamic response including deflections and stresses of simply supported prestressed concrete beams with openings. Using modal analysis, a design method was presented based on the natural frequencies of prestressed beams with openings.

8.2 Conclusions

Based on the theoretical and experimental results from this investigation, the following conclusions may be drawn:

1- The agreement between the results from the experiments and from the finite element analysis is quite favourable for both static and dynamic analyses.

For the static study:

2- Horizontal location of the opening has a significant effect on the local deflection of the opening chords, with only a minor effect on the global beam deflection in the elastic stage. In the non-linear stage, the beam maximum deflection increases significantly as the opening moves towards the interior support. The opening edge should

be located a distance equal to at least the depth of the beam from such support in order to avoid excessive deflections.

3- The vertical location of the opening greatly affects the beam maximum deflection at the transfer stage, while at the working stage, this effect is insignificant.

4- The opening width has a significant effect on the beam deflection in the working and ultimate stages of loading, with a minor effect in the transfer stage.

5- An increase in the opening depth increases the deflection due to vertically applied load, as well as the camber due to the prestressing force.

6- The horizontal stresses in the vicinity of the opening are significantly influenced by the location and size of the opening. Moving the opening towards the continuous interior support has the effect of increasing the horizontal stresses in the vicinity of the opening in the working and ultimate stages but not in the transfer stage. The vertical location of the opening affects the horizontal stress distribution in the opening region during the three stages of loading. Increasing the opening width has the effect of reducing the stress concentration due to prestressing at the edges of the opening, but it augments the horizontal stresses at the opening edges during the working and ultimate stages.

7- The horizontal stress distribution at the solid section above the continuous interior support is not significantly affected by the presence of the opening if its edge is located a distance equal to the depth of the beam from such support.

8- The prestressing force creates a vertical splitting stress at the opening edges with a maximum value at the centre of the opening regardless of the location of the prestressing force. Depth of opening has a significant influence on this stress while the opening width has almost no effect on this stress.

9- Vertically applied load gives rise to a vertical splitting stress at the upper right and the lower left corners of the opening, and a vertical compressive stress at the other two corners of the opening, with almost no stresses at the middle of the opening edges when the two chords have the same dimensions and as long as the opening edges are not cracked. The vertical location of the opening has a direct effect on determining the value of the splitting stress due to the vertical load, while the horizontal location has almost no effect on this stress.

10- The shear force at an opening in rectangular and I-beams is carried by the top and bottom chords of the opening according to the root ratio given by Eq. (7.2.1). However, for an opening in a non-symmetric section such as in a T- beam, the shear is distributed according to the inertia ratio.

11- Prestressed concrete beams with openings may collapse in different modes of failure according to the dimensions and locations of the opening and according to the reinforcement at the opening edges and chords. The failure may be: strut failure; mechanism failure; shear failure in the opening chords; or, tension failure of the tension chord.

For the dynamic study:

12- The fundamental frequency of a simply supported beam with shear openings is less than that for a solid beam. When the opening is located in the maximum bending field, the fundamental frequency exceeds that of the solid beam. The change in the fundamental frequency of such beams affects the overall response.

13- Having an opening in a location where there is a node (zero displacement) in a certain mode shape leads to a sudden reduction in the natural frequency associated with that mode shape.

14- Increasing the opening width or depth has the effect of decreasing the fundamental frequency of beams with a shear opening, while for beams with a bending opening, as the opening width increases, the fundamental frequency increases up to a certain limit, then it decreases with further increase in the opening width.

15- Horizontal location of an opening has a significant influence on the natural

frequencies of prestressed concrete continuous beams with openings. The fundamental frequency decreases significantly with increase in the opening width or depth when the opening is located in the maximum moment - maximum shear field, and especially for beams with unequal spans.

16- Examining the mode shapes of continuous two-span prestressed concrete beams with openings, shows that the maximum displacement occurs at the opening region even if the opening is located in the shear span of the longer span.

17- Having two openings in the same span of a two equal-span continuous beam effects a significant decrease in the third natural frequency, while in the case of one opening in each span, the first and second natural frequencies are significantly decreased.

18- Vierendeel action is quite evident in the deflected shape of the opening chords when the beam is subjected to harmonic loading.

19- The ratio of mid-span stresses for beams with openings to those of the solid beam, when they are subjected to harmonic loading, depends on the ratio between their natural frequencies.

20- Horizontal stress in the opening chords consist of two parts, one due to the primary moment resulting directly from the exciting load, and the second due to the

secondary moment, resulting from the shear force in the opening chords.

21- The modal analysis procedure presented herein gives an accurate method to determine the deflections and stresses at the critical sections outside the opening and in the vicinity of the opening, once the natural frequencies of beams with openings are determined.

8.3 Recommendations for Future Research:

Future research may include the following:

(1) The effect of the amount and arrangement of reinforcement around the opening on the behaviour of prestressed concrete beams with openings.

(2) The effective width of the flange in a T-beam which can be used in Eq. (7.2.1) so that the same equation can be applied not only to rectangular and I-beams but also for T-beams.

(3) The effect of lateral prestressing at the opening edges on the ultimate capacity of prestressed beams with openings.

(4) The behaviour of prestressed concrete beams with openings subjected to fatigue loading.

**Table 3.1 Characteristics of Rectangular Beams
Used in the Non-Linear Analysis**

BEAM IDENTIFICATION	BEAM DIMENSIONS		DIMENSIONS OF OPENING		LOCATION OF OPENING		ECCENTRICITY AND PRESTRESSING FORCE	
	H (in)	b (in)	W (in)	h (in)	l (in)	C (in)	e (in)	F (kip)
BI1A	10	4	12	3	39	5	1.57	31.2
BI1B	10	4	12	3	34	5	1.57	31.2
BI1C	10	4	12	3	29	5	1.57	31.2
BI2A	10	4	16	3	32	6	1.82	26.5
BI2B	10	4	16	3	32	5	1.82	26.5
BI2C	10	4	16	3	32	4	1.82	26.5
BI3A	10	4	12	3	34	5	1.57	31.2
BI3B	10	4	16	3	32	5	1.57	31.2
BI3C	10	4	20	3	30	5	1.57	31.2
BI4A	10	4	16	3	32	5	1.57	31.2
BI4B	10	4	16	4	32	5	1.57	31.2
BI4C	10	4	16	5	32	5	1.57	31.2

Note: 1 in.=25.4 mm; 1 kip=4.45 kN

Table 3.2 Characteristics of T- and I- Beams

Used in the Non-Linear Analysis

BEAM IDENTIFICATION	BEAM DIMENSIONS				DIMENSIONS OF OPENING		LOCATION OF OPENING		ECCENTRICITY AND PRESTRESSING FORCE	
	H (in)	b (in)	B (in)	t (in)	W (in)	h (in)	l (in)	C (in)	e (in)	F (kip)
BII1A	12	4	18	2	18	4	33	6.5	3.16	40.5
BII1B	12	4	18	2	18	4	27	6.5	3.16	40.5
BII1C	12	4	18	2	18	4	21	6.5	3.16	40.5
BII2A	12	4	18	2	18	4	27	6.5	3.16	40.5
BII2B	12	4	18	2	18	4	27	5.0	3.16	40.5
BII2C	12	4	18	2	18	4	27	3.5	3.16	40.5
BII3A	12	4	18	2	12	4	27	6.5	3.16	40.5
BII3B	12	4	18	2	18	4	27	6.5	3.16	40.5
BII3C	12	4	18	2	24	4	27	6.5	3.16	40.5
BII4A	12	4	18	2	18	3	27	6.5	3.16	40.5
BII4B	12	4	18	2	18	4	27	6.5	3.16	40.5
BII4C	12	4	18	2	18	5	27	6.5	3.16	40.5
BIII1A	14	4	18	2	18	5	27	7.0	2.44	66.1
BIII1B	14	4	18	2	18	5	23	7.0	2.44	66.1
BIII1C	14	4	18	2	18	5	18	7.0	2.44	66.1

Note: 1 in.=25.4 mm; 1 kip=4.45 kN

**Table 3.3 Characteristics of Beams with Rectangular Section
(Parametric Study for Shear Distribution)**

BEAM IDENTIFICATION	BEAM DIMENSIONS		DIMENSIONS OF OPENING		LOCATION OF OPENING	
	H (in)	b (in)	W (in)	h (in)	l (in)	C (in)
R ₁	10	4	12	3	19	2.5
R ₂	10	4	12	3	19	4.0
R ₃	10	4	12	3	19	4.5
R ₄	10	4	12	3	19	5.5
R ₅	10	4	12	3	19	6.0
R ₆	10	4	16	3	17	2.5
R ₇	10	4	16	3	17	3.0
R ₈	10	4	16	3	17	3.5
R ₉	10	4	16	3	17	4.0
R ₁₀	10	4	16	3	17	4.5
R ₁₁	10	4	16	3	17	5.5
R ₁₂	10	4	16	3	17	6.0
R ₁₃	10	4	16	3	17	6.5
R ₁₄	10	4	20	3	15	2.5
R ₁₅	10	4	20	3	15	4.0
R ₁₆	10	4	20	3	15	4.5
R ₁₇	10	4	20	3	15	5.5
R ₁₈	10	4	20	3	15	6.0

Note: 1 in. = 25.4 mm

**Table 3.4: Characteristics of Beams with T- and I- Section
(Parametric Study for Shear Distribution)**

BEAM IDENTIFICATION	BEAM DIMENSIONS			DIMENSIONS OF OPENING		LOCATION OF OPENING	
	H (in)	b (in)	B (in)	W (in)	h (in)	l (in)	C (in)
T ₁	12	4	18	18	4	15	5.5
T ₂	12	4	18	18	4	15	6.5
T ₃	12	4	18	18	4	15	7.5
T ₄	12	4	18	18	3.5	15	5.75
T ₅	12	4	18	18	3.5	15	6.75
I ₁	14	4	18	18	4	24	4.5
I ₂	14	4	18	18	4	24	5.5
I ₃	14	4	18	18	4	24	6.5
I ₄	14	4	18	18	4	24	7.5

Note: 1 in. = 25.4 mm

TABLE 4.1 Characteristics of the Tested Rectangular Beams

BEAM IDENTIFICATION	BEAM DIMENSIONS		DIMENSIONS OF OPENING		LOCATION OF OPENING		ECCENTRICITY AND PRESTRESSING FORCE		CONCRETE COMPRESSIVE STRENGTH
	H (in)	b (in)	W (in)	h (in)	l (in)	C (in)	e (in)	F (kip)	
BI1A	10	4	12	3	39	5	1.428	33.4	5900
BI1B, BI3A	10	4	12	3	34	5	1.566	31.19	6300
BI2A	10	4	16	3	32	6	1.824	26.5	7200
BI2B, BI3B	10	4	16	3	32	5	1.888	31.78	6200
BI2C	10	4	16	3	32	4	1.87	26.18	6600
BI3C	10	4	20	3	30	5	1.77	26.0	6100

Note: 1 in=25.4 mm; 1 kip=4.45 kN; 1 psi=6.89 kPa

TABLE 4.2 Characteristics of the Tested T- and I- Beams

BEAM IDENTIFICATION	BEAM DIMENSIONS				DIMENSIONS OF OPENING		LOCATION OF OPENING		ECCENTRICITY AND PRESTRESSING FORCE		CONCRETE COMPRESSIVE STRENGTH
	H (in)	b (in)	B (in)	t (in)	W (in)	h (in)	l (in)	C (in)	e (in)	F (kip)	
BI11A	12	4	18	2	18	4	33	6.5	3.34	43.56	6330
BI11B, BI12A BI13B, BI14B	12	4	18	2	18	4	27	6.5	3.23	38.43	7780
BI11C	12	4	18	2	18	4	21	6.5	3.16	40.46	7700
BI12B	12	4	18	2	18	4	27	5	3.31	38.84	7000
BI14C	12	4	18	2	18	5	27	6.5	2.8	42.44	7200
BI11A	14	4	18	2	18	5	27	7	2.44	66.11	6800
BI11C	14	4	18	2	18	5	18	7	2.18	60.66	6020

Note: 1 in=25.4 mm; 1 kip=4.45 kN; 1 psi=6.89 kPa

Table 6.1 Percentage Change In First Three Natural Frequencies as Compared to Those of Solid Beam

Type of Cross Section	Natural Frequency	Percentage Change in Frequency					
		Opening in Shear Span		Opening in Mid-Span		Opening Close to Interior Support	
		Equal	Unequal	Equal	Unequal	Equal	Unequal
Rectangular-Section	ω_1	-7	-9	+5	+7	-10	-26
	ω_2	-3	-1	+2	-37	-20	+1
	ω_3	+1	-4	-34	-7	+1	-20
T-Section	ω_1	-9	-13	-1	-4	-13	-27
	ω_2	-5	-5	-4	-34	-19	-7
	ω_3	-4	-3	-34	-4	-7	-11
I-Section	ω_1	-13	-16	+1	-3	-24	-36
	ω_2	-5	-9	-8	-39	-17	-8
	ω_3	-12	-6	-26	-4	-11	-11

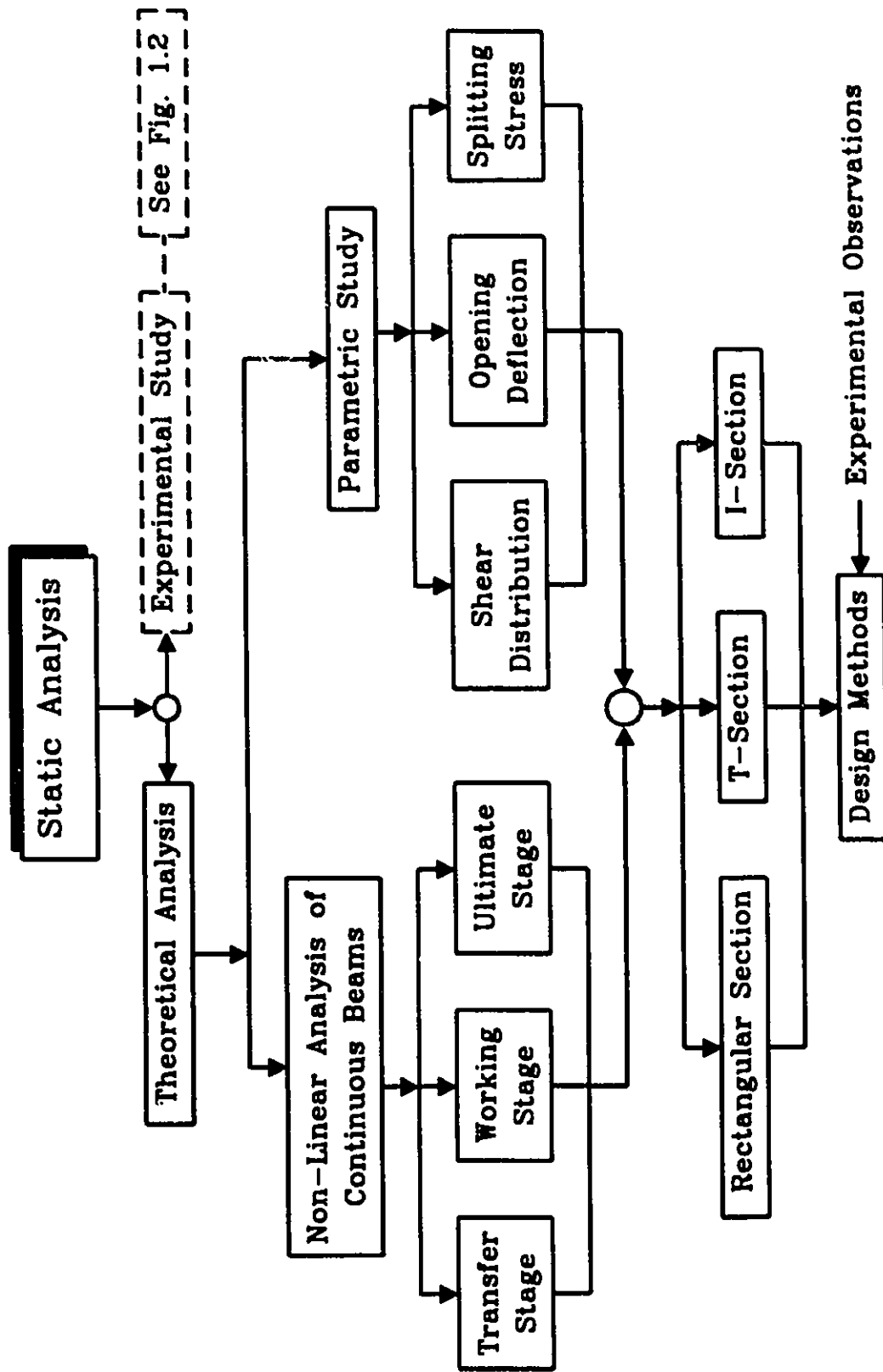
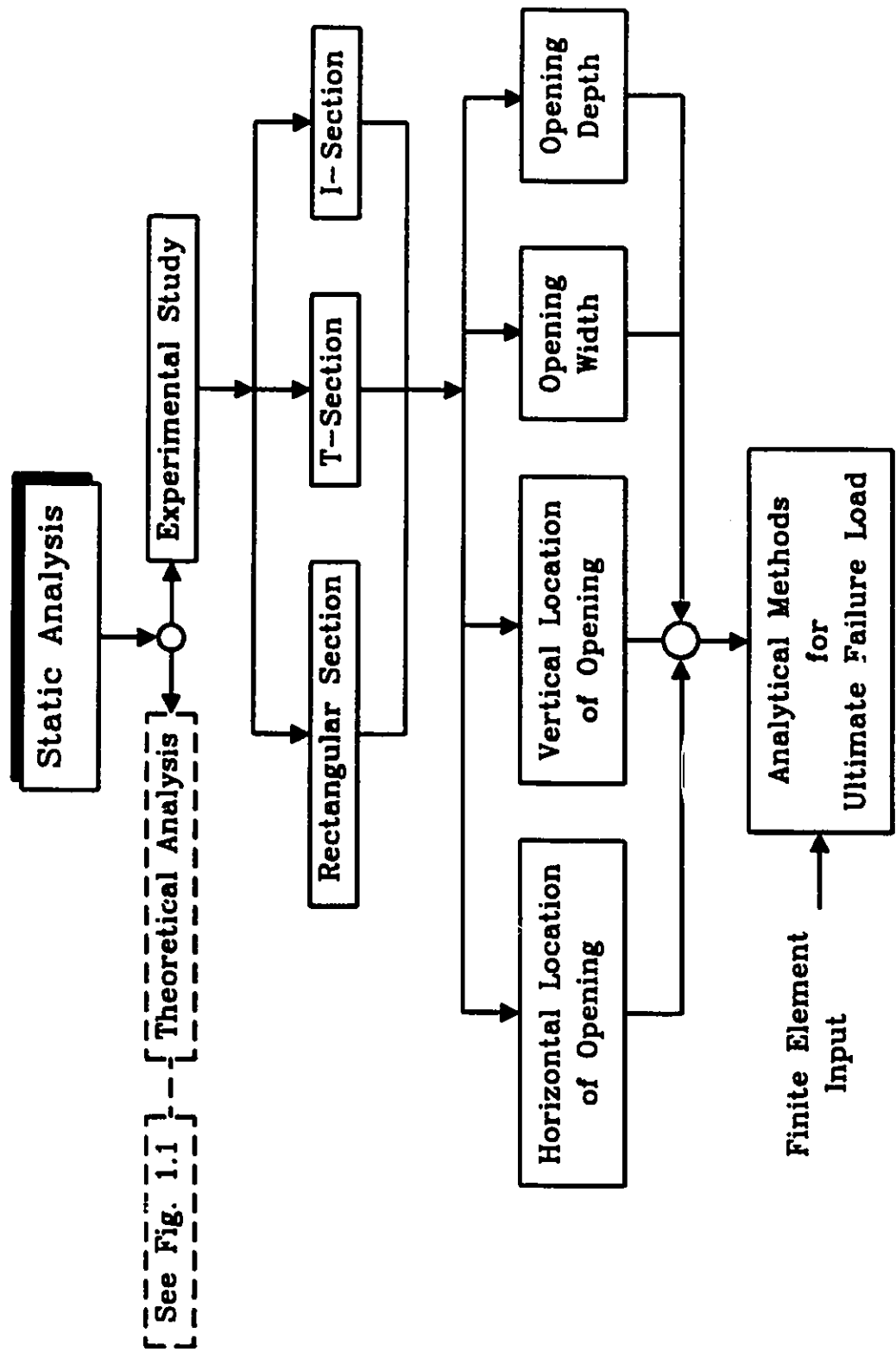


FIG. 1.1 STATIC ANALYSIS LAYOUT (THEORETICAL ANALYSIS)



[See Fig. 1.1] -- [Theoretical Analysis]

FIG. 1.2 STATIC ANALYSIS LAYOUT (EXPERIMENTAL STUDY)

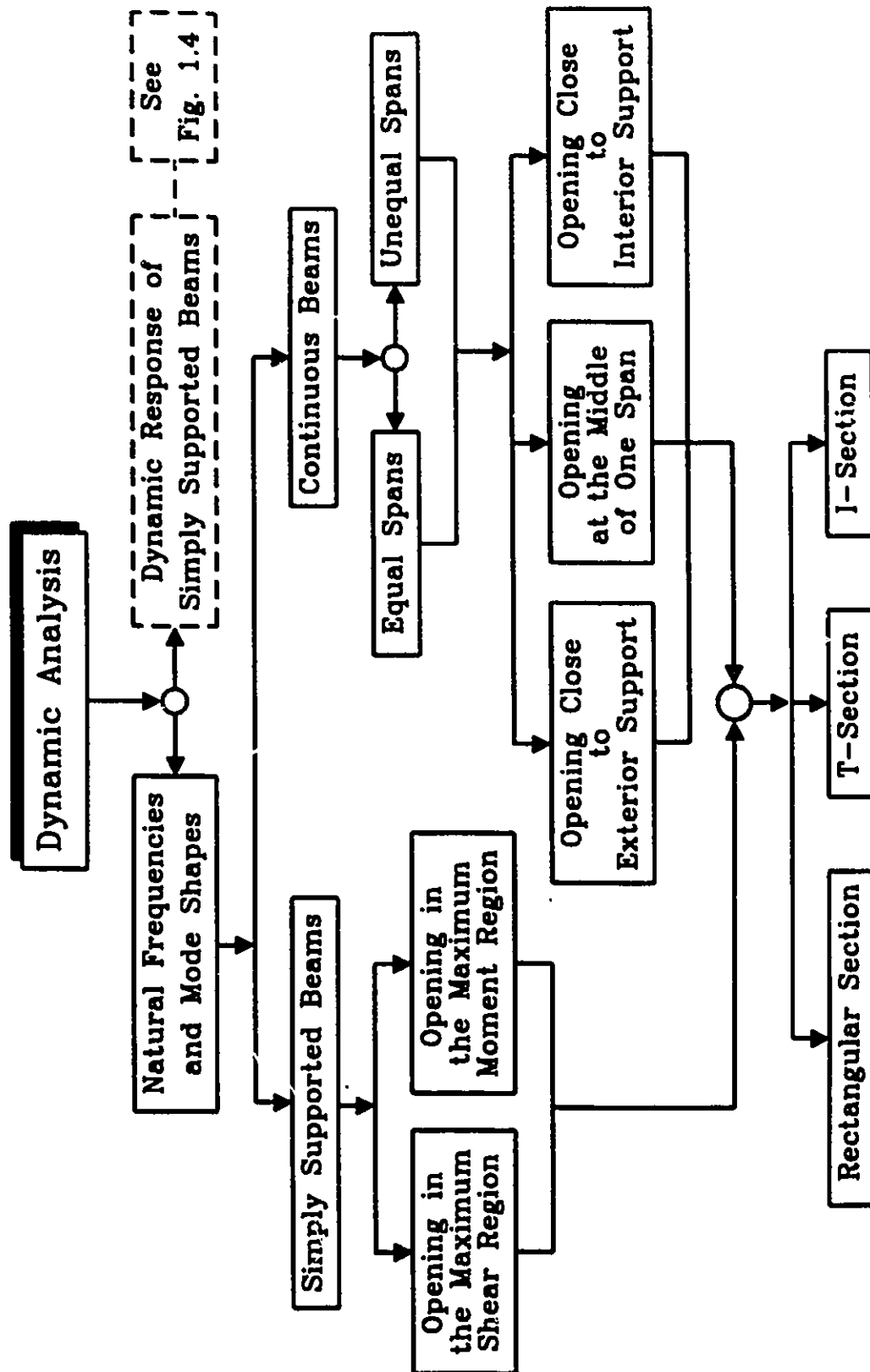


FIG. 1.3 DYNAMIC ANALYSIS LAYOUT (NATURAL FREQUENCIES)

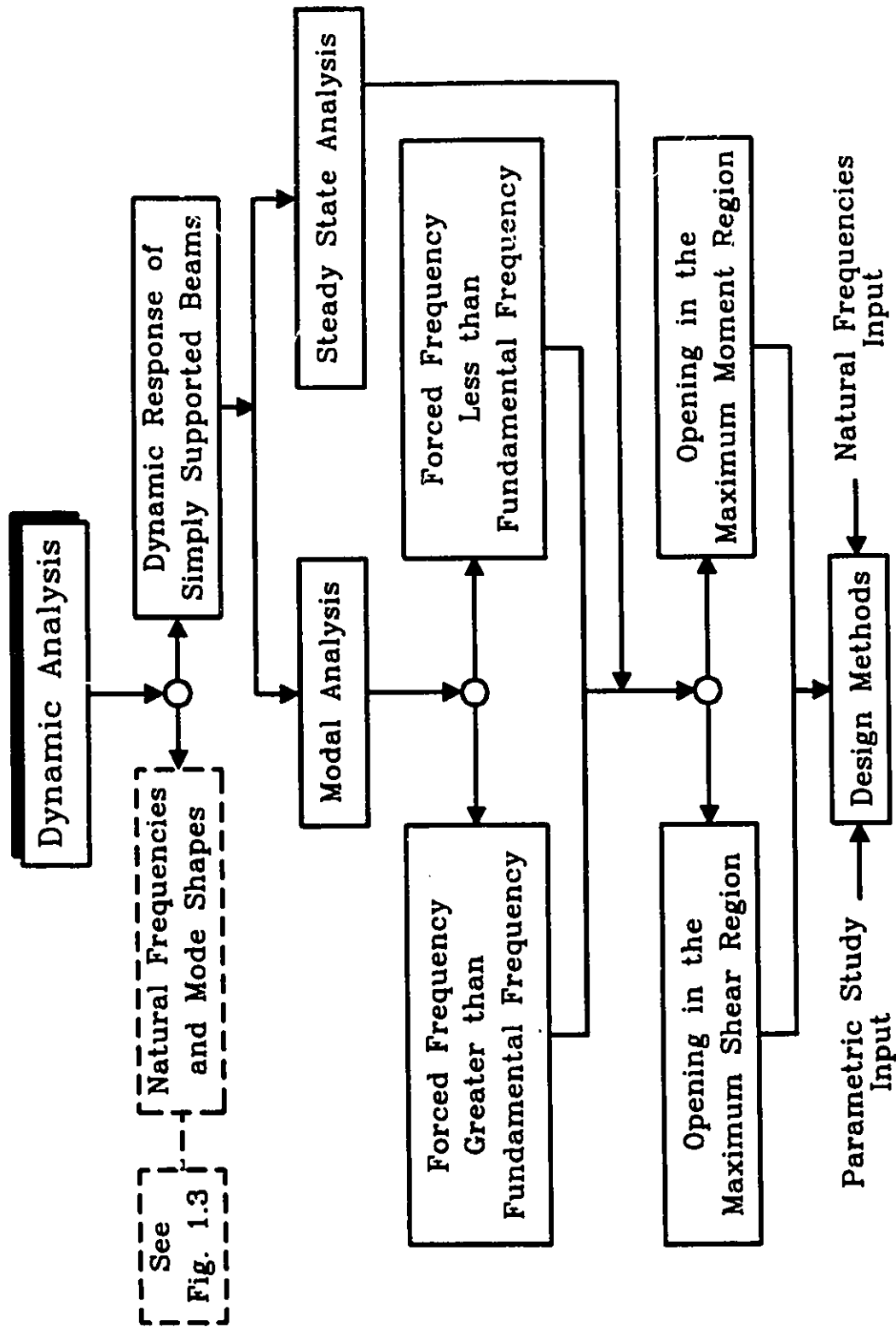


FIG. 1.4 DYNAMIC ANALYSIS LAYOUT (DYNAMIC RESPONSE)

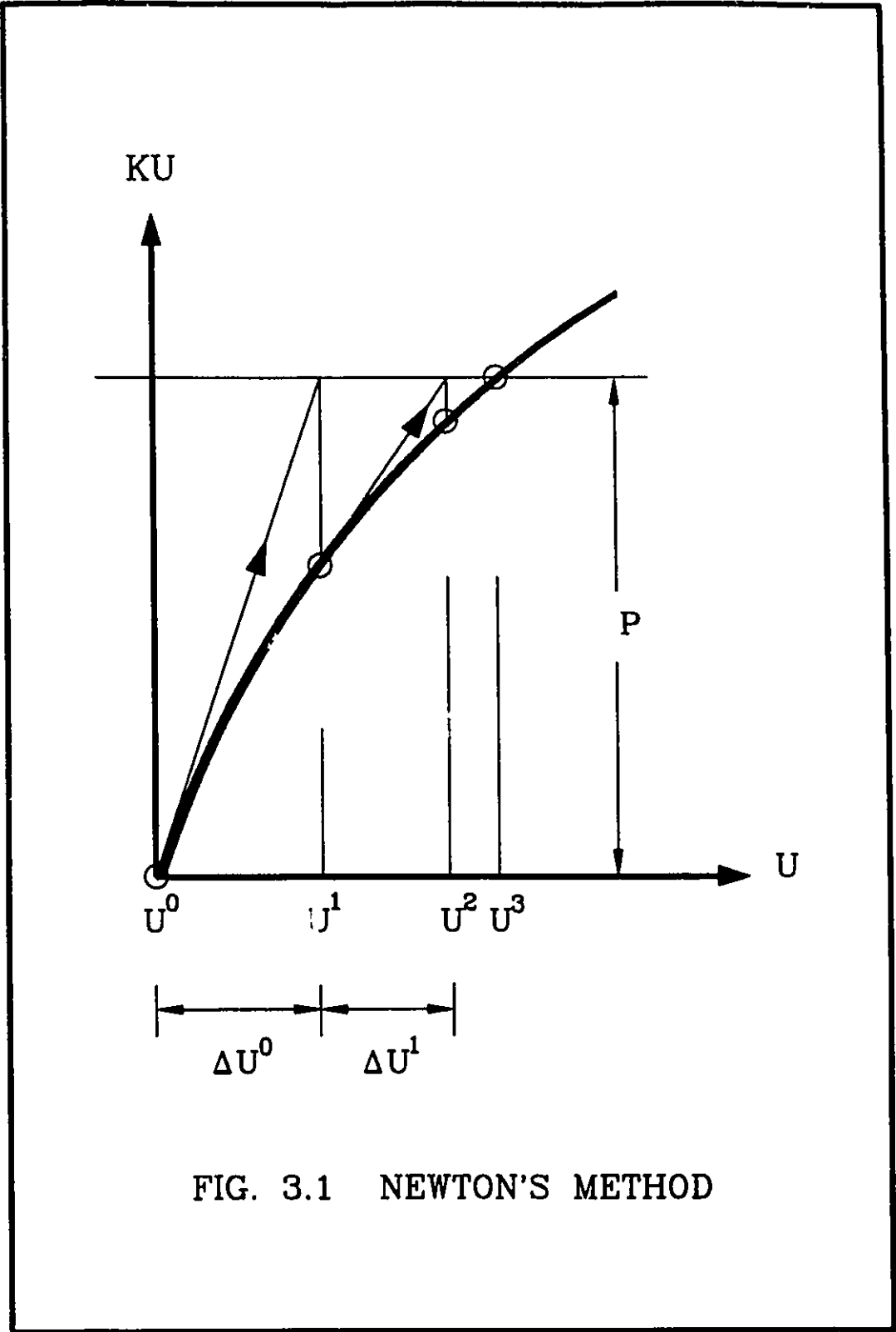
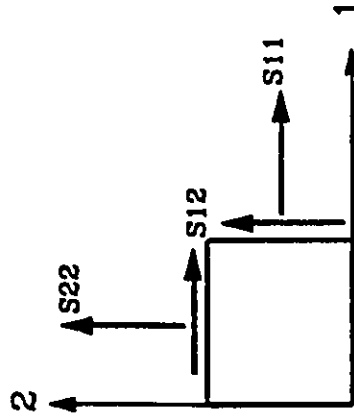
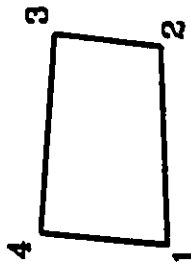
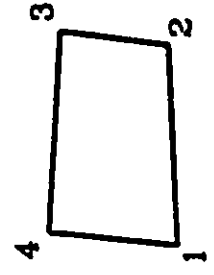
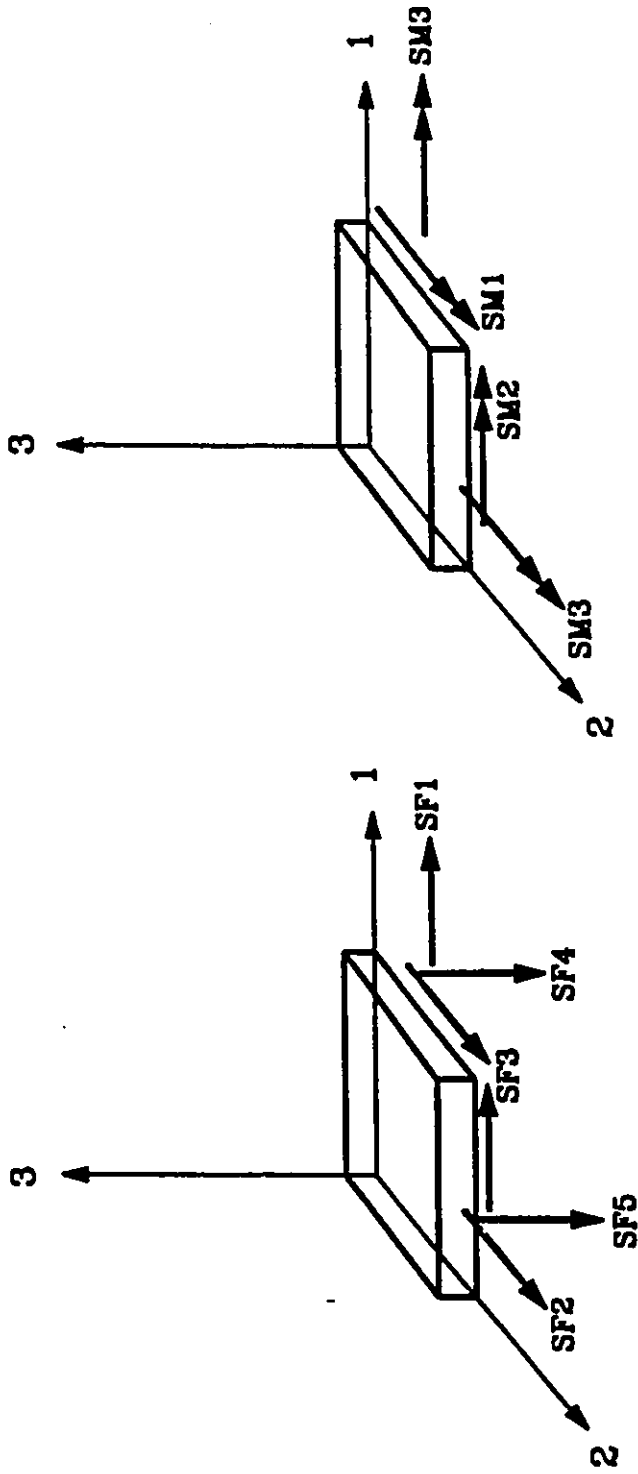


FIG. 3.1 NEWTON'S METHOD



- Four Nodes Element
- Degrees of Freedom : U_1, U_2
- Output Stresses : S_{11}, S_{22}, S_{12}
- REBAR Option Available in Two Directions

FIG. 3.2 PLANE STRESS ELEMENT CPS4



- Four Nodes Element
- Degrees of Freedom : $U_1, U_2, U_3, \Phi_1, \Phi_2, \Phi_3$
- Output Forces : $SF_1, SF_2, SF_3, SF_4, SF_5$
- Output Moments : SM_1, SM_2, SM_3
- Stress Components : S_{11}, S_{22}, S_{12}
- REBAR Option Available in Two Directions

FIG. 3.3 SHELL ELEMENT S4R

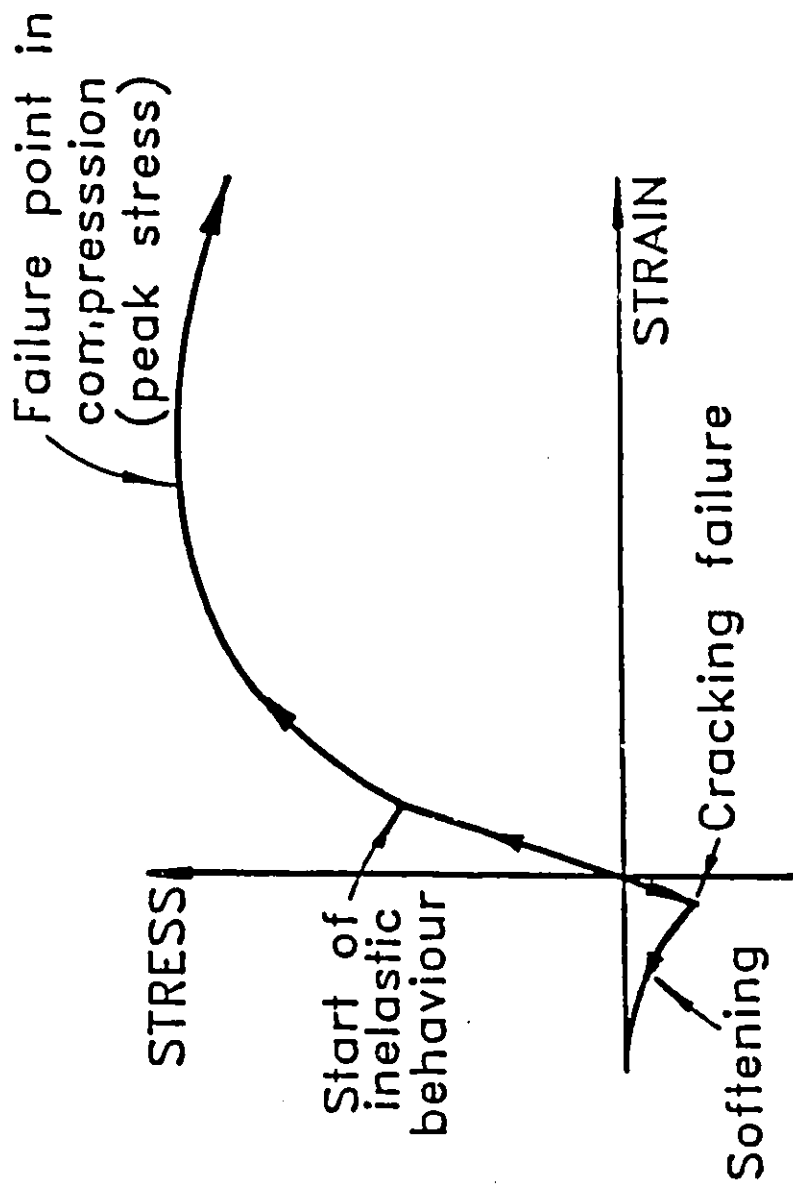


FIG. 3.4 UNIAXIAL BEHAVIOUR OF PLAIN CONCRETE

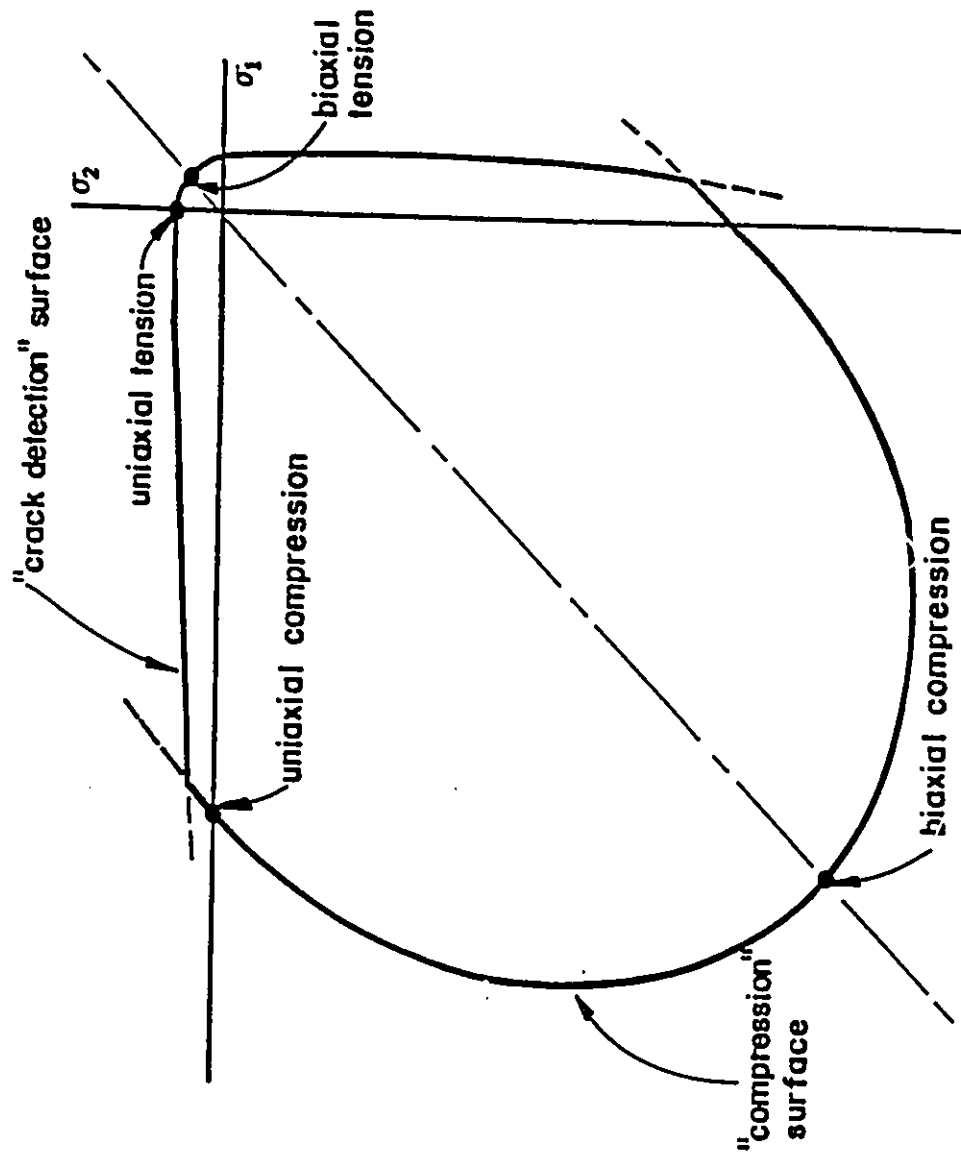


FIG. 3.5 YIELD AND FAILURE SURFACES OF CONCRETE IN PLANE STRESS

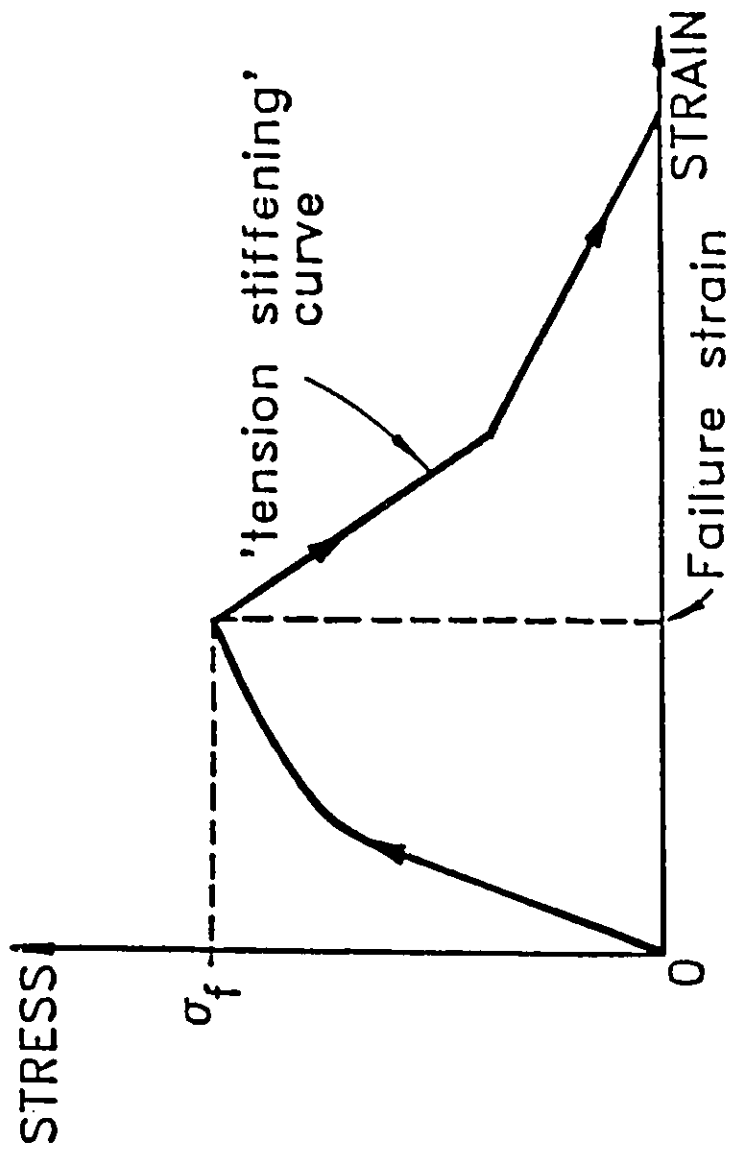
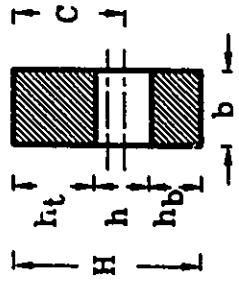


FIG. 3.6 TENSION STIFFENING OF CONCRETE



SEC. X-X

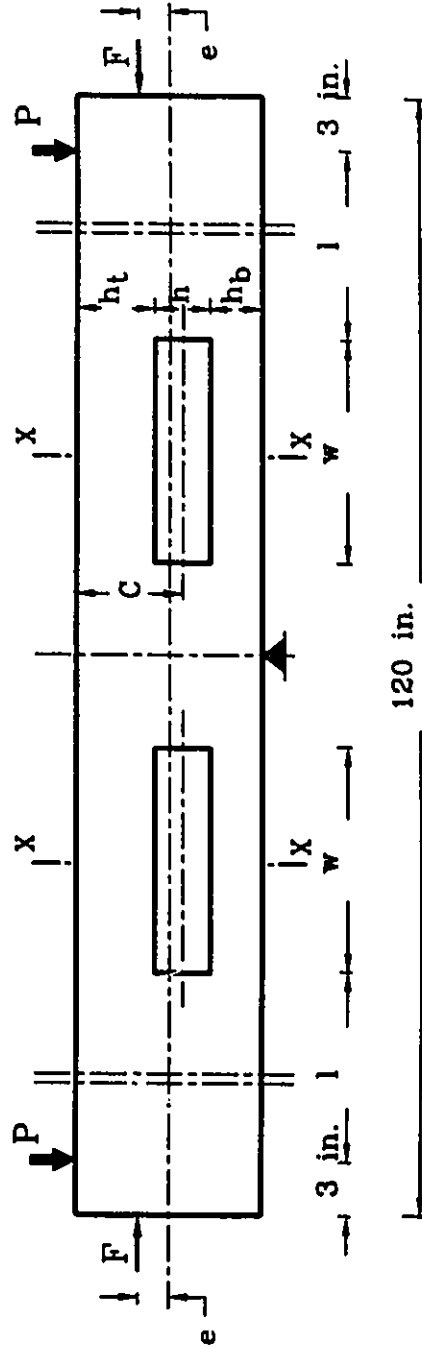


FIG. 3.7 TYPICAL RECTANGULAR BEAM LAYOUT

Note: 1 in.=25.4 mm

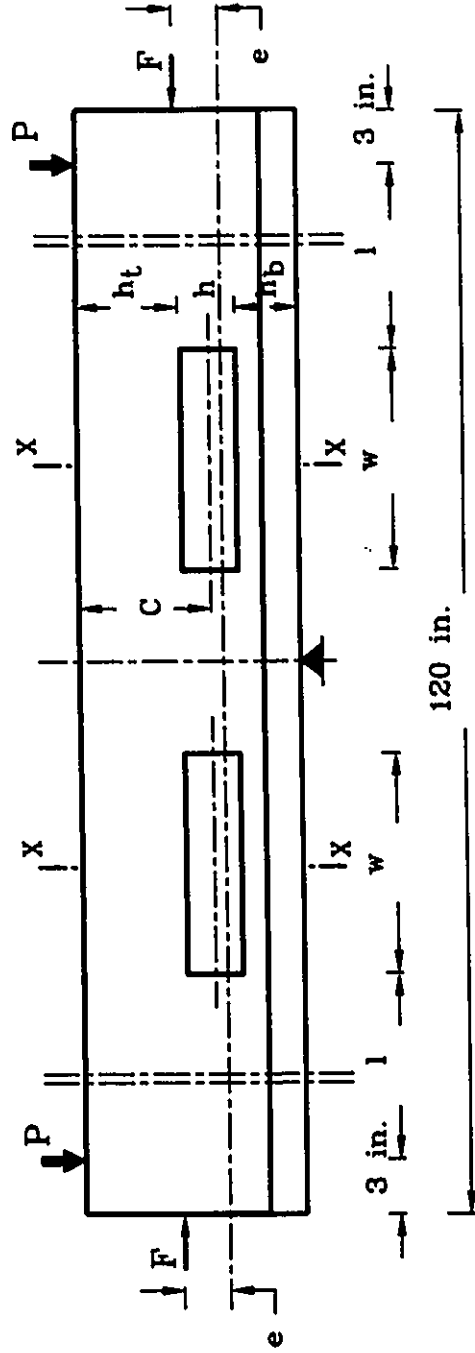
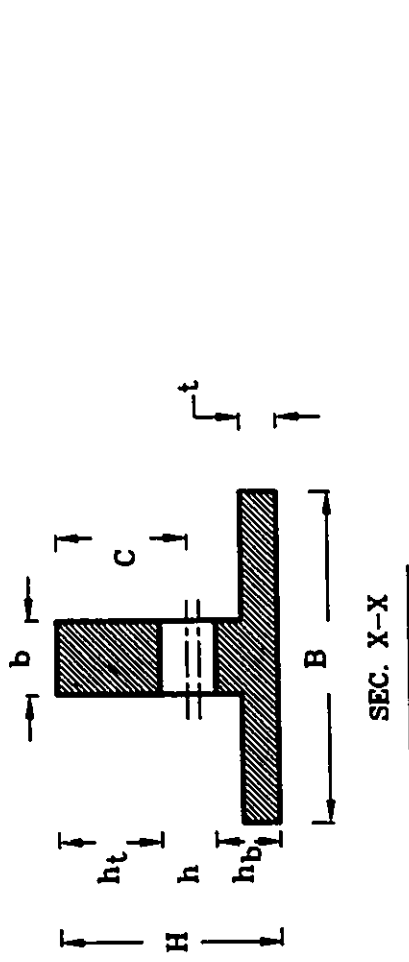
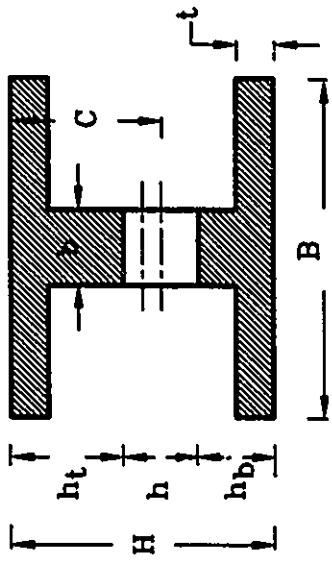


FIG. 3.8 TYPICAL T-BEAM LAYOUT

Note: 1 in.=25.4 mm



SEC. X-X

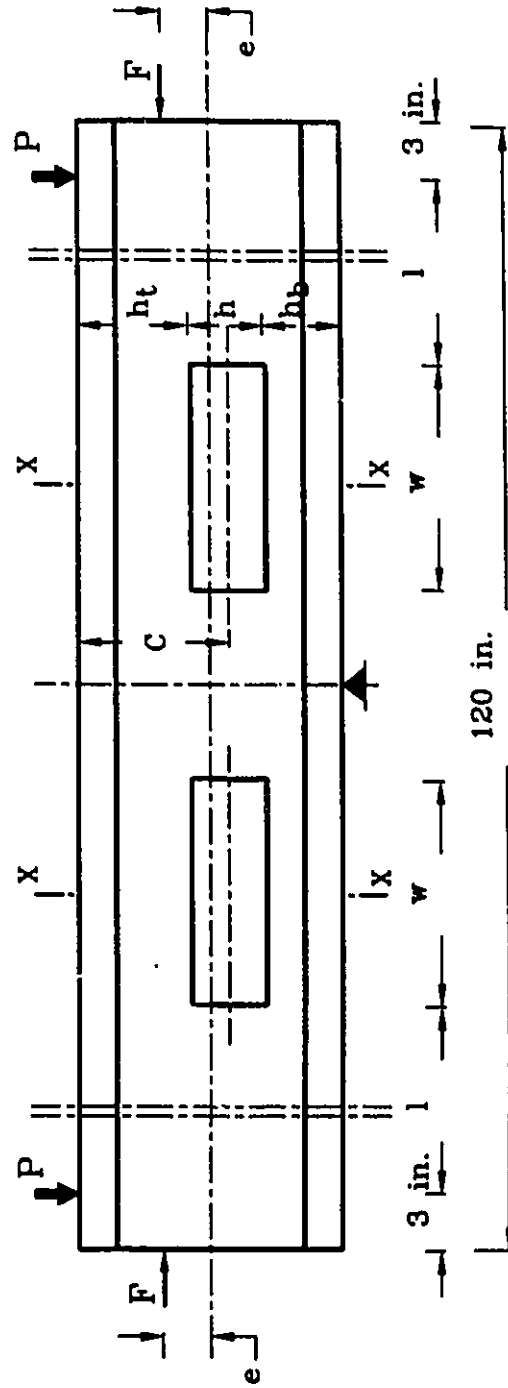


FIG. 3.9 TYPICAL I-BEAM LAYOUT

Note: 1 in.=25.4 mm

	(I) Rectangular Beams	(II) T-Beams	(III) I-Beams
Horizontal (1) Location of Opening	BI1A (M/VH = 4.5) BI1B (M/VH = 4.0) BI1C (M/VH = 3.5)	BII1A (M/VH = 3.5) BII1B (M/VH = 3.0) BII1C (M/VH = 2.5)	BIII1A (M/VH = 2.6) BIII1B (M/VH = 2.3) BIII1C (M/VH = 1.9)
Vertical (2) Location of Opening	BI2A (C = 6.0 in.) BI2B (C = 5.0 in.) BI2C (C = 4.0 in.)	BII2A (C = 6.5 in.) BII2B (C = 5.0 in.) BII2C (C = 3.5 in.)	
Width (3) of Opening	BI3A (W = 12 in.) BI3B (W = 16 in.) BI3C (W = 20 in.)	BII3A (W = 12 in.) BII3B (W = 18 in.) BII3C (W = 24 in.)	
Depth (4) of Opening	BI4A (h = 3 in.) BI4B (h = 4 in.) BI4C (h = 5 in.)	BII4A (h = 3 in.) BII4B (h = 4 in.) BII4C (h = 5 in.)	

Note: 1 in. = 25.4 mm

FIG. 3.10 DEFINITION OF THE BEAMS USED IN THE NON-LINEAR ANALYSIS

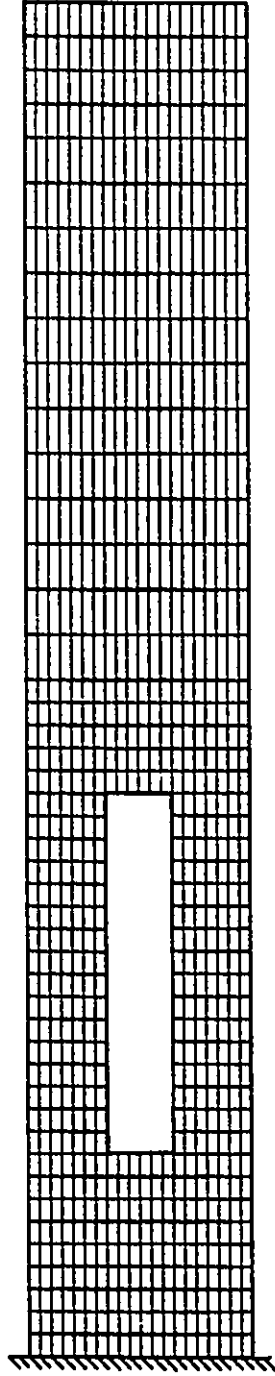


FIG. 3.11 TYPICAL FINITE ELEMENT MESH FOR A RECTANGULAR BEAM

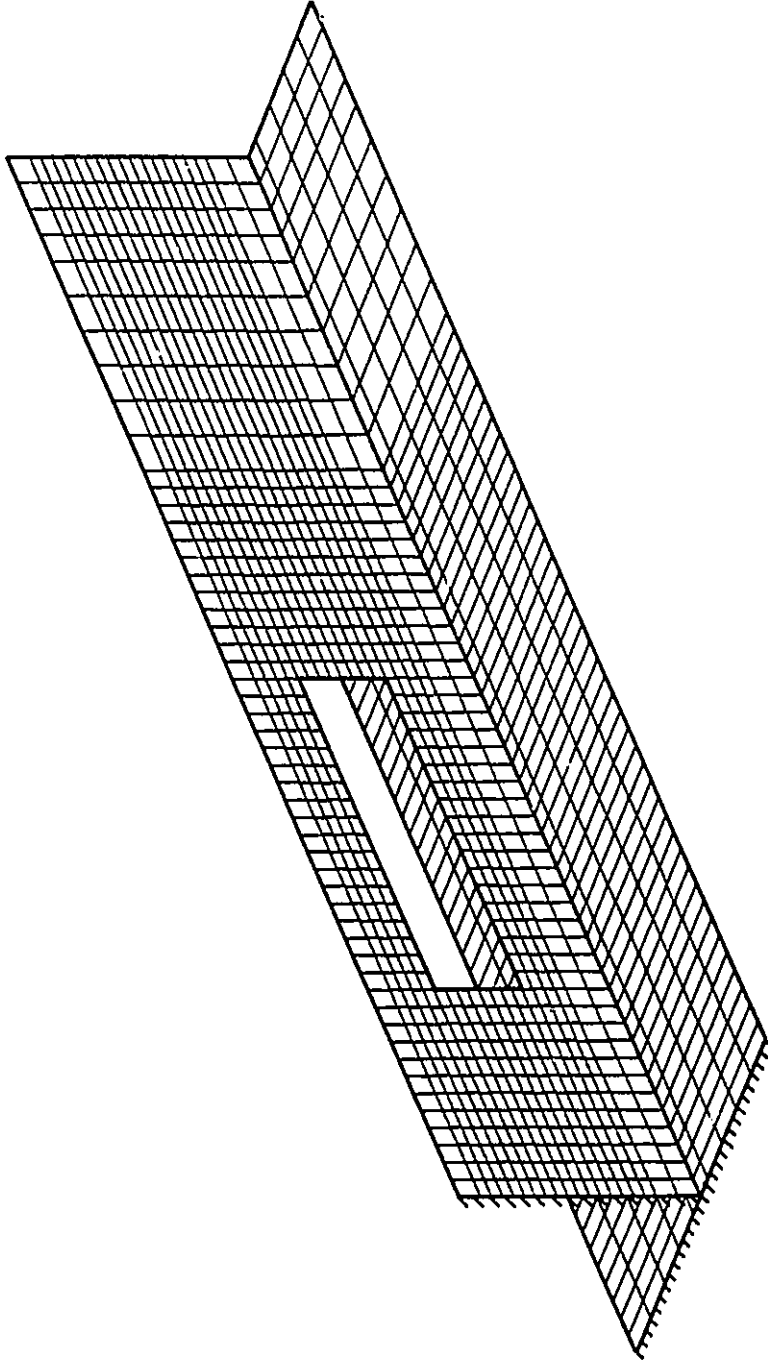


FIG. 3.12 TYPICAL FINITE ELEMENT MESH FOR A T-BEAM

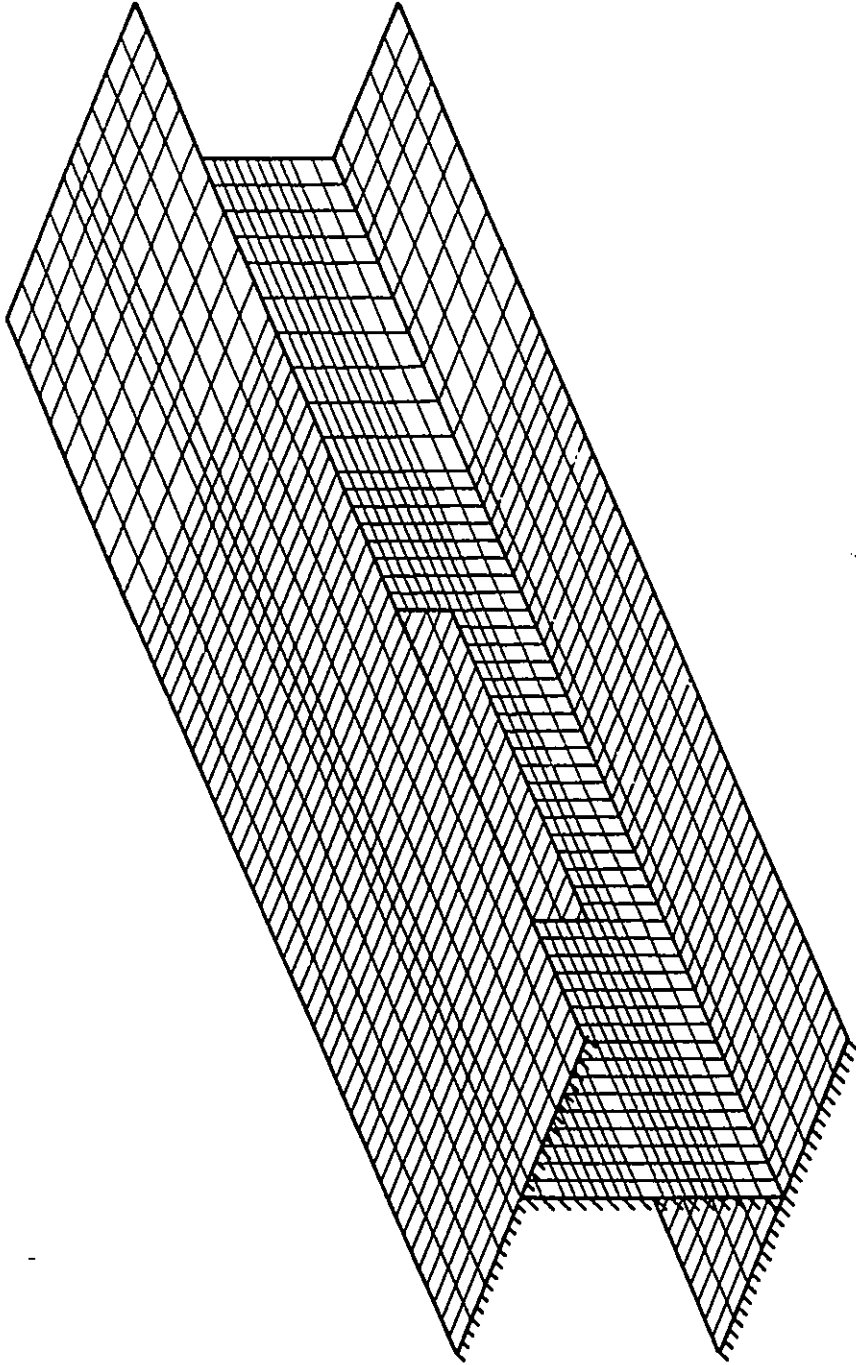
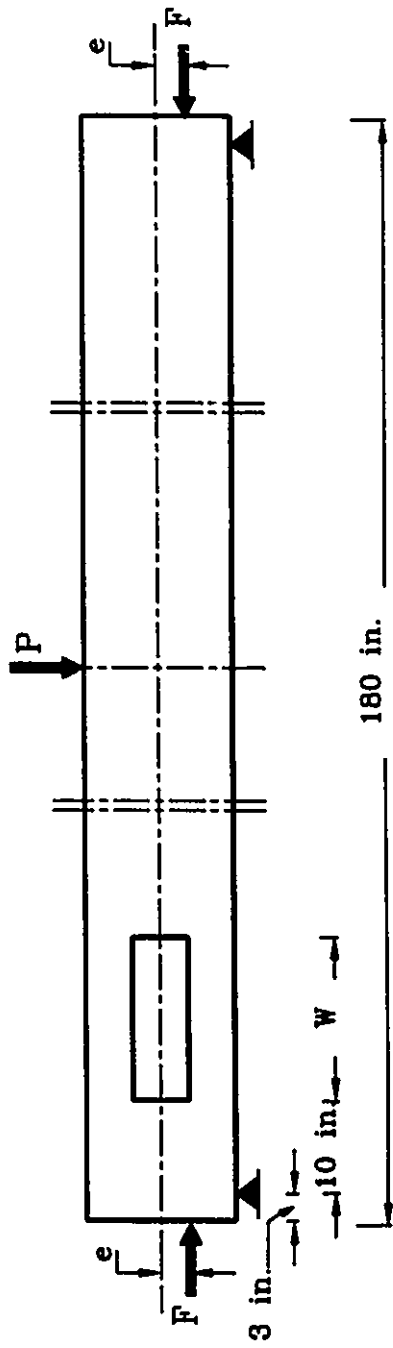
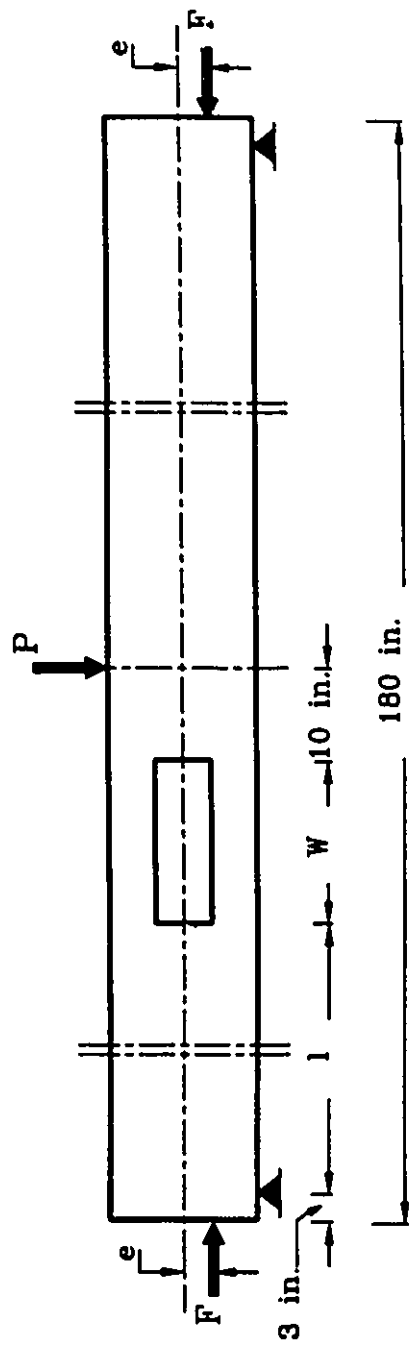


FIG. 3.13 TYPICAL FINITE ELEMENT MESH FOR AN I-BEAM



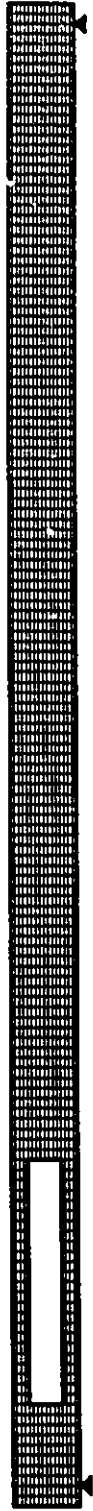
(a)



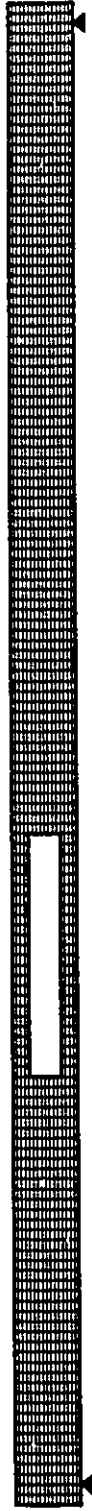
(b)

FIG. 3.14 SIMPLY SUPPORTED BEAMS USED IN THE DYNAMIC ANALYSIS
 (a) OPENING IN HIGH SHEAR REGION; AND (b) OPENING IN HIGH MOMENT REGION

Note: 1 in. = 25.4 mm

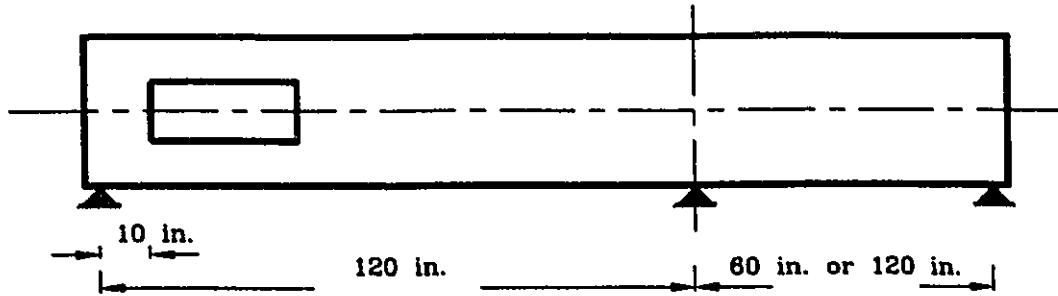


(a)

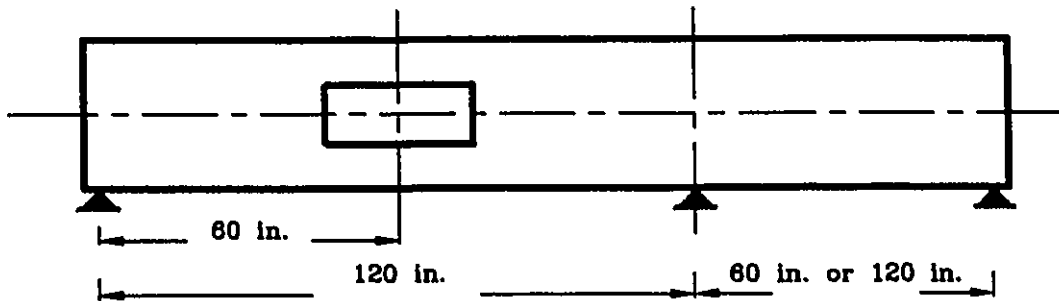


(b)

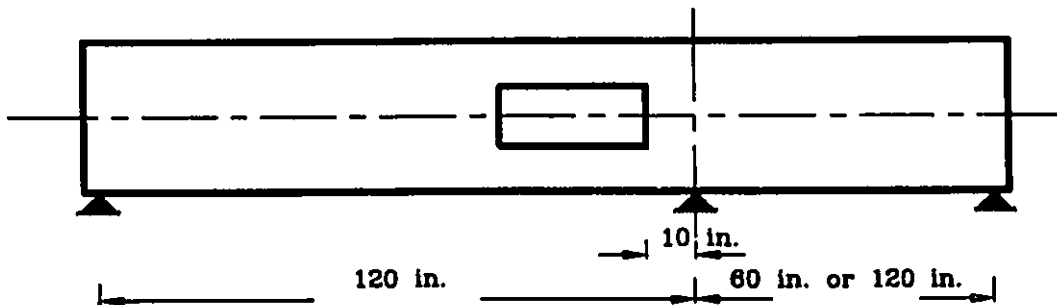
FIG. 3.15 TYPICAL FINITE ELEMENT MESH FOR A SIMPLY SUPPORTED BEAM
(a) WITH OPENING IN HIGH SHEAR REGION; AND (b) WITH OPENING IN HIGH MOMENT REGION



(a)



(b)



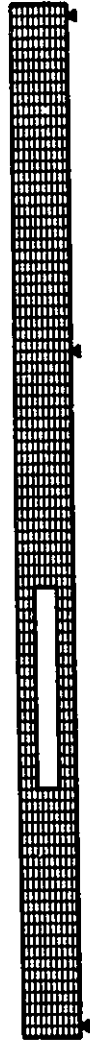
(c)

FIG. 3.16 OPENING LOCATIONS IN THE ANALYZED CONTINUOUS BEAMS

Note: 1 in.=25.4 mm



(a)



(b)

FIG. 3.17 TYPICAL FINITE ELEMENT MESH FOR A CONTINUOUS BEAM

(a) WITH EQUAL SPANS; AND (b) WITH UNEQUAL SPANS

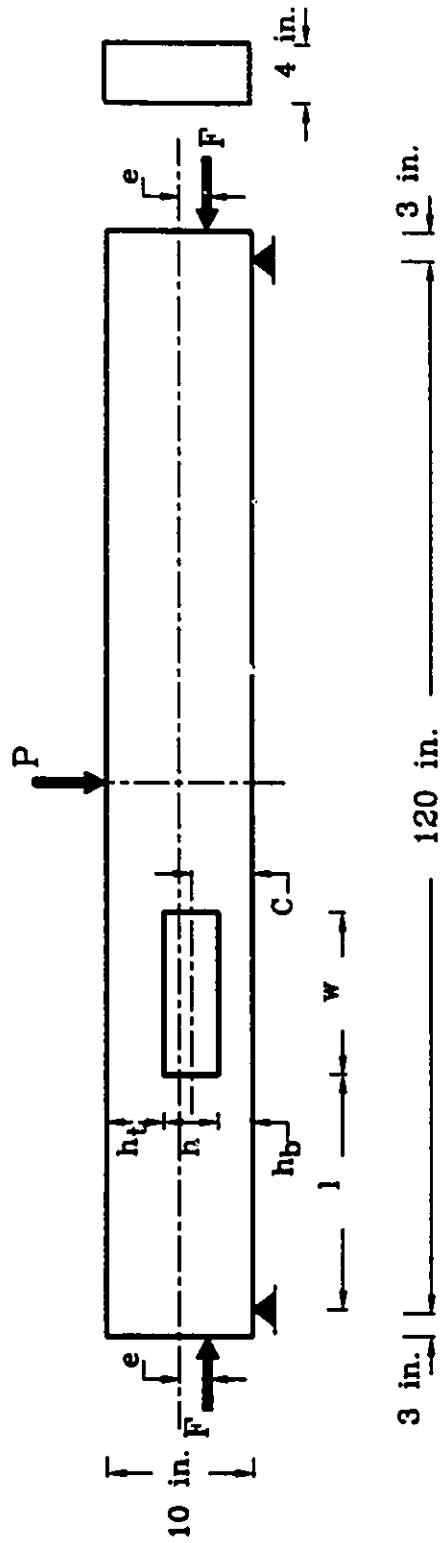


FIG. 3.18 TYPICAL LAYOUT OF SIMPLY SUPPORTED BEAMS
USED IN THE PARAMETRIC STUDY

Note: 1 in. = 25.4 mm

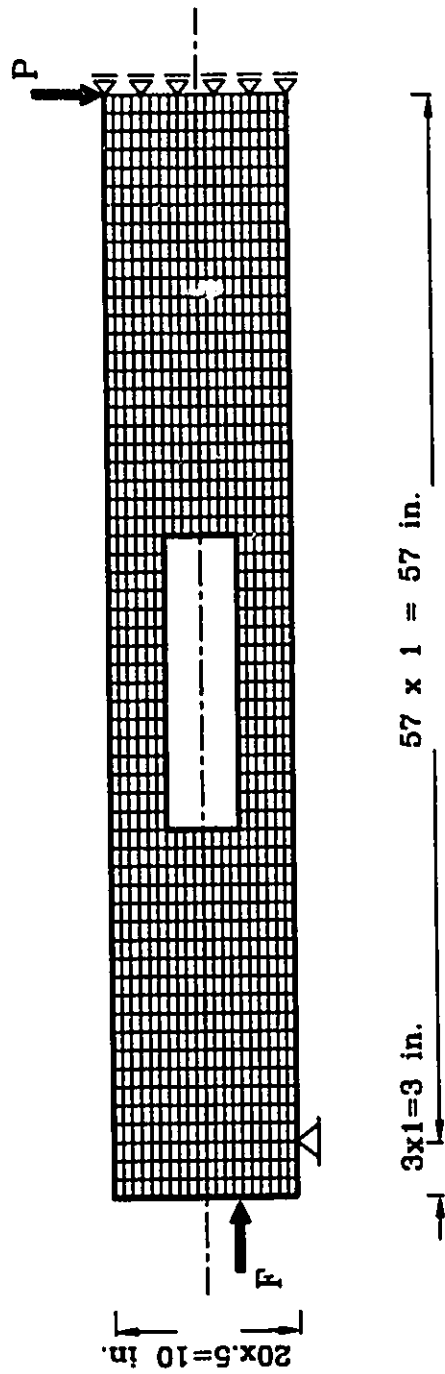


FIG. 3.19 TYPICAL FINITE ELEMENT MESH
 FOR SIMPLY SUPPORTED BEAM

Note: 1 in. = 25.4 mm

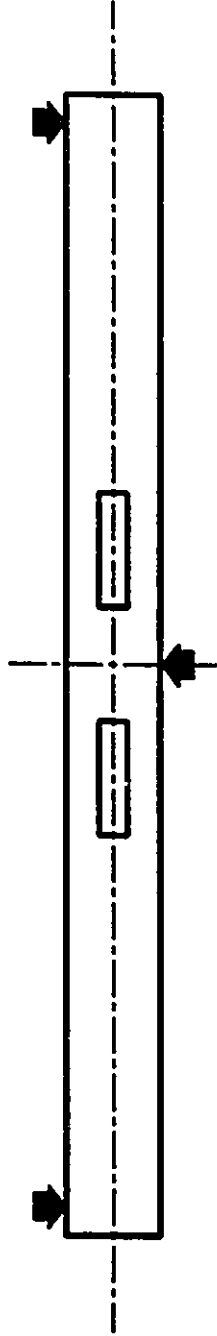


FIG. 4.1 a TEST ARRANGEMENT TO STUDY THE EFFECT OF CONTINUITY

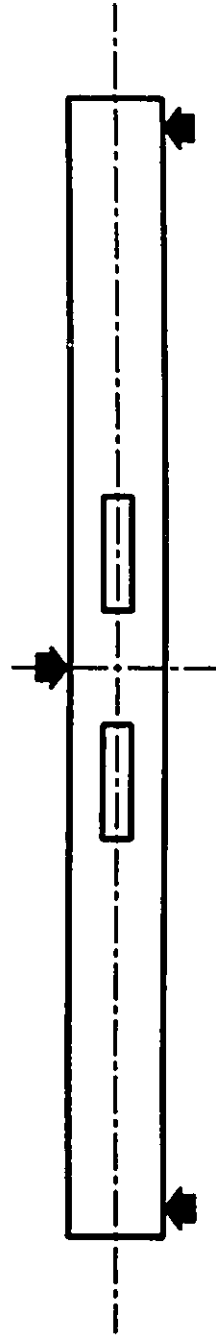


FIG. 4.1 b ACTUAL TEST ARRANGEMENT TO SIMULATE (a) ABOVE



FIG. 4.2 TEST SET-UP FOR A RECTANGULAR BEAM



FIG. 4.3 TEST SET-UP FOR A T-BEAM



FIG. 4.4 TEST SET-UP FOR AN I-BEAM

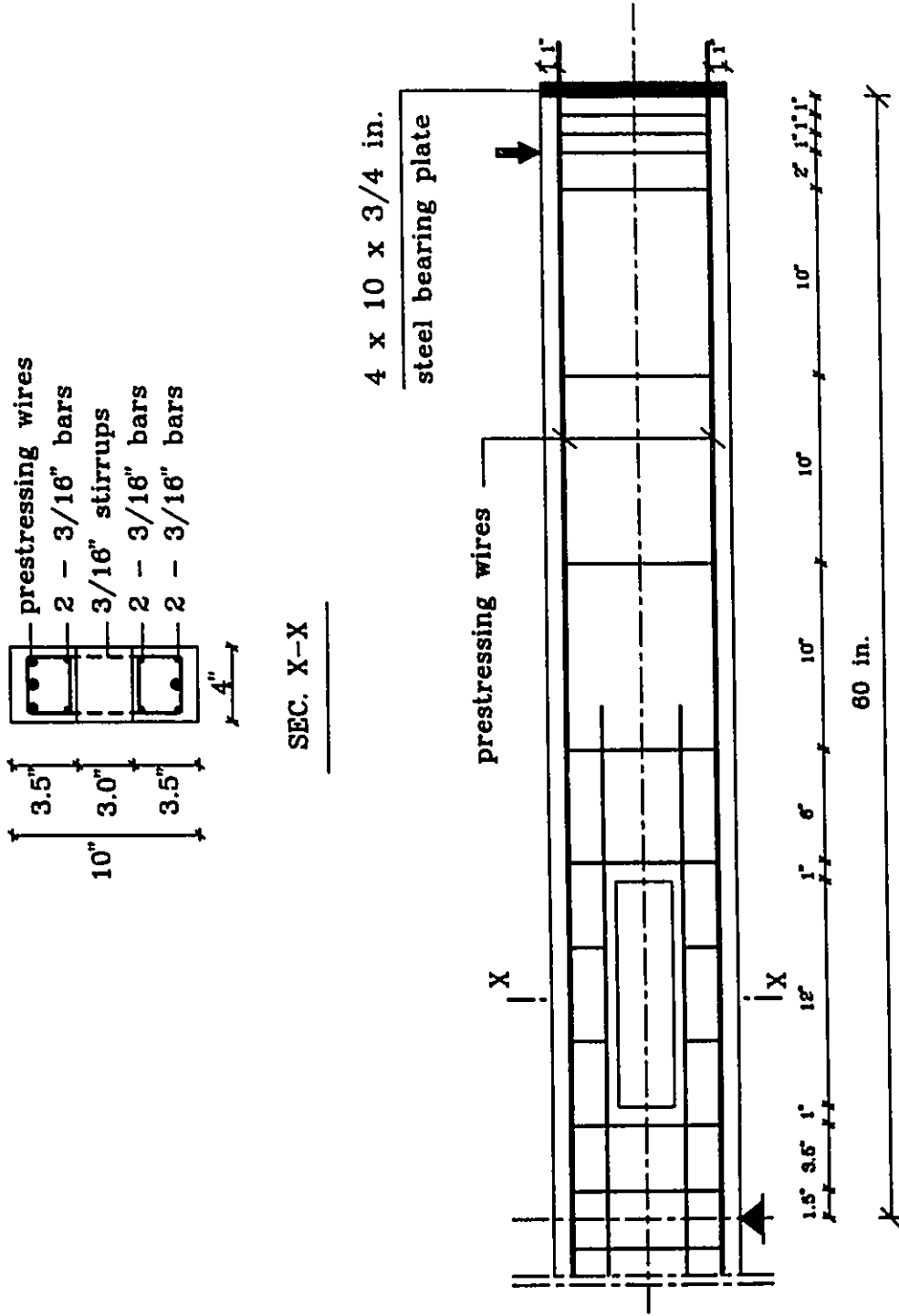


FIG. 4.5 REINFORCEMENT DETAILS FOR BEAM BI1A

Note: 1 in. = 25.4 mm

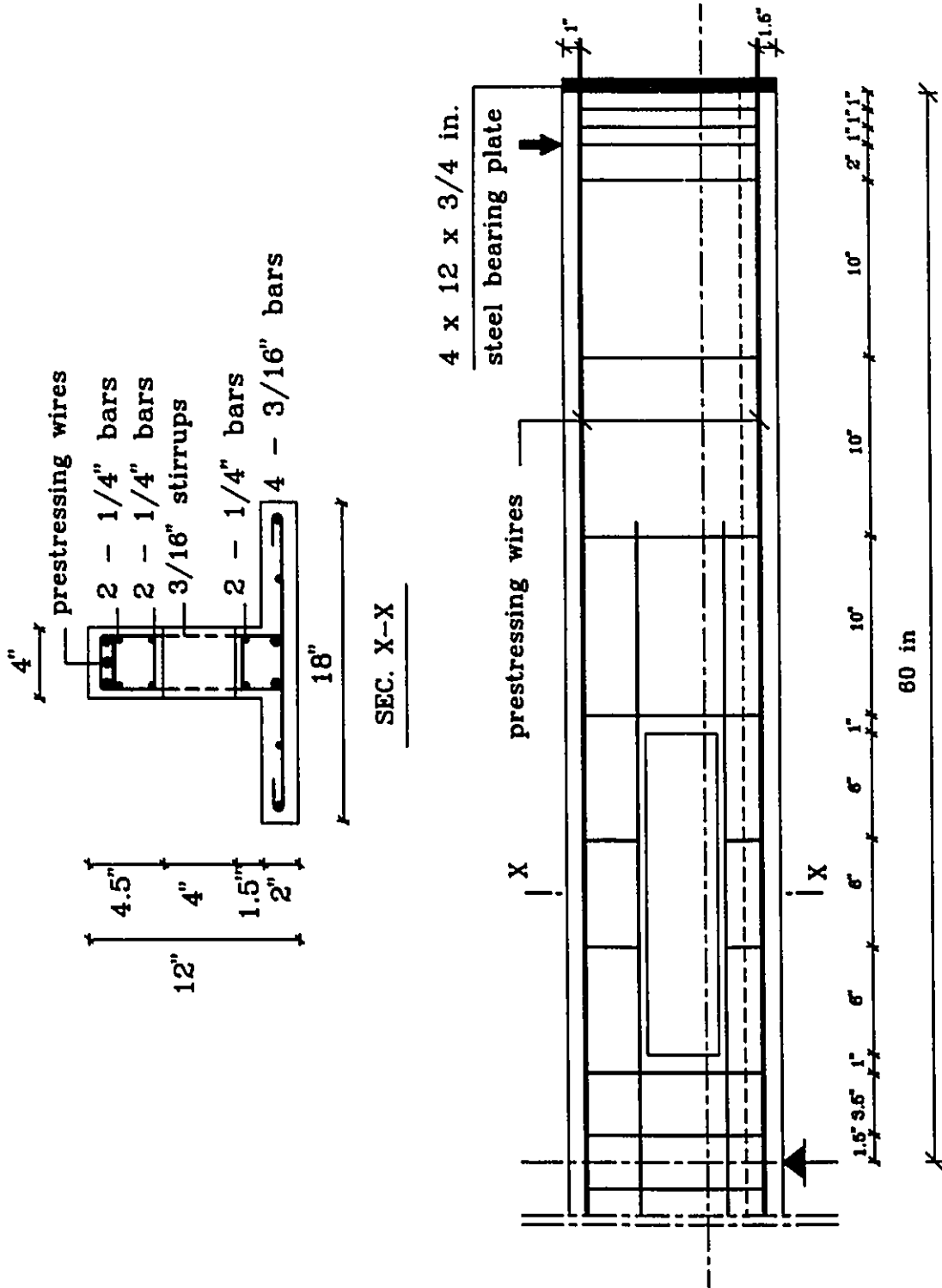


FIG. 4.6 REINFORCEMENT DETAILS FOR BEAM BIII1A

Note: 1 in. = 25.4 mm

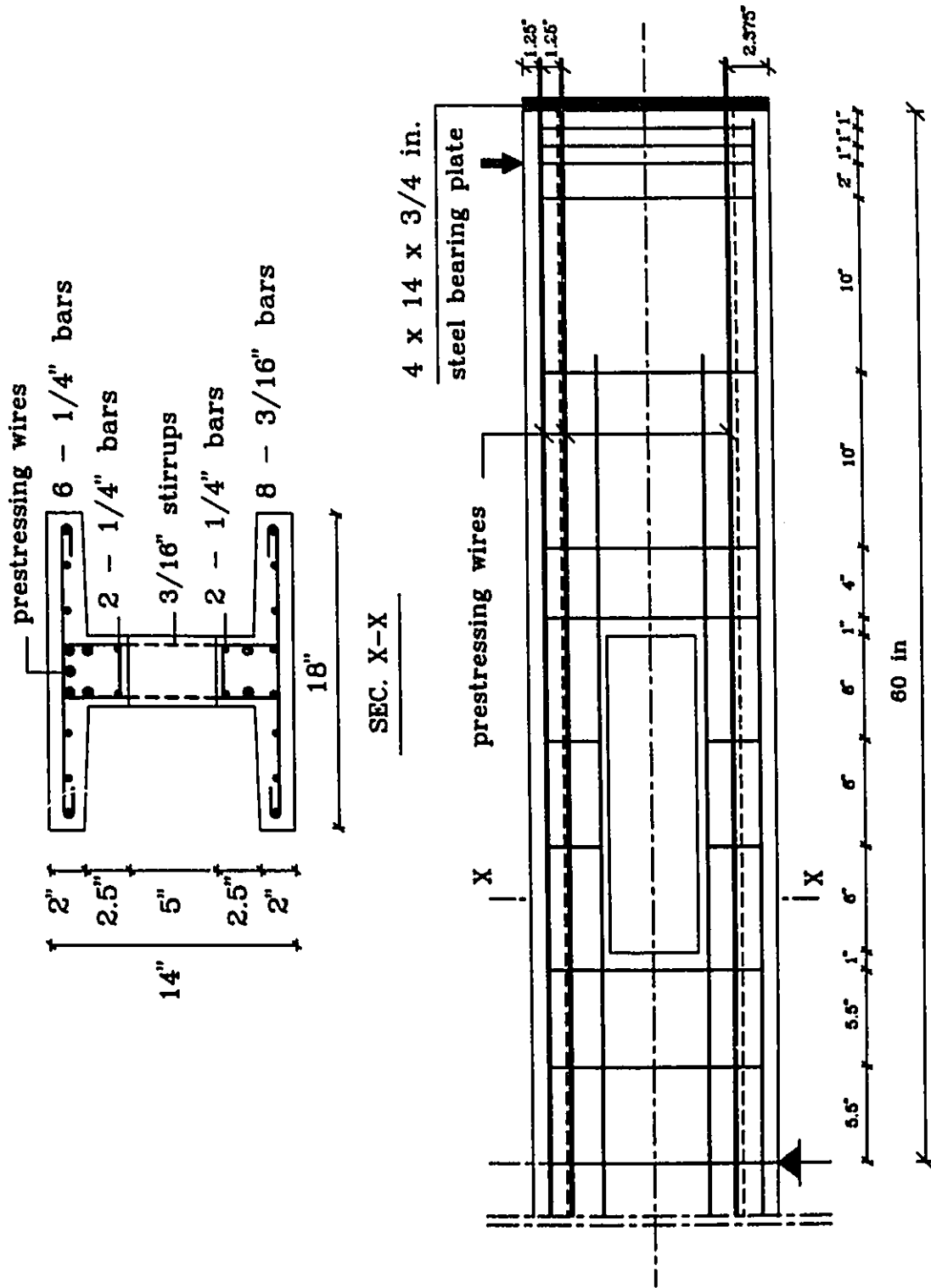


FIG. 4.7 REINFORCEMENT DETAILS FOR BEAM BIII1A

Note: 1 in.=25.4 mm

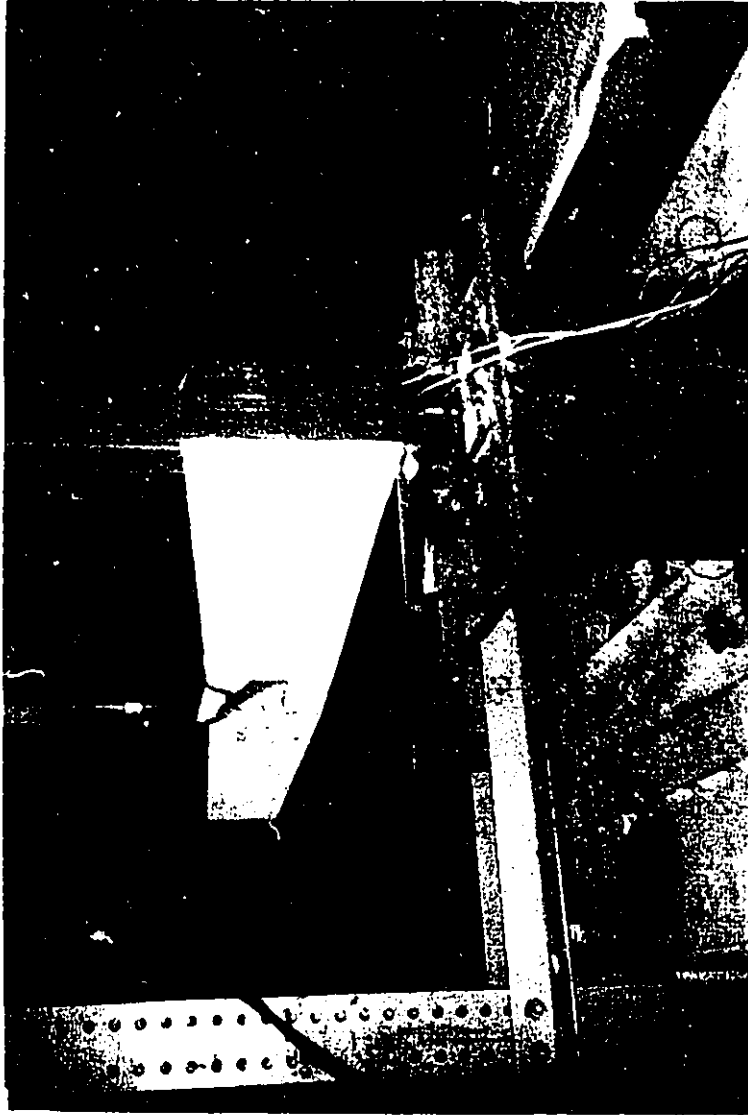


FIG. 4.8 a UNJACKED END OF THE FIRST TYPE OF PRESTRESSING WIRES

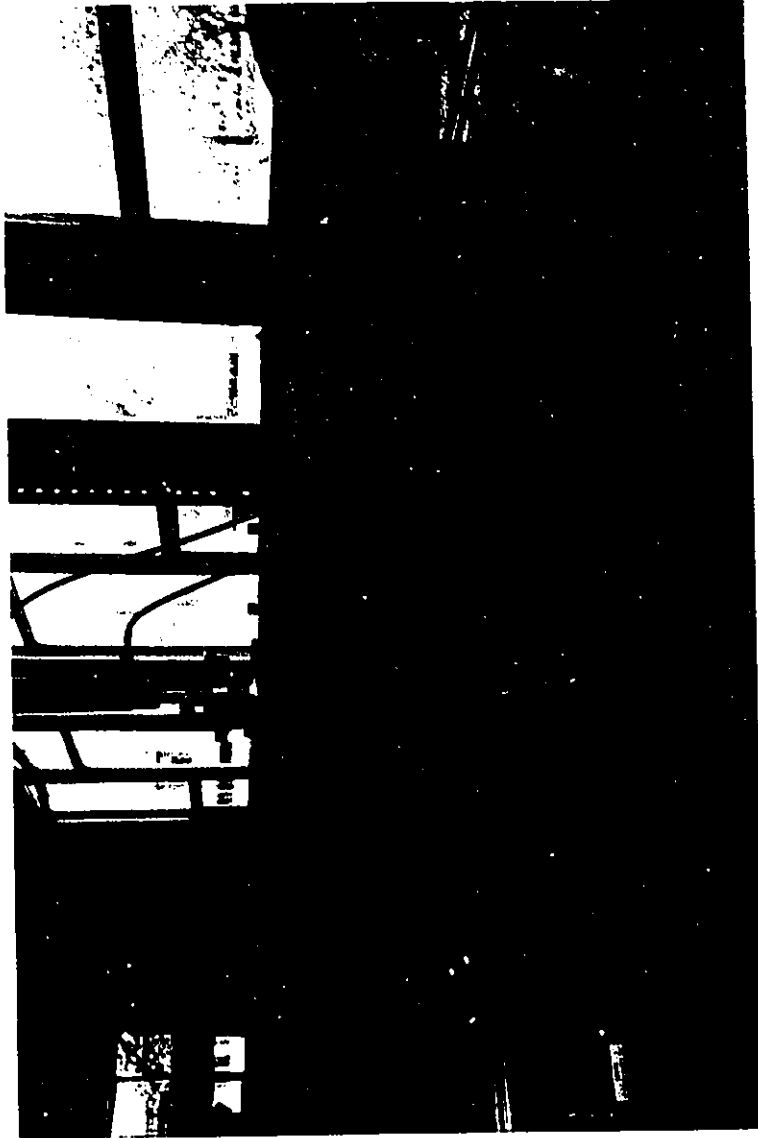


FIG. 4.8 b JACKED END OF THE FIRST TYPE OF PRESTRESSING WIRES



FIG. 4.9 a UNJACKED END OF THE SECOND TYPE OF PRESTRESSING WIRES

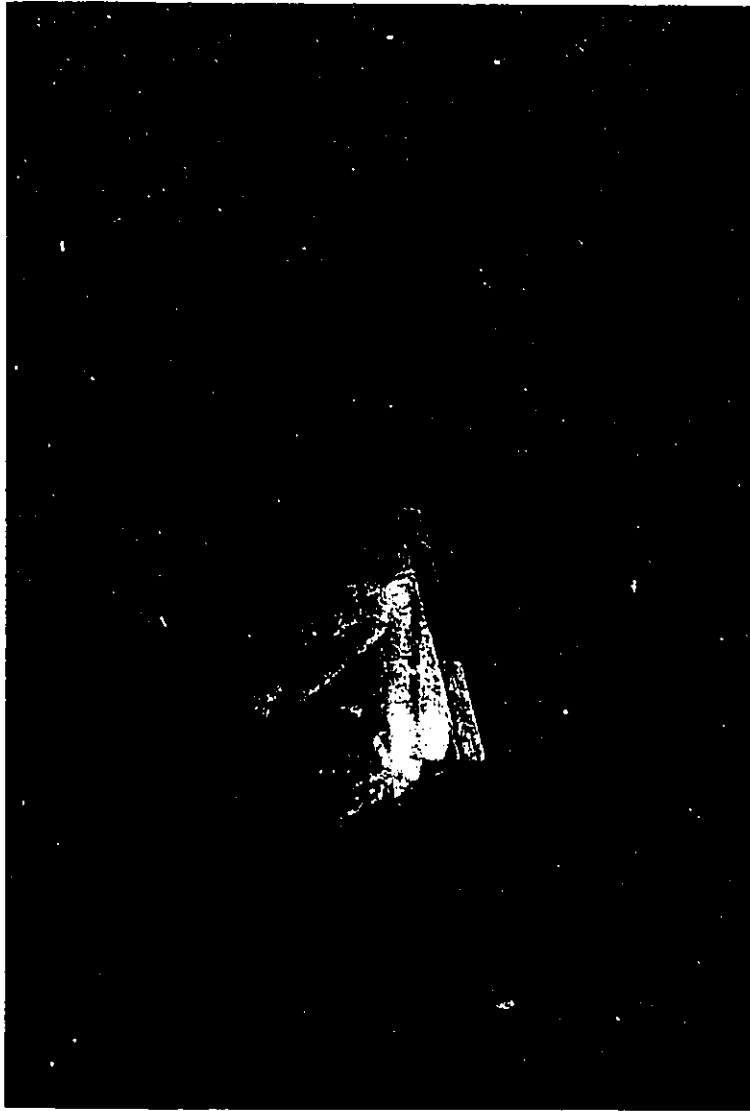


FIG. 4.9 b JACKED END OF THE SECOND TYPE OF PRESTRESSING WIRES

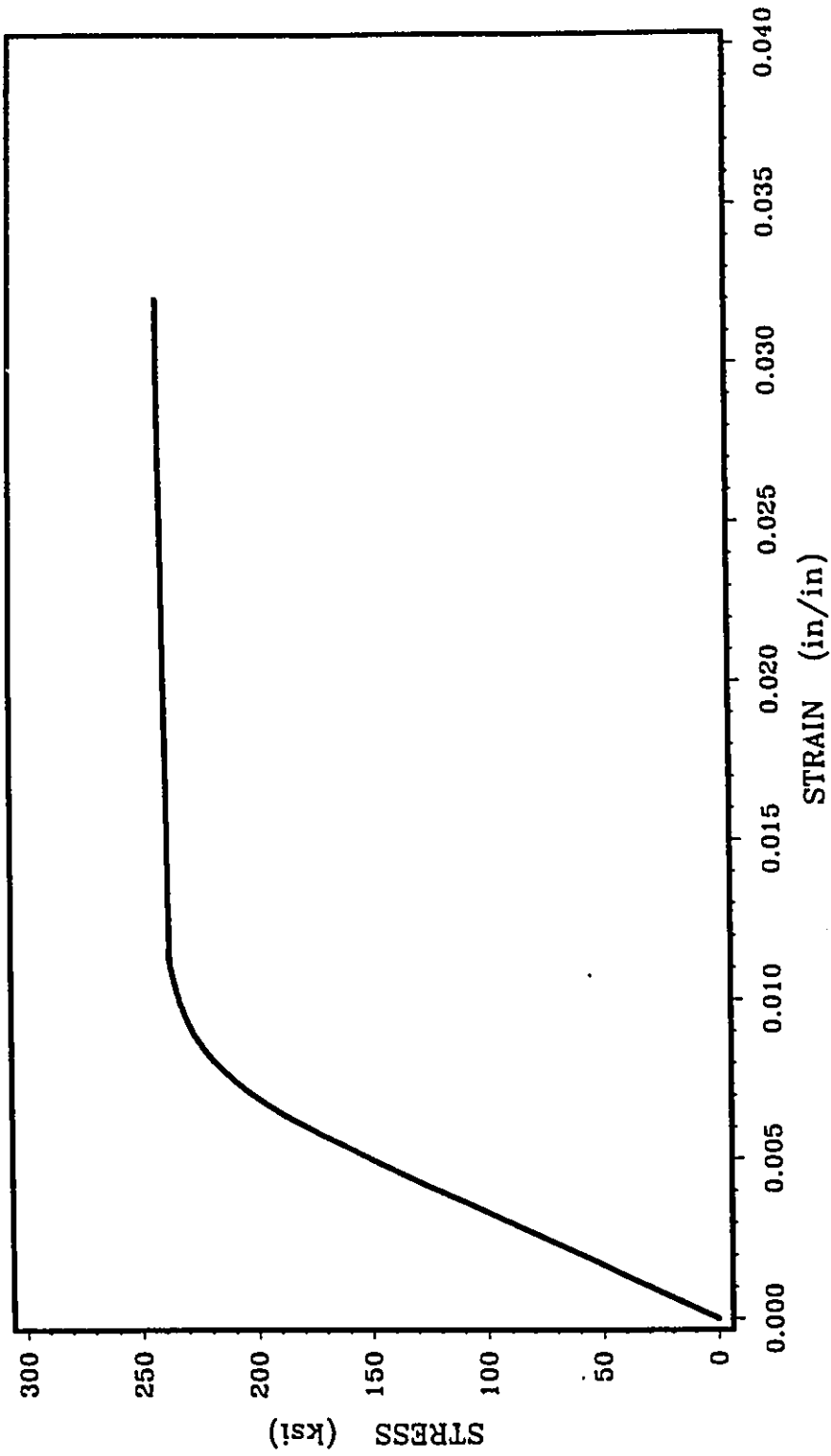


FIG. 4.10 TYPICAL STRESS-STRAIN CURVE
FOR THE PRESTRESSING STEEL
(TYPE 1)

Note: 1 ksi=6.89 MPa



FIG. 4.11 NON-PRESTRESSING REINFORCEMENT OF A T-BEAM

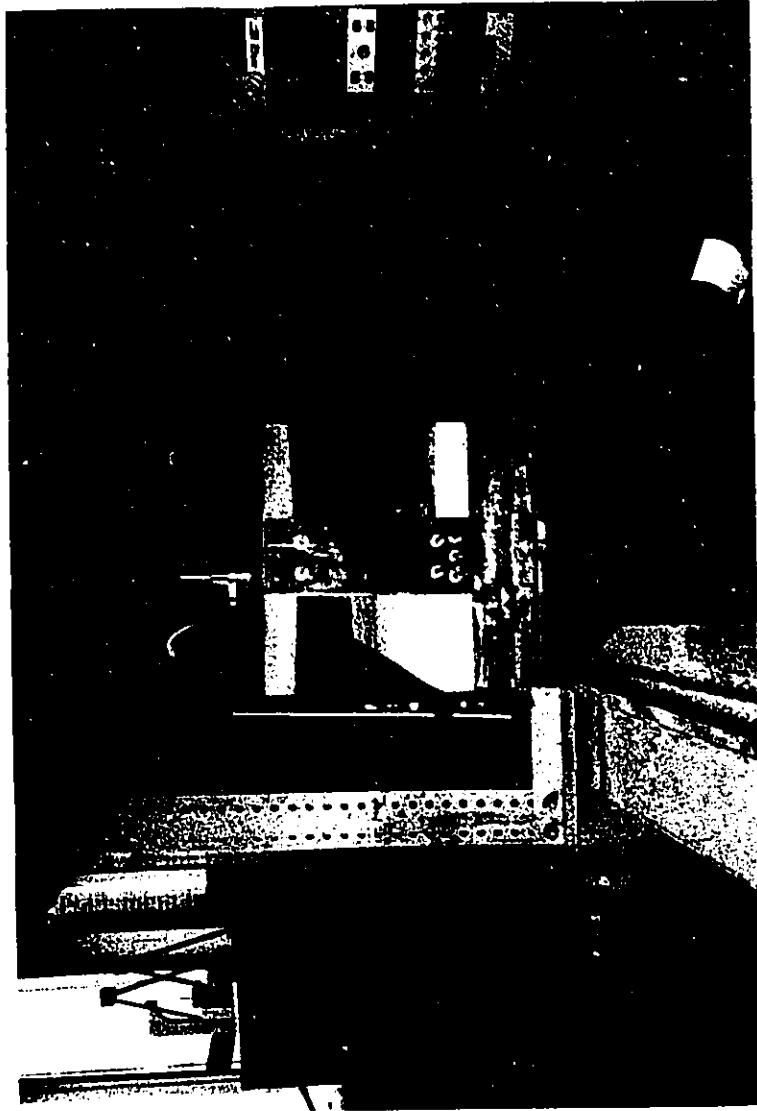


FIG. 4.12 END-PLATE FOR AN I-BEAM

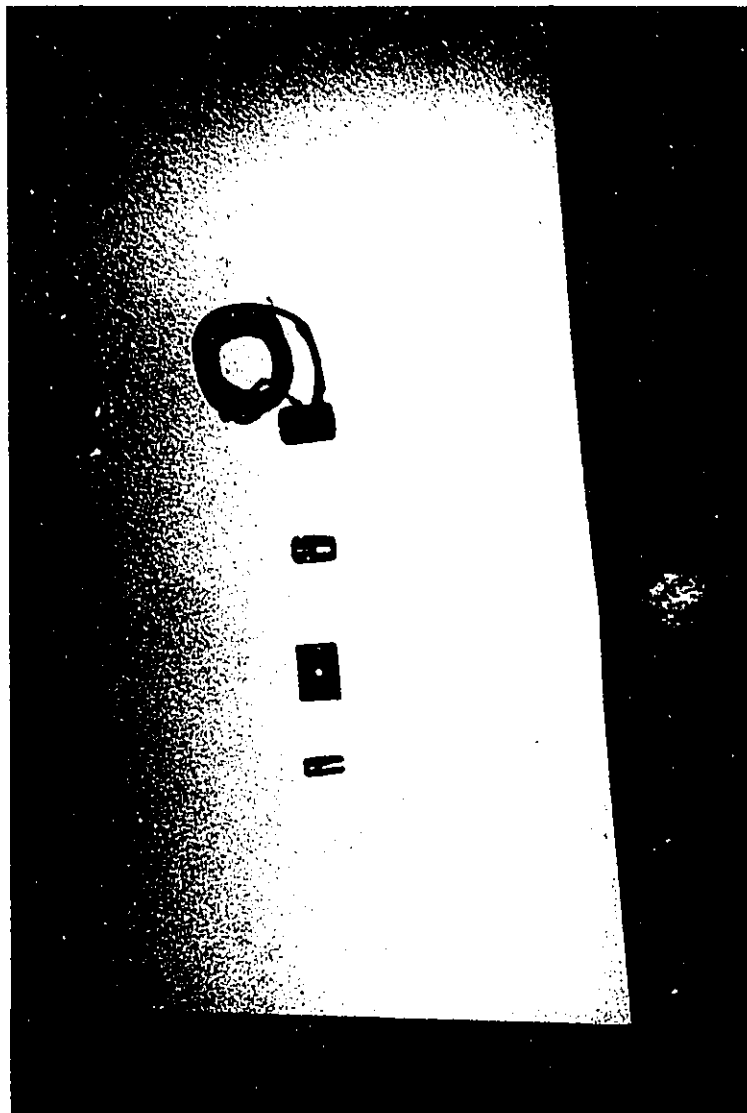


FIG. 4.13 ANCHORAGE UNITS AND LOAD CELL USED IN PRESTRESSING

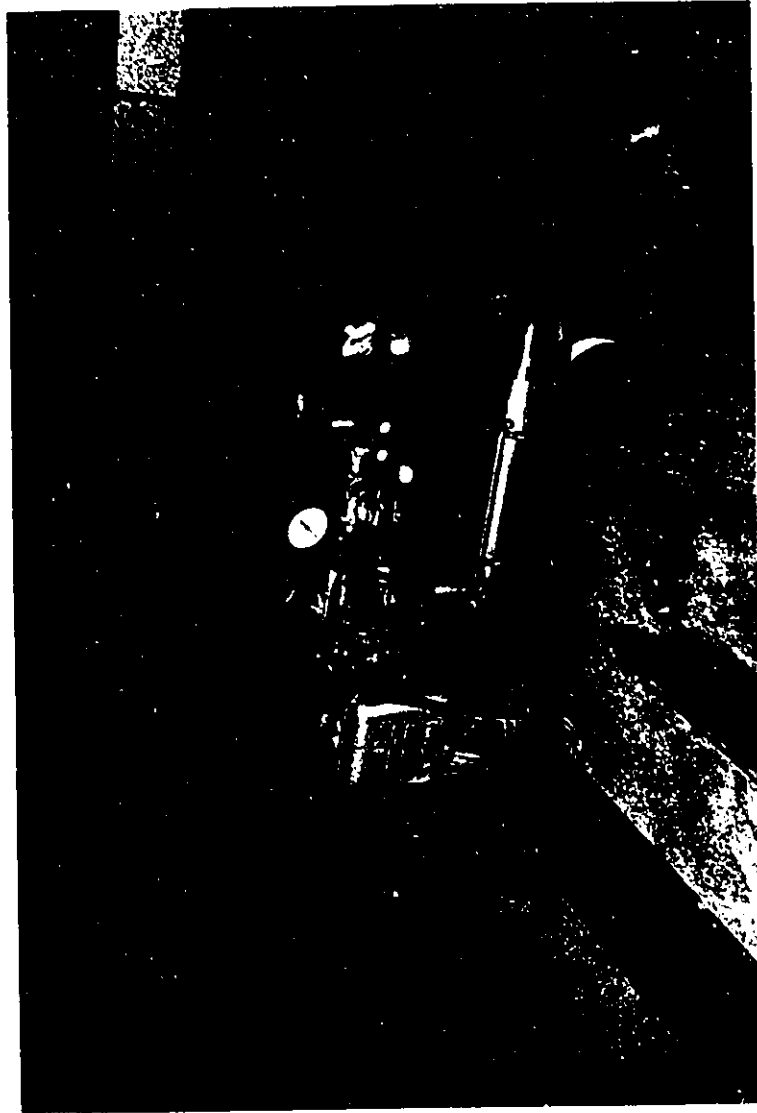


FIG. 4.14 THE PRESTRESSING HYDRAULIC JACK

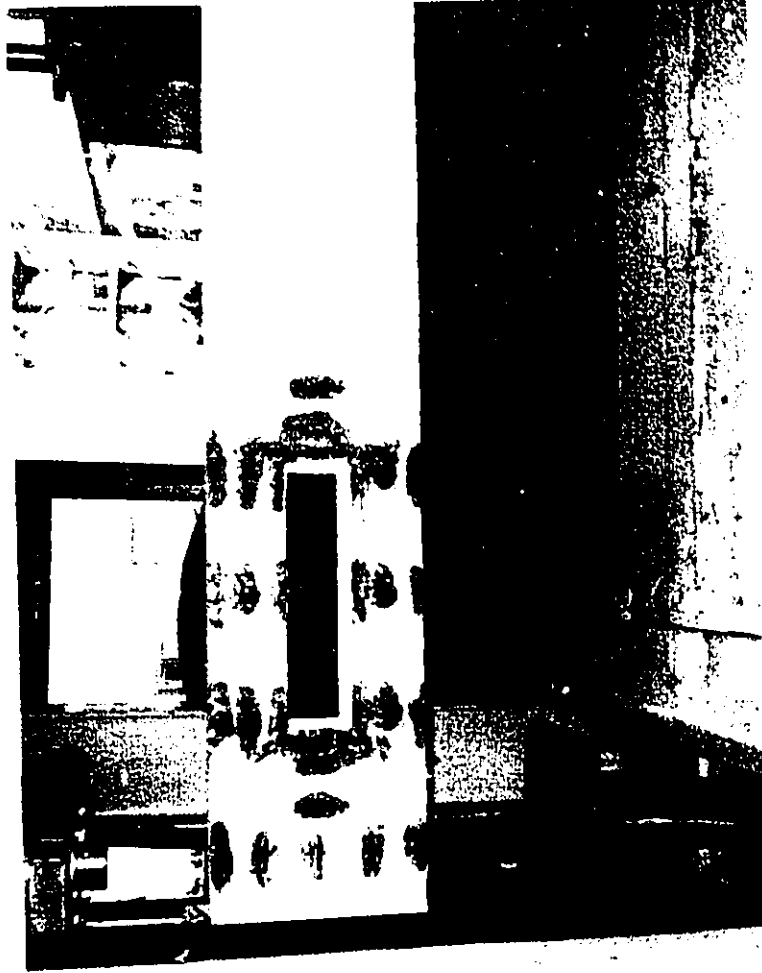


FIG. 4.15 ELECTRIC STRAIN GAUGES ON A RECTANGULAR BEAM

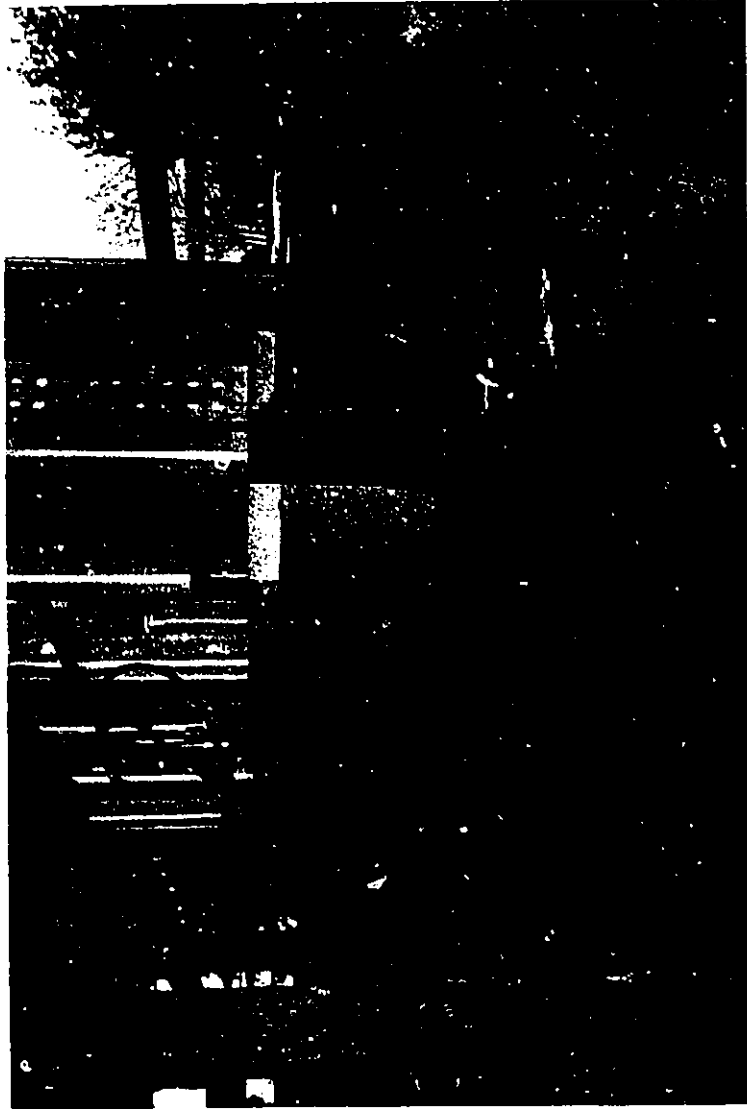


FIG. 4.16 ELECTRIC STRAIN GAUGES ON A T-BEAM

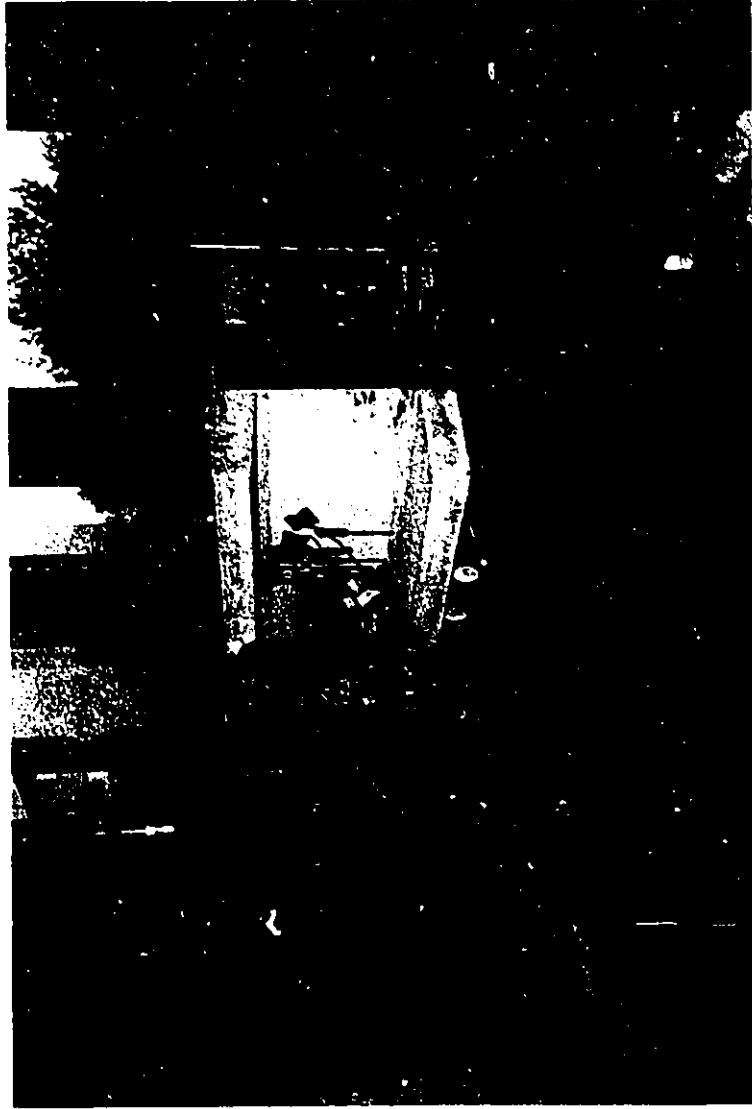


FIG. 4.17 ELECTRIC STRAIN GAUGES ON AN I-BEAM

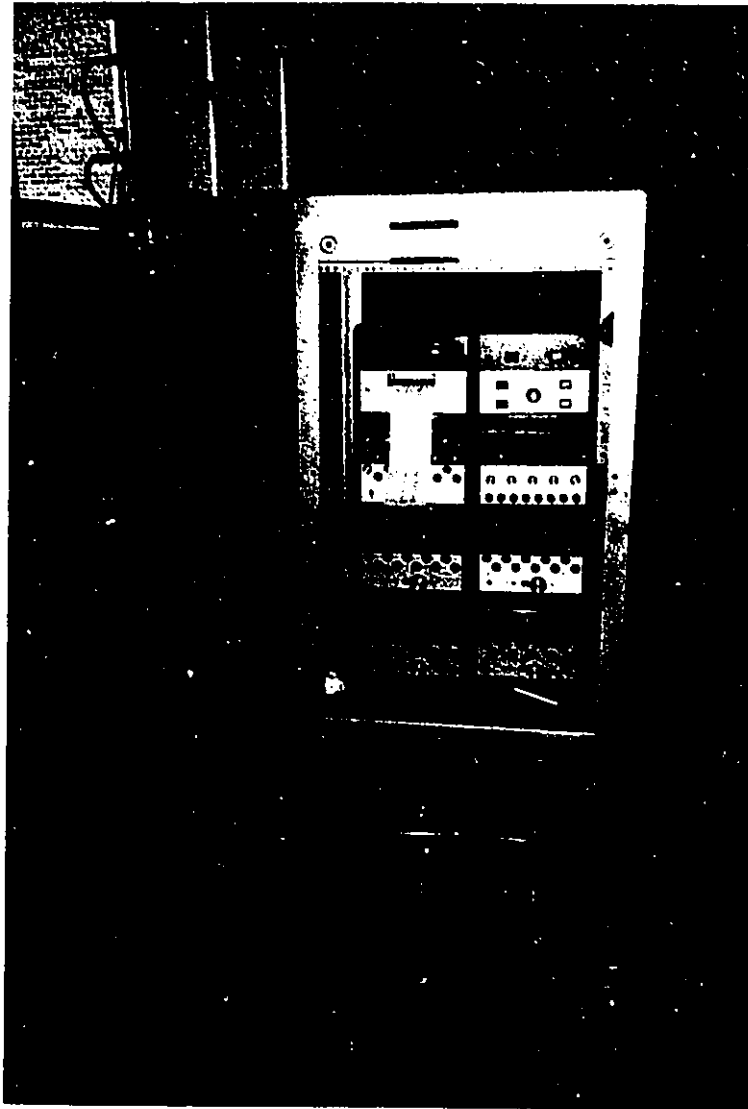


FIG. 4.18 THE AUTOMATIC STRAIN INDICATOR

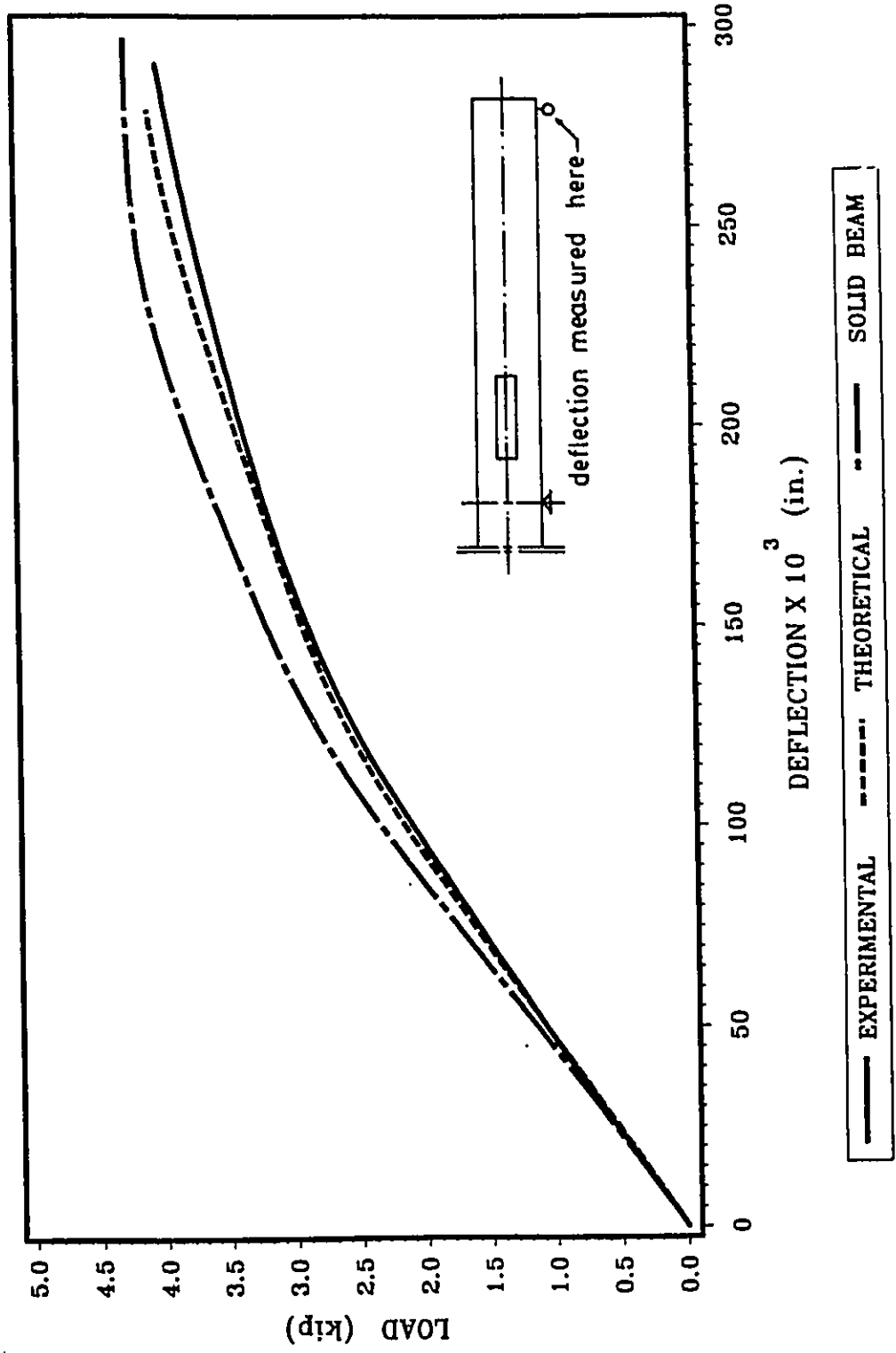


FIG. 5.1 LOAD-DEFLECTION RELATIONSHIP FOR BI1A

Note: 1 in.=25.4 mm, 1 kip=4.45 kN

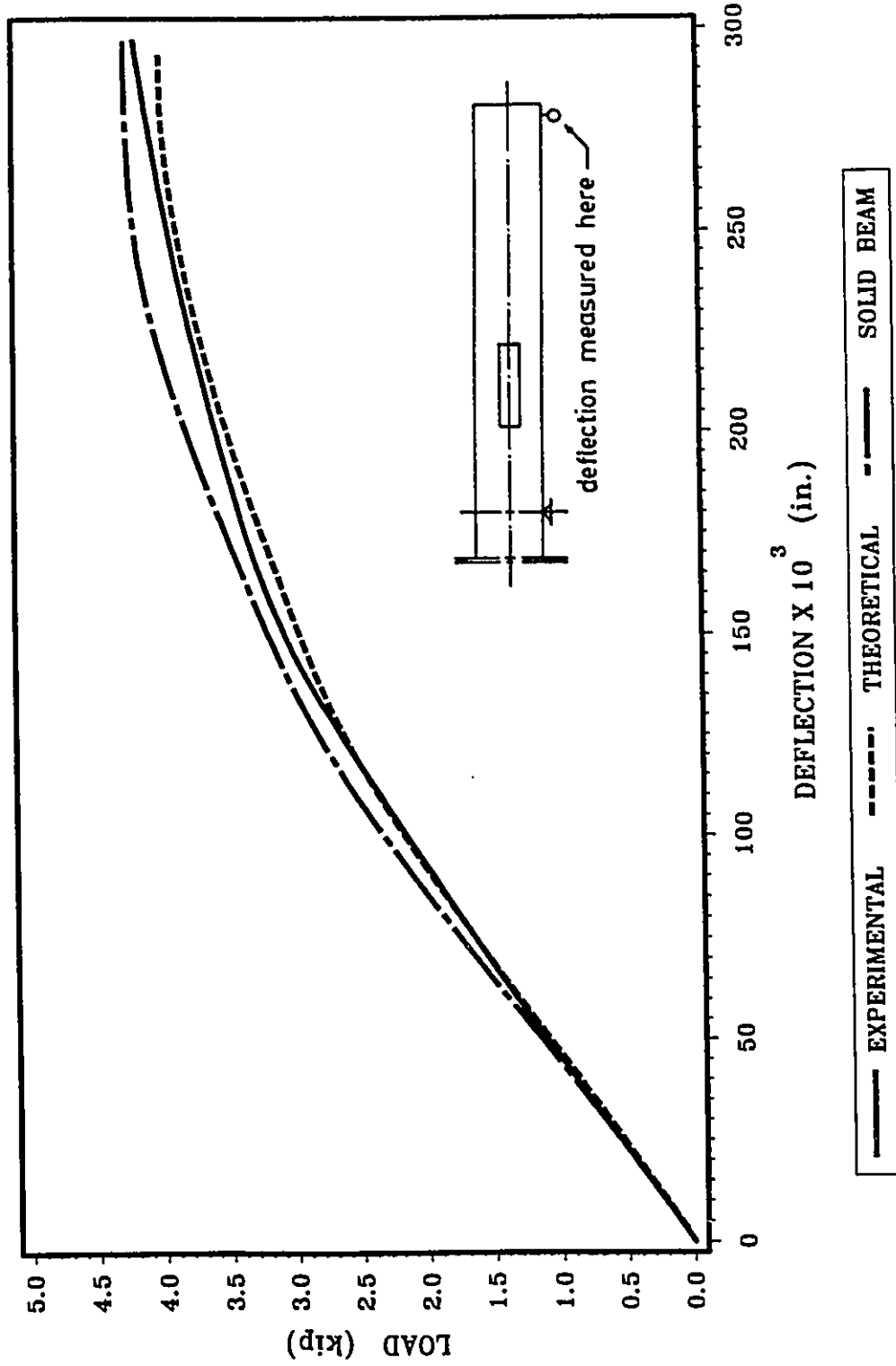


FIG. 5.2 LOAD-DEFLECTION RELATIONSHIP FOR BI1B

Note: 1 in.=25.4 mm, 1 kip=4.45 kN

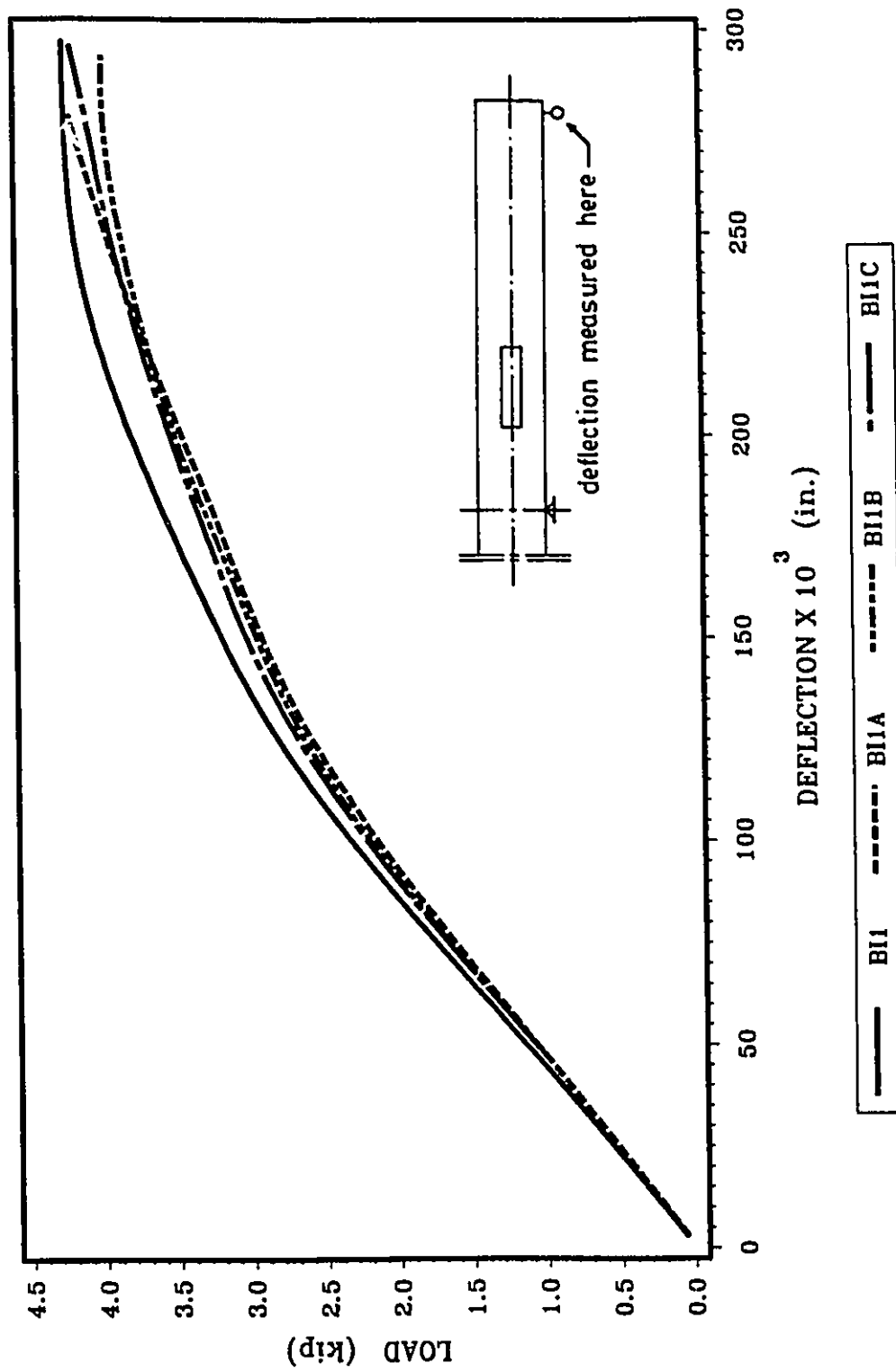


FIG. 5.3 LOAD-DEFLECTION RELATIONSHIP FOR BI1, BI1A, BI1B & BI1C

Note: 1 in.=25.4 mm, 1 kip=4.45 kN

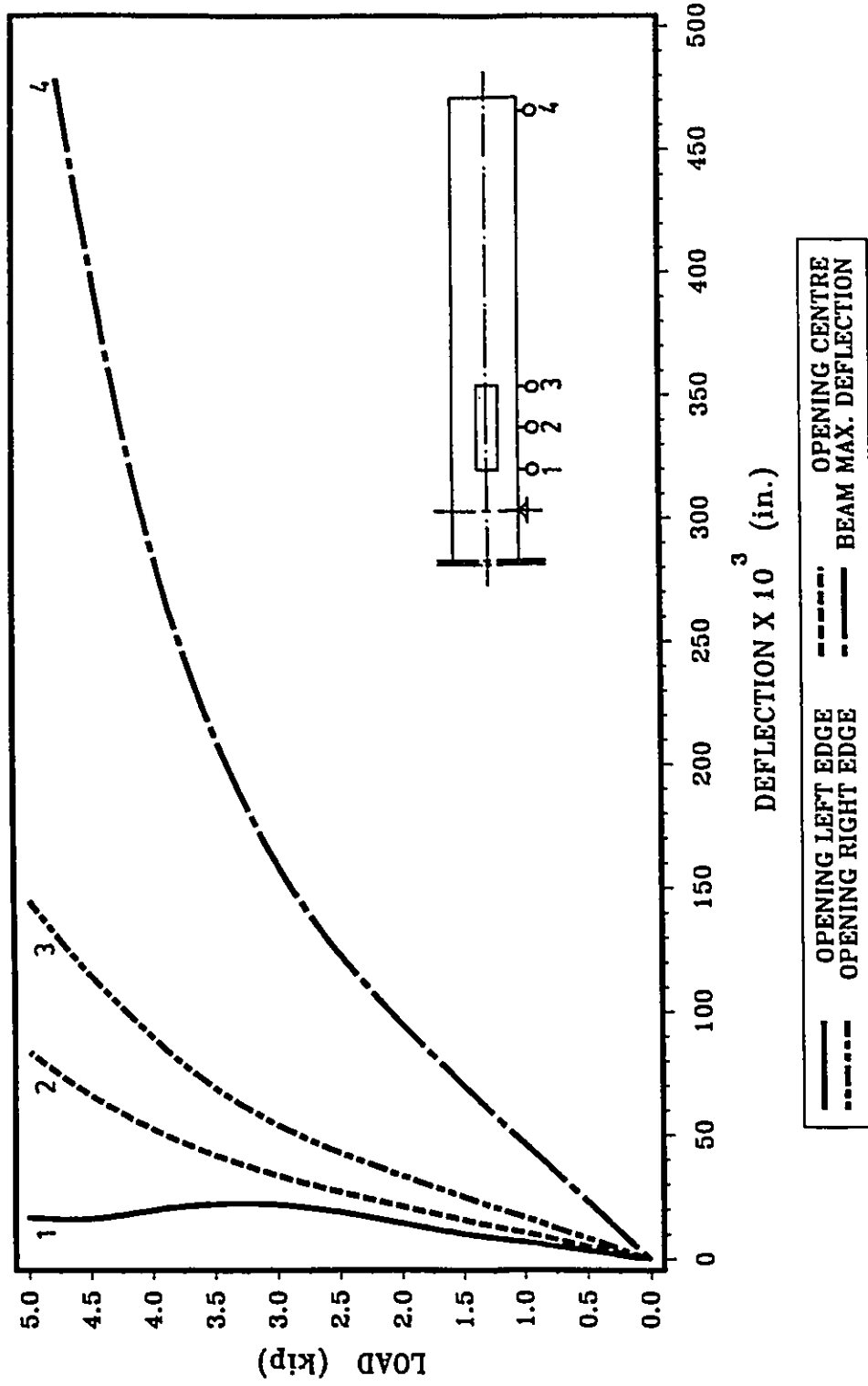


FIG. 5.4 OPENING DEFLECTION FOR BI1A
(EXPERIMENTAL)

Note: 1 in.=25.4 mm, 1 kip= 4.45 kN

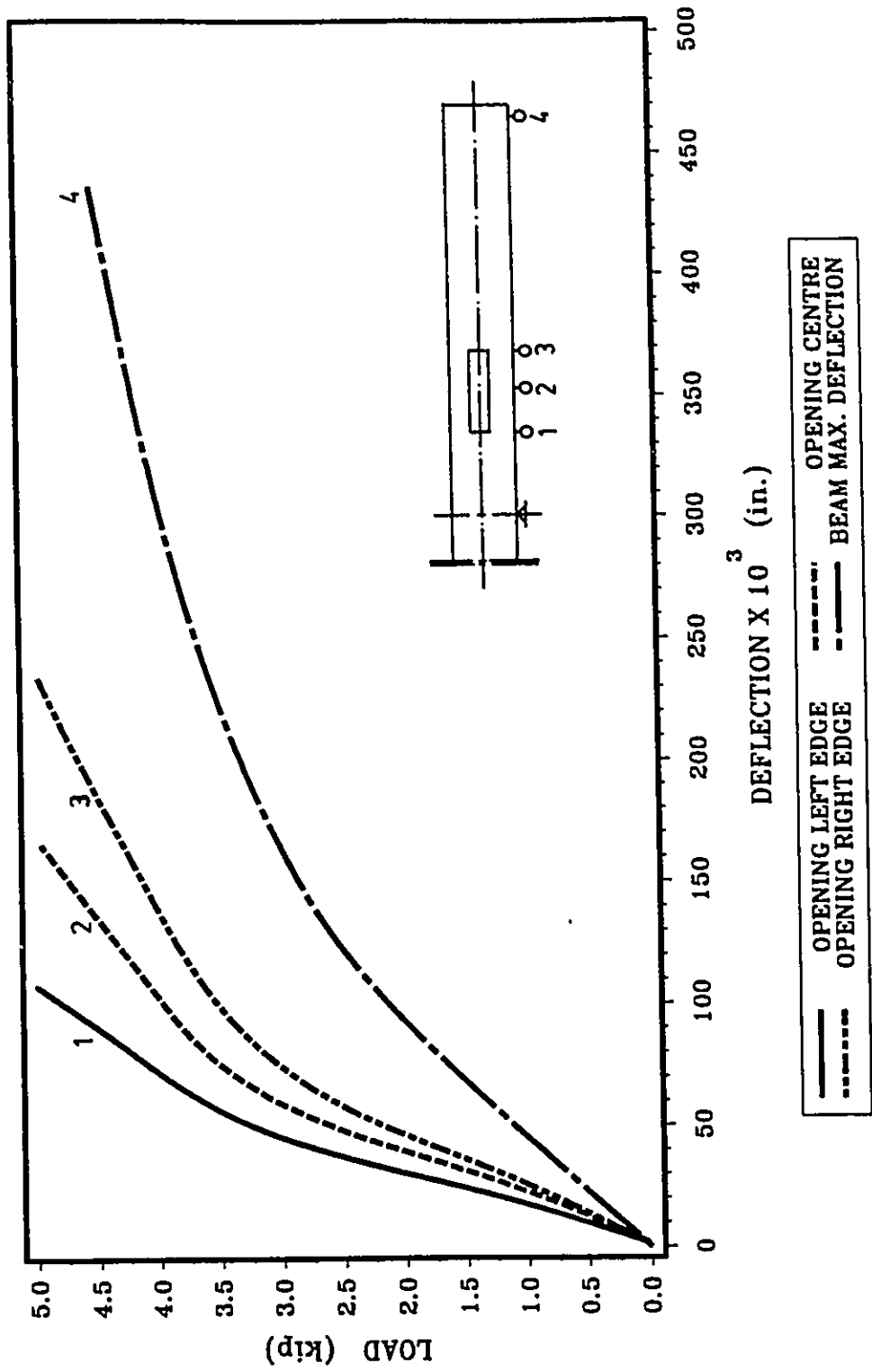


FIG. 5.5 OPENING DEFLECTION FOR BI1B
(EXPERIMENTAL)

Note: 1 in.=25.4 mm, 1 kip=4.45 kN

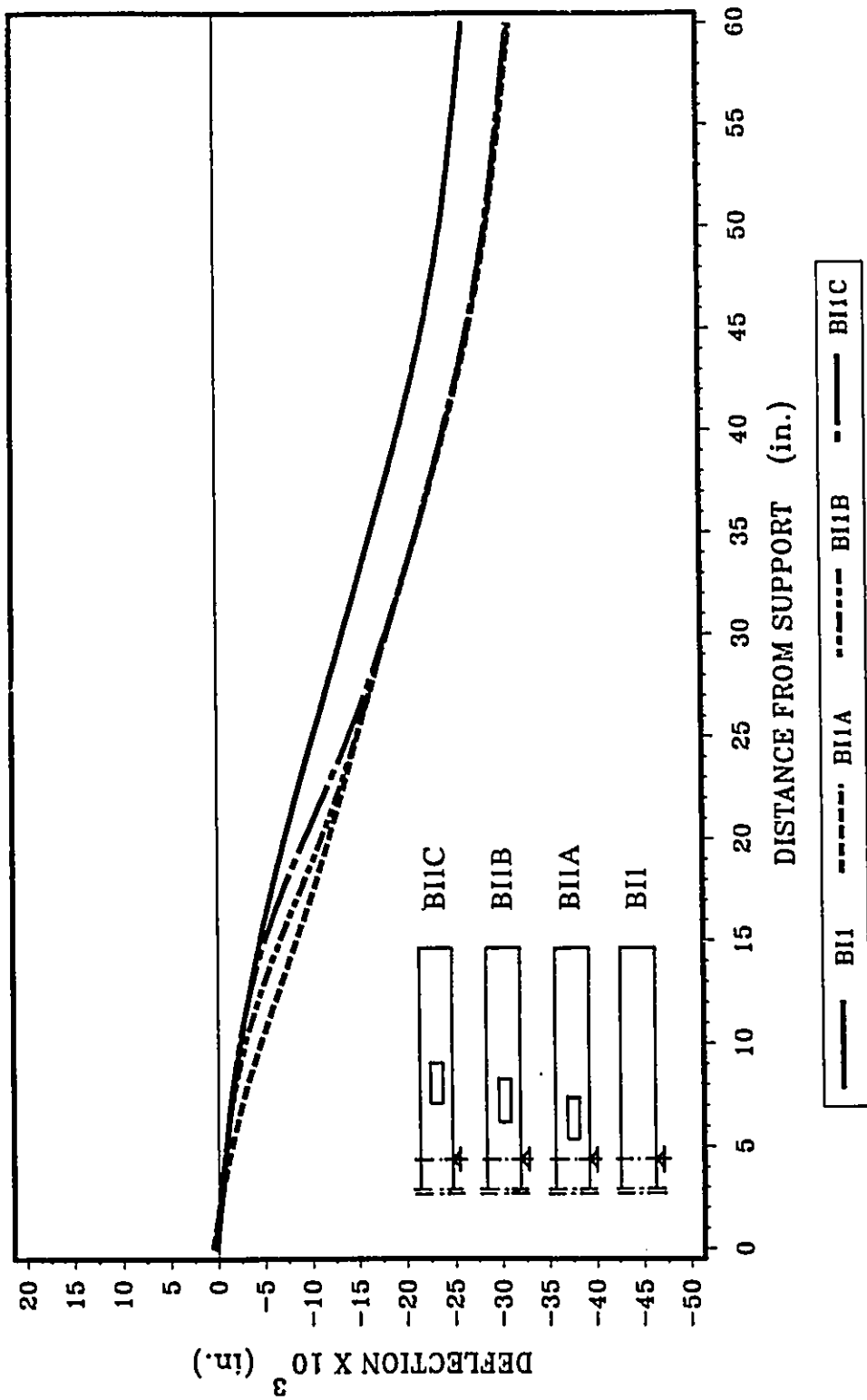


FIG. 5.6 DEFLECTED SHAPE FOR BI1, BI1A, BI1B & BI1C
(P = 2 kip)

Note: 1 in.=25.4 mm, 1 kip=4.45 kN

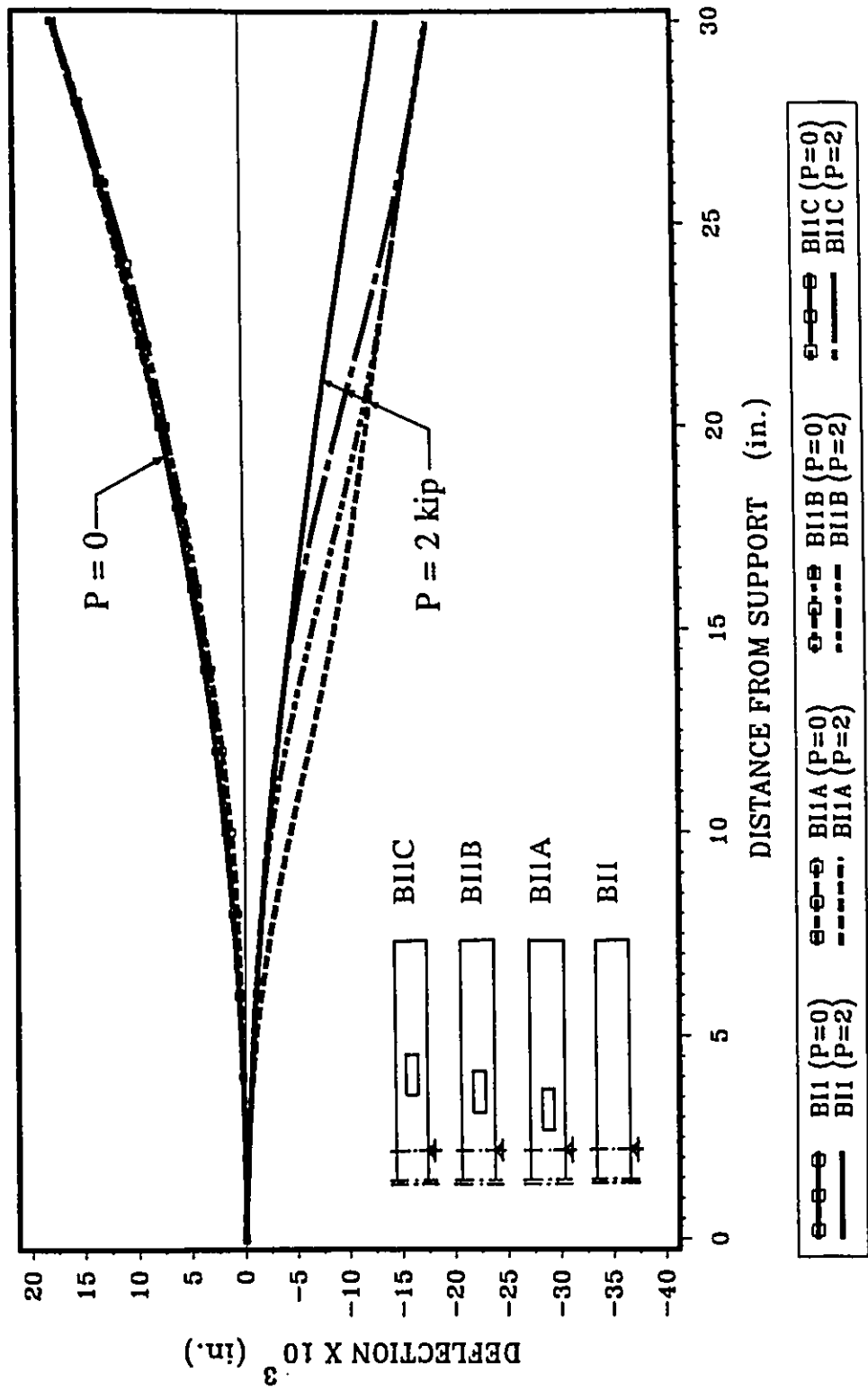


FIG. 5.7 DEFLECTED SHAPE FOR BI1, BI1A, BI1B & BI1C
(P = 0 & P = 2 kip)

Note: 1 in.=25.4 mm, 1 kip=4.45 kN

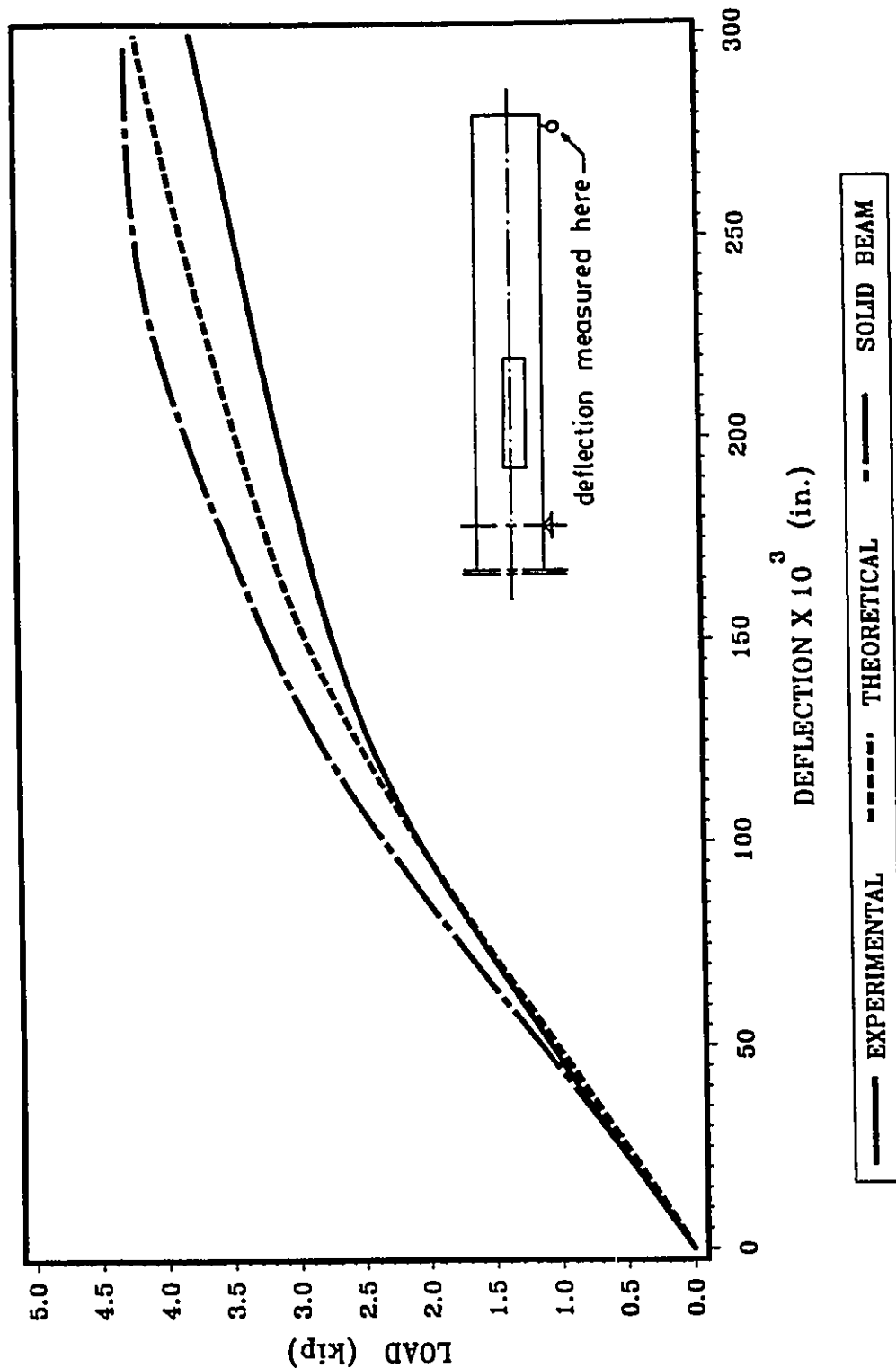


FIG. 5.8 LOAD-DEFLECTION RELATIONSHIP FOR BI2A

Note: 1 in.=25.4 mm, 1 kip=4.45 kN

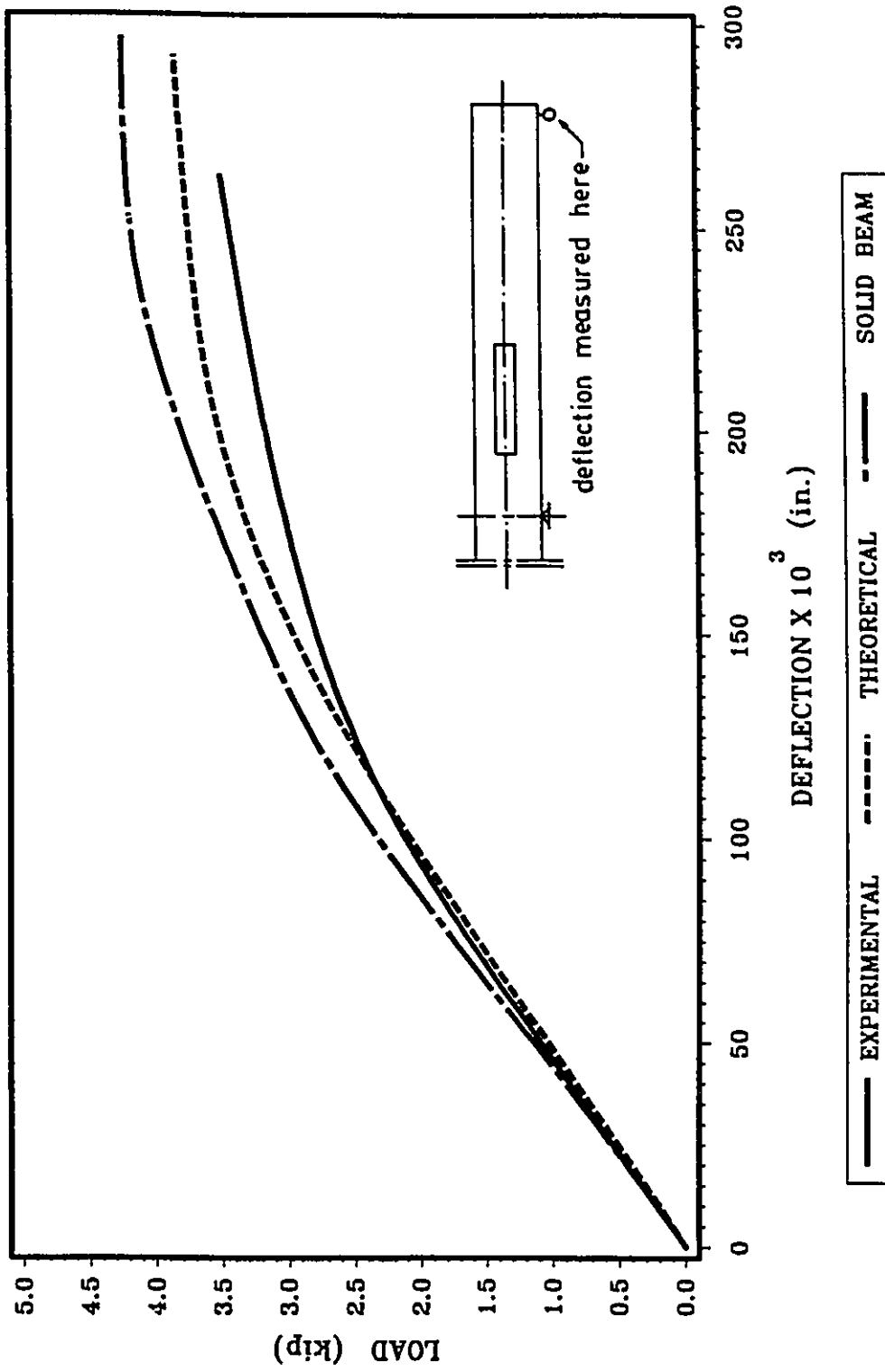


FIG. 5.9 LOAD-DEFLECTION RELATIONSHIP FOR BI2B

Note: 1 in.=25.4 mm, 1 kip=4.45 kN

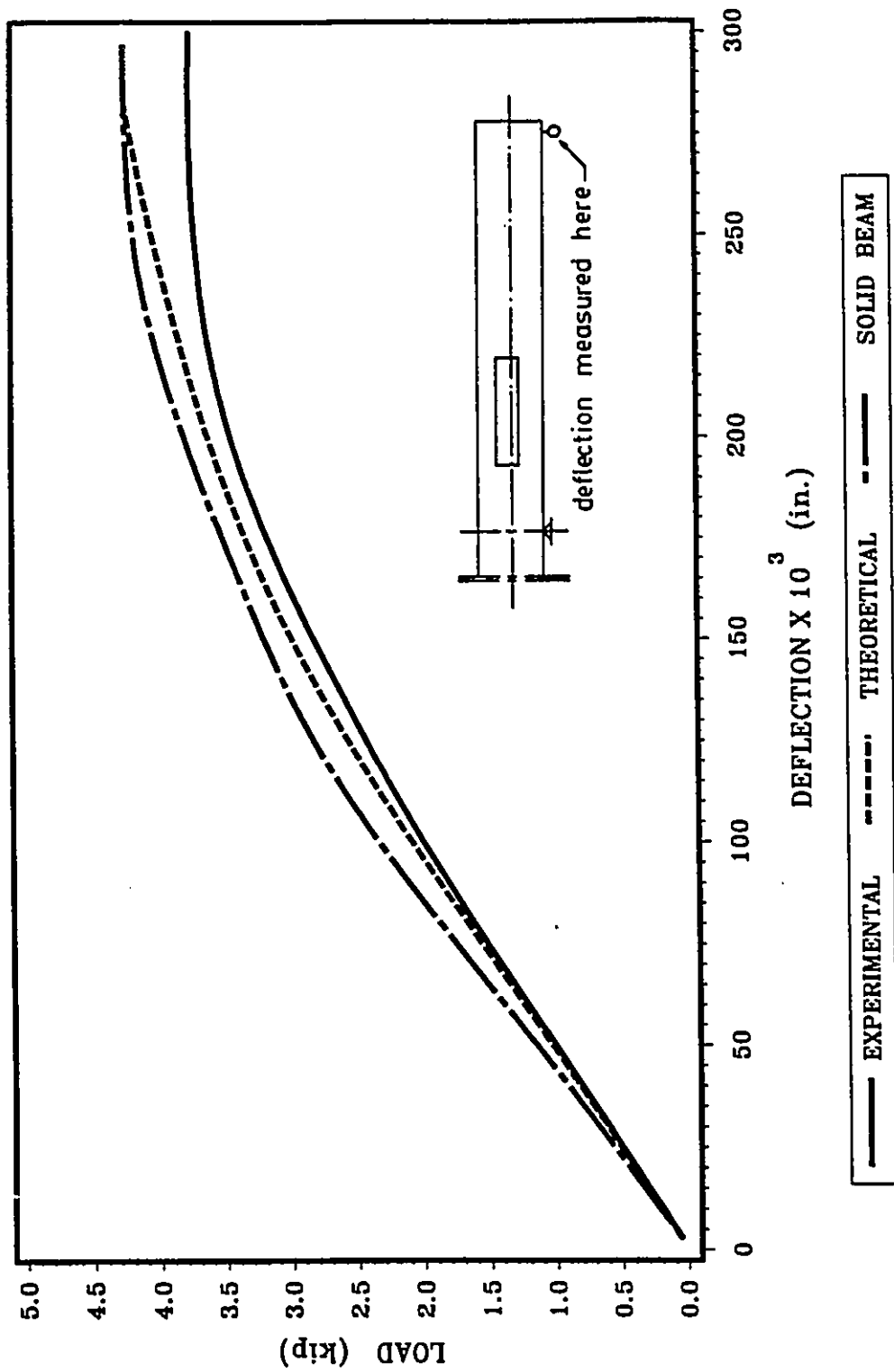


FIG. 5.10 LOAD-DEFLECTION RELATIONSHIP FOR BI2C

Note: 1 in.=25.4 mm, 1 kip=4.45 kN

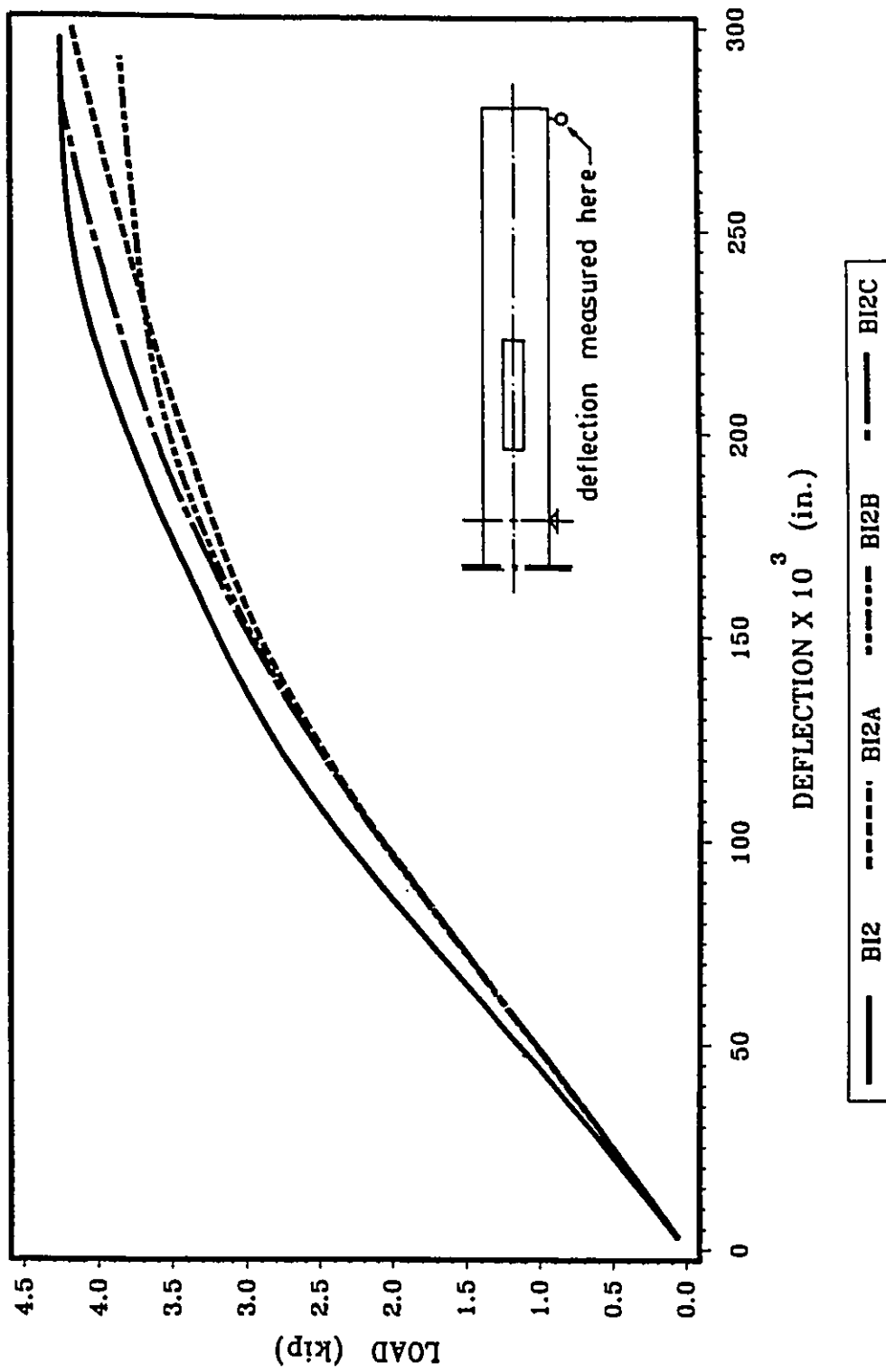


FIG. 5.1.1 LOAD-DEFLECTION RELATIONSHIP FOR BI2, BI2A, BI2B & BI2C

Note: 1 in.=25.4 mm, 1 kip=4.45 kN

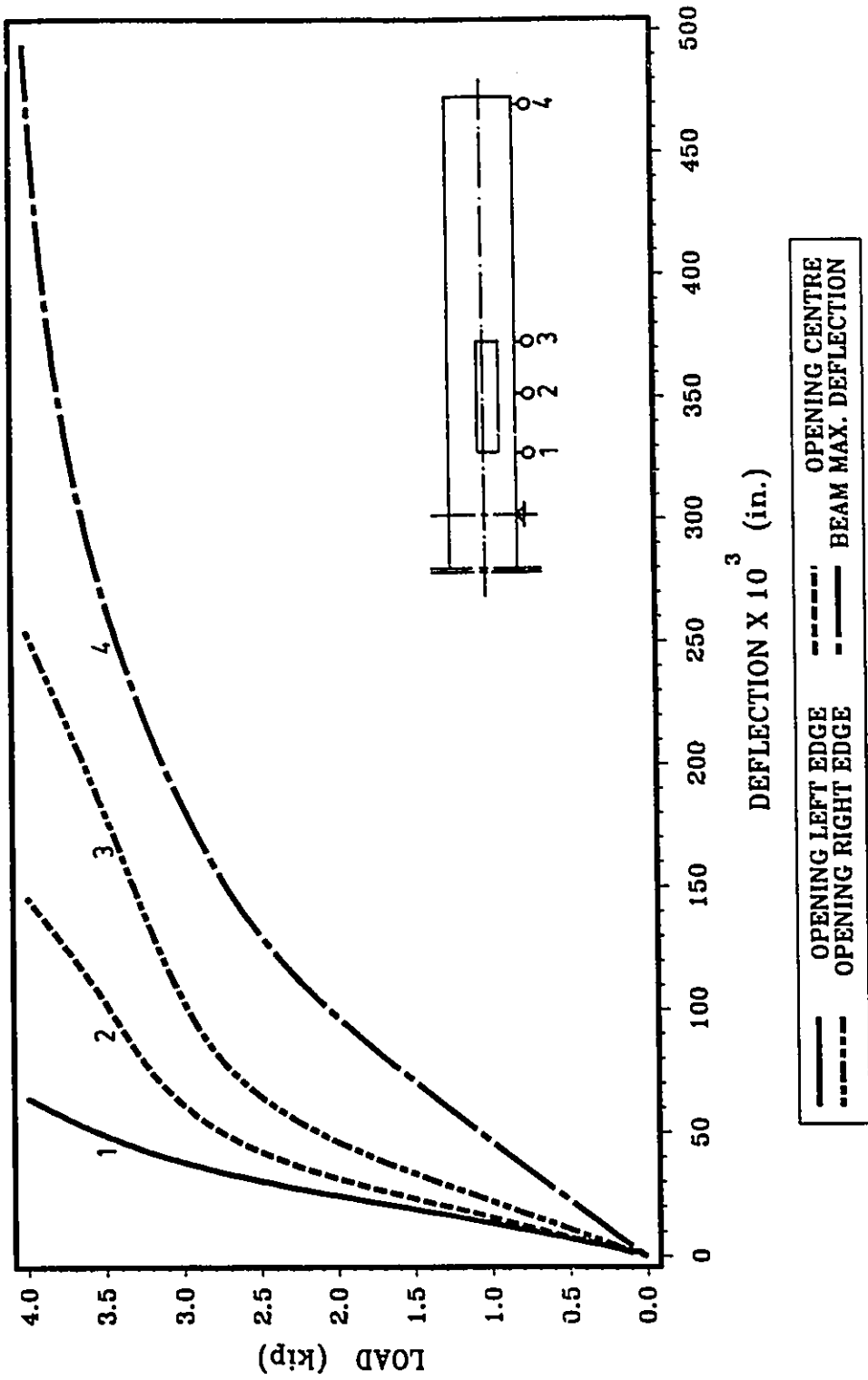


FIG. 5.12 OPENING DEFLECTION FOR B12A
(EXPERIMENTAL)

Note: 1 in.=25.4 mm, 1 kip= 4.45 kN

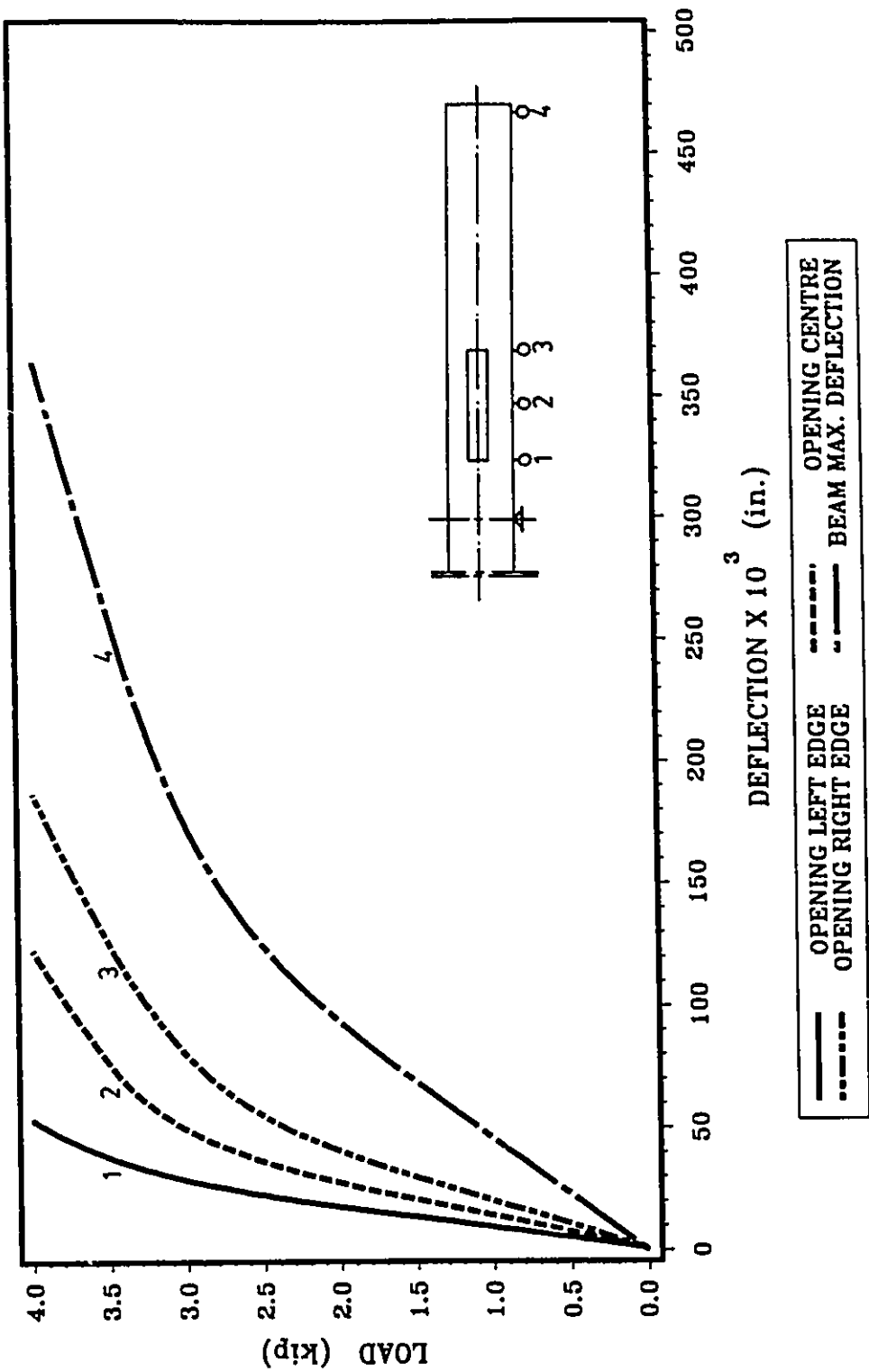


FIG. 5.13 OPENING DEFLECTION FOR BI2B
(EXPERIMENTAL)

Note: 1 in. = 25.4 mm, 1 kip = 4.45 kN

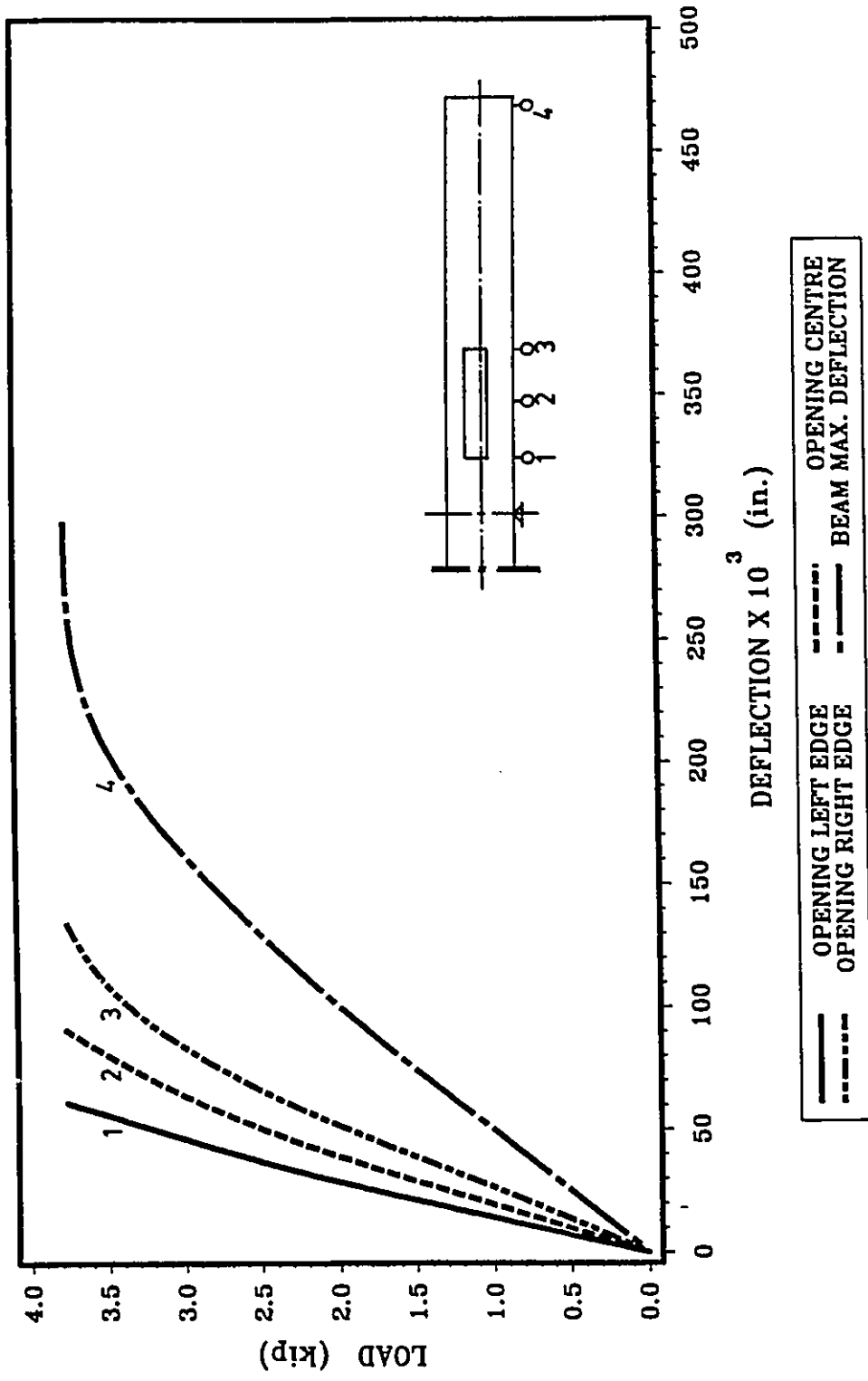


FIG. 5.14 OPENING DEFLECTION FOR BI2C
(EXPERIMENTAL)

Note: 1 in. = 25.4 mm, 1 kip = 4.45 kN

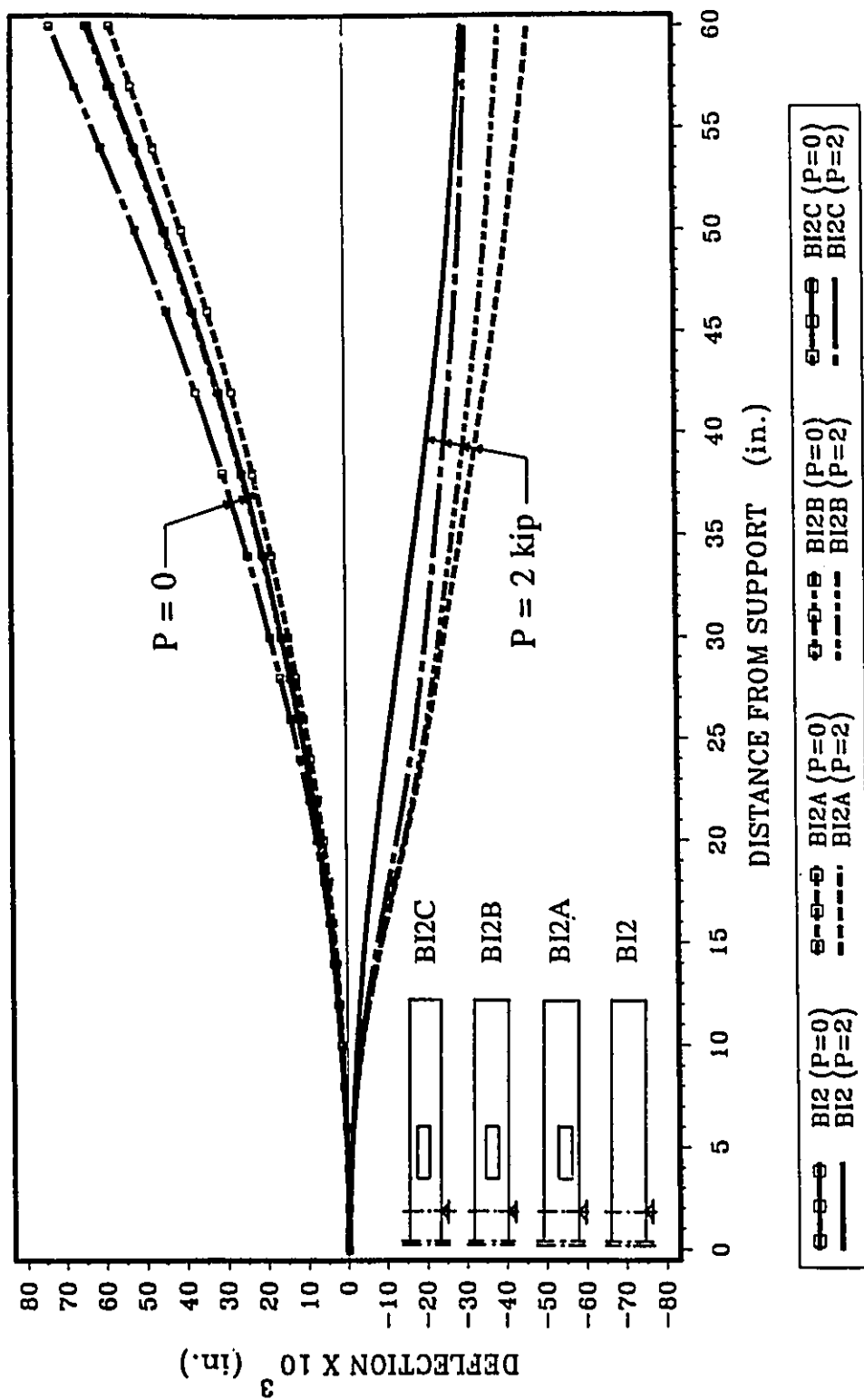


FIG. 5.15 DEFLECTED SHAPE FOR B12, B12A, B12B & B12C
(P = 0 & P = 2 kip)

Note: 1 in.=25.4 mm, 1 kip=4.45 kN

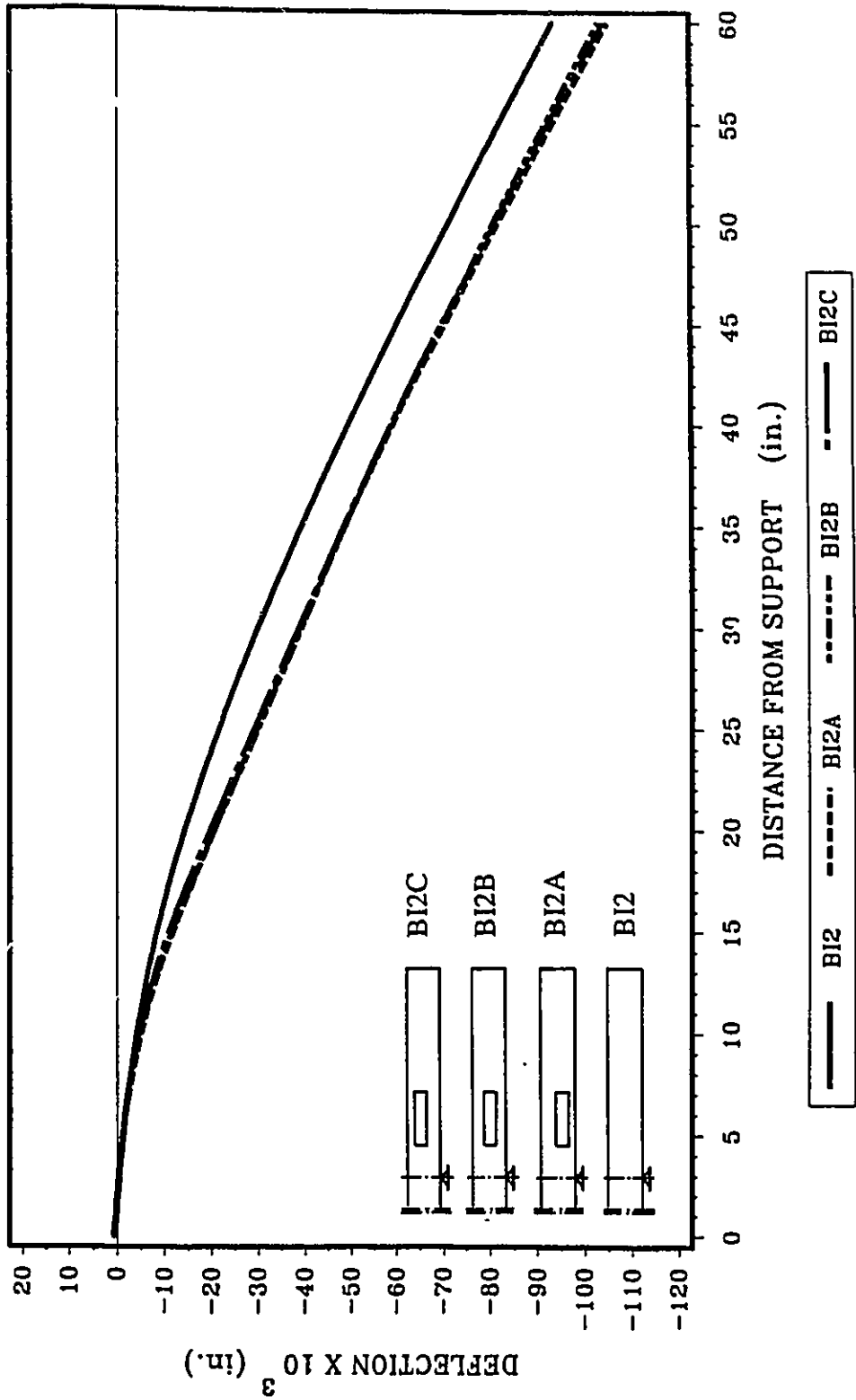


FIG. 5.16 DEFLECTED SHAPE FOR BI2, BI2A, BI2B & BI2C
(DUE TO P = 2 kip)

Note: 1 in.=25.4 mm, 1 kip=4.45 kN

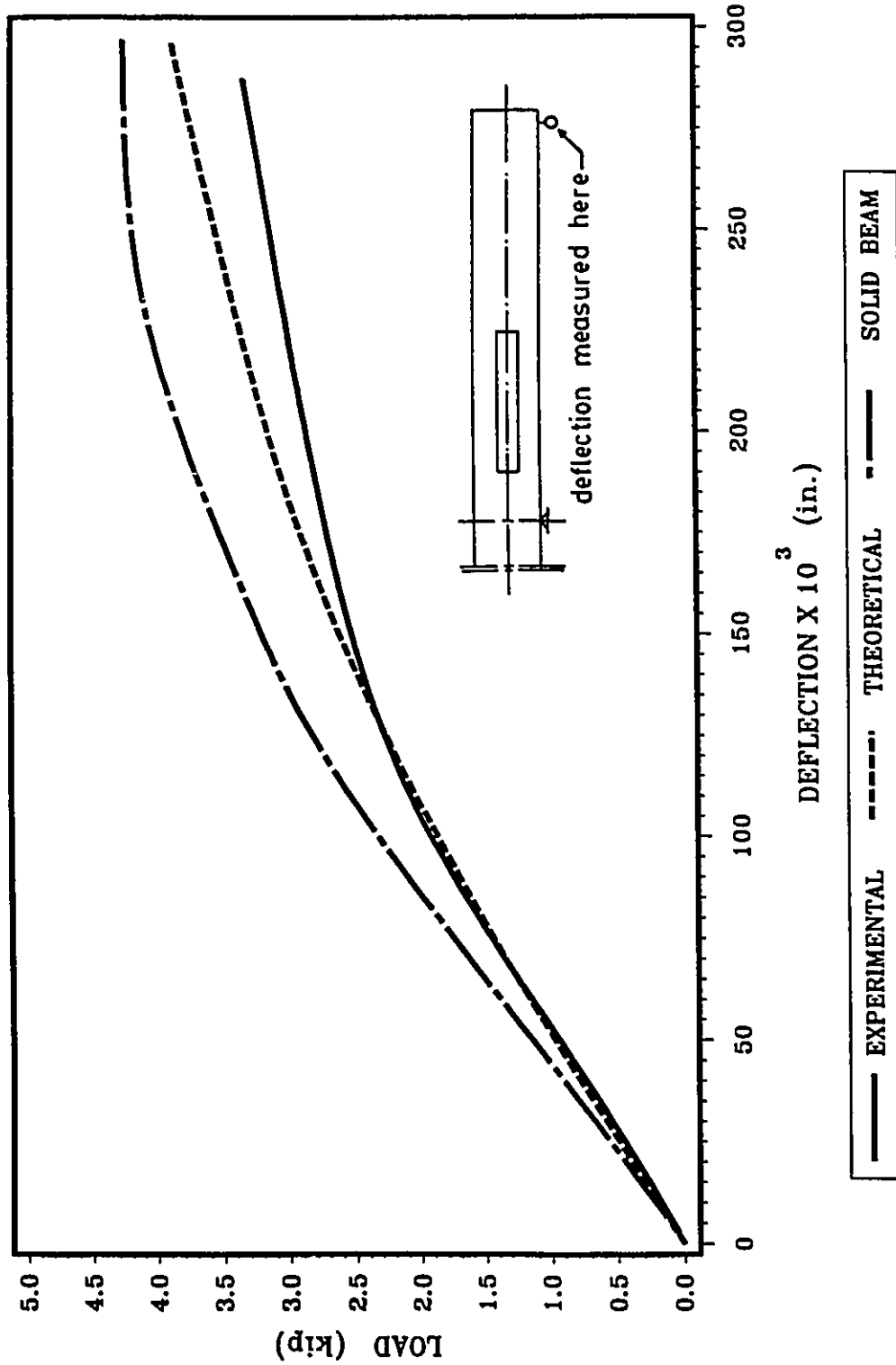


FIG. 5.17 LOAD-DEFLECTION RELATIONSHIP FOR BI3C

Note: 1 in.=25.4 mm, 1 kip=4.45 kN

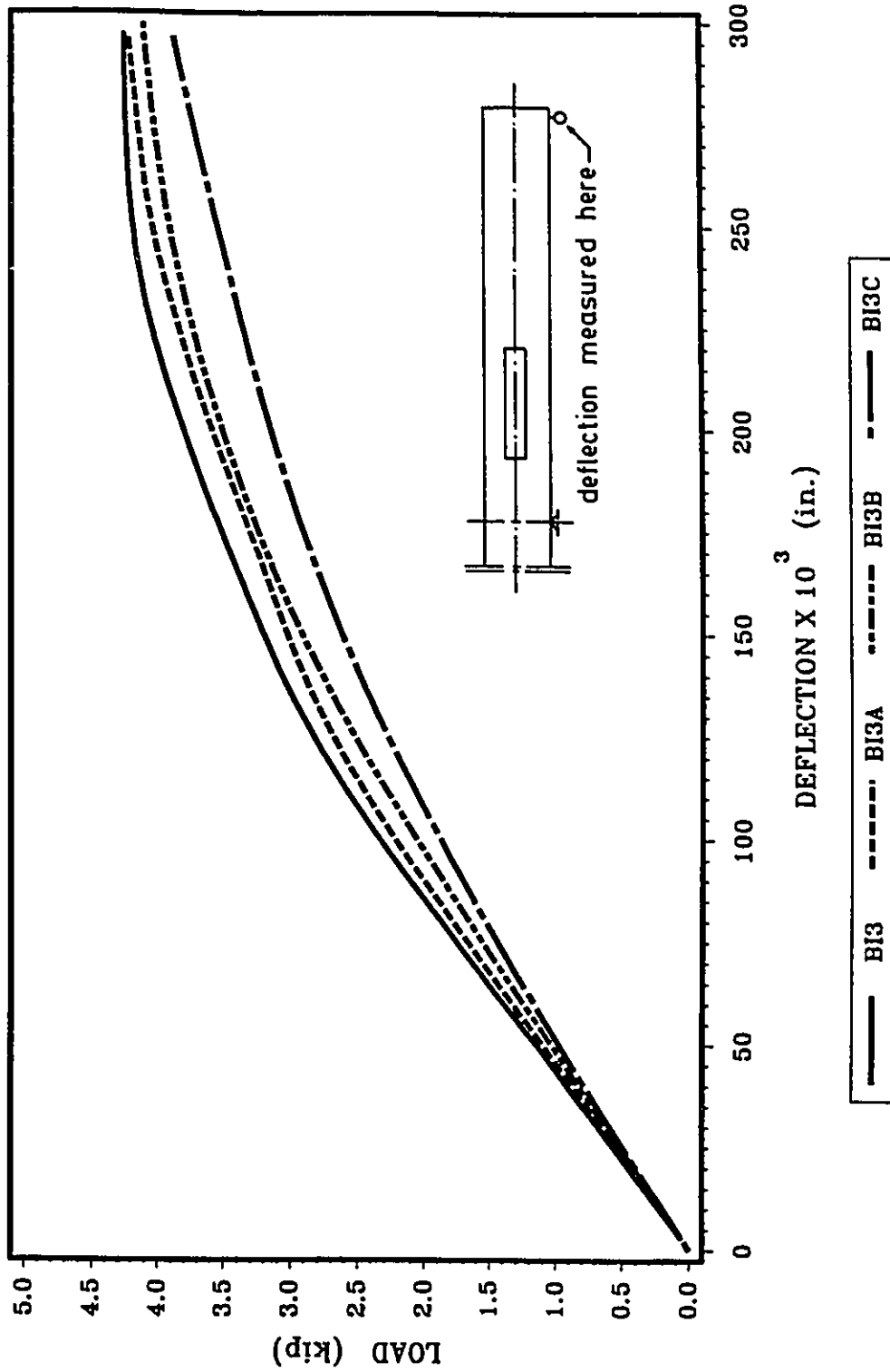


FIG. 5.18 LOAD-DEFLECTION RELATIONSHIP FOR BI3, BI3A, BI3B & BI3C

Note: 1 in.=25.4 mm, 1 kip=4.45 kN

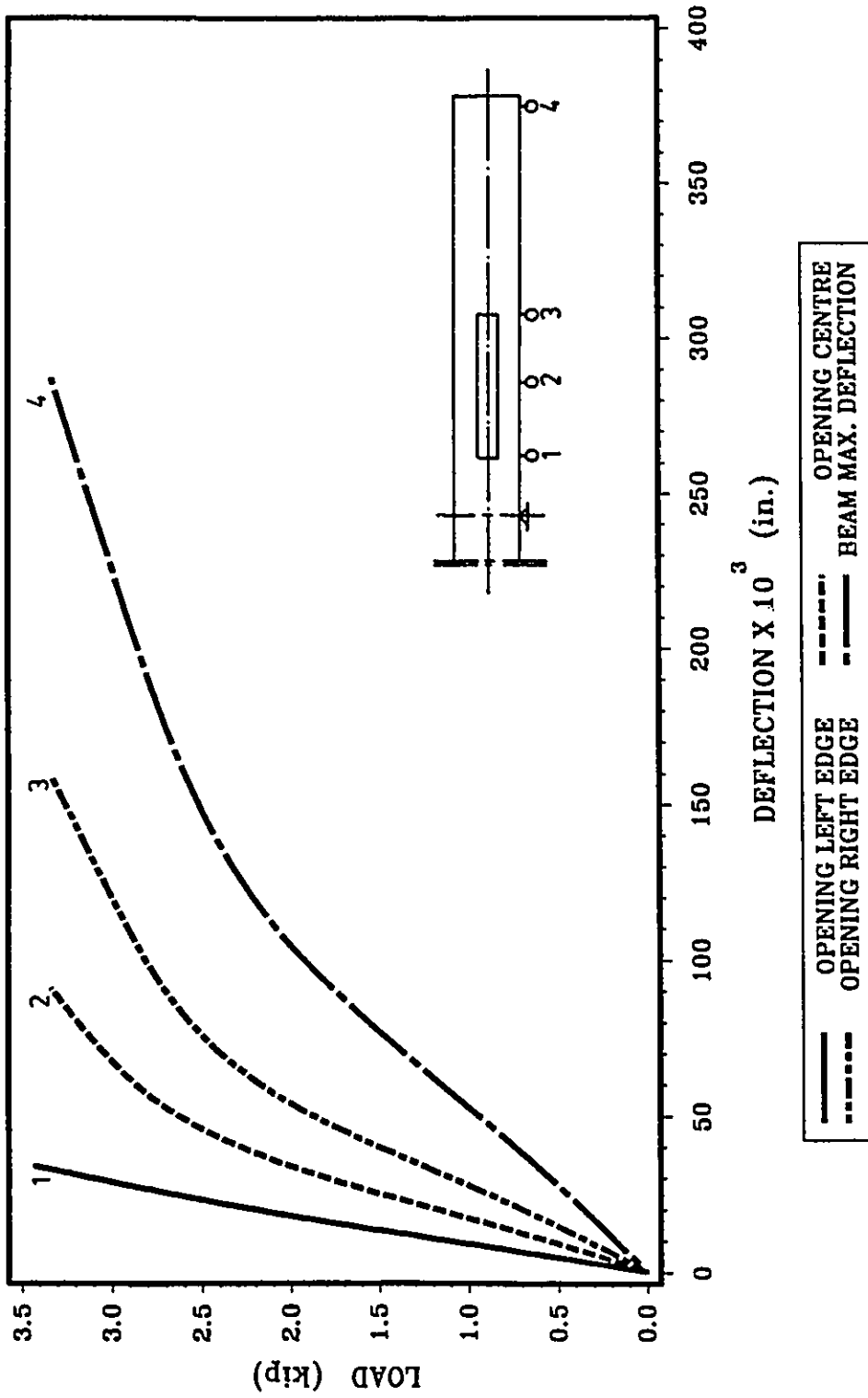


FIG. 5.19 OPENING DEFLECTION FOR B13C
(EXPERIMENTAL)

Note: 1 in.=25.4 mm, 1 kip= 4.45 kN

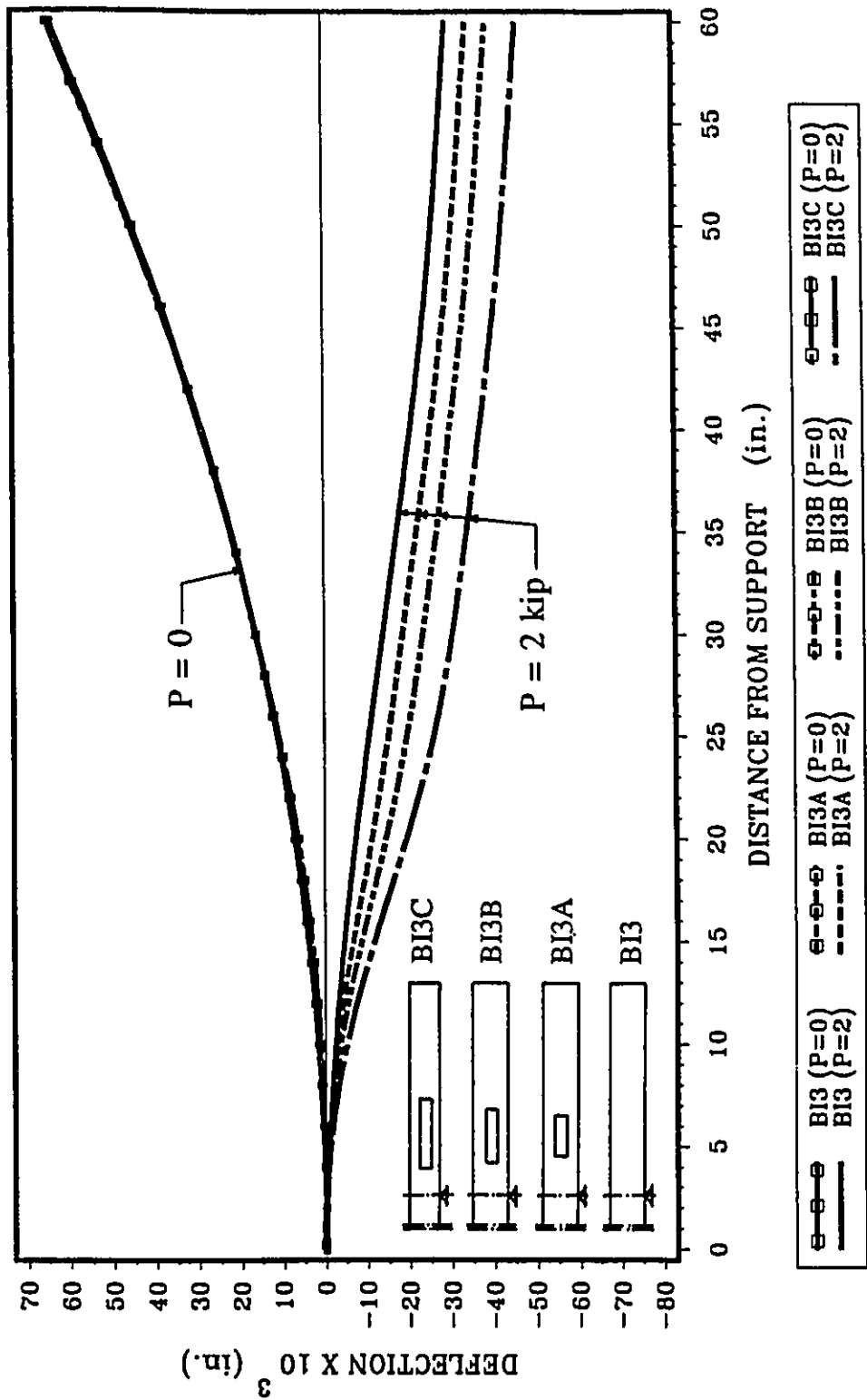


FIG. 5.20 DEFLECTED SHAPE FOR B13, B13A, B13B & B13C
(P = 0 & P = 2 kip)

Note: 1 in.=25.4 mm, 1 kip=4.45 kN

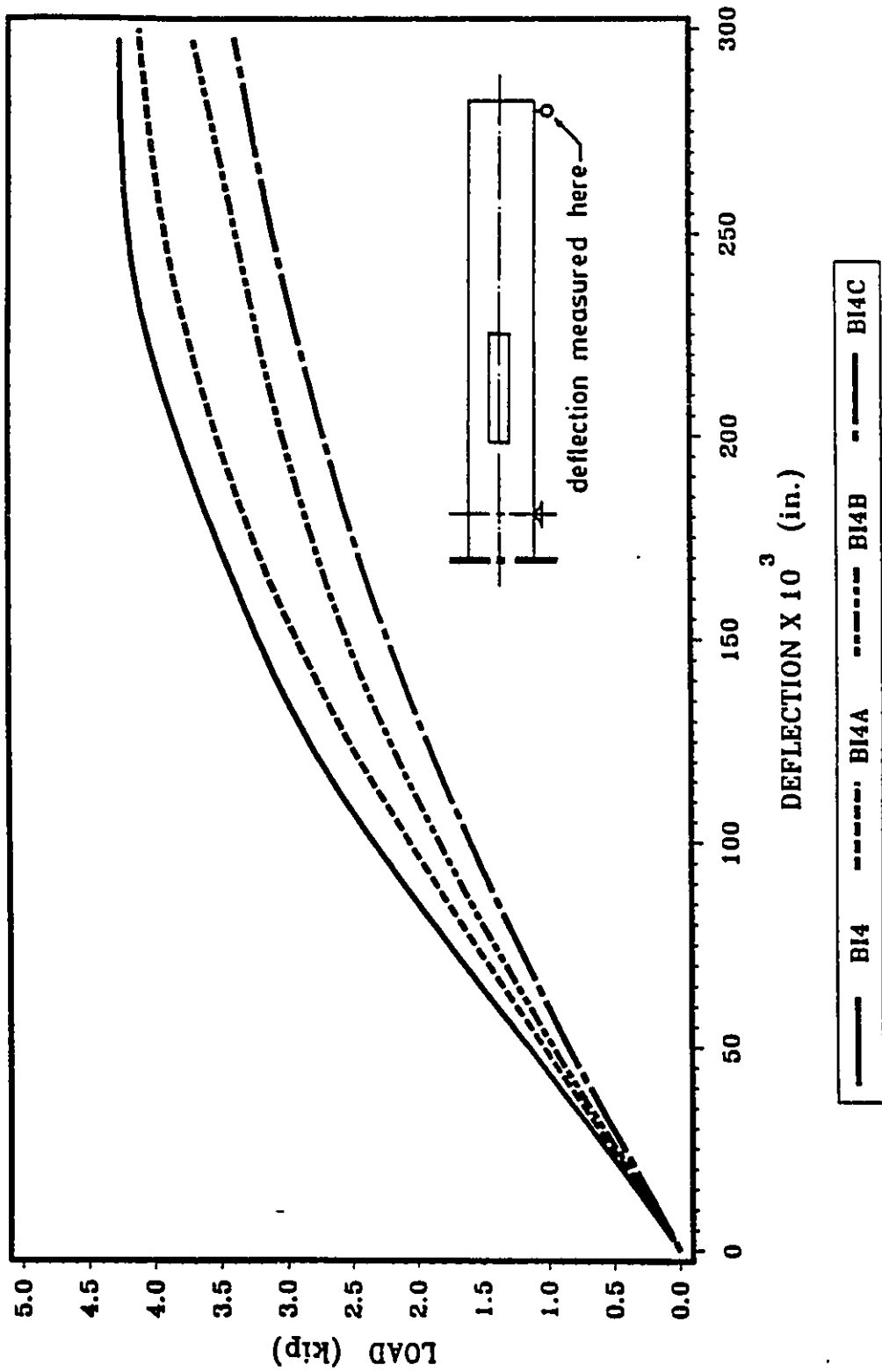


FIG. 5.21 LOAD-DEFLECTION RELATIONSHIP FOR BI4, BI4A, BI4B & BI4C

Note: 1 in.=25.4 mm, 1 kip=4.45 kN

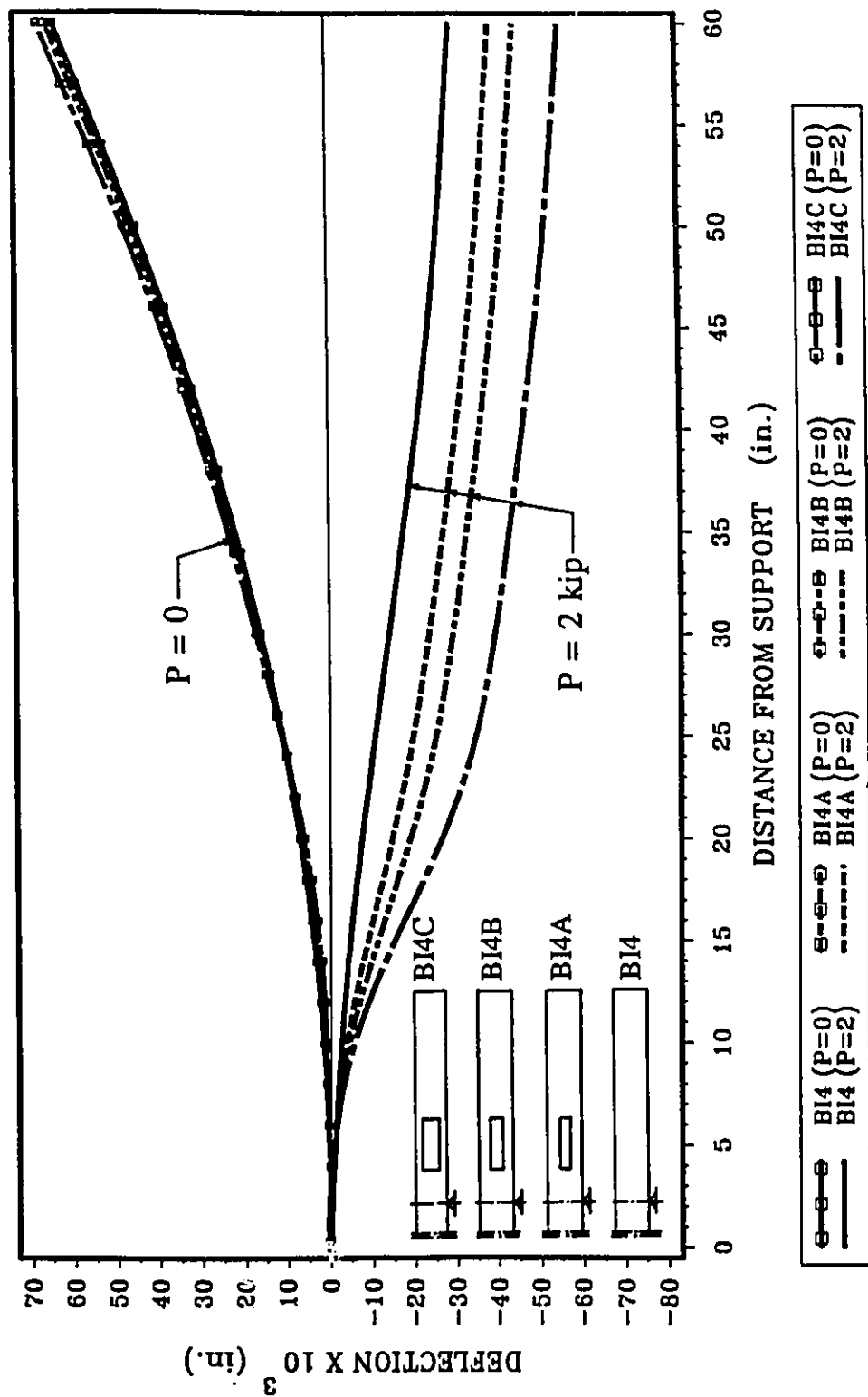


FIG. 5.22 DEFLECTED SHAPE FOR BI4, BI4A, BI4B & BI4C
(P = 0 & P = 2 kip)

Note: 1 in.=25.4 mm, 1 kip=4.45 kN

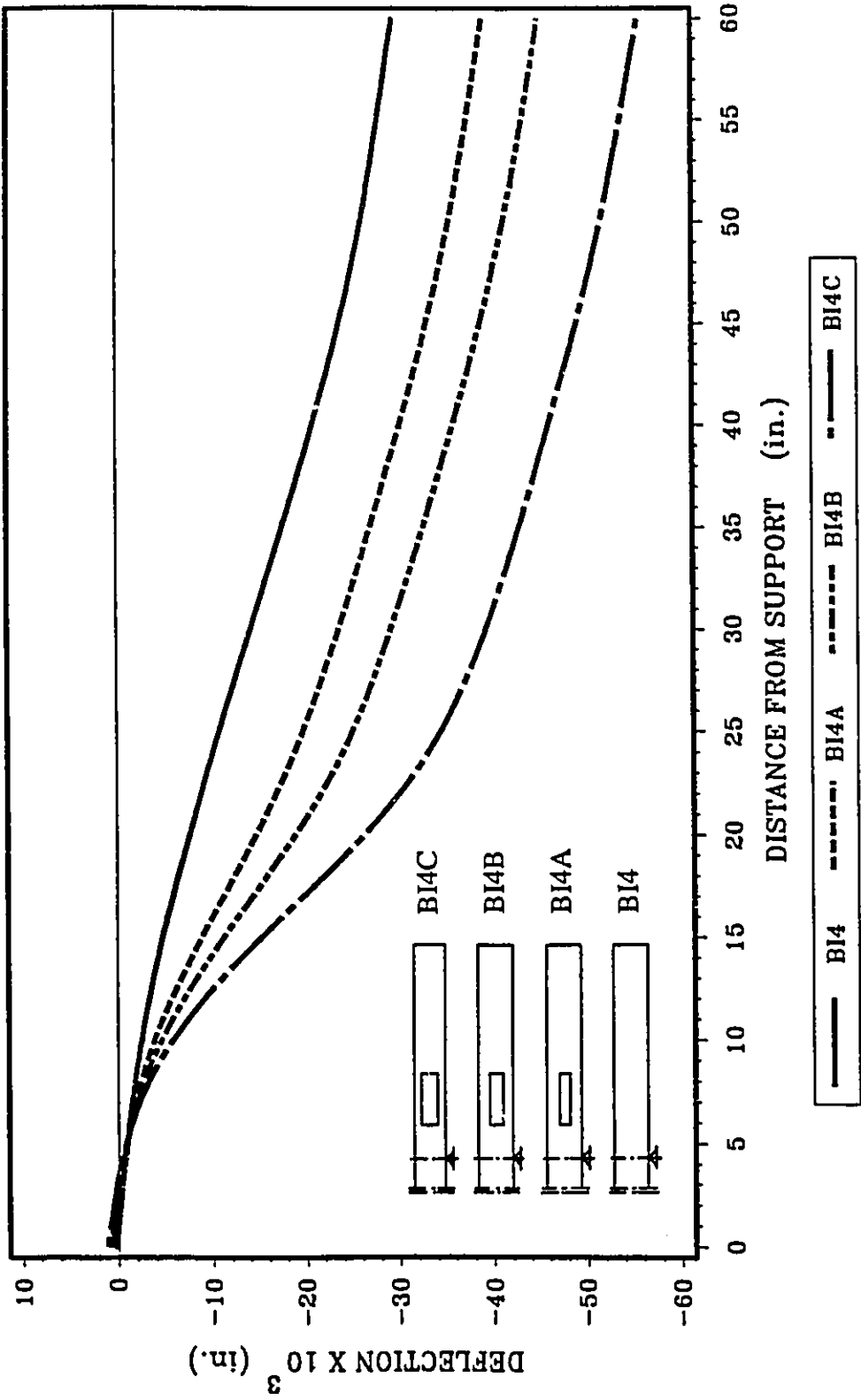


FIG. 5.23 DEFLECTED SHAPE FOR BI4, BI4A, BI4B & BI4C
(P = 2 kip)

Note: 1 in.=25.4 mm, 1 kip=4.45 kN

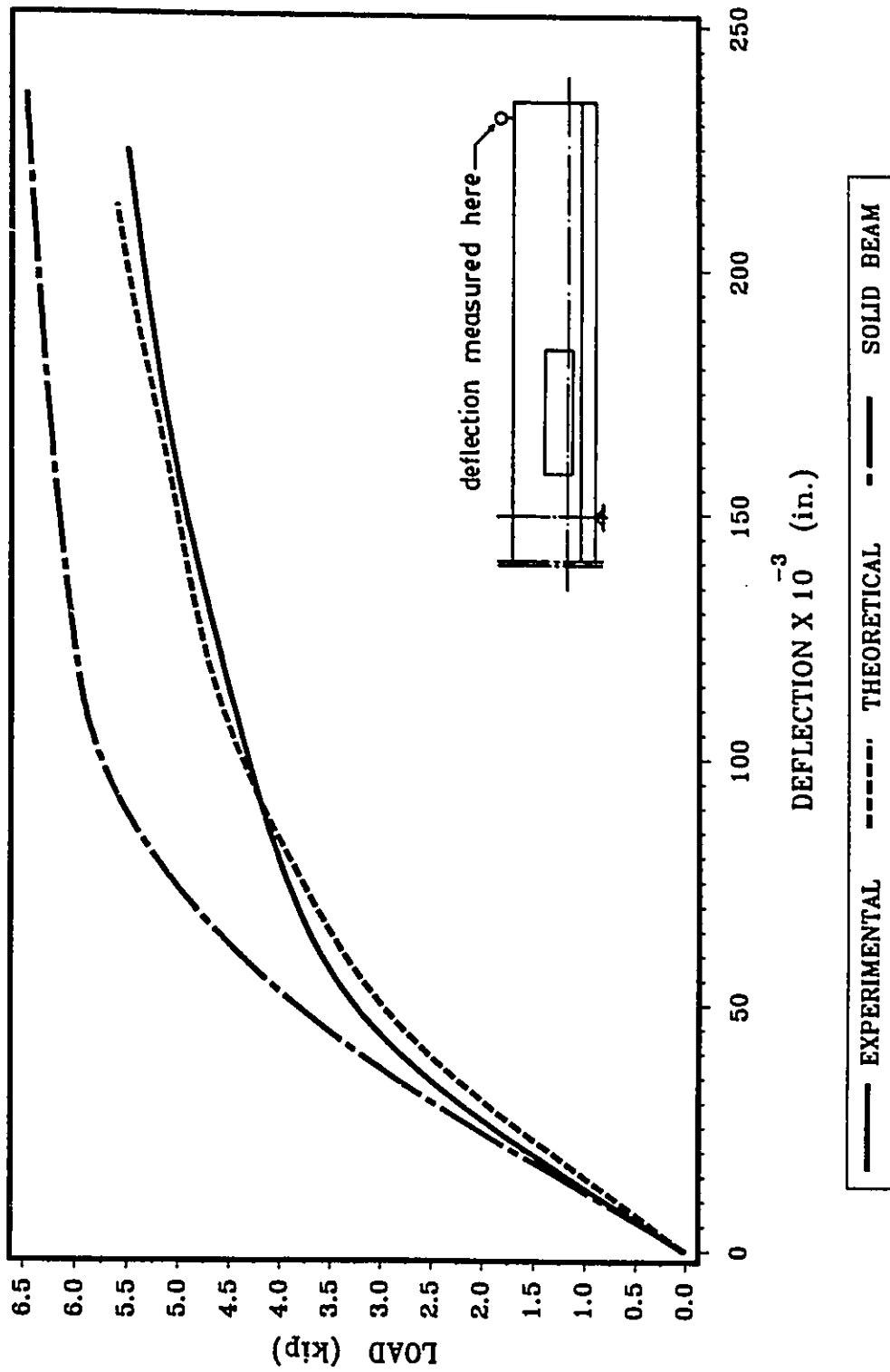


FIG. 5.24 LOAD-DEFLECTION RELATIONSHIP FOR BII1A

Note: 1 in.=25.4 mm, 1 kip=4.45 kN

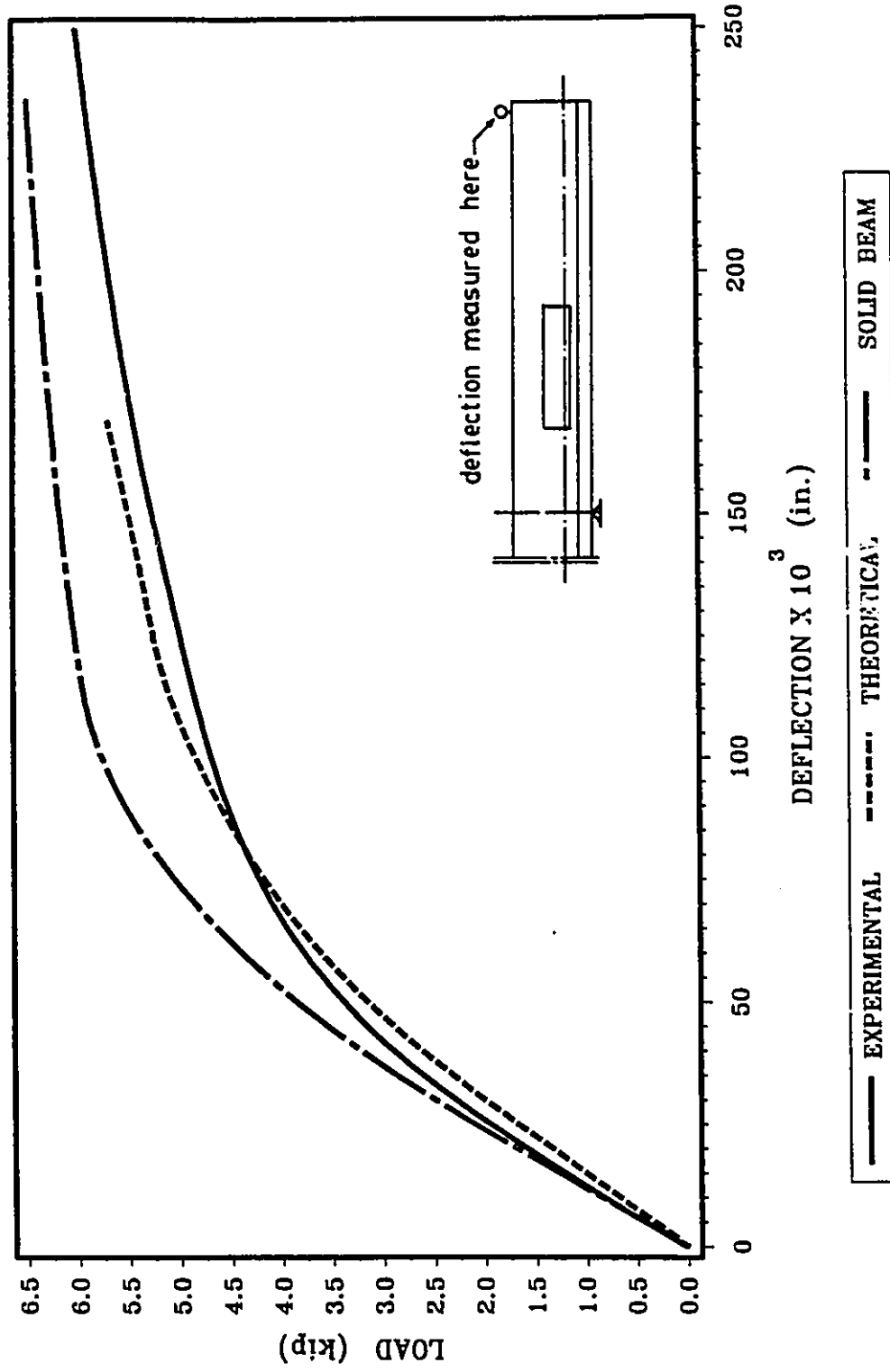


FIG. 5.25 LOAD-DEFLECTION RELATIONSHIP FOR BII1B

Note: 1 in.=25.4 mm, 1 kip=4.45 kN

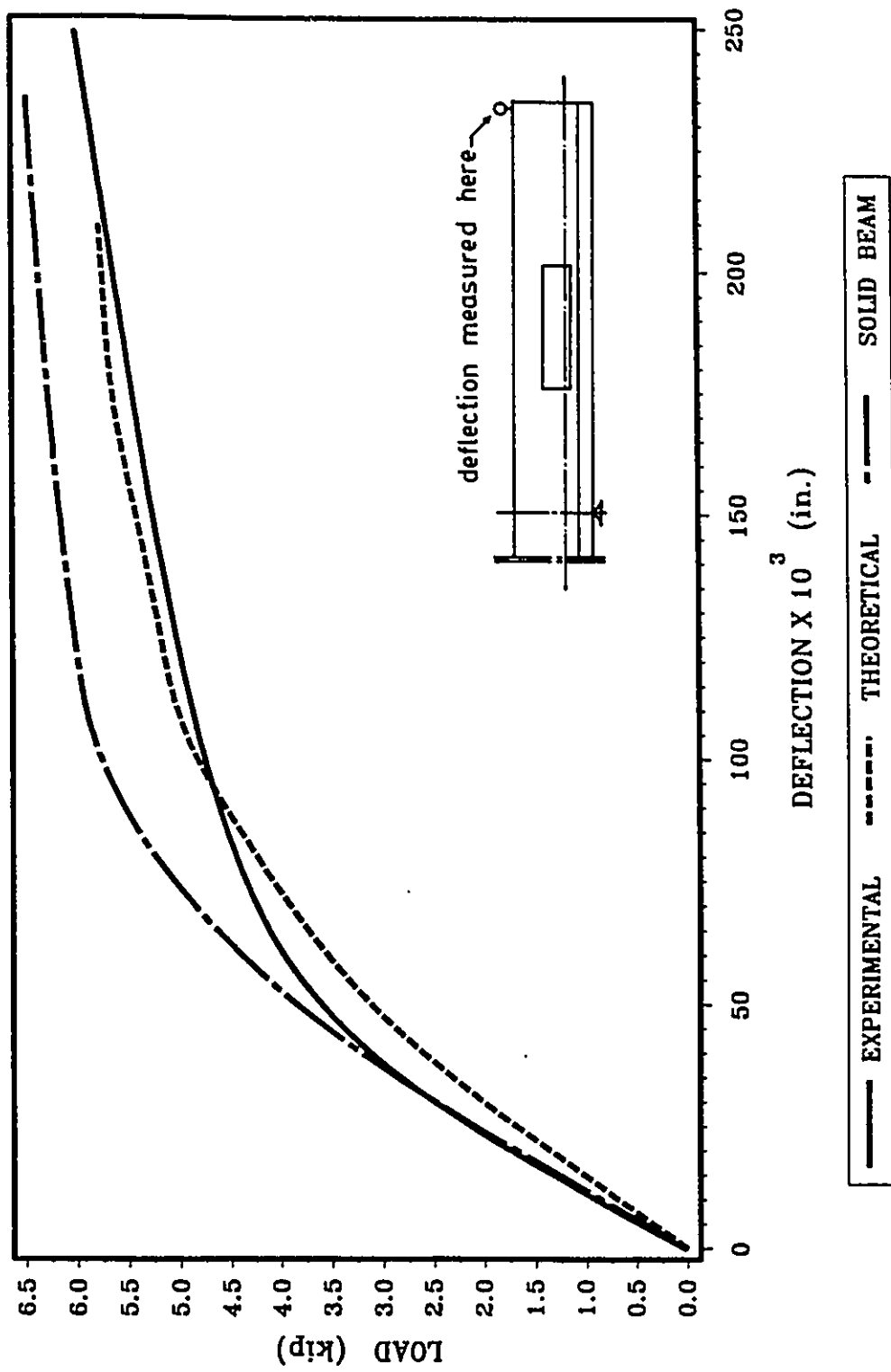


FIG. 5.26 LOAD-DEFLECTION RELATIONSHIP FOR BII1C

Note: 1 in.=25.4 mm, 1 kip=4.45 kN

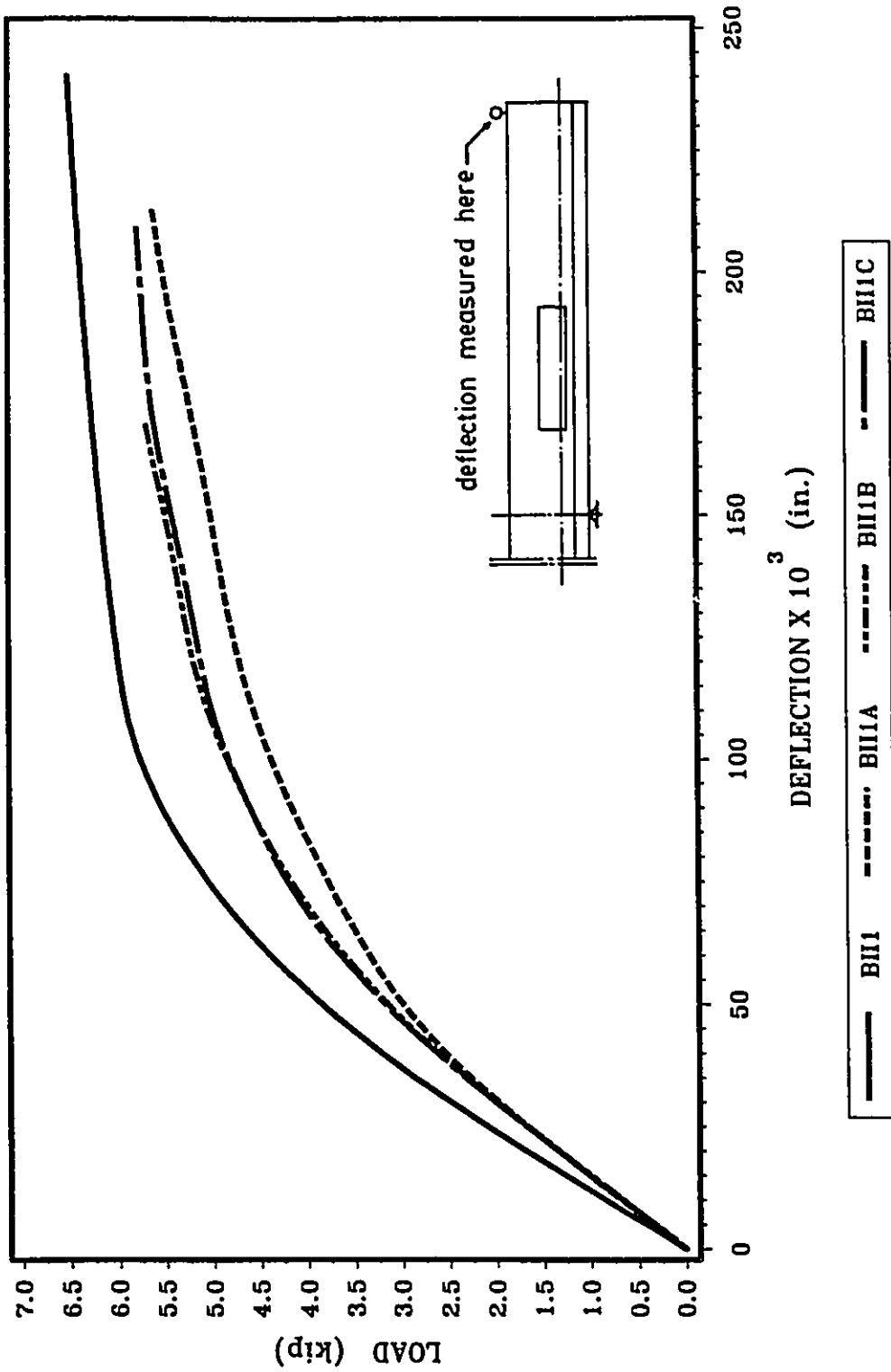


FIG. 5.27 LOAD-DEFLECTION RELATIONSHIP FOR BII1, BII1A, BII1B & BII1C

Note: 1 in.=25.4 mm, 1 kip=4.45 kN

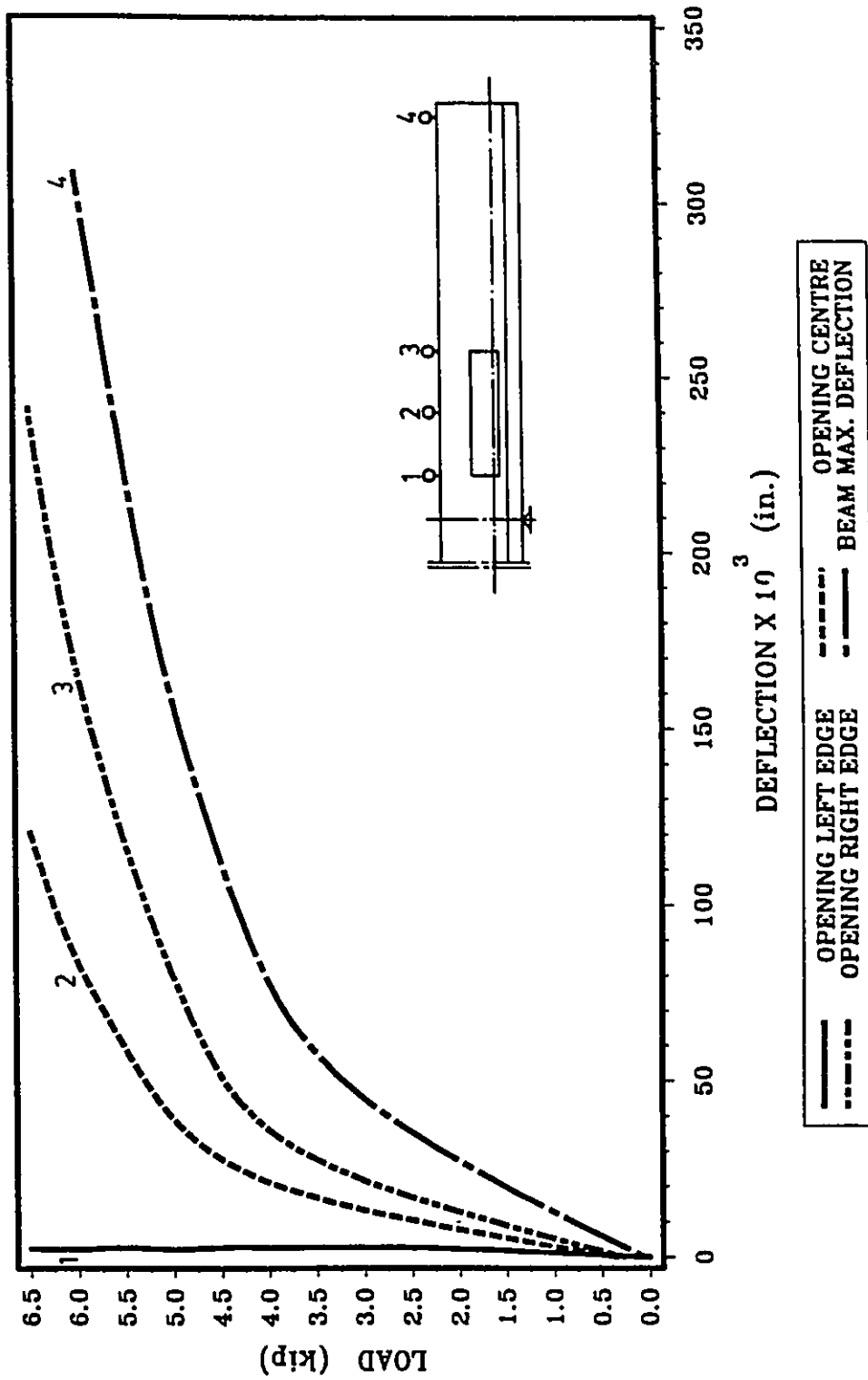


FIG. 5.28 OPENING DEFLECTION FOR BII1A
(EXPERIMENTAL)

Note: 1 in. = 25.4 mm, 1 kip = 4.45 kN

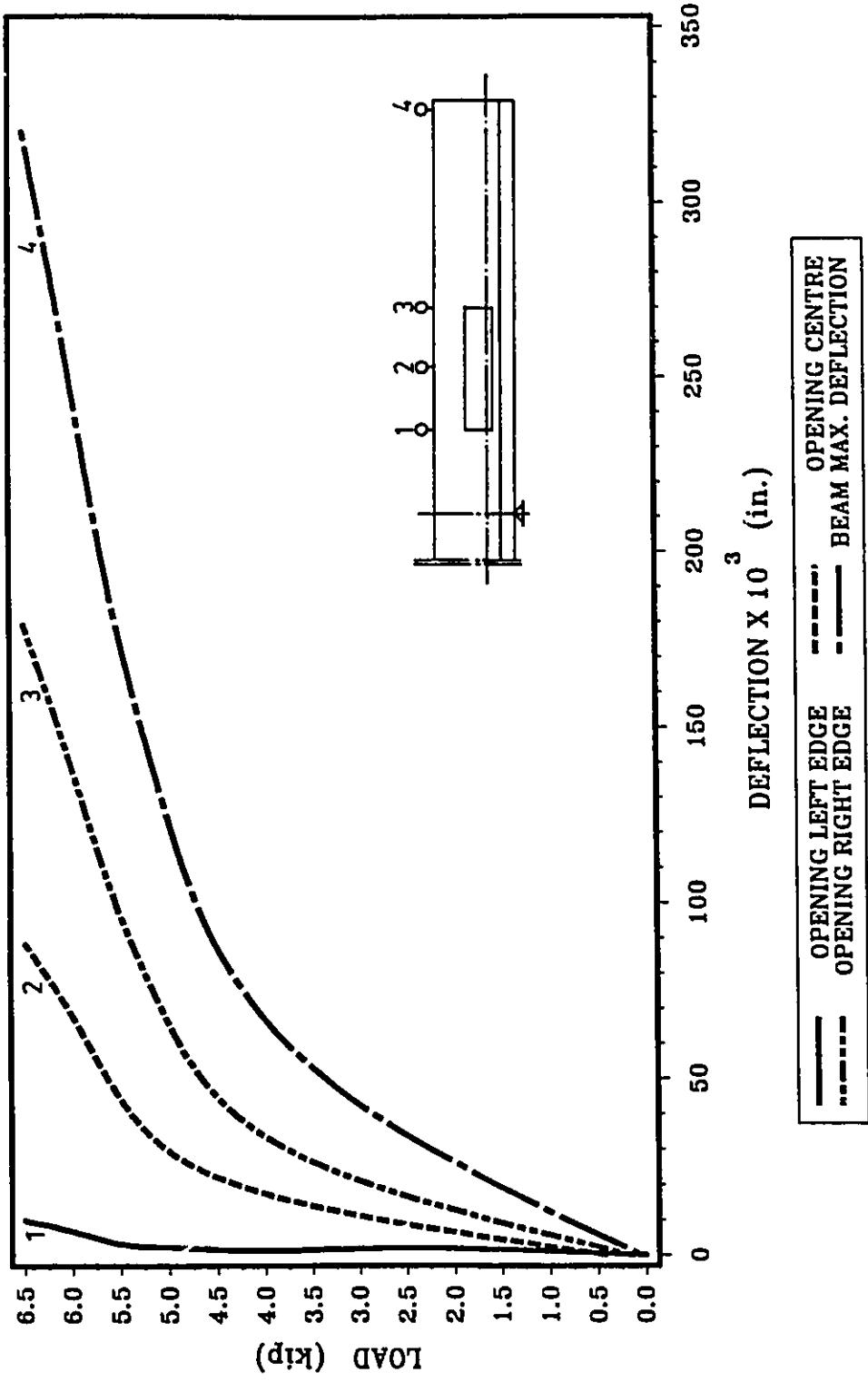


FIG. 5.29 OPENING DEFLECTION FOR BII1B
(EXPERIMENTAL)

Note: 1 in.=25.4 mm, 1 kip= 4.45 kN

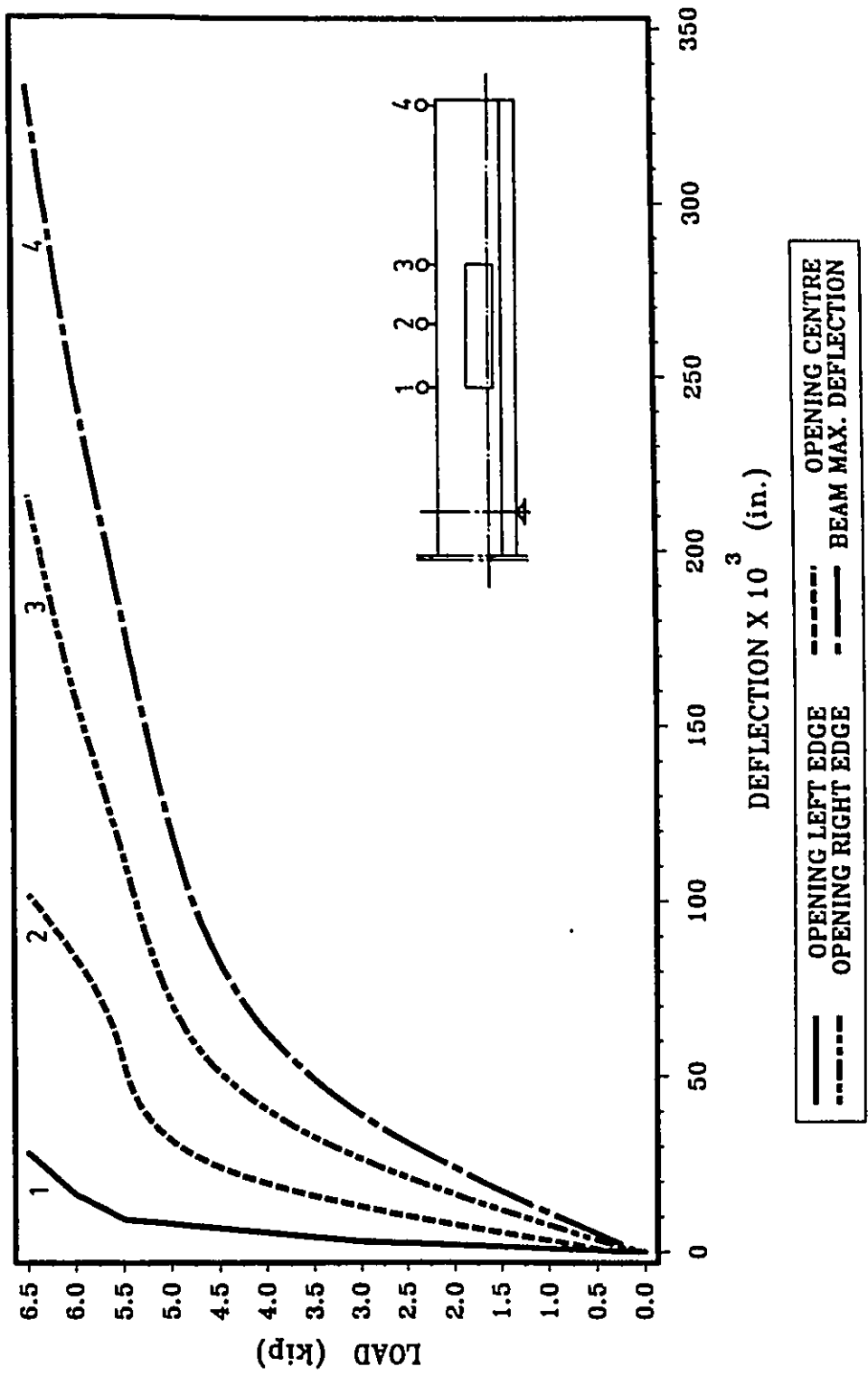


FIG. 5.30 OPENING DEFLECTION FOR RII1C
(EXPERIMENTAL)

Note: 1 in.=25.4 mm, 1 kip= 4.45 kN

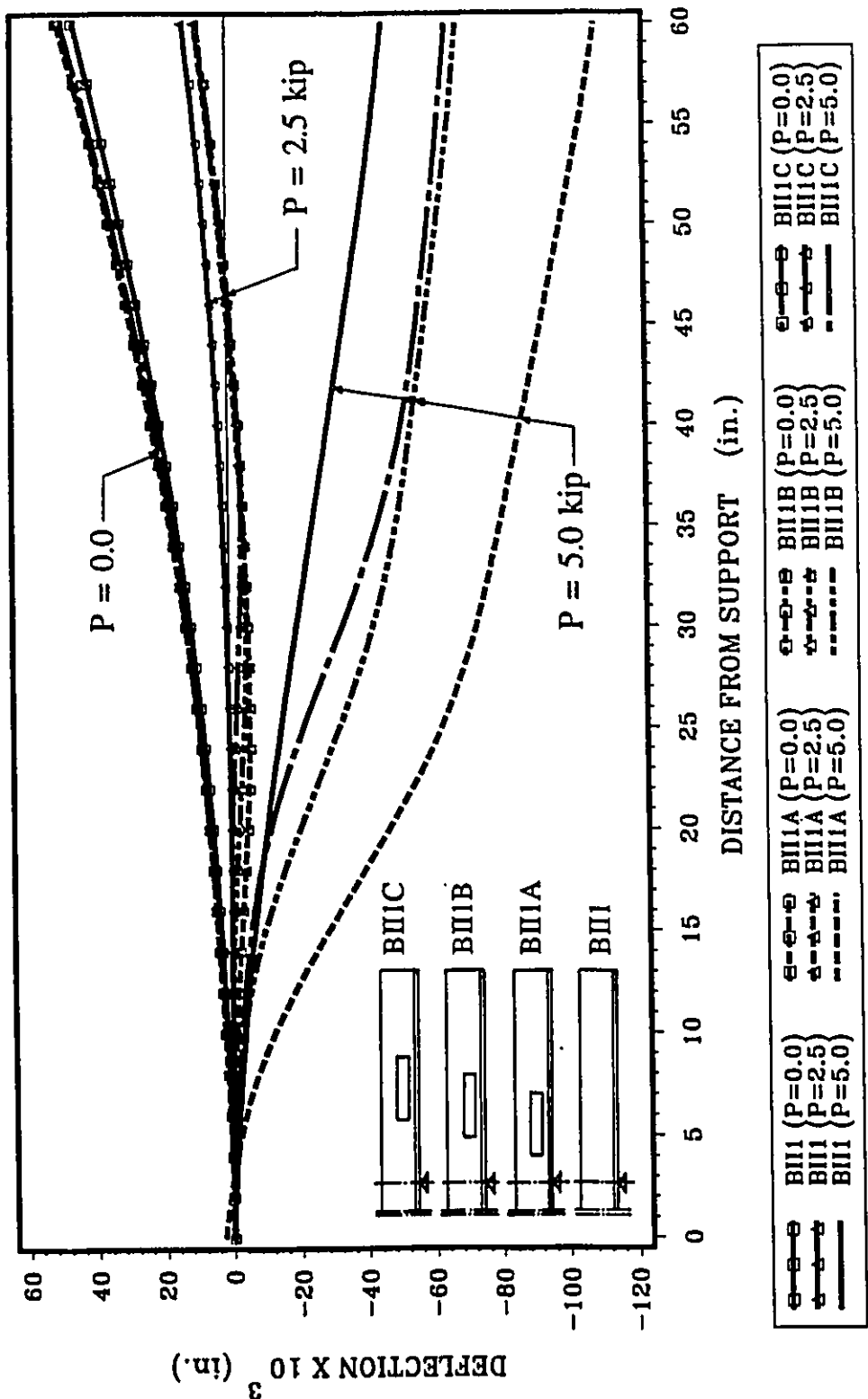


FIG. 5.31 DEFLECTED SHAPE FOR BII1, BII1A, BII1B & BII1C
 (P = 0, P = 2.5 & P = 5 kip)

Note: 1 in.=25.4 mm, 1 kip=4.45 kN

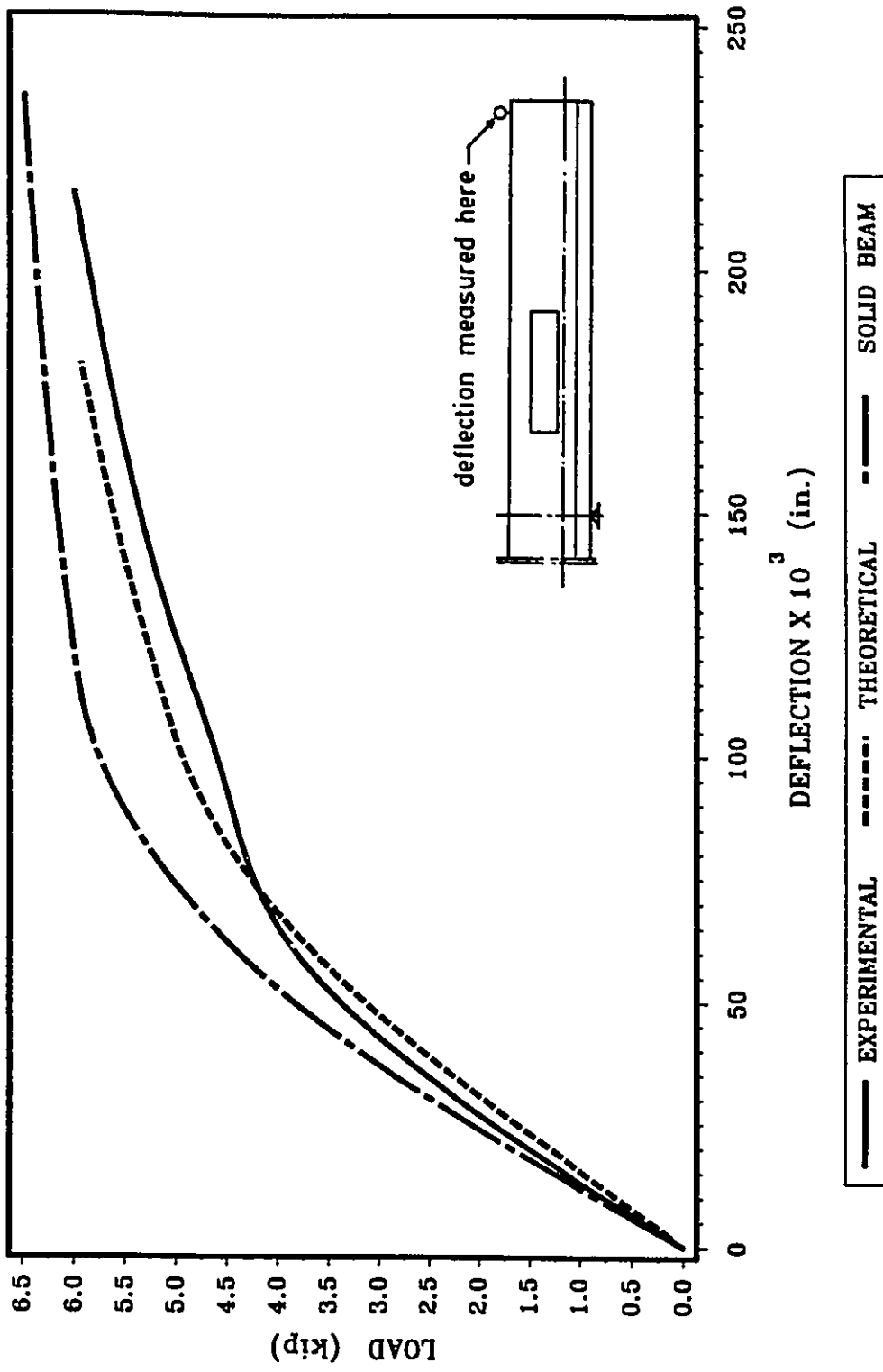


FIG. 5.32 LOAD--DEFLECTION RELATIONSHIP FOR BII2B

Note: 1 in.=25.4 mm, 1 kip=4.45 kN

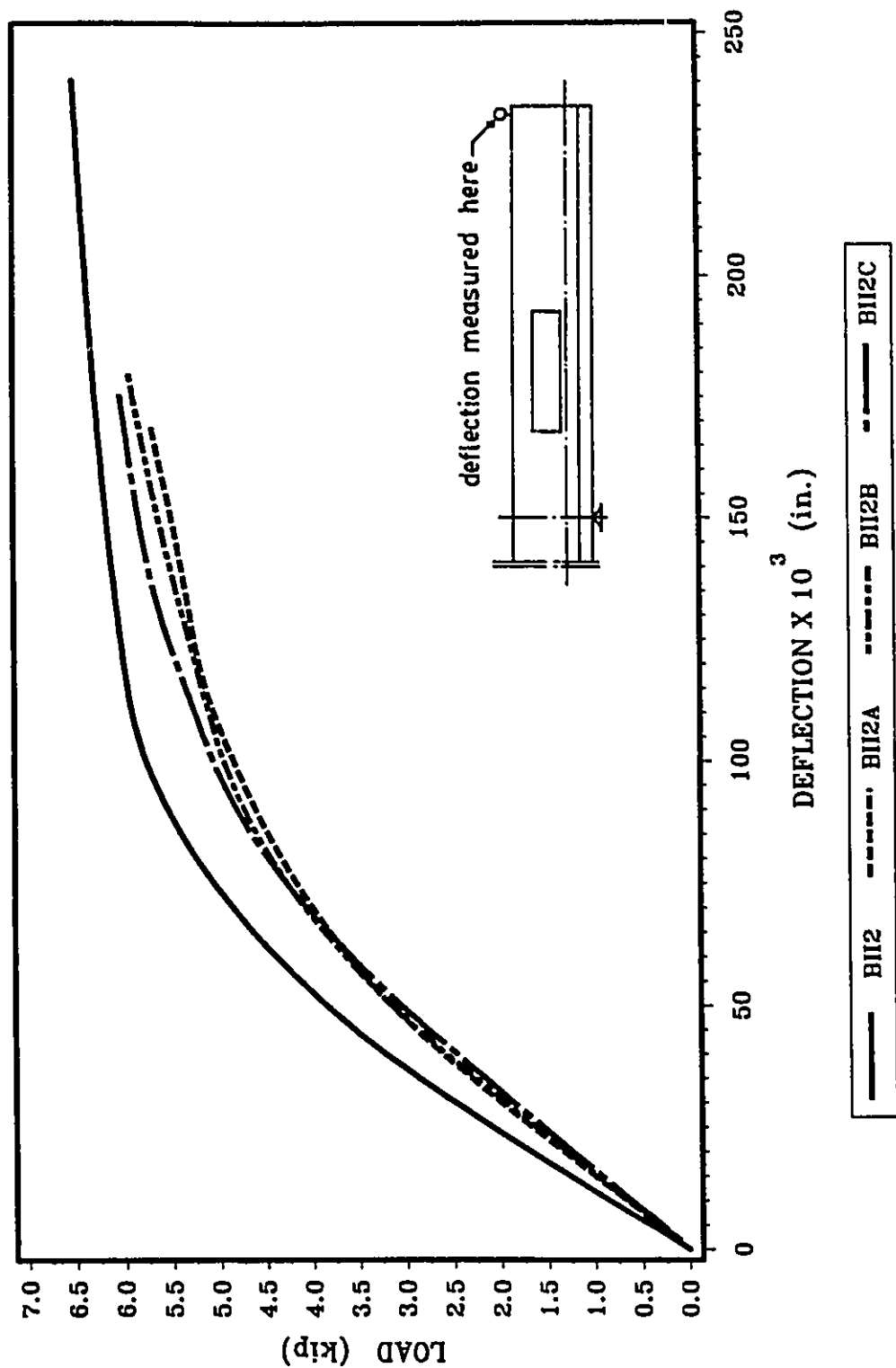


FIG. 5.33 LOAD-DEFLECTION RELATIONSHIP FOR BII2, BII2A, BII2B & BII2C

Note: 1 in.=25.4 mm, 1 kip=4.45 kN

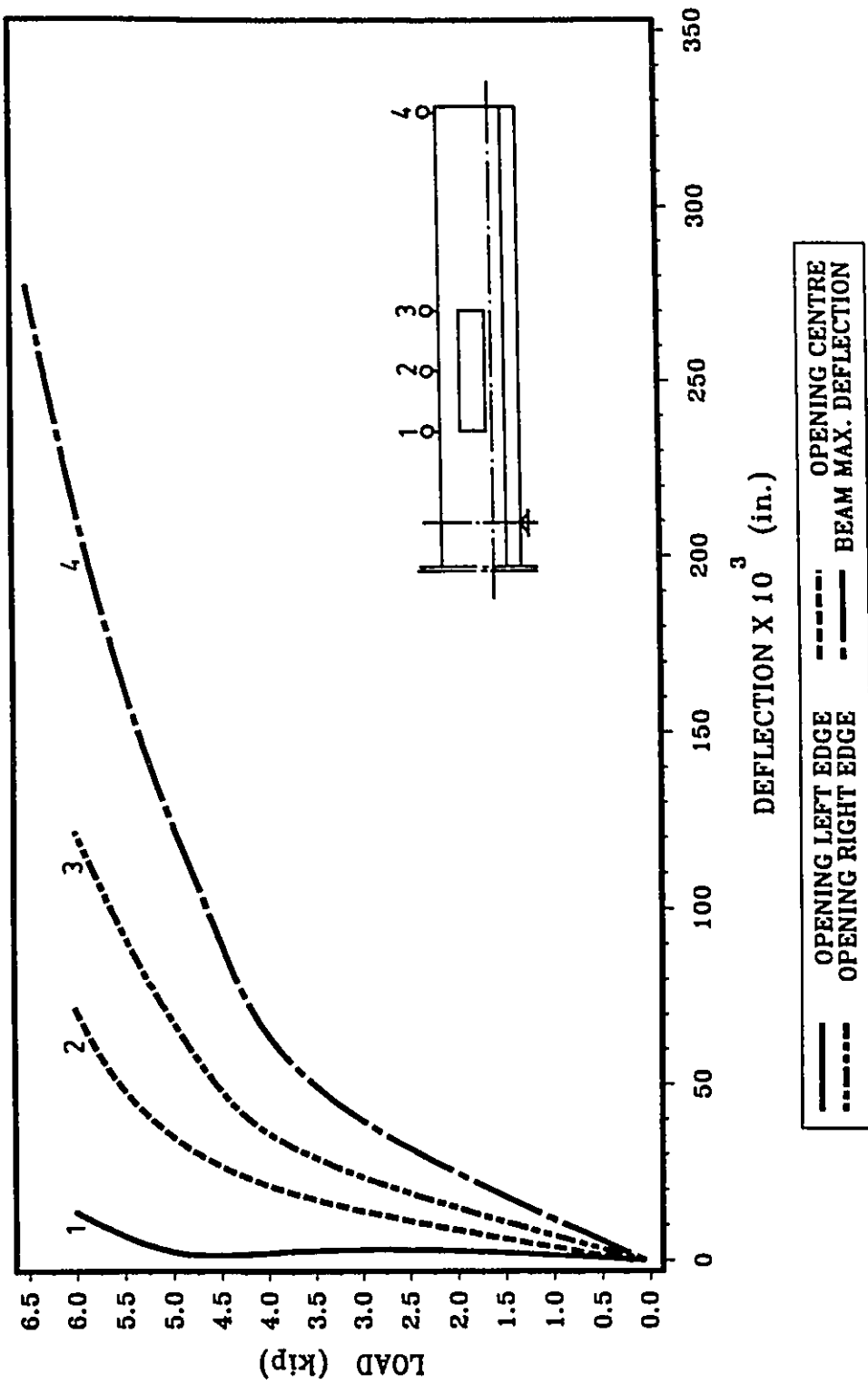


FIG. 5.34 OPENING DEFLECTION FOR B112B
(EXPERIMENTAL)

Note: 1 in.=25.4 mm, 1 kip= 4.45 kN

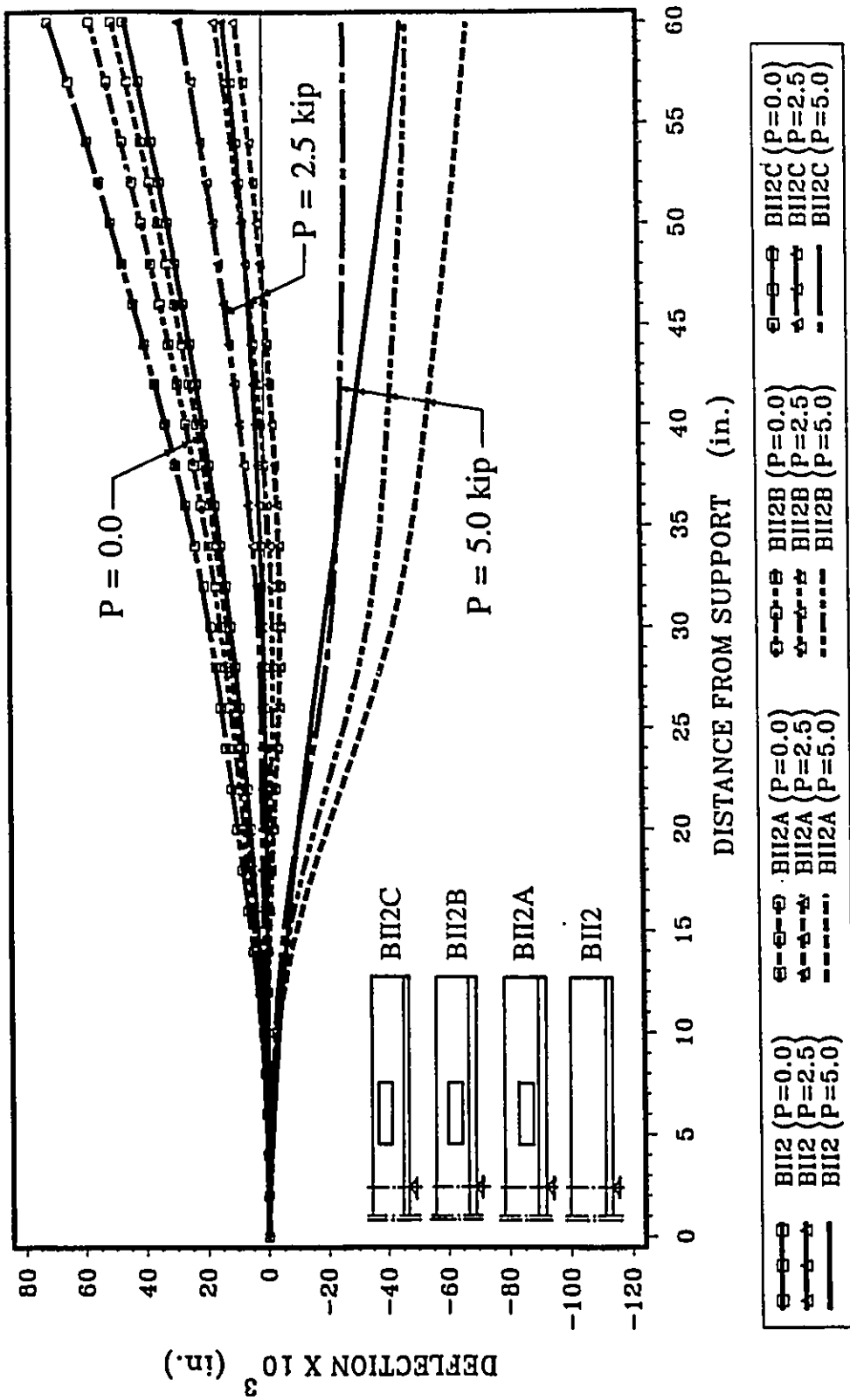


FIG. 5.35 DEFLECTED SHAPE FOR BII2, BII2A, BII2B & BII2C
 (P = 0, P = 2.5 & P = 5 kip)

Note: 1 in.=25.4 mm, 1 kip=4.45 kN

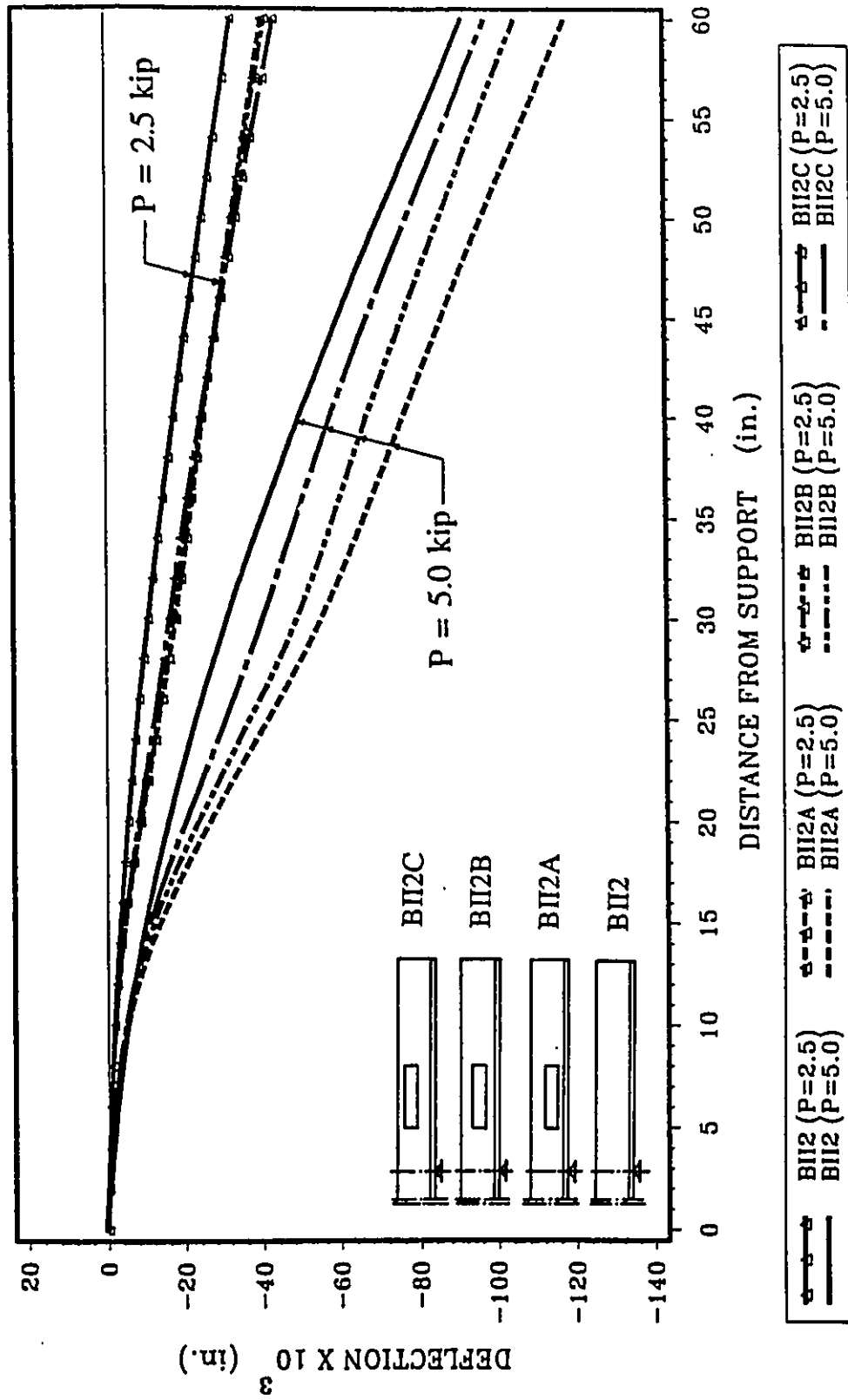


FIG. 5.36 DEFLECTED SHAPE FOR BII2, BII2A, BII2B & BII2C
(DUE TO P = 2.5 & P = 5 kip)

Note: 1 in.=25.4 mm, 1 kip=4.45 kN

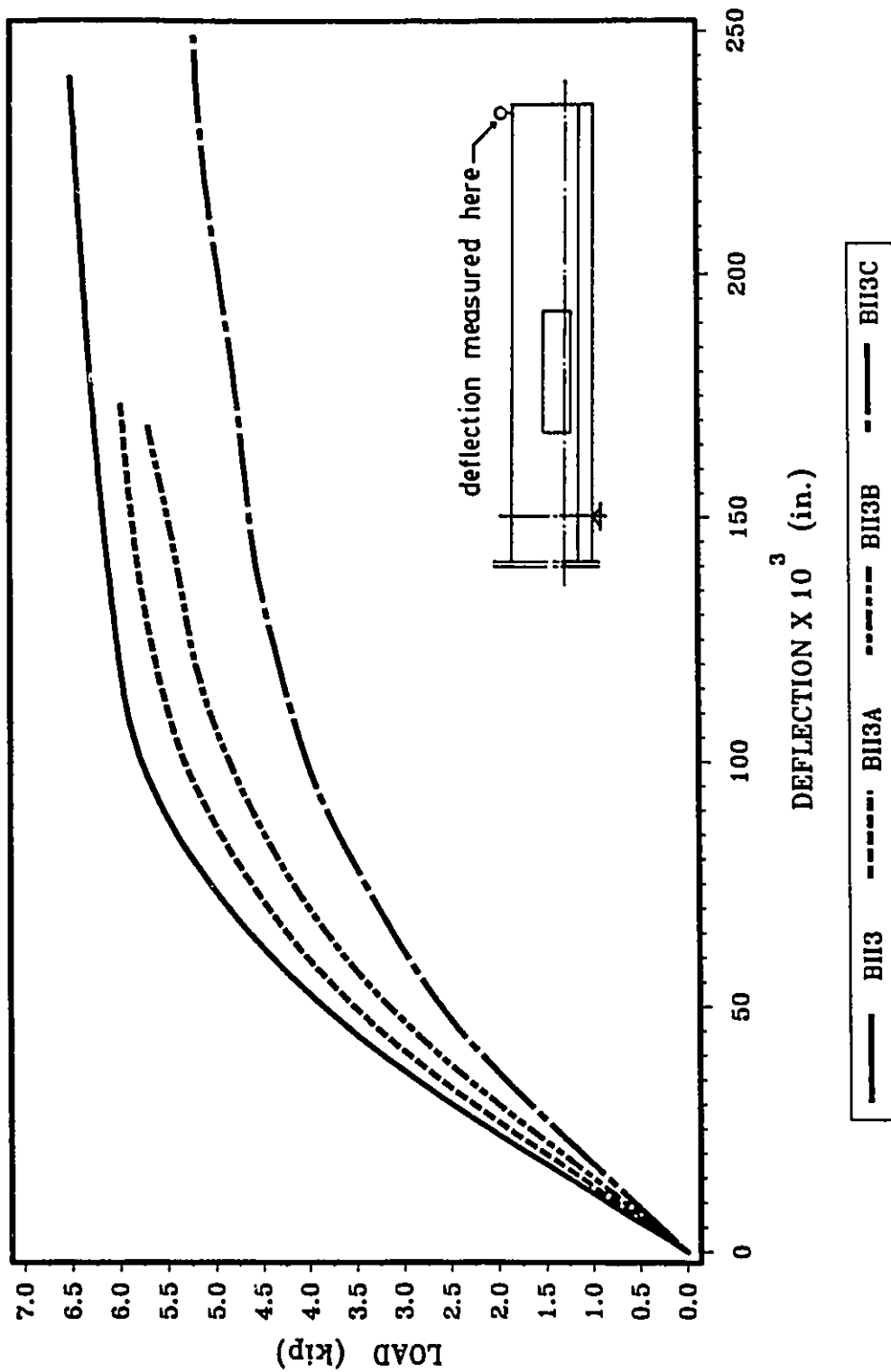


FIG. 5.37 LOAD-DEFLECTION RELATIONSHIP FOR BI13, BI3A, BI3B & BI3C

Note: 1 in.=25.4 mm, 1 kip=4.45 kN

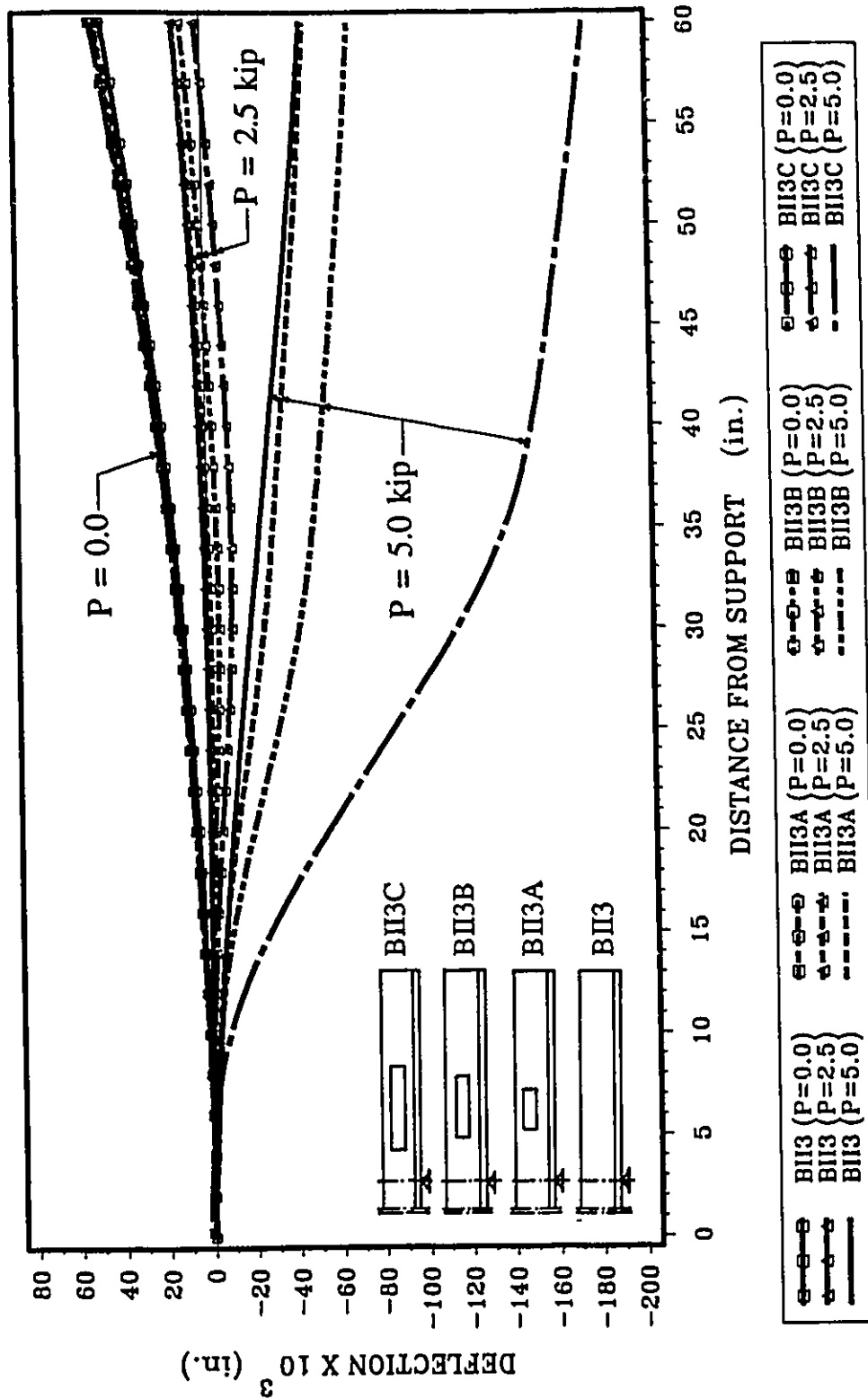


FIG. 5.38 DEFLECTED SHAPE FOR BI13, BI3A, BI3B & BI3C
(P = 0, P = 2.5 & P = 5 kip)

Note: 1 in.=25.4 mm, 1 kip=4.45 kN

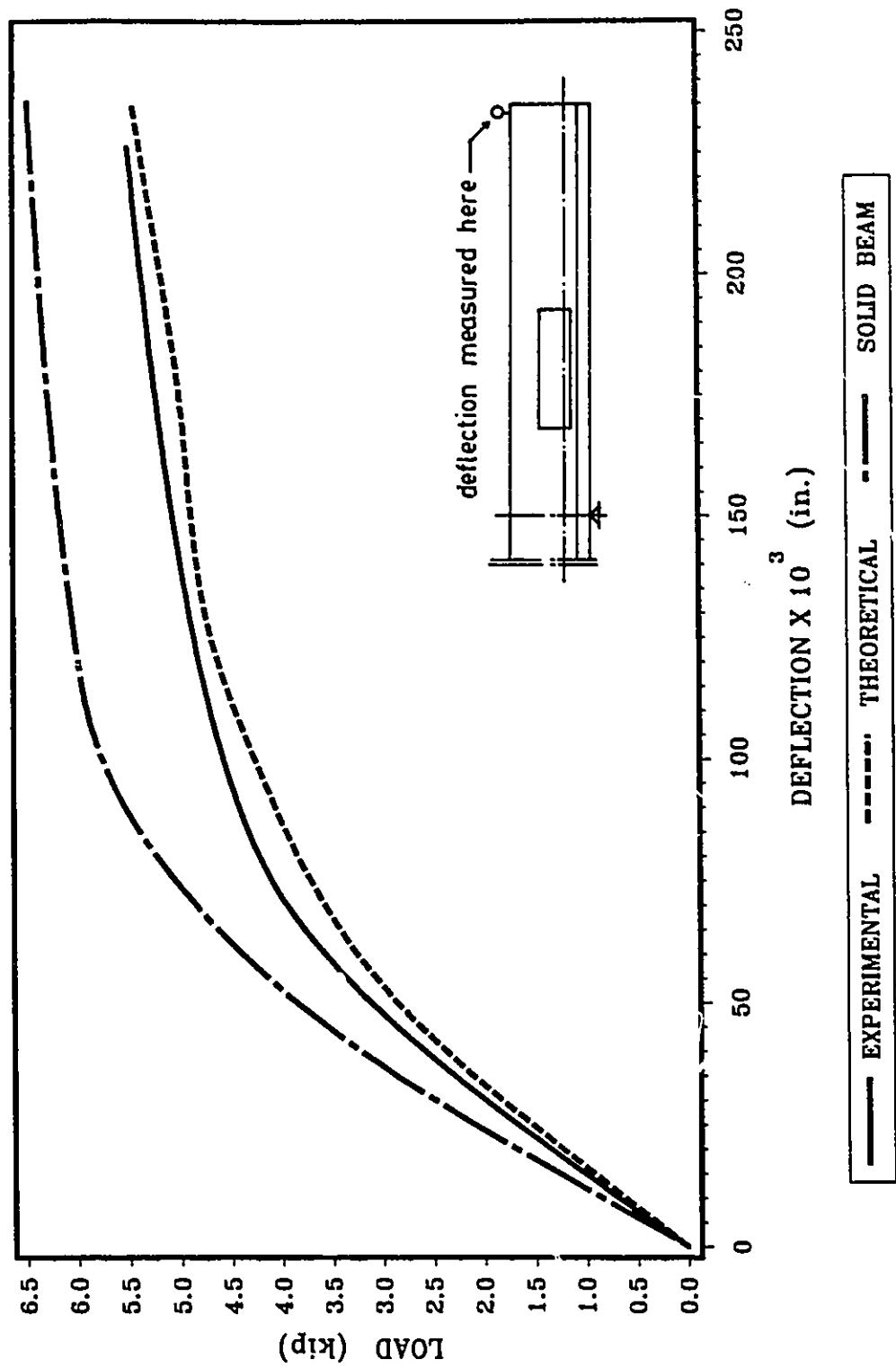


FIG. 5.39 LOAD-DEFLECTION RELATIONSHIP FOR BII4C

Note: 1 in.=25.4 mm, 1 kip=4.45 kN

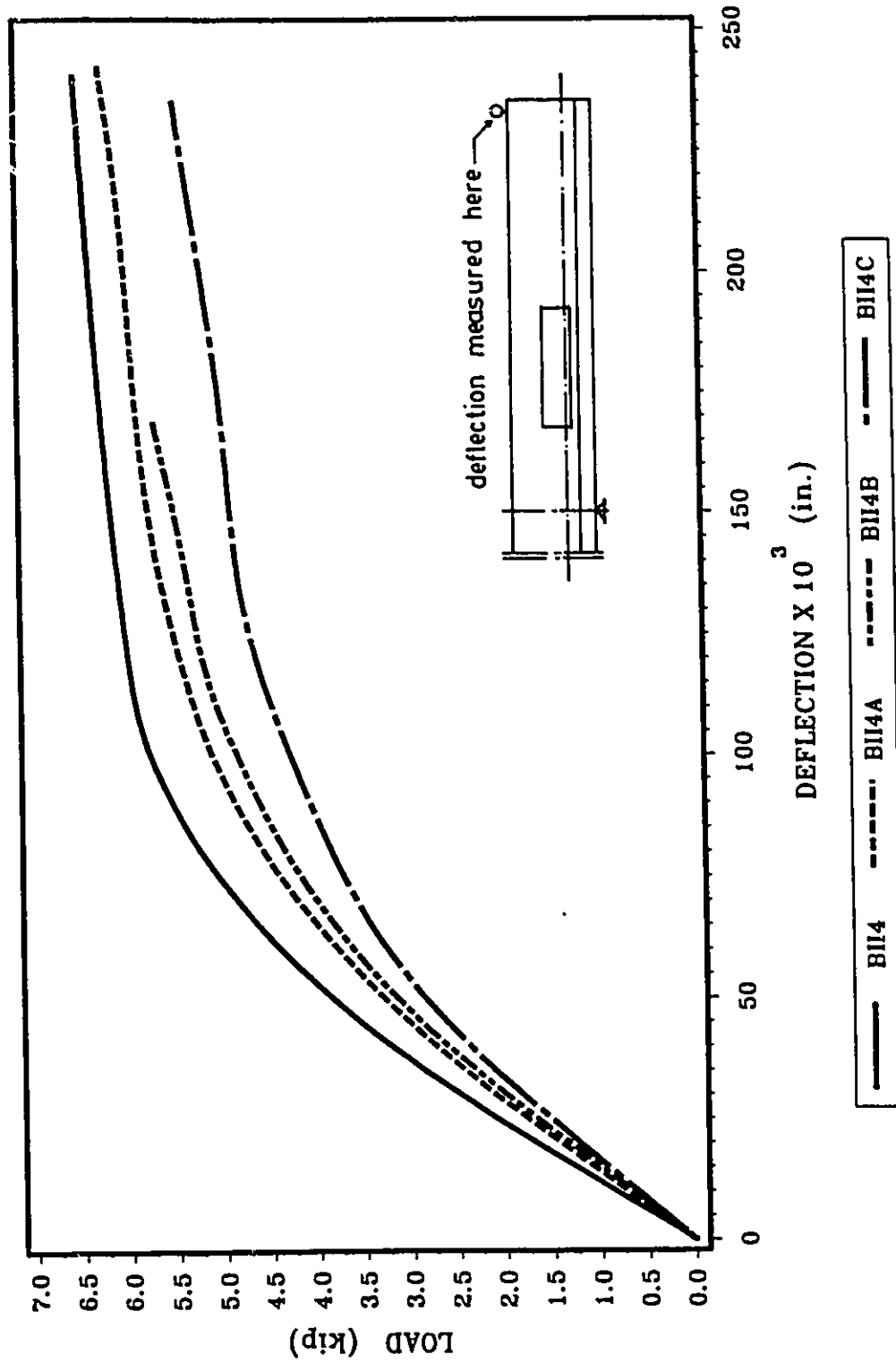


FIG. 5.40 LOAD-DEFLECTION RELATIONSHIP FOR BII4, BII4A, BII4B & BII4C

Note: 1 in.=25.4 mm, 1 kip=4.45 kN

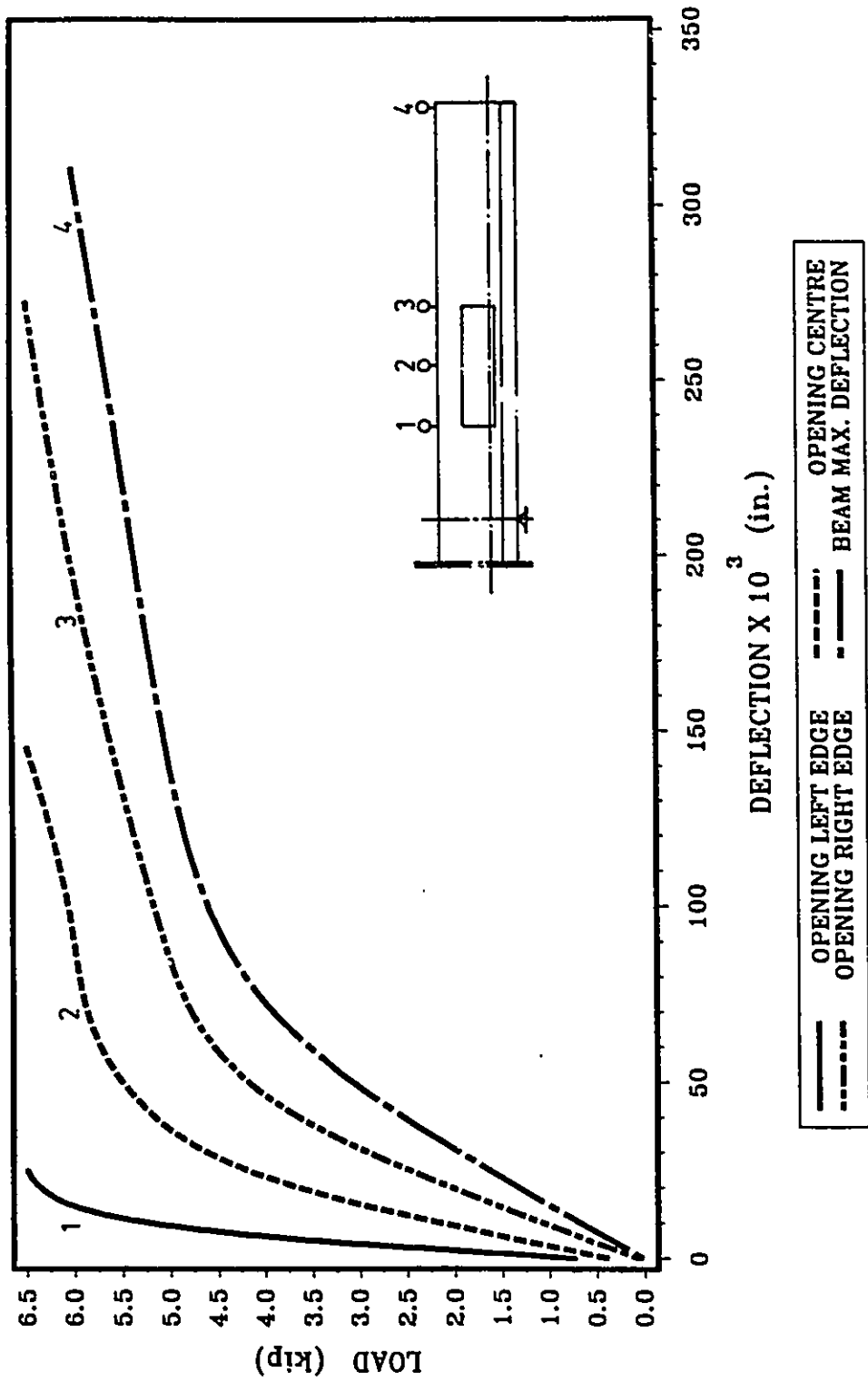


FIG. 5.41 OPENING DEFLECTION FOR BII4C
(EXPERIMENTAL)

Note: 1 in.=25.4 mm, 1 kip= 4.45 kN

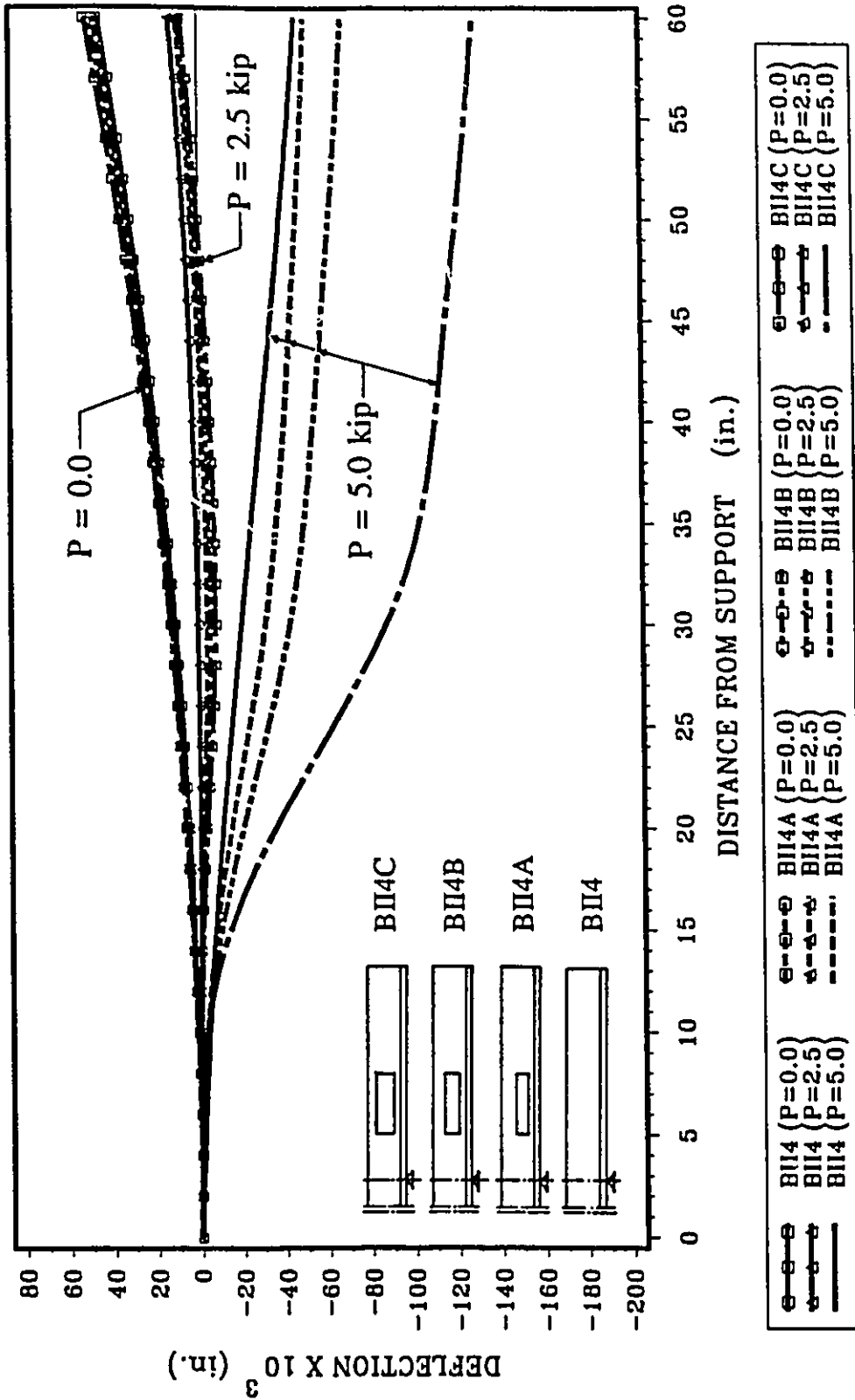


FIG. 5.42 DEFLECTED SHAPE FOR BII4, BII4A, BII4B & BII4C
($P = 0$, $P = 2.5$ & $P = 5$ kip)

Note: 1 in. = 25.4 mm, 1 kip = 4.45 kN

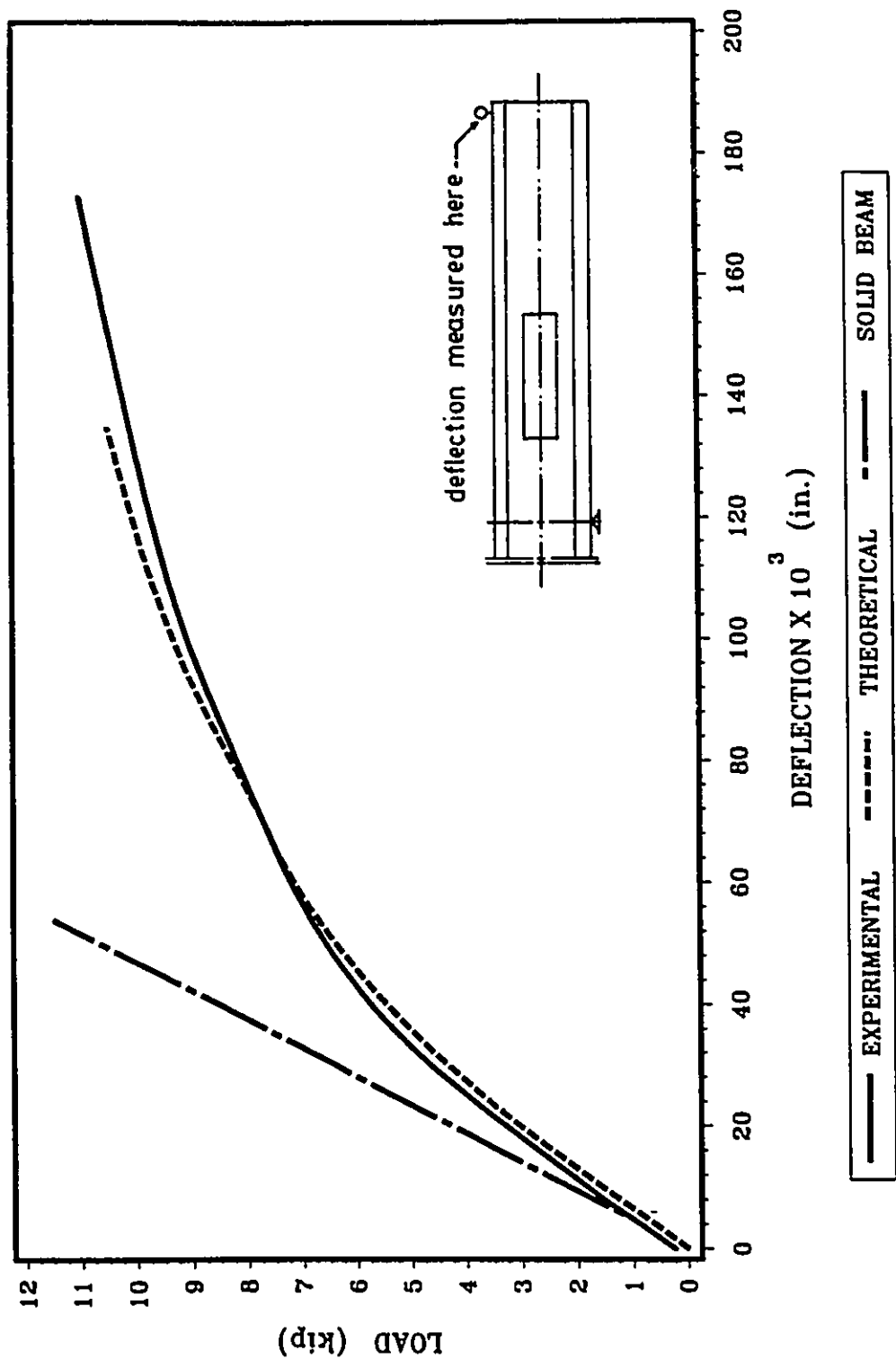


FIG. 5.43 LOAD-DEFLECTION RELATIONSHIP FOR BI111A

Note: 1 in.=25.4 mm, 1 kip=4.45 kN

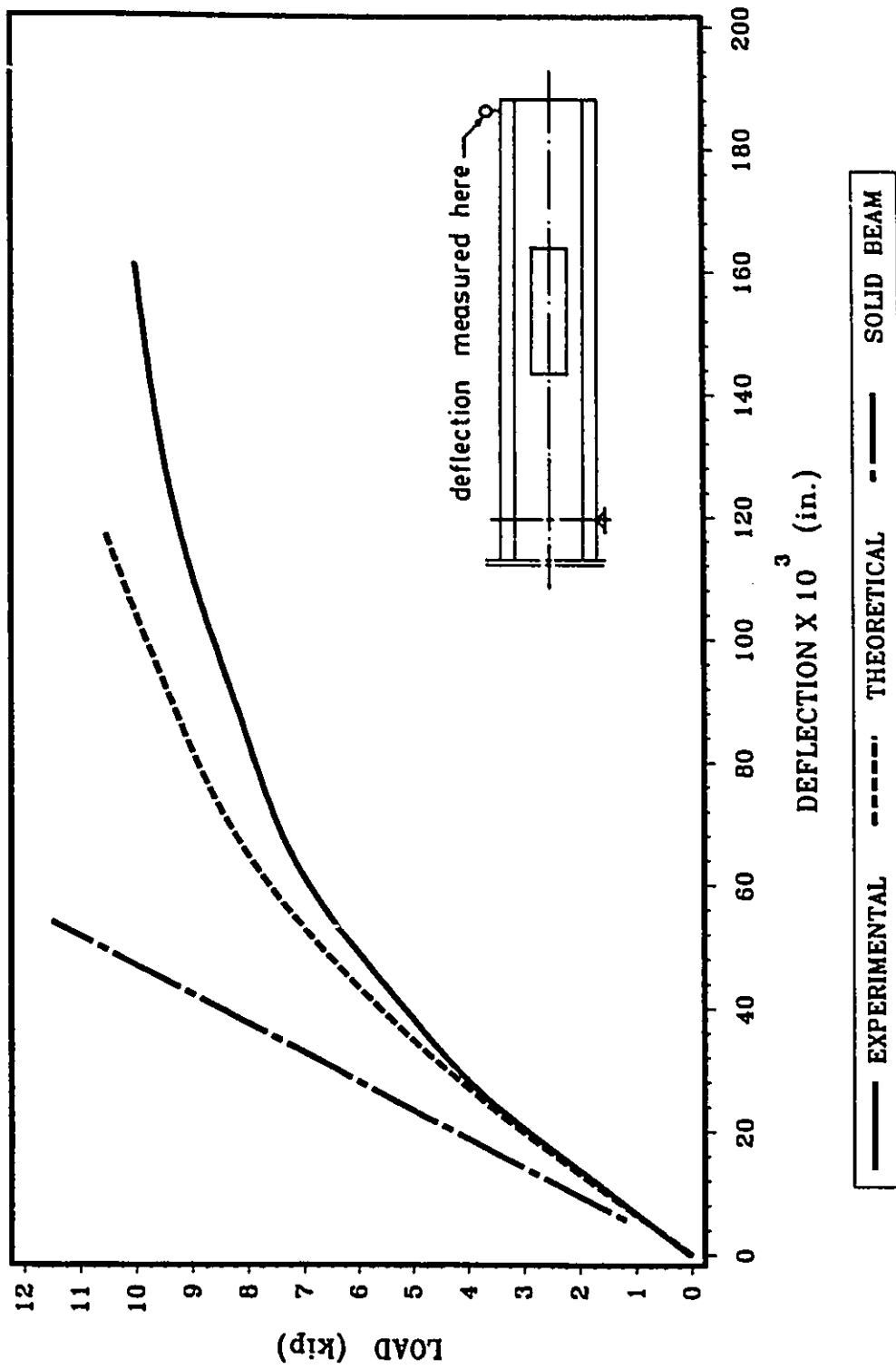


FIG. 5.44 LOAD-DEFLECTION RELATIONSHIP FOR BIII1C

Note: 1 in.=25.4 mm, 1 kip=4.45 kN

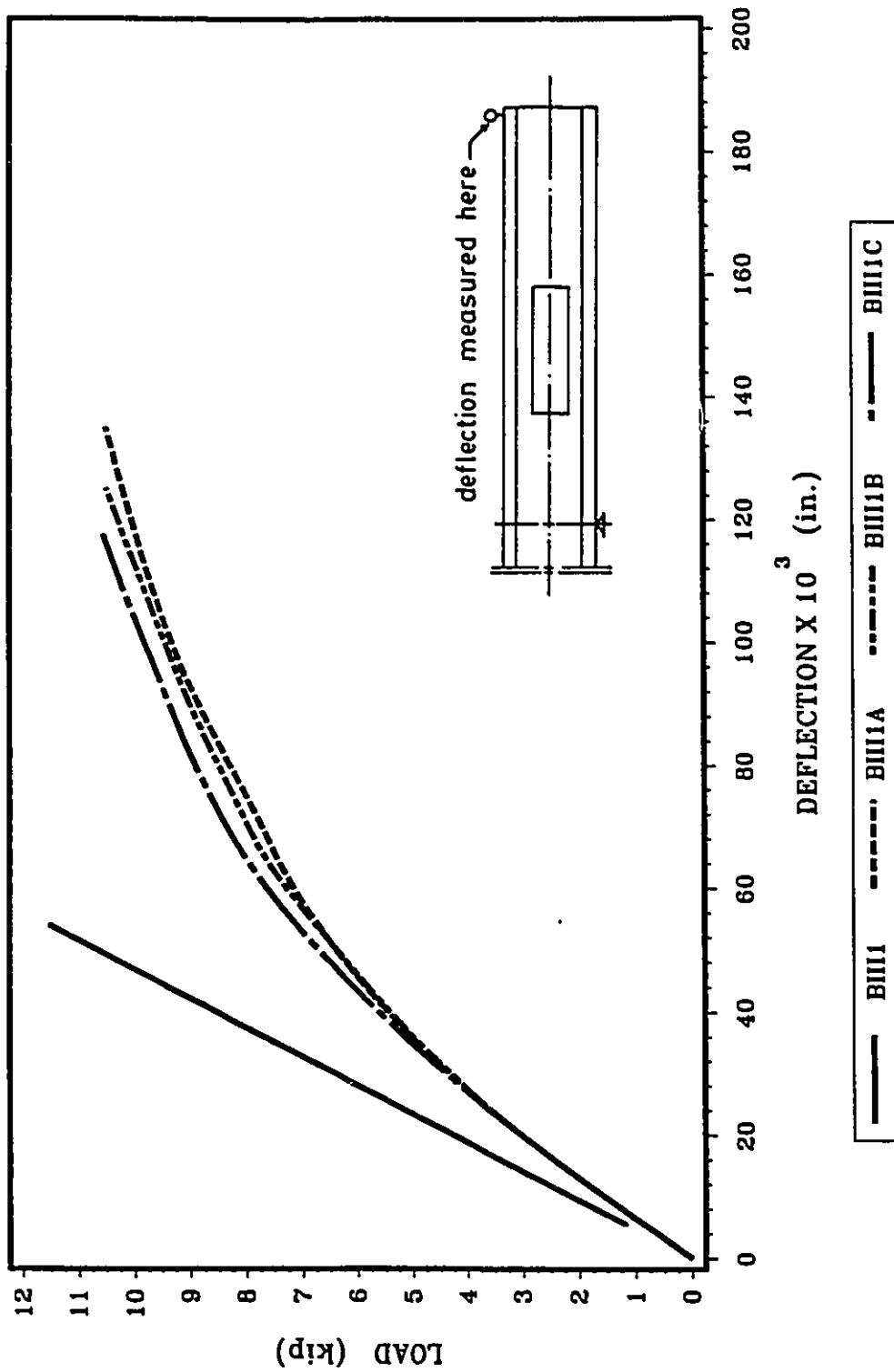


FIG. 5.45 LOAD-DEFLECTION RELATIONSHIP FOR BIII1, BIII1A, BIII1B & BIII1C

Note: 1 in.=25.4 mm, 1 kip=4.45 kN

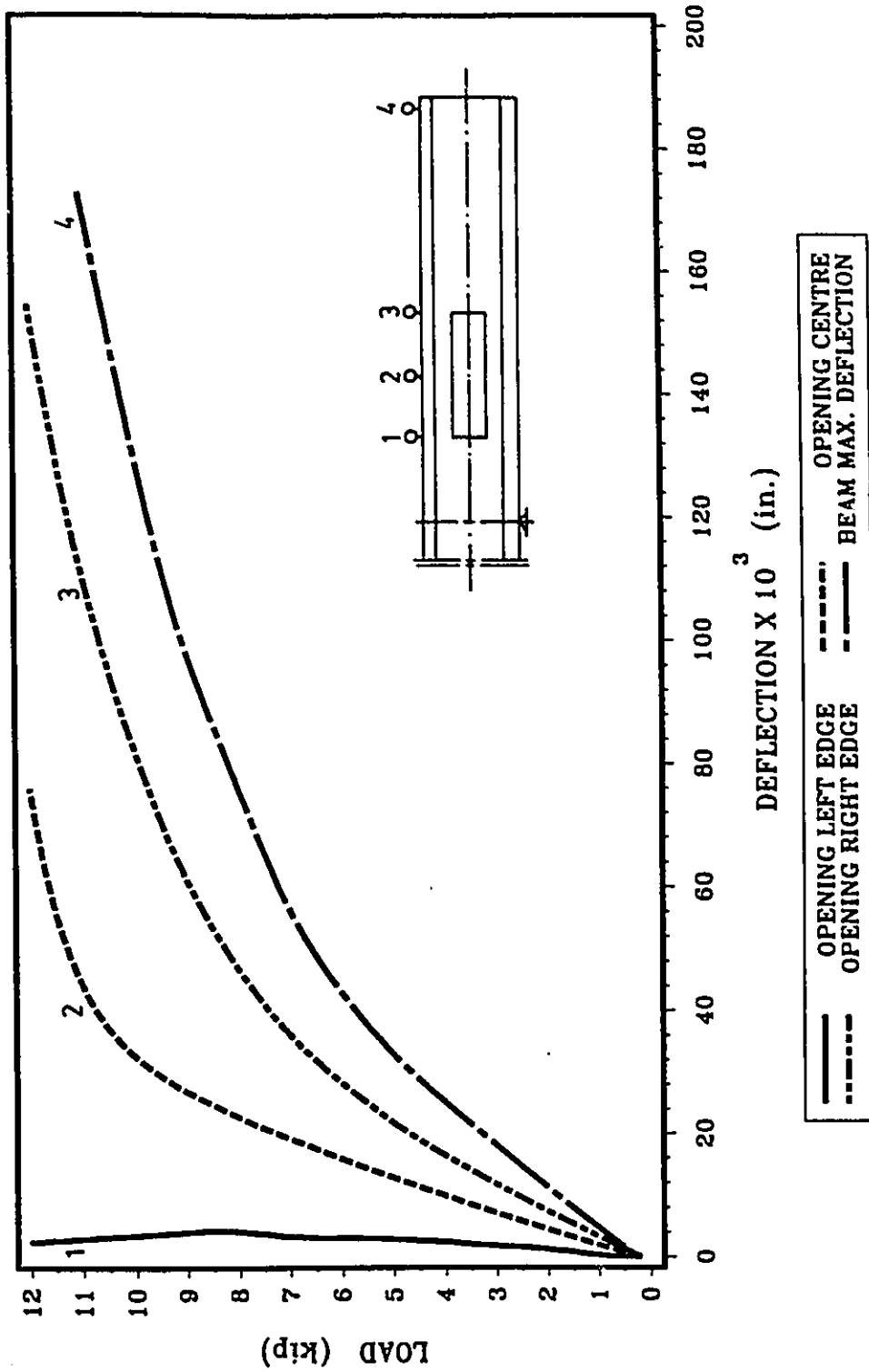


FIG. 5.46 OPENING DEFLECTION FOR BI11A
(EXPERIMENTAL)

Note: 1 in. = 25.4 mm, 1 kip = 4.45 kN

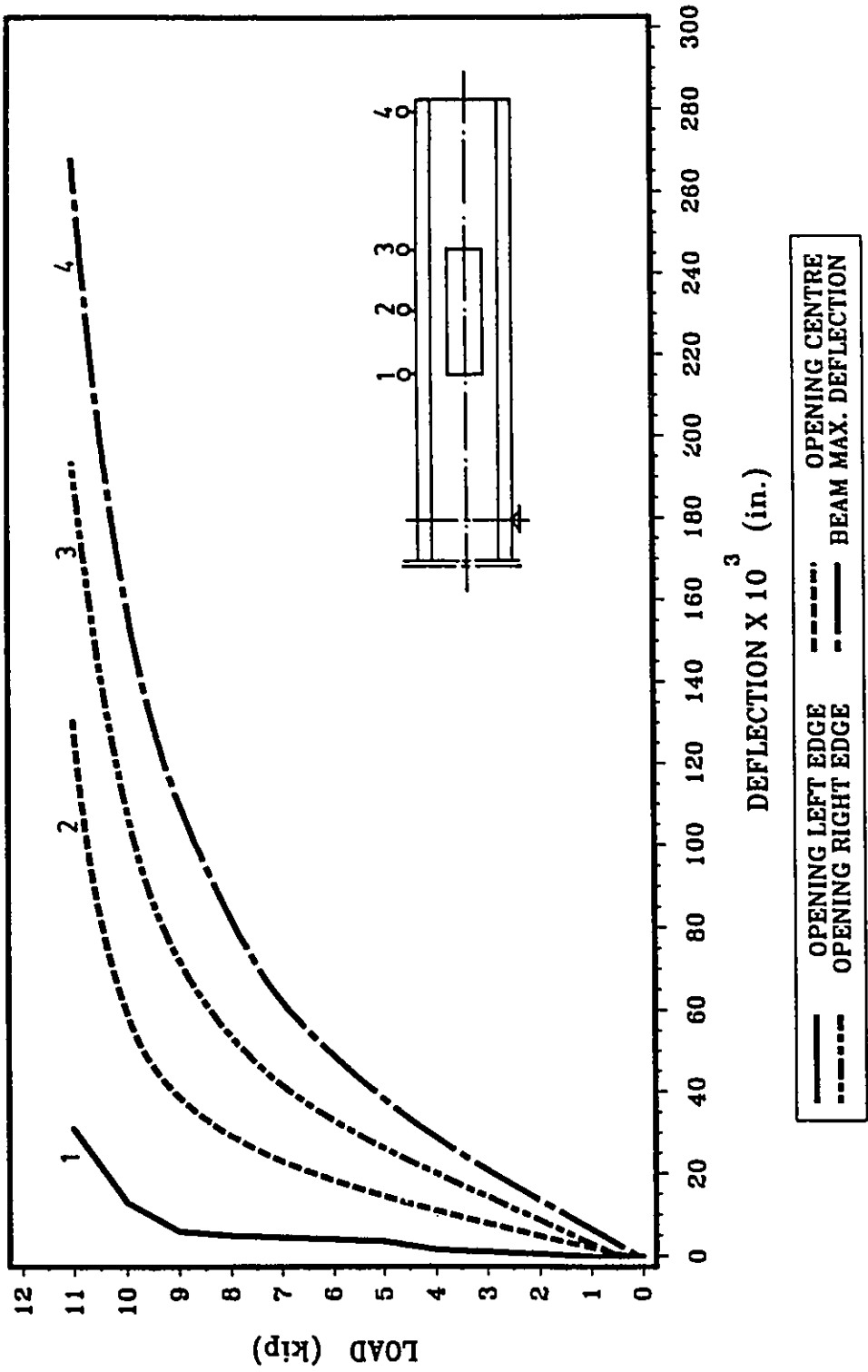


FIG. 5.47 OPENING DEFLECTION FOR BI11C
(EXPERIMENTAL)

Note: 1 in.=25.4 mm, 1 kip= 4.45 kN

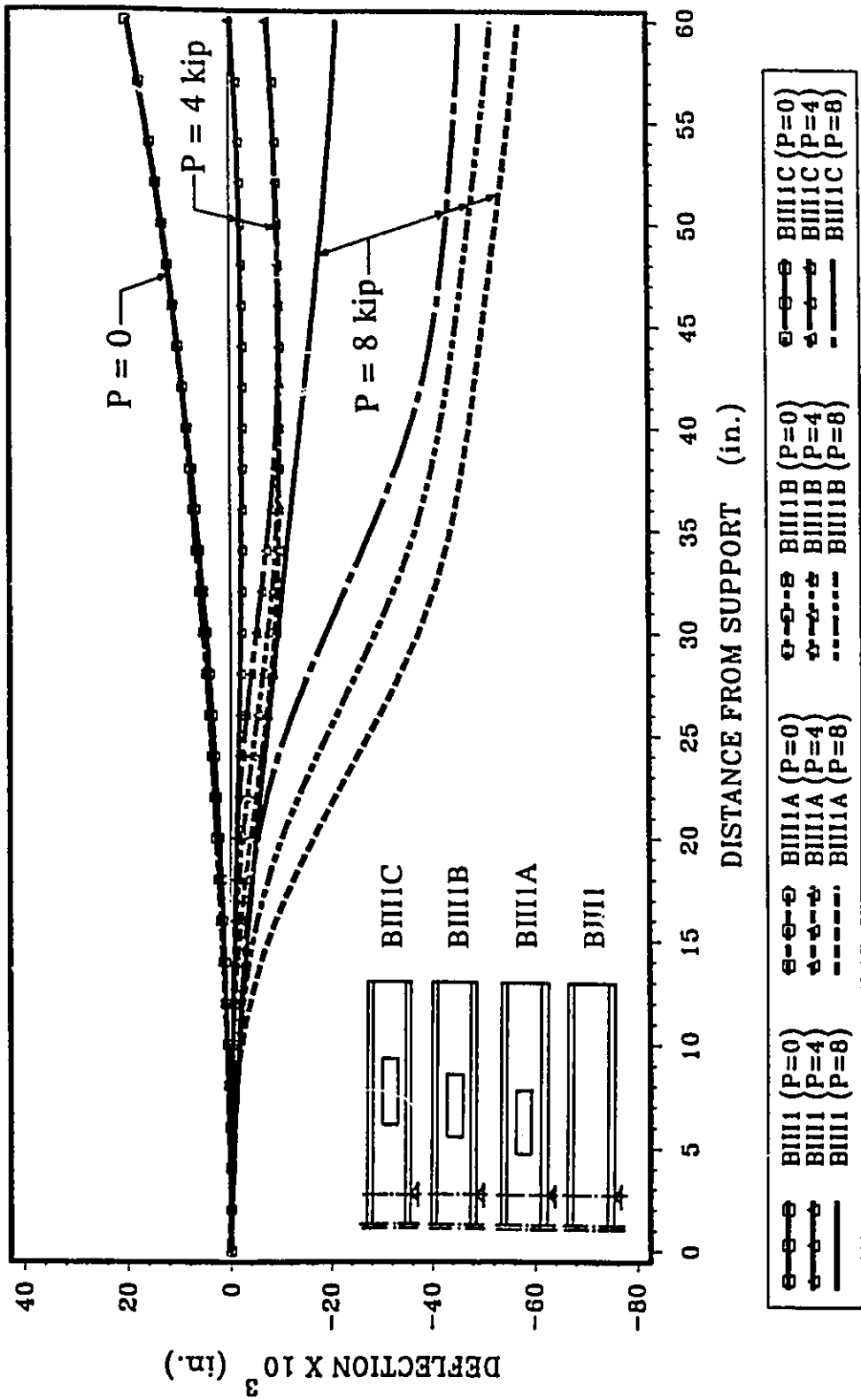
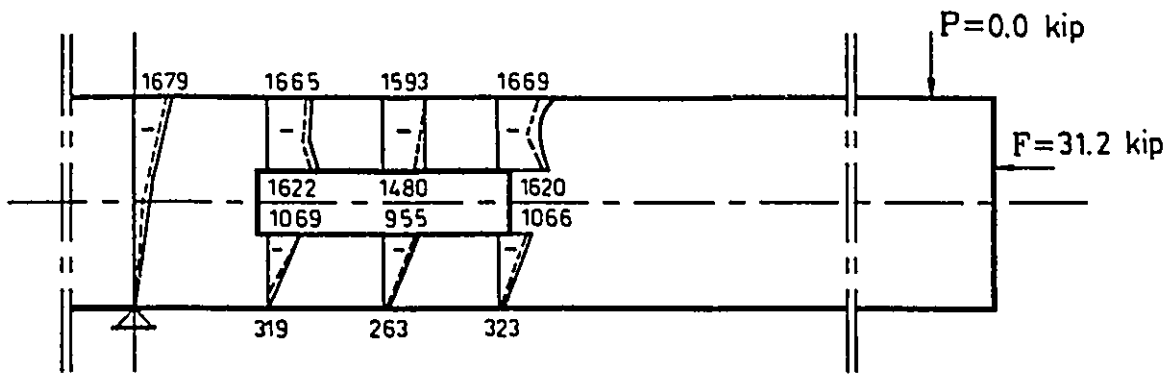
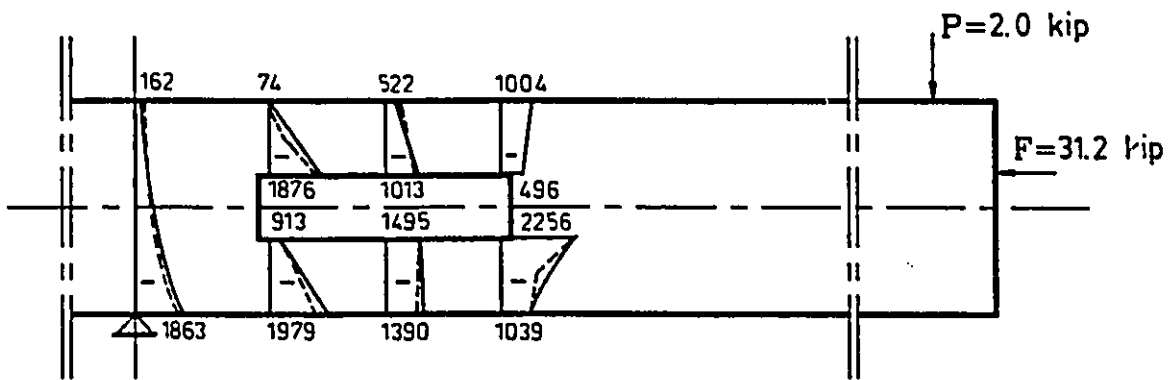


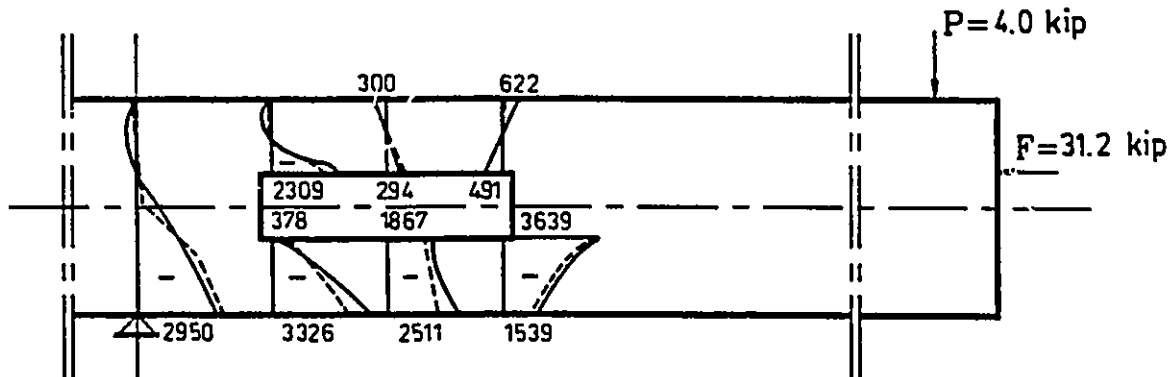
FIG. 5.48 DEFLECTED SHAPE FOR BIII1, BIII1A, BIII1B & BIII1C
(P = 0, P = 4 & P = 8 kip)



(a) TRANSFER STAGE



(b) WORKING STAGE



(c) ULTIMATE STAGE

--- Experimental
 ——— Theoretical

FIG. 5.49 HORIZONTAL STRESS DISTRIBUTION FOR BEAM BI1A

Note: stresses are shown in psi; 1 psi=6.89 kPa; 1 kip=4.45 kN

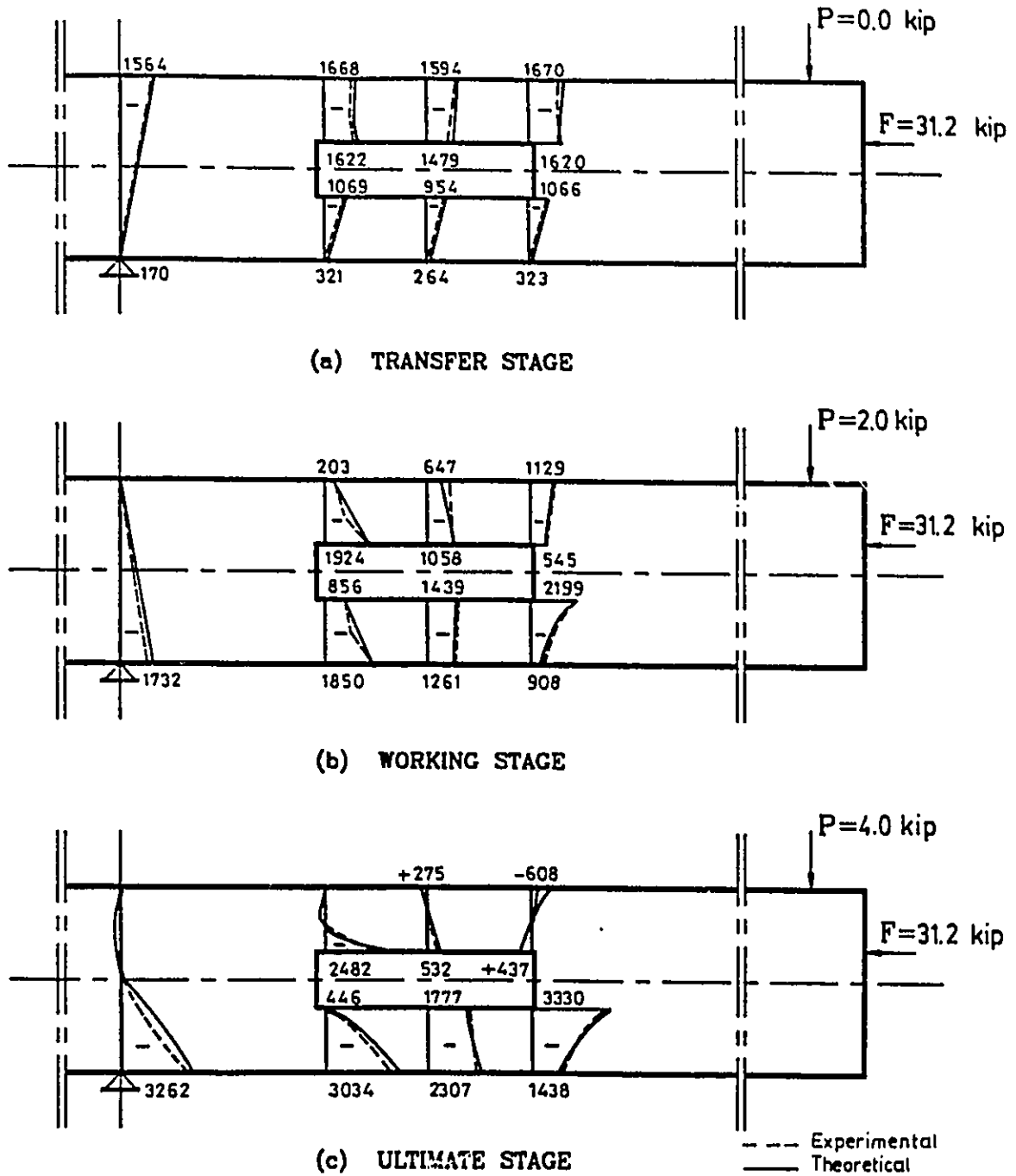
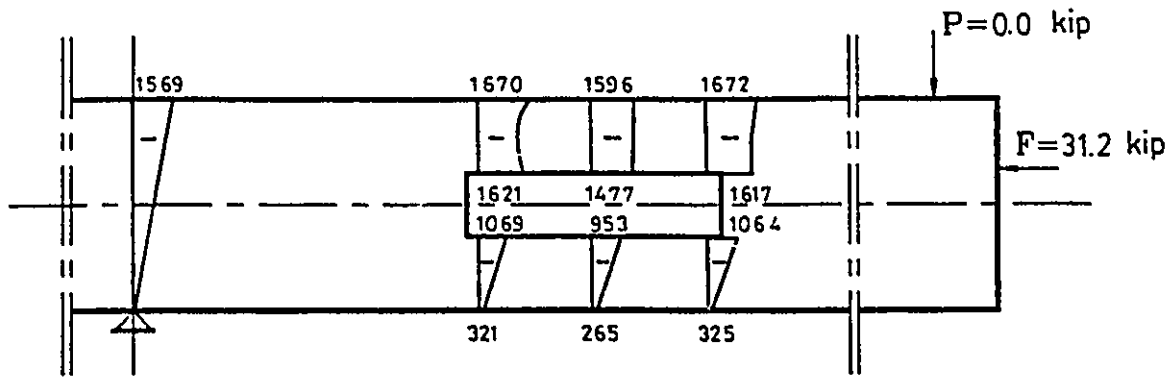
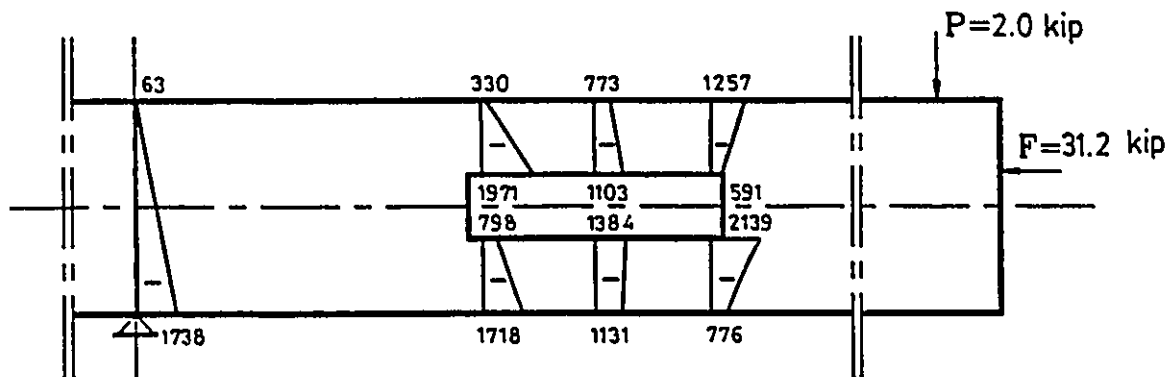


FIG. 5.50 HORIZONTAL STRESS DISTRIBUTION FOR BEAMS BIIB& BI3A

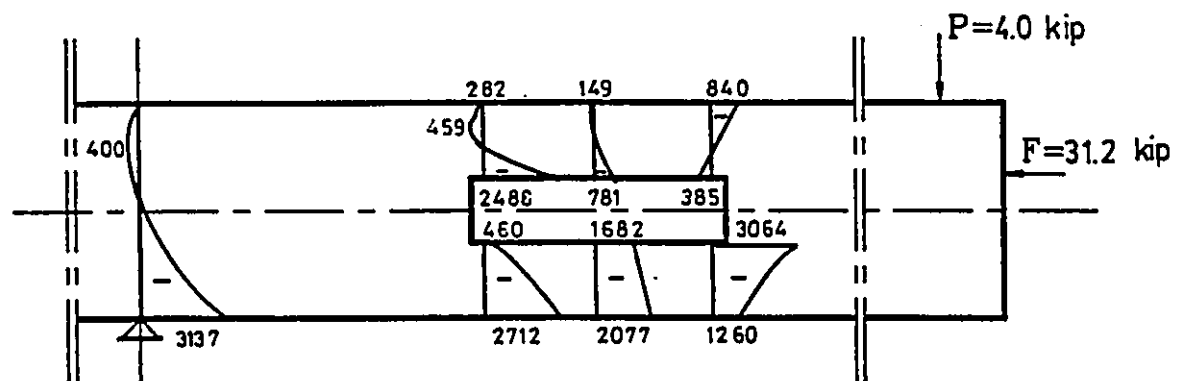
Note: stresses are shown in psi; 1 psi=6.89 Kpa; 1 kip=4.45 kN



(a) TRANSFER STAGE



(b) WORKING STAGE



(c) ULTIMATE STAGE

FIG. 5.51 HORIZONTAL STRESS DISTRIBUTION FOR BEAM BI1C

Note: stresses are shown in psi; 1 psi=6.89 Kpa; 1 kip=4.45 kN

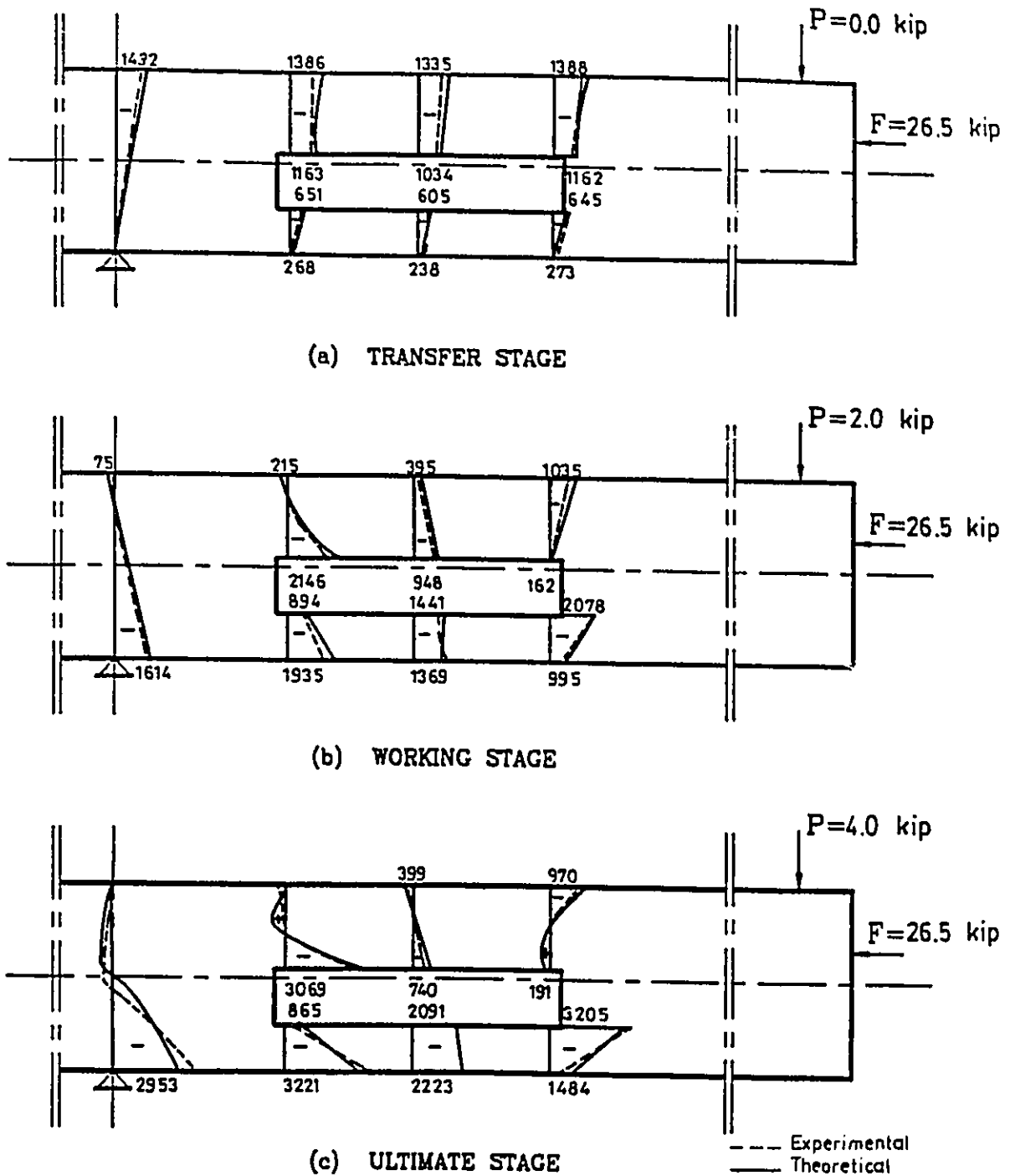
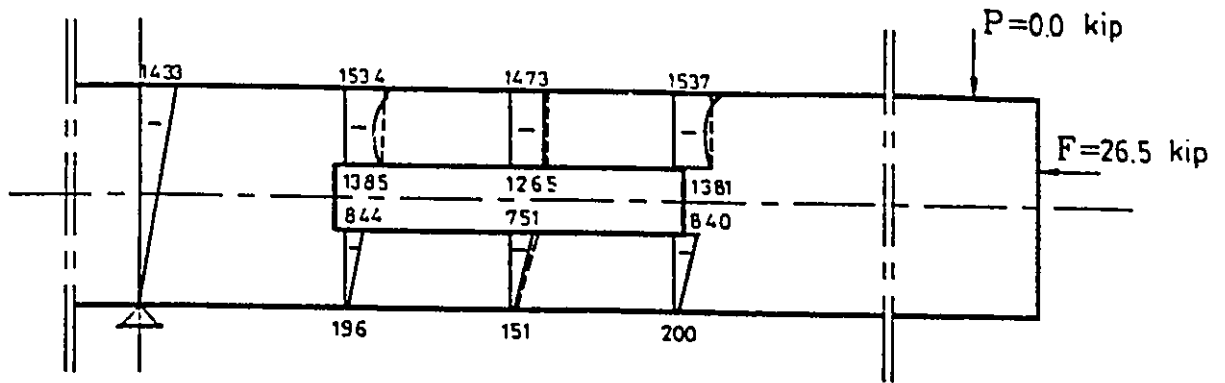
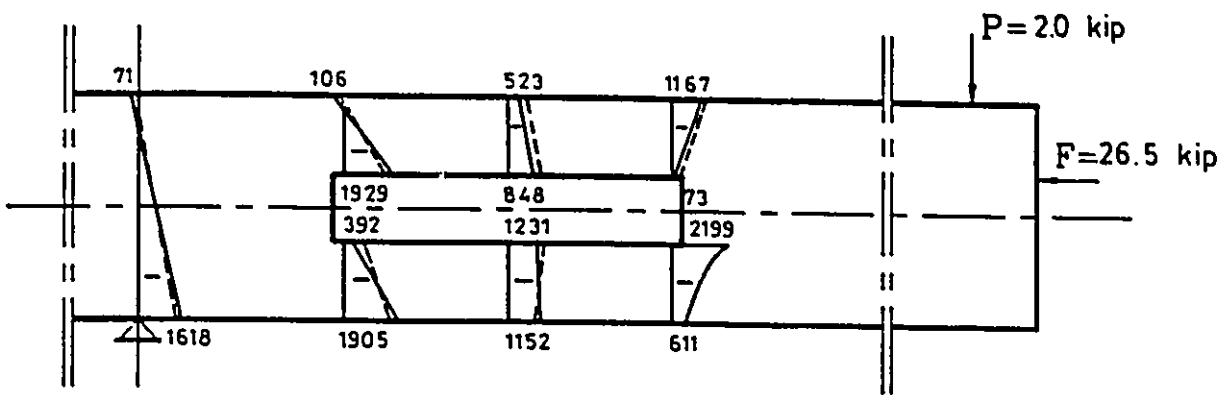


FIG. 5.52 HORIZONTAL STRESS DISTRIBUTION FOR BEAM B12A

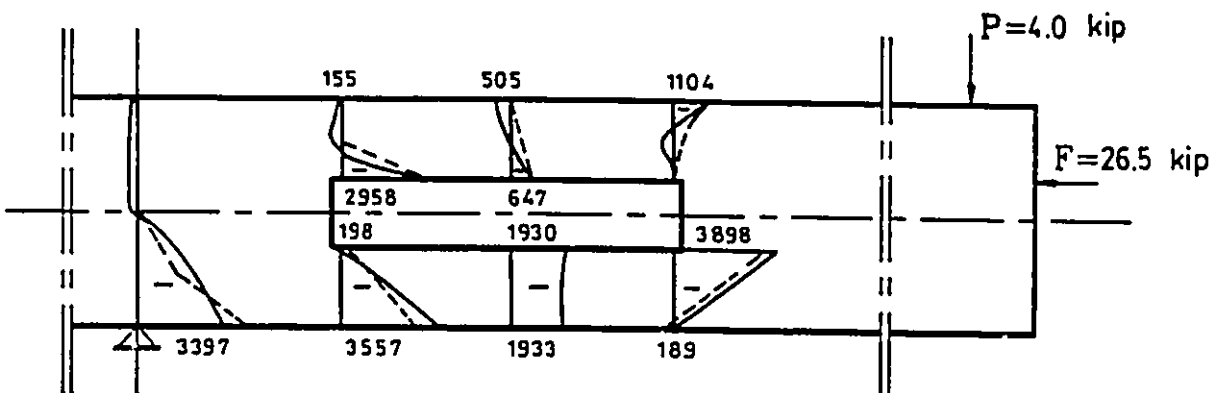
Note: stresses are shown in psi; 1 psi=6.89 Kpa; 1 kip=4.45 kN



(a) TRANSFER STAGE



(b) WORKING STAGE

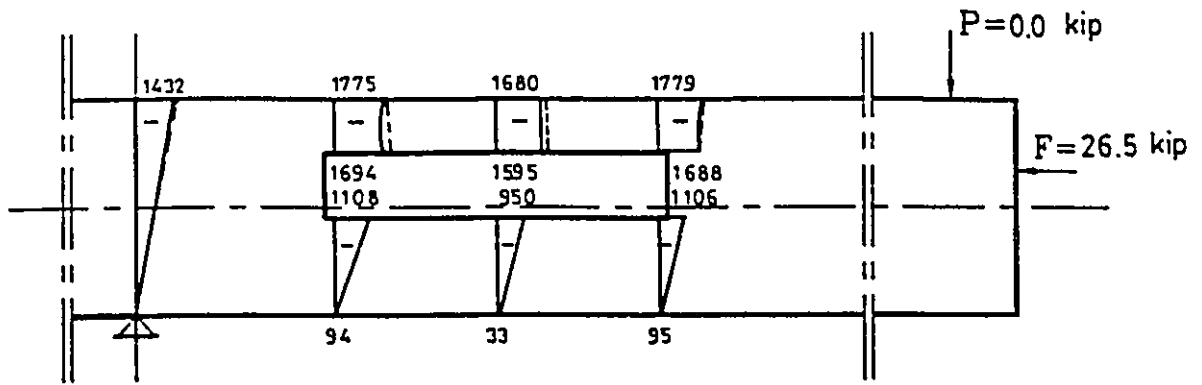


(c) ULTIMATE STAGE

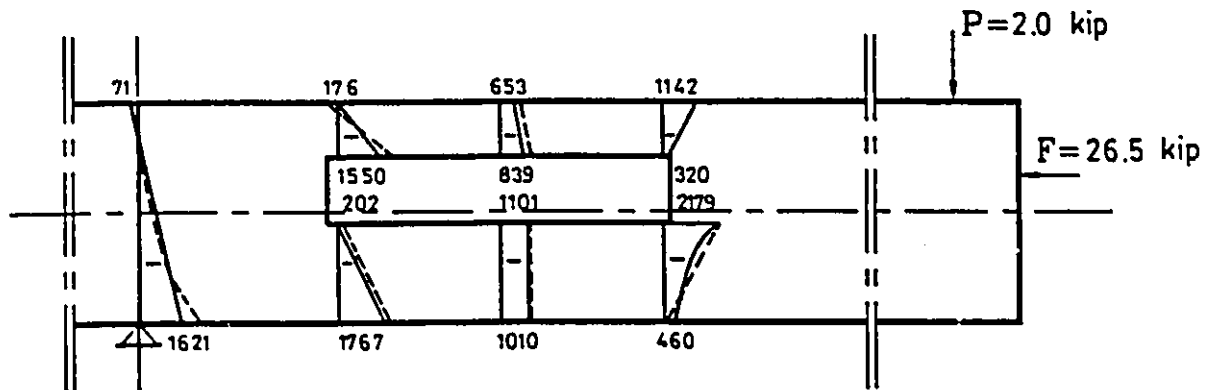
--- Experimental
 ——— Theoretical

FIG. 5.53 HORIZONTAL STRESS DISTRIBUTION FOR BEAM B12B

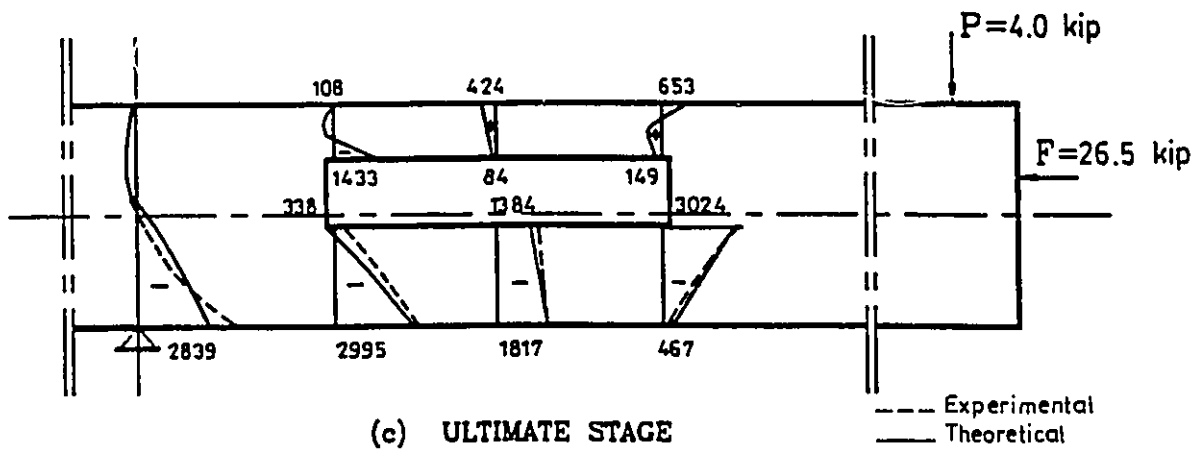
Note: stresses are shown in psi; 1 psi=6.89 Kpa; 1 kip=4.45 kN



(a) TRANSFER STAGE



(b) WORKING STAGE



(c) ULTIMATE STAGE

--- Experimental
 ——— Theoretical

FIG. 5.54 HORIZONTAL STRESS DISTRIBUTION FOR BEAM B12C

Note: stresses are shown in psi; 1 psi=6.89 kPa; 1 kip=4.45 kN

— Finite Element
 - - - Beam Theory

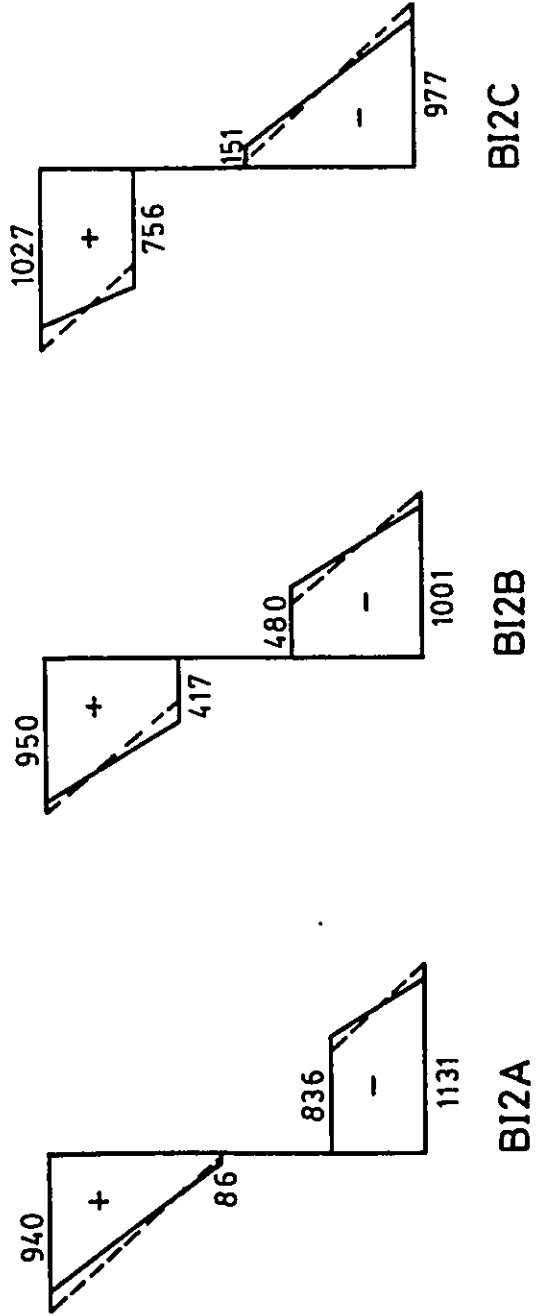
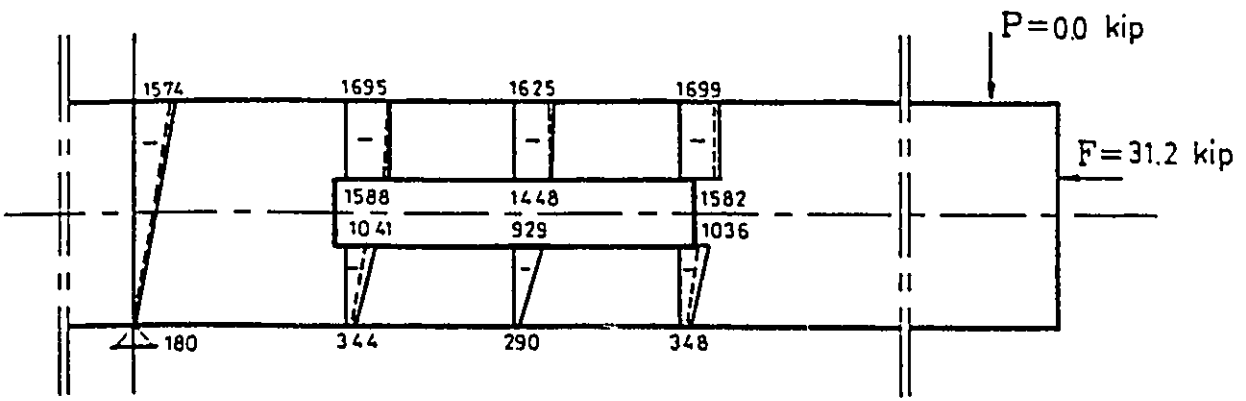
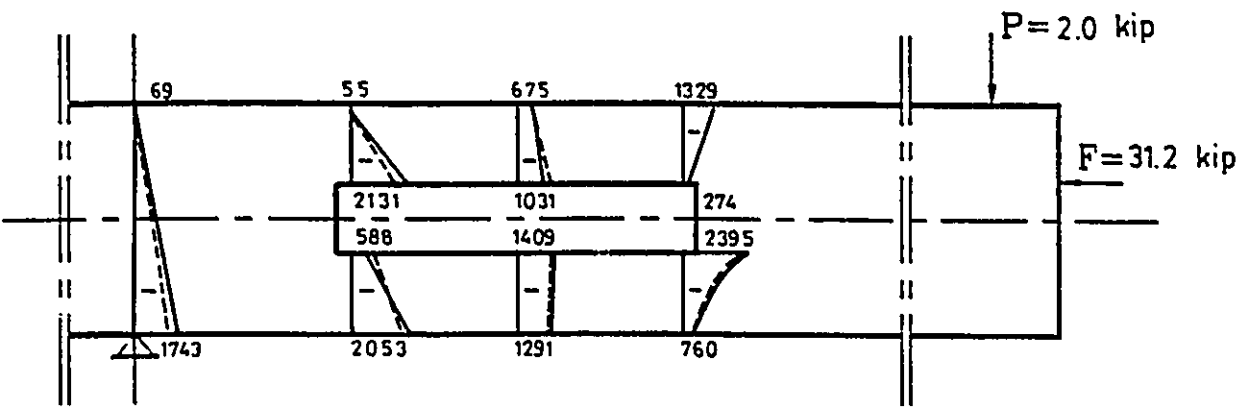


FIG. 5.55 HORIZONTAL STRESS DISTRIBUTION AT MID-OPENING FOR GROUP BI2
 (P = 2 kip)

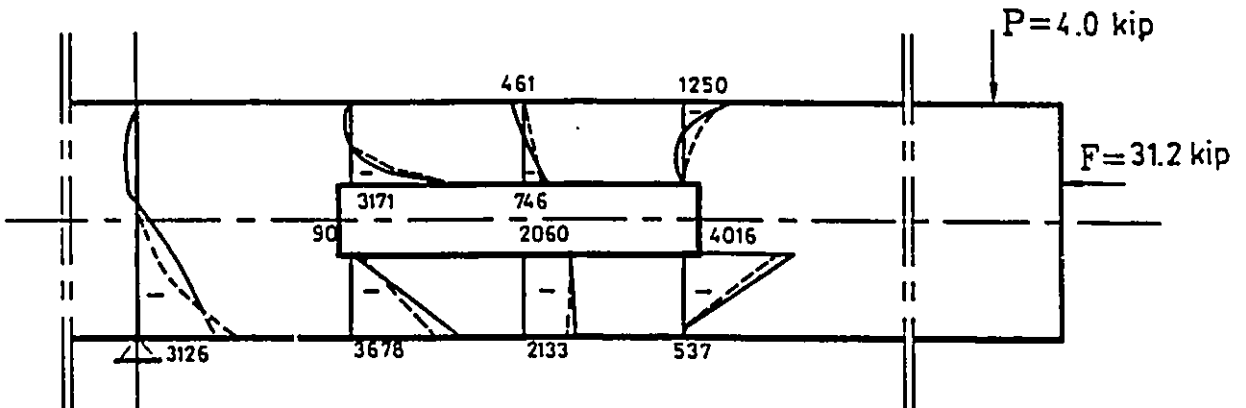
Note: stresses are shown in psi; 1 psi=6.89 kPa; 1 kip=4.45 kN



(a) TRANSFER STAGE



(b) WORKING STAGE



(c) ULTIMATE STAGE

--- Experimental
 ——— Theoretical

FIG. 5.56 HORIZONTAL STRESS DISTRIBUTION FOR BEAMS BI3B & BI4A

Note: stresses are shown in psi; 1 psi=6.89 kPa; 1 kip=4.45 kN

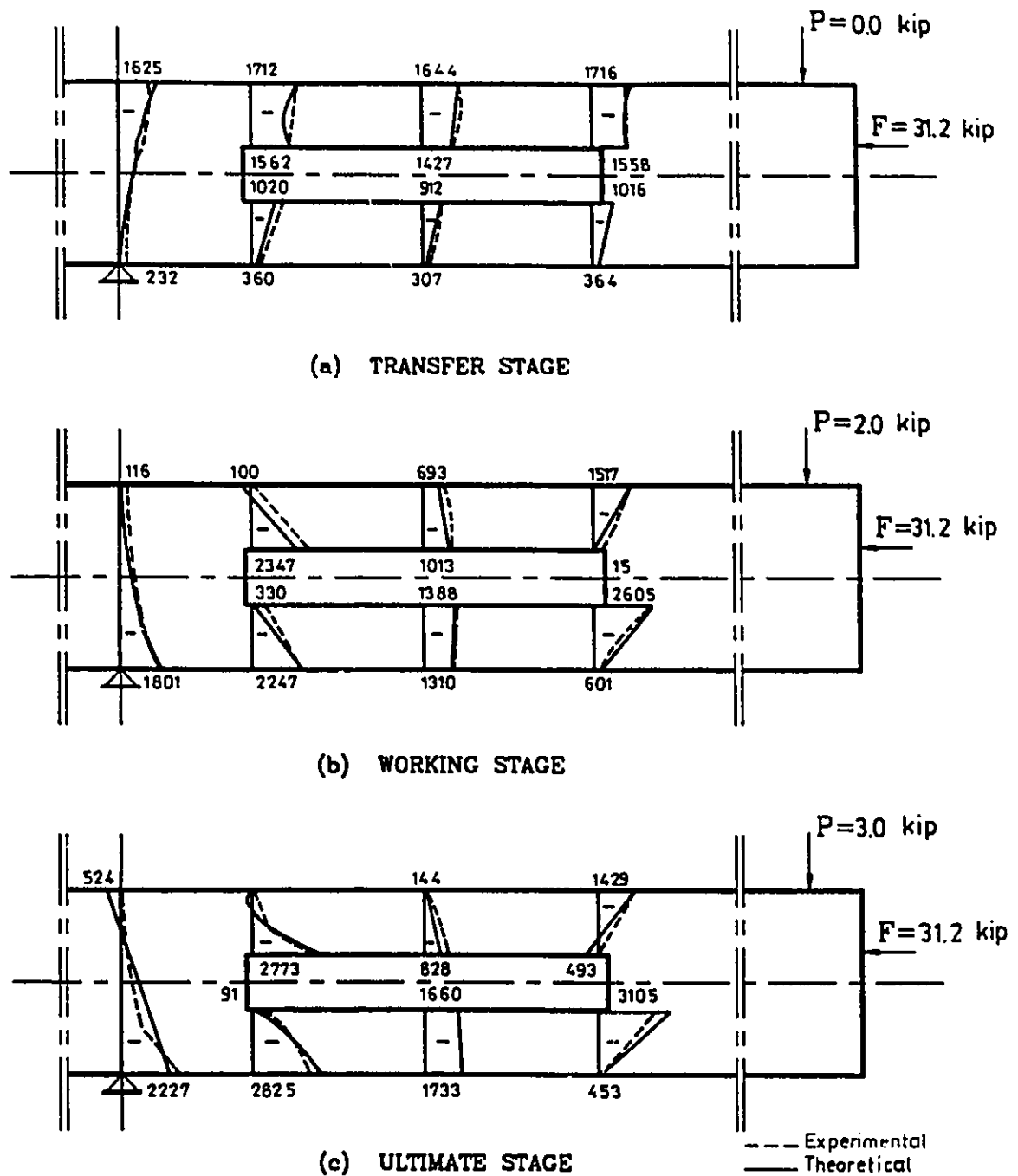
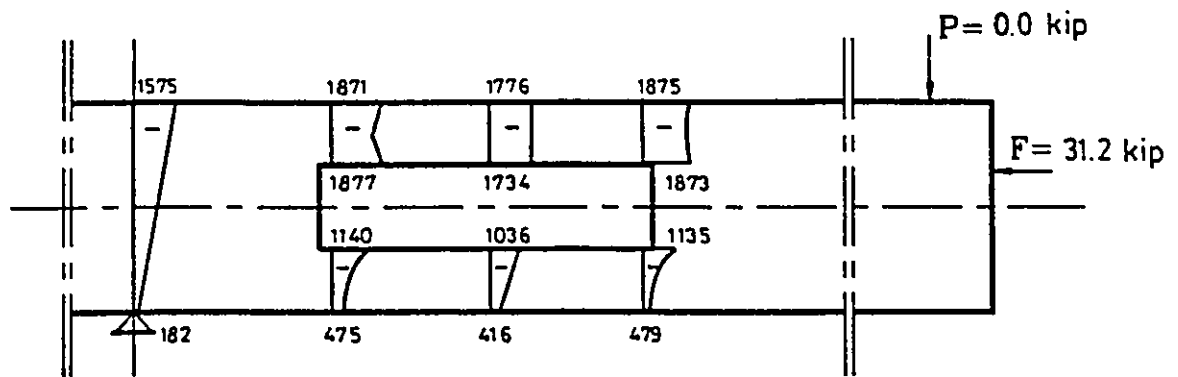
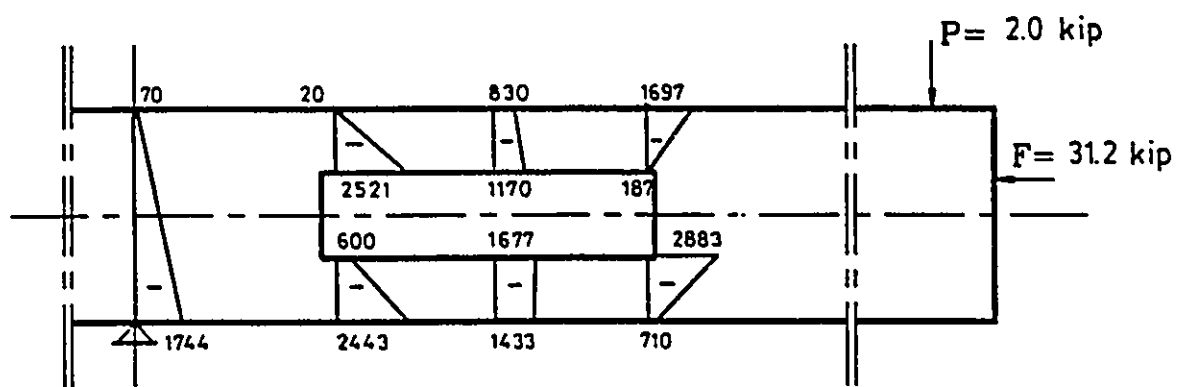


FIG. 5.57 HORIZONTAL STRESS DISTRIBUTION FOR BEAM B13C

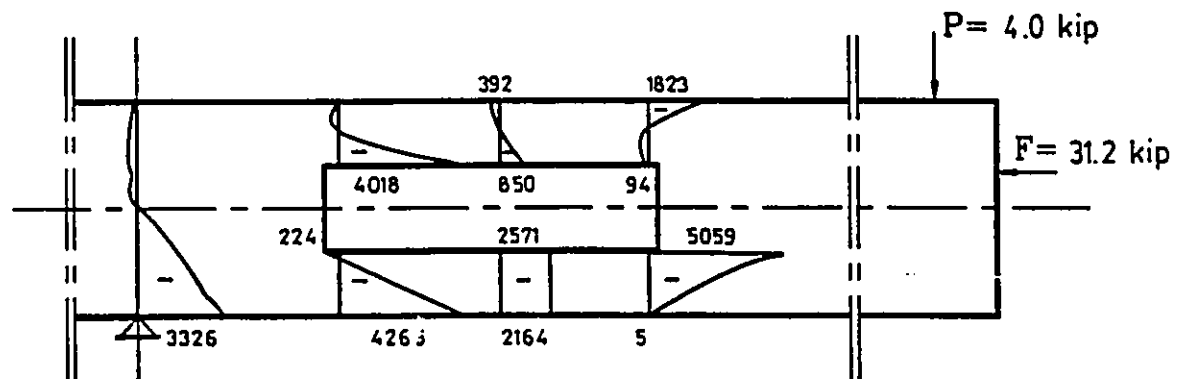
Note: stresses are shown in psi; 1 psi=6.89 kPa; 1 kip=4.45 kN



(a) TRANSFER STAGE



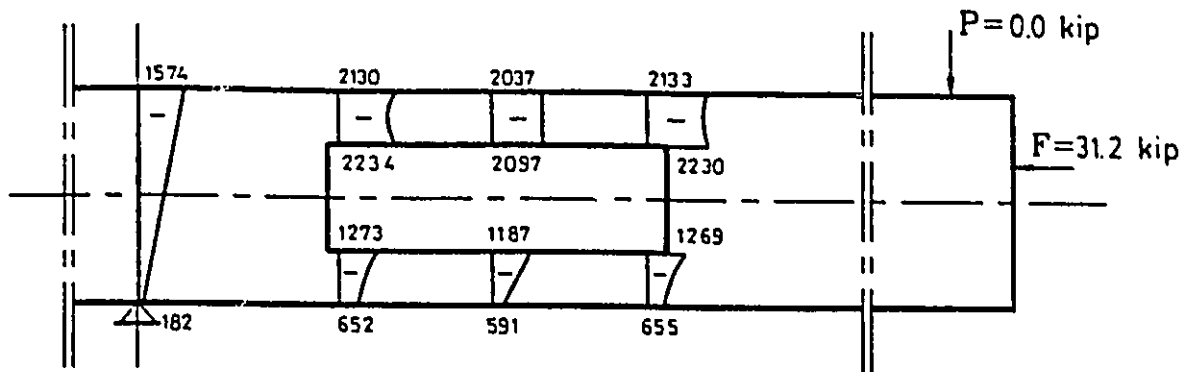
(b) WORKING STAGE



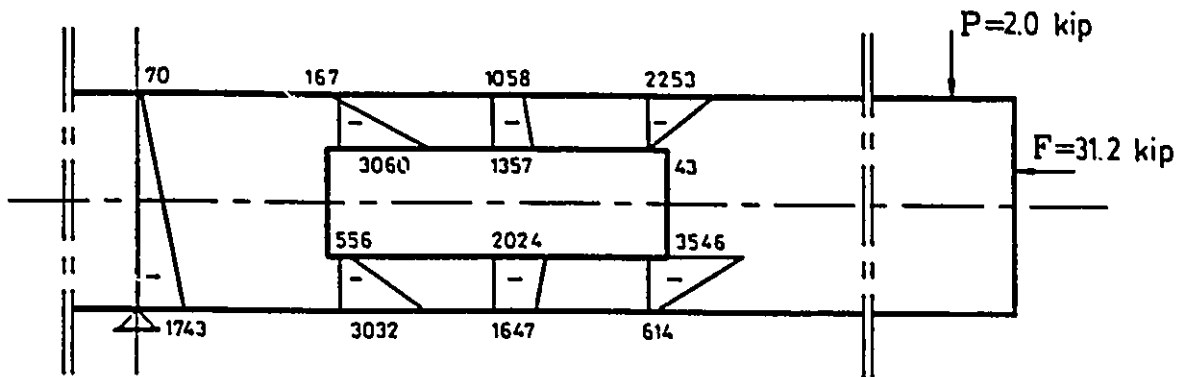
(c) ULTIMATE STAGE

FIG. 5.58 HORIZONTAL STRESS DISTRIBUTION FOR BEAM BI4B

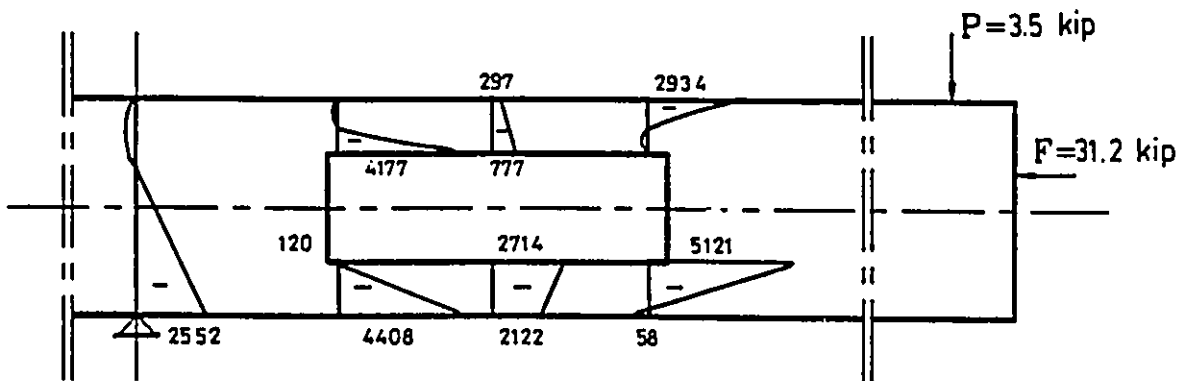
Note: stresses are shown in psi; 1 psi=6.89 kPa; 1 kip=4.45 kN



(a) TRANSFER STAGE



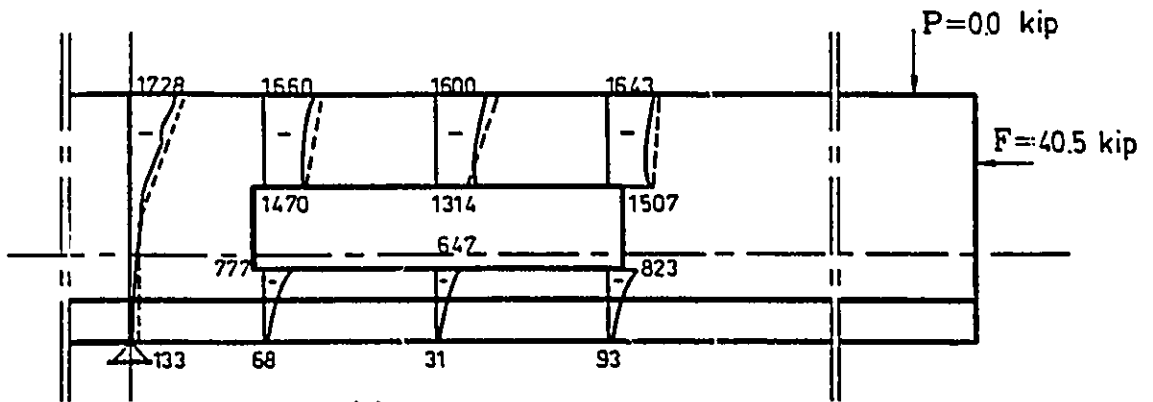
(b) WORKING STAGE



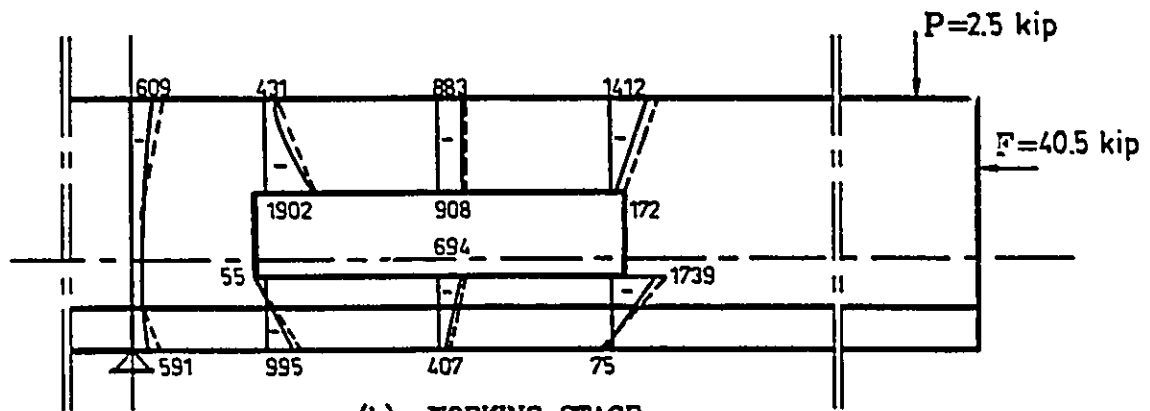
(c) ULTIMATE STAGE

FIG. 5.59 HORIZONTAL STRESS DISTRIBUTION FOR BEAM BI4C

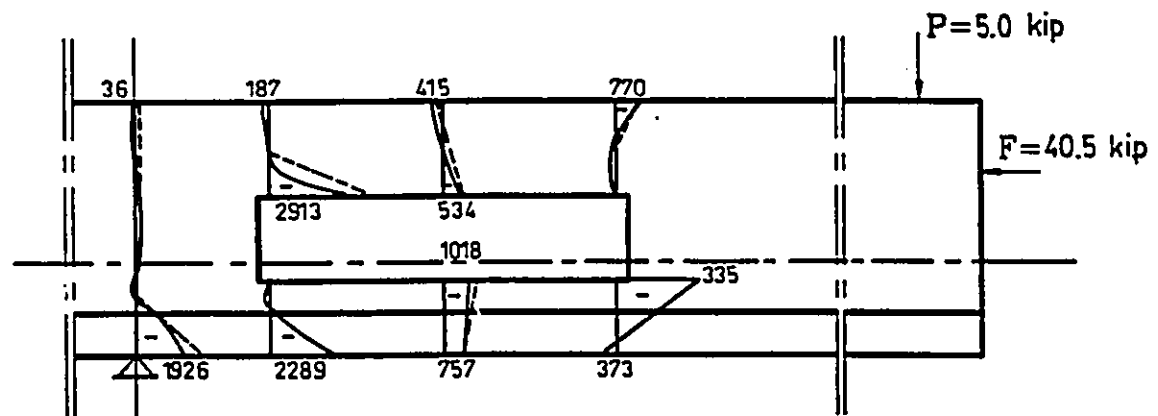
Note: stresses are shown in psi; 1 psi=6.89 kPa; 1 kip=4.45 kN



(a) TRANSFER STAGE



(b) WORKING STAGE



(c) ULTIMATE STAGE

--- Experimental
 ——— Theoretical

FIG. 5.60 HORIZONTAL STRESS DISTRIBUTION FOR BEAM BII1A

Note: stresses are shown in psi; 1 psi=6.89 kPa; 1 kip=4.45 kN

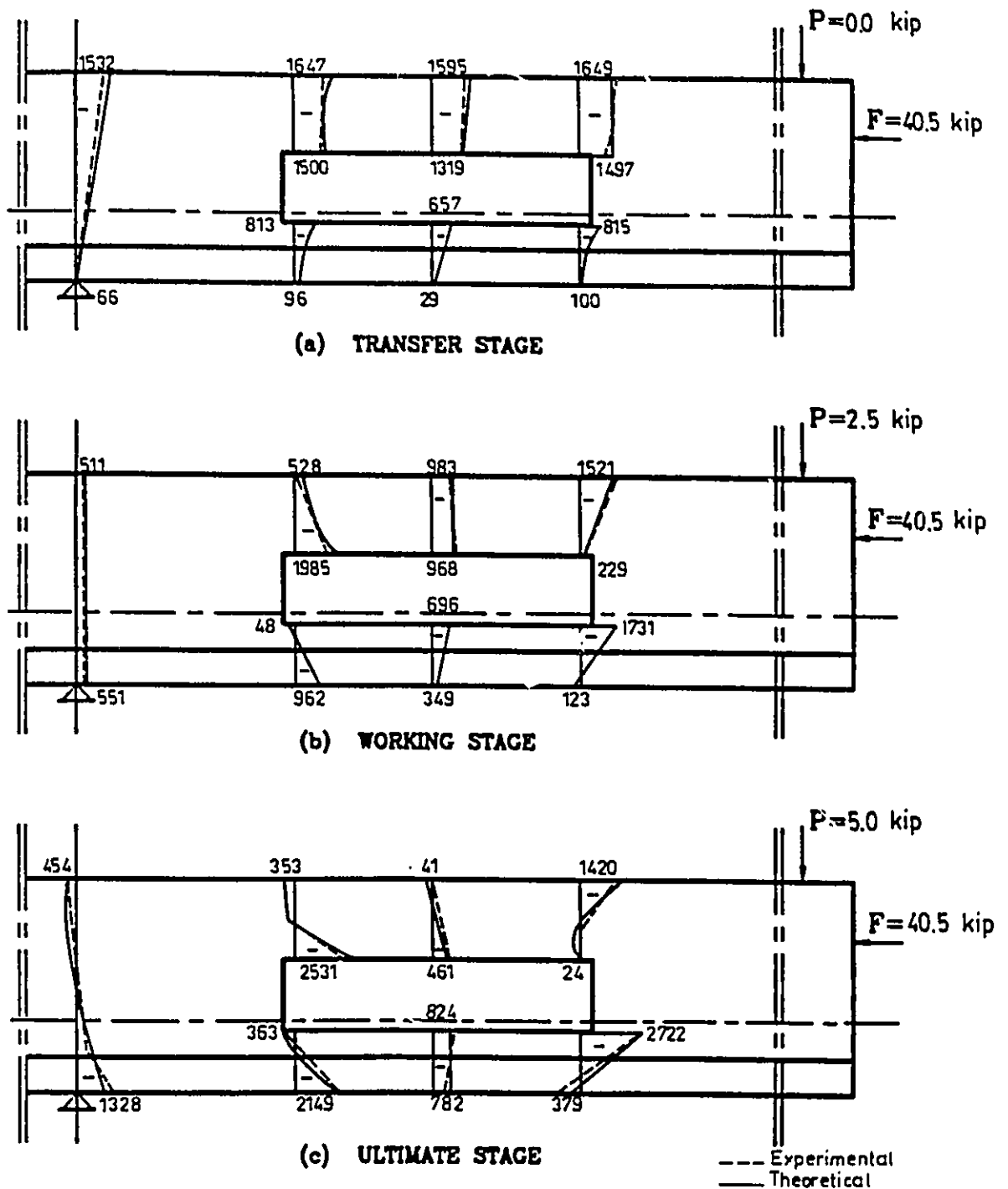


FIG. 5.61 HORIZONTAL STRESS DISTRIBUTION FOR BEAMS
BII1B, BII2A, BII3B & BII4B

Note: stresses are shown in psi; 1 psi=6.89 kPa; 1 kip=4.45 kN

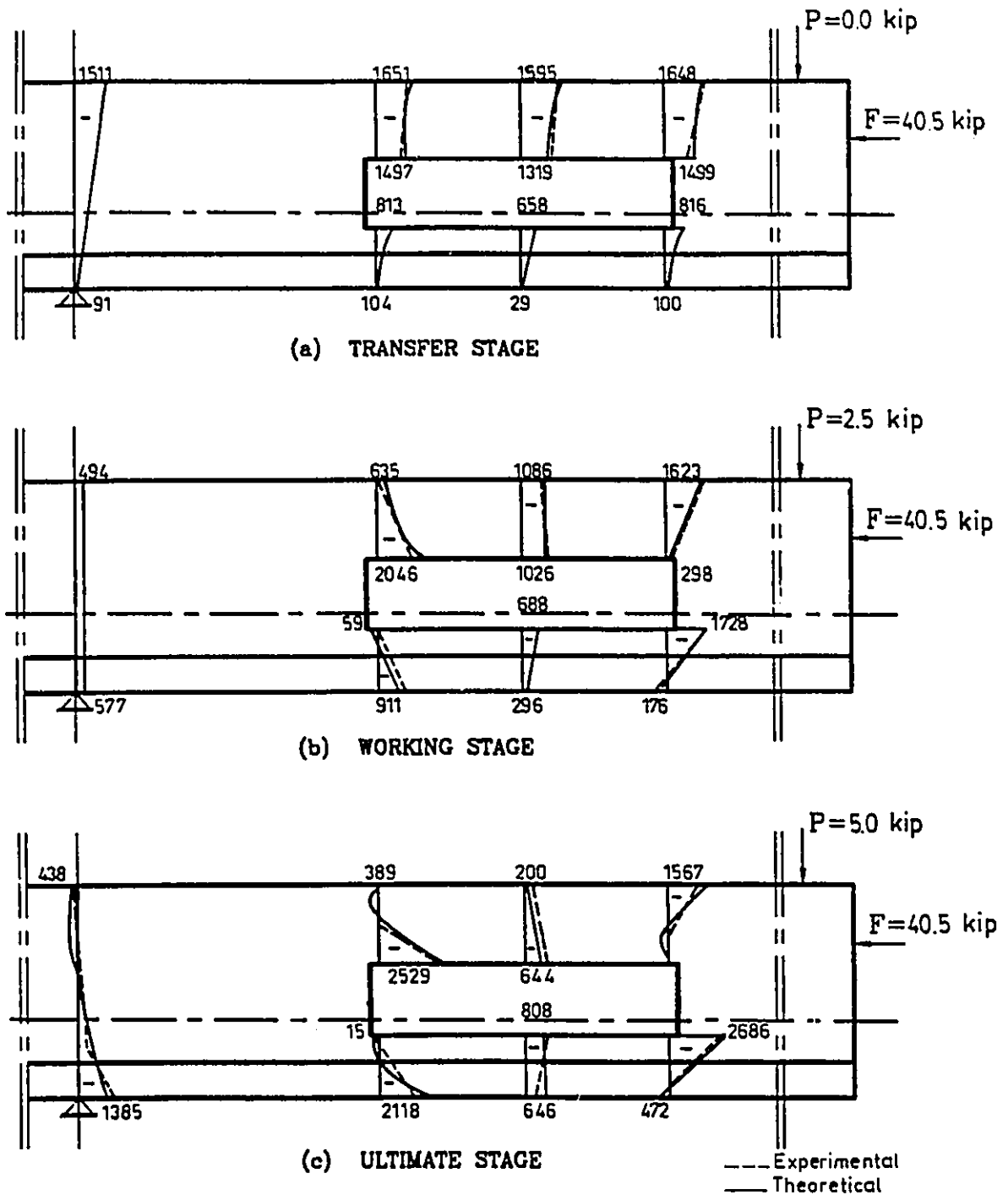


FIG. 5.62 HORIZONTAL STRESS DISTRIBUTION FOR BEAM BIIIC

Note: stresses are shown in psi; 1 psi=6.89 kPa; 1 kip=4.45 kN

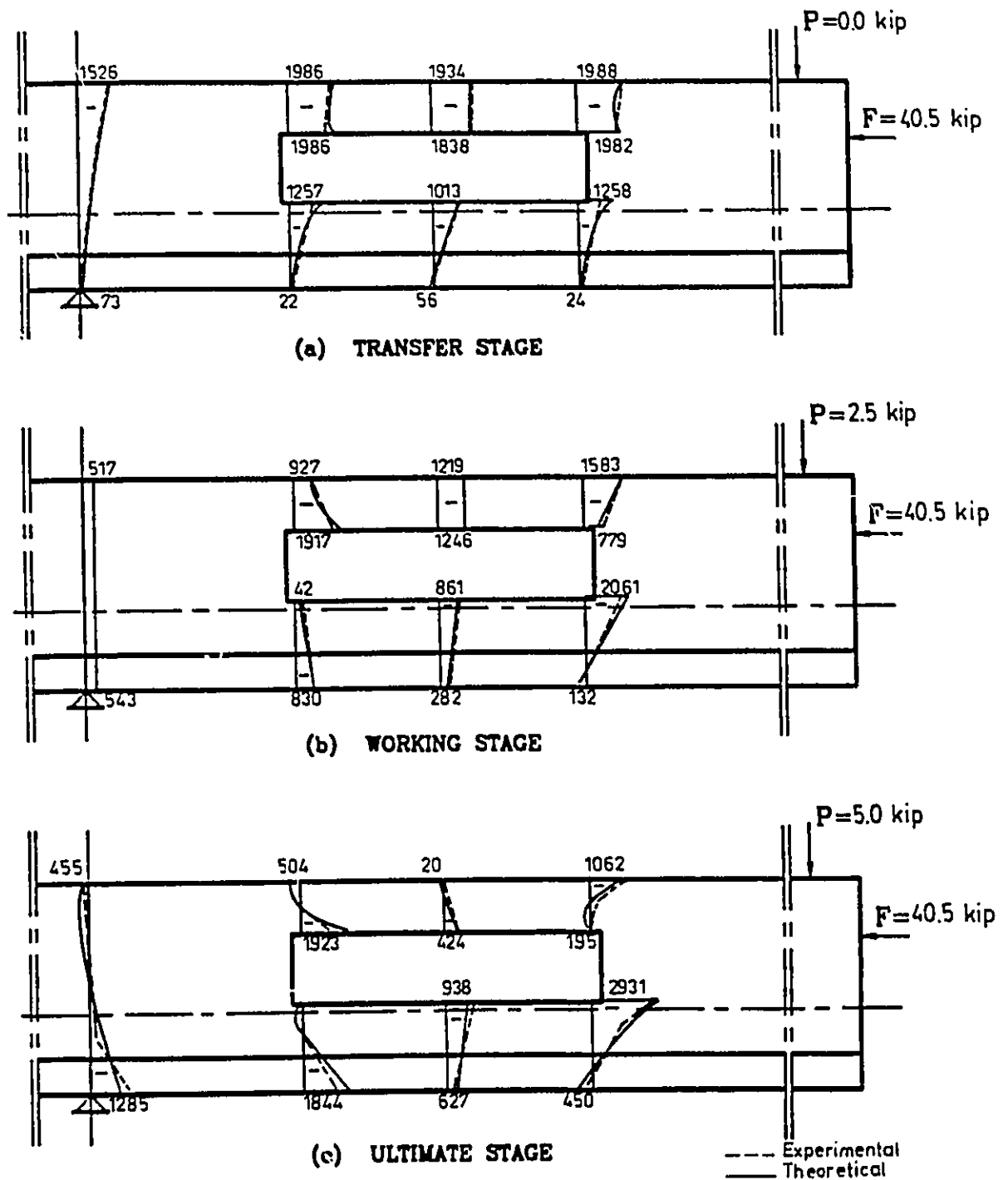


FIG. 5.63 HORIZONTAL STRESS DISTRIBUTION FOR BEAM BII2B

Note: stresses are shown in psi; 1 psi=6.89 kPa; 1 kip=4.45 kN

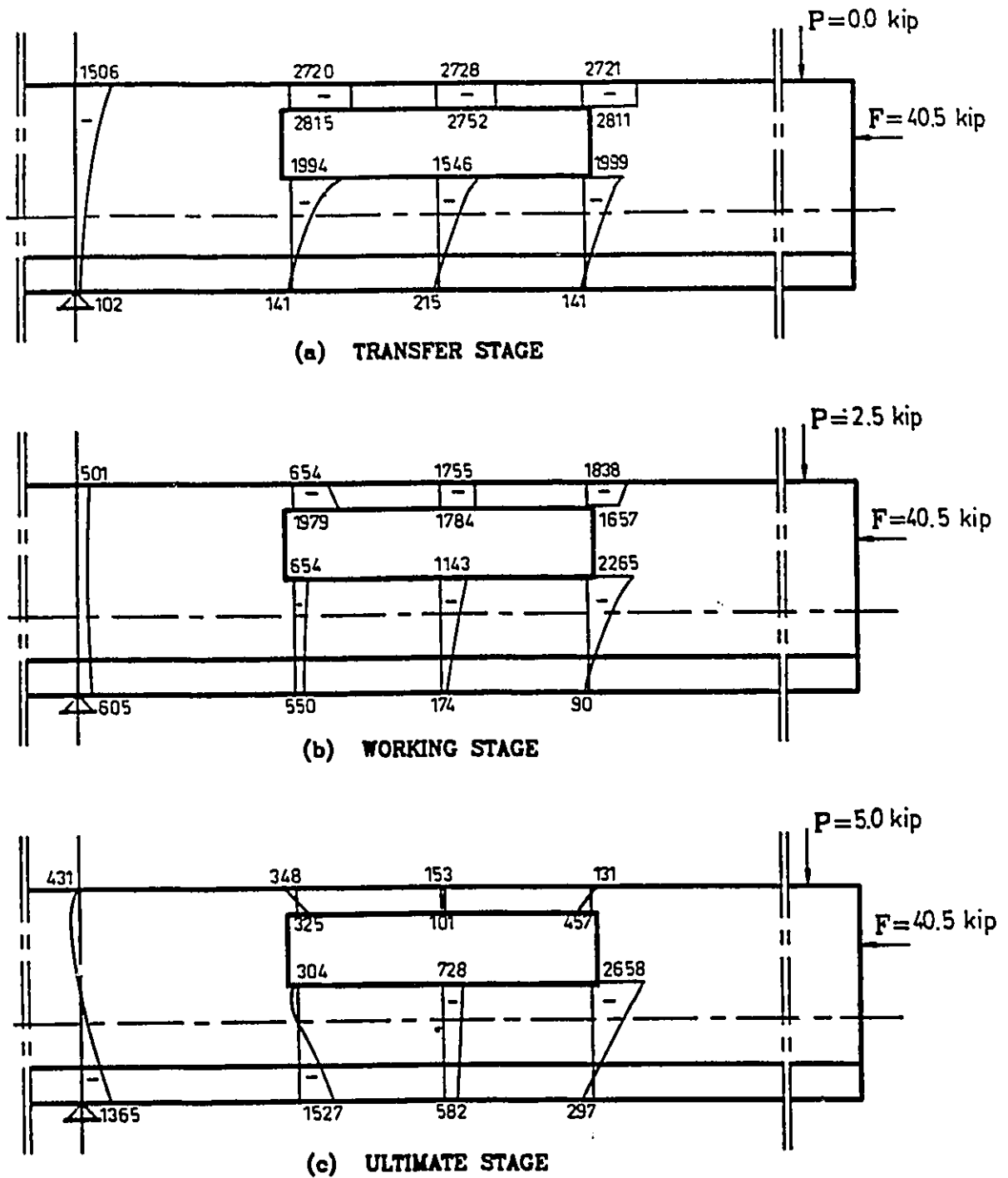


FIG. 5.64 HORIZONTAL STRESS DISTRIBUTION FOR BEAM BII2C

Note: stresses are shown in psi; 1 psi=6.89 kPa; 1 kip=4.45 kN

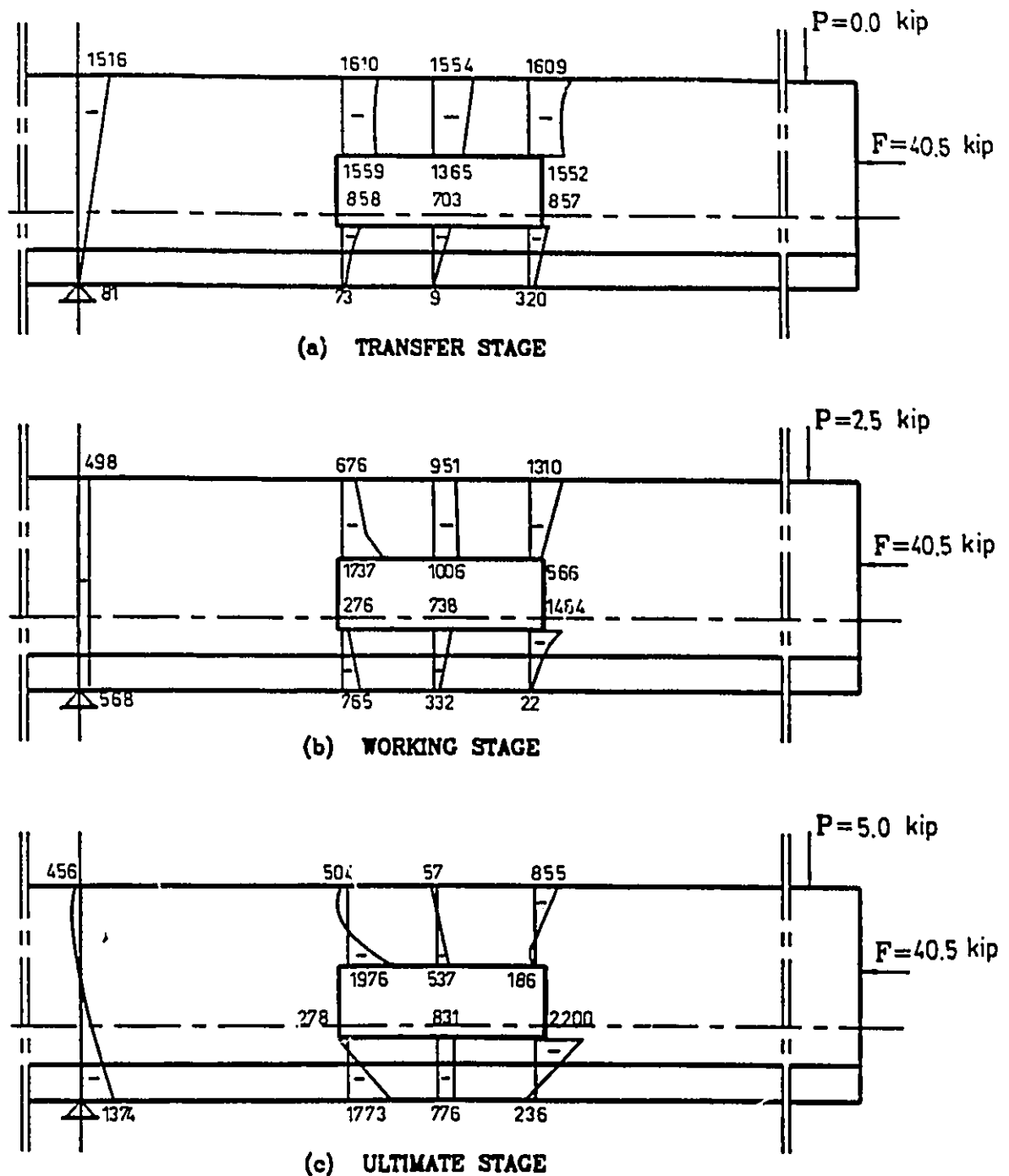


FIG. 5.65 HORIZONTAL STRESS DISTRIBUTION FOR BEAM BI13A

Note: stresses are shown in psi; 1 psi=6.89 kPa; 1 kip=4.45 kN

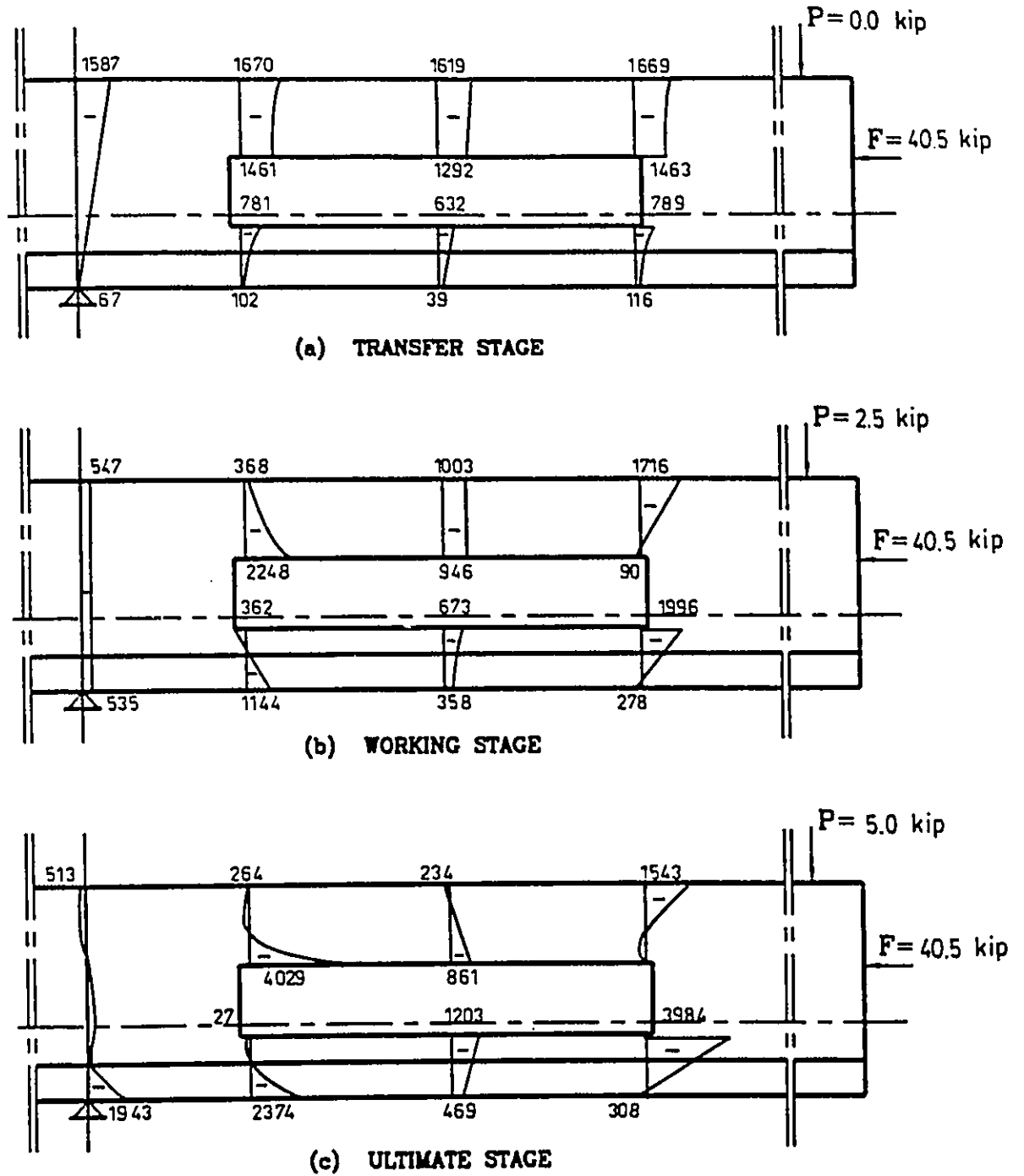


FIG. 5.66 HORIZONTAL STRESS DISTRIBUTION FOR BEAM BII3C

Note: stresses are shown in psi; 1 psi=6.89 kPa; 1 kip=4.45 kN

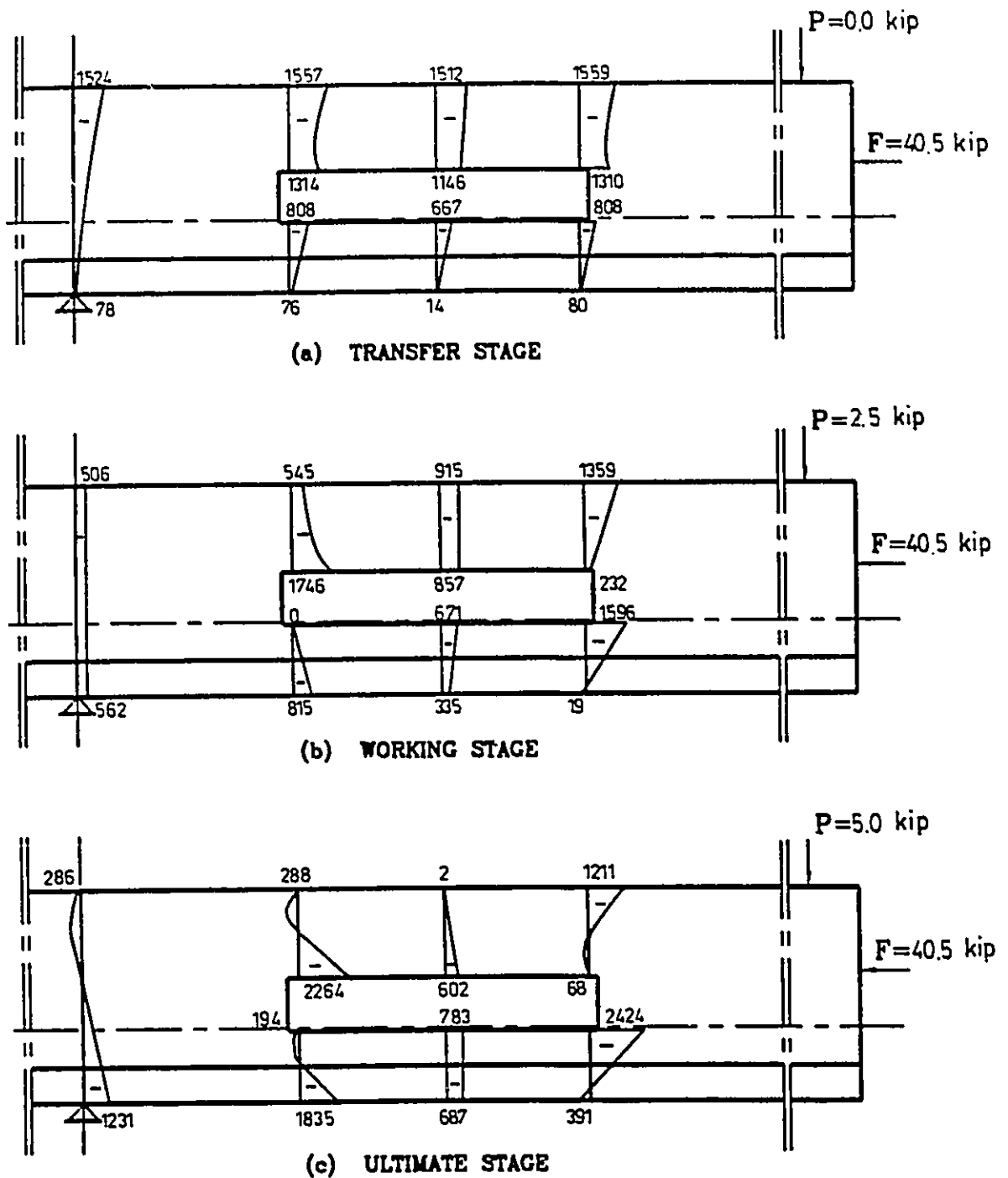


FIG. 5.67 HORIZONTAL STRESS DISTRIBUTION FOR BEAM BII4A

Note: stresses are shown in psi; 1 psi=6.89 kPa; 1 kip=4.45 kN

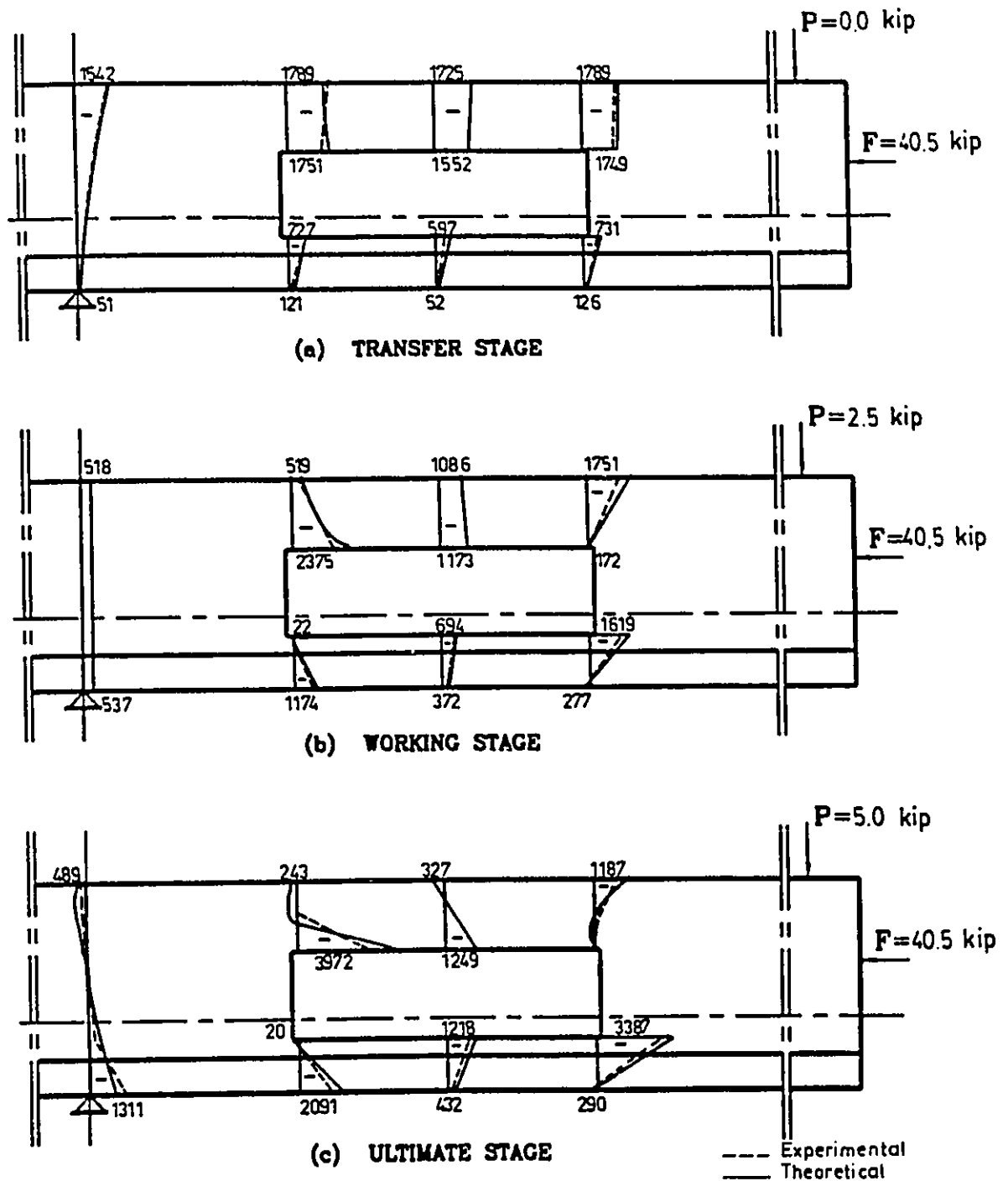


FIG. 5.68 HORIZONTAL STRESS DISTRIBUTION FOR BEAM BII4C

Note: stresses are shown in psi; 1 psi=6.89 kPa; 1 kip=4.45 kN

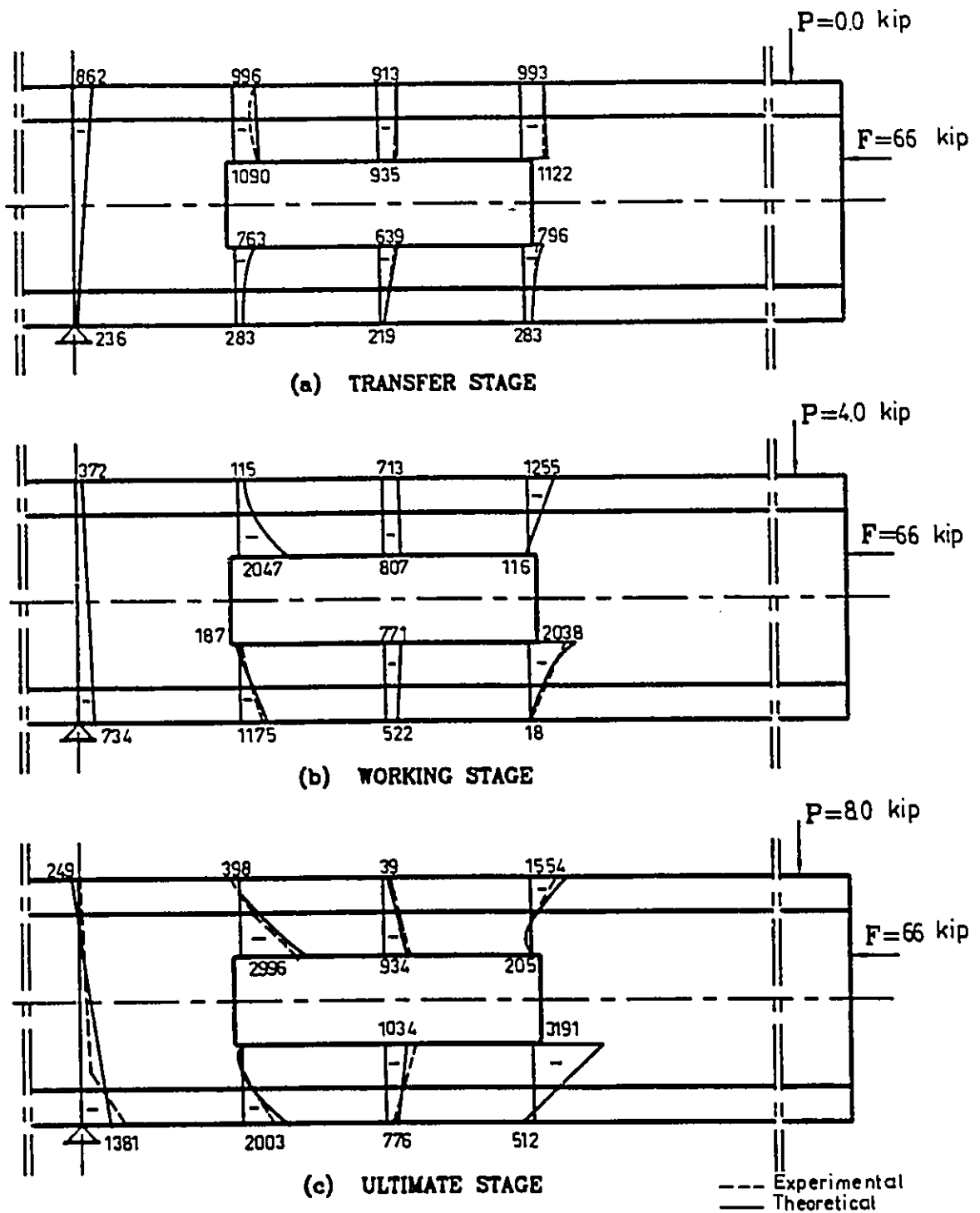


FIG. 5.69 HORIZONTAL STRESS DISTRIBUTION FOR BEAM BIII1A

Note: stresses are shown in psi; 1 psi=6.89 kPa; 1 kip=4.45 kN

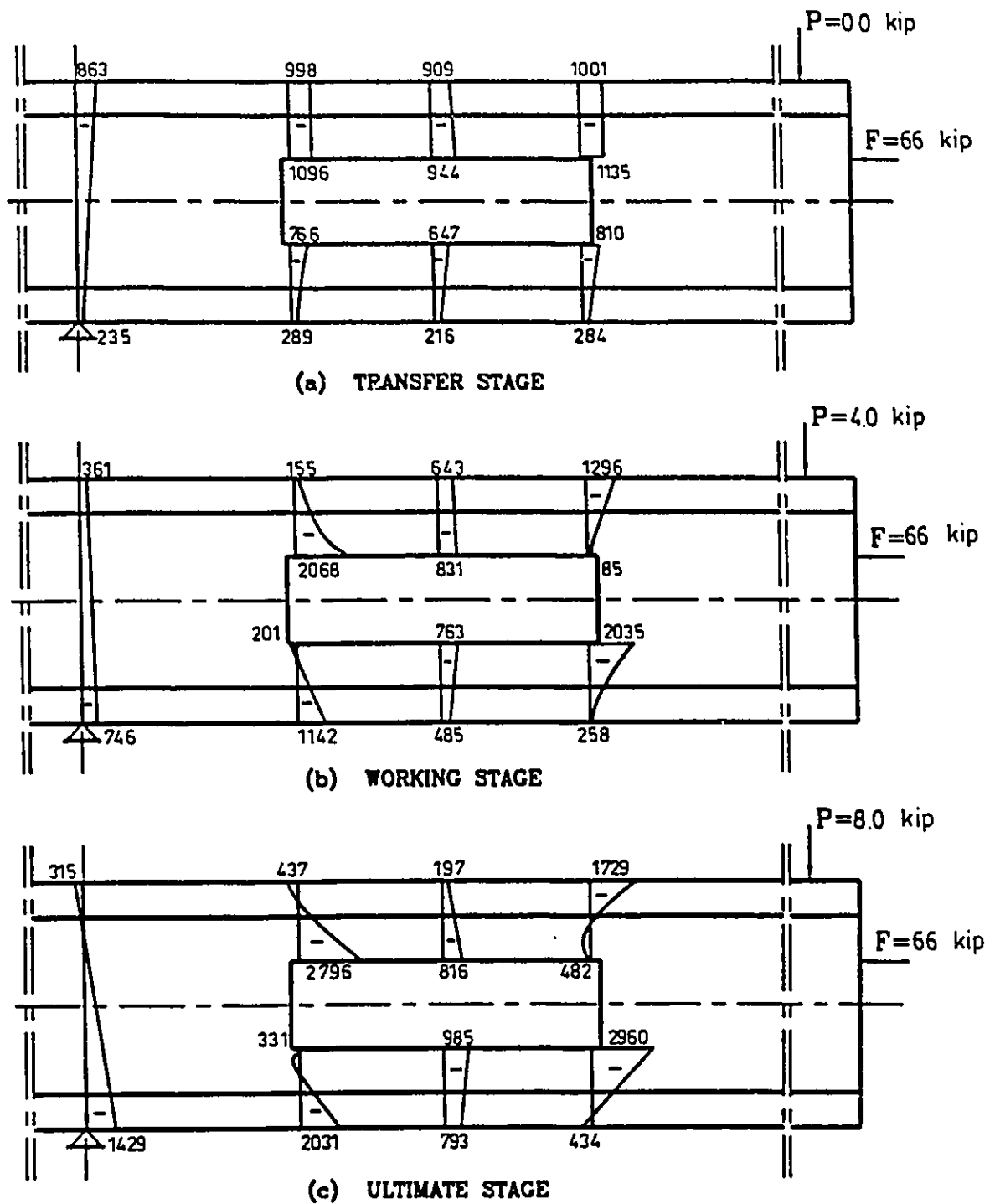


FIG. 5.70 HORIZONTAL STRESS DISTRIBUTION FOR BEAM BIII1B

Note: stresses are shown in psi; 1 psi=6.89 kPa; 1 kip=4.45 kN

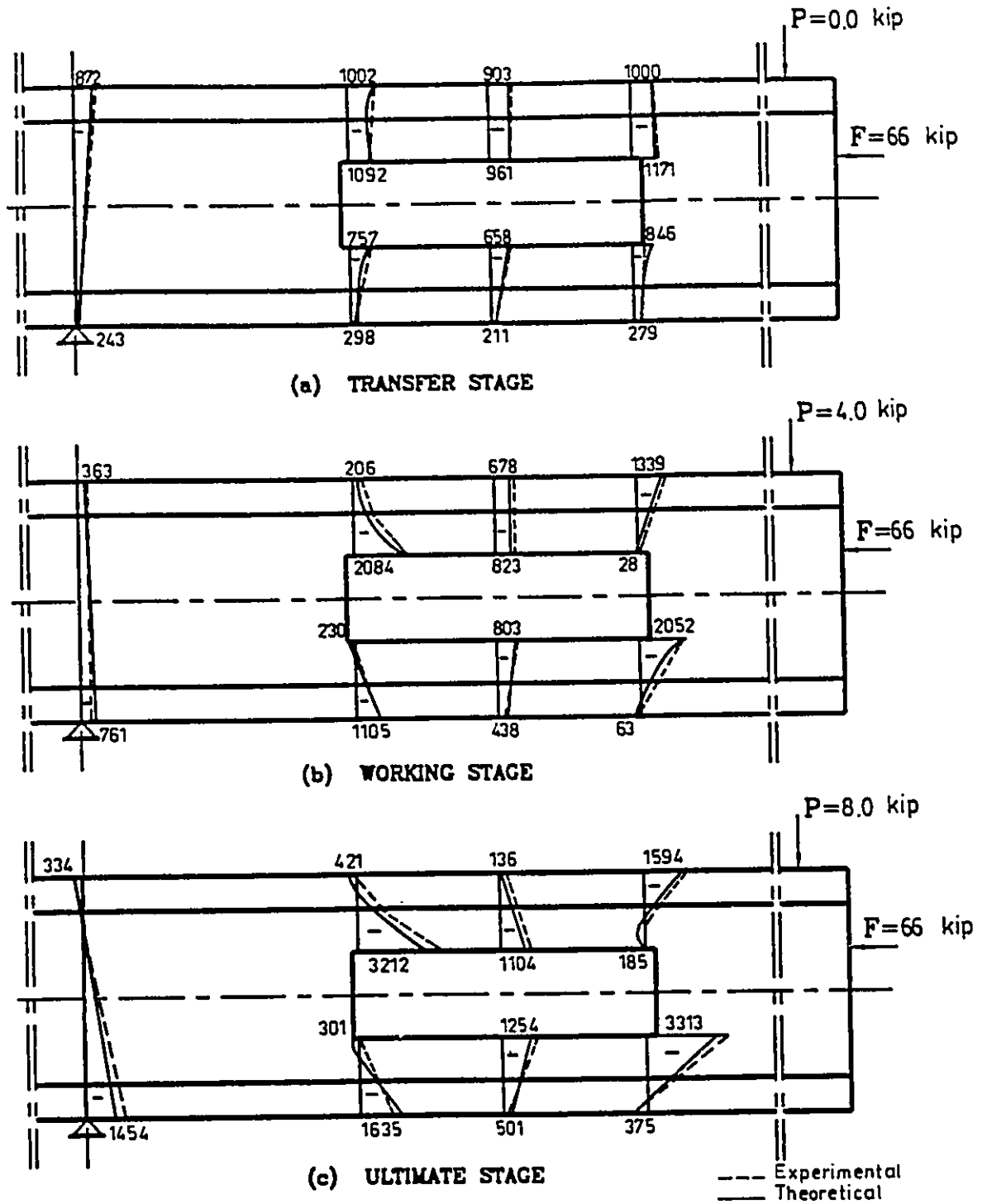
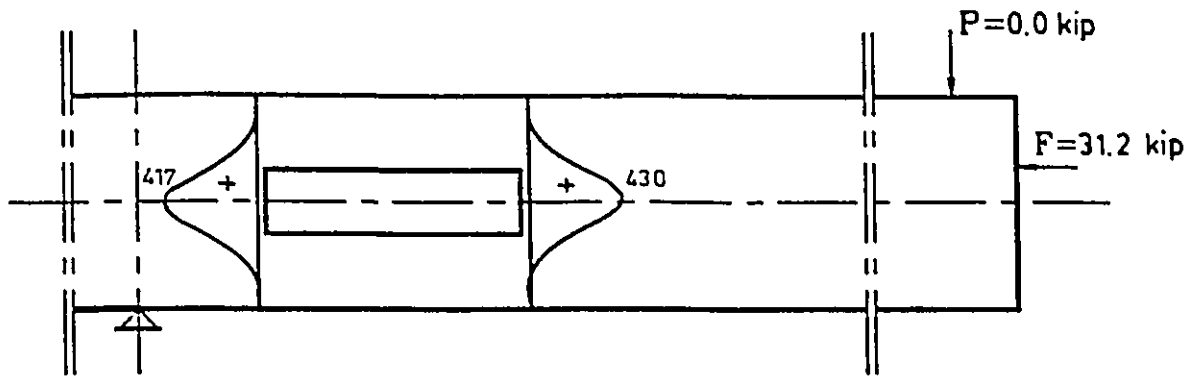
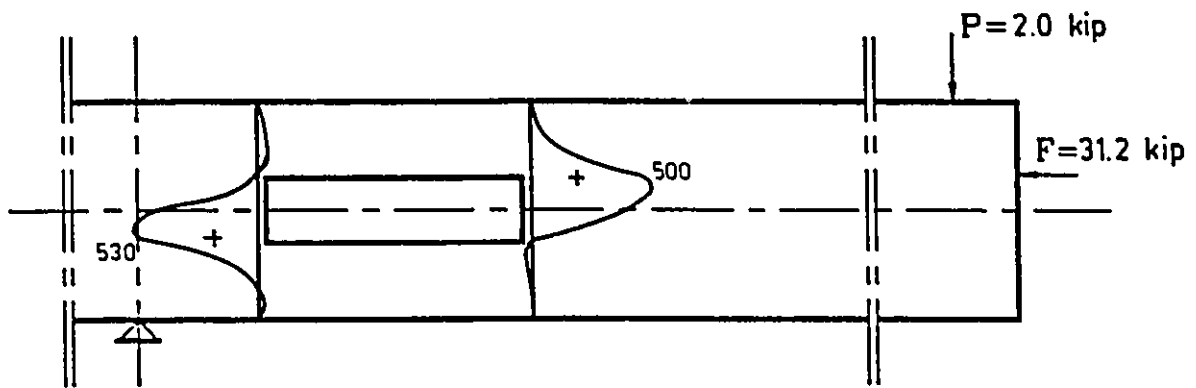


FIG. 5.71 HORIZONTAL STRESS DISTRIBUTION FOR BEAM BIII C

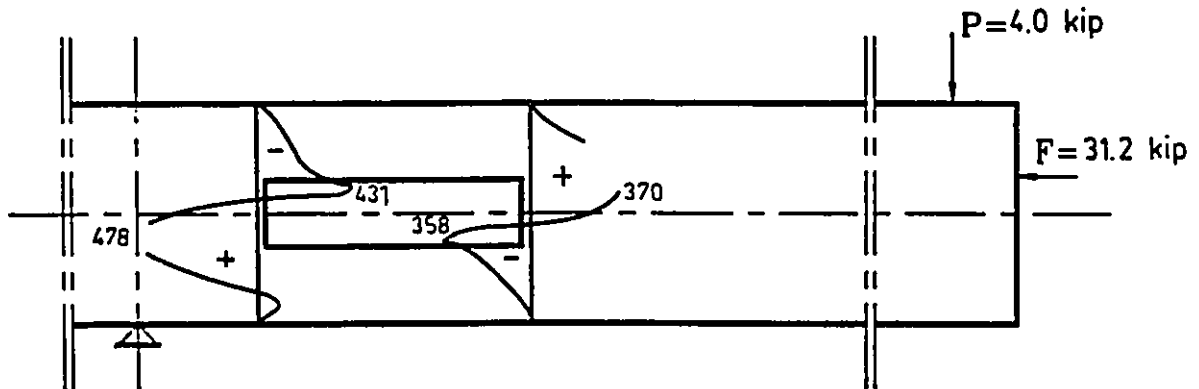
Note: stresses are shown in psi; 1 psi=6.89 kPa; 1 kip=4.45 kN



(a) TRANSFER STAGE



(b) WORKING STAGE



(c) ULTIMATE STAGE

FIG. 5.72 VERTICAL STRESS DISTRIBUTION FOR BEAM B11A

Note: stresses are shown in psi; 1 psi=6.89 kPa; 1 kip=4.45 kN

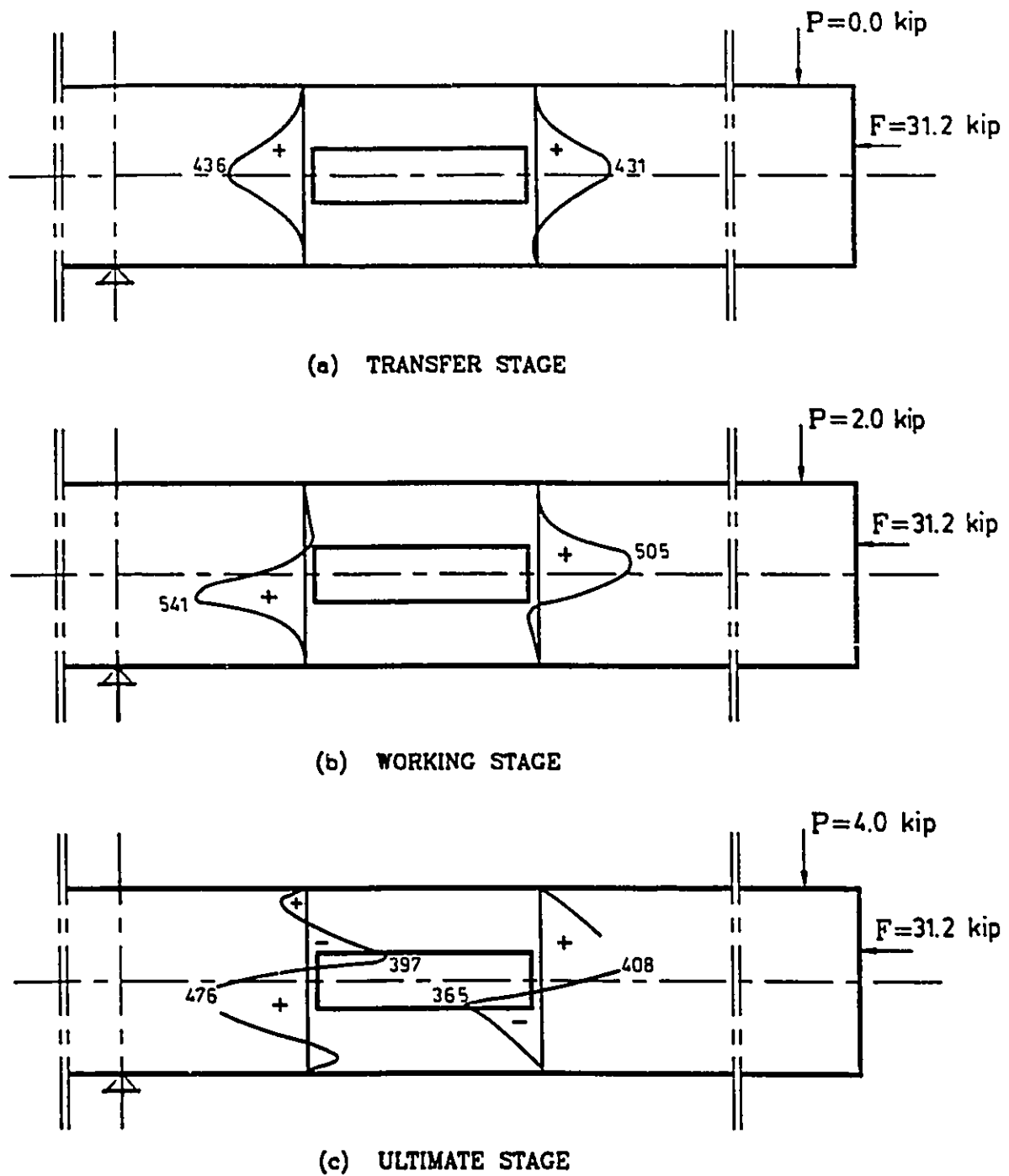
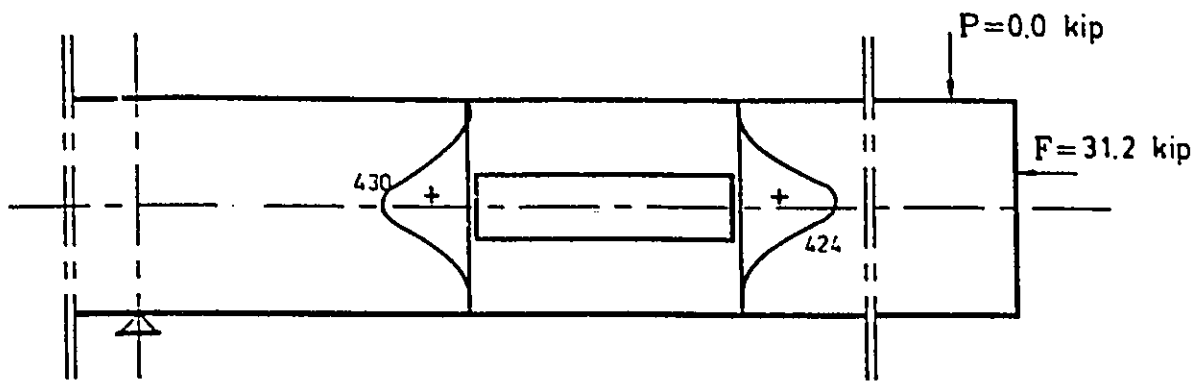
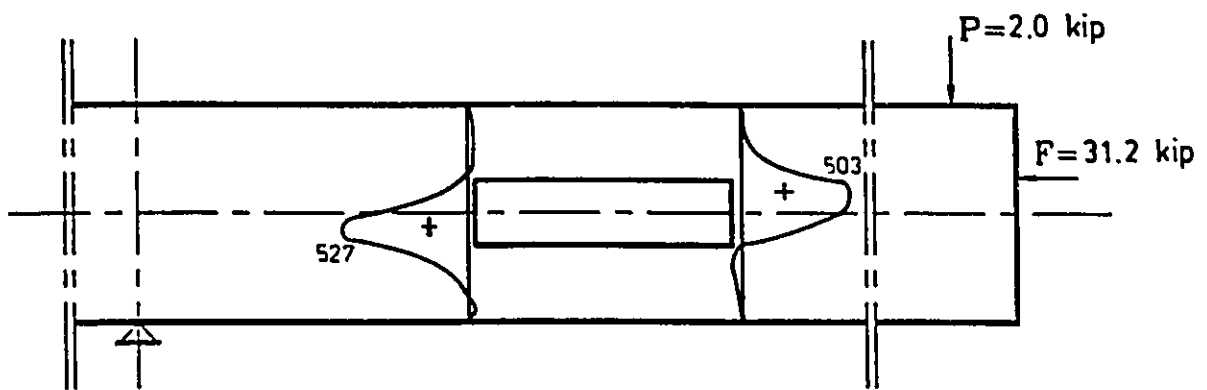


FIG. 5.73 VERTICAL STRESS DISTRIBUTION FOR BEAMS BI1B & BI3A

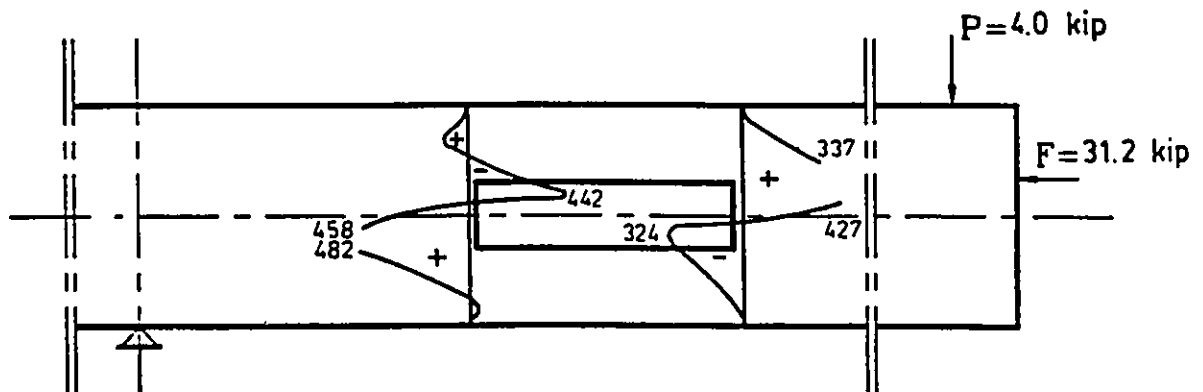
Note: stresses are shown in psi; 1 psi=6.89 kPa; 1 kip=4.45 kN



(a) TRANSFER STAGE



(b) WORKING STAGE



(c) ULTIMATE STAGE

FIG. 5.74 VERTICAL STRESS DISTRIBUTION FOR BEAM BI1C

Note: stresses are shown in psi; 1 psi=6.89 kPa; 1 kip=4.45 kN

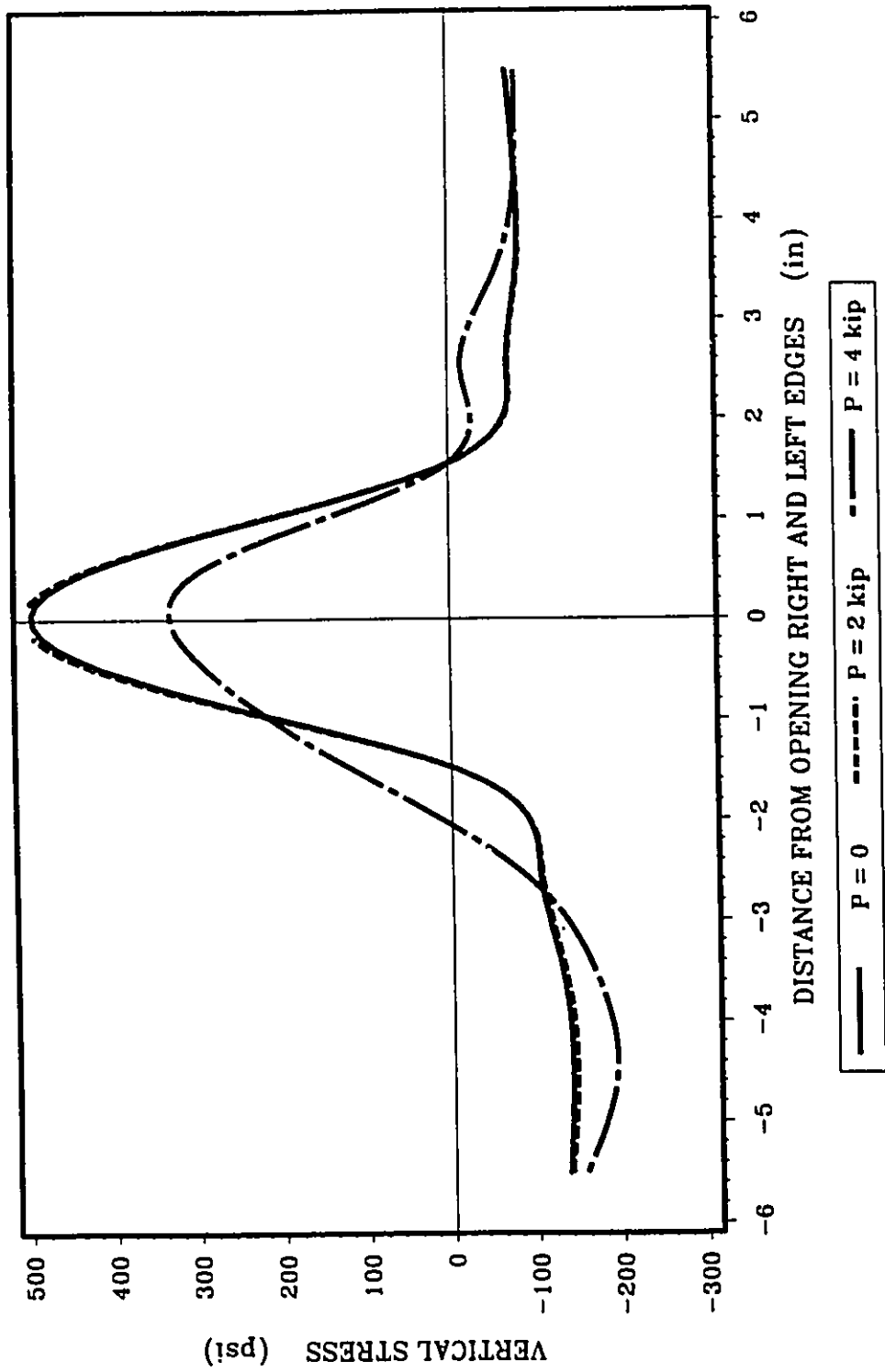


FIG. 5.75 VERTICAL STRESS DISTRIBUTION AT THE OPENING FOR BEAM B11A

Note: 1 in.=25.4 mm; 1 kip=4.45 kN; 1 psi=6.89 kPa

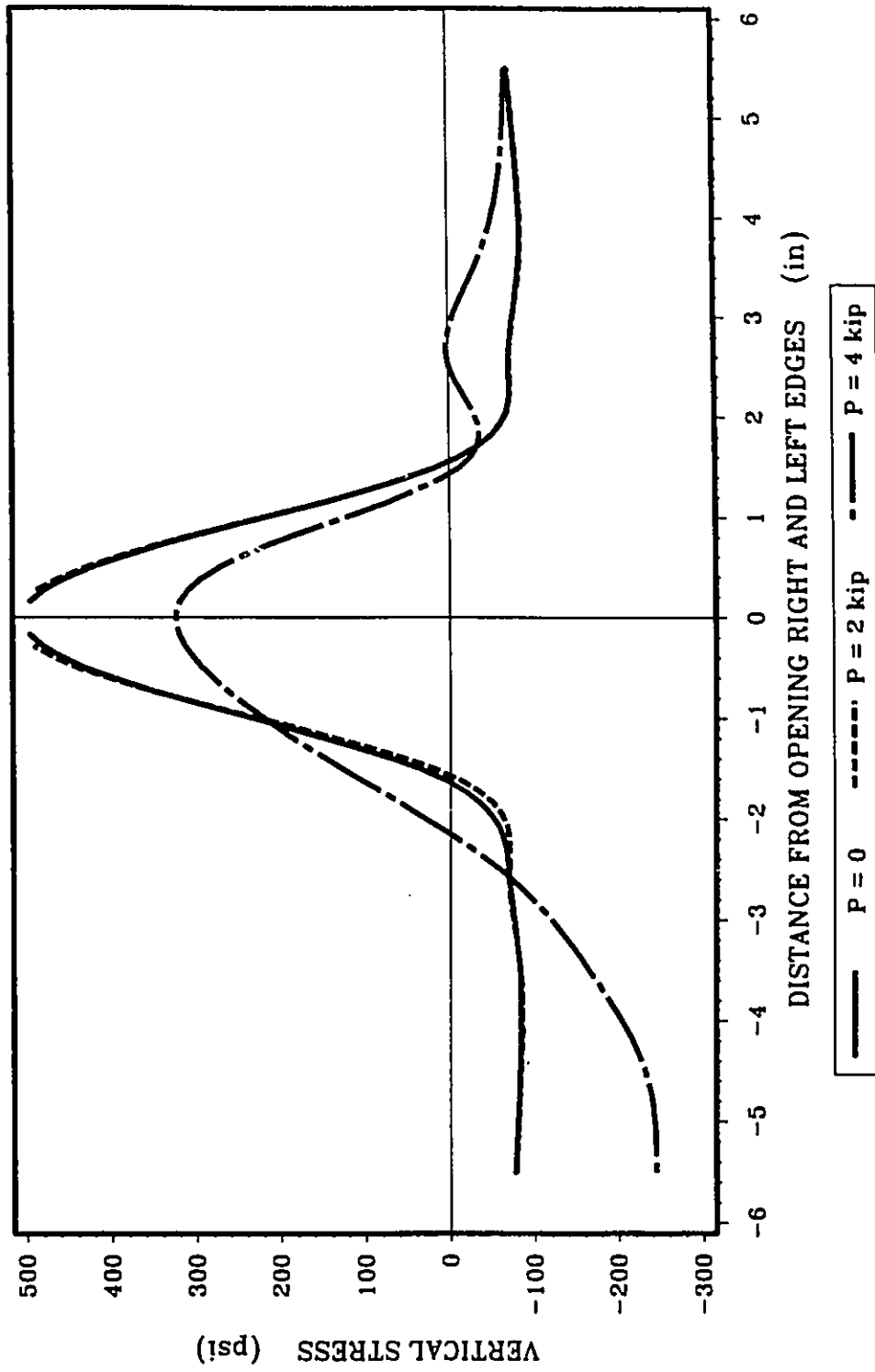


FIG. 5.76 VERTICAL STRESS DISTRIBUTION AT THE OPENING FOR BEAM BI1B

Note: 1 in.=25.4 mm; 1 kip=4.45 kN; 1 psi=6.89 kPa

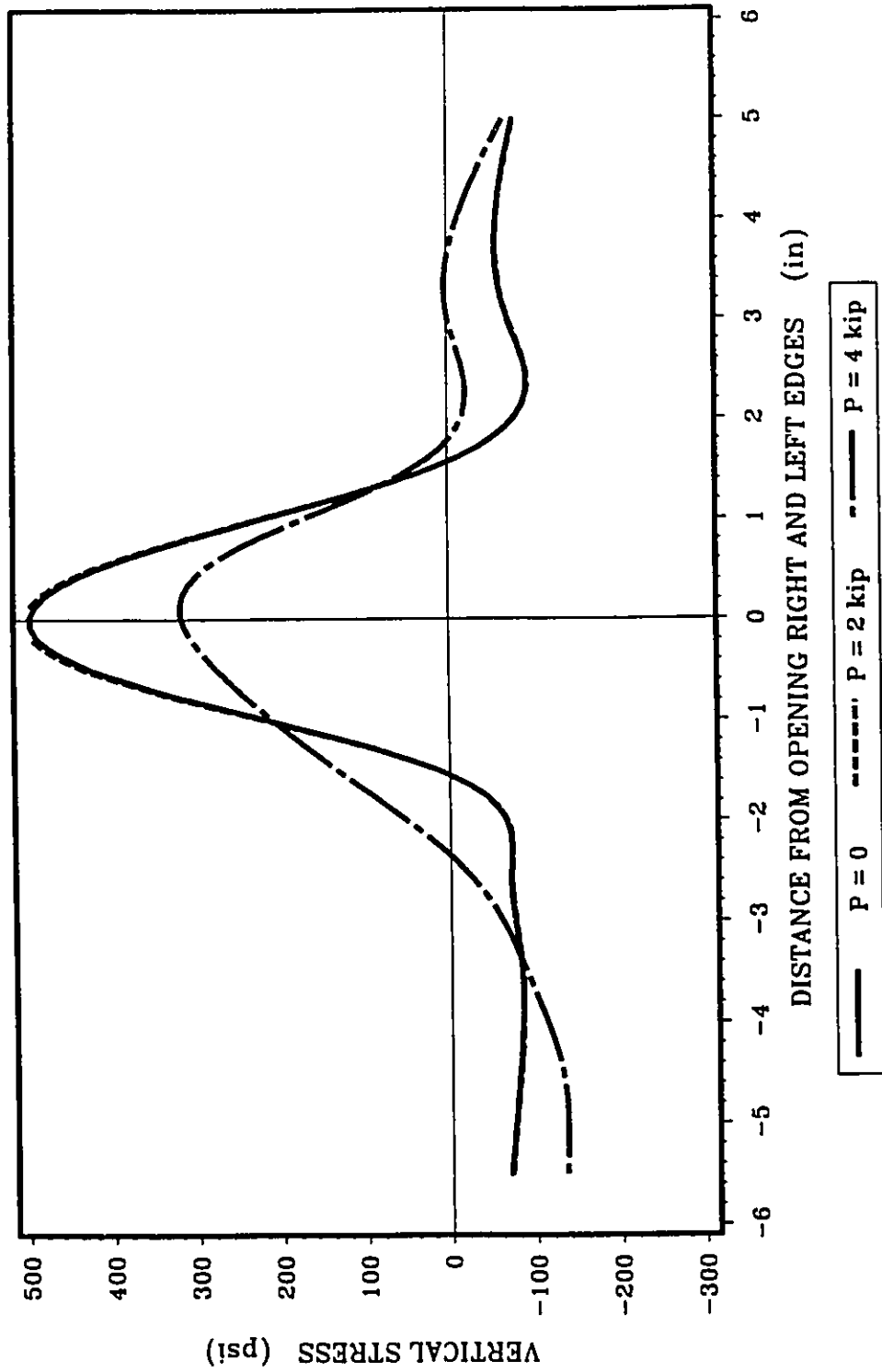
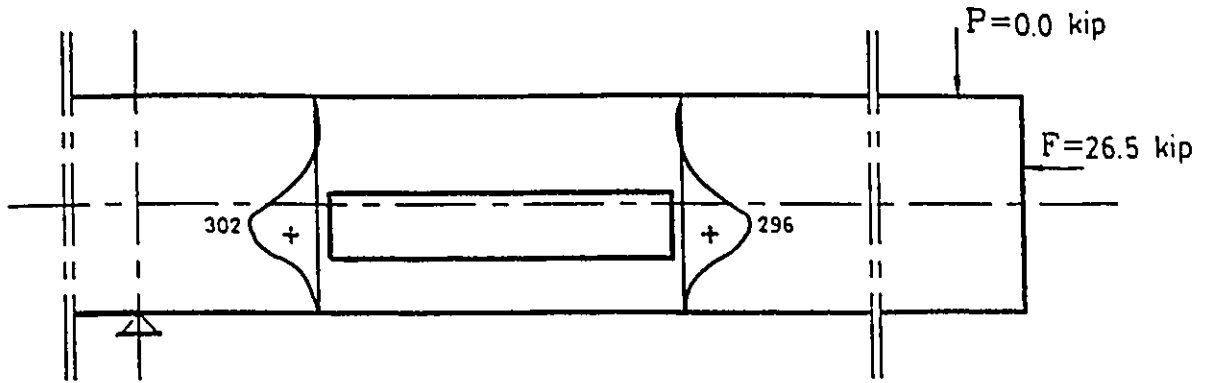
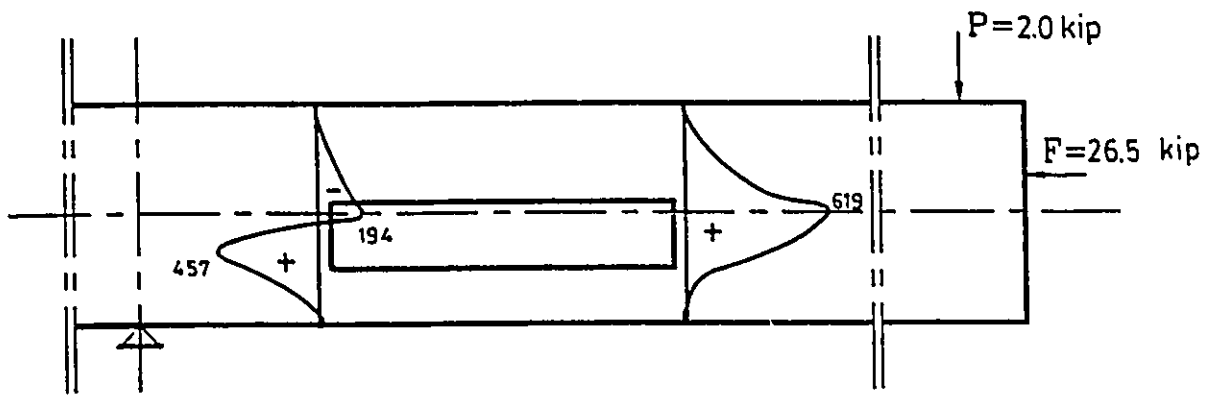


FIG. 5.77 VERTICAL STRESS DISTRIBUTION AT THE OPENING FOR BEAM BI1C

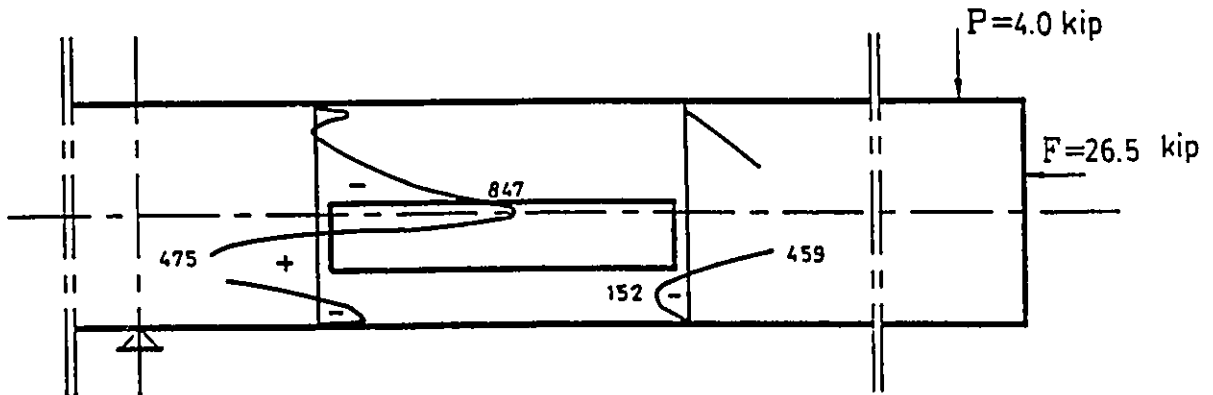
Note: 1 in.=25.4 mm; 1 kip=4.45 kN; 1 psi=6.89 kPa



(a) TRANSFER STAGE



(b) WORKING STAGE



(c) ULTIMATE STAGE

FIG. 5.78 VERTICAL STRESS DISTRIBUTION FOR BEAM B12A

Note: stresses are shown in psi; 1 psi=6.89 kPa; 1 kip=4.45 kN

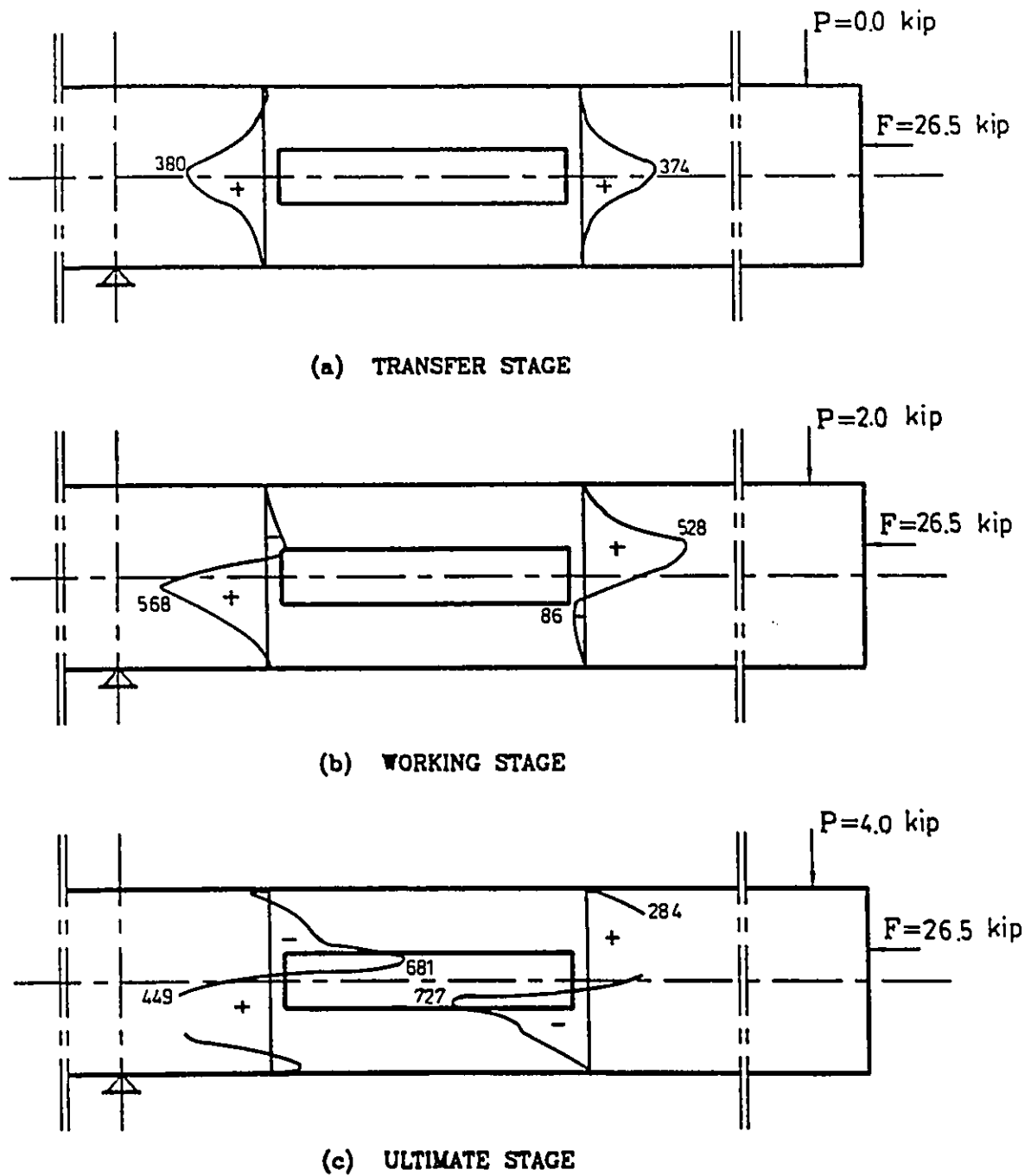
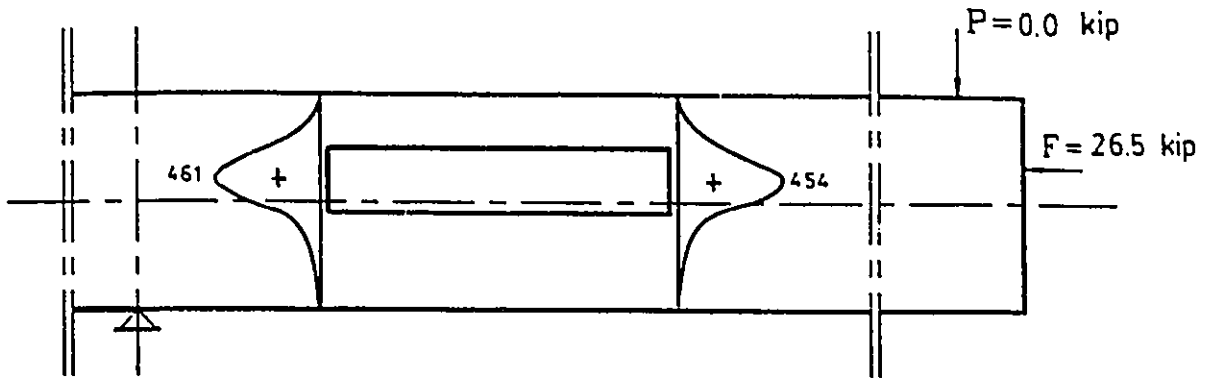
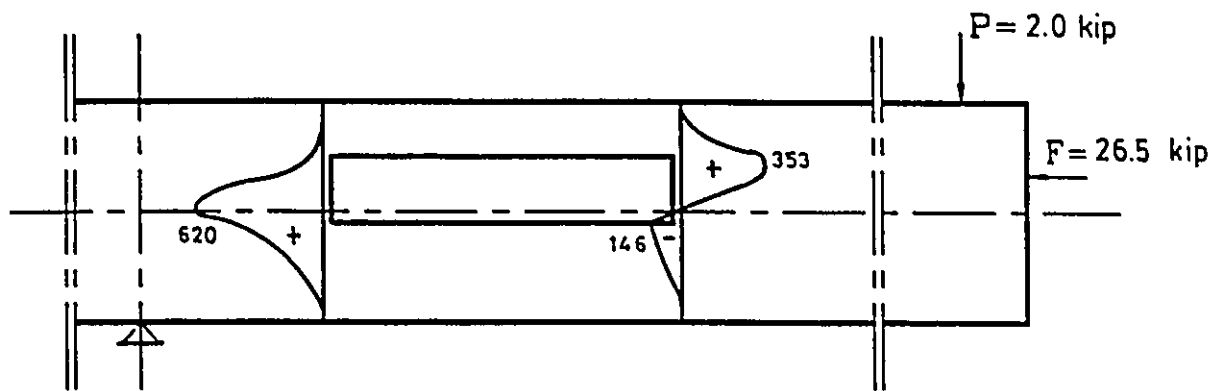


FIG. 5.79 VERTICAL STRESS DISTRIBUTION FOR BEAM B12B

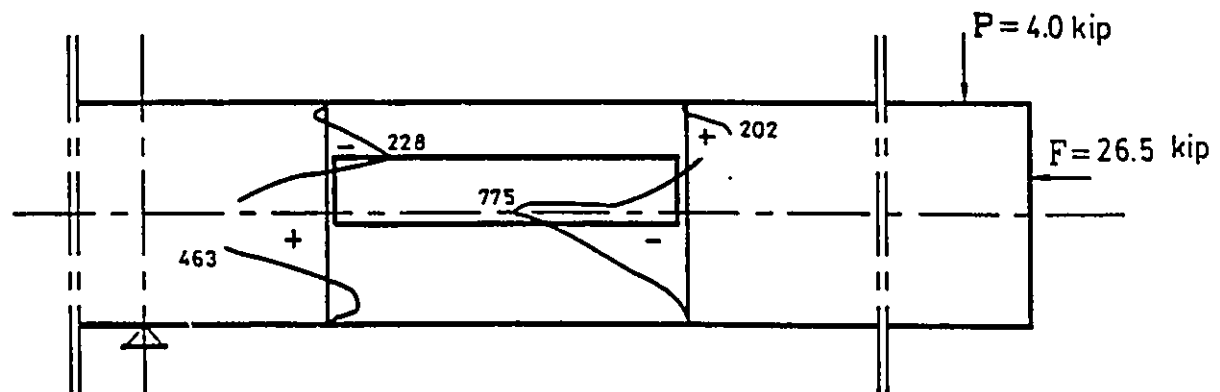
Note: stresses are shown in psi; 1 psi=6.89 kPa; 1 kip=4.45 kN



(a) TRANSFER STAGE



(b) WORKING STAGE



(c) ULTIMATE STAGE

FIG. 5.80 VERTICAL STRESS DISTRIBUTION FOR BEAM B12C

Note: stresses are shown in psi; 1 psi=6.89 kPa; 1 kip=4.45 kN

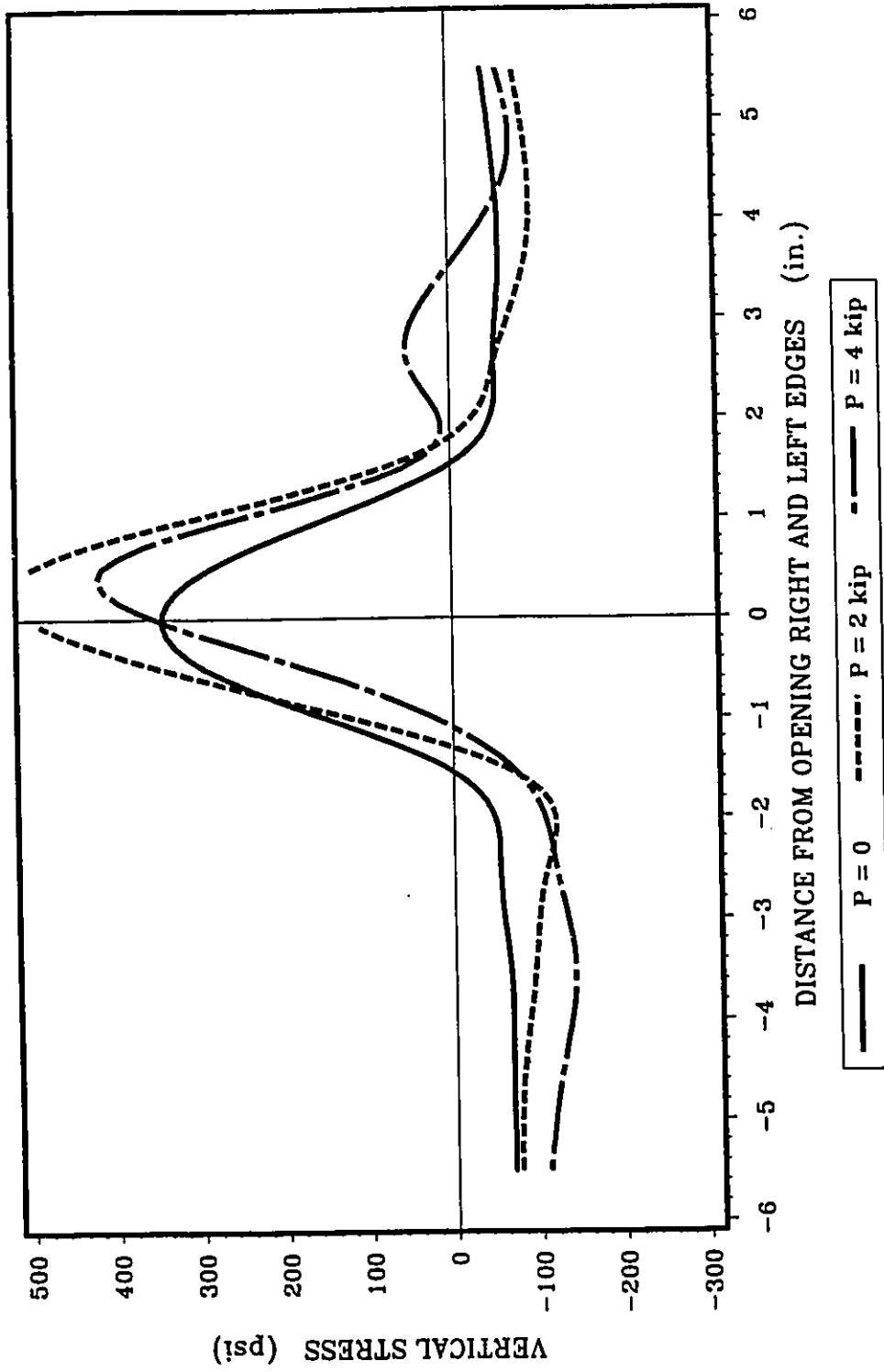


FIG. 5.81 VERTICAL STRESS DISTRIBUTION AT THE OPENING FOR BEAM B12A

Note: 1 in.=25.4 mm; 1 kip=4.45 kN; 1 psi=6.89 kPa

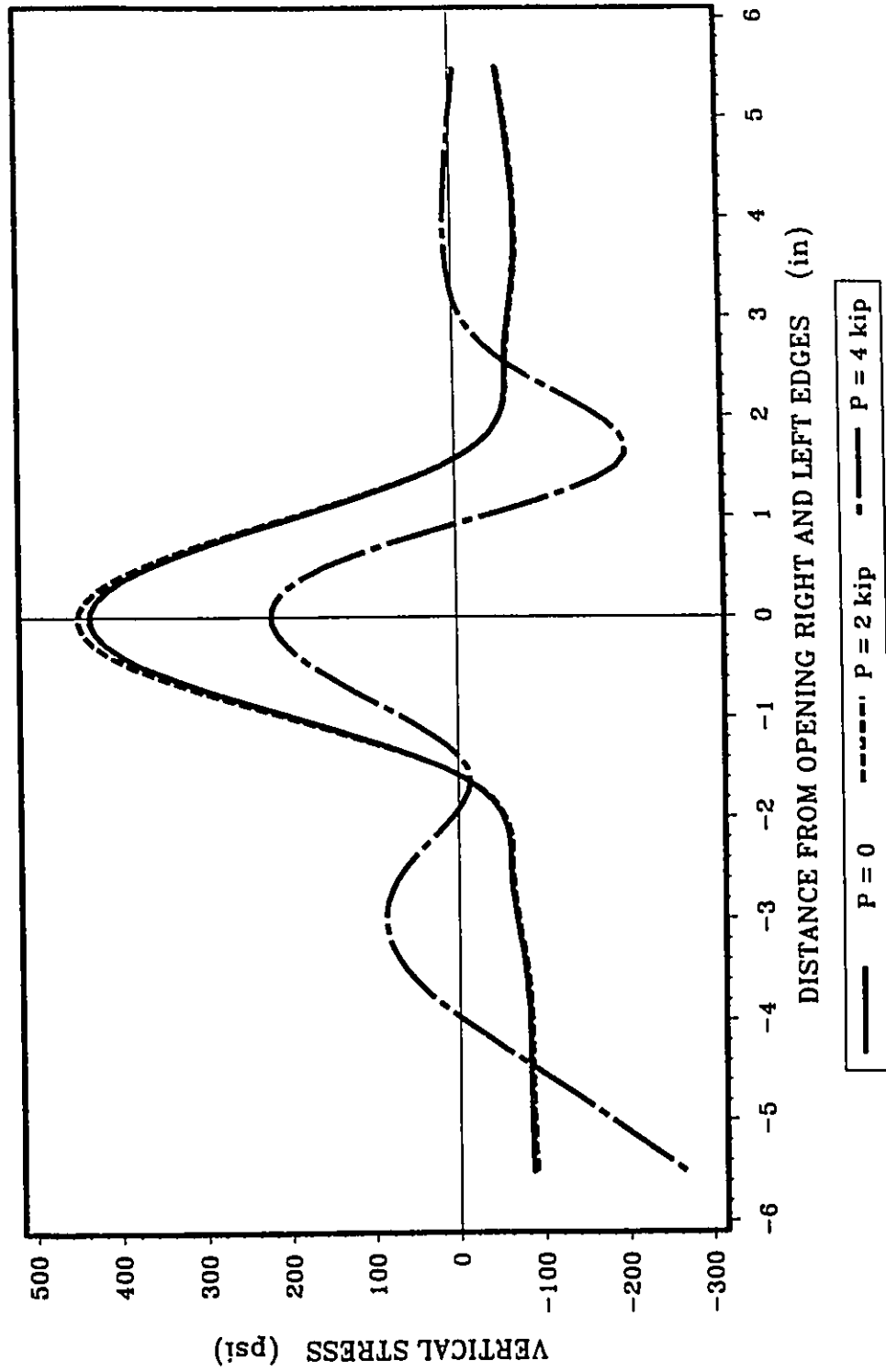


FIG. 5.82 VERTICAL STRESS DISTRIBUTION AT THE OPENING FOR BEAM BI2B

Note: 1 in.=25.4 mm; 1 kip=4.45 kN; 1 psi=6.89 kPa

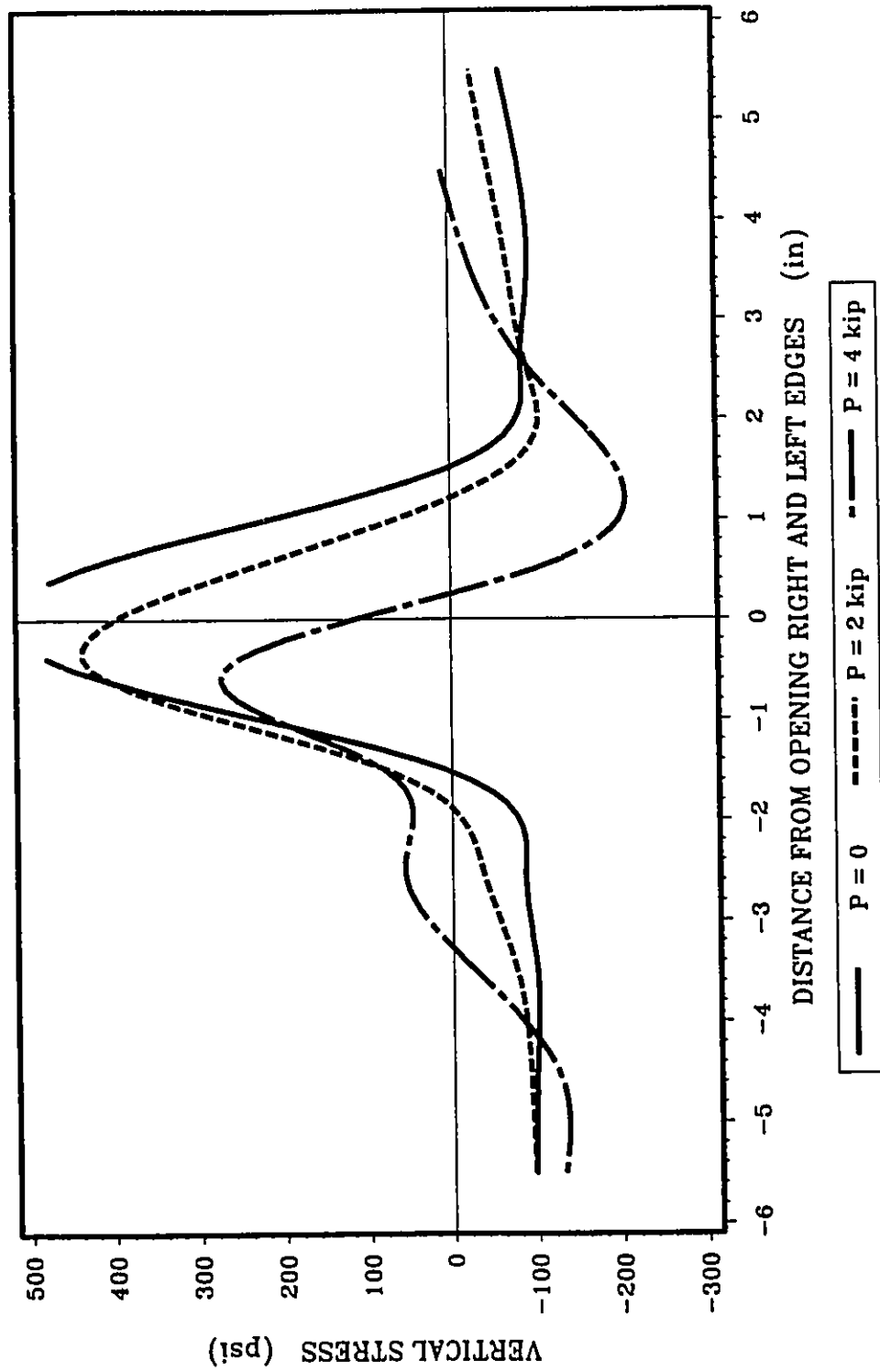


FIG. 5.83 VERTICAL STRESS DISTRIBUTION AT THE OPENING FOR BEAM BI2C

Note: 1 in.=25.4 mm; 1 kip=4.45 kN; 1 psi=6.89 kPa

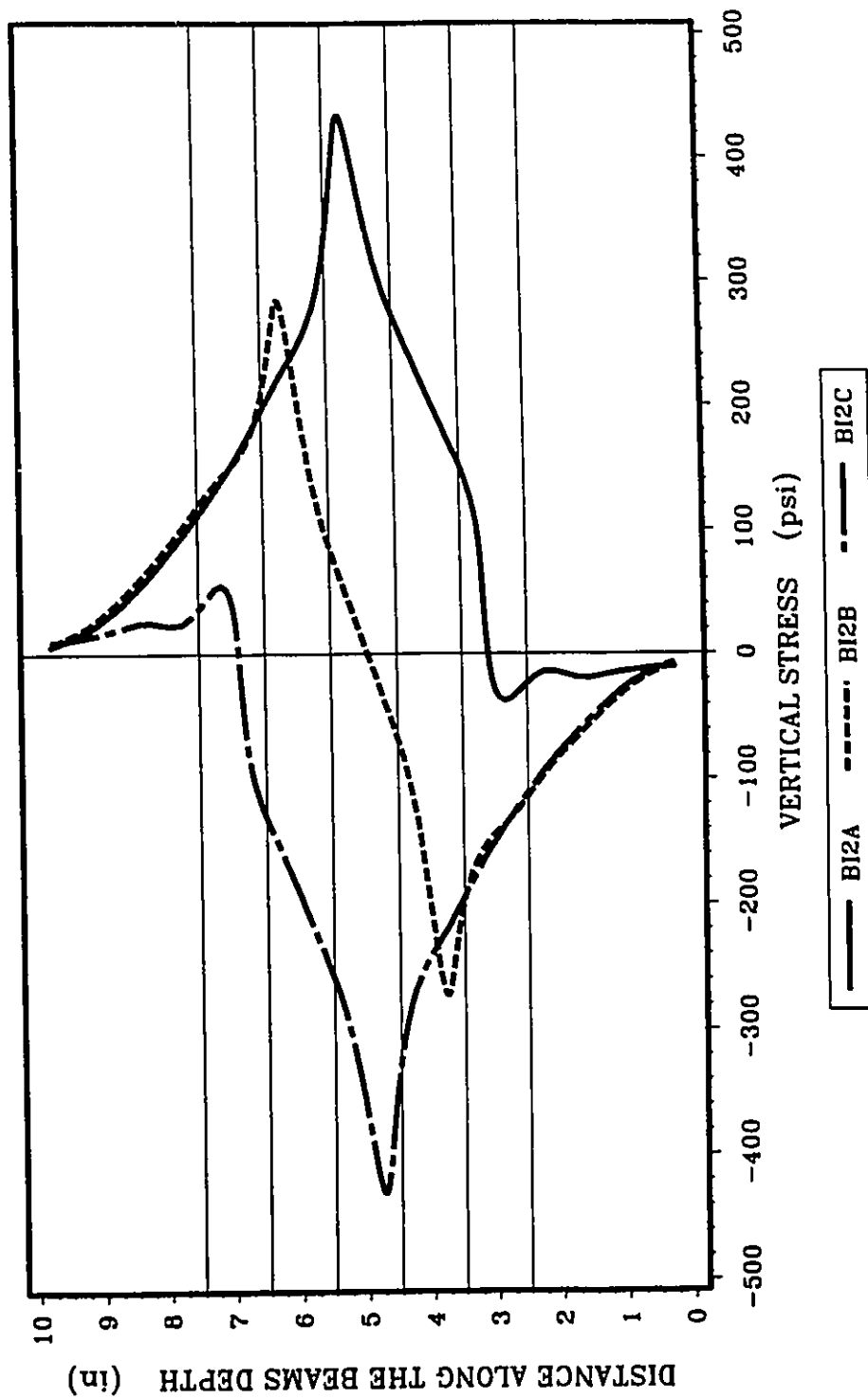
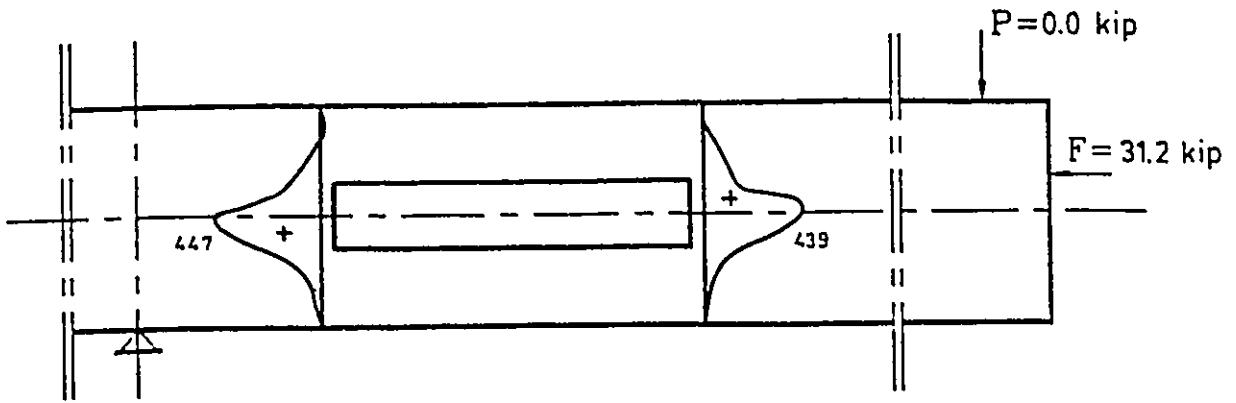
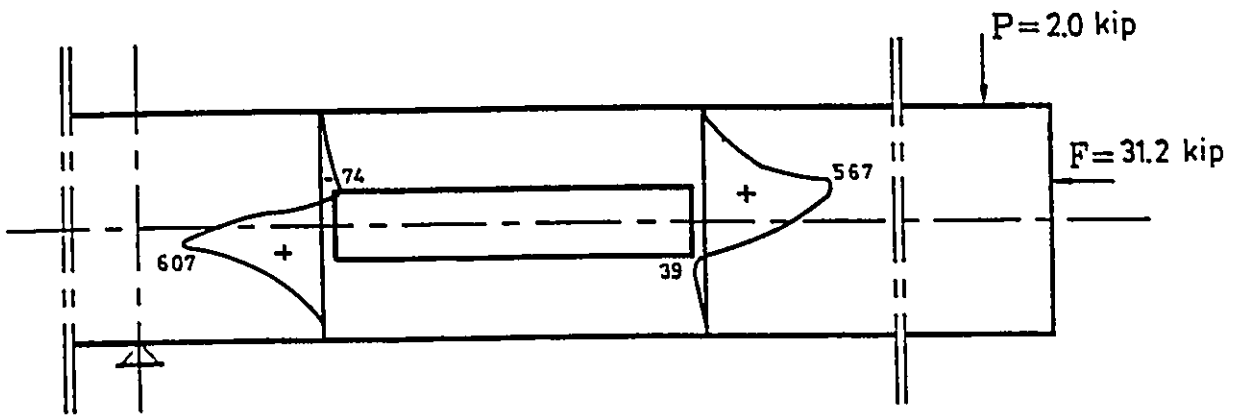


FIG. 5.84 VERTICAL STRESS DISTRIBUTION AT THE OPENING EDGES FOR GROUP BI2
(P = 2 kip)

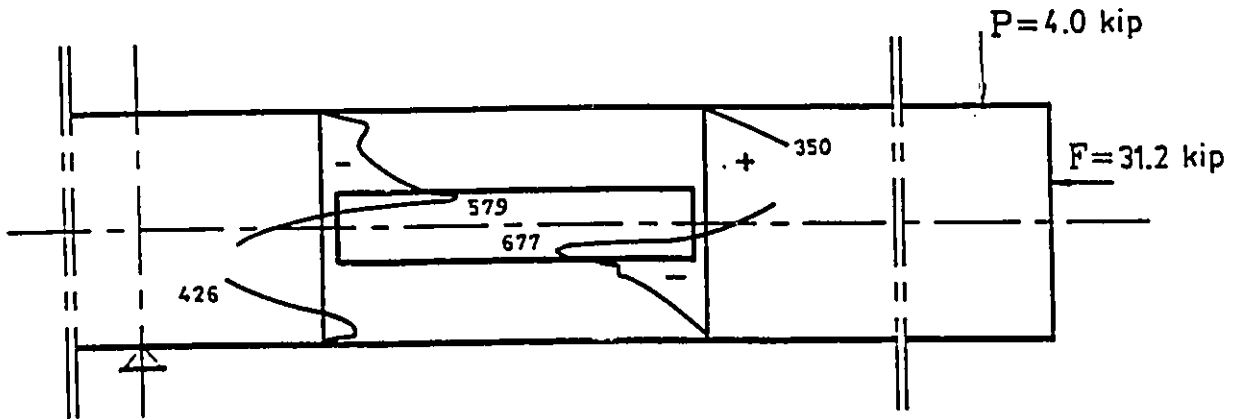
Note: 1 in.=25.4 mm; 1 kip=4.45 kN; 1 psi=6.89 kPa



(a) TRANSFER STAGE



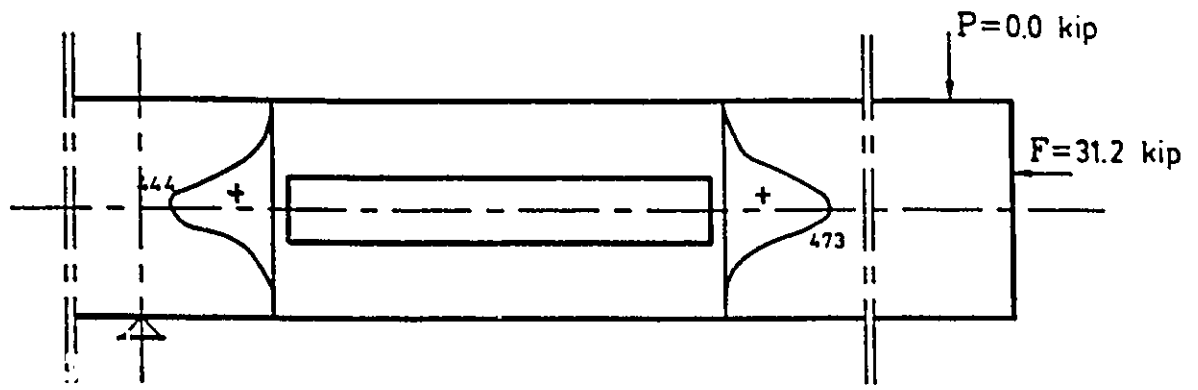
(b) WORKING STAGE



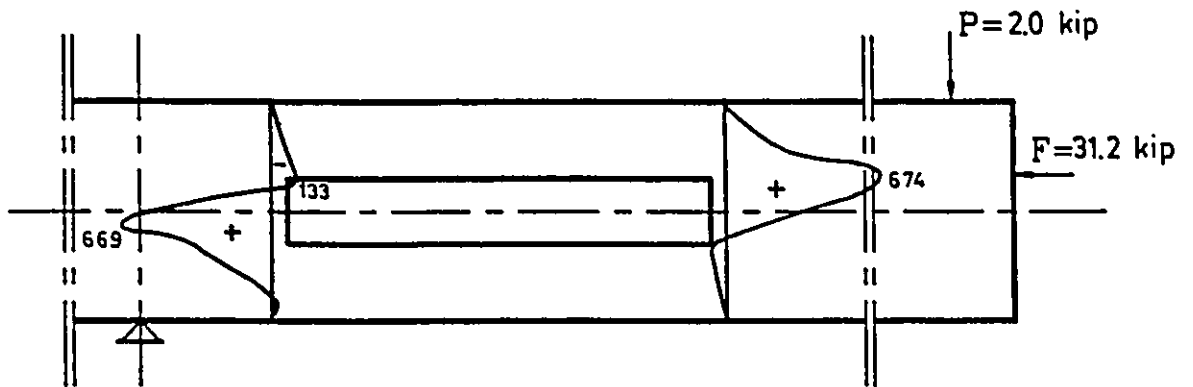
(c) ULTIMATE STAGE

FIG. 5.85 VERTICAL STRESS DISTRIBUTION FOR BEAM B13B

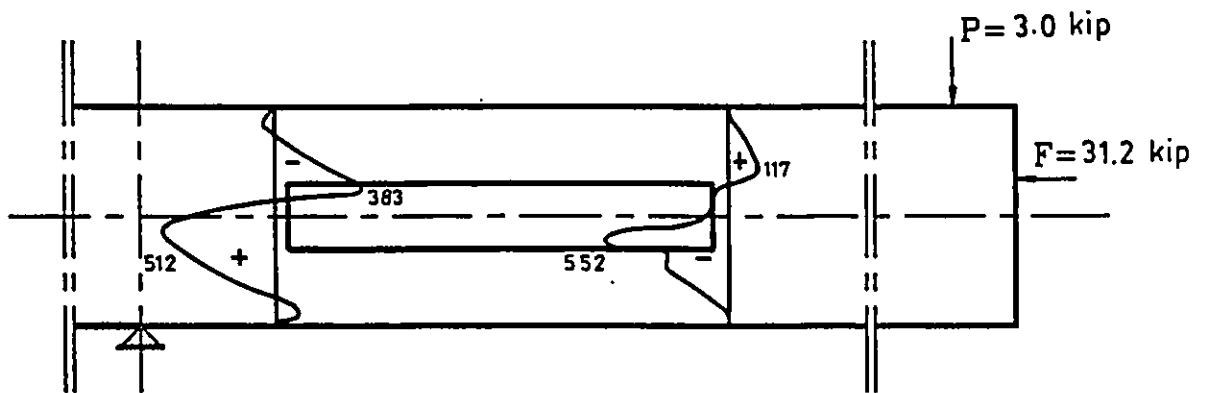
Note: stresses are shown in psi; 1 psi=6.89 kPa; 1 kip=4.45 kN



(a) TRANSFER STAGE



(b) WORKING STAGE



(c) ULTIMATE STAGE

FIG. 5.86 VERTICAL STRESS DISTRIBUTION FOR BEAM B13C

Note: stresses are shown in psi; 1 psi=6.89 kPa; 1 kip=4.45 kN

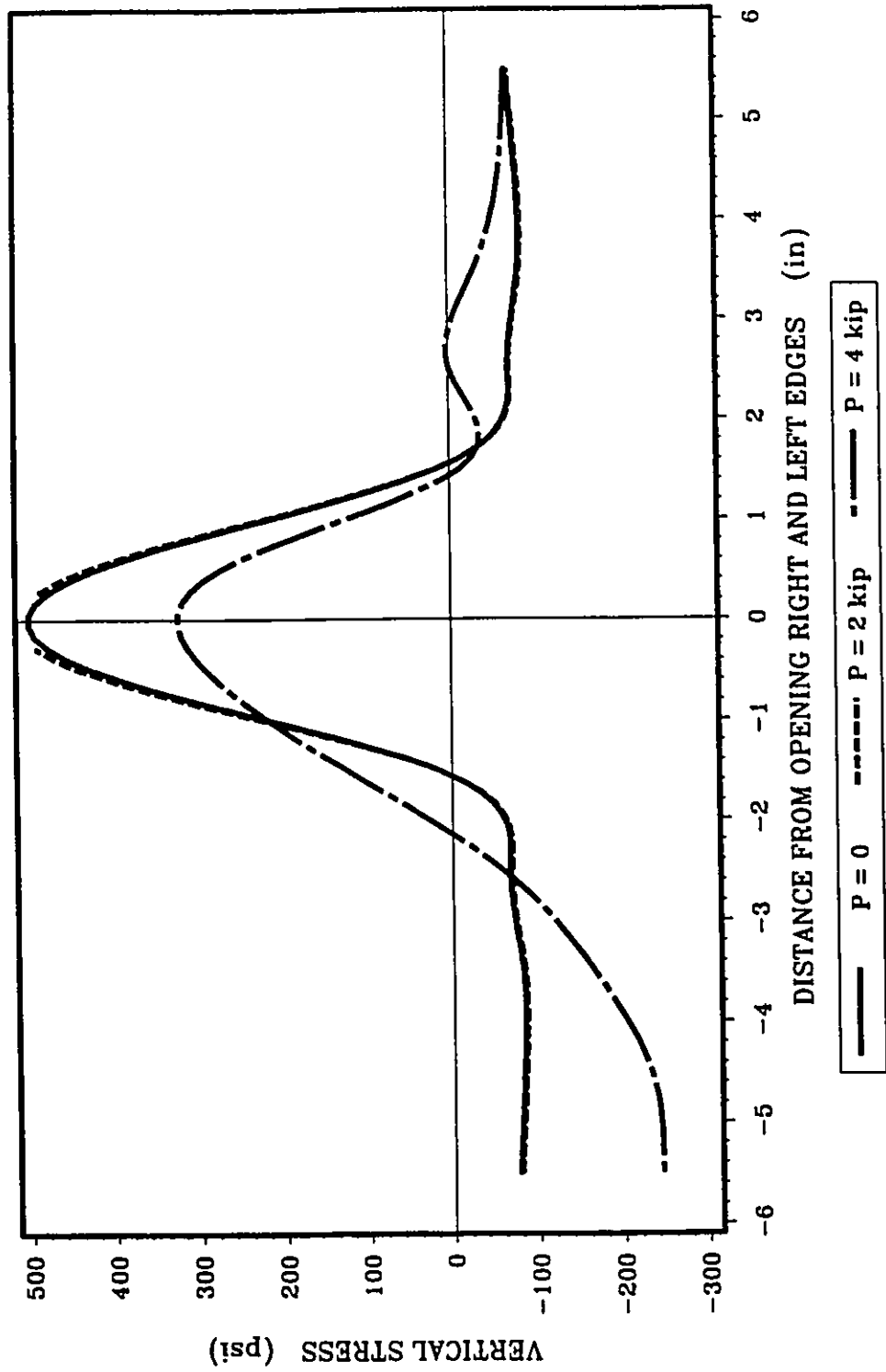


FIG. 5.87 VERTICAL STRESS DISTRIBUTION AT THE OPENING FOR BEAM B13A

Note: 1 in.=25.4 mm; 1 kip=4.45 kN; 1 psi=6.89 kPa

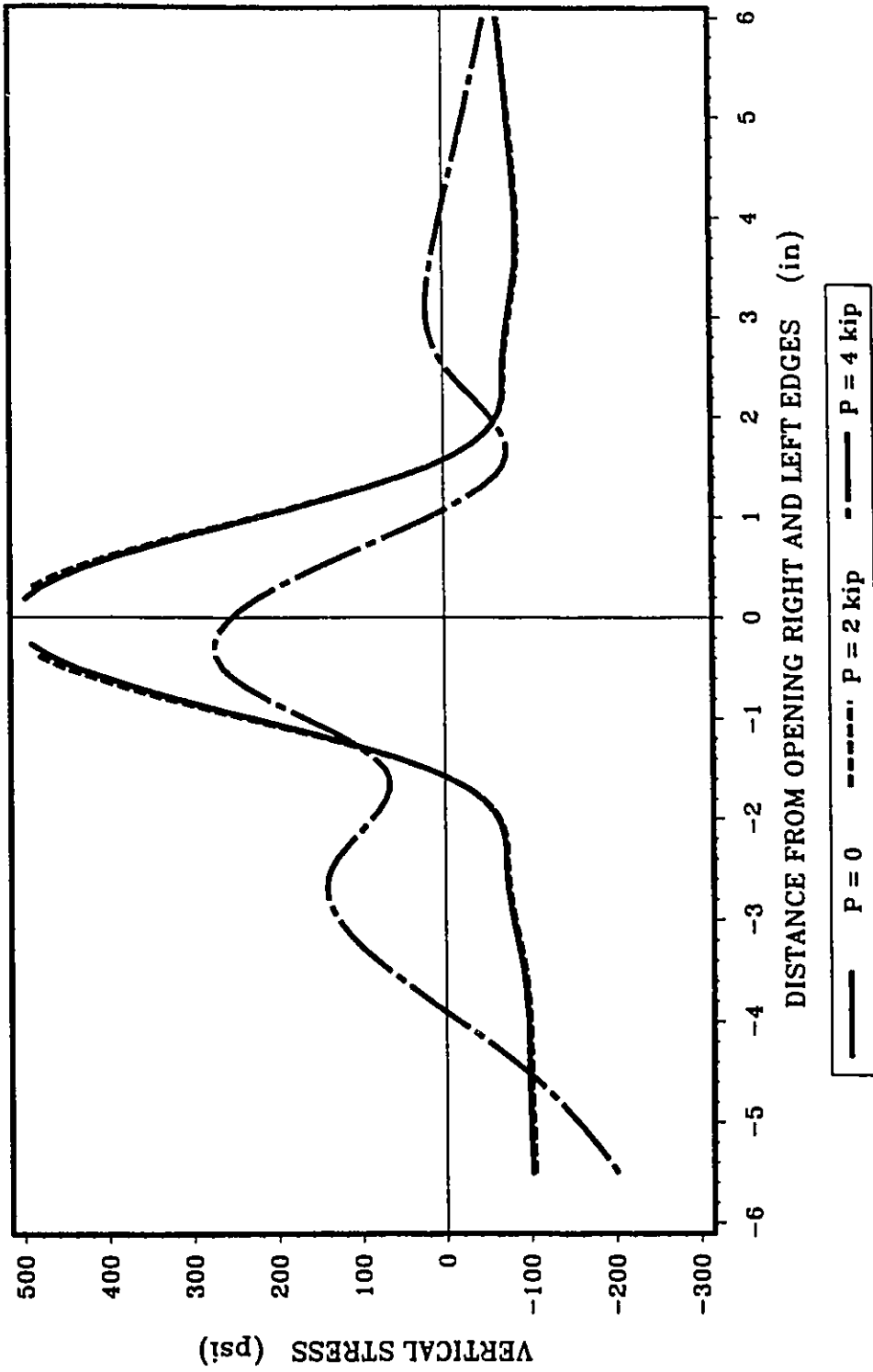


FIG. 5.88 VERTICAL STRESS DISTRIBUTION AT THE OPENING FOR BEAM BI3B

Note: 1 in.=25.4 mm; 1 kip=4.45 kN; 1 psi=6.89 kPa

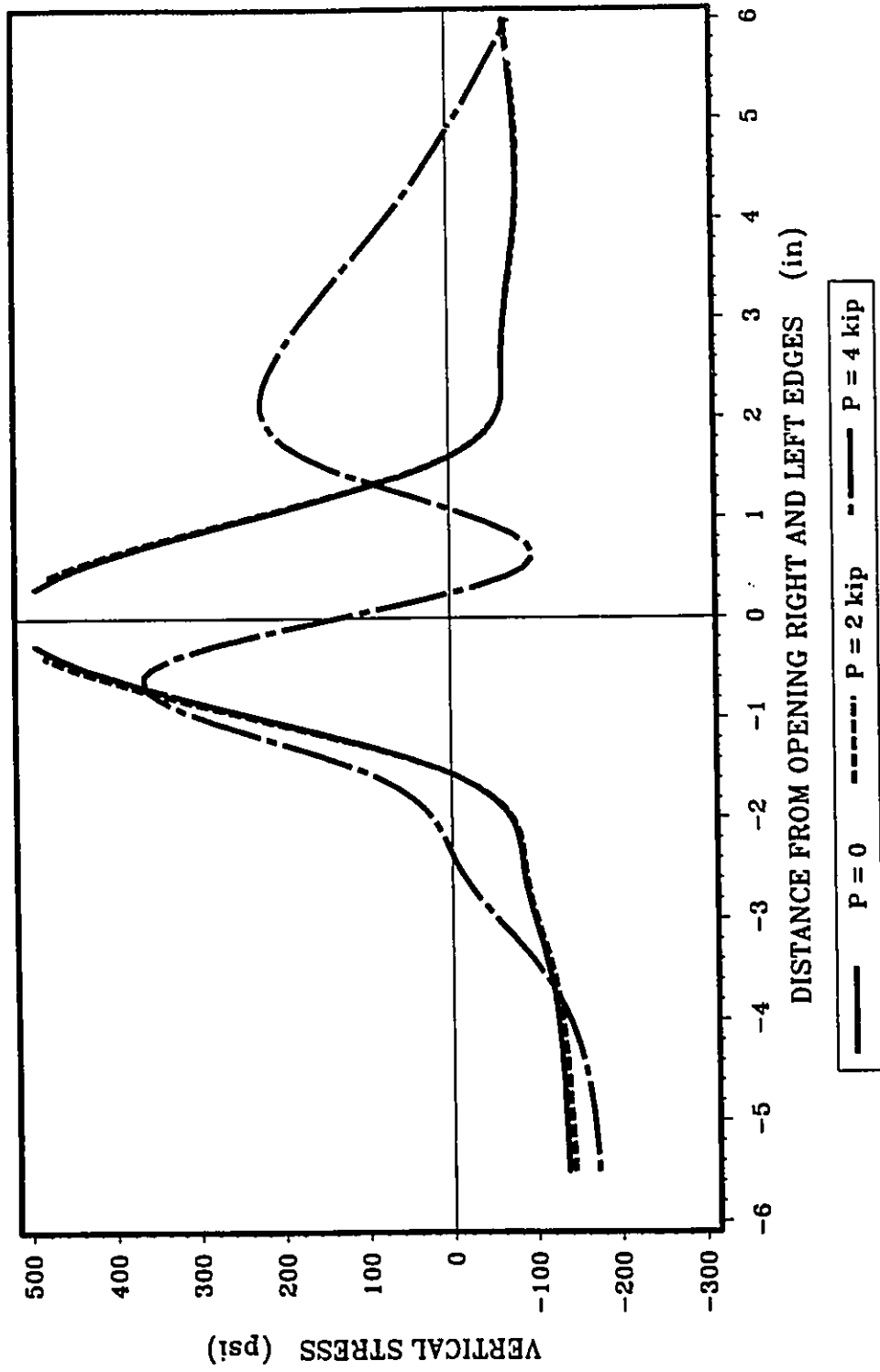


FIG. 5.89 VERTICAL STRESS DISTRIBUTION AT THE OPENING FOR BEAM B13C

Note: 1 in.=25.4 mm; 1 kip=4.45 kN; 1 psi=6.89 kPa

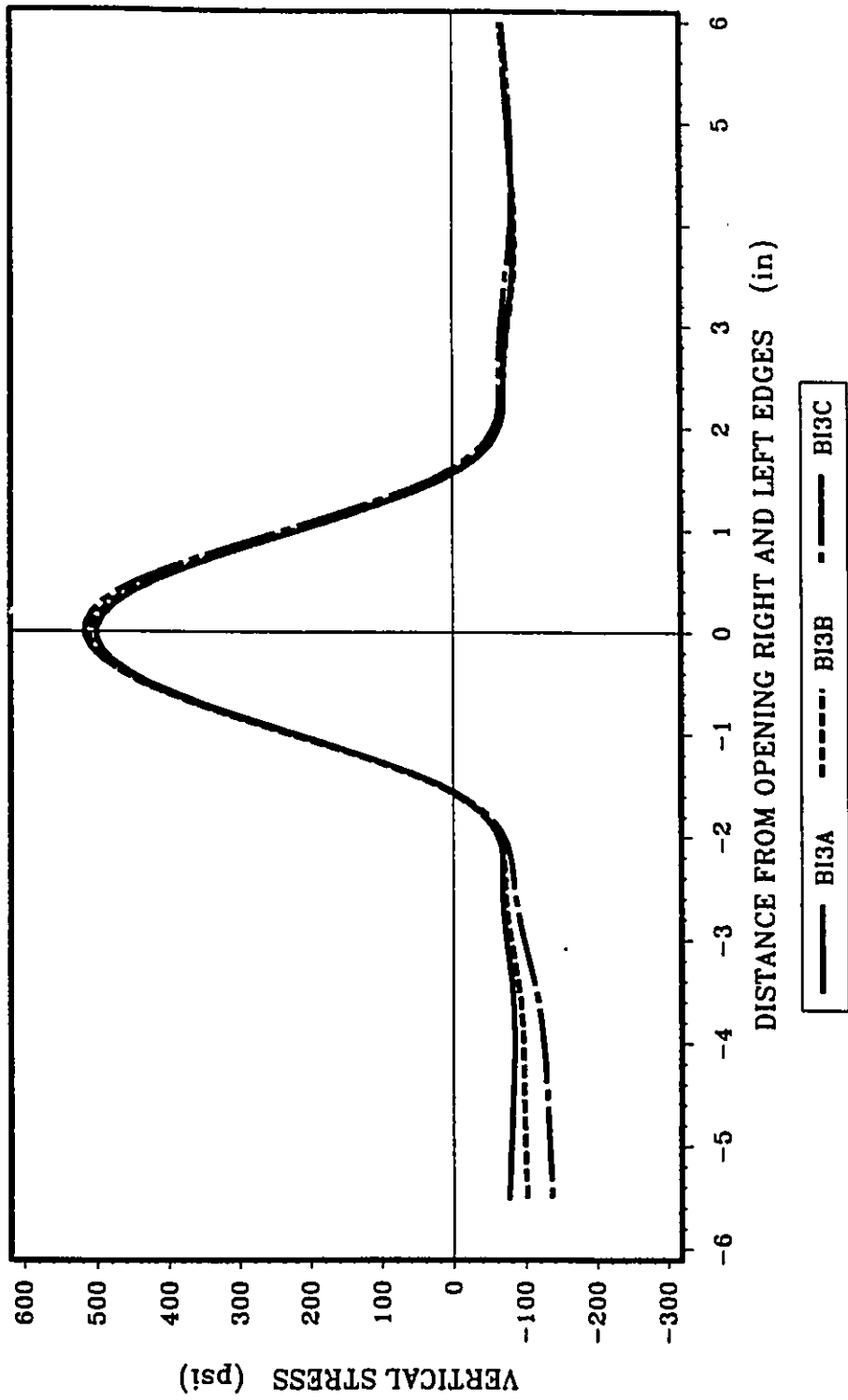


FIG. 5.90 VERTICAL STRESS DISTRIBUTION AT THE OPENING FOR GROUP B13
(P = 0)

Note: 1 in.=25.4 mm; 1 psi=6.89 kPa

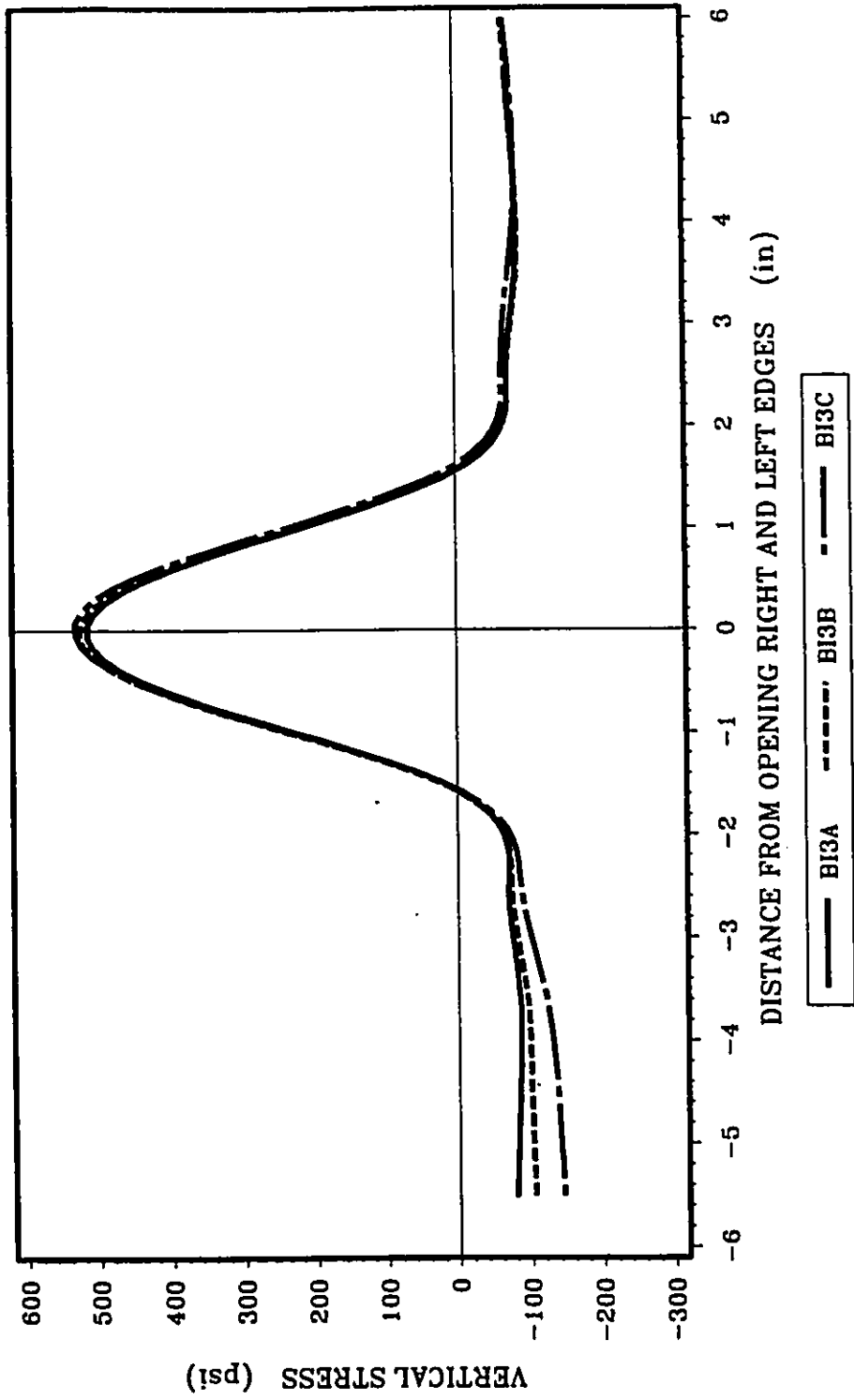


FIG. 5.91 VERTICAL STRESS DISTRIBUTION AT THE OPENING FOR GROUP B13
(P = 2 kip)

Note: 1 in.=25.4 mm; 1 psi=6.89 kPa

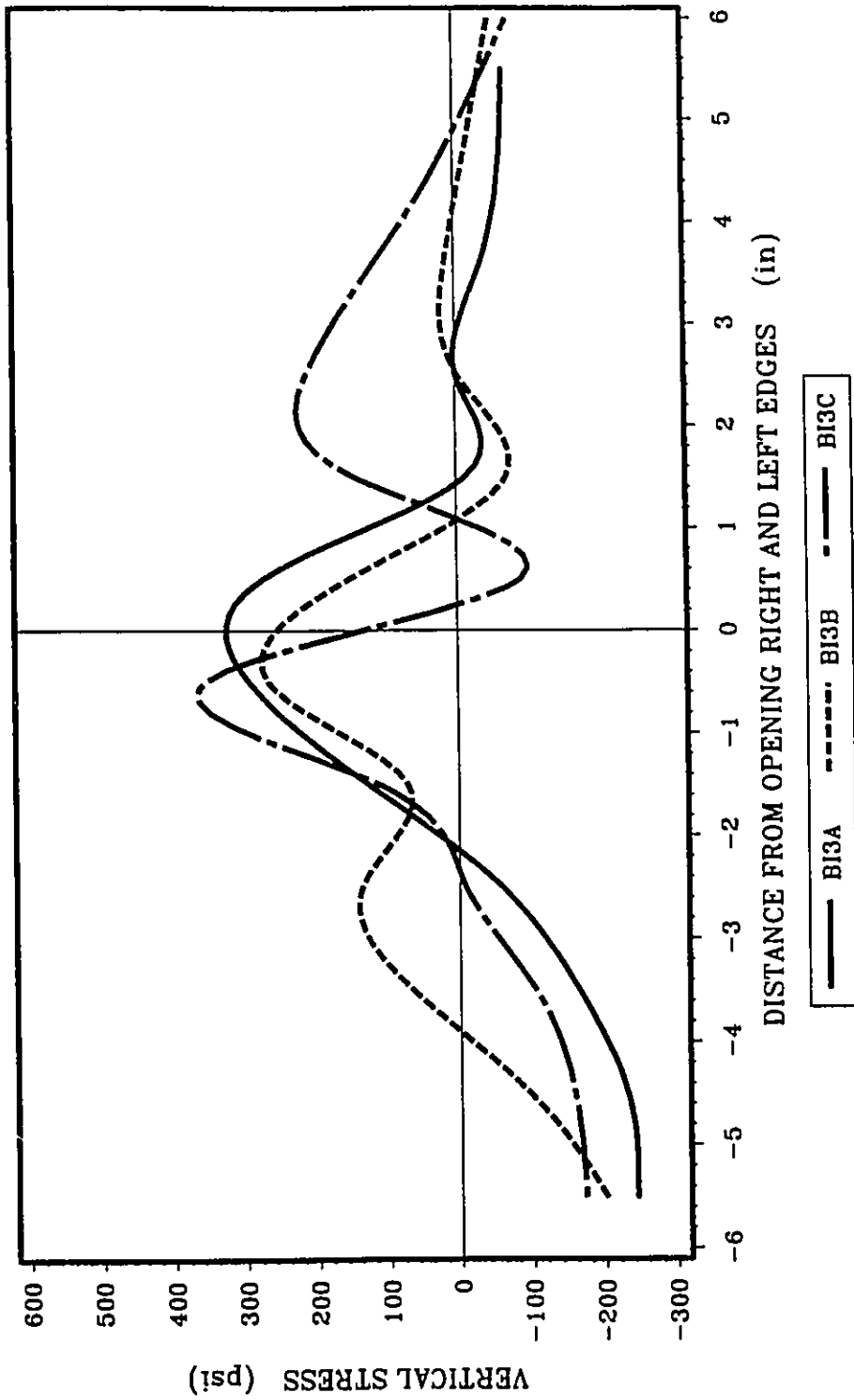
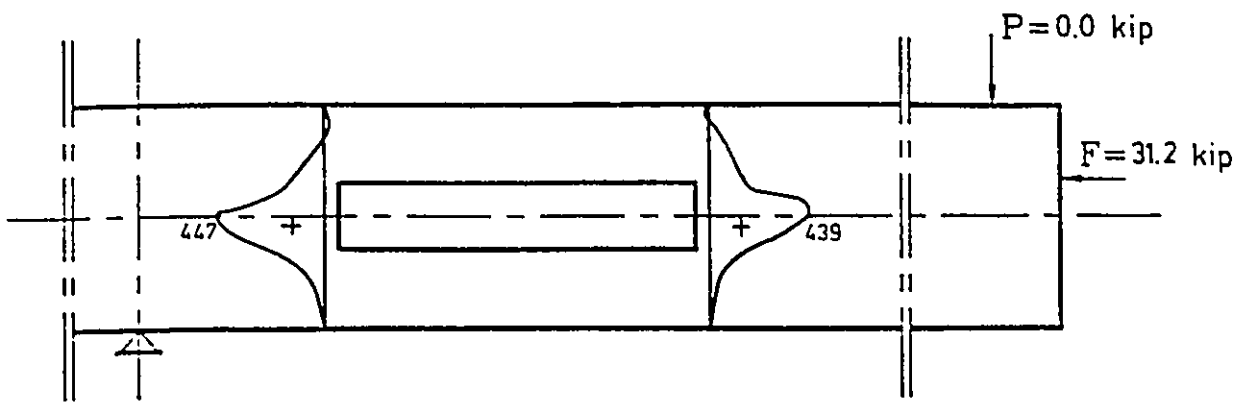
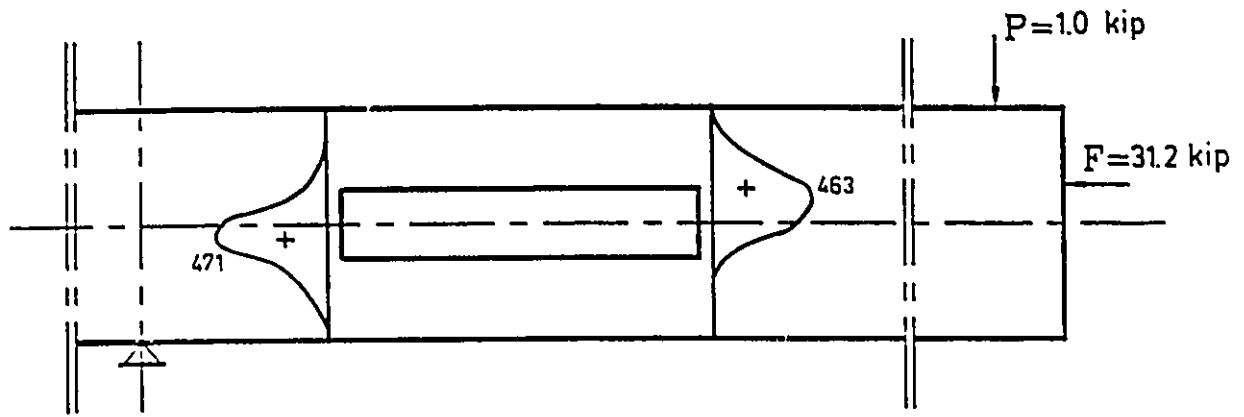


FIG. 5.92 VERTICAL STRESS DISTRIBUTION AT THE OPENING FOR GROUP B13
(P = 4 kip)

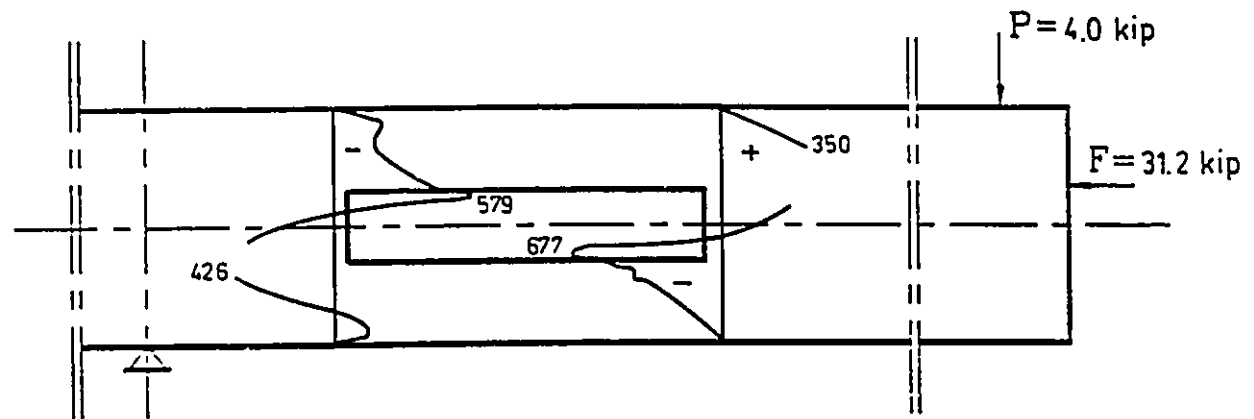
Note: 1 in.=25.4 mm; 1 psi=6.89 kPa



(a) TRANSFER STAGE



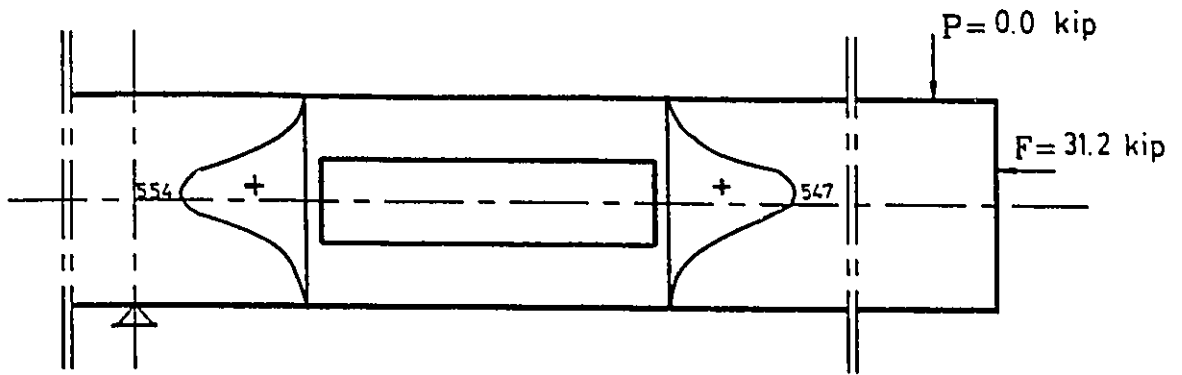
(b) WORKING STAGE



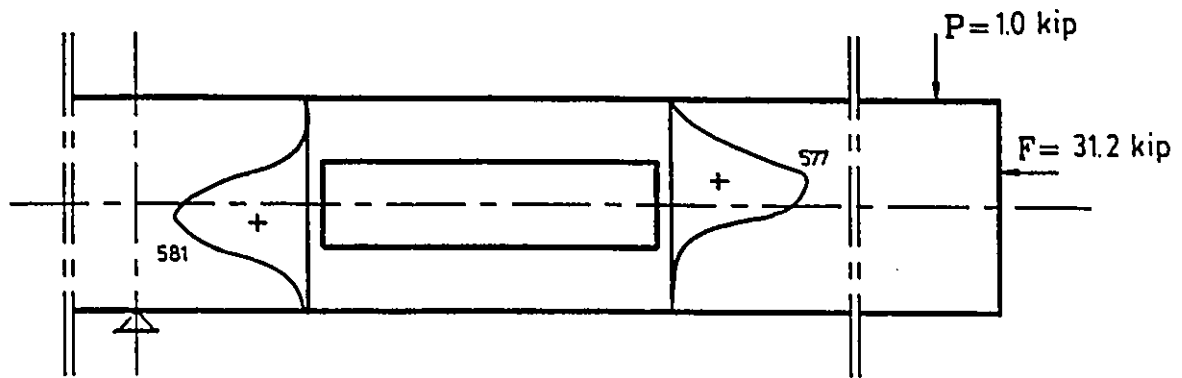
(c) ULTIMATE STAGE

FIG. 5.93 VERTICAL STRESS DISTRIBUTION FOR BEAM B14A

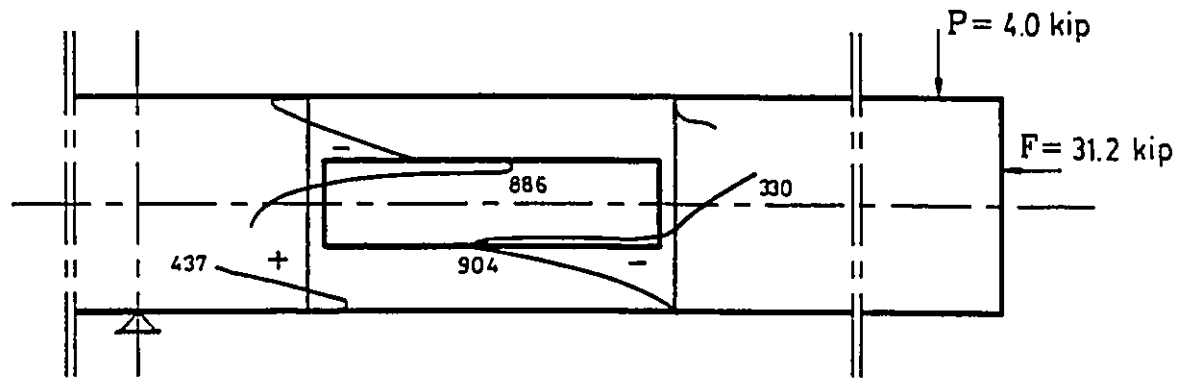
Note: stresses are shown in psi; 1 psi=6.89 kPa; 1 kip=4.45 kN



(a) TRANSFER STAGE



(b) WORKING STAGE



(c) ULTIMATE STAGE

FIG. 5.94 VERTICAL STRESS DISTRIBUTION FOR BEAM BI4B

Note: stresses are shown in psi; 1 psi=6.89 kPa; 1 kip=4.45 kN

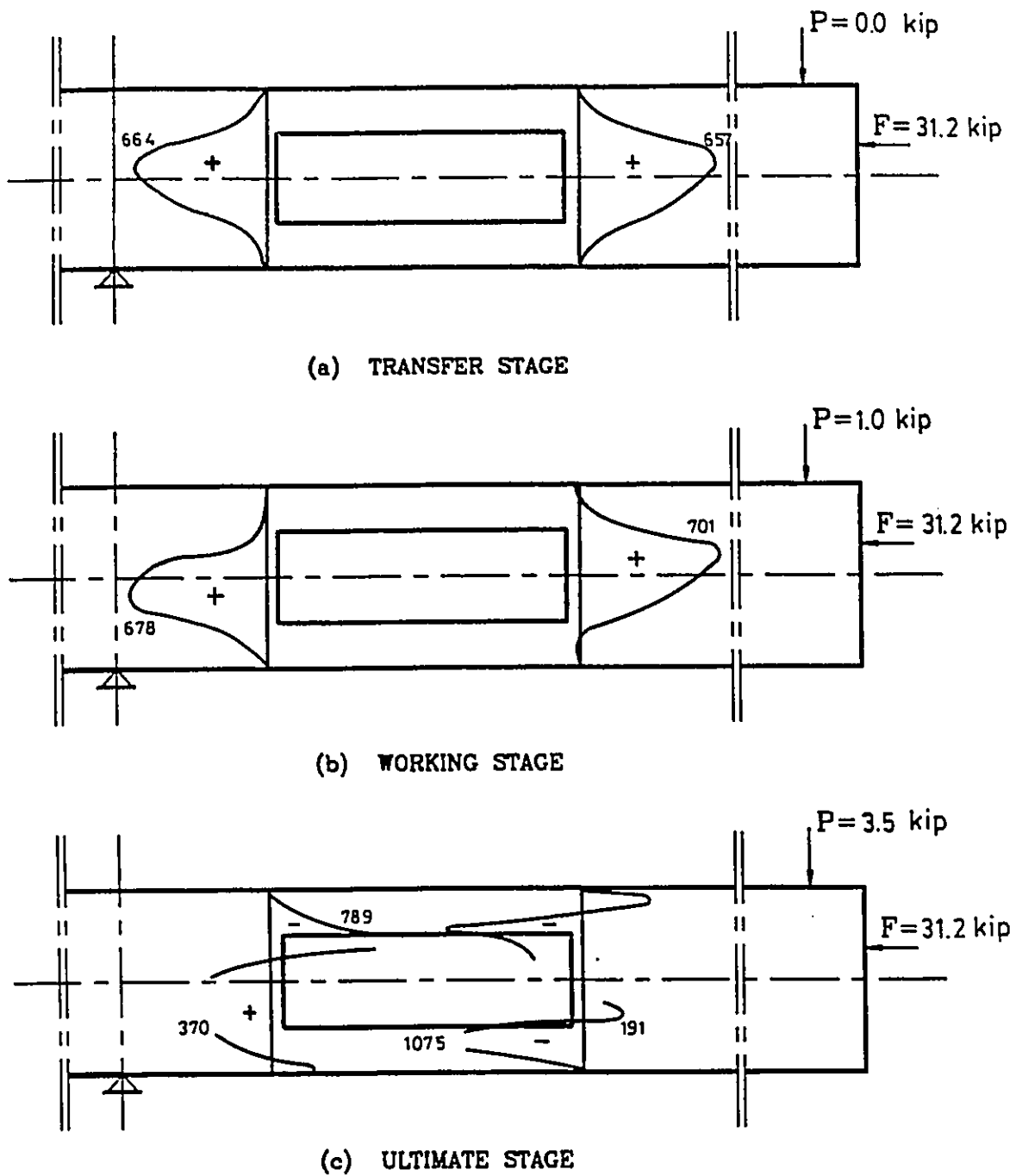


FIG. 5.95 VERTICAL STRESS DISTRIBUTION FOR BEAM BI4C

Note: stresses are shown in psi; 1 psi=6.89 kPa; 1 kip=4.45 kN

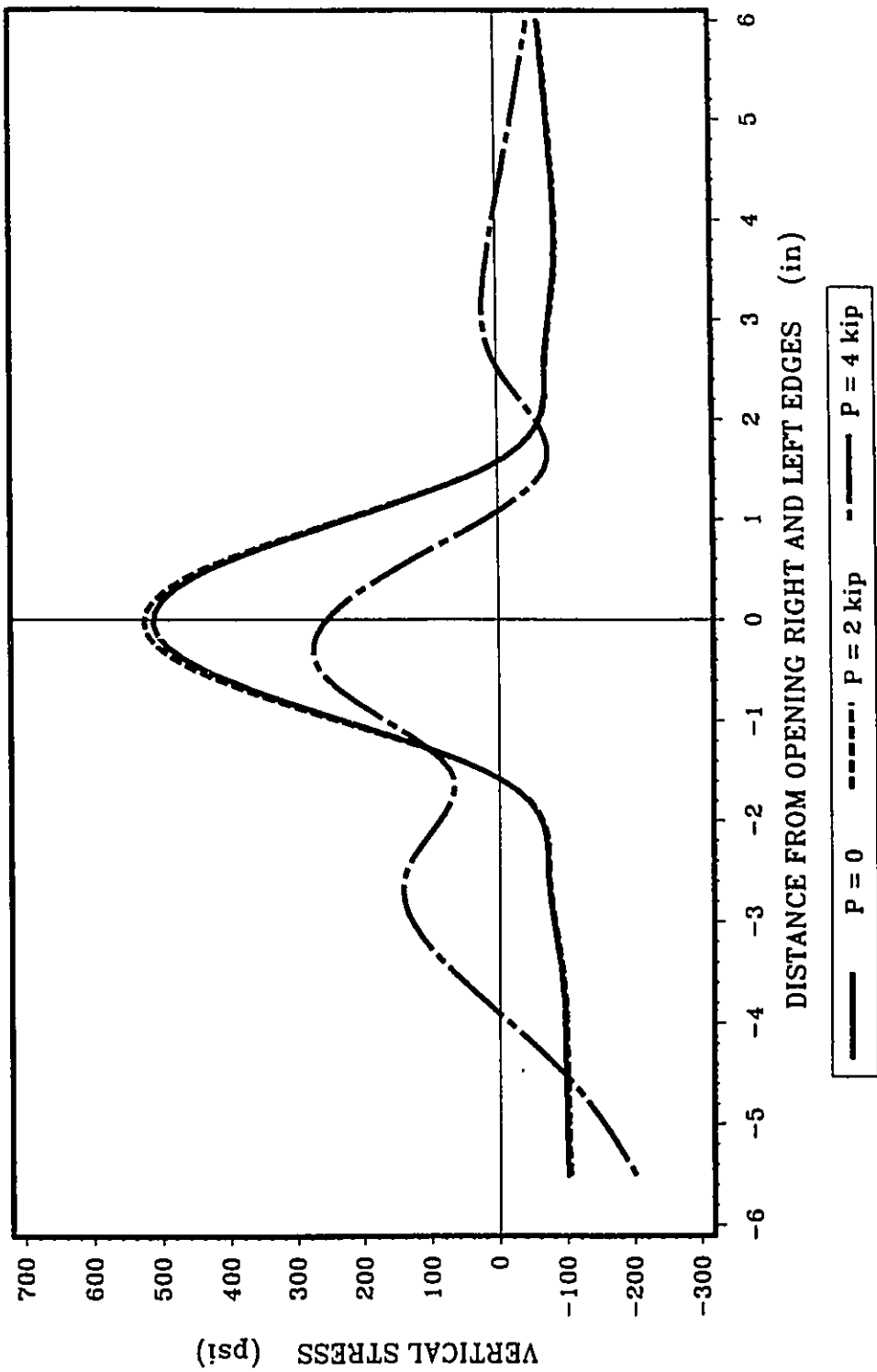


FIG. 5.96 VERTICAL STRESS DISTRIBUTION AT THE OPENING FOR BEAM BI4A

Note: 1 in.=25.4 mm; 1 kip=4.45 kN; 1 psi=6.89 kPa

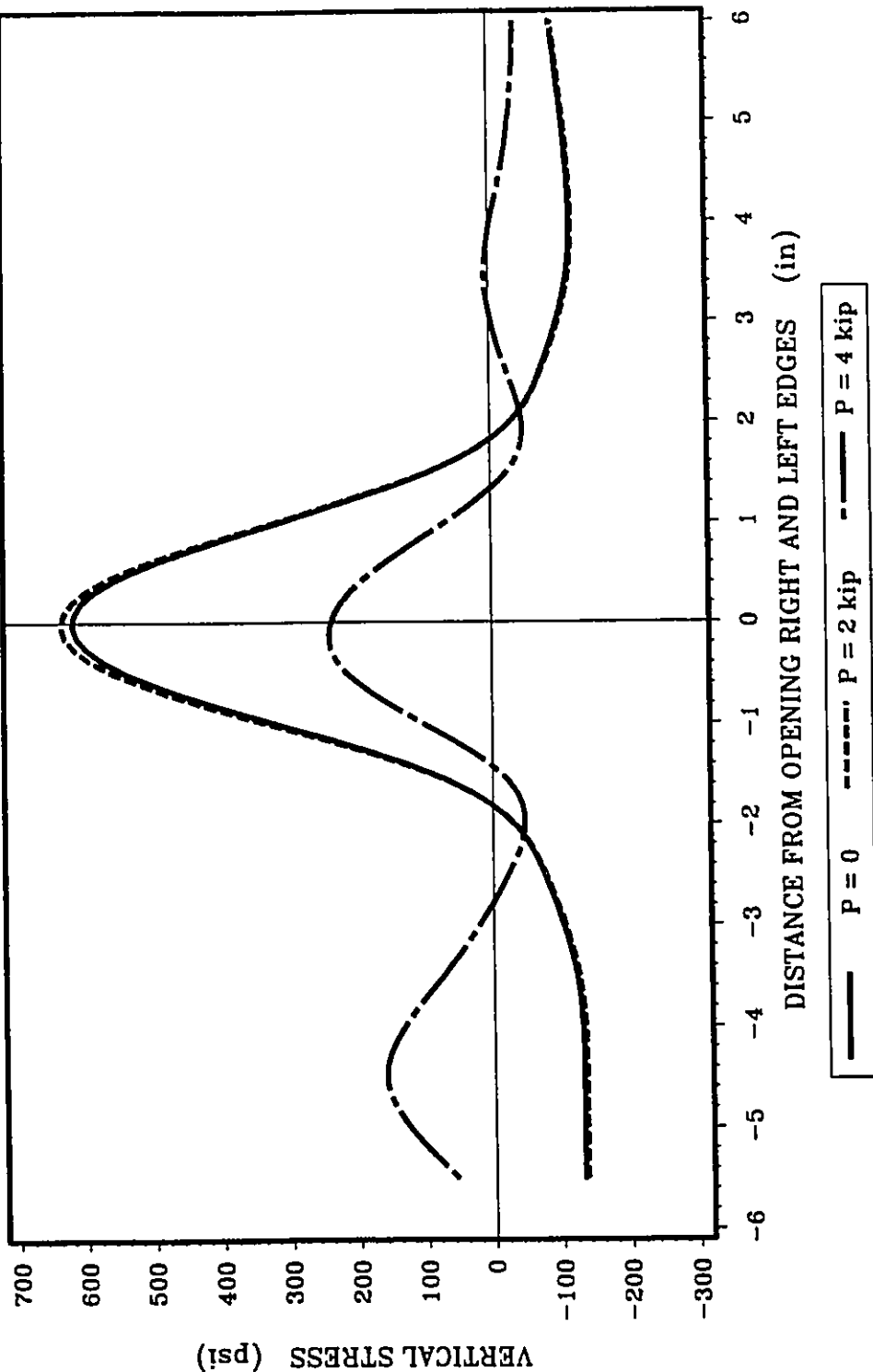


FIG. 5.97 VERTICAL STRESS DISTRIBUTION AT THE OPENING FOR BEAM BI4B

Note: 1 in.=25.4 mm; 1 kip=4.45 kN; 1 psi=6.89 kPa

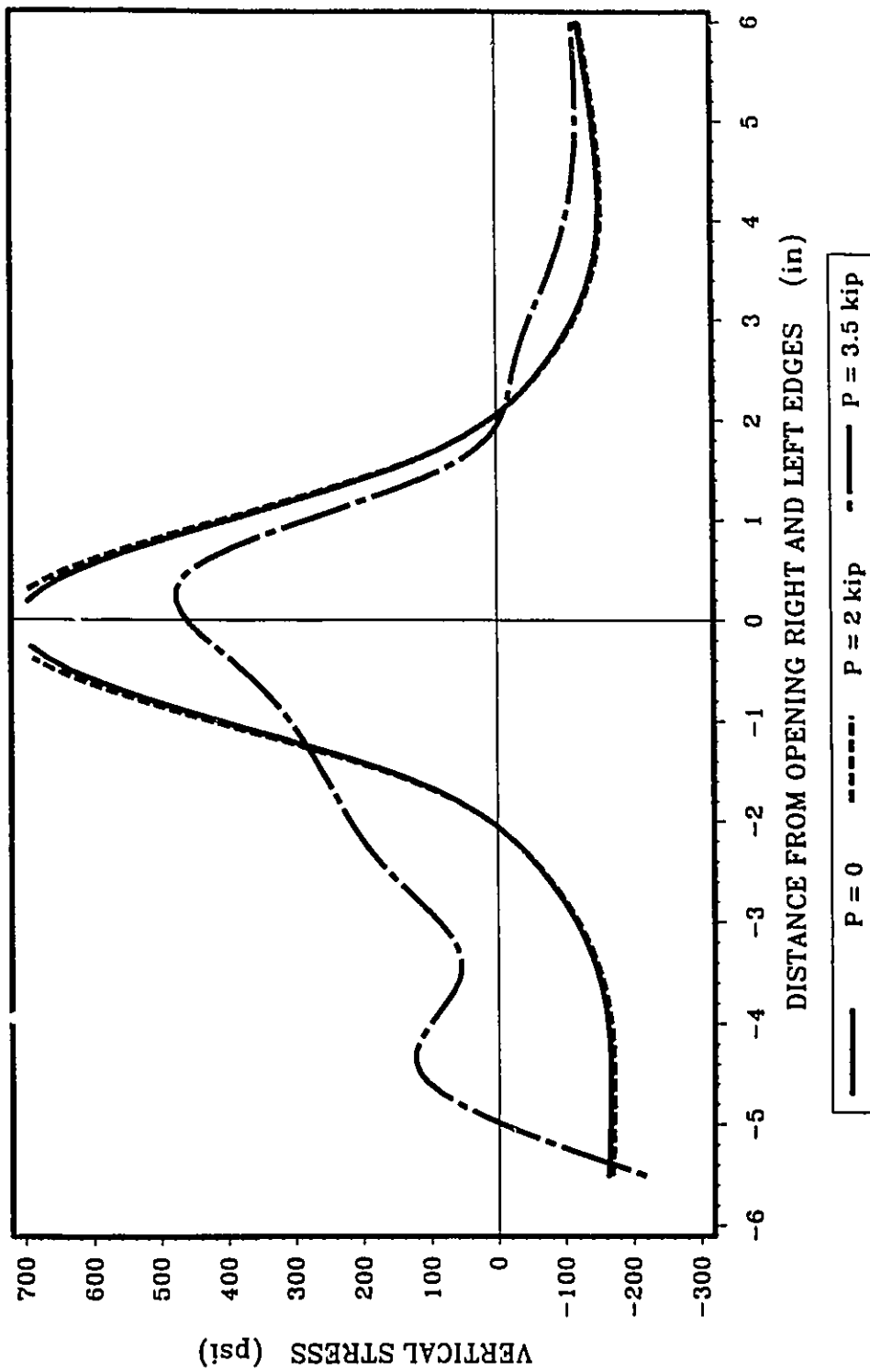


FIG. 5.98 VERTICAL STRESS DISTRIBUTION AT THE OPENING FOR BEAM B14C

Note: 1 in.=25.4 mm; 1 kip=4.45 kN; 1 psi=6.89 kPa

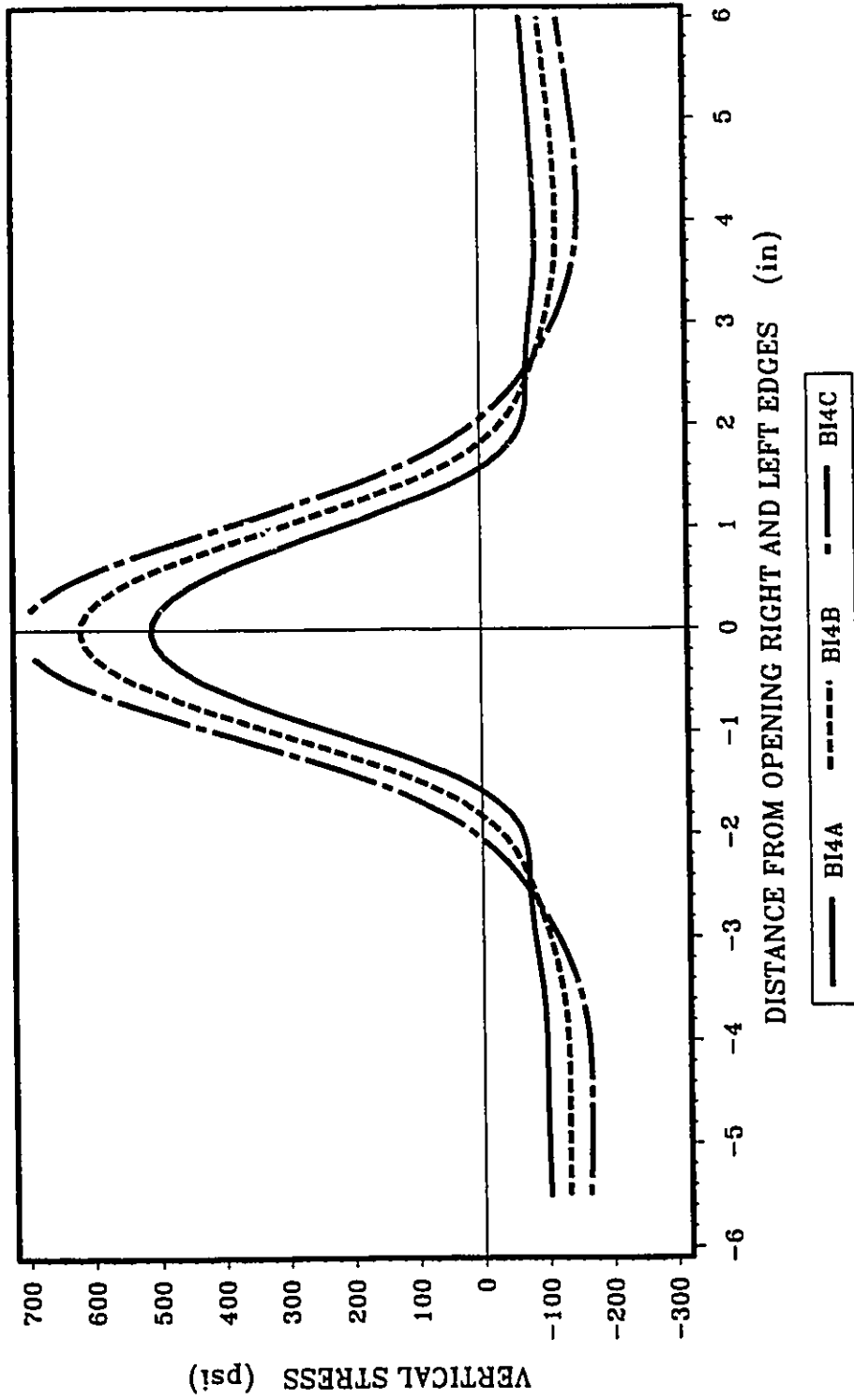


FIG. 5.99 VERTICAL STRESS DISTRIBUTION AT THE OPENING FOR GROUP BI4
(P = 0)

Note: 1 in.=25.4 mm; 1 psi=6.89 kPa

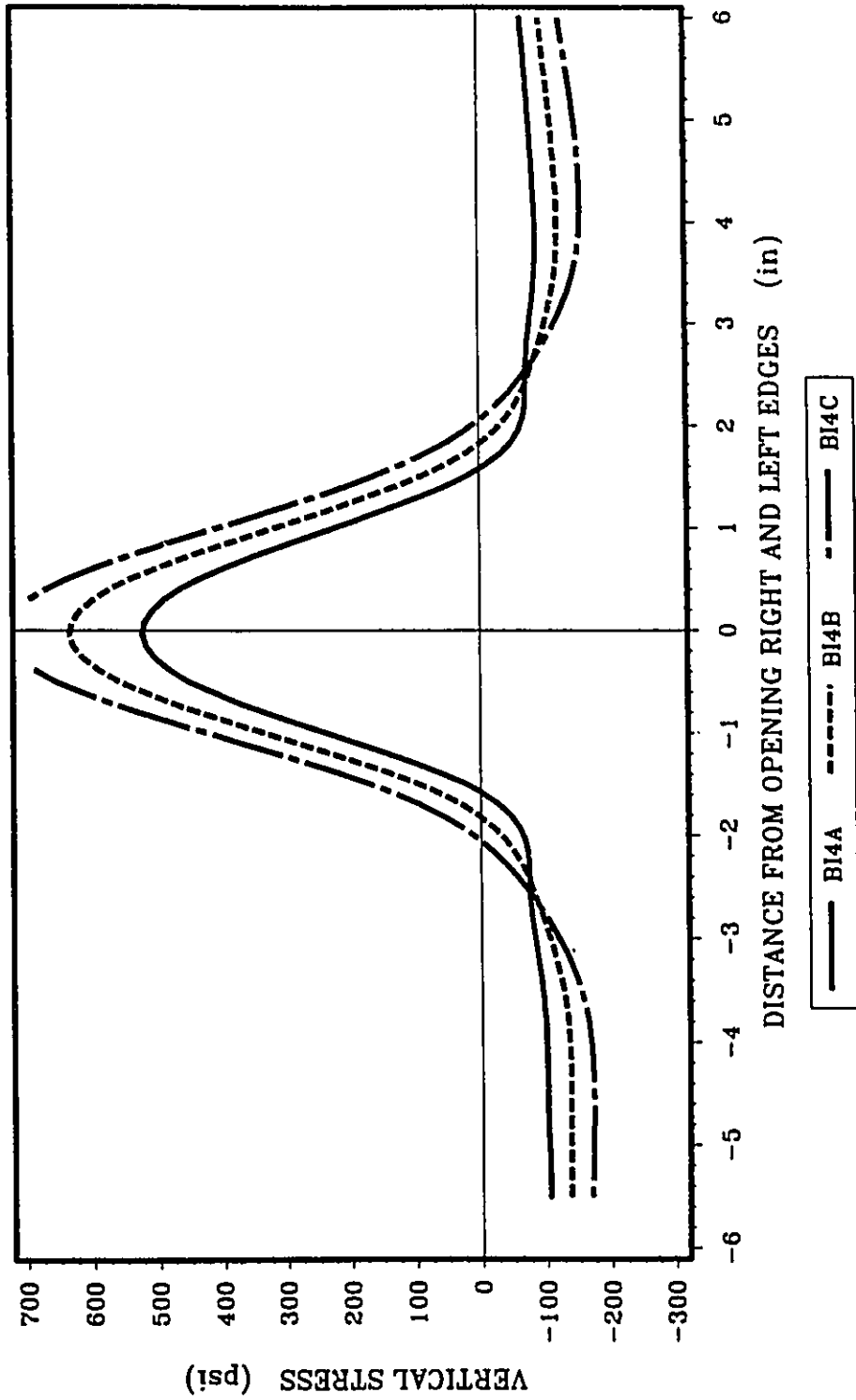


FIG. 5.100 VERTICAL STRESS DISTRIBUTION AT THE OPENING FOR GROUP BI4
(P = 2 kip)

Note: 1 in.=25.4 mm; 1 psi=6.89 kPa

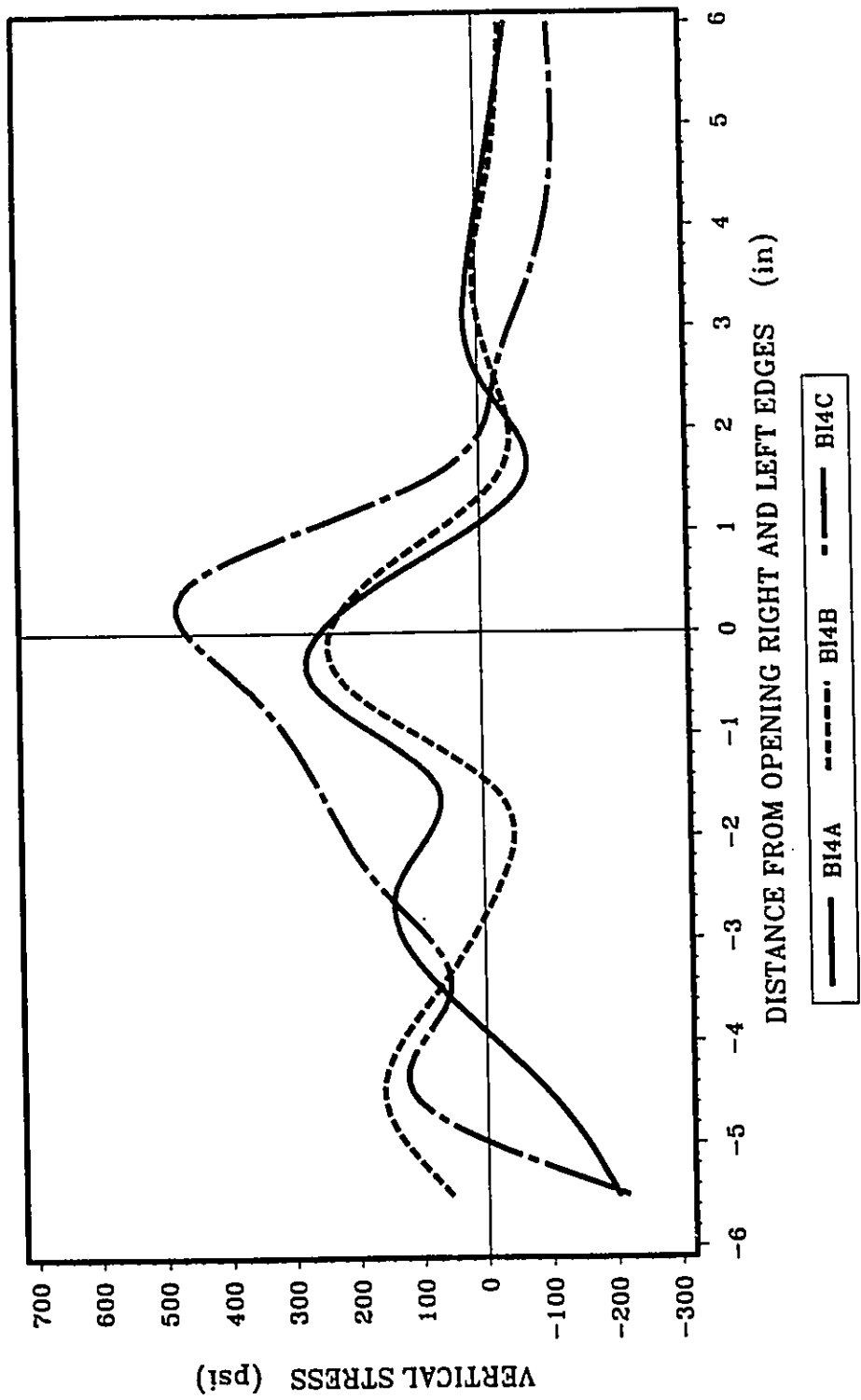


FIG. 5.101 VERTICAL STRESS DISTRIBUTION AT THE OPENING FOR GROUP BI4
(P = 3.5 kip)

Note: 1 in.=25.4 mm; 1 psi=6.89 kPa

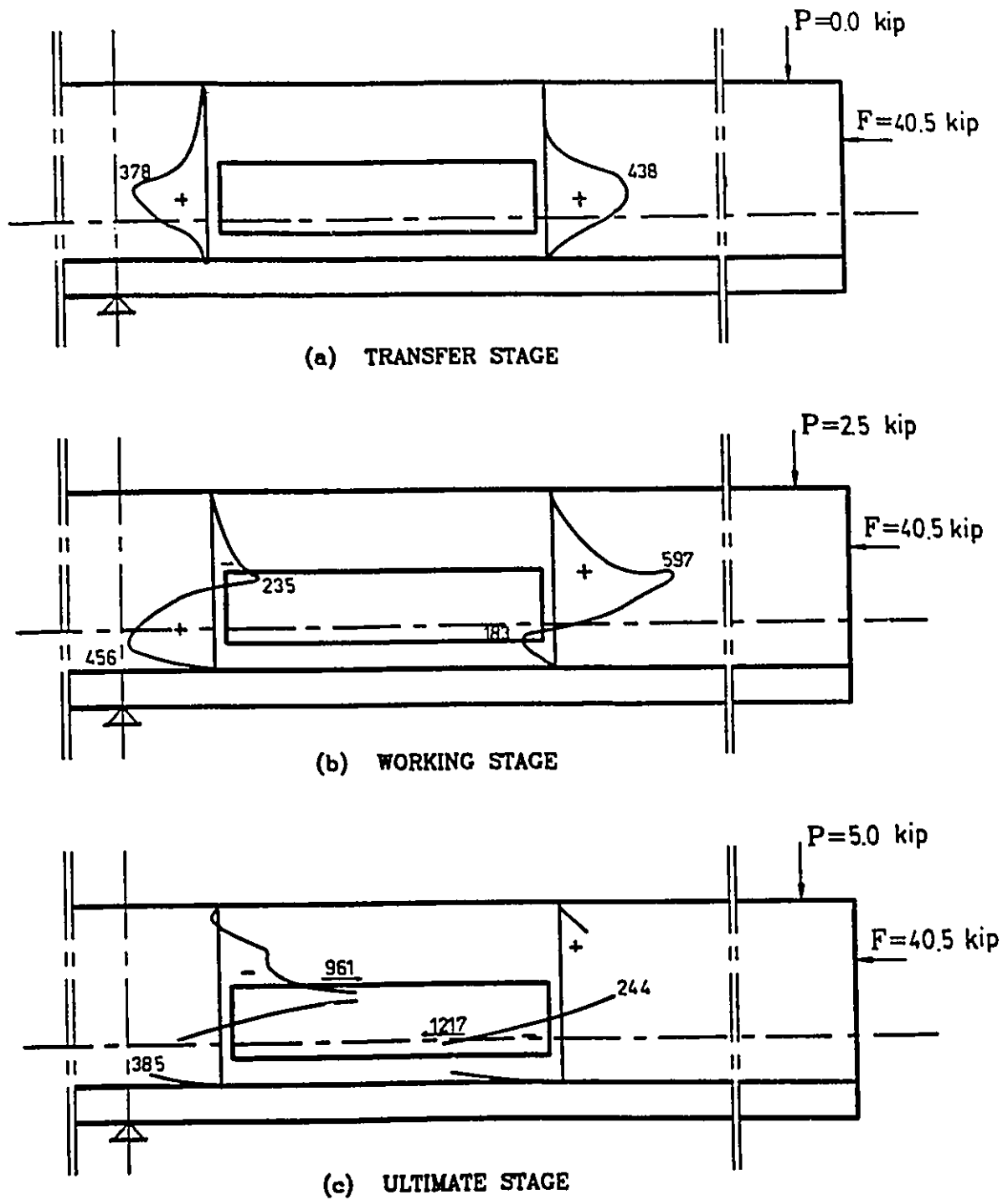


FIG. 5.102 VERTICAL STRESS DISTRIBUTION FOR BEAM BII1A

Note: stresses are shown in psi; 1 psi=6.89 kPa; 1 kip=4.45 kN

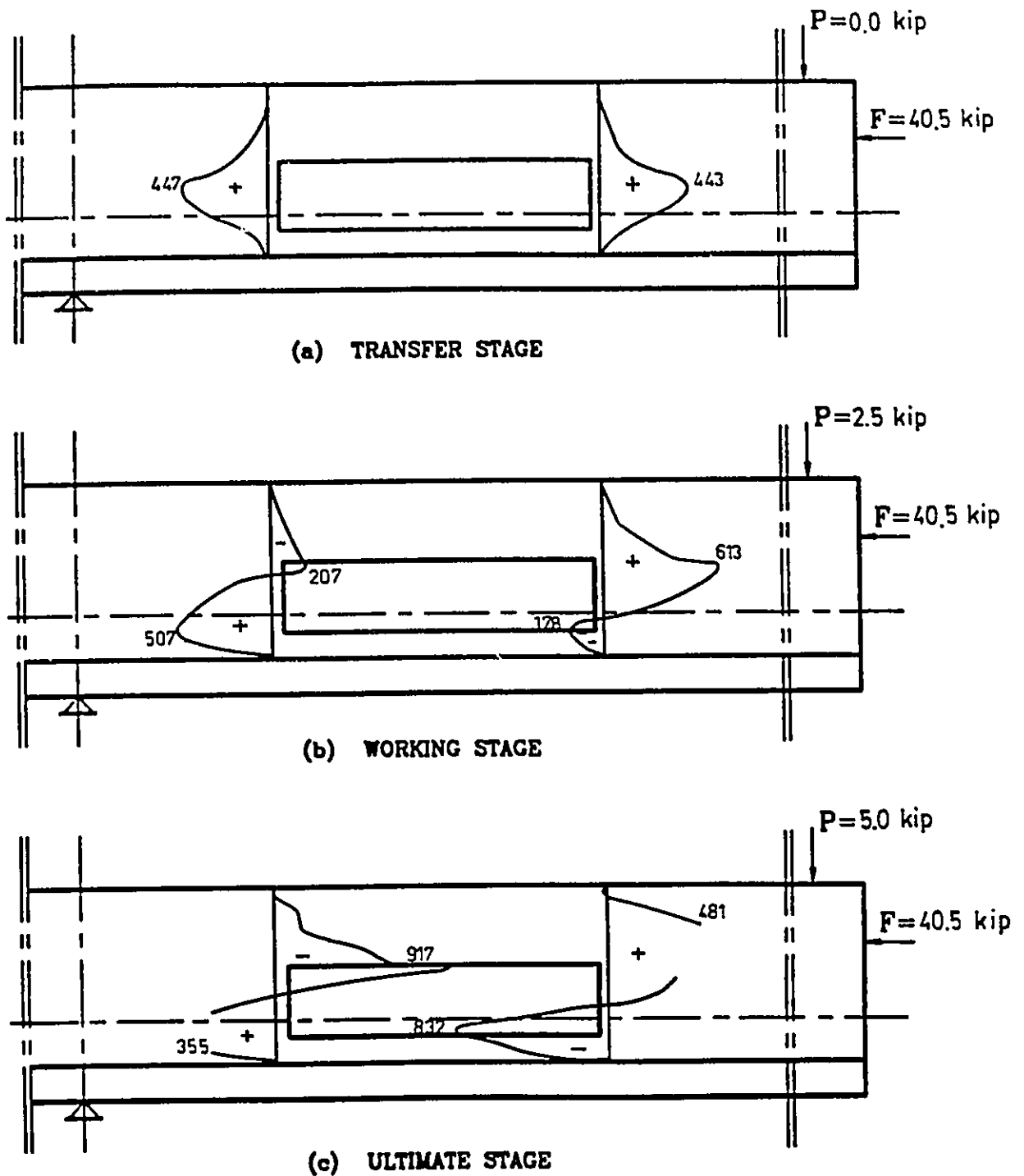


FIG. 5.103 VERTICAL STRESS DISTRIBUTION FOR BEAMS
BII1B, BII2A, BII3B & BII4B

Note: stresses are shown in psi; 1 psi=6.89 kPa; 1 kip=4.45 kN

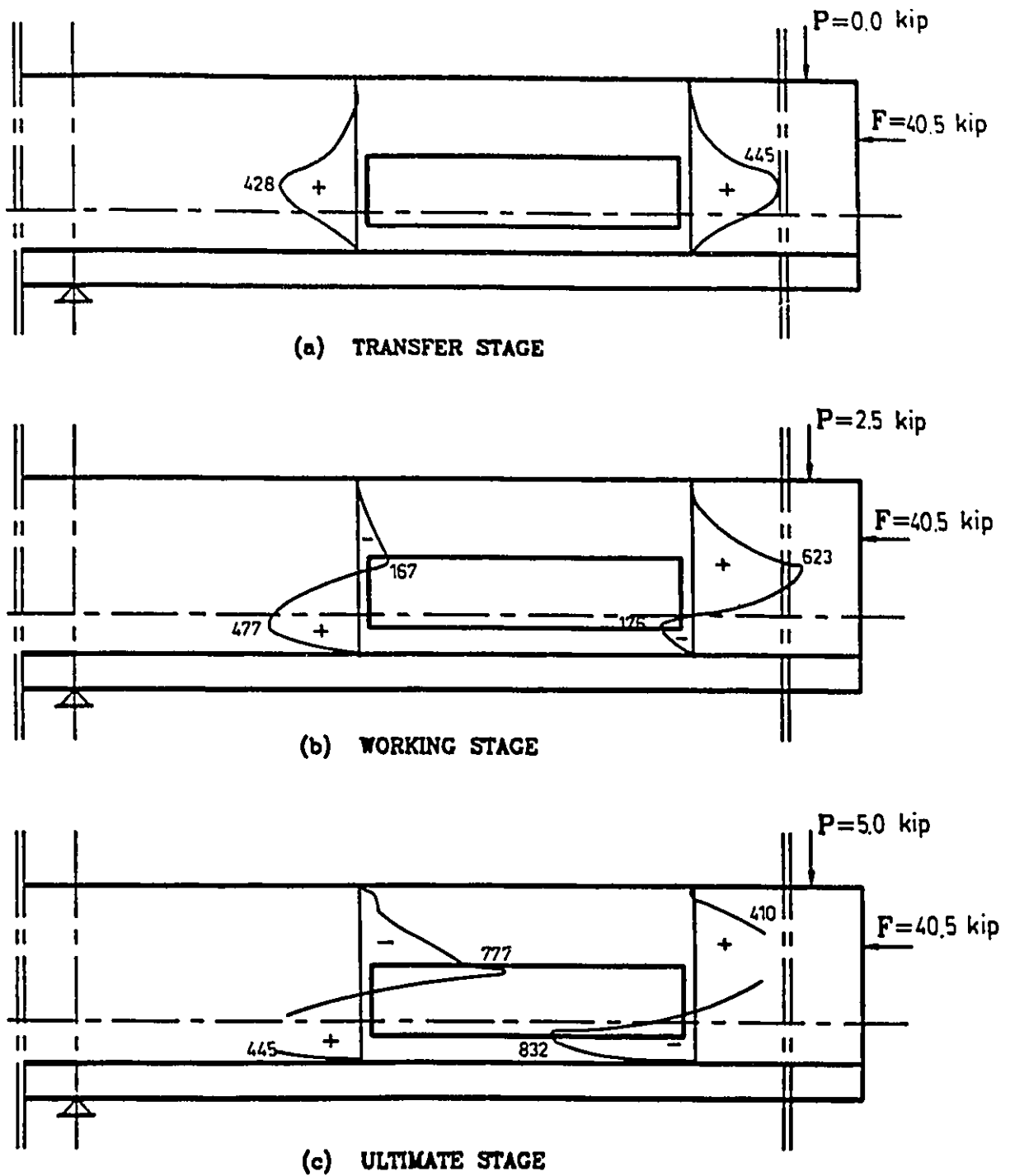


FIG. 5.104 VERTICAL STRESS DISTRIBUTION FOR BEAM BIIIc

Note: stresses are shown in psi; 1 psi=6.89 kPa; 1 kip=4.45 kN

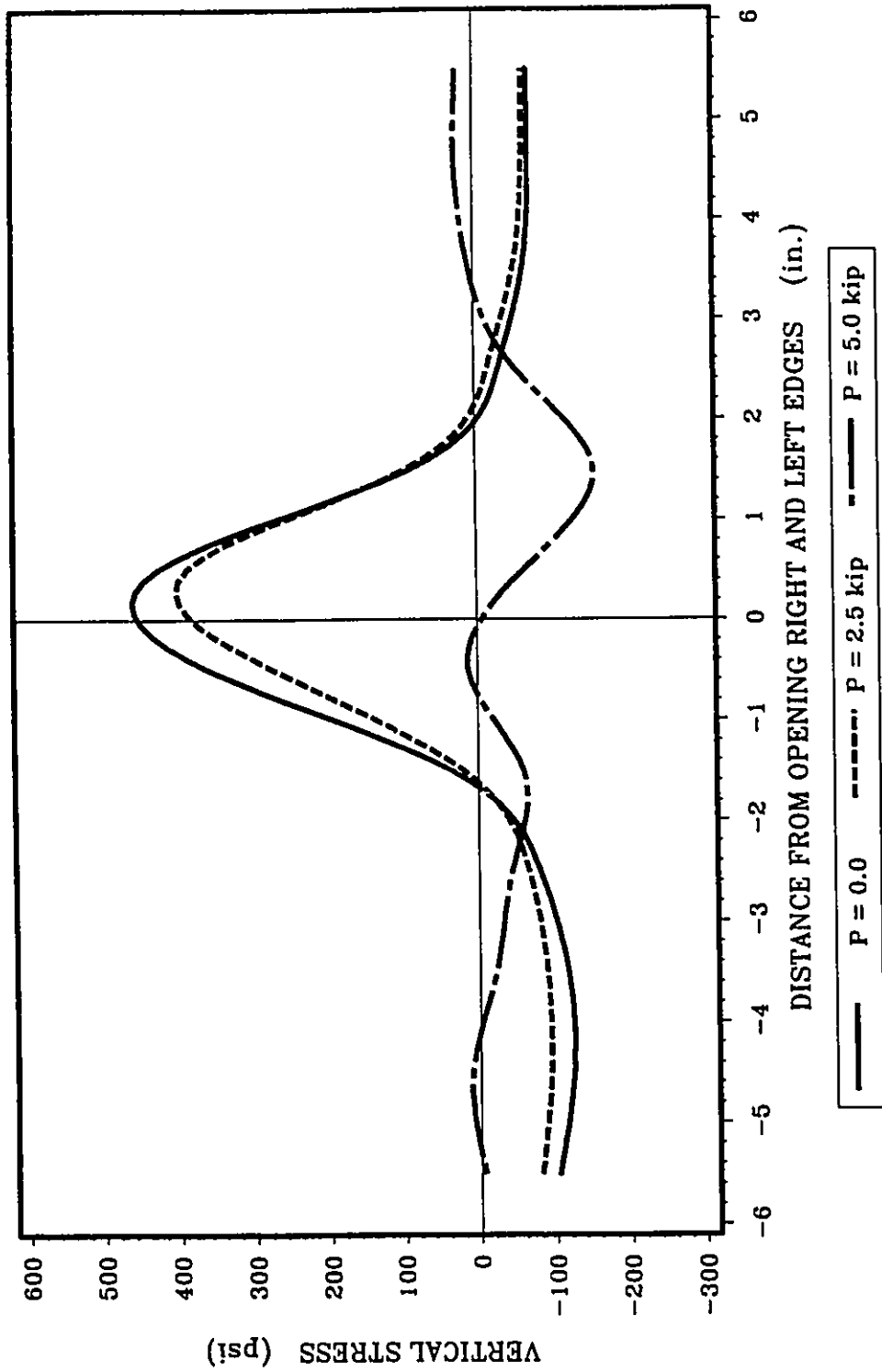


FIG. 5.105 VERTICAL STRESS DISTRIBUTION AT THE OPENING FOR BEAM BII1A

Note: 1 in.=25.4 mm; 1 kip=4.45 kN; 1 psi=6.89 kPa

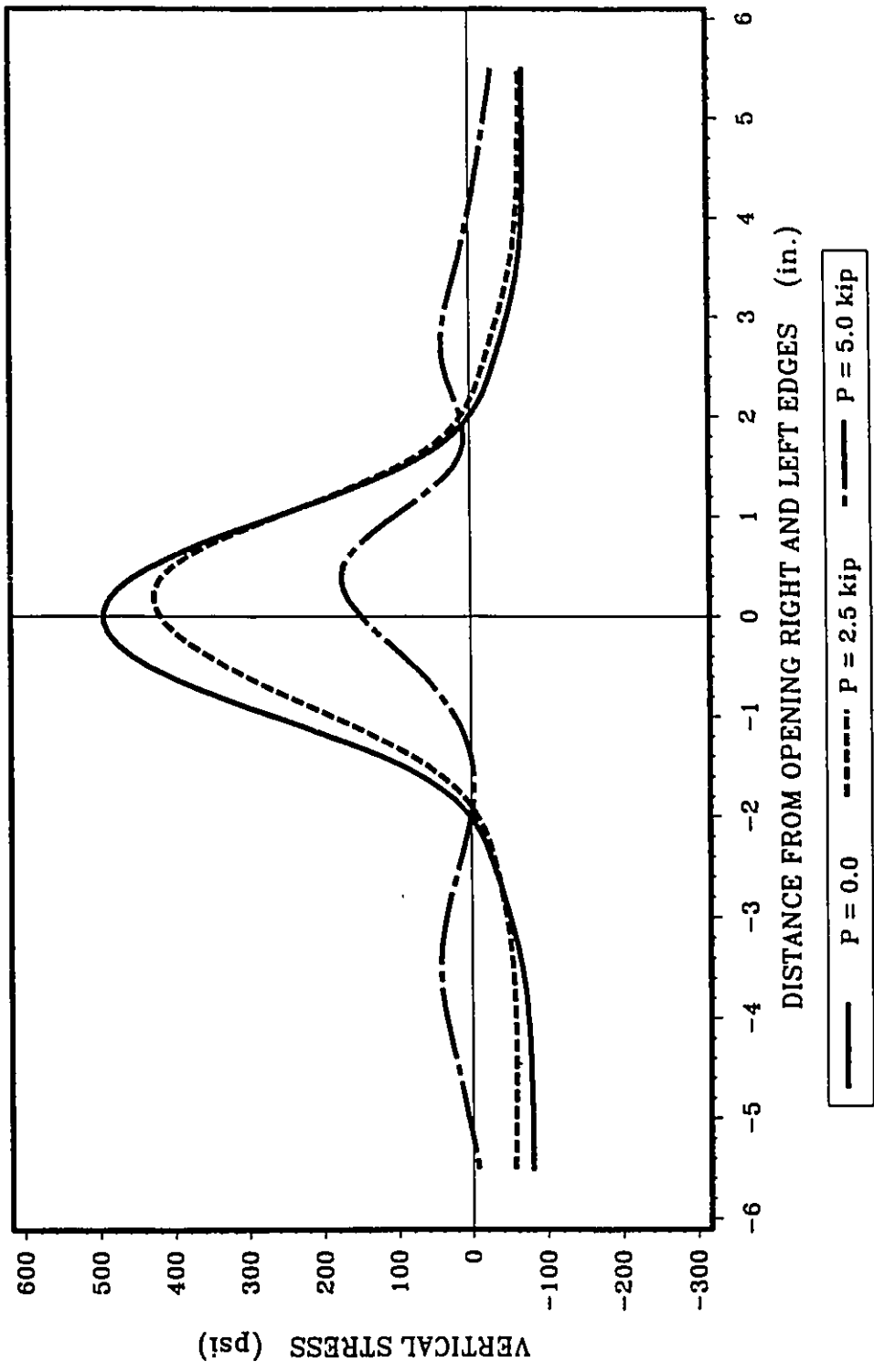


FIG. 5.106 VERTICAL STRESS DISTRIBUTION AT THE OPENING FOR BEAM BII1B

Note: 1 in.=25.4 mm; 1 kip=4.45 kN; 1 psi=6.89 kPa

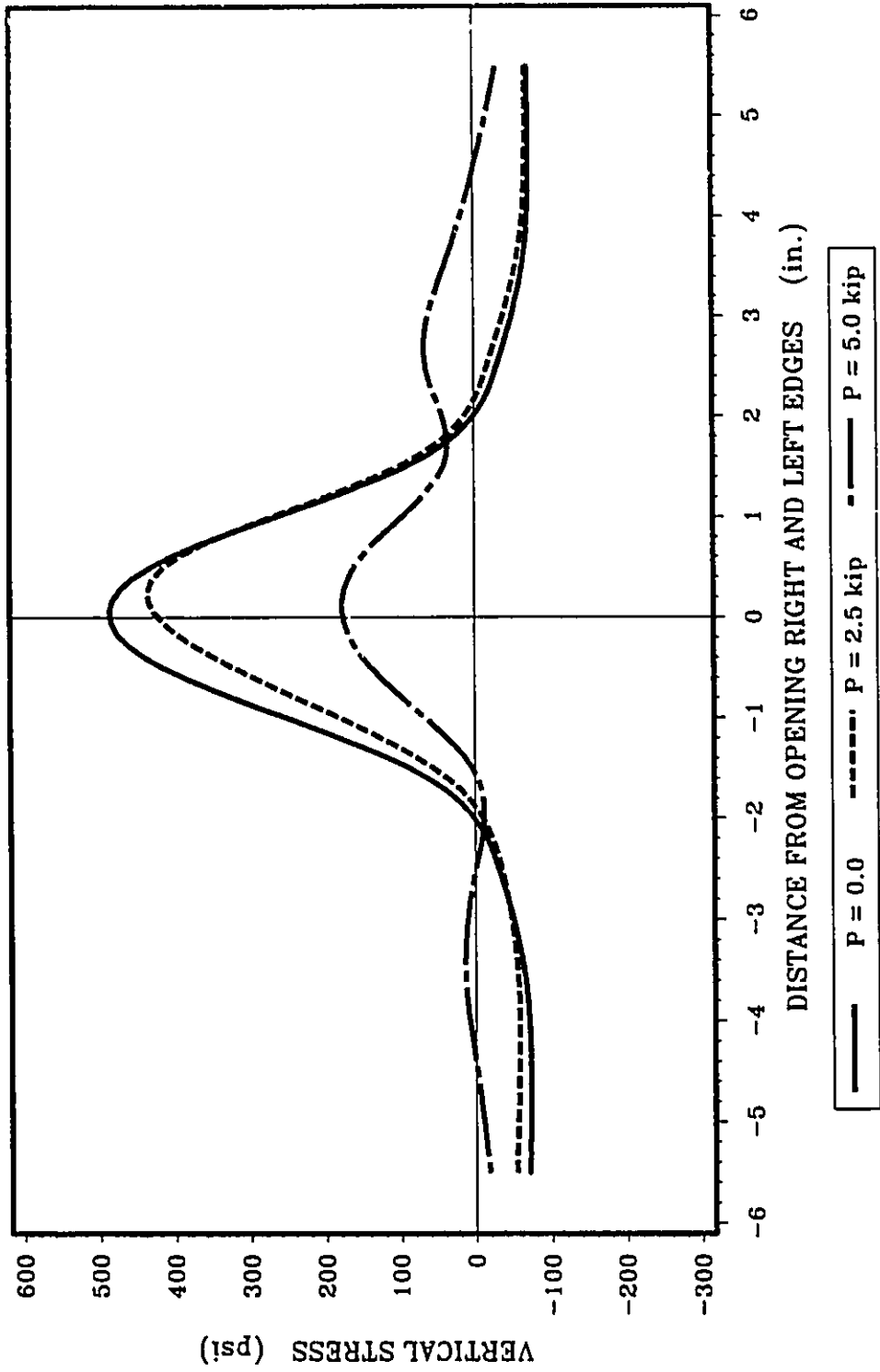


FIG. 5.107 VERTICAL STRESS DISTRIBUTION AT THE OPENING FOR BEAM BI1C

Note: 1 in. = 25.4 mm; 1 kip = 4.45 kN; 1 psi = 6.89 kPa

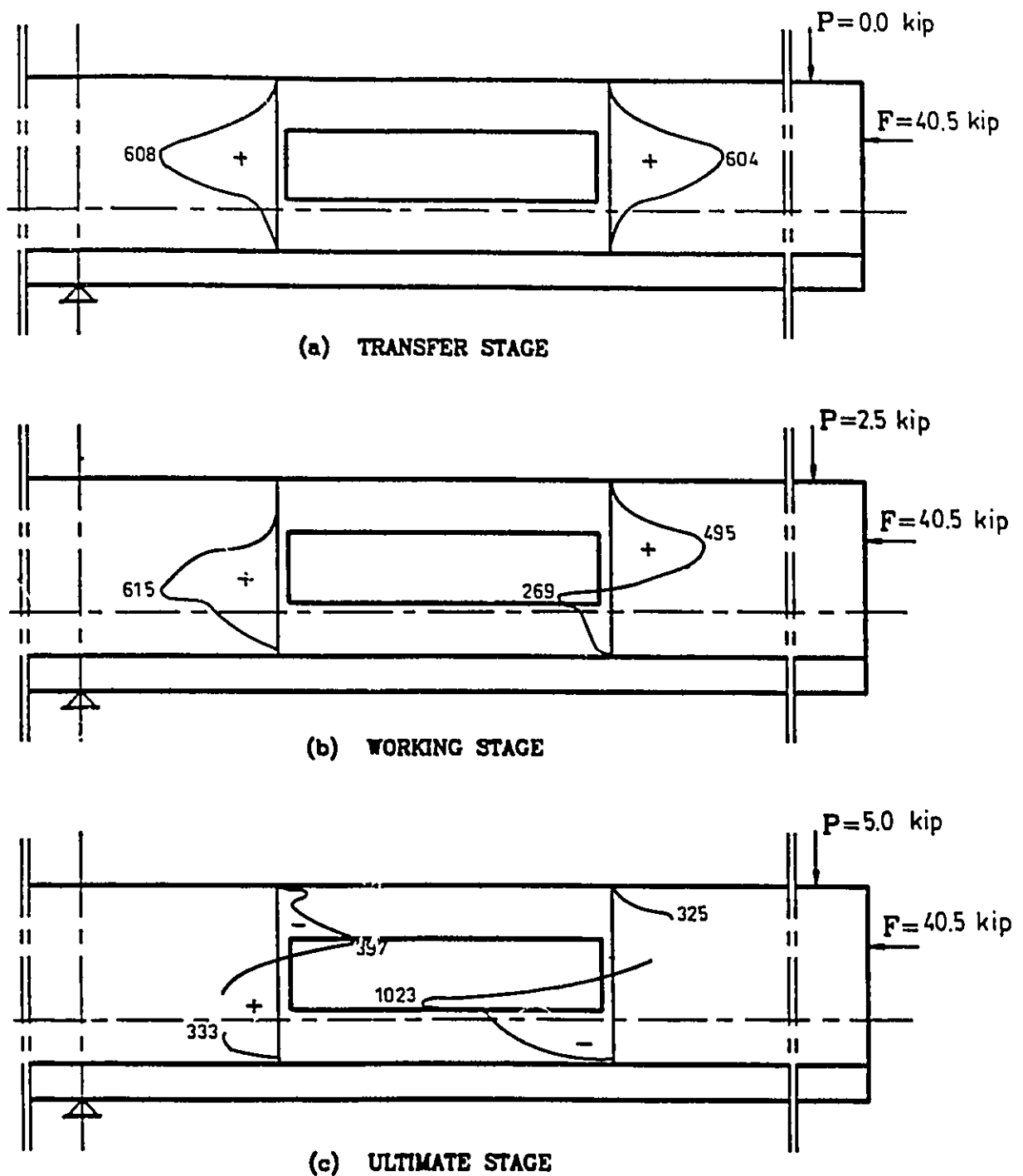


FIG. 5.108 VERTICAL STRESS DISTRIBUTION FOR BEAM BII2B

Note: stresses are shown in psi; 1 psi=6.89 kPa; 1 kip=4.45 kN

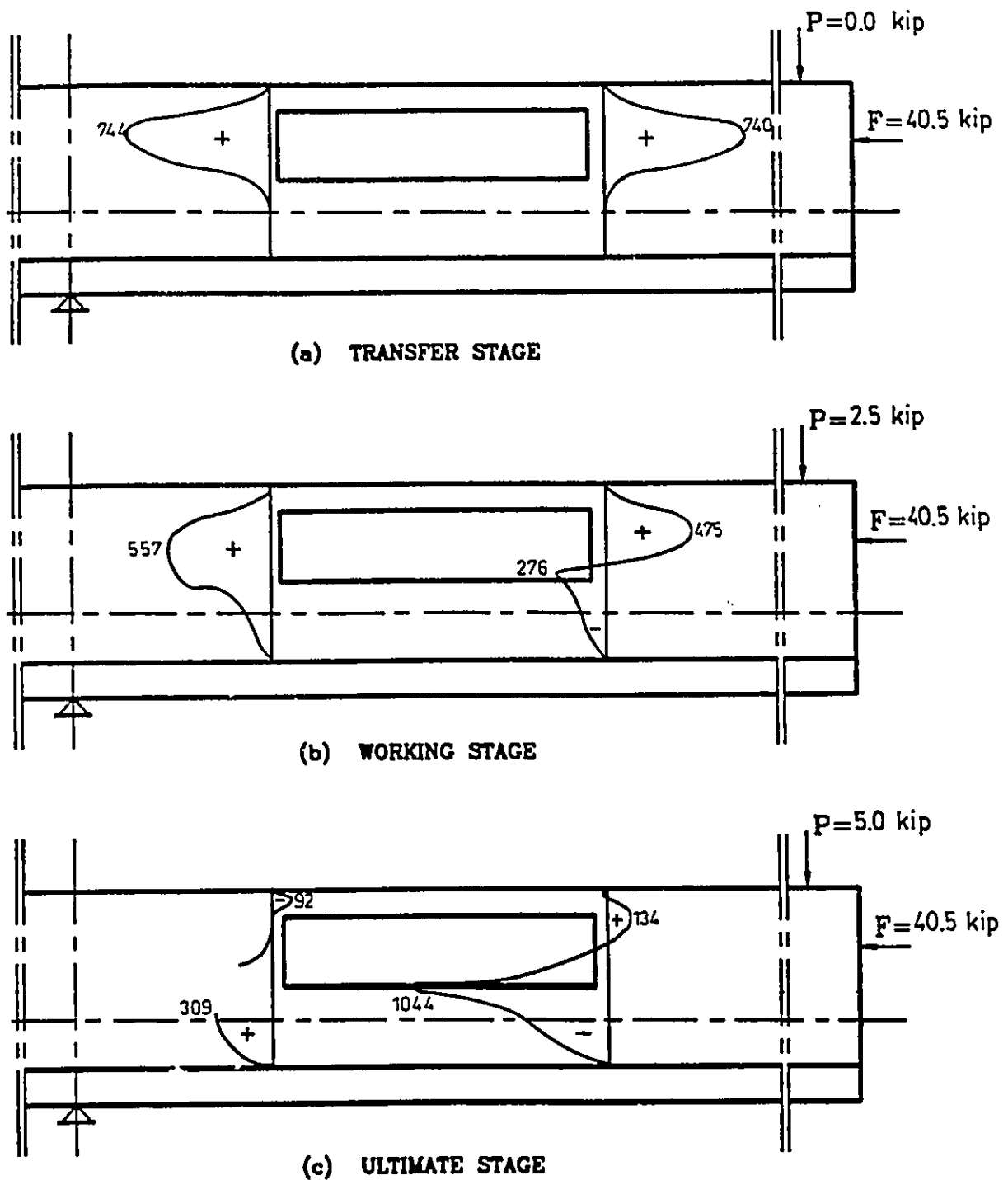


FIG. 5.109 VERTICAL STRESS DISTRIBUTION FOR BEAM BI12C

Note: stresses are shown in psi; 1 psi=6.89 kPa; 1 kip=4.45 kN

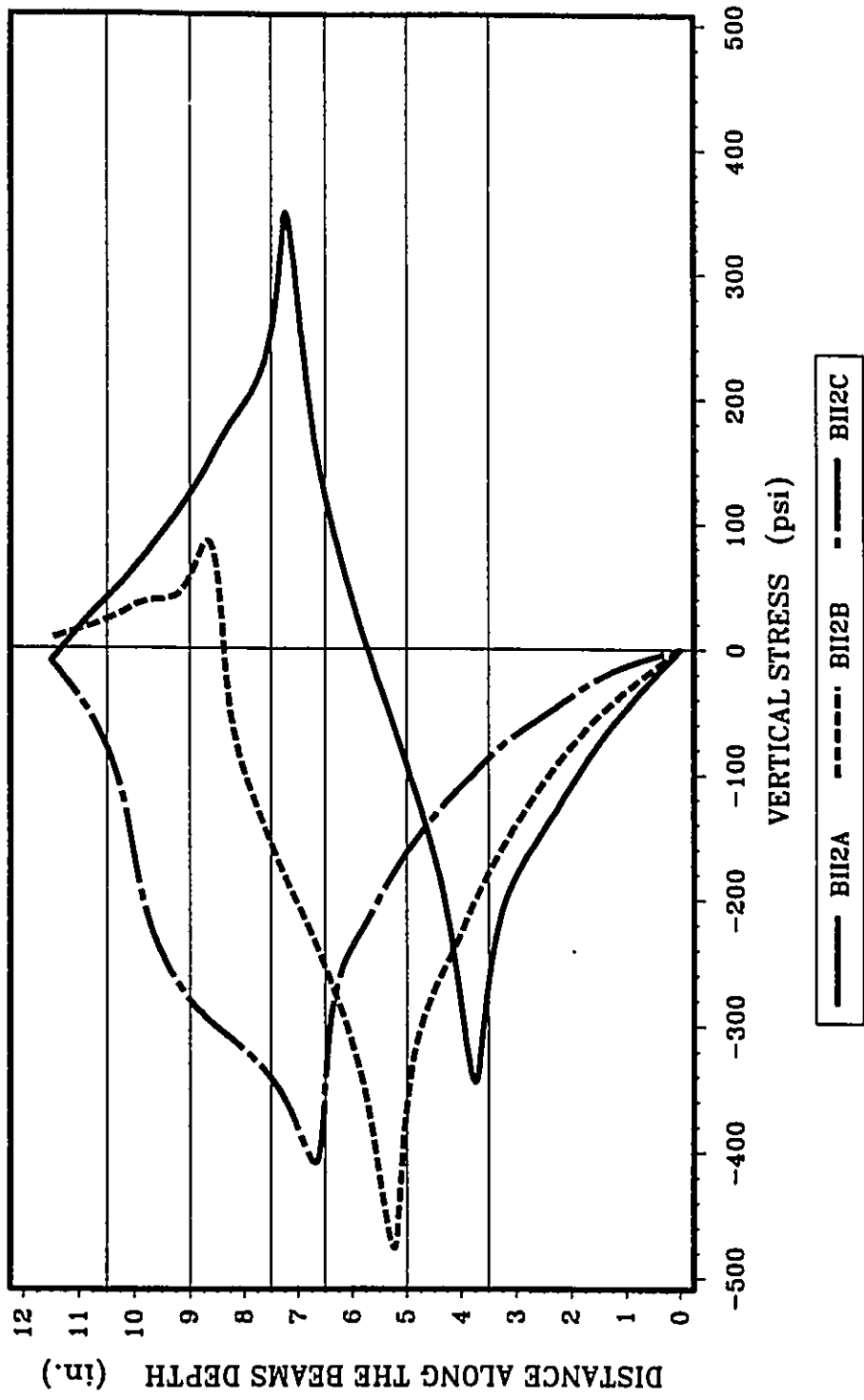


FIG. 5.110 VERTICAL STRESS DISTRIBUTION AT THE OPENING EDGES FOR GROUP BII2
(P = 2.5 kip)

Note: 1 in.=25.4 mm; 1 kip=4.45 kN; 1 psi=6.89 kPa

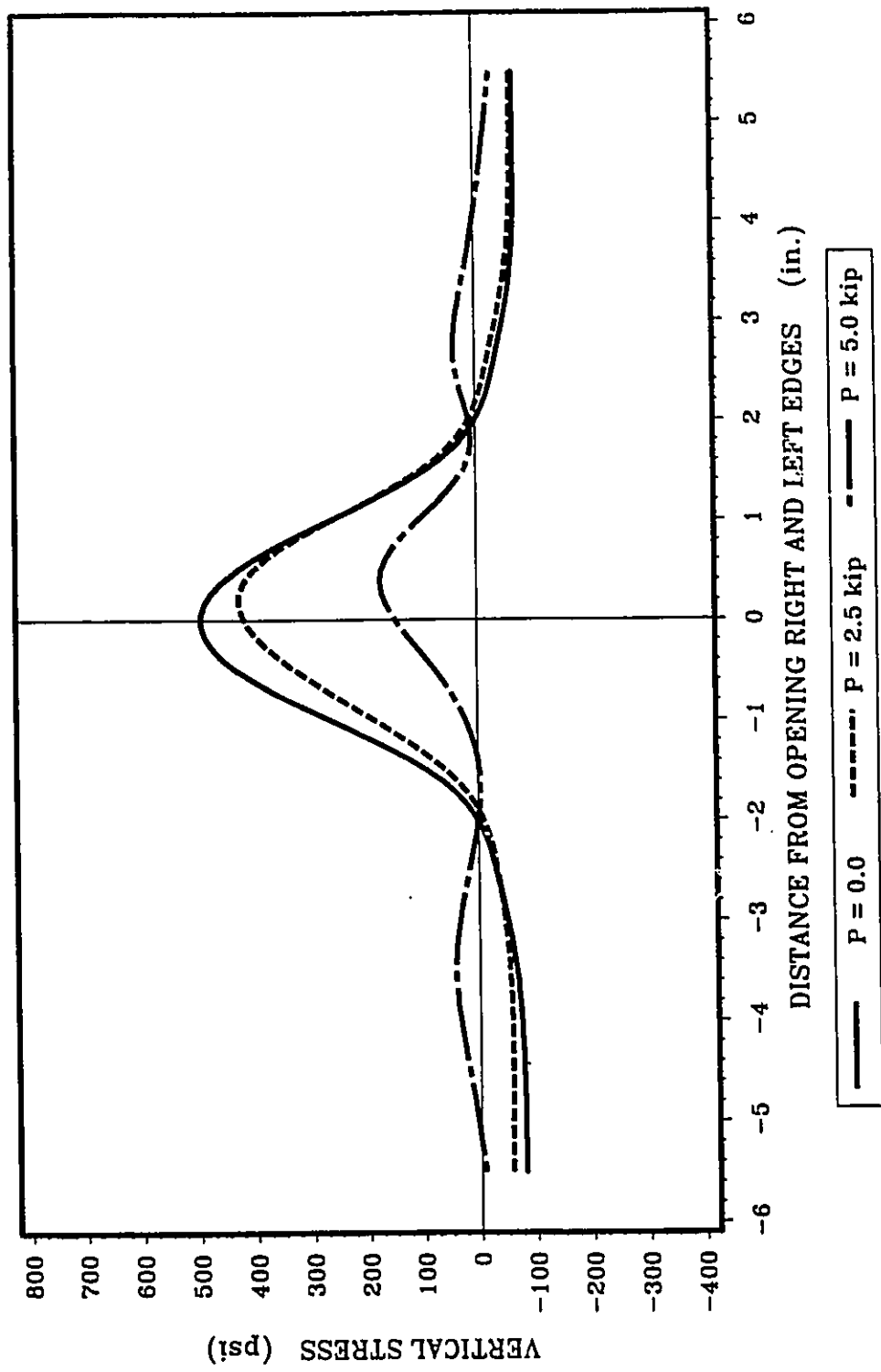


FIG. 5.111 VERTICAL STRESS DISTRIBUTION AT THE OPENING FOR BEAM BII2A

Note: 1 in.=25.4 mm; 1 kip=4.45 kN; 1 psi=6.89 kPa

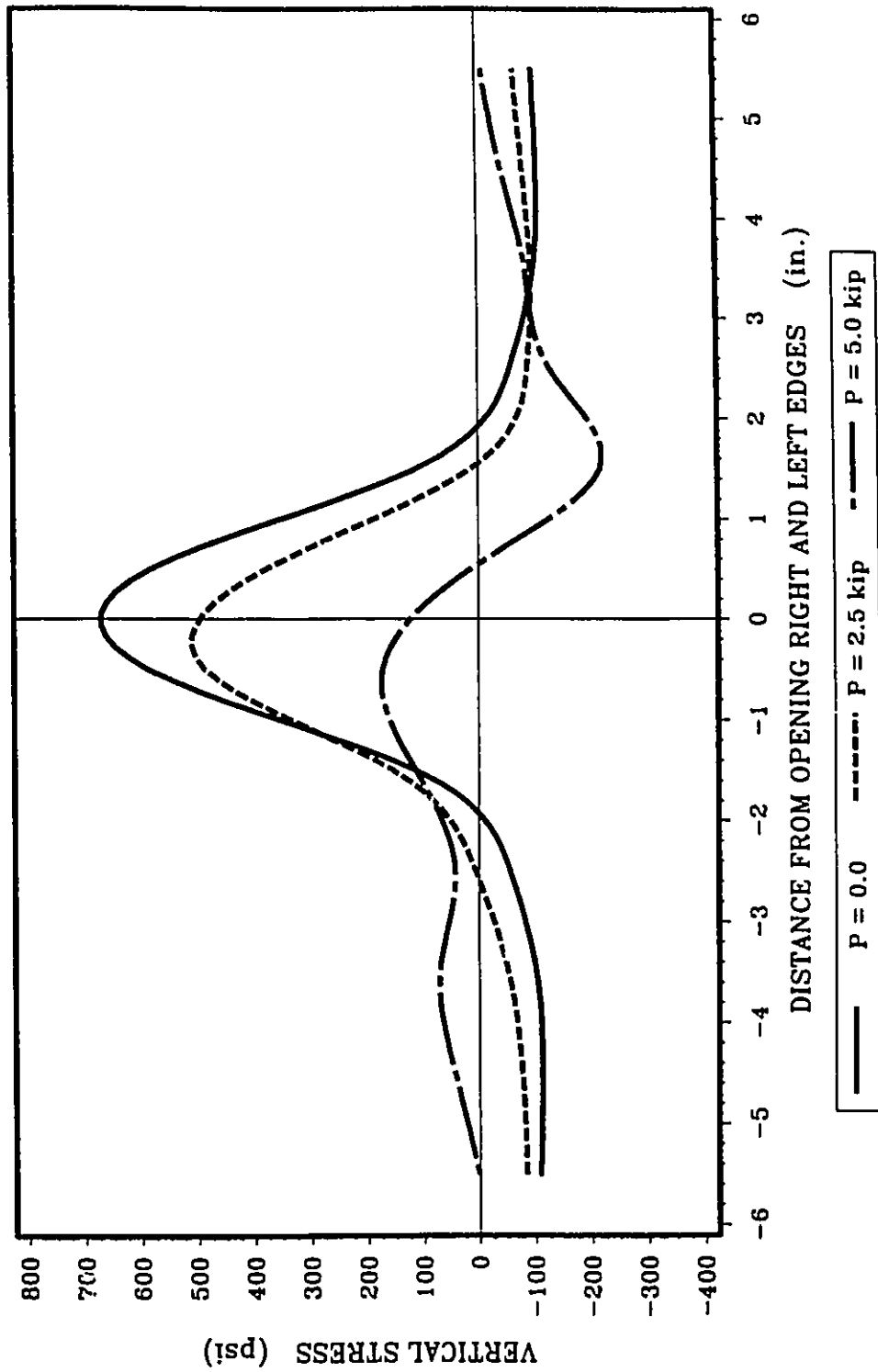


FIG. 5.112 VERTICAL STRESS DISTRIBUTION AT THE OPENING FOR BEAM BII2B

Note: 1 in.=25.4 mm; 1 kip=4.45 kN; 1 psi=6.89 kPa

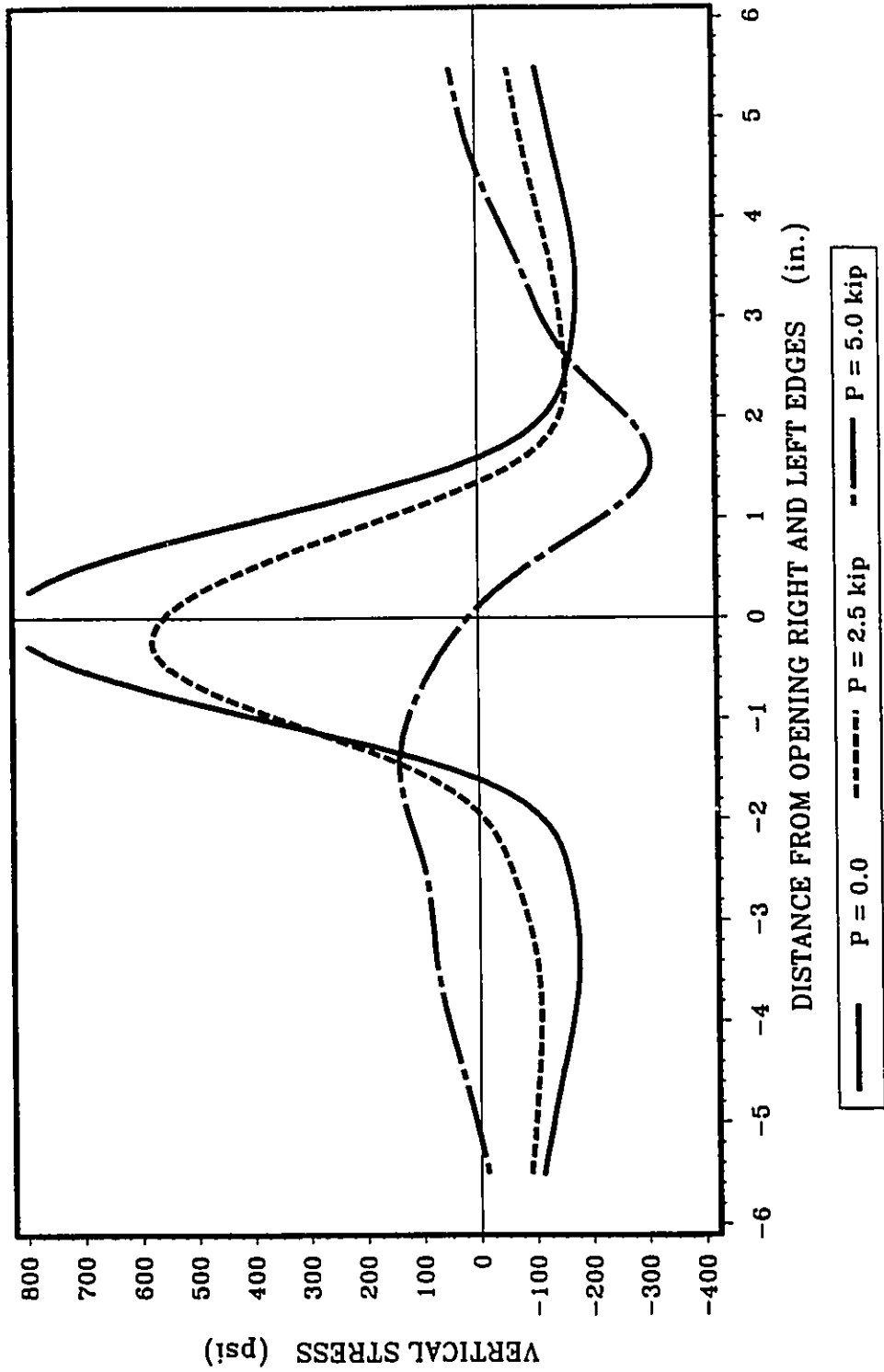


FIG. 5.1.13 VERTICAL STRESS DISTRIBUTION AT THE OPENING FOR BEAM BII2C

Note: 1 in.=25.4 mm; 1 kip=4.45 kN; 1 psi=6.89 kPa

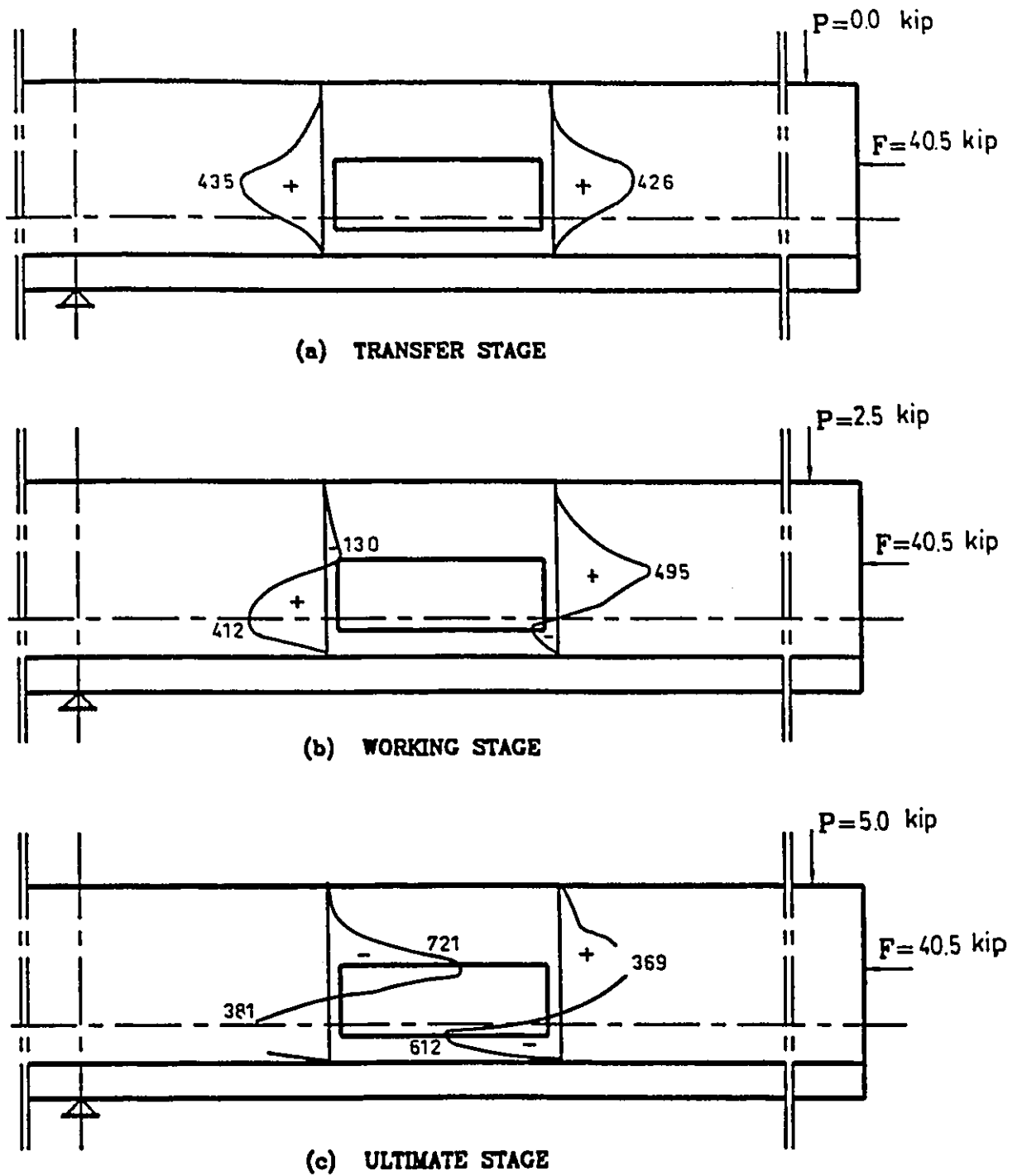


FIG. 5.114 VERTICAL STRESS DISTRIBUTION FOR BEAM BII3A

Note: stresses are shown in psi; 1 psi=6.89 kPa; 1 kip=4.45 kN

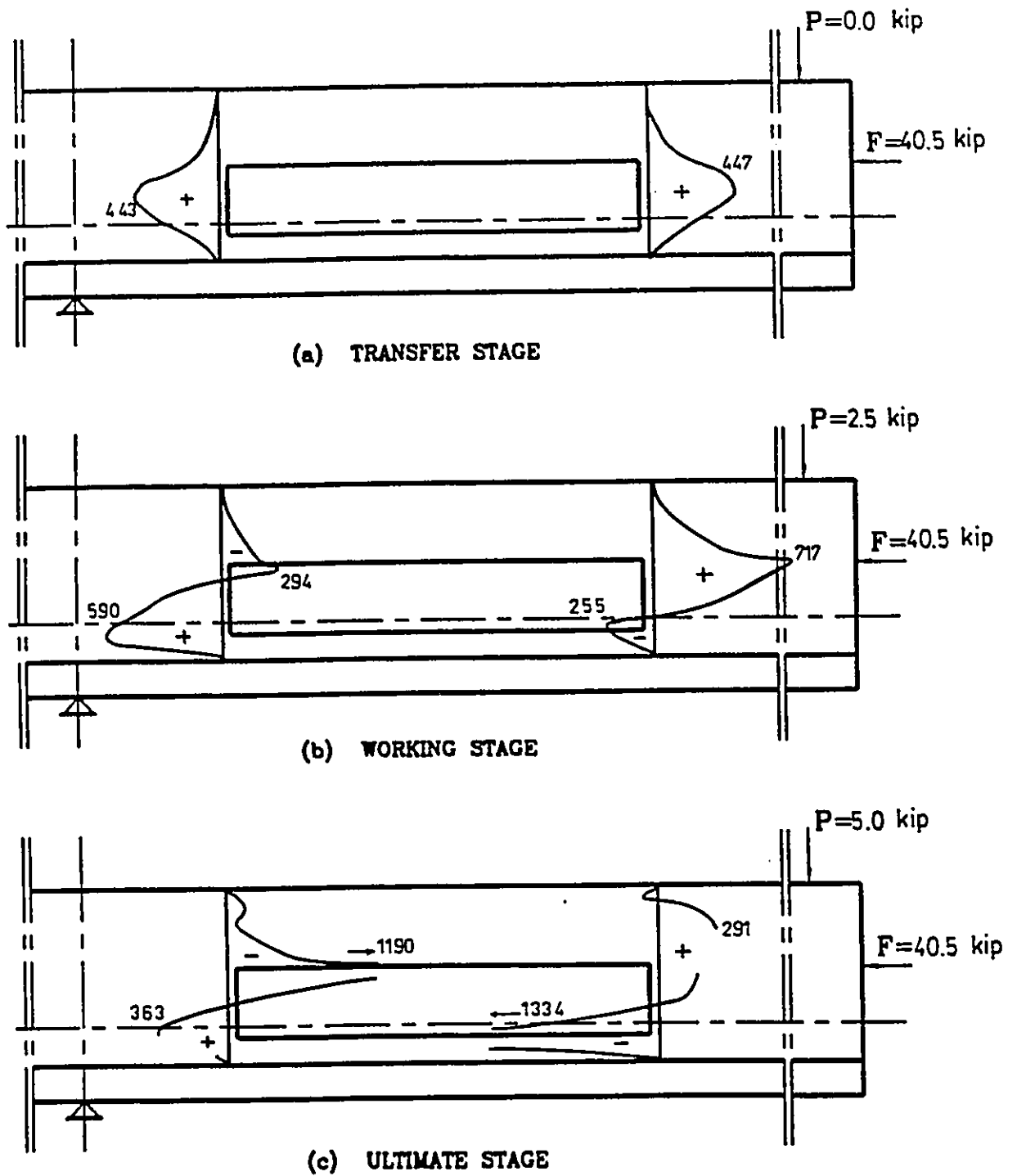


FIG. 5.115 VERTICAL STRESS DISTRIBUTION FOR BEAM BI3C

Note: stresses are shown in psi; 1 psi=6.89 kPa; 1 kip=4.45 kN

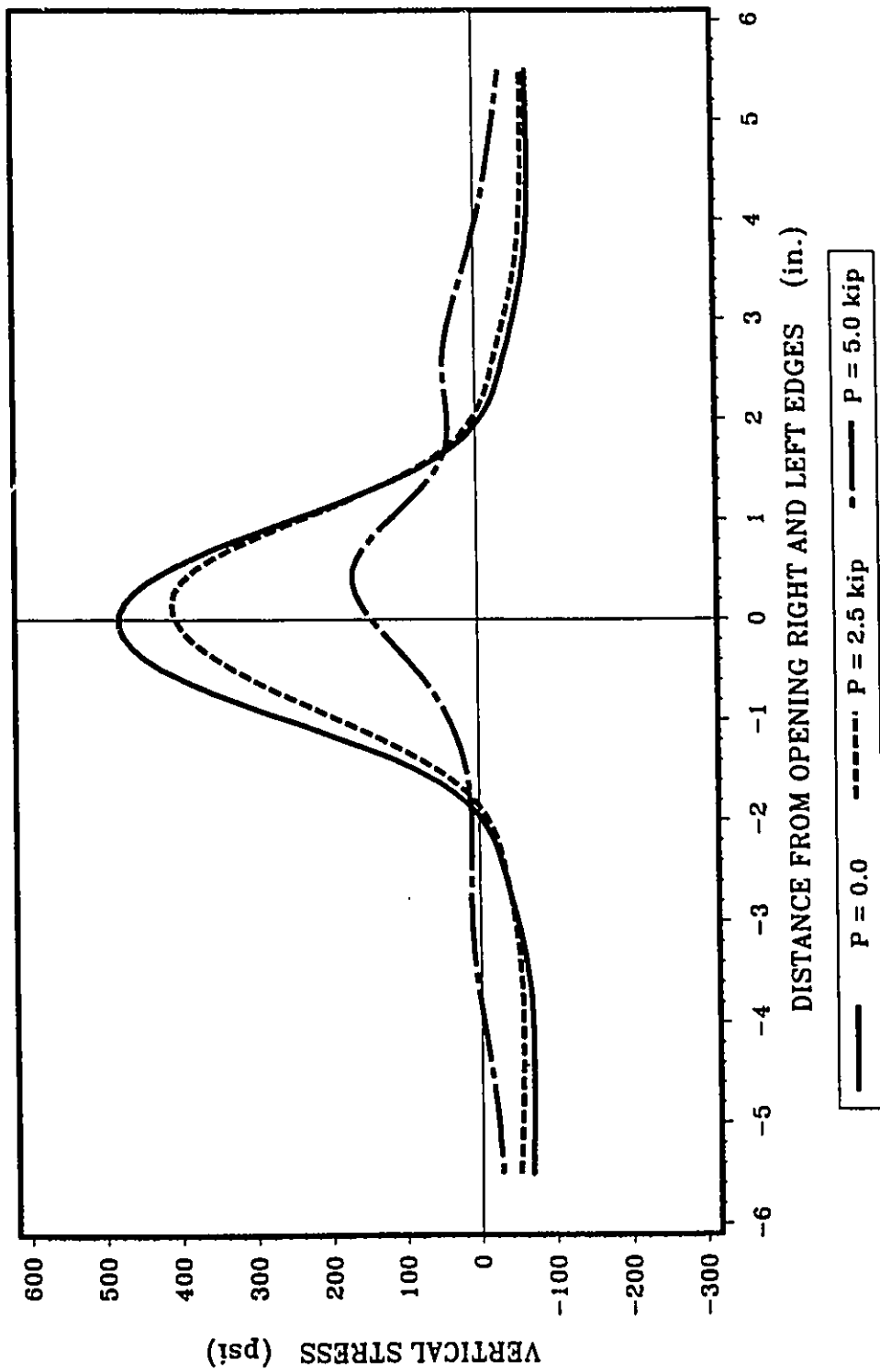


FIG. 5.116 VERTICAL STRESS DISTRIBUTION AT THE OPENING FOR BEAM BII3A

Note: 1 in.=25.4 mm; 1 kip=4.45 kN; 1 psi=6.89 kPa

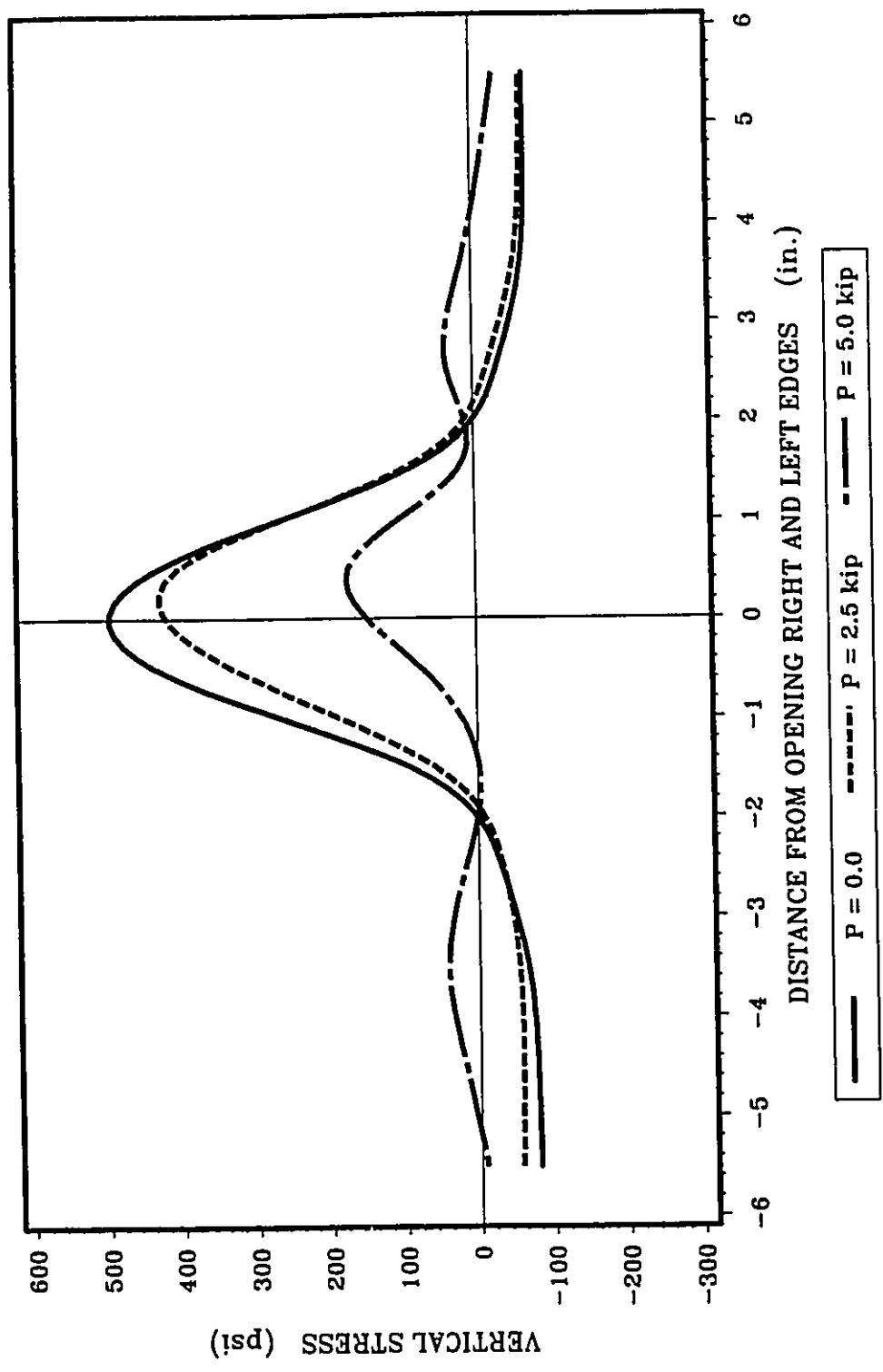


FIG. 5.1.17 VERTICAL STRESS DISTRIBUTION AT THE OPENING FOR BEAM BI3B

Note: 1 in.=25.4 mm; 1 kip=4.45 kN; 1 psi=6.89 kPa

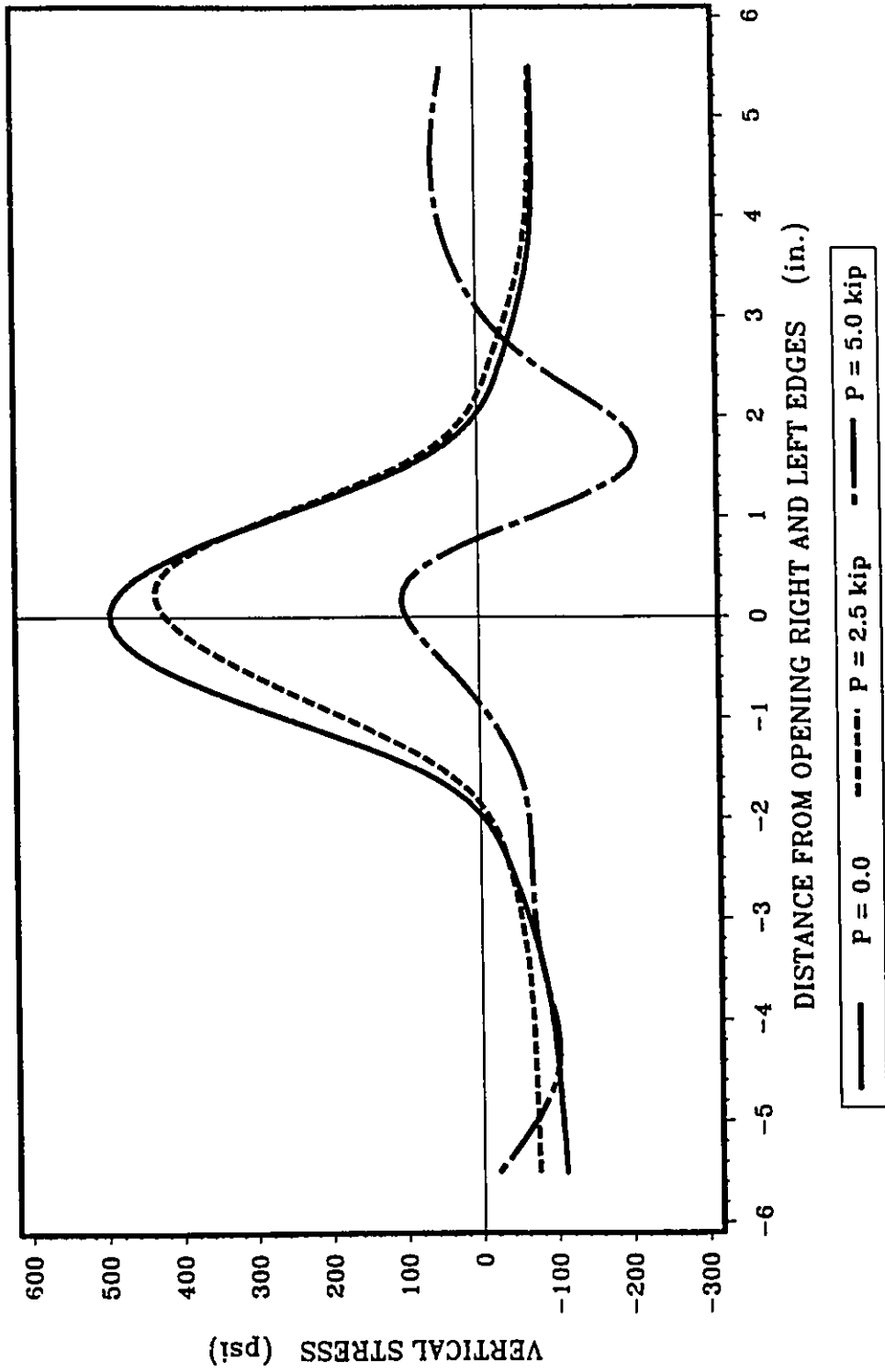


FIG. 5.118 VERTICAL STRESS DISTRIBUTION AT THE OPENING FOR BEAM BI3C

Note: 1 in.=25.4 mm; 1 kip=4.45 kN; 1 psi=6.89 kPa

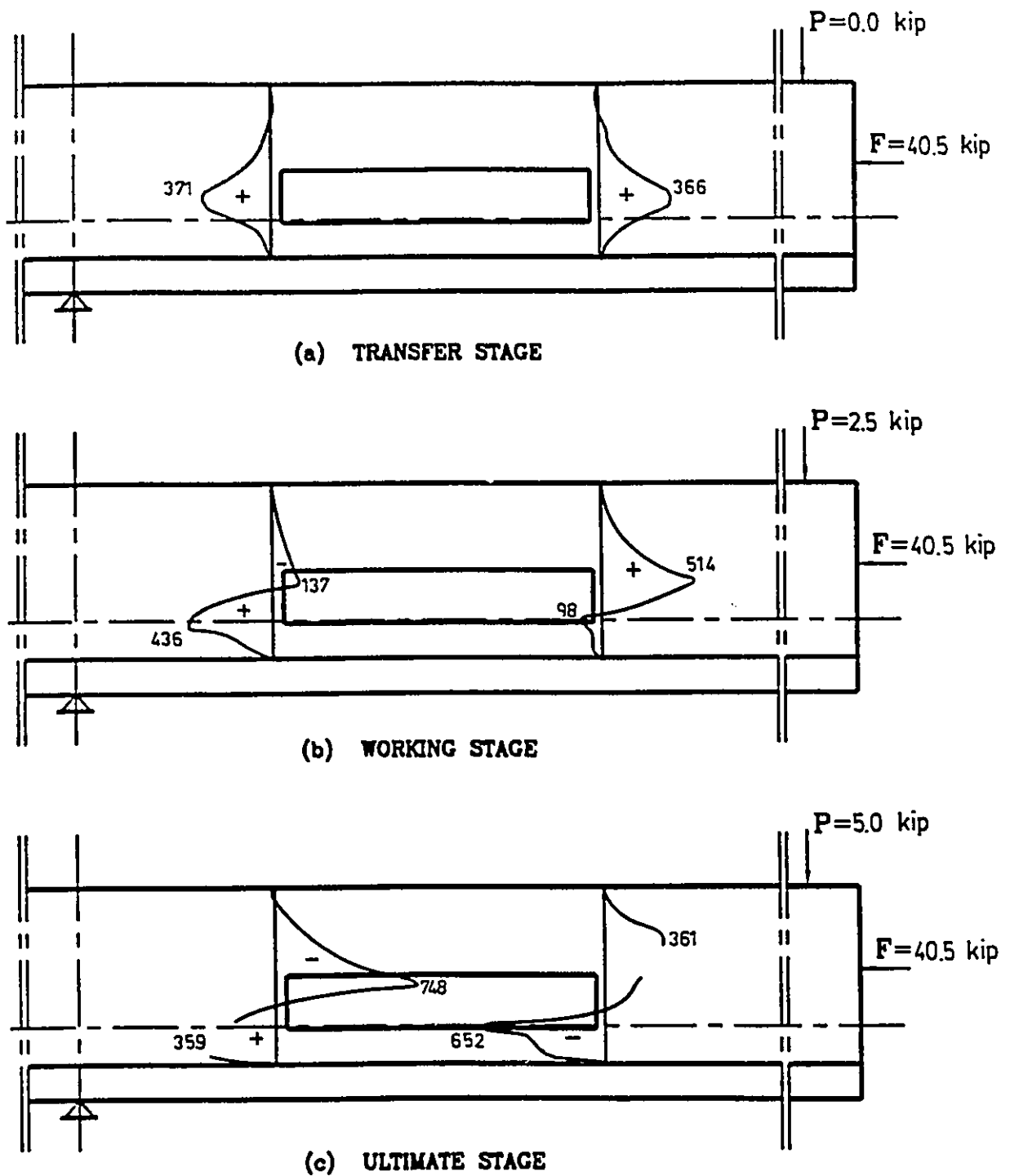


FIG. 5.119 VERTICAL STRESS DISTRIBUTION FOR BEAM BII4A

Note: stresses are shown in psi; 1 psi=6.89 kPa; 1 kip=4.45 kN

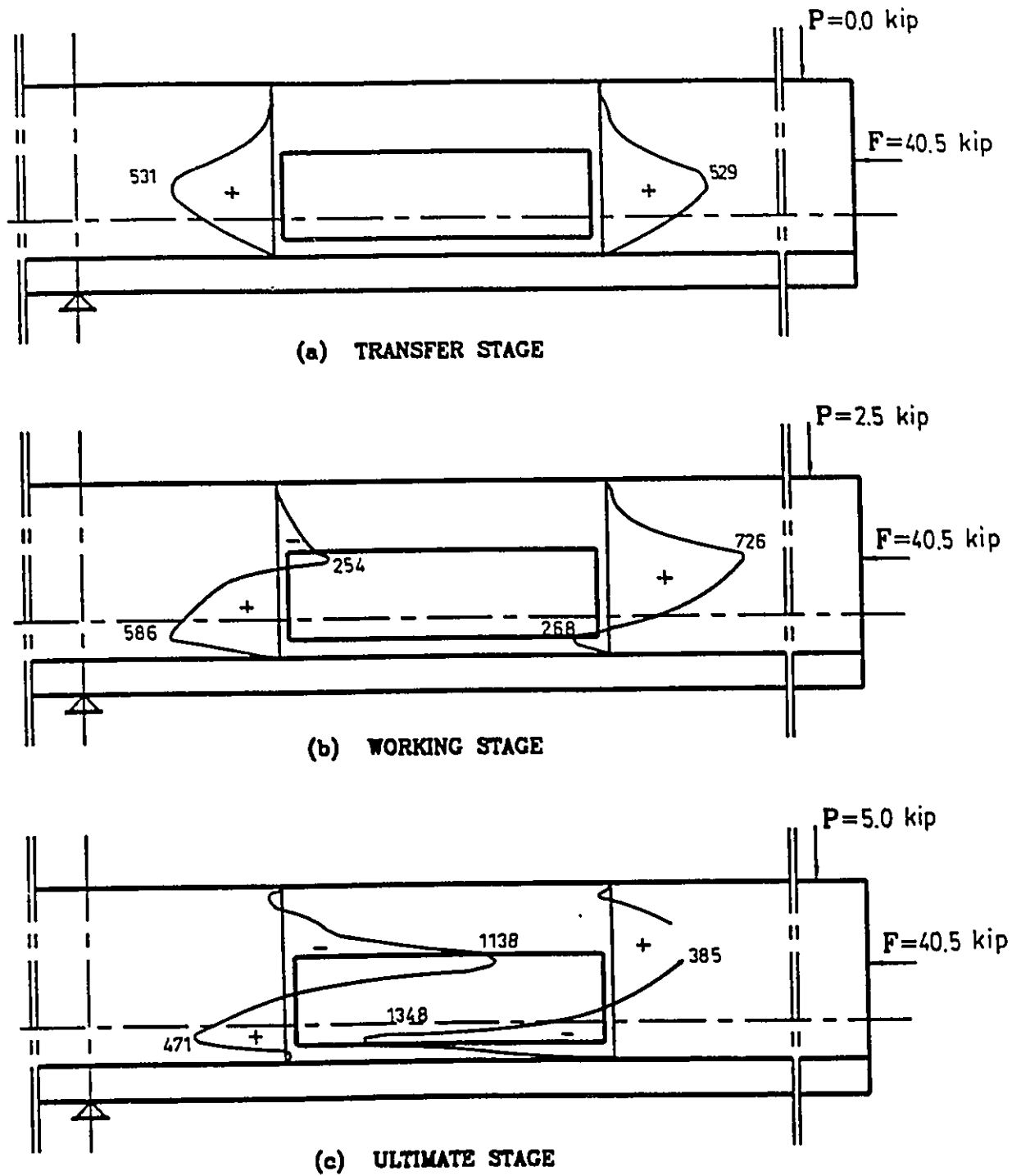


FIG. 5.120 VERTICAL STRESS DISTRIBUTION FOR BEAM BI4C

Note: stresses are shown in psi; 1 psi=6.89 kPa; 1 kip=4.45 kN

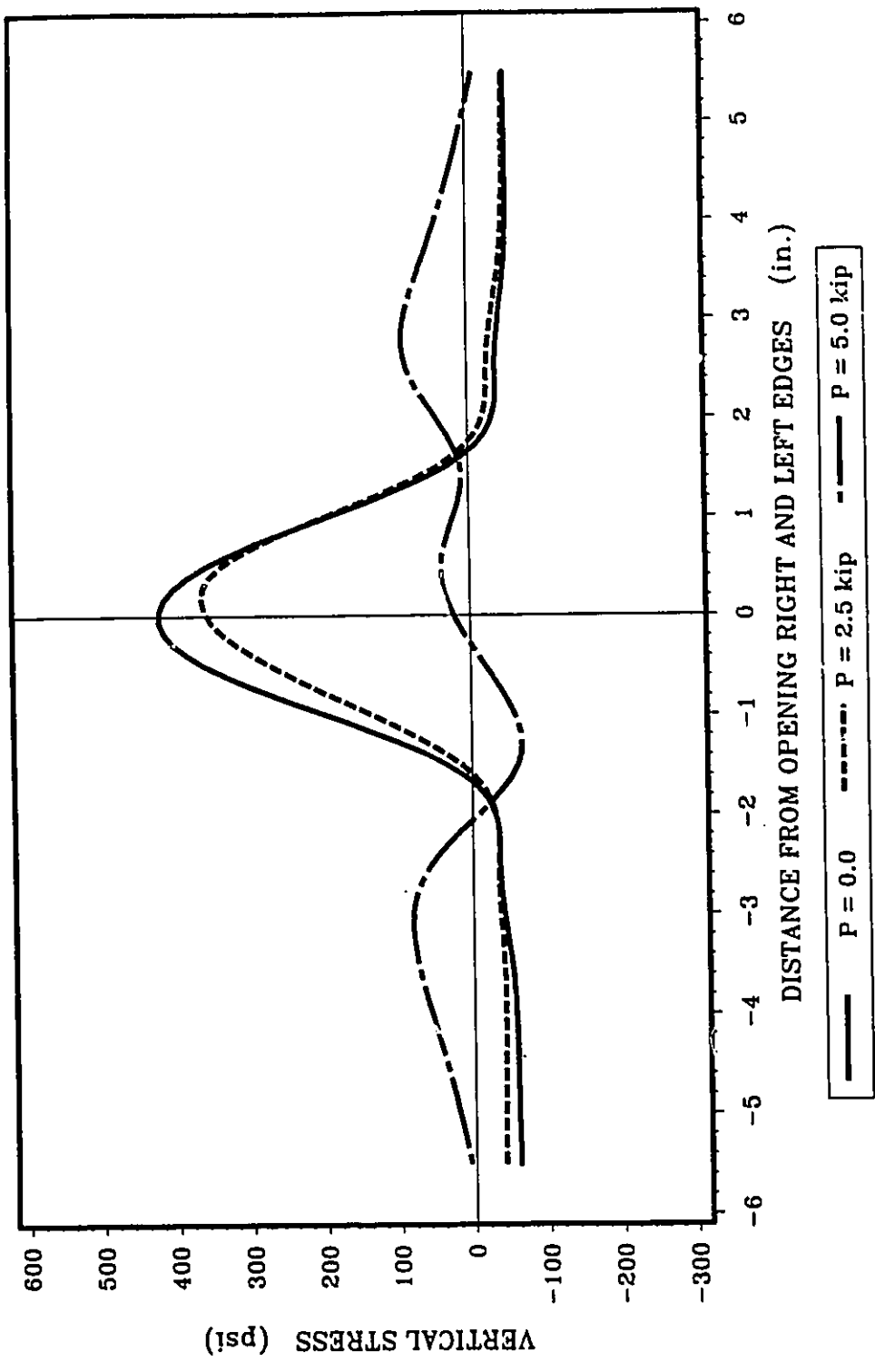


FIG. 5.121 VERTICAL STRESS DISTRIBUTION AT THE OPENING FOR BEAM BII4A

Note: 1 in.=25.4 mm; 1 kip=4.45 kN; 1 psi=6.89 kPa

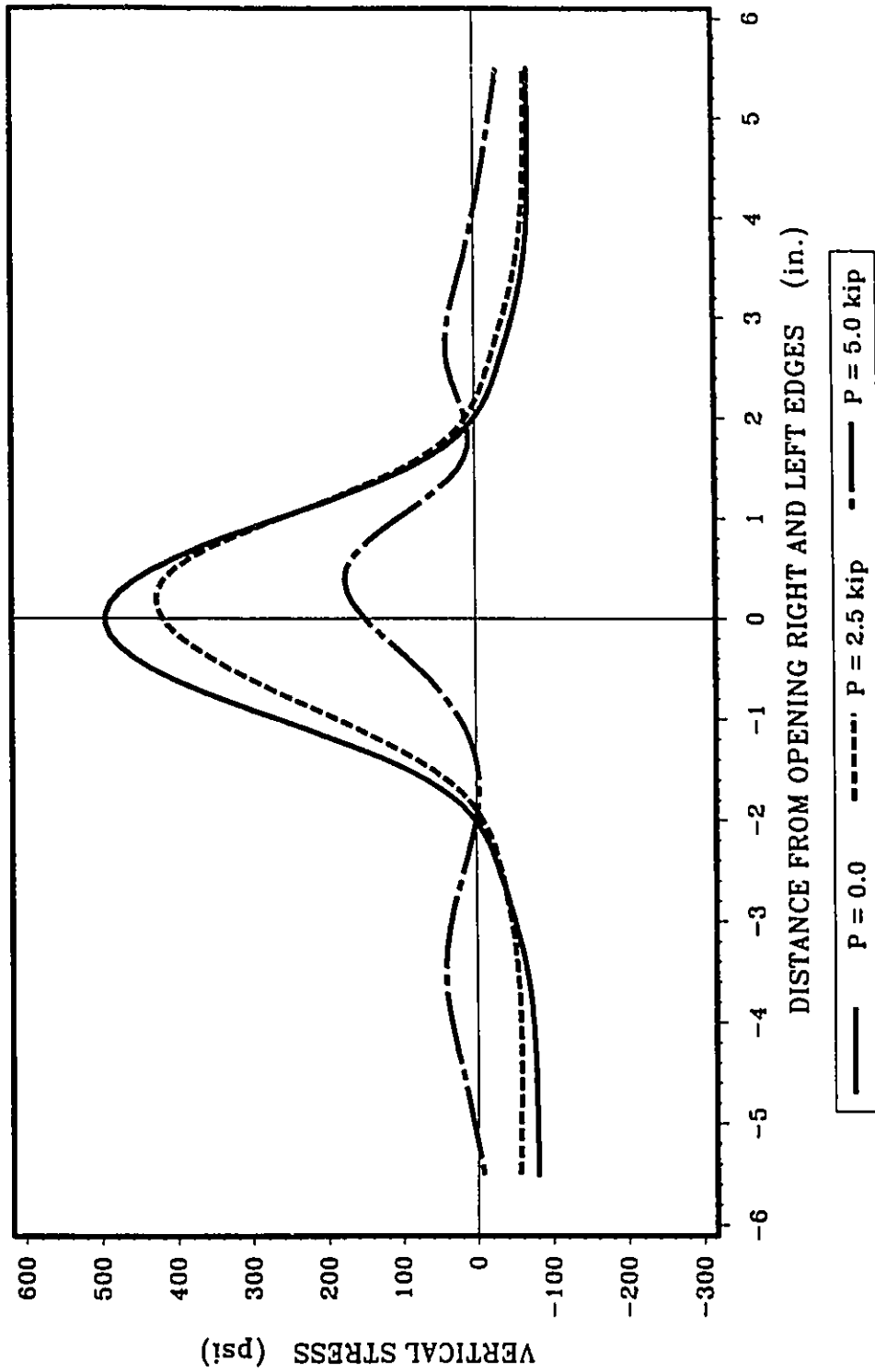


FIG. 5.122 VERTICAL STRESS DISTRIBUTION AT THE OPENING FOR BEAM BII4B

Note: 1 in.=25.4 mm; 1 kip=4.45 kN; 1 psi=6.89 kPa

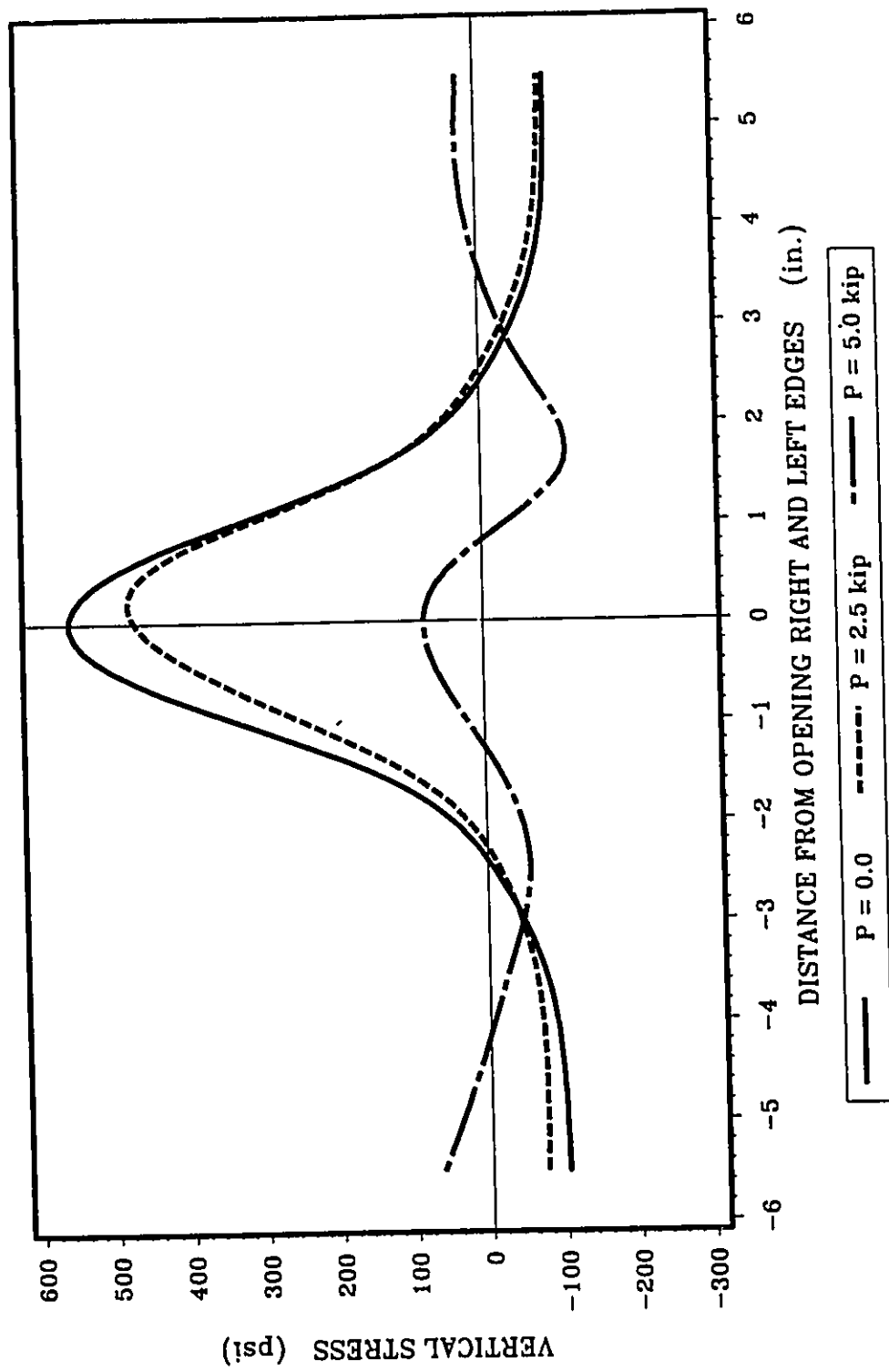


FIG. 5.123 VERTICAL STRESS DISTRIBUTION AT THE OPENING FOR BEAM BII4C

Note: 1 in. = 25.4 mm; 1 kip = 4.45 kN; 1 psi = 6.89 kPa

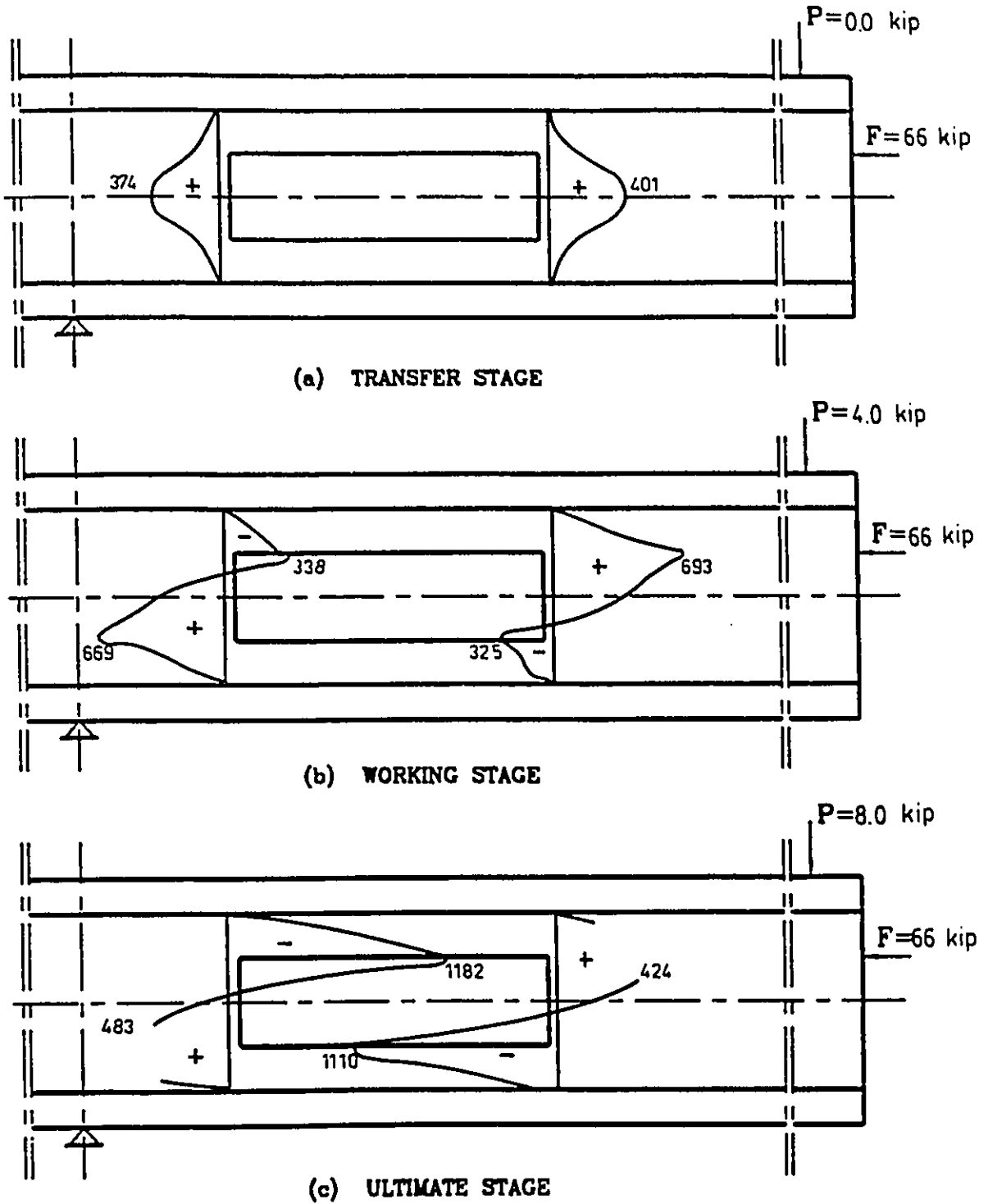


FIG. 5.124 VERTICAL STRESS DISTRIBUTION FOR BEAM BIII1A

Note: stresses are shown in psi; 1 psi=6.89 kPa; 1 kip=4.45 kN

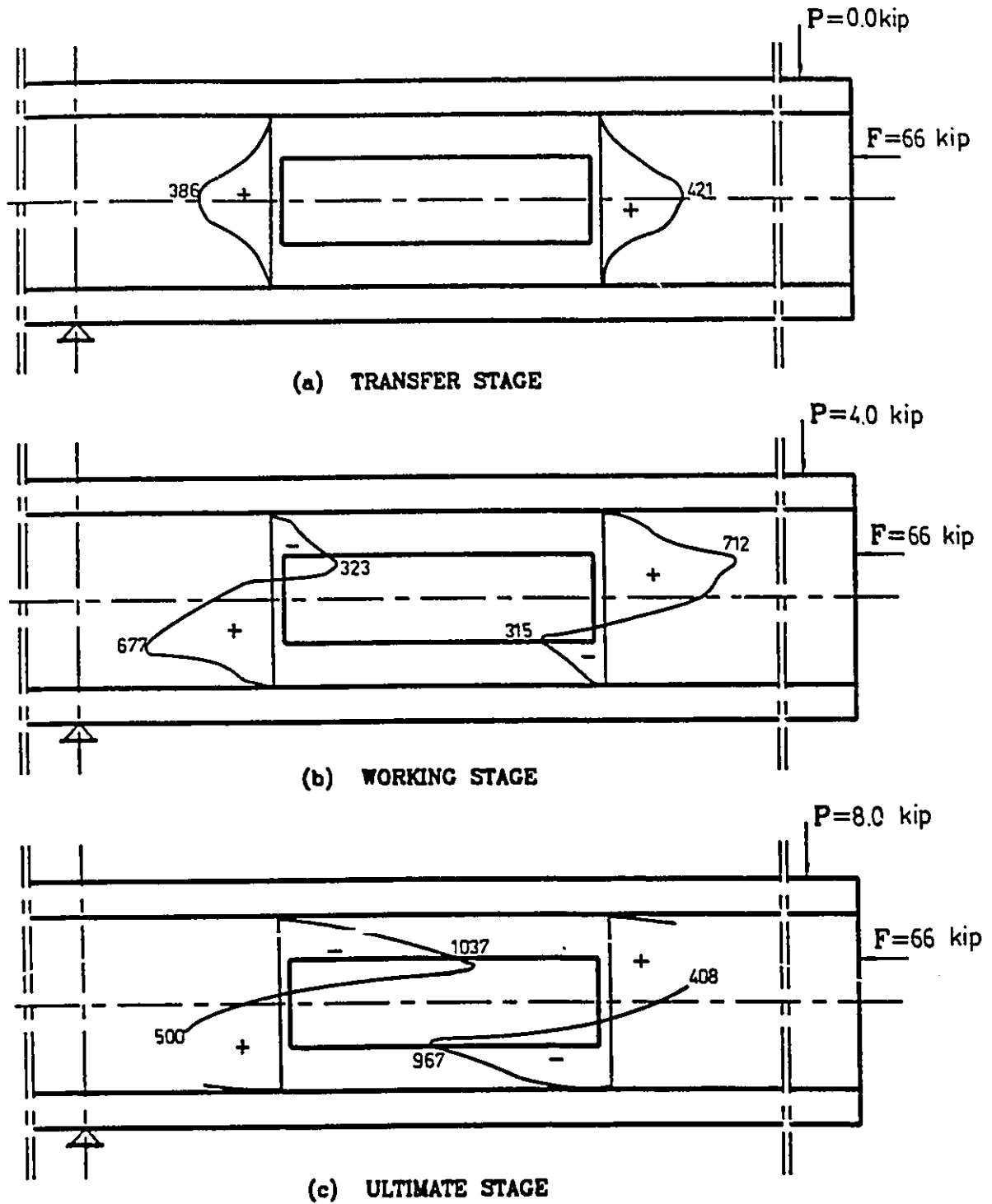


FIG. 5.125 VERTICAL STRESS DISTRIBUTION FOR BEAM BIII1B

Note: stresses are shown in psi; 1 psi=6.89 kPa; 1 kip=4.45 kN

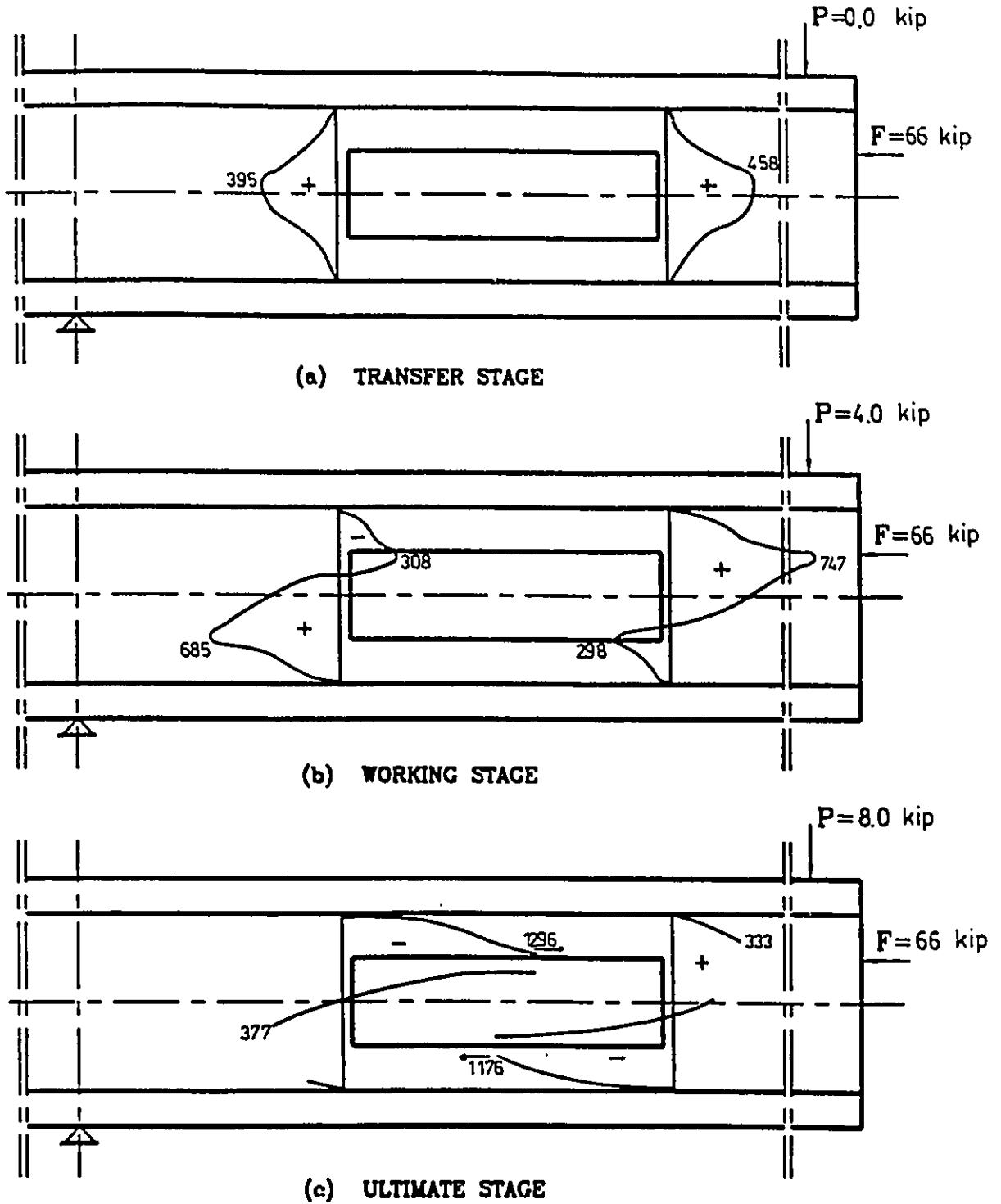


FIG. 5.126 VERTICAL STRESS DISTRIBUTION FOR BEAM BIIIIC

Note: stresses are shown in psi; 1 psi=6.89 kPa; 1 kip=4.45 kN

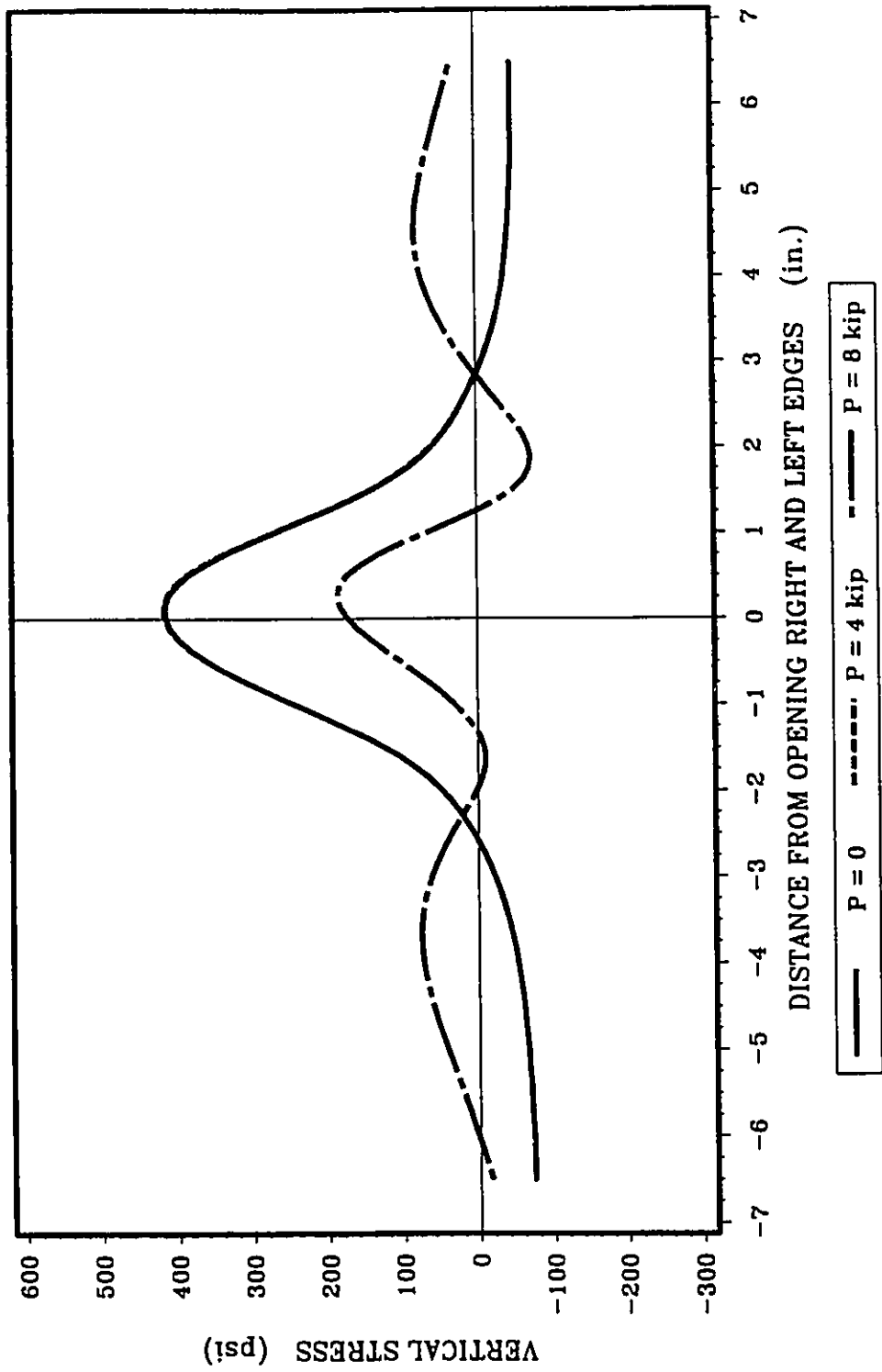


FIG. 5.127 VERTICAL STRESS DISTRIBUTION AT THE OPENING FOR BEAM BIII1A

Note: 1 in.=25.4 mm; 1 kip=4.45 kN; 1 psi=6.89 kPa

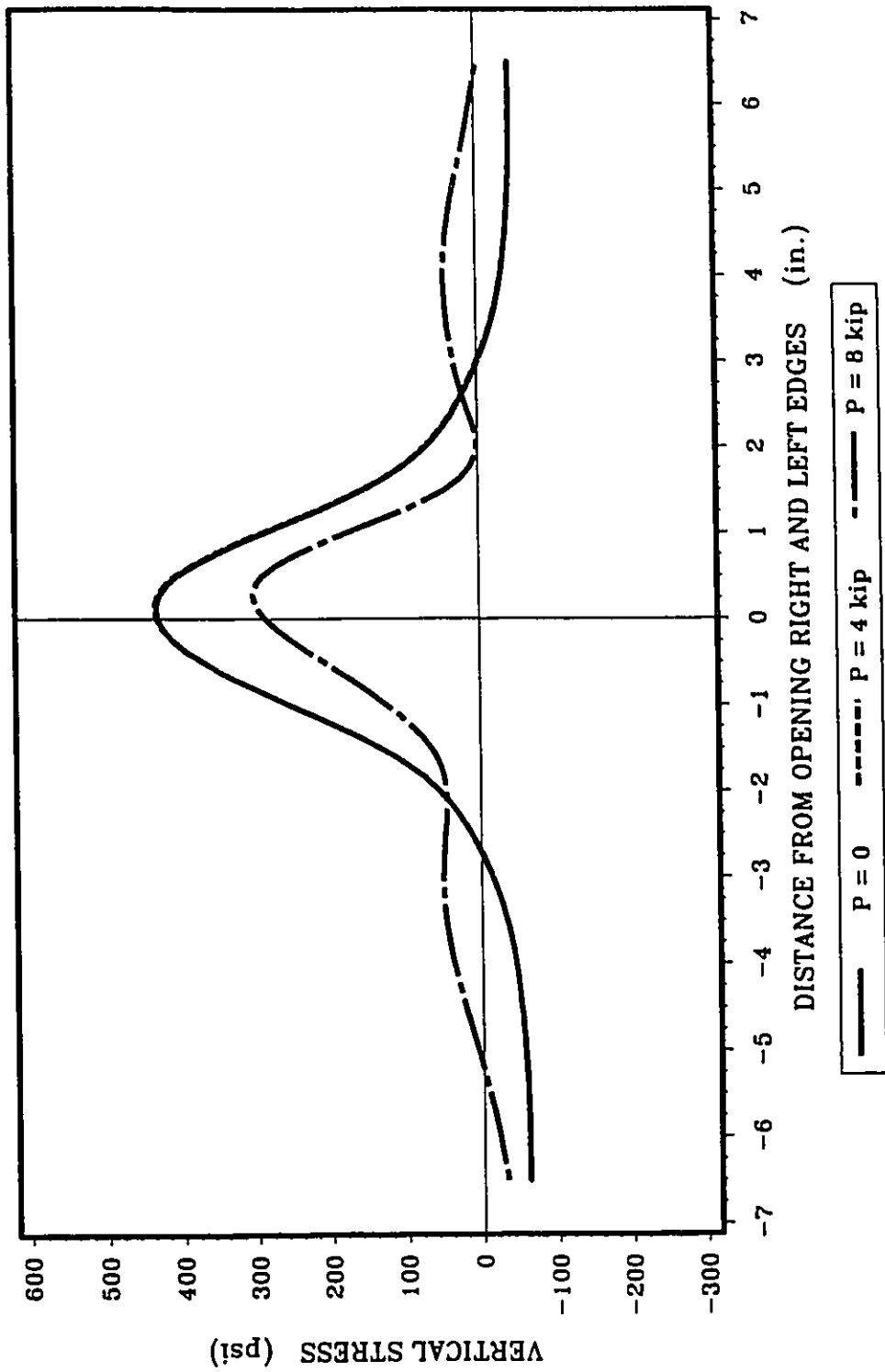


FIG. 5.128 VERTICAL STRESS DISTRIBUTION AT THE OPENING FOR BEAM BIII1B

Note: 1 in.=25.4 mm; 1 kip=4.45 kN; 1 psi=6.89 kPa

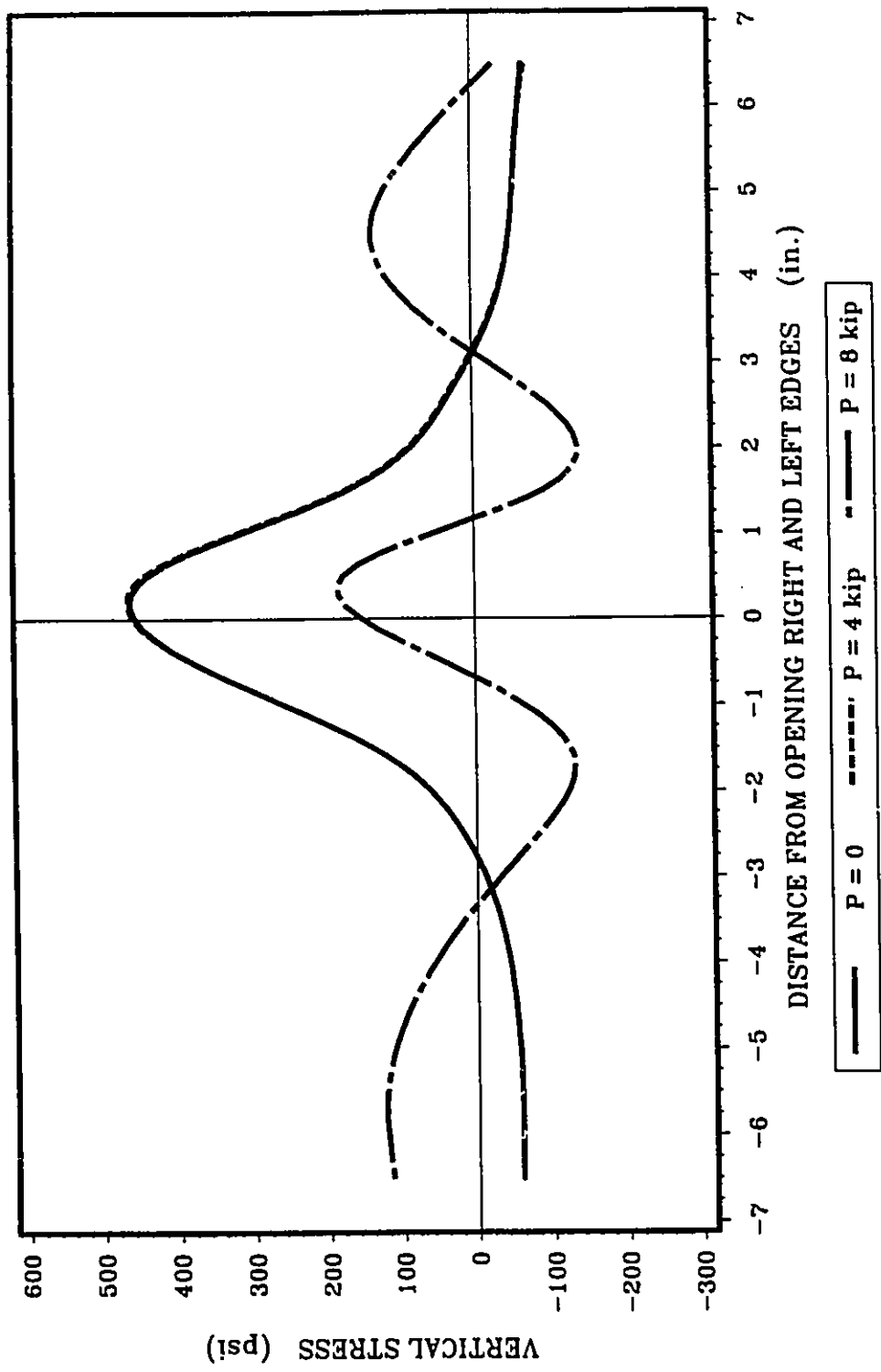
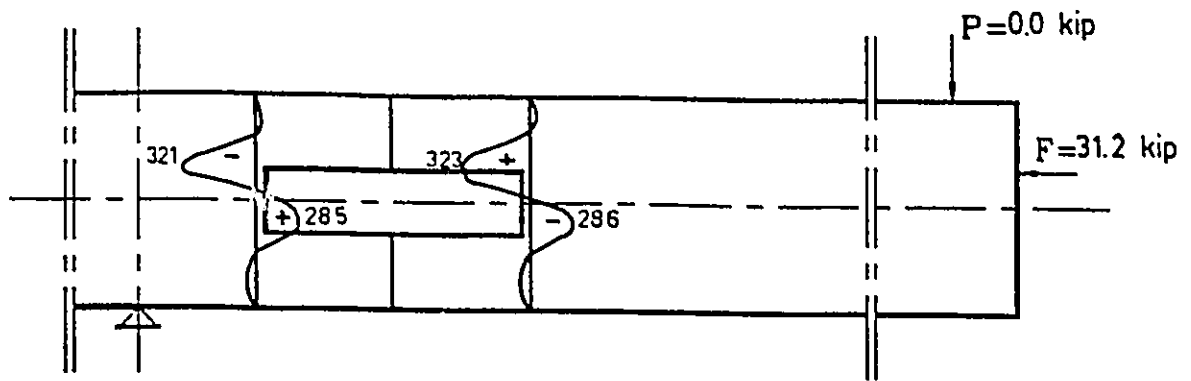
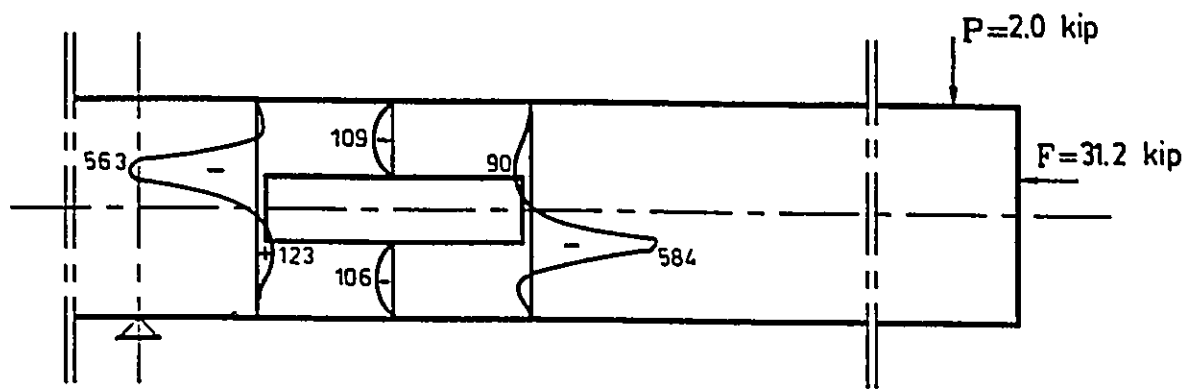


FIG. 5.129 VERTICAL STRESS DISTRIBUTION AT THE OPENING FOR BEAM BIII1C

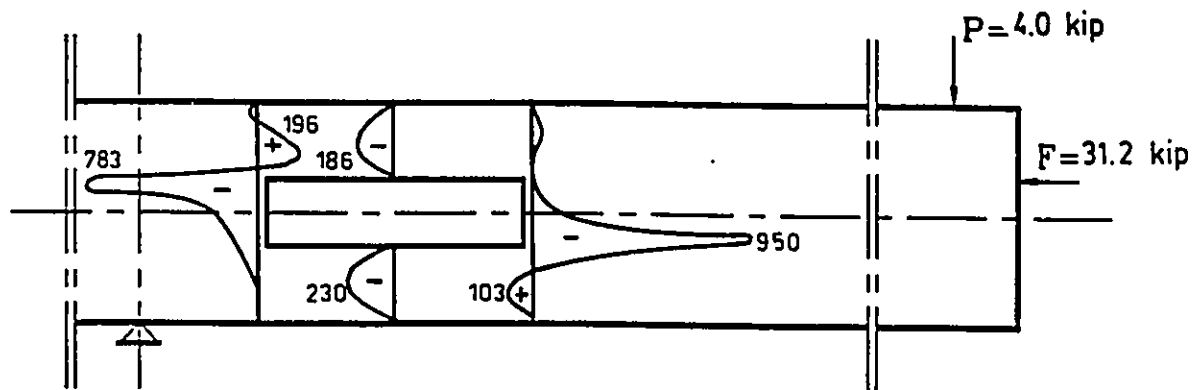
Note: 1 in.=25.4 mm; 1 kip=4.45 kN; 1 psi=6.89 kPa



(a) TRANSFER STAGE



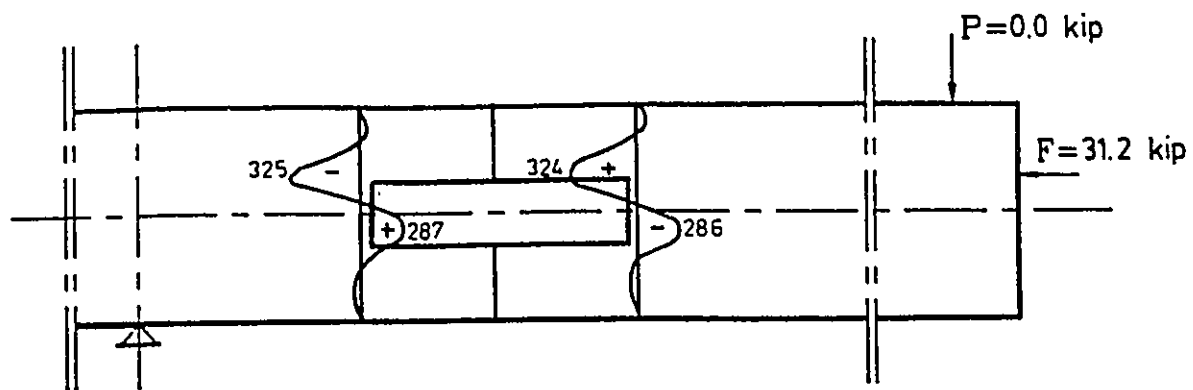
(b) WORKING STAGE



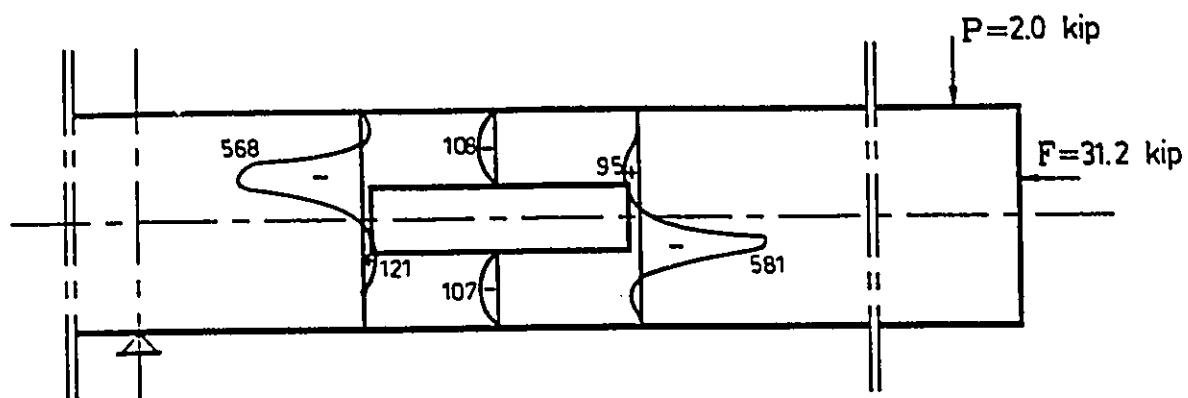
(c) ULTIMATE STAGE

FIG. 5.130 SHEAR STRESS DISTRIBUTION FOR BEAM B11A

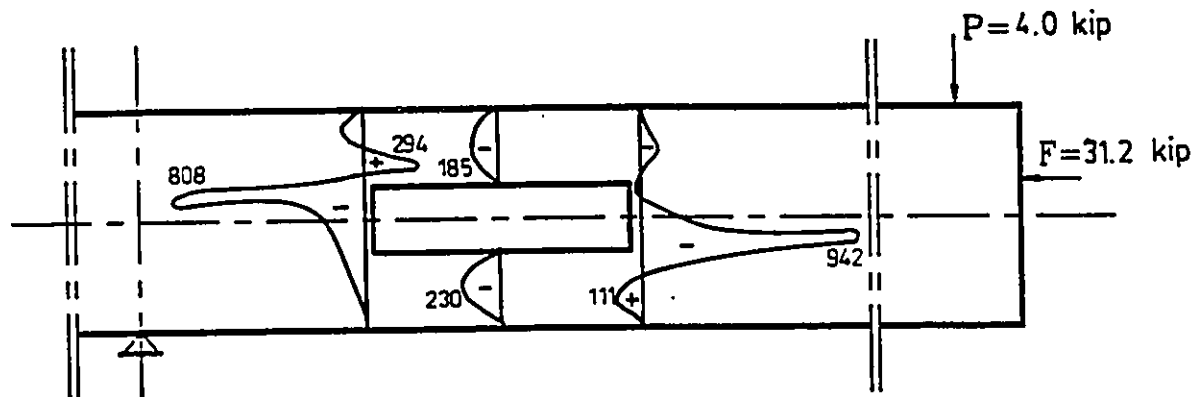
Note: stresses are shown in psi; 1 psi=6.89 kPa; 1 kip=4.45 kN



(a) TRANSFER STAGE



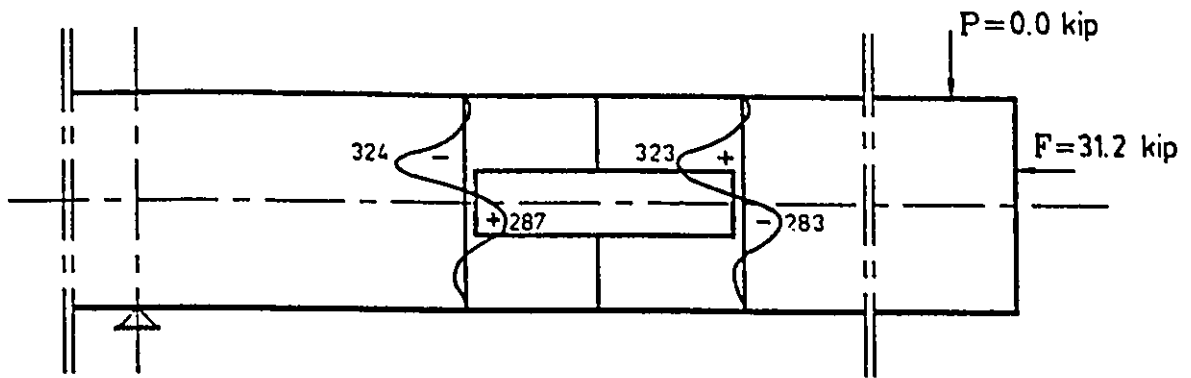
(b) WORKING STAGE



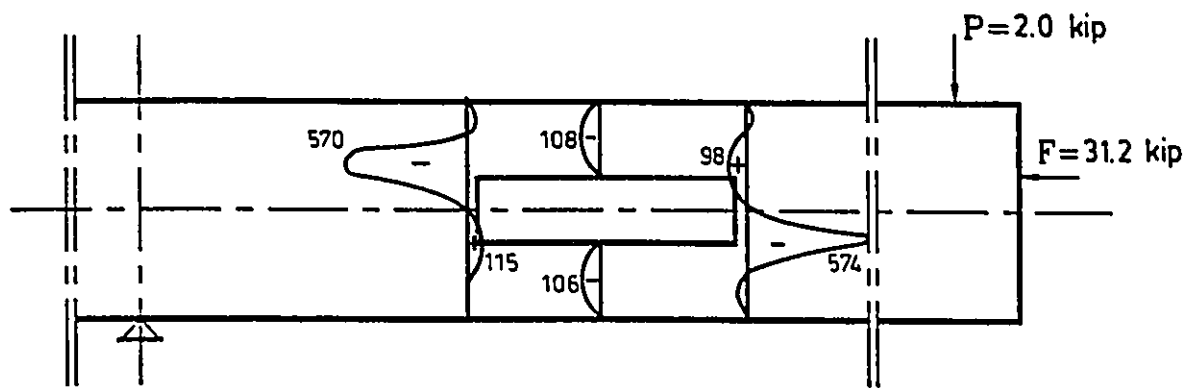
(c) ULTIMATE STAGE

FIG. 5.131 SHEAR STRESS DISTRIBUTION FOR BEAMS BIIB& BI3A

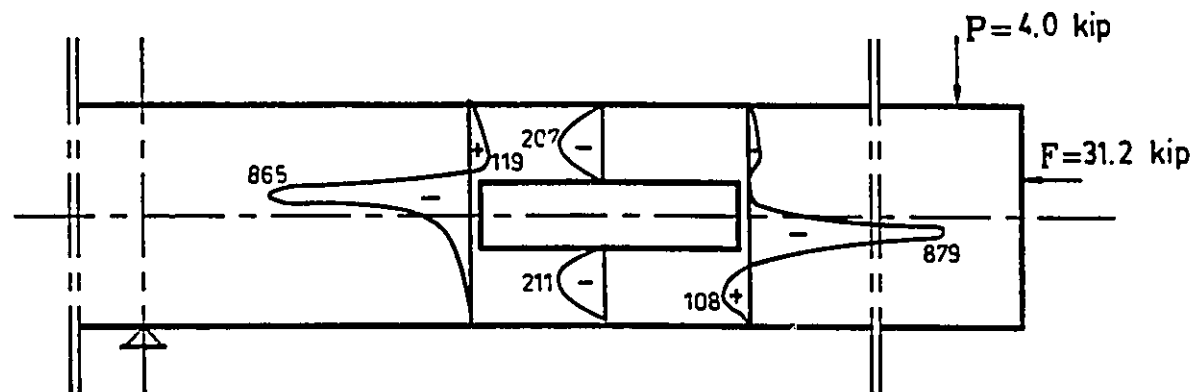
Note: stresses are shown in psi; 1 psi=6.89 kPa; 1 kip=4.45 kN



(a) TRANSFER STAGE



(b) WORKING STAGE



(c) ULTIMATE STAGE

FIG. 5.132 SHEAR STRESS DISTRIBUTION FOR BEAM B11C

Note: stresses are shown in psi; 1 psi=6.89 kPa; 1 kip=4.45 kN

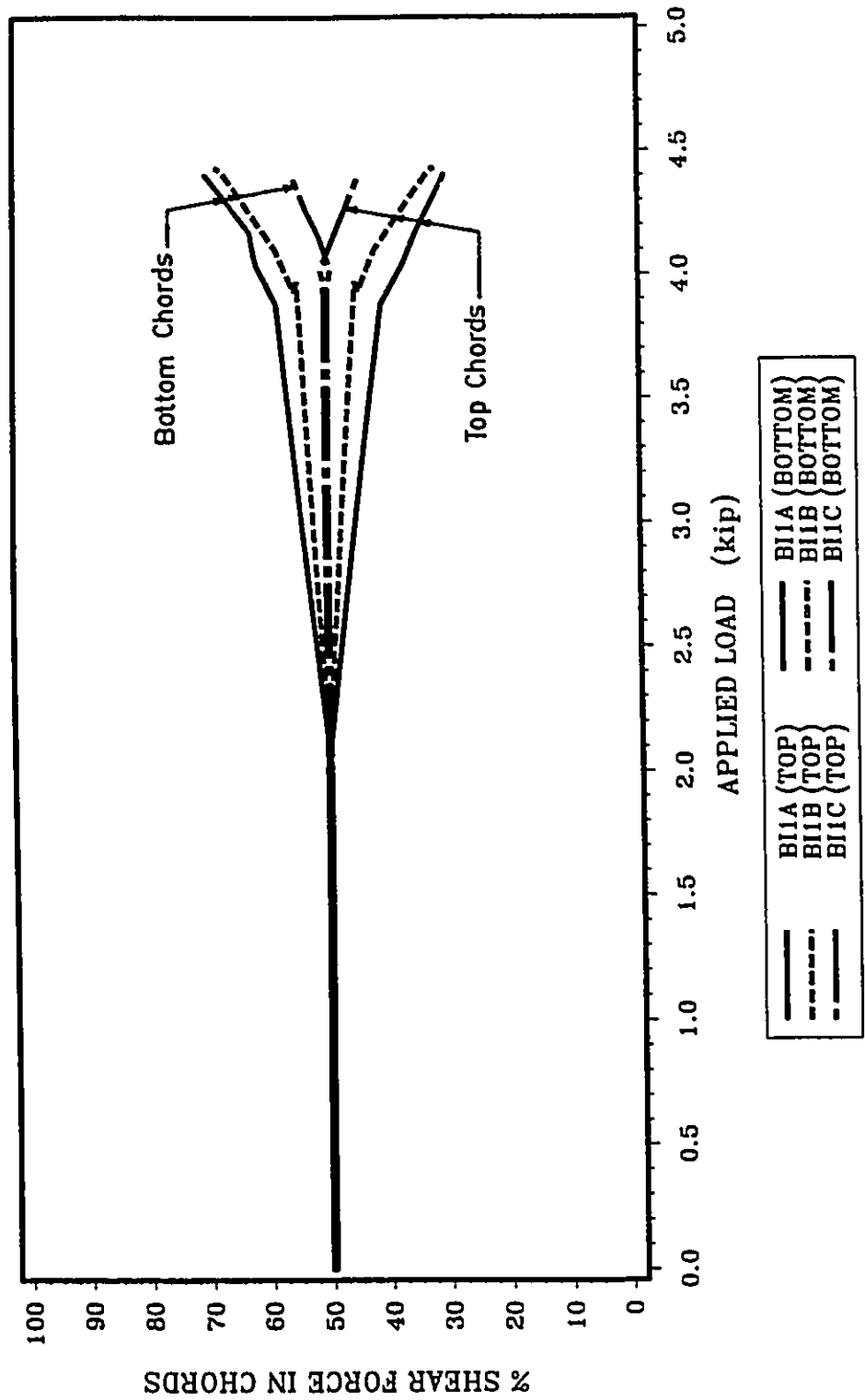
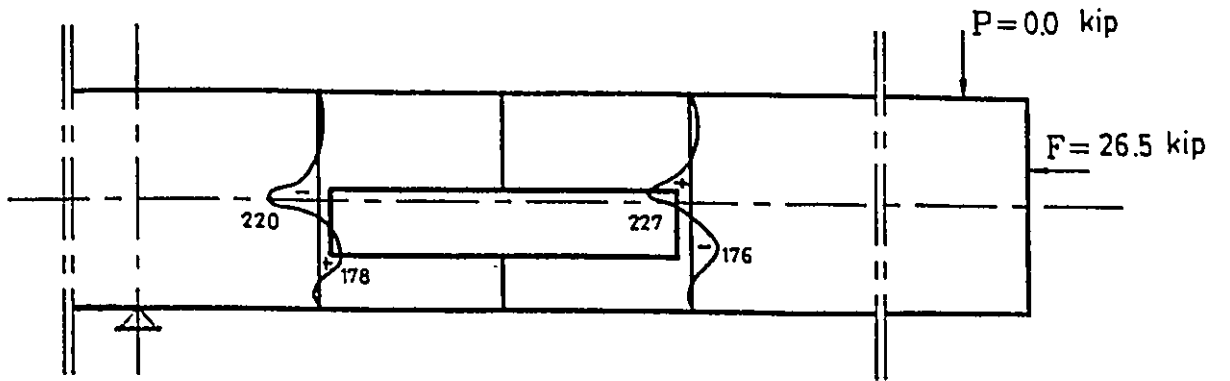
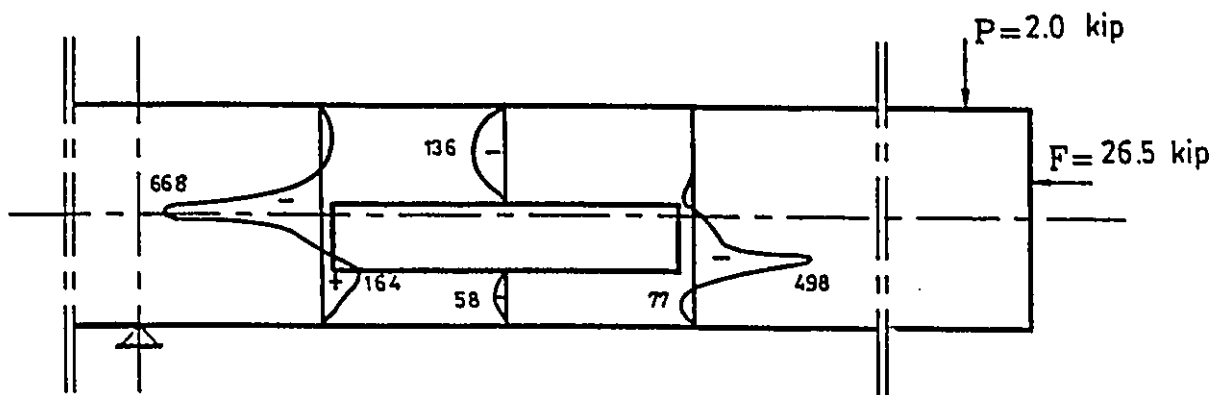


FIG. 5.133 DISTRIBUTION OF SHEAR FORCE BETWEEN TOP AND BOTTOM CHORDS FOR GROUP BI1

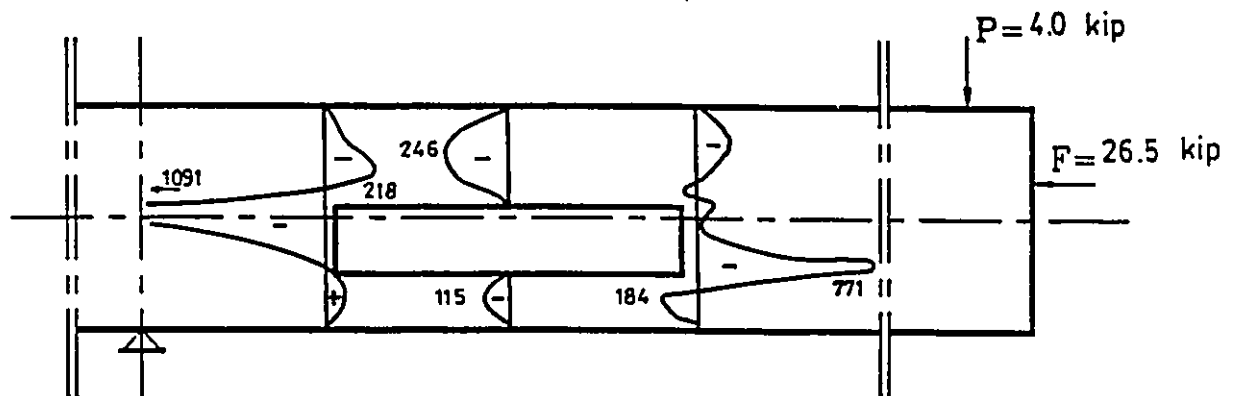
Note: 1 kip=4.45 kN



(a) TRANSFER STAGE



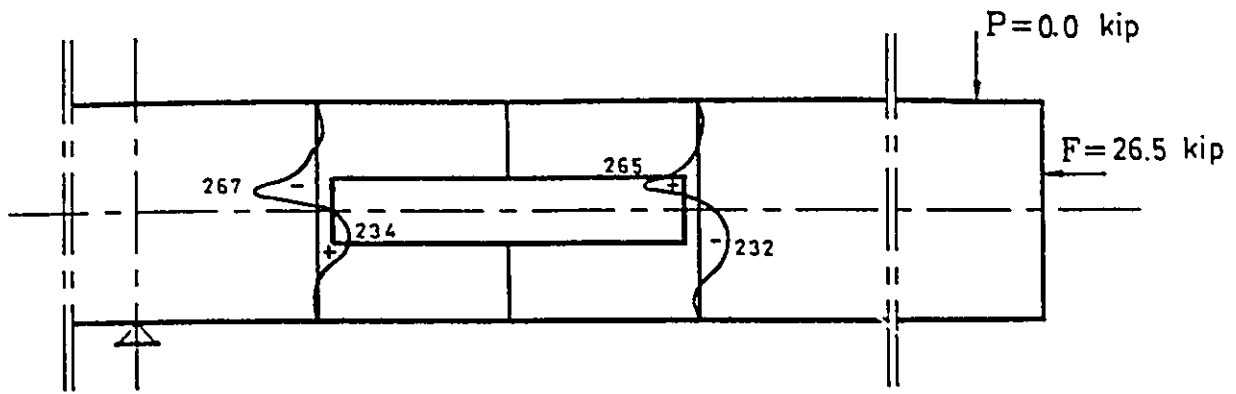
(b) WORKING STAGE



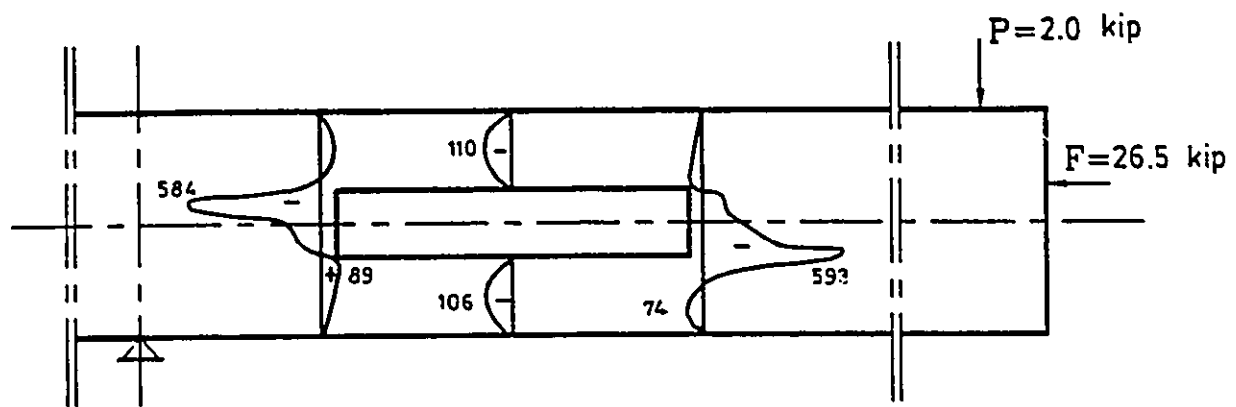
(c) ULTIMATE STAGE

FIG. 5.134 SHEAR STRESS DISTRIBUTION FOR BEAM B12A

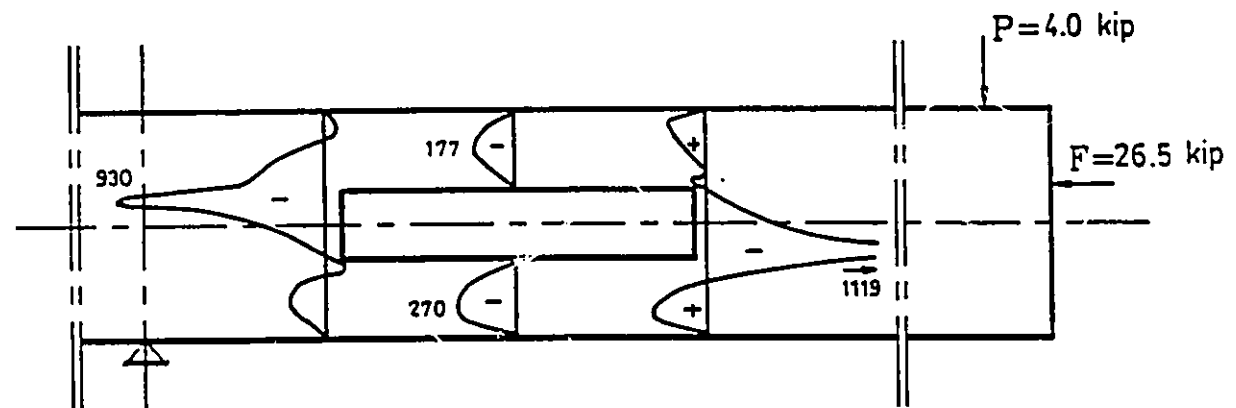
Note: stresses are shown in psi; 1 psi=6.89 kPa; 1 kip=4.45 kN



(a) TRANSFER STAGE



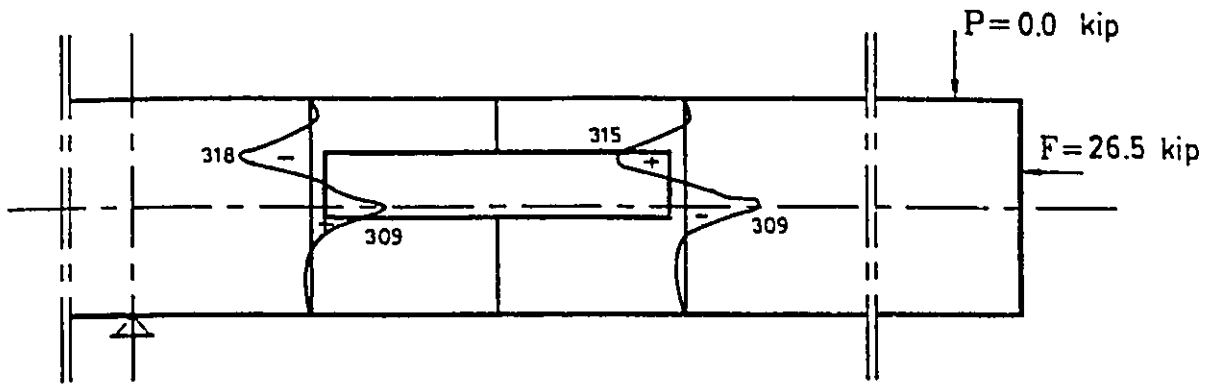
(b) WORKING STAGE



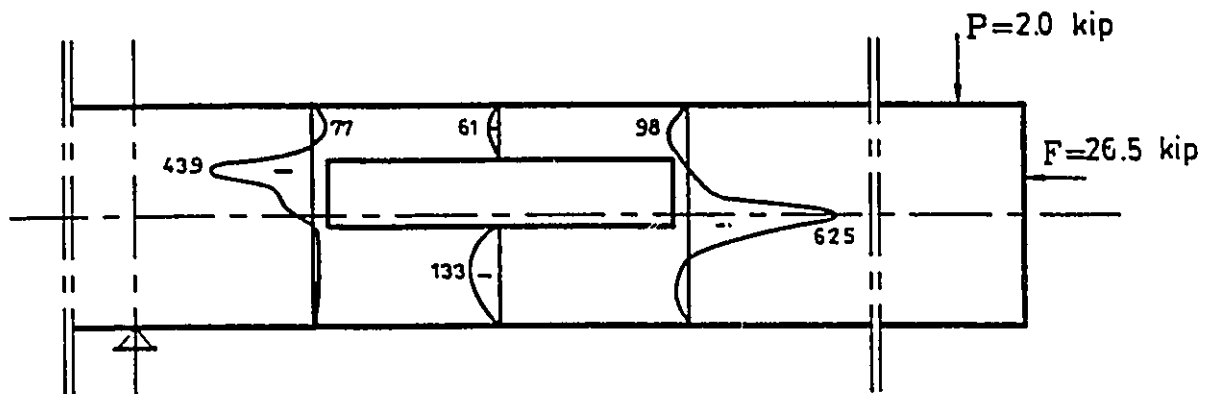
(c) ULTIMATE STAGE

FIG. 5.135 SHEAR STRESS DISTRIBUTION FOR BEAM B12B

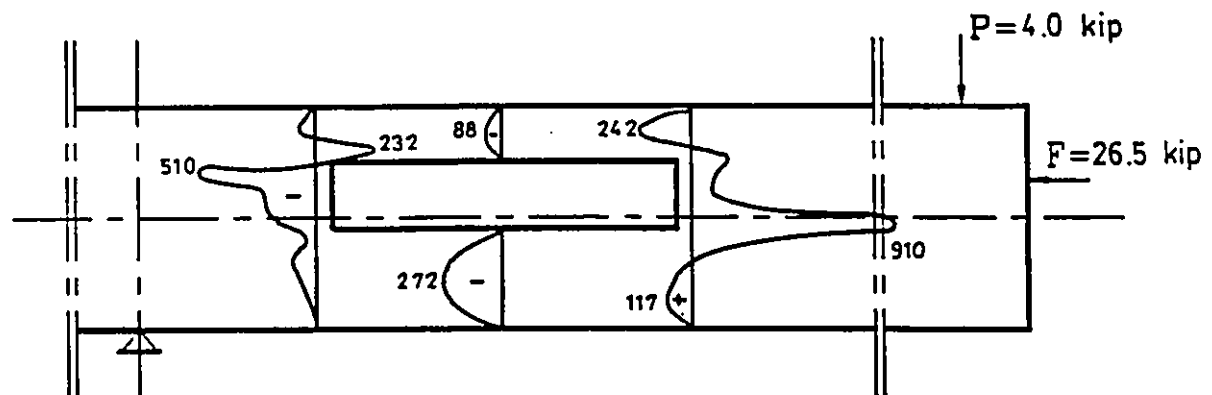
Note: stresses are shown in psi; 1 psi=6.89 kPa; 1 kip=4.45 kN



(a) TRANSFER STAGE



(b) WORKING STAGE



(c) ULTIMATE STAGE

FIG. 5.136 SHEAR STRESS DISTRIBUTION FOR BEAM B12C

Note: stresses are shown in psi; 1 psi=6.89 kPa; 1 kip=4.45 kN

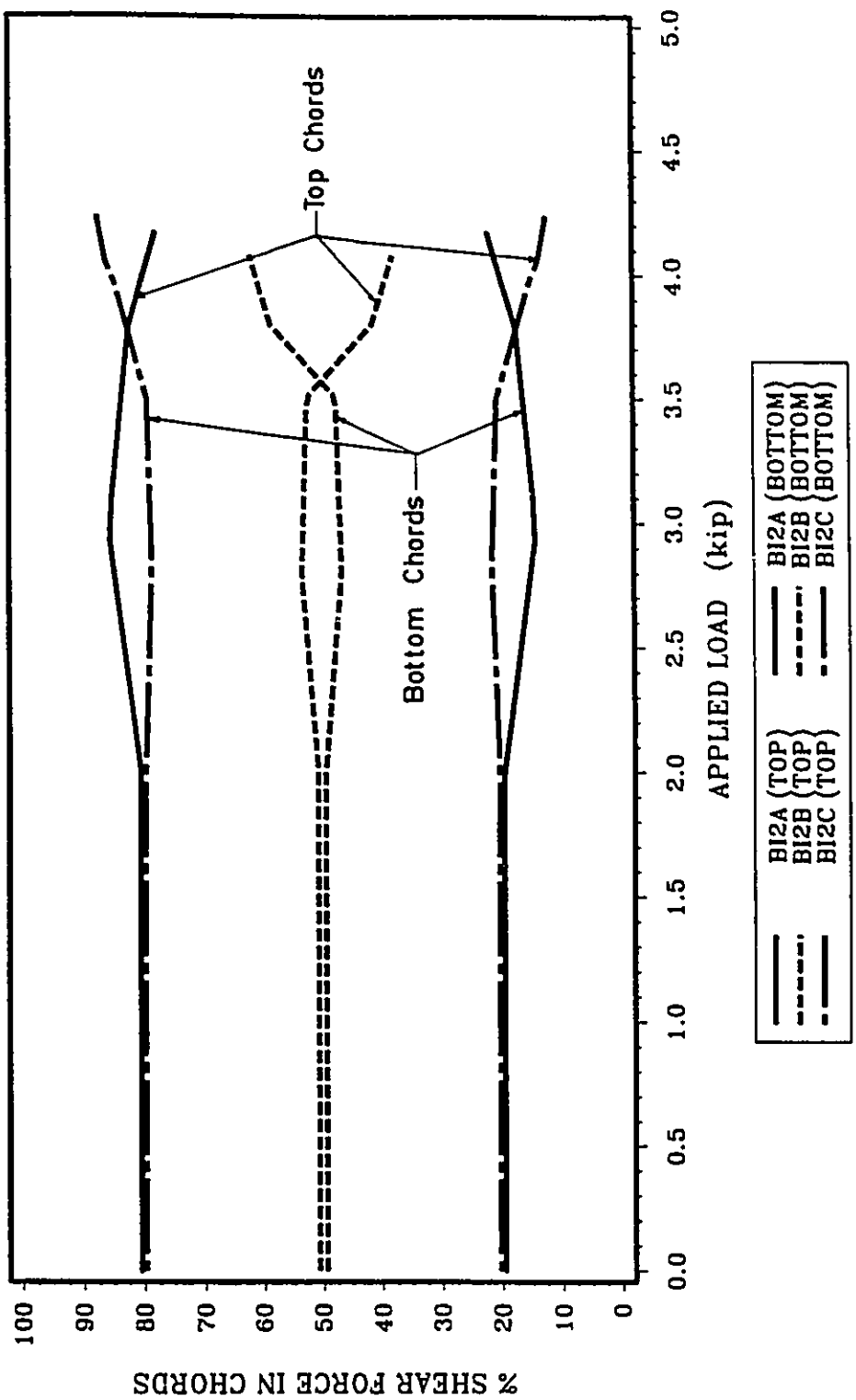
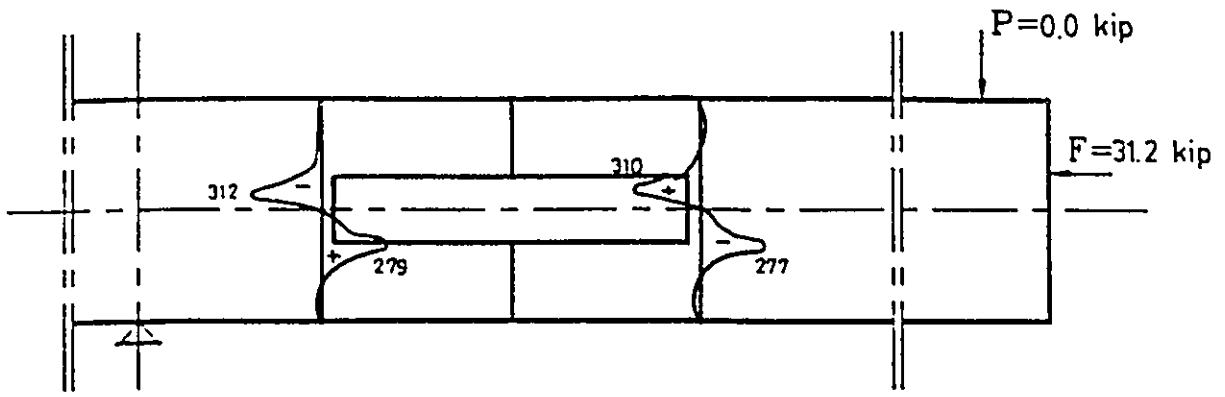
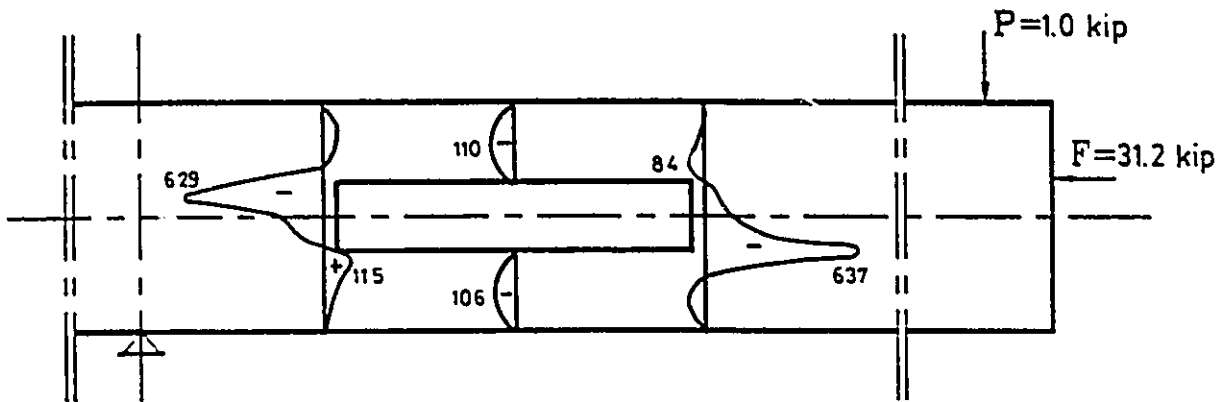


FIG. 5.137 DISTRIBUTION OF SHEAR FORCE BETWEEN TOP AND BOTTOM CHORDS FOR GROUP BI2

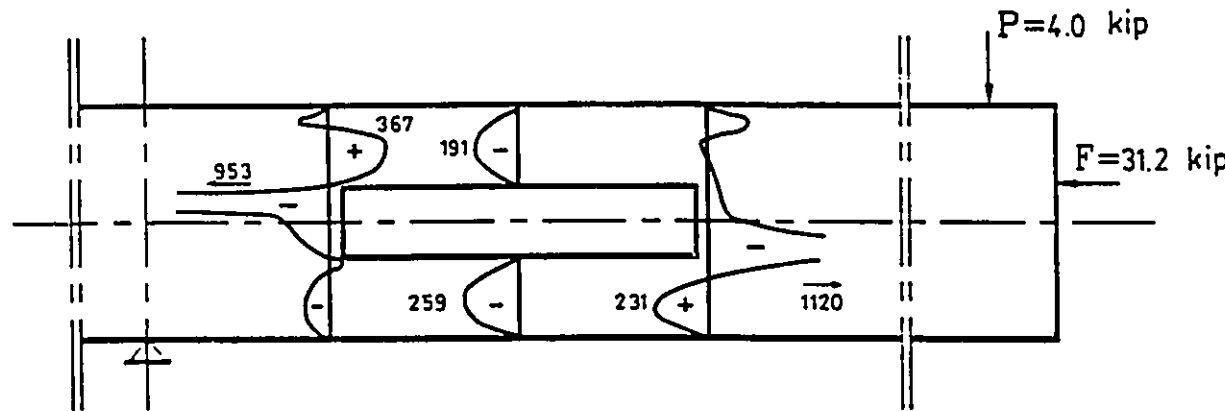
Note: 1 kip=4.45 kN



(a) TRANSFER STAGE



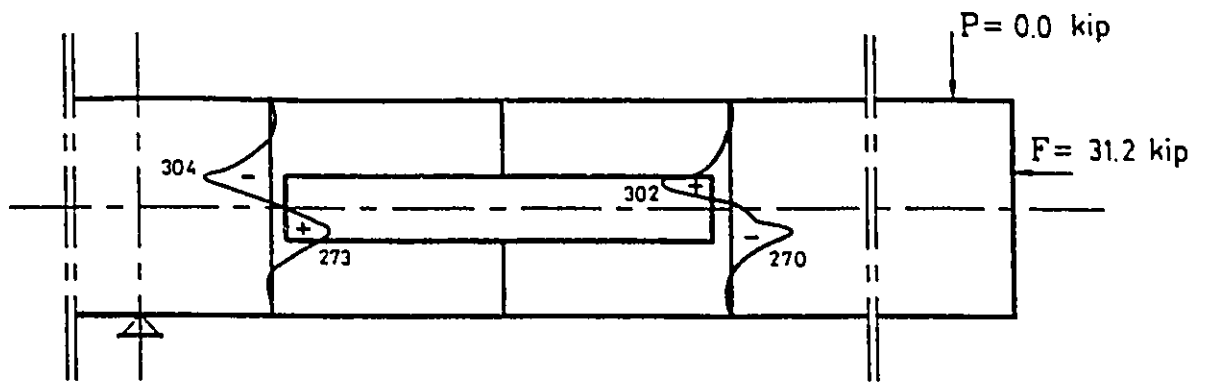
(b) WORKING STAGE



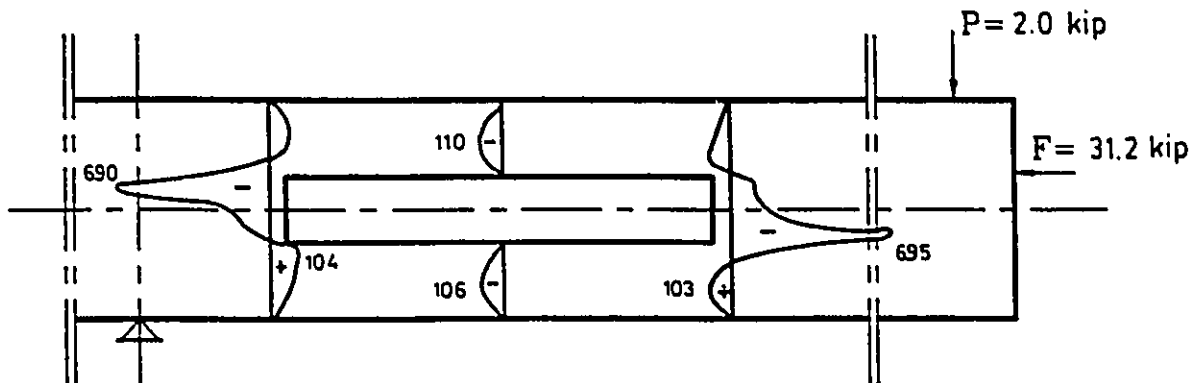
(c) ULTIMATE STAGE

FIG. 5.138 SHEAR STRESS DISTRIBUTION FOR BEAM B13B

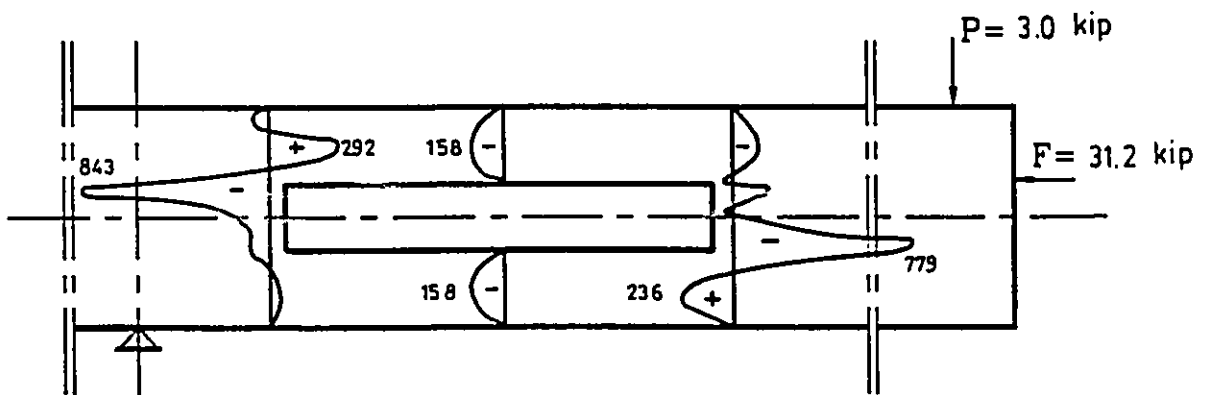
Note: stresses are shown in psi; 1 psi=6.89 kPa; 1 kip=4.45 kN



(a) TRANSFER STAGE



(b) WORKING STAGE



(c) ULTIMATE STAGE

FIG. 5.139 SHEAR STRESS DISTRIBUTION FOR BEAM B13C

Note: stresses are shown in psi; 1 psi=6.89 kPa; 1 kip=4.45 kN

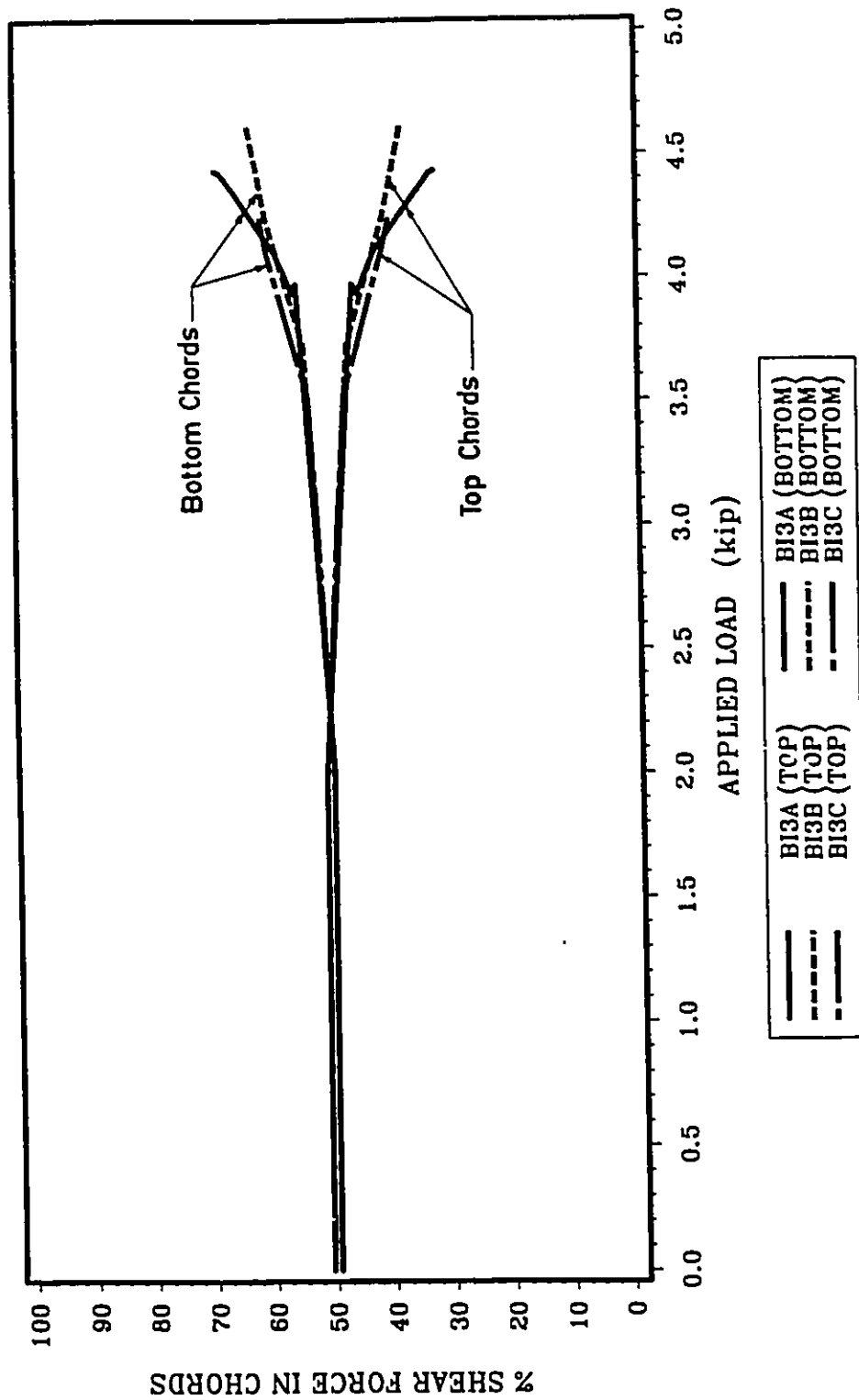
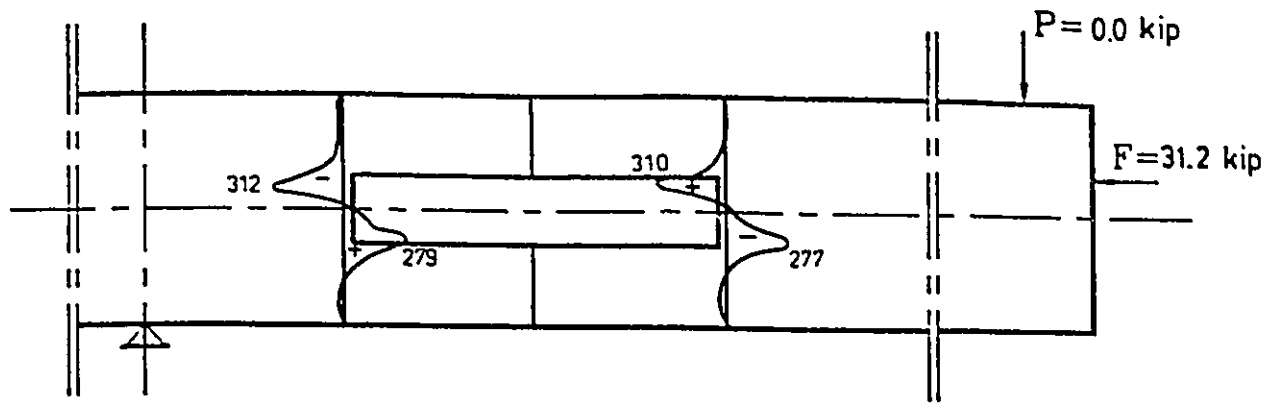
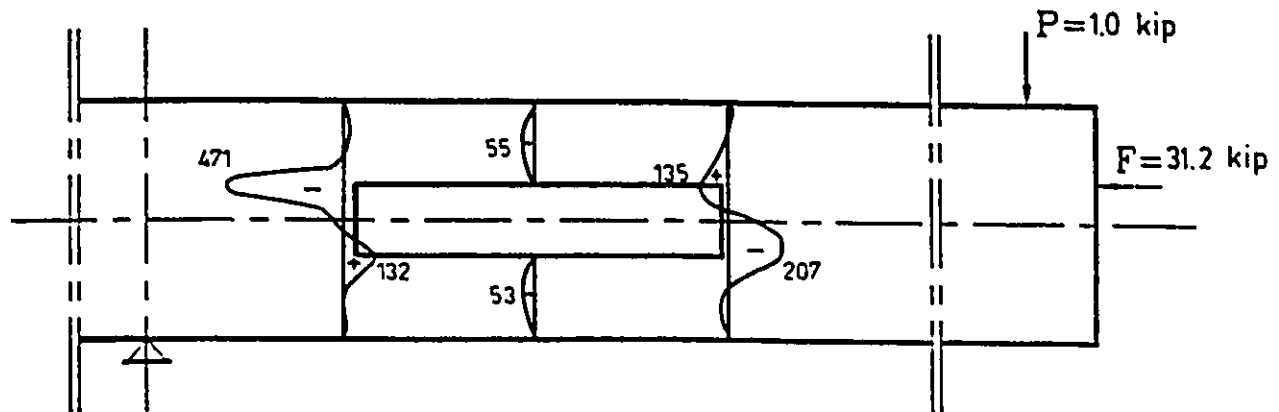


FIG. 5.140 DISTRIBUTION OF SHEAR FORCE BETWEEN TOP AND BOTTOM CHORDS FOR GROUP B13

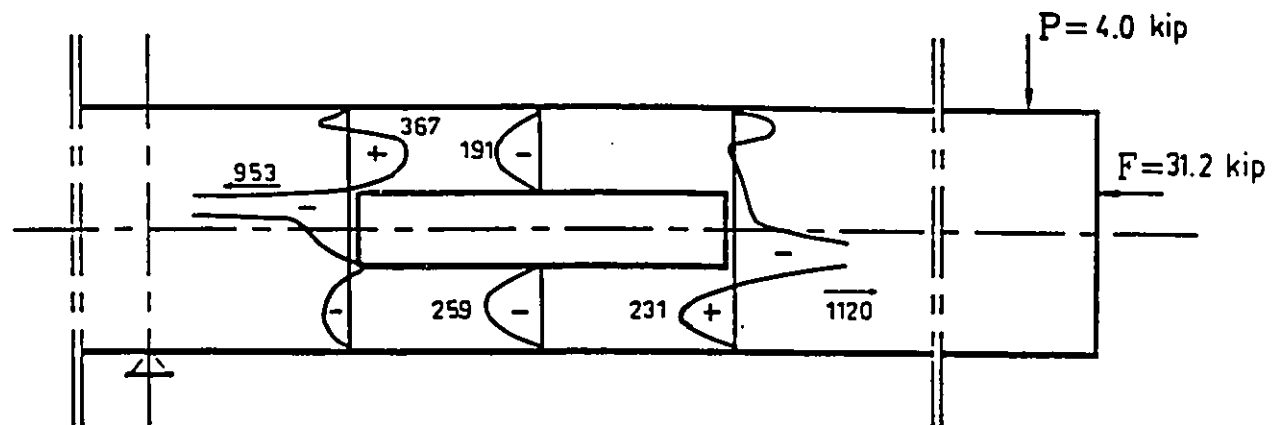
Note: 1 kip=4.45 kN



(a) TRANSFER STAGE



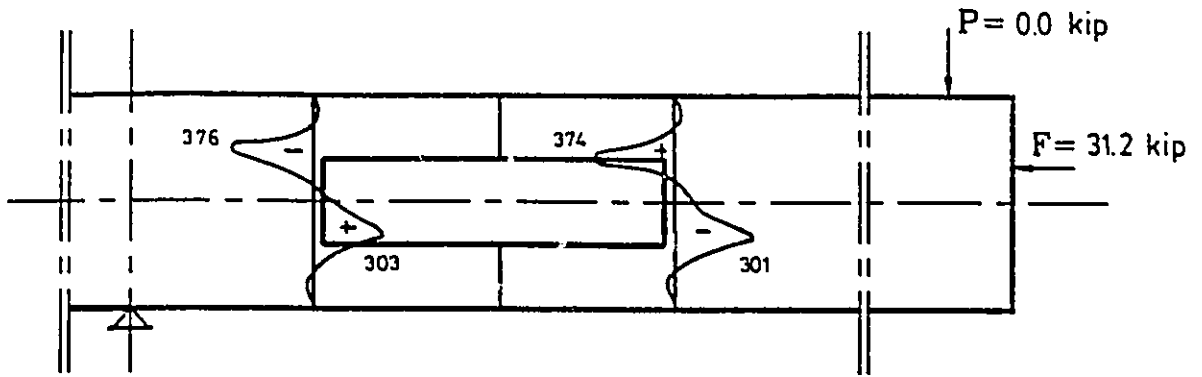
(b) WORKING STAGE



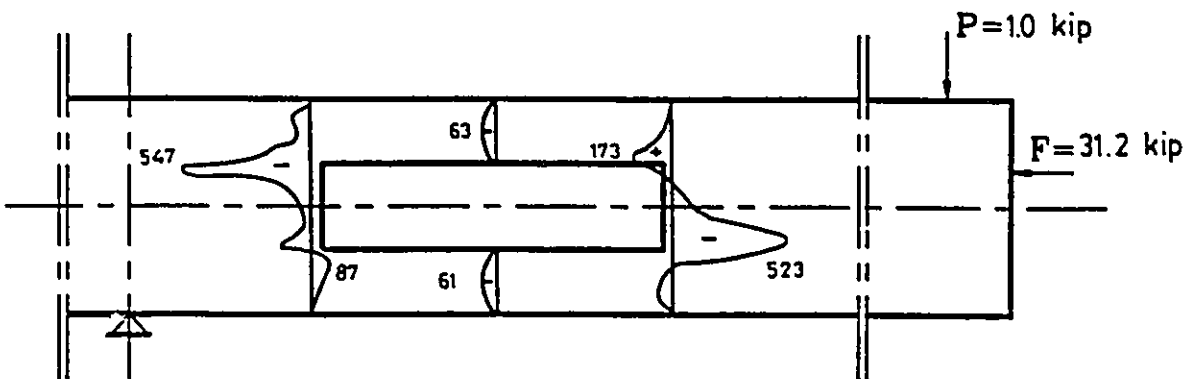
(c) ULTIMATE STAGE

FIG. 5.141 SHEAR STRESS DISTRIBUTION FOR BEAM B14A

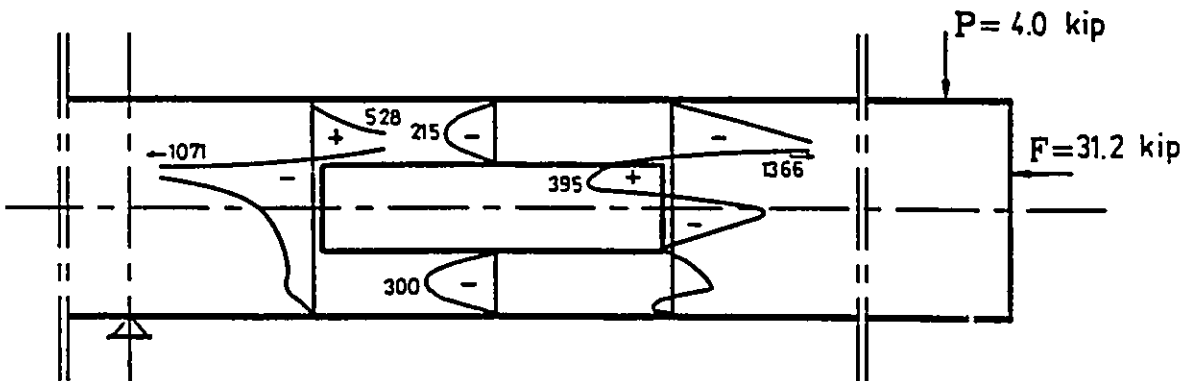
Note: stresses are shown in psi; 1 psi=6.89 kPa; 1 kip=4.45 kN



(a) TRANSFER STAGE



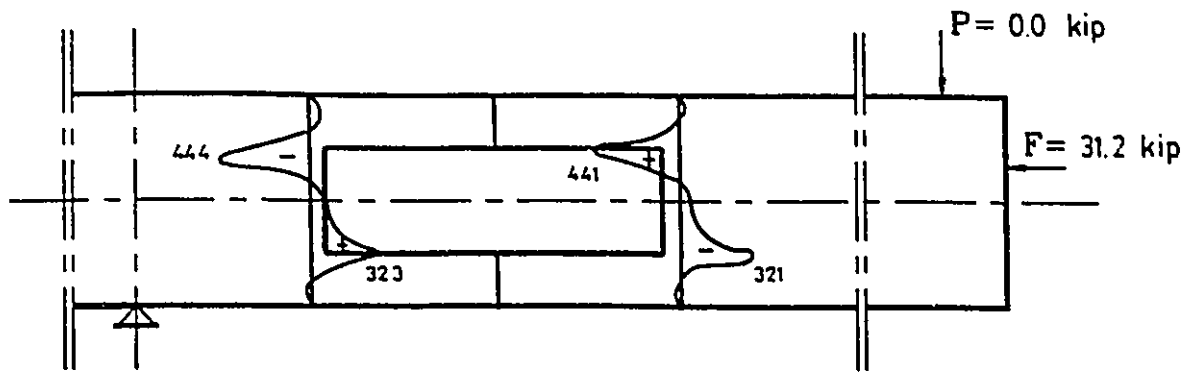
(b) WORKING STAGE



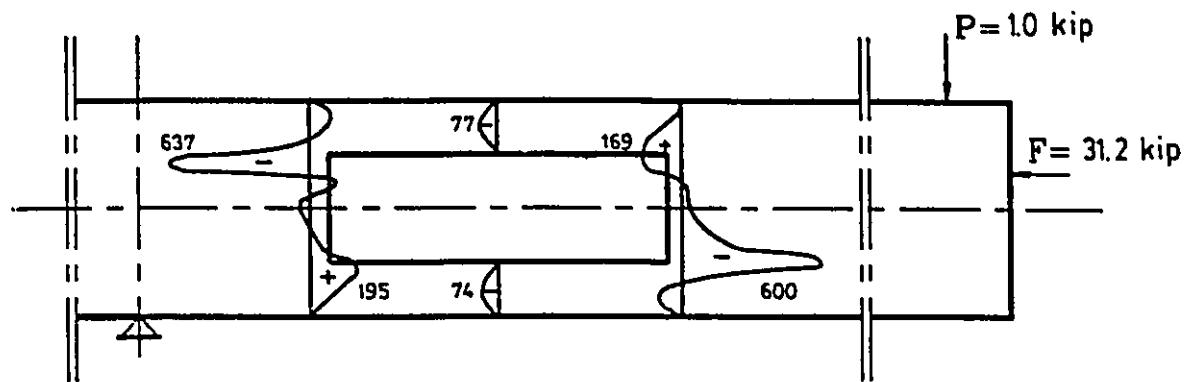
(c) ULTIMATE STAGE

FIG. 5.142 SHEAR STRESS DISTRIBUTION FOR BEAM BI4B

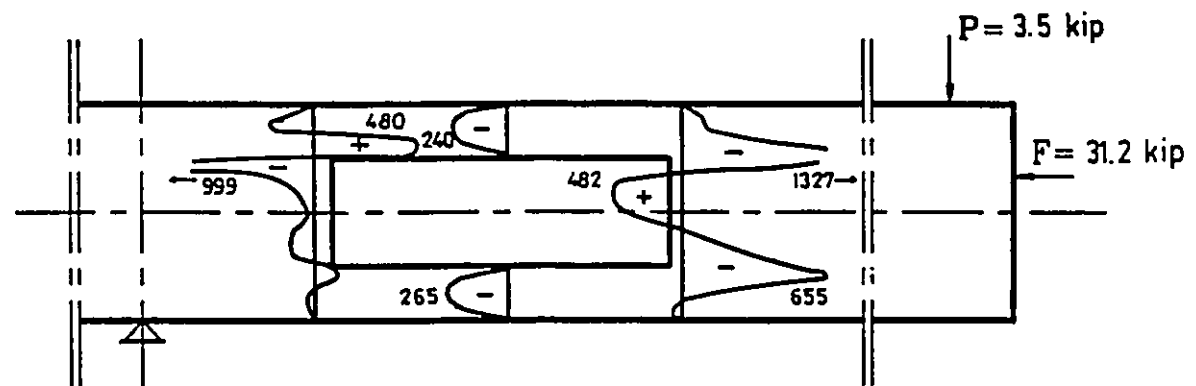
Note: stresses are shown in psi; 1 psi=6.89 kPa; 1 kip=4.45 kN



(a) TRANSFER STAGE



(b) WORKING STAGE



(c) ULTIMATE STAGE

FIG. 5.143 SHEAR STRESS DISTRIBUTION FOR BEAM B14C

Note: stresses are shown in psi; 1 psi=6.89 kPa; 1 kip=4.45 kN

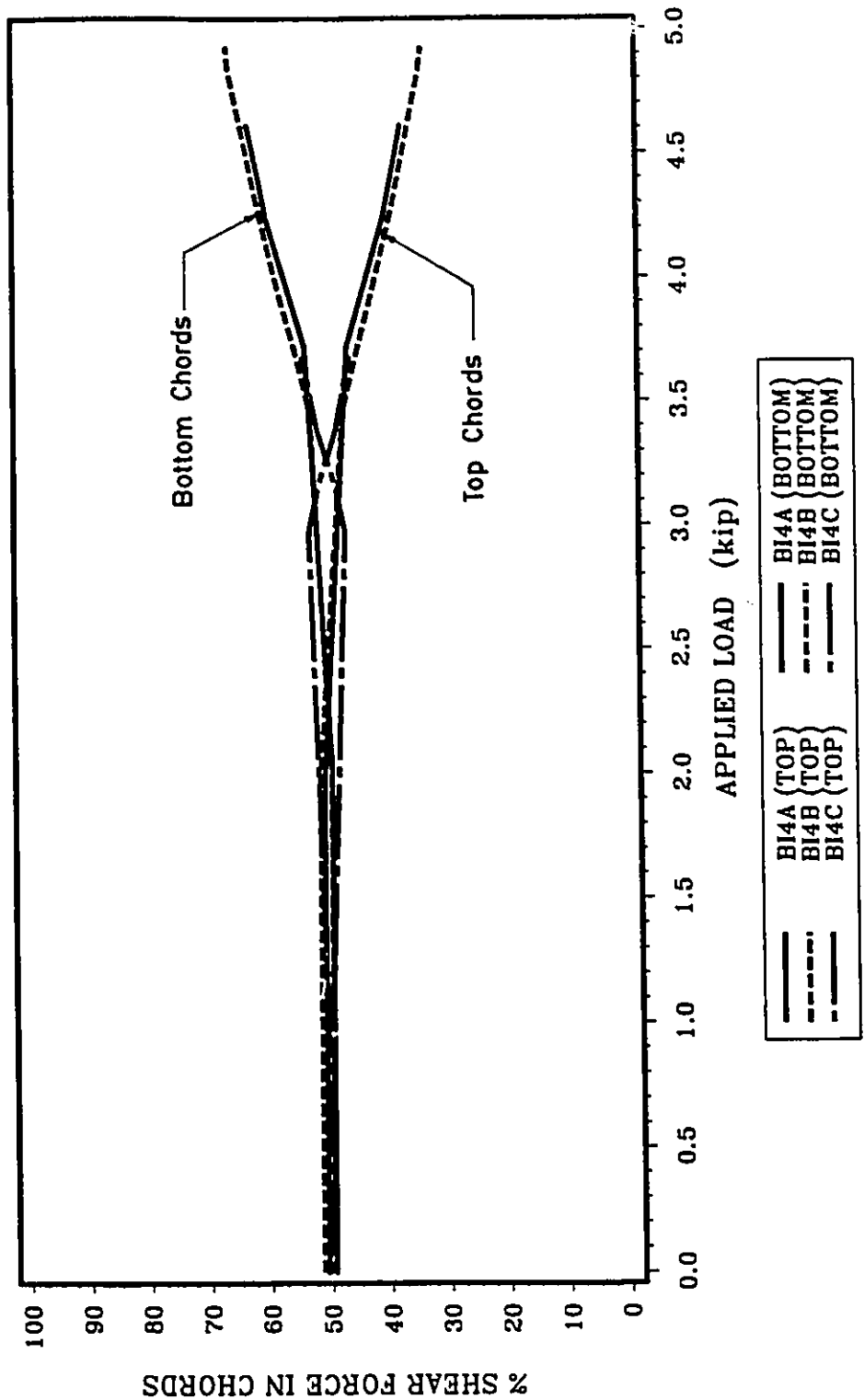


FIG. 5.144 DISTRIBUTION OF SHEAR FORCE BETWEEN TOP AND BOTTOM CHORDS FOR GROUP BI4

Note: 1 kip=4.45 kN

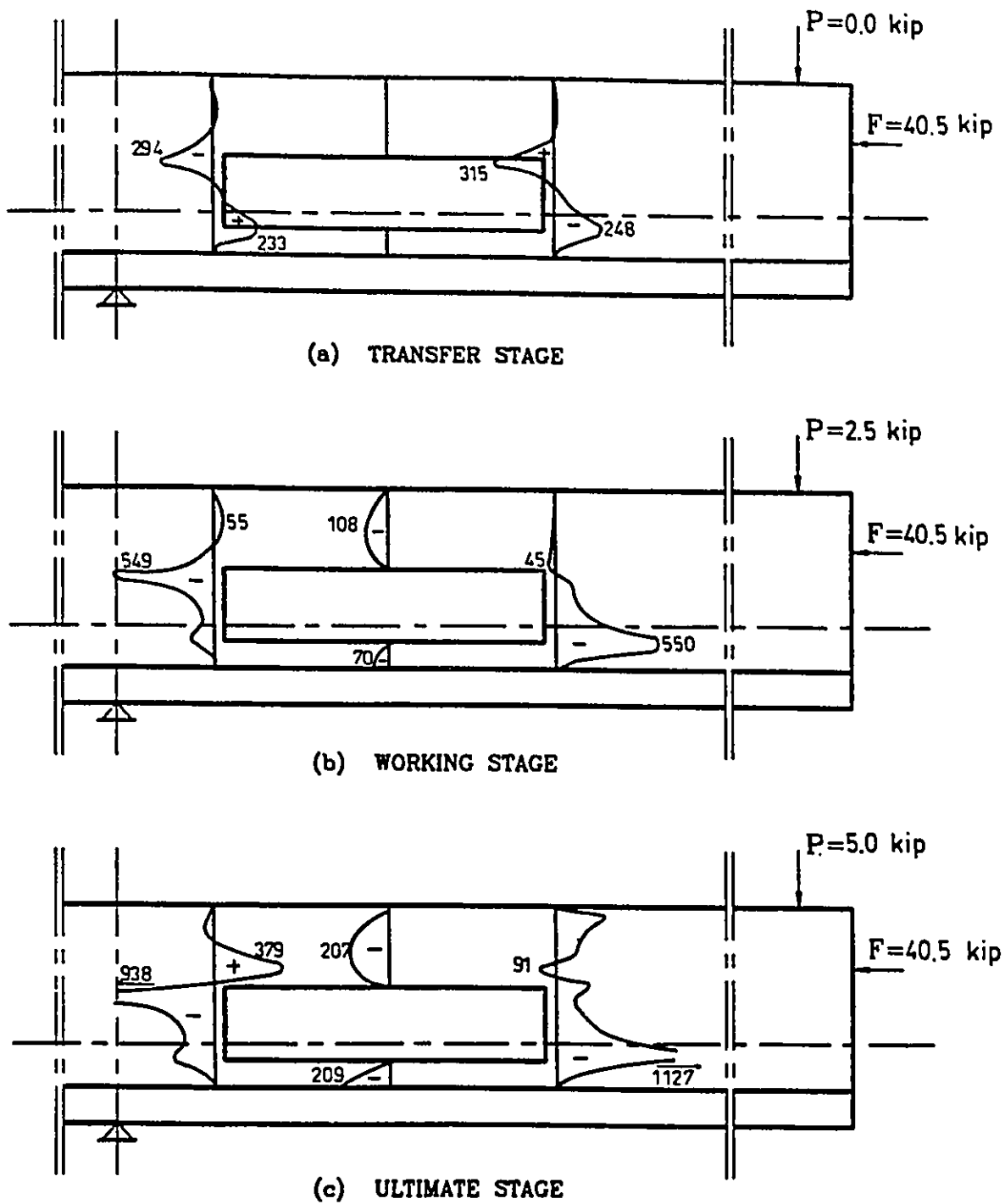


FIG. 5.145 SHEAR STRESS DISTRIBUTION FOR BEAM B11A

Note: stresses are shown in psi; 1 psi=6.89 kPa; 1 kip=4.45 kN

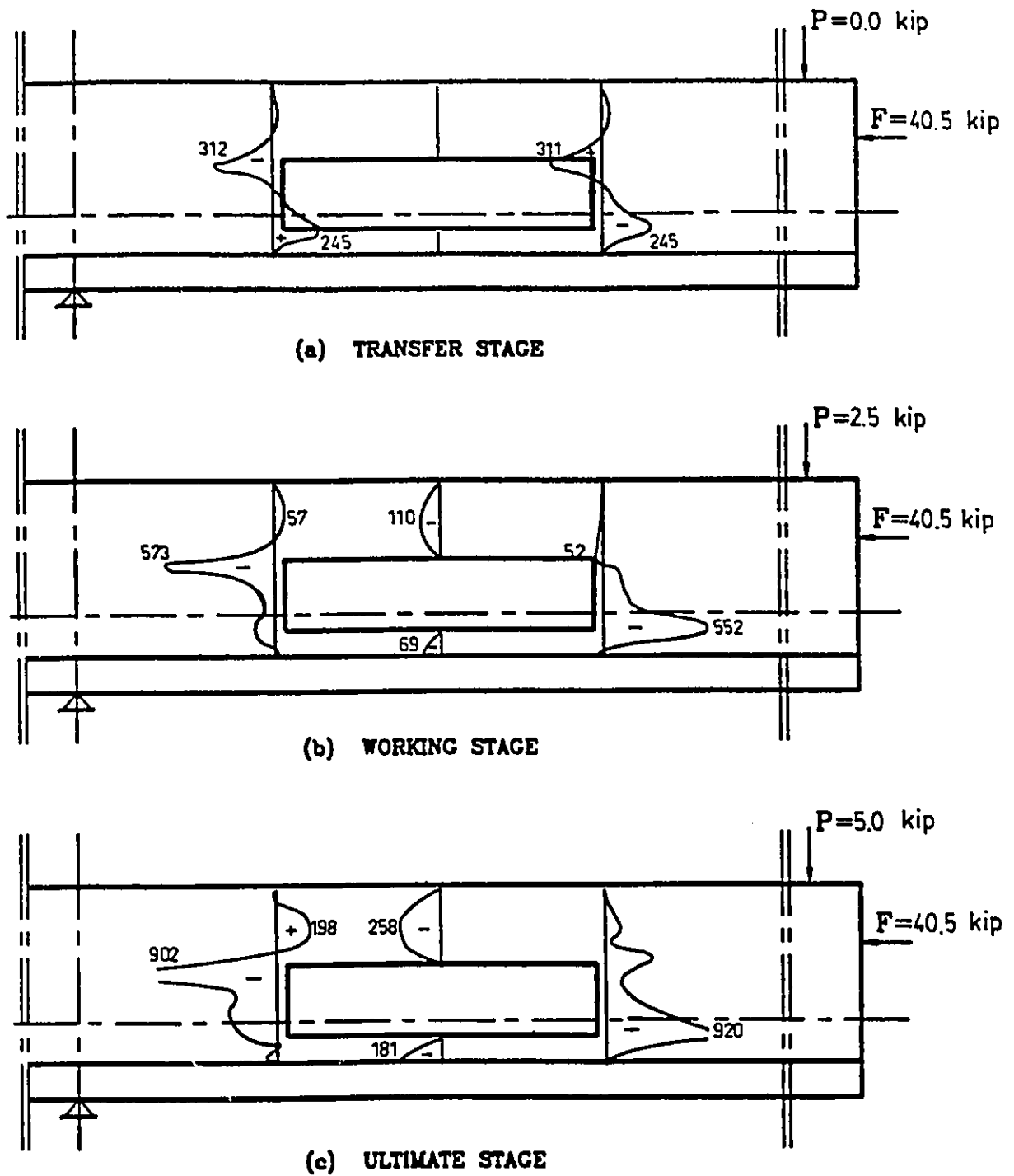


FIG. 5.146 SHEAR STRESS DISTRIBUTION FOR BEAMS
BII1B, BII2A, BII3B & BII4B

Note: stresses are shown in psi; 1 psi=6.89 kPa; 1 kip=4.45 kN

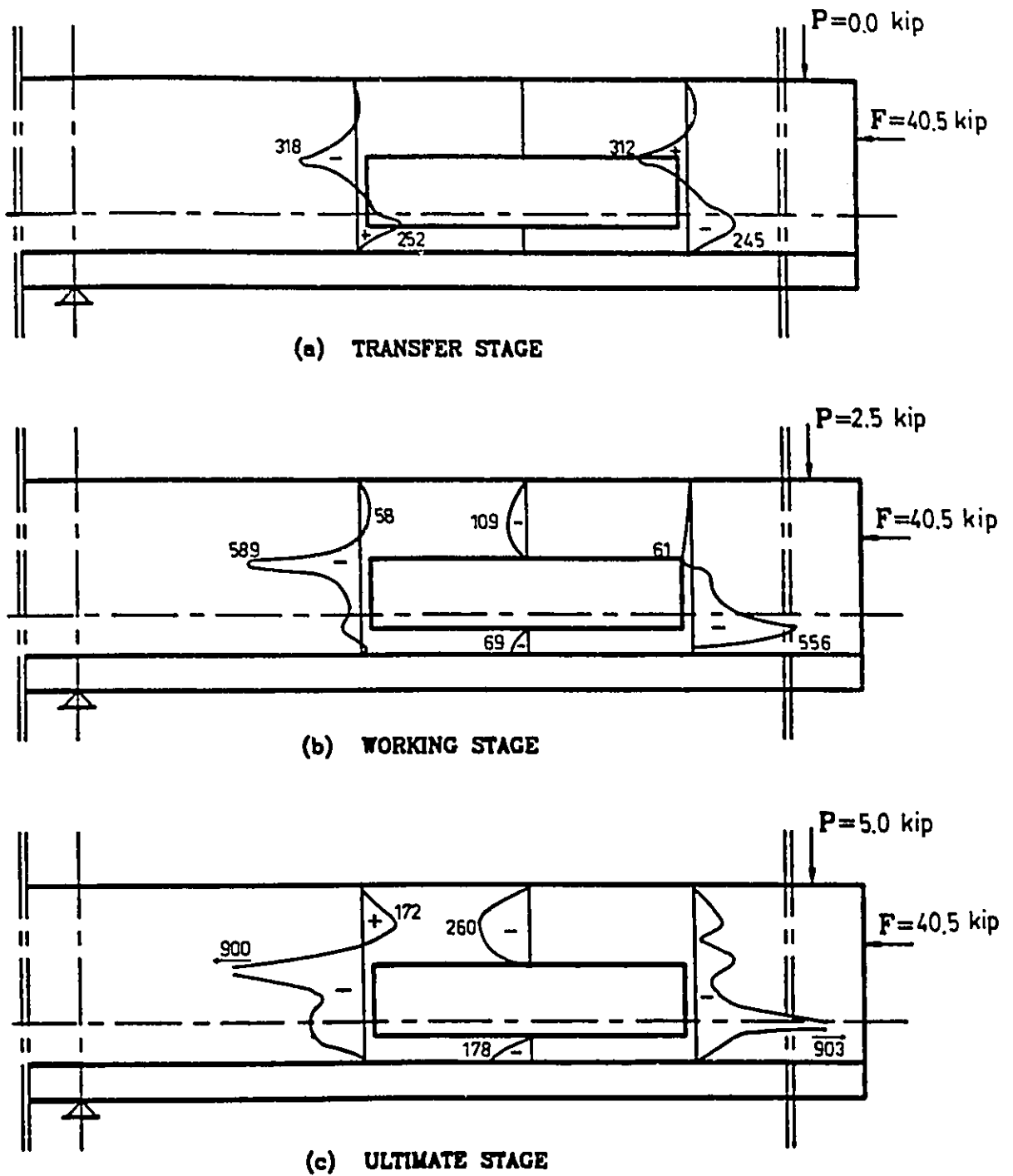


FIG. 5.147 SHEAR STRESS DISTRIBUTION FOR BEAM BIIc

Note: stresses are shown in psi; 1 psi=6.89 kPa; 1 kip=4.45 kN

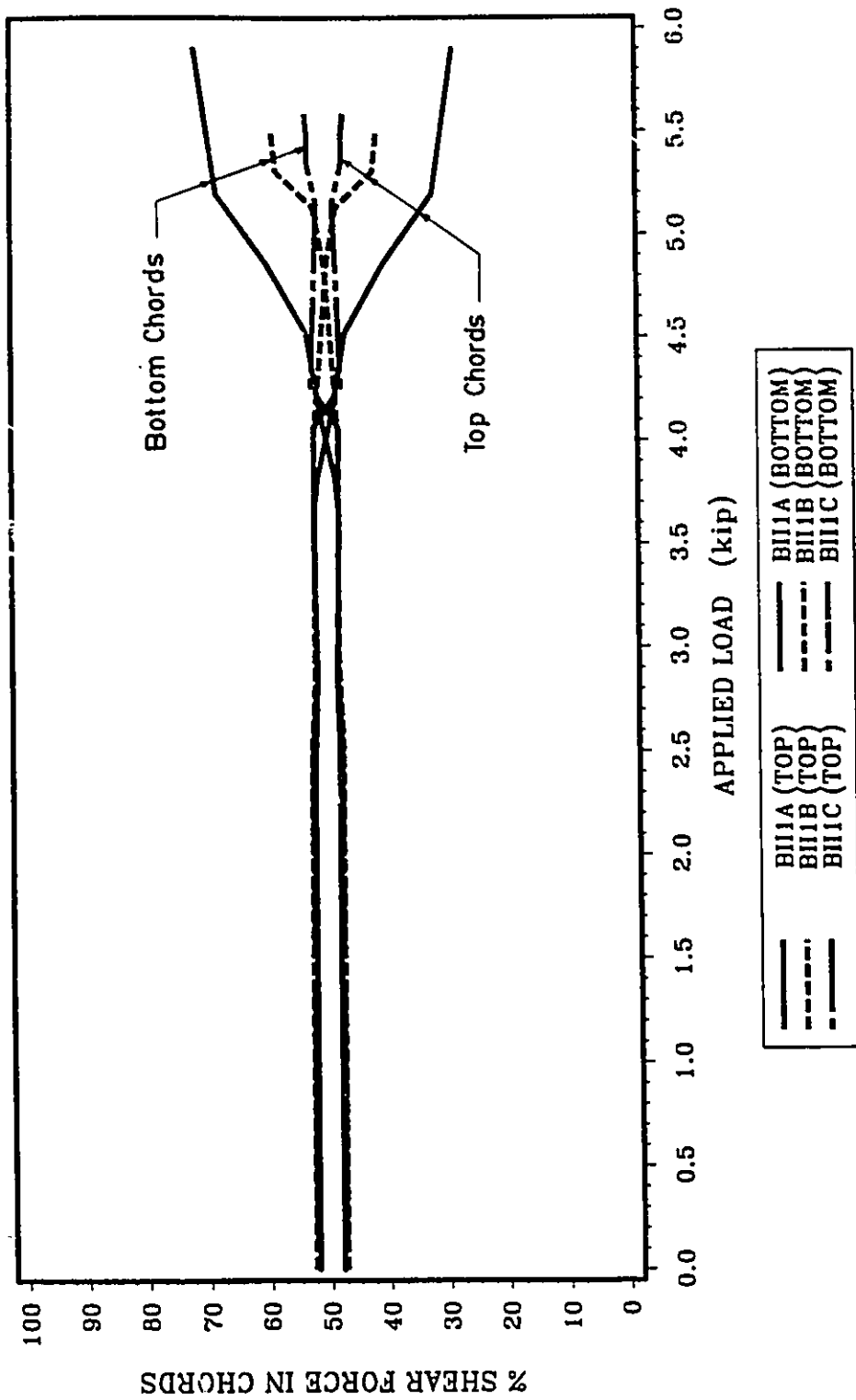


FIG. 5.148 DISTRIBUTION OF SHEAR FORCE BETWEEN TOP AND BOTTOM CHORDS FOR GROUP BII1

Note: 1 kip=4.45 kN

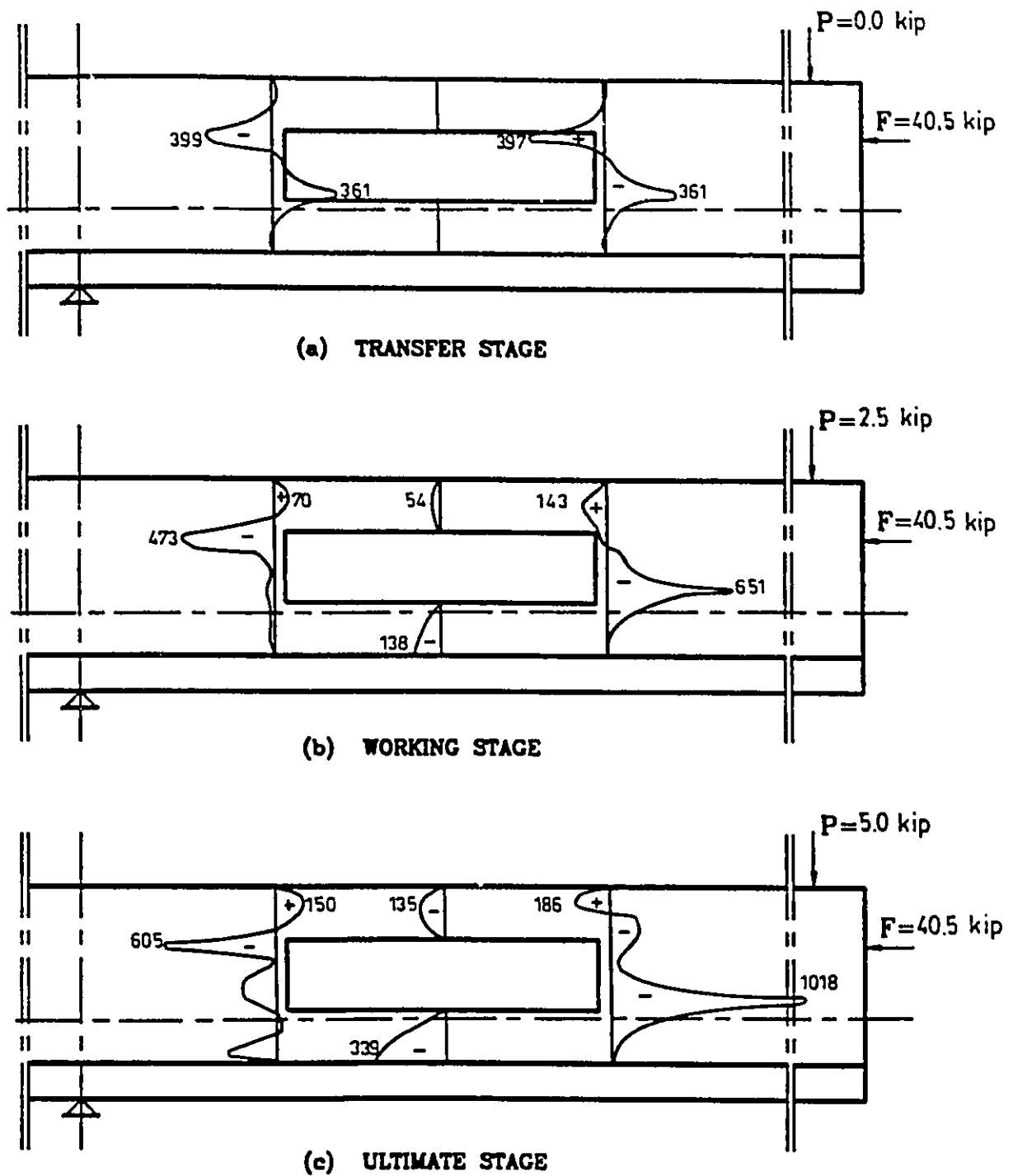


FIG. 5.149 SHEAR STRESS DISTRIBUTION FOR BEAM B112B

Note: stresses are shown in psi; 1 psi=6.89 kPa; 1 kip=4.45 kN

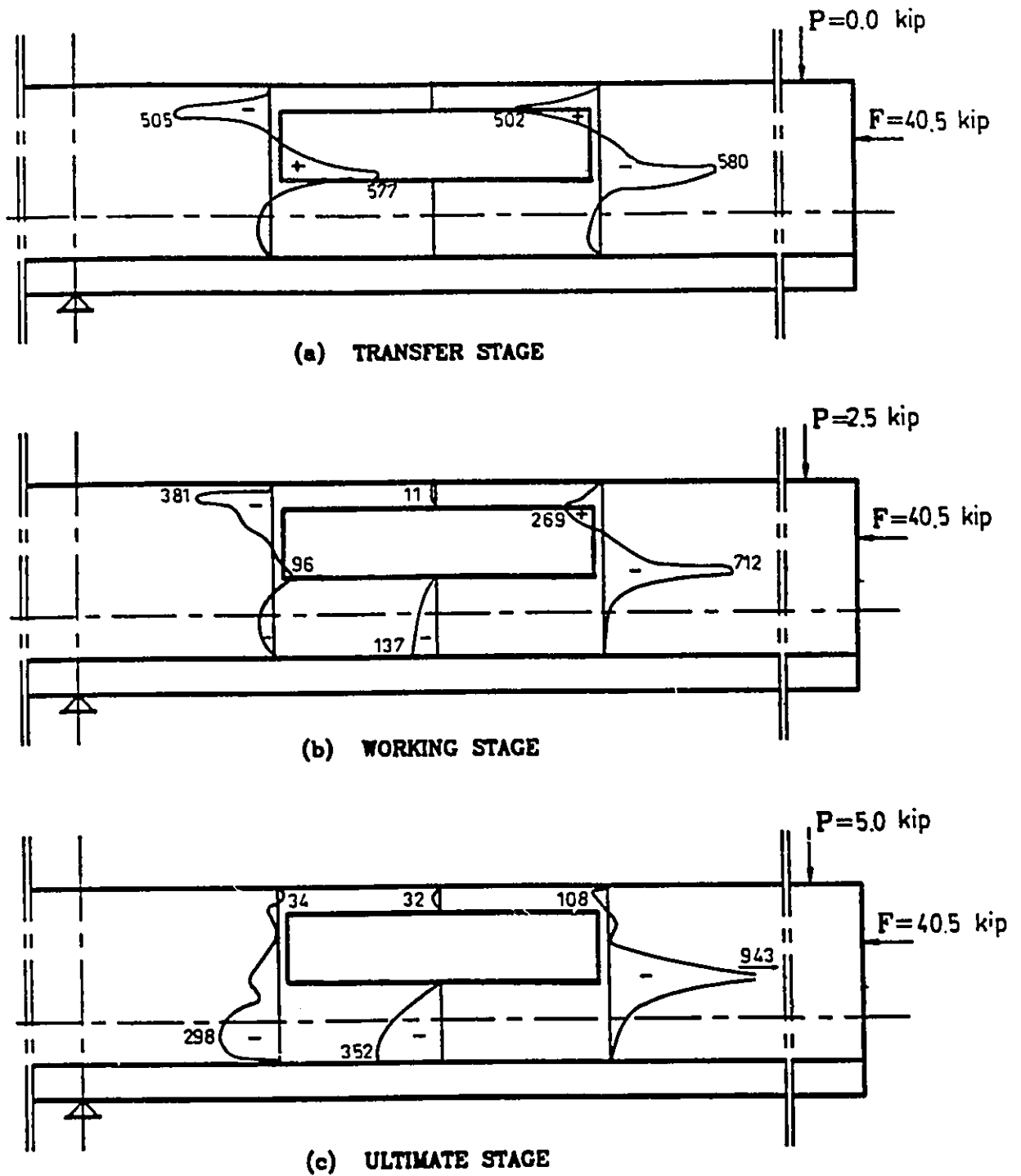


FIG. 5.150 SHEAR STRESS DISTRIBUTION FOR BEAM BE2C

Note: stresses are shown in psi; 1 psi=6.89 kPa; 1 kip=4.45 kN

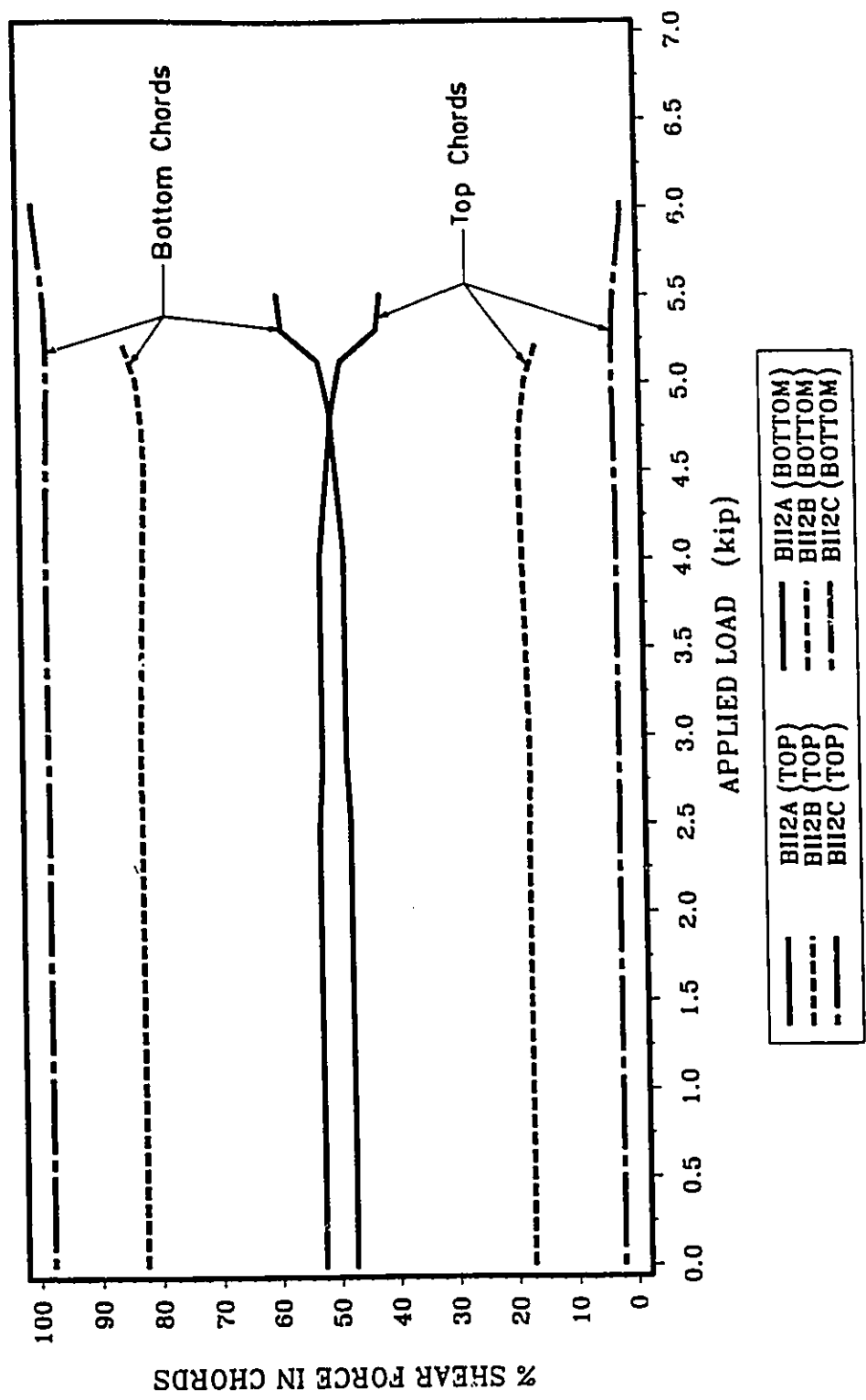


FIG. 5.151 DISTRIBUTION OF SHEAR FORCE BETWEEN TOP AND BOTTOM CHORDS FOR GROUP BII2

Note: 1 kip=4.45 kN

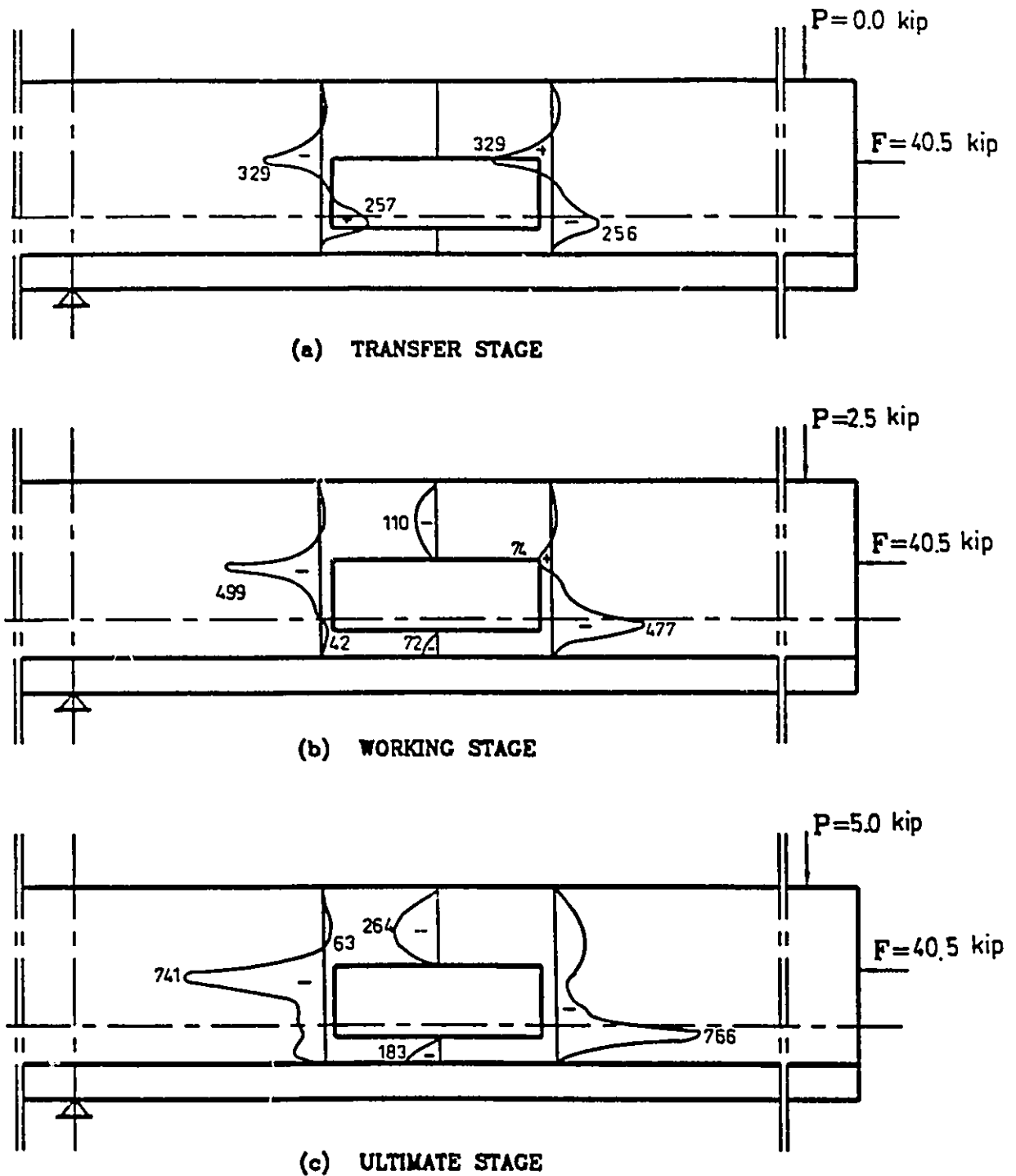


FIG. 5.152 SHEAR STRESS DISTRIBUTION FOR BEAM BII3A

Note: stresses are shown in psi; 1 psi=6.89 kPa; 1 kip=4.45 kN

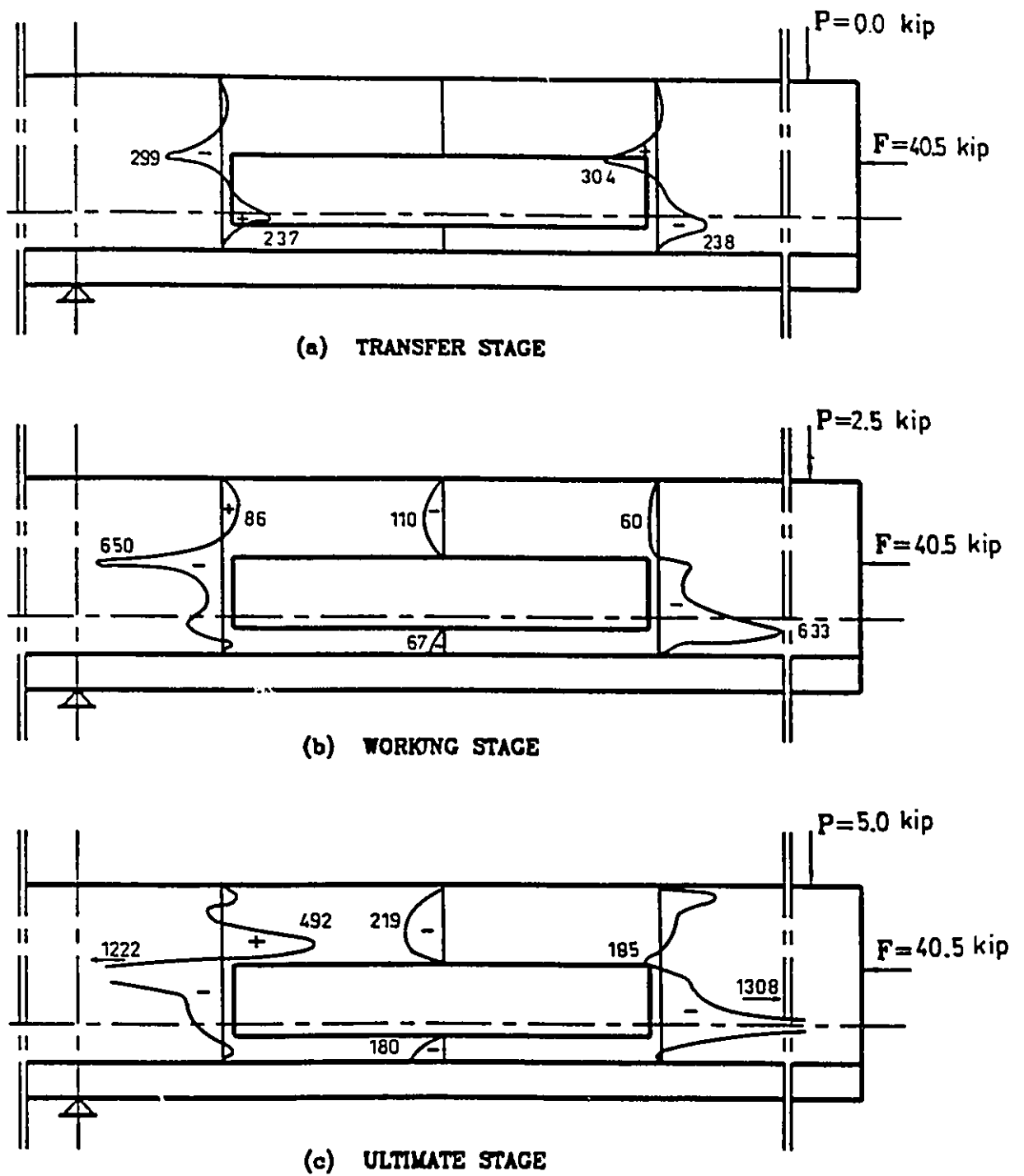


FIG. 5.153 SHEAR STRESS DISTRIBUTION FOR BEAM B113C

Note: stresses are shown in psi; 1 psi=6.89 kPa; 1 kip=4.45 kN

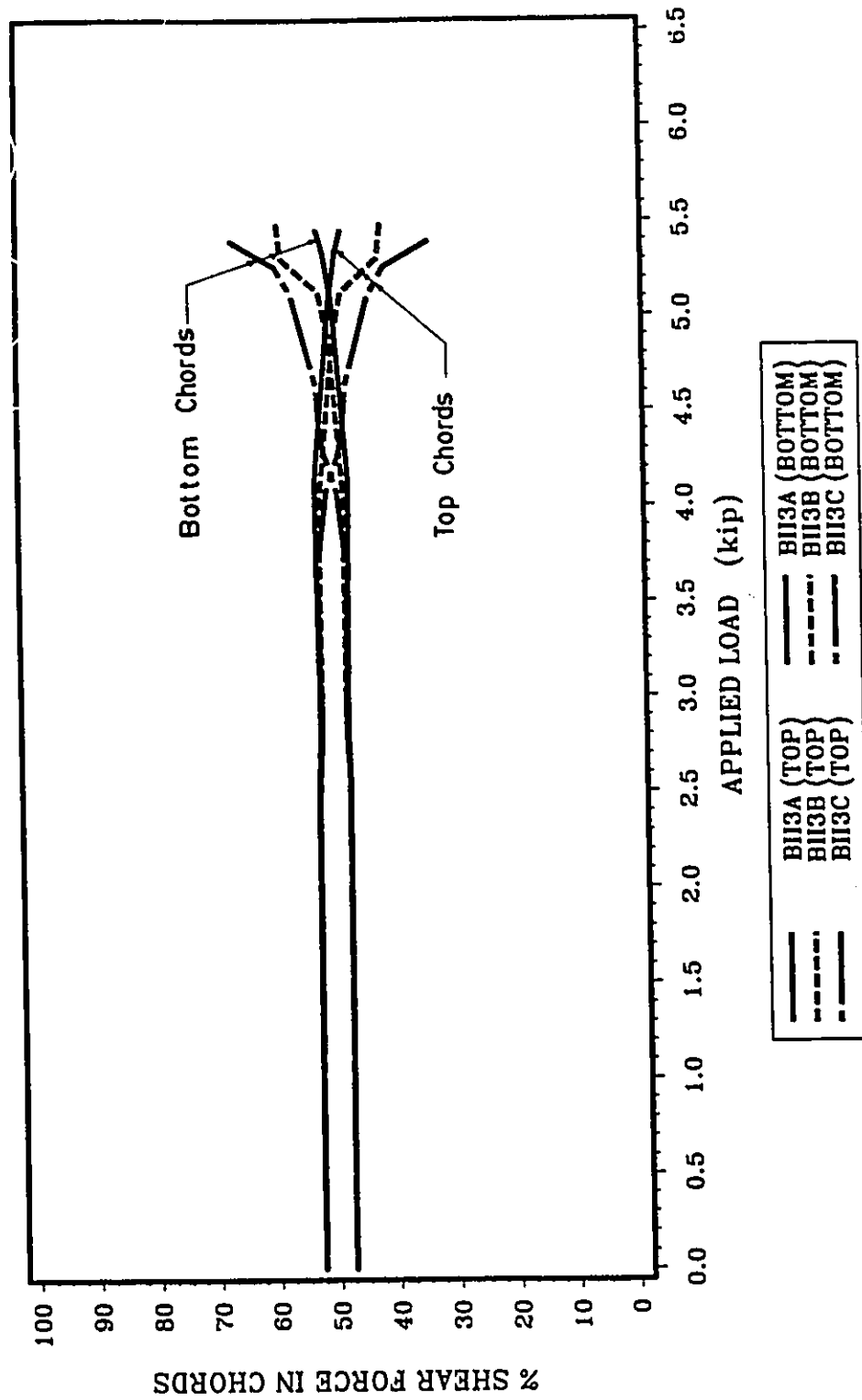


FIG. 5.154 DISTRIBUTION OF SHEAR FORCE BETWEEN TOP AND BOTTOM CHORDS FOR GROUP BII3

Note: 1 kip=4.45 kN

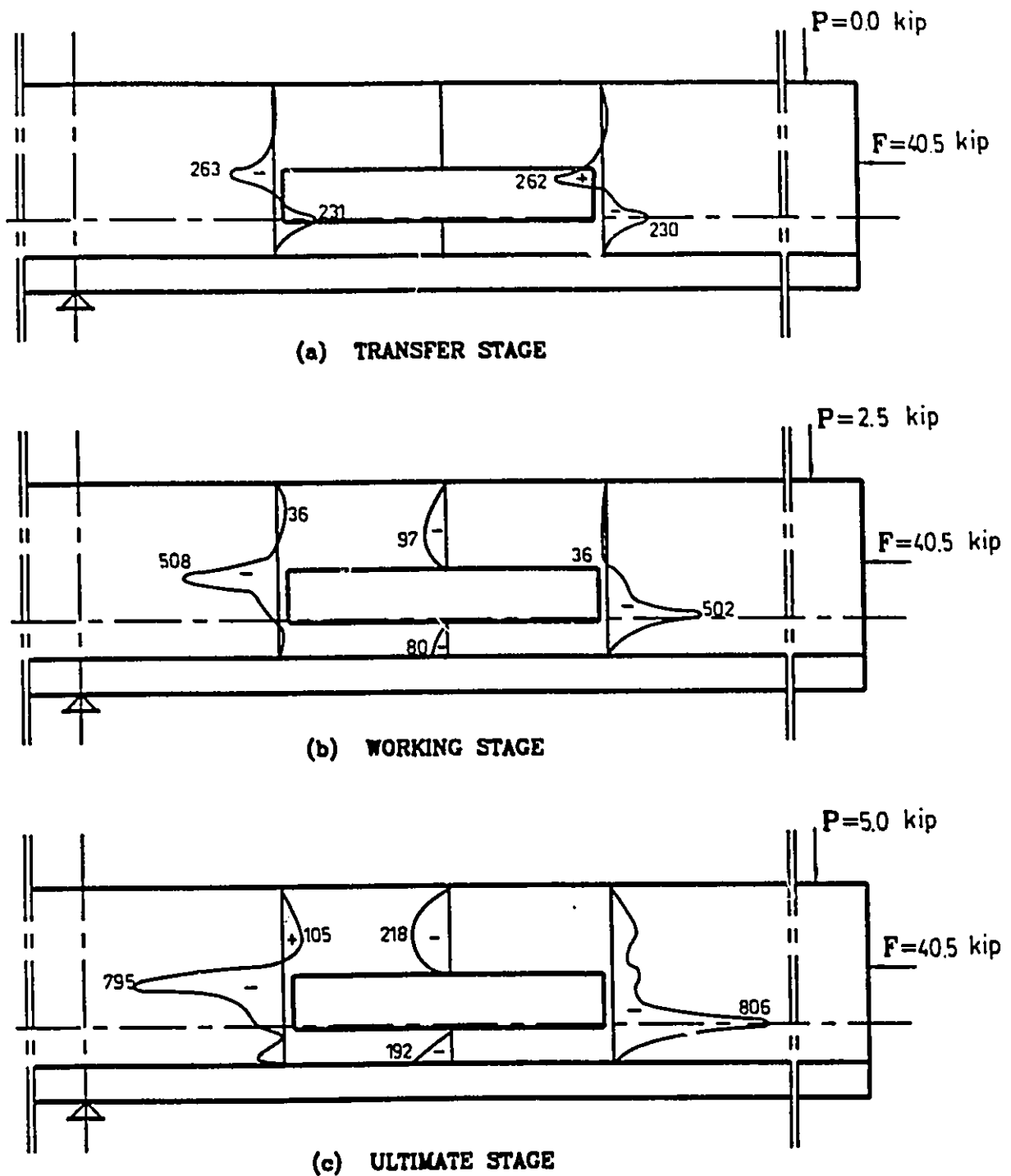


FIG. 5.155 SHEAR STRESS DISTRIBUTION FOR BEAM BII4A

Note: stresses are shown in psi; 1 psi=6.89 kPa; 1 kip=4.45 kN

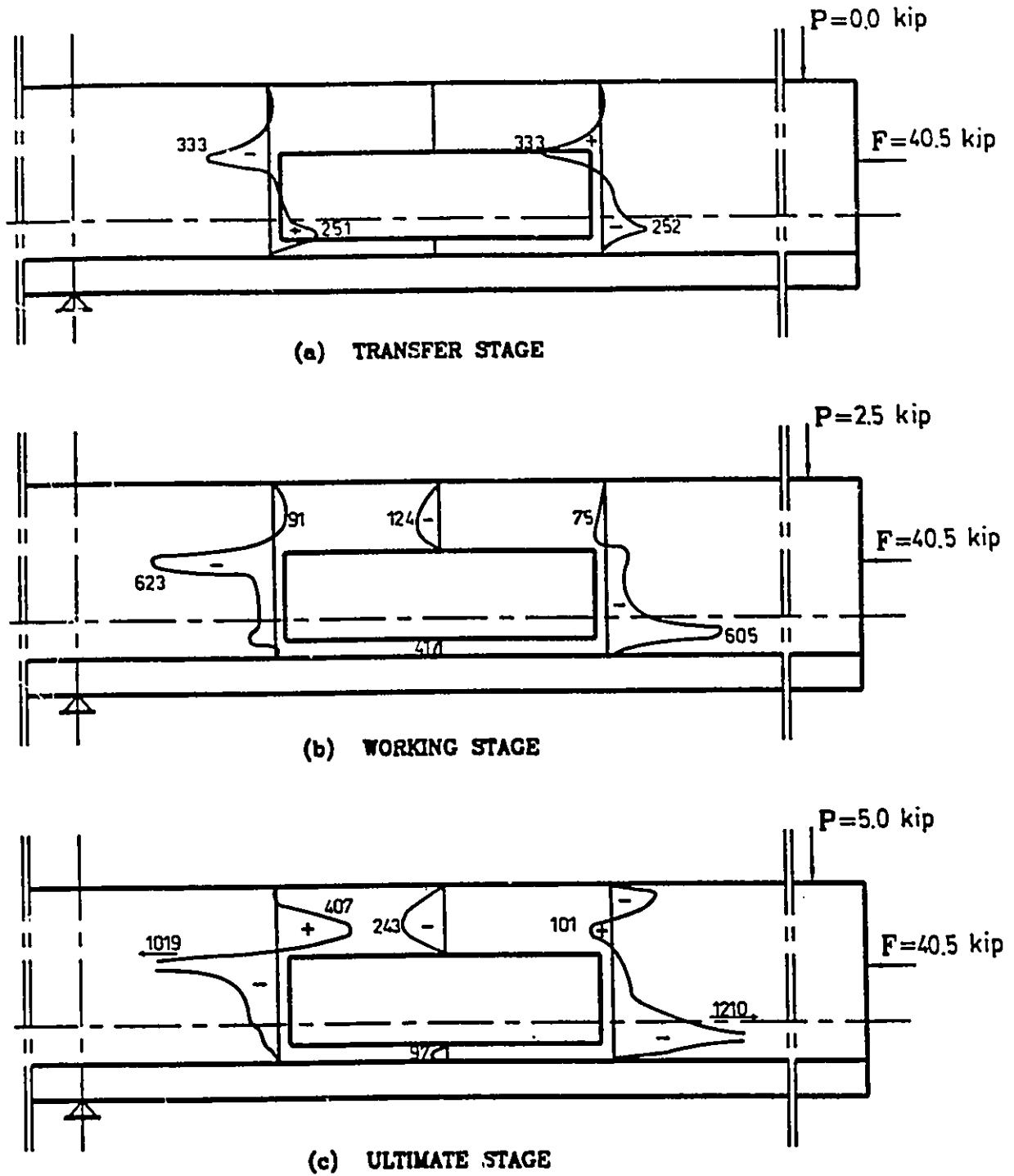


FIG. 5.156 SHEAR STRESS DISTRIBUTION FOR BEAM BII4C

Note: stresses are shown in psi; 1 psi=6.89 kPa; 1 kip=4.45 kN

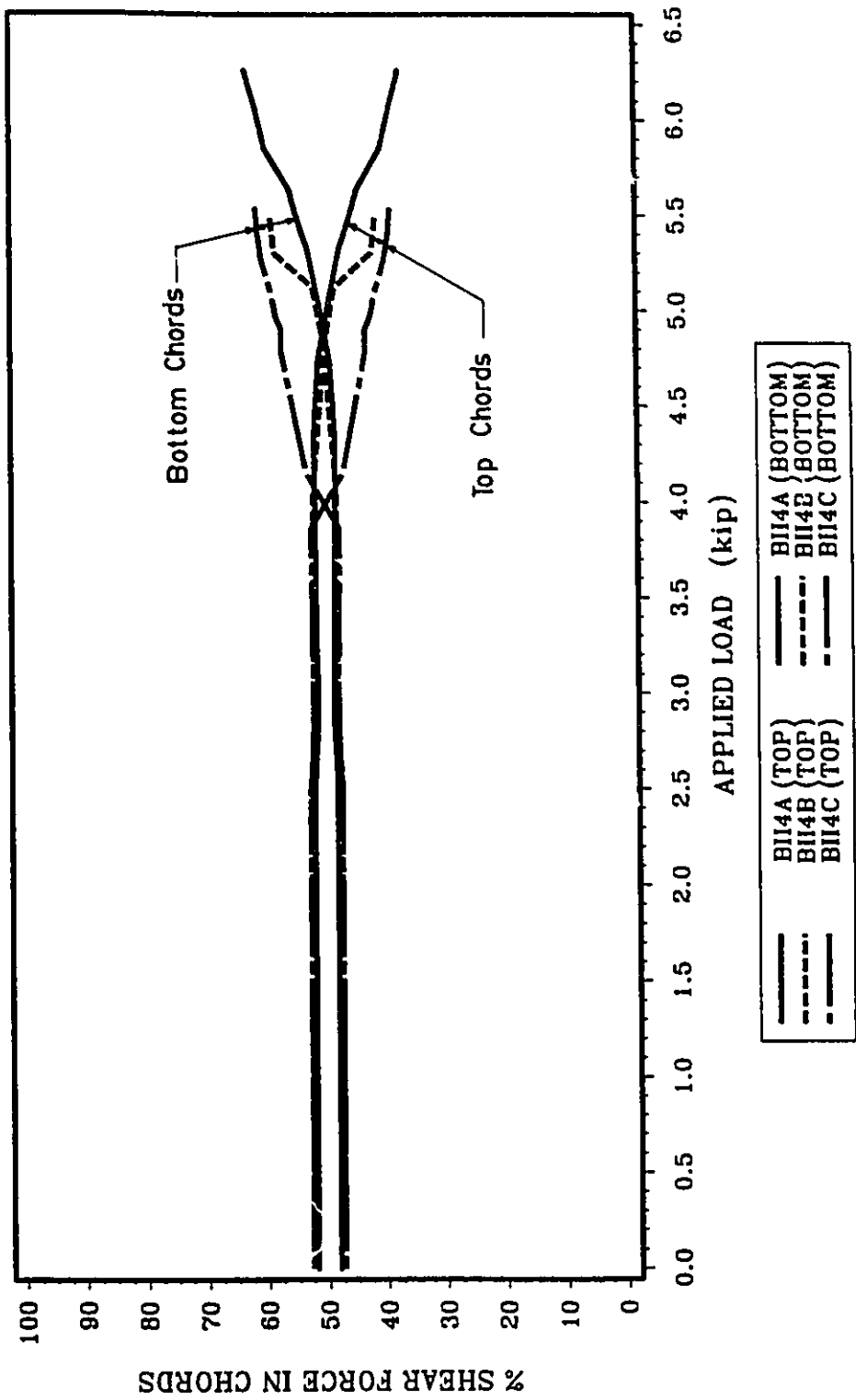


FIG. 5.157 DISTRIBUTION OF SHEAR FORCE BETWEEN TOP AND BOTTOM CHORDS FOR GROUP BII4

Note: 1 kip=4.45 kN

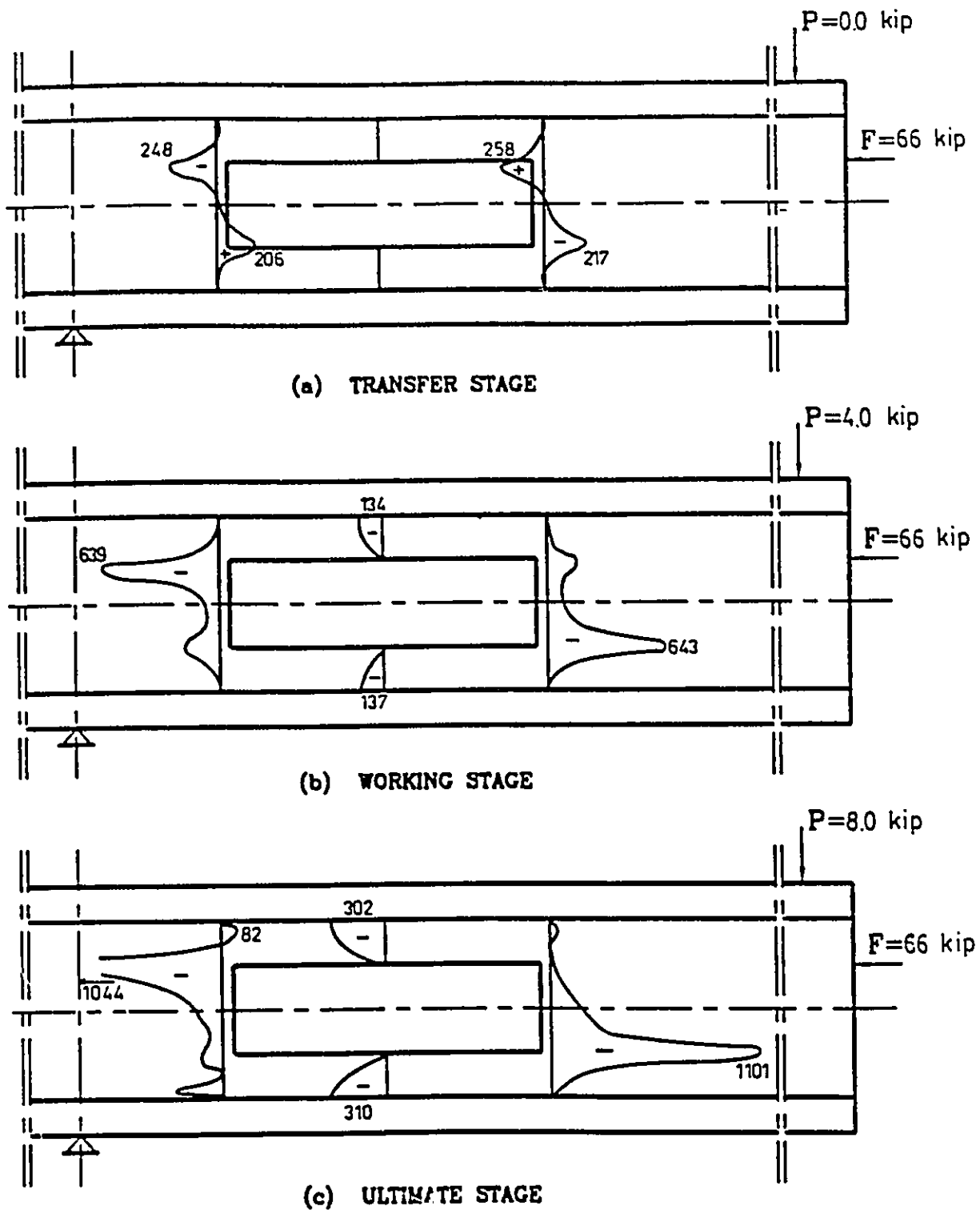


FIG. 5.158 SHEAR STRESS DISTRIBUTION FOR BEAM BIII1A

Note: stresses are shown in psi; 1 psi=6.89 kPa; 1 kip=4.45 kN

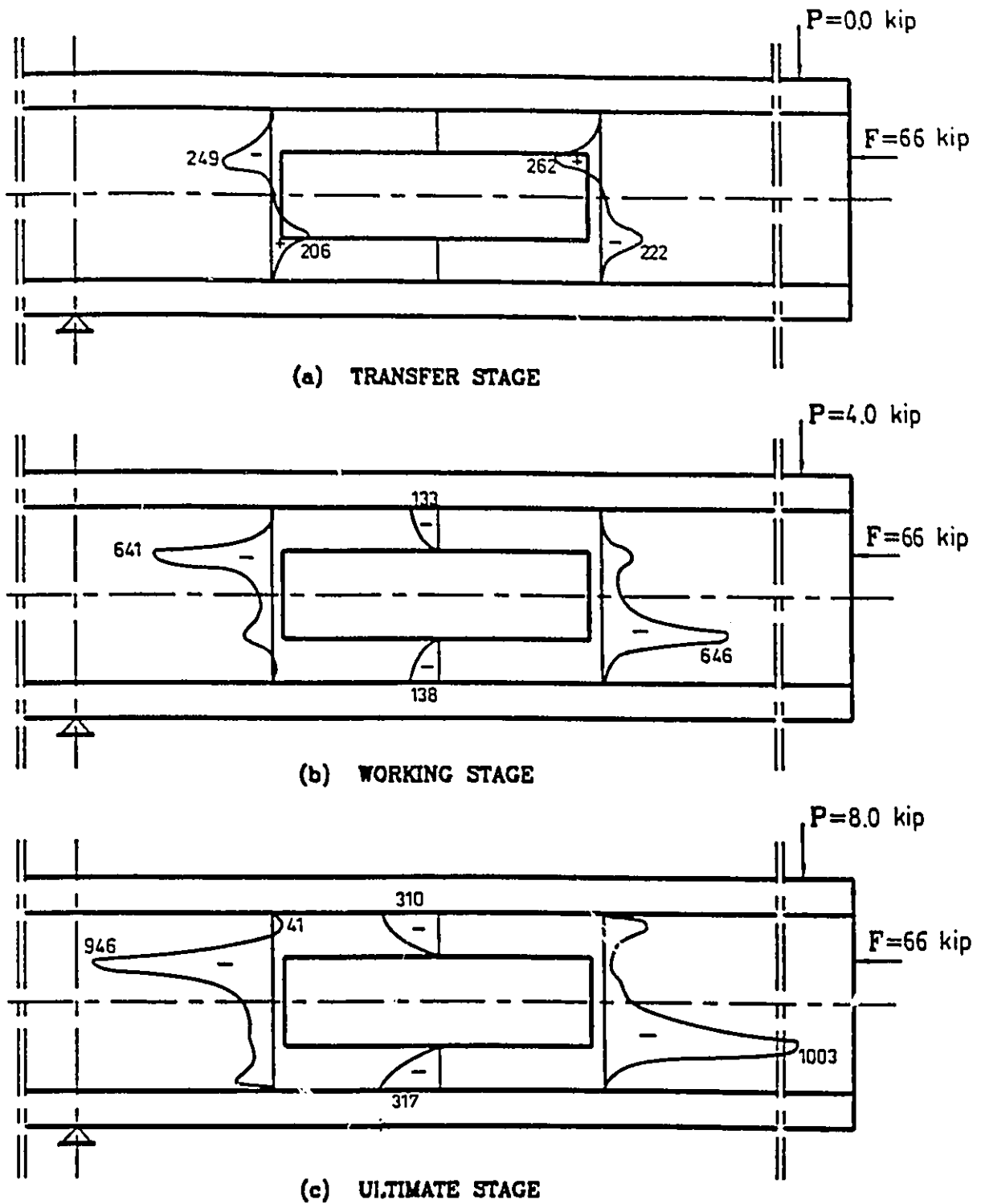


FIG. 5.159 SHEAR STRESS DISTRIBUTION FOR BEAM BIII1B

Note: stresses are shown in psi; 1 psi=6.89 kPa; 1 kip=4.45 kN

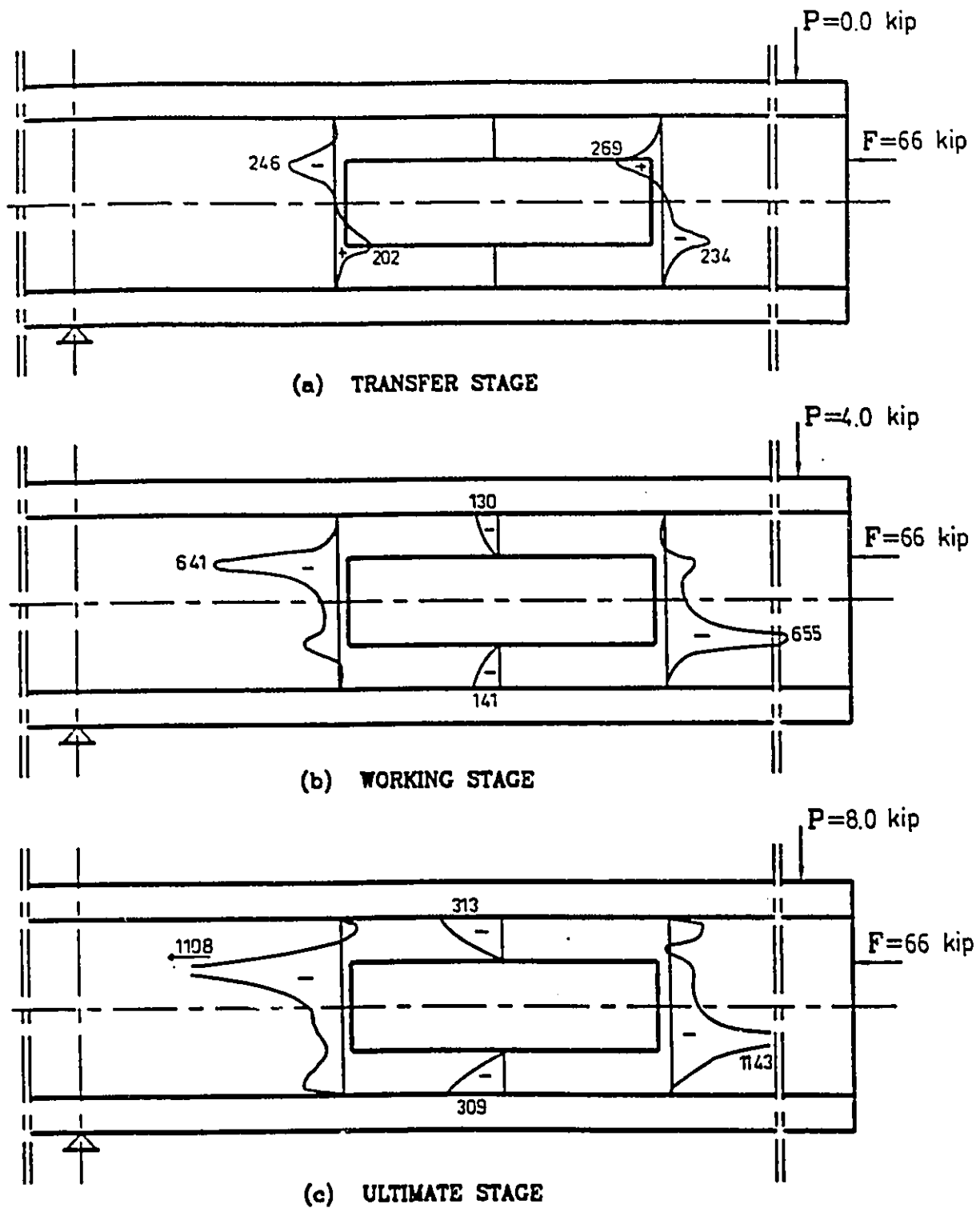


FIG. 5.160 SHEAR STRESS DISTRIBUTION FOR BEAM BIII1C

Note: stresses are shown in psi; 1 psi=6.89 kPa; 1 kip=4.45 kN

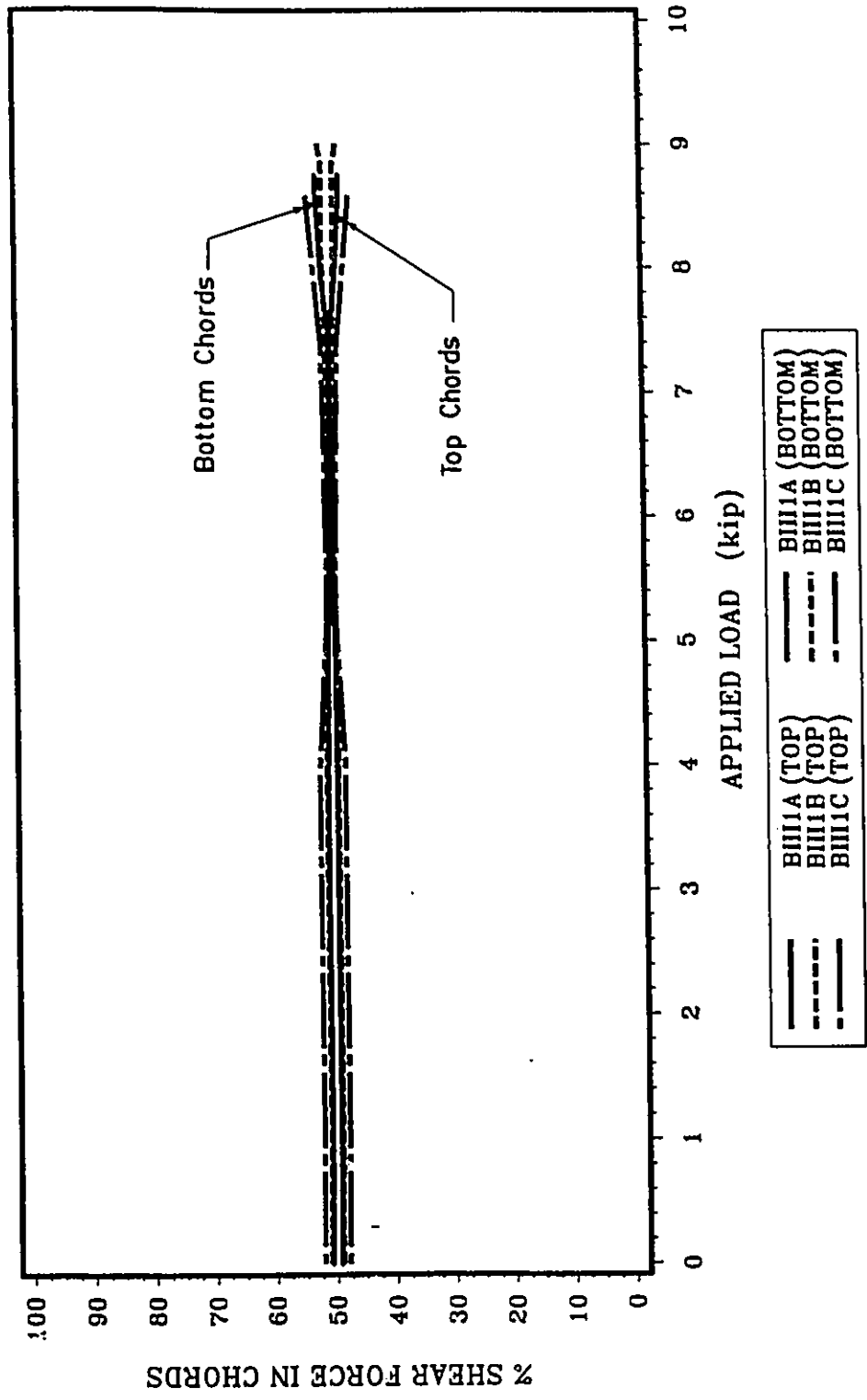


FIG. 5.161 DISTRIBUTION OF SHEAR FORCE BETWEEN TOP AND BOTTOM CHORDS FOR GROUP BIII1

Note: 1 kip=4.45 kN



FIG. 5.162 CRACK PATTERN FOR BEAM B11A



FIG. 5.163 a FAILURE MODE FOR BEAM B11A

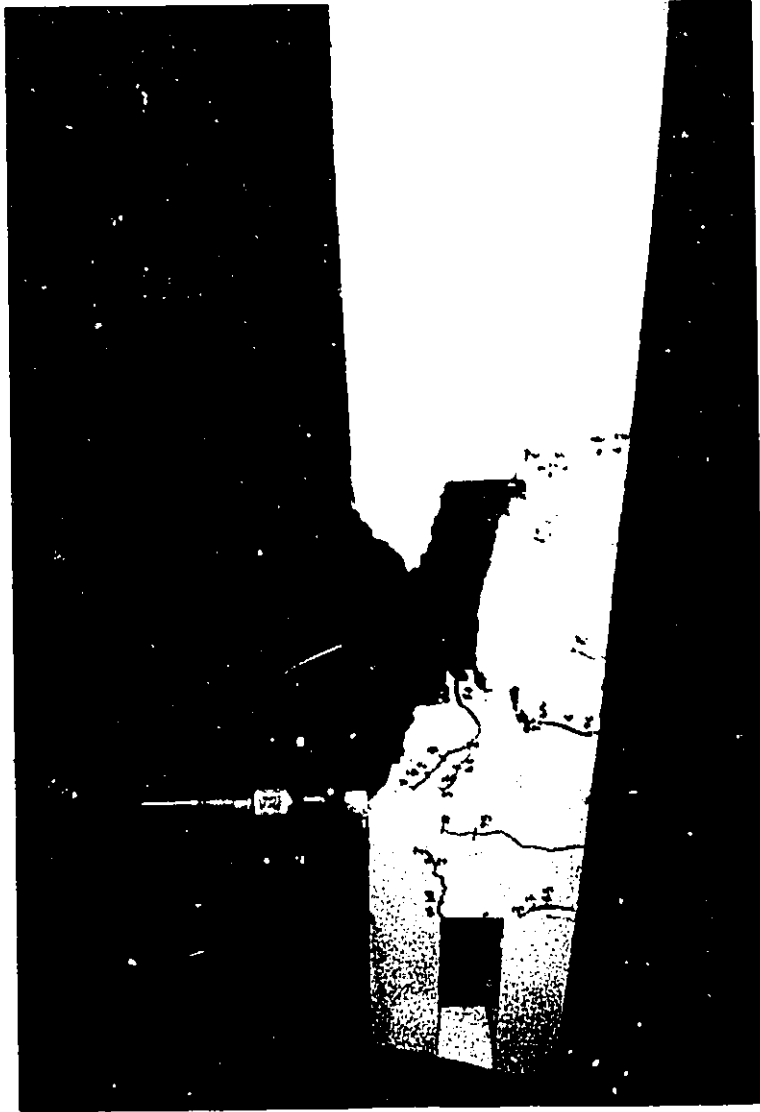


FIG. 5.163 b FAILURE MODE FOR BEAM BI1A



FIG. 5.164 CRACK PATTERN FOR BEAM BI1B



FIG. 5.165 a FAILURE MODE FOR BEAM BIIB

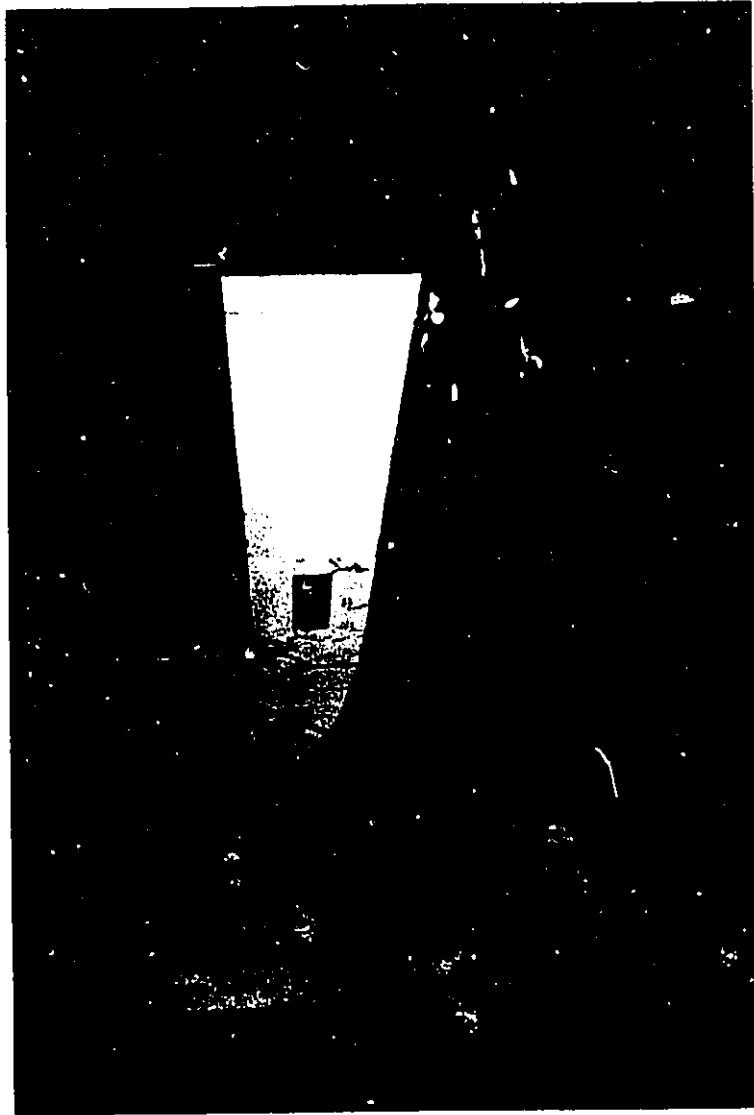


FIG. 5.165 b FAILURE MODE FOR BEAM BIIB



FIG. 5.165 c FAILURE MODE FOR BEAM BIIB

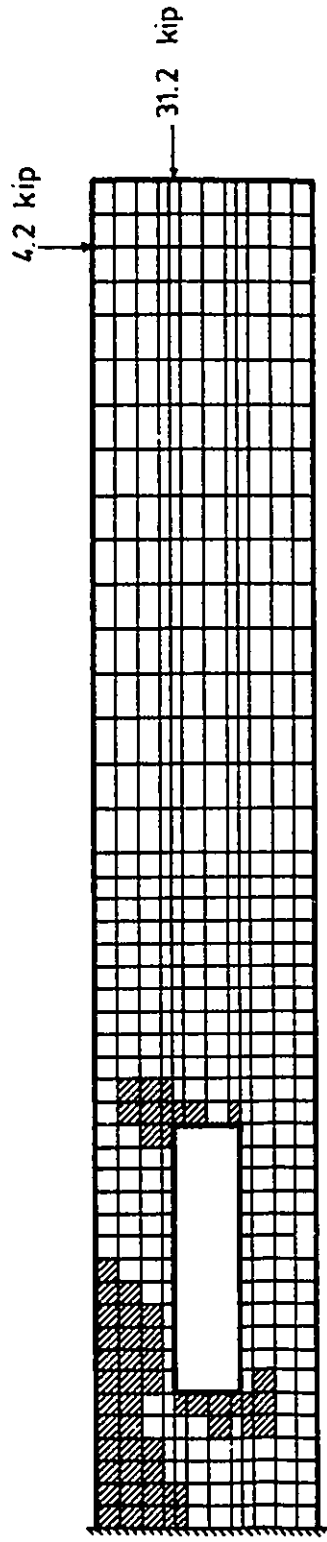


FIG. 5.166 THEORETICAL CRACK PATTERN FOR BEAM B11A

Note: cracked areas are hatched; 1 kip=4.45 kN

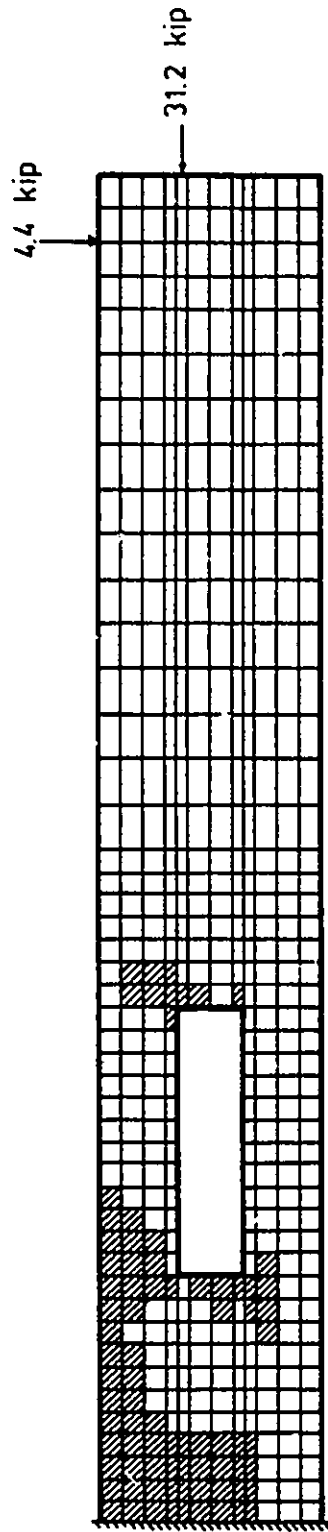


FIG. 5.167 THEORETICAL CRACK PATTERN FOR BEAM BIIB

Note: cracked areas are hatched; 1 kip=4.45 kN

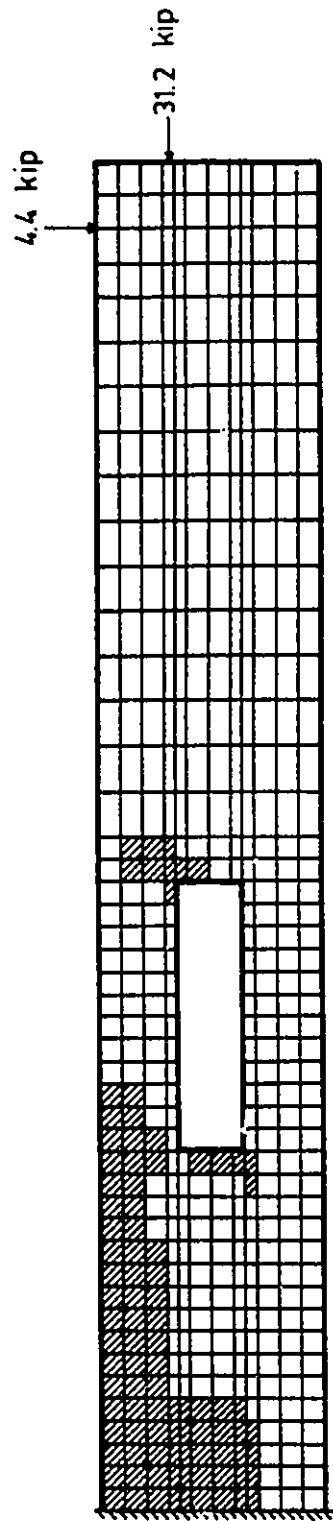


FIG. 5.168 THEORETICAL CRACK PATTERN FOR BEAM BIIC

Note: cracked areas are hatched; 1 kip=4.45 kN

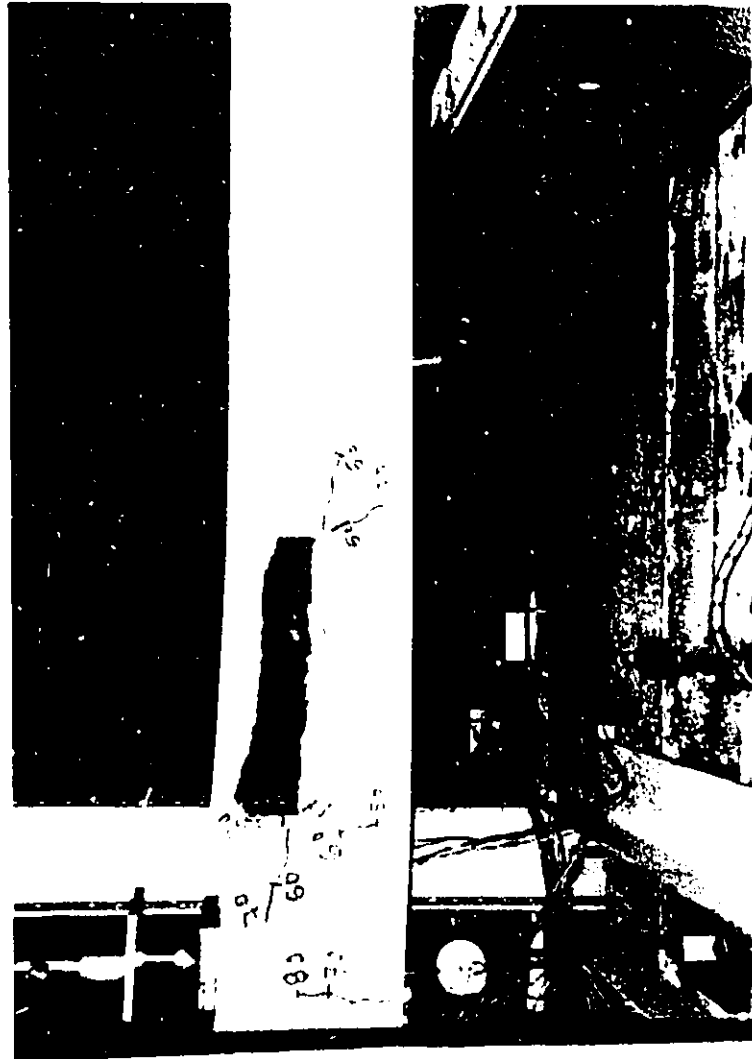


FIG. 5.169 a CRACK PATTERN AND FAILURE MODE FOR BEAM B12A

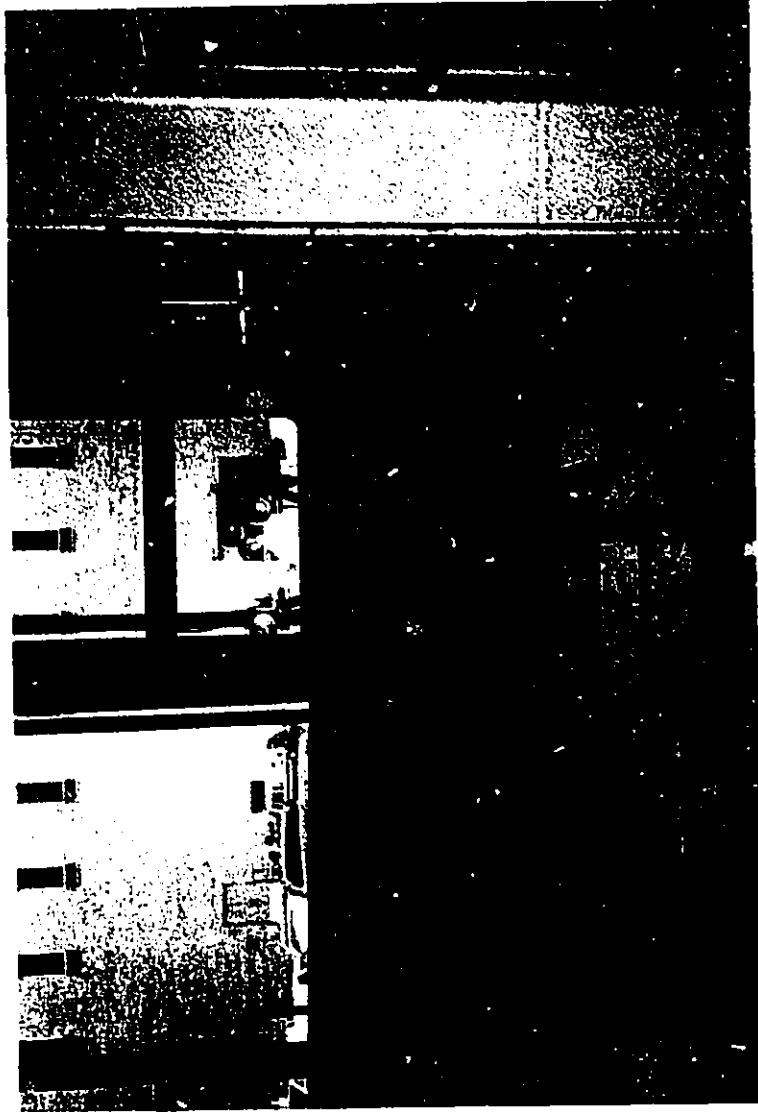


FIG. 5.169 b CRACK PATTERN AND FAILURE MODE FOR BEAM BI2A



FIG. 5.170 CRACK PATTERN FOR BEAM BI2B

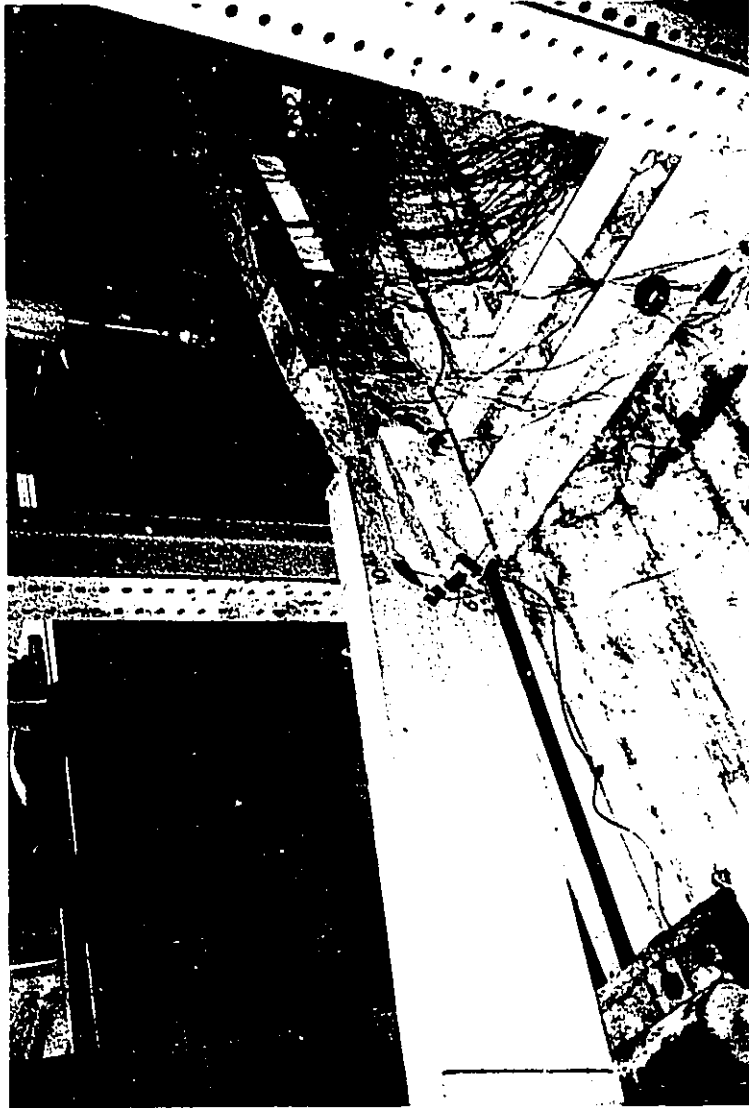


FIG. 5.171 a FAILURE MODE FOR BEAM BI2B



FIG. 5.171 b FAILURE MODE FOR BEAM BI2B



FIG. 5.172 a CRACK PATTERN FOR BEAM BI2C



FIG. 5.172 b CRACK PATTERN FOR BEAM BI2C



FIG. 5.173 a FAILURE MODE FOR BEAM BI2C



FIG. 5.173 b FAILURE MODE FOR BEAM BI2C

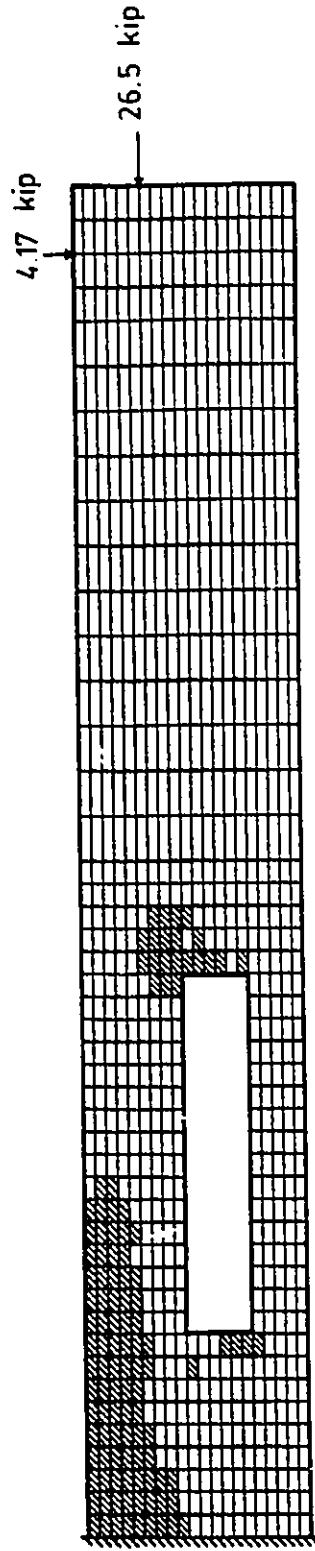


FIG. 5.174 THEORETICAL CRACK PATTERN FOR BEAM B12A

Note: cracked areas are hatched; 1 kip=4.45 kN

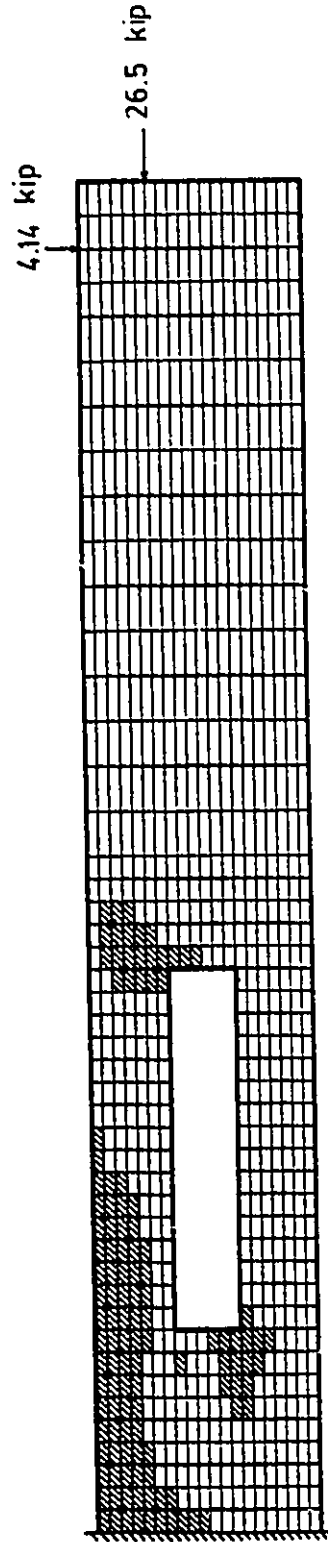


FIG. 5.175 THEORETICAL CRACK PATTERN FOR BEAM BI2B

Note: cracked areas are hatched; 1 kip=4.45 kN

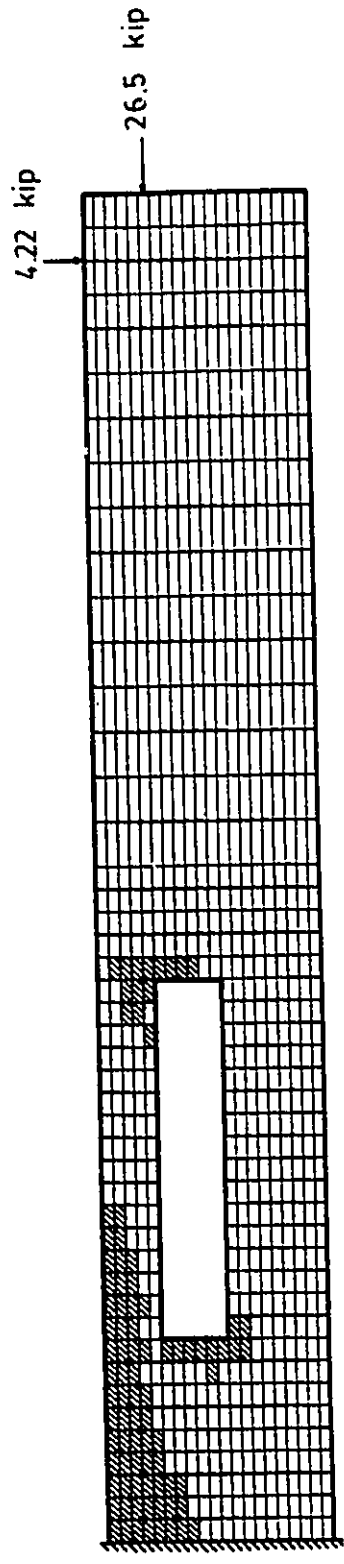


FIG. 5.176 THEORETICAL CRACK PATTERN FOR BEAM B12C

Note: cracked areas are hatched; 1 kip=4.45 kN



FIG. 5.177 a CRACK PATTERN FOR BEAM BI3C

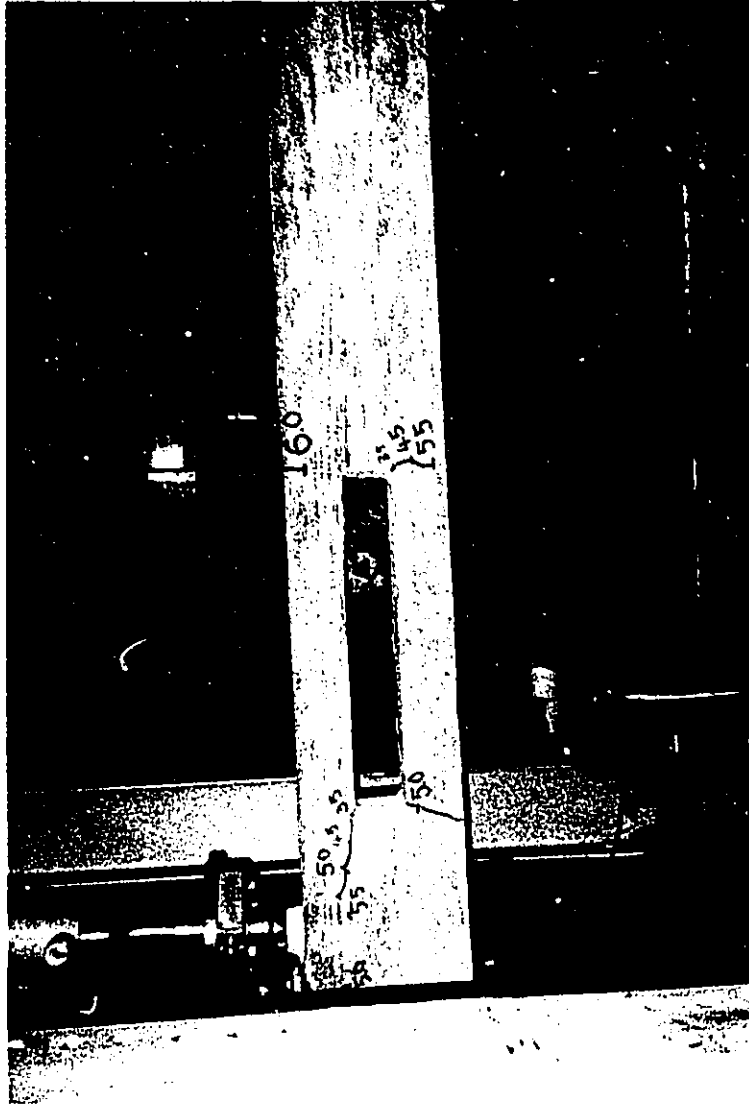


FIG. 5.177 b CRACK PATTERN FOR BEAM BI3C

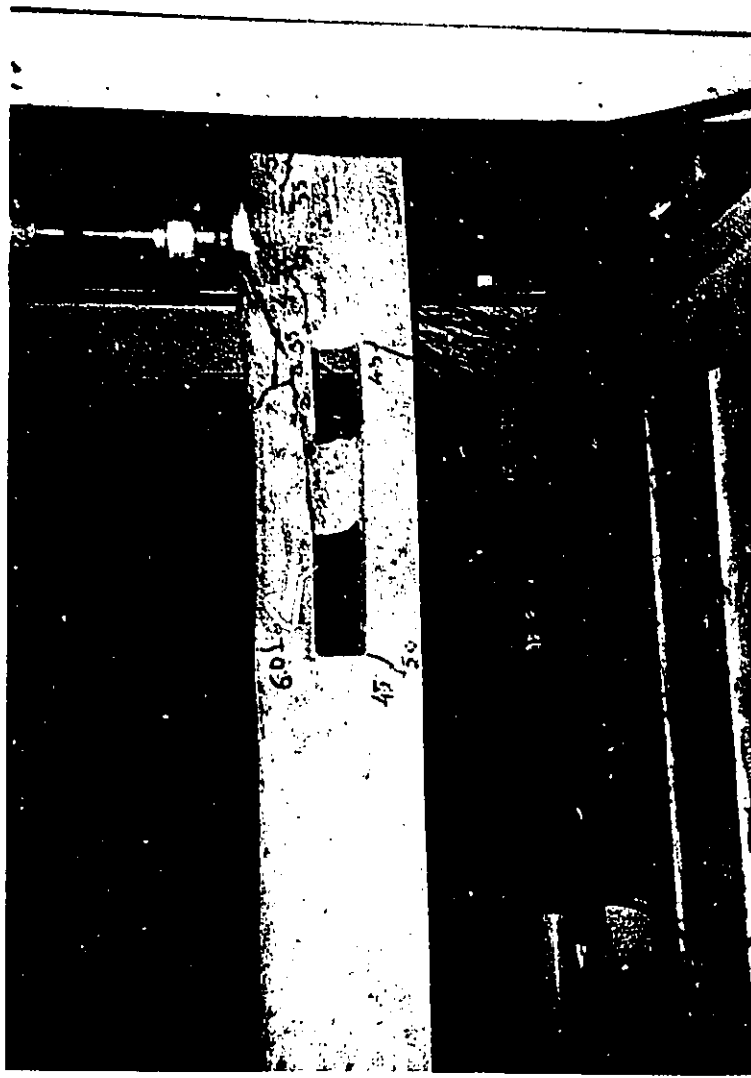


FIG. 5.178 FAILURE MODE FOR BEAM B13C

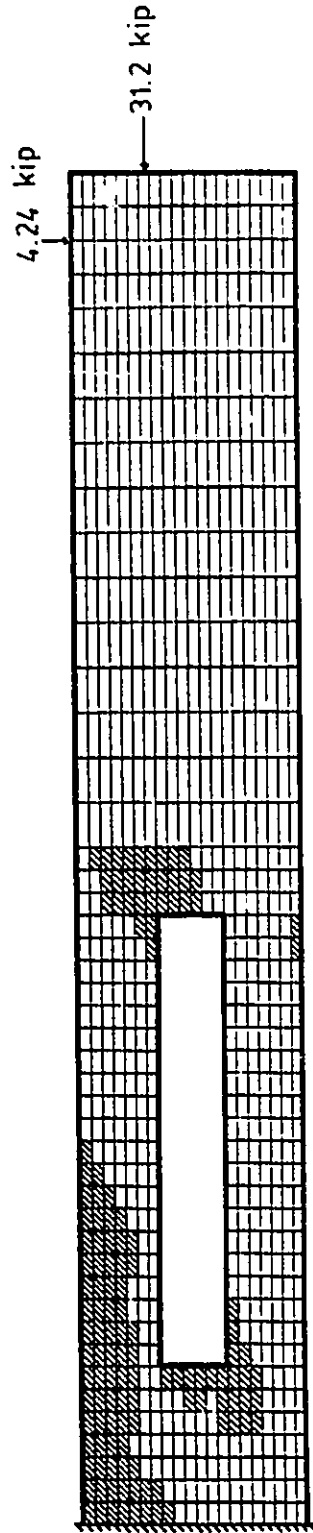


FIG. 5.179 THEORETICAL CRACK PATTERN FOR BEAM B13C

Note: cracked areas are hatched; 1 kip=4.45 kN

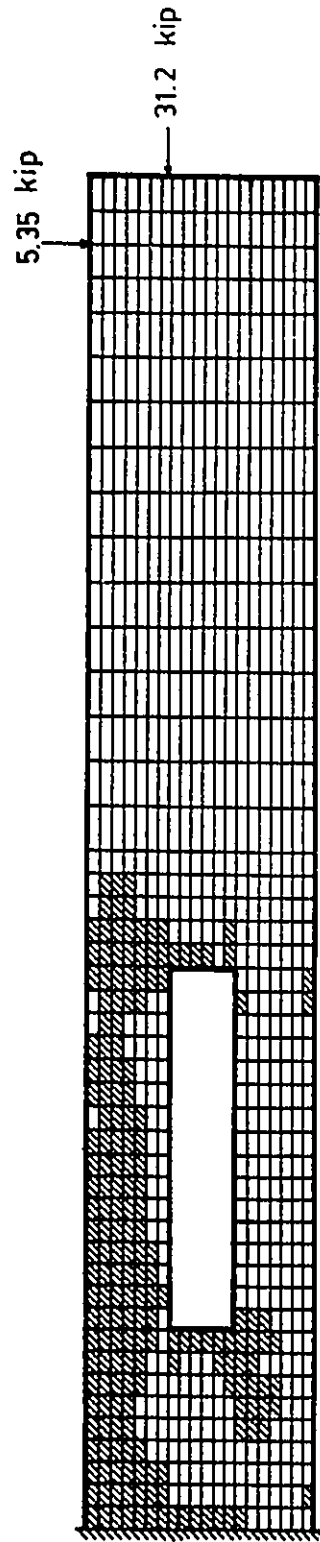


FIG. 5.180 THEORETICAL CRACK PATTERN FOR BEAM BI4A

Note: cracked areas are hatched; 1 kip=4.45 kN

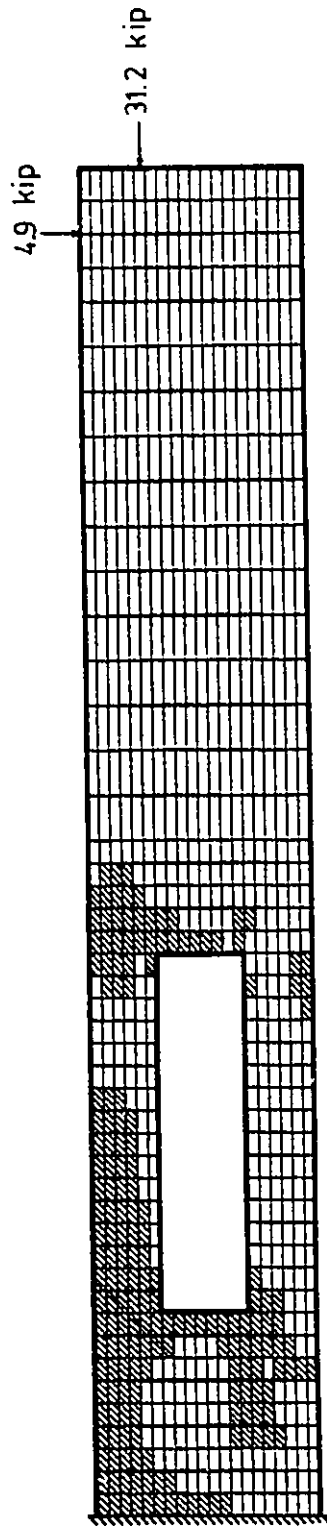


FIG. 5.181 THEORETICAL CRACK PATTERN FOR BEAM BI4B

Note: cracked areas are hatched; 1 kip=4.45 kN

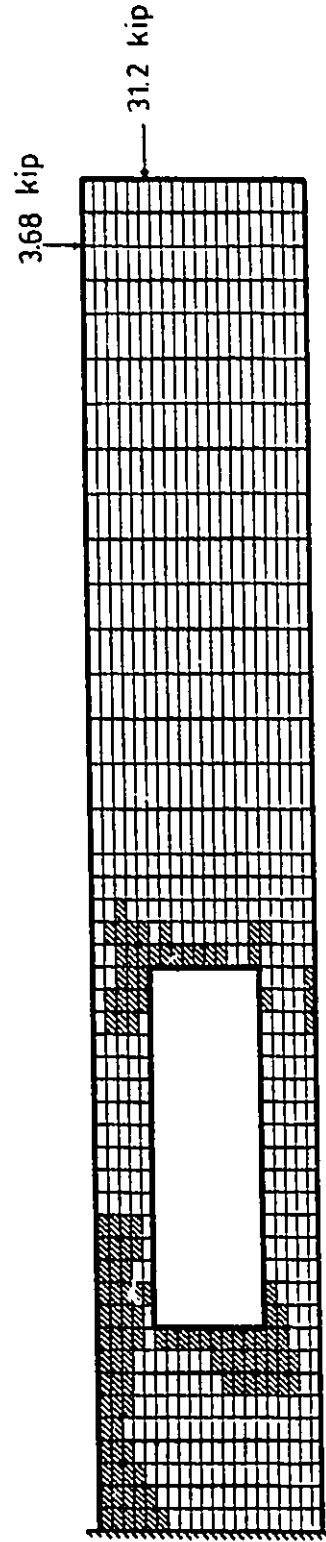


FIG. 5.182 THEORETICAL CRACK PATTERN FOR BEAM B14C

Note: cracked areas are hatched; 1 kip=4.45 kN



FIG. 5.183 a CRACK PATTERN FOR BEAM BIIIa



FIG. 5.183 b CRACK PATTERN FOR BEAM BIIIa



FIG. 5.183 c. CRACK PATTERN FOR BEAM BIIIa

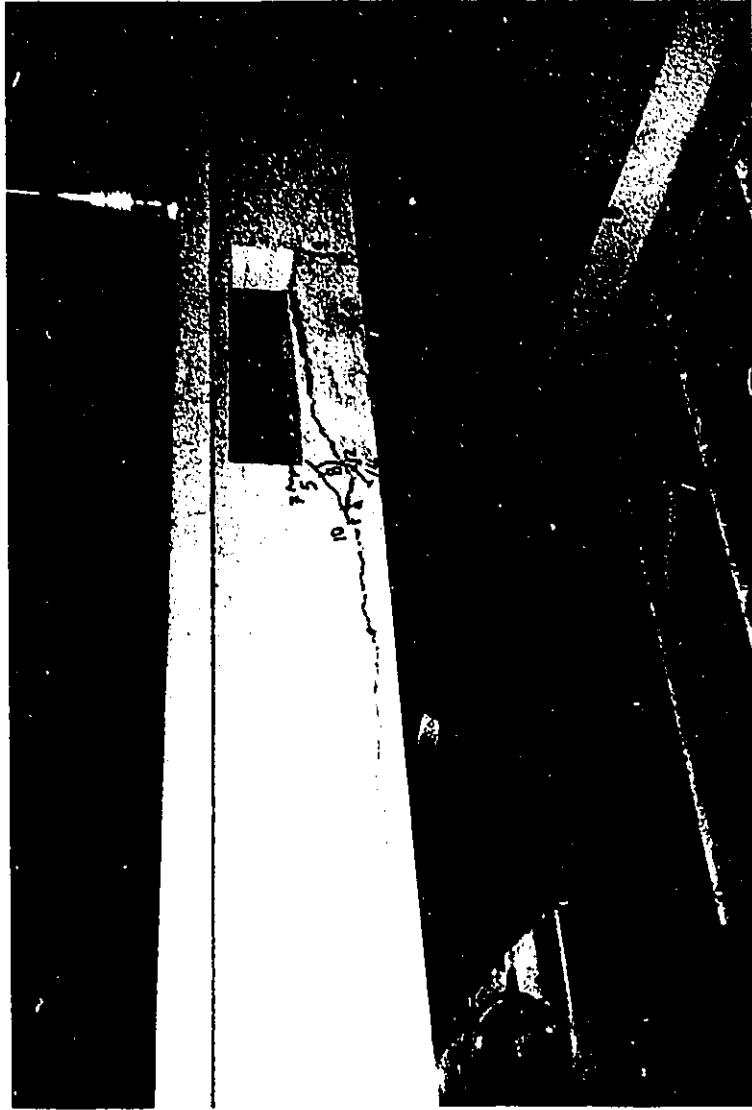


FIG. 5.184 a FAILURE MODE FOR BEAM BIIIa

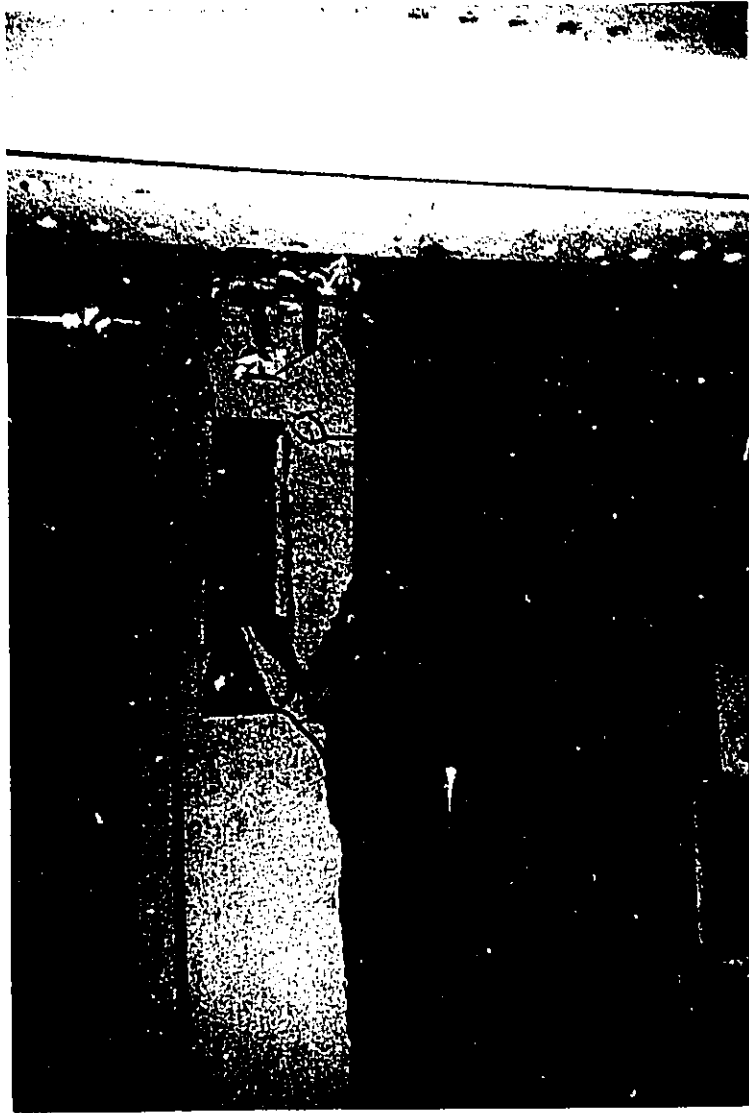


FIG. 5.184 b FAILURE MODE FOR BEAM BIIIa



FIG. 5.185 a CRACK PATTERN FOR BEAM BIIIIB



FIG. 5.185 b CRACK PATTERN FOR BEAM BIIIIB



FIG. 5.185 c CRACK PATTERN FOR BEAM BIII B

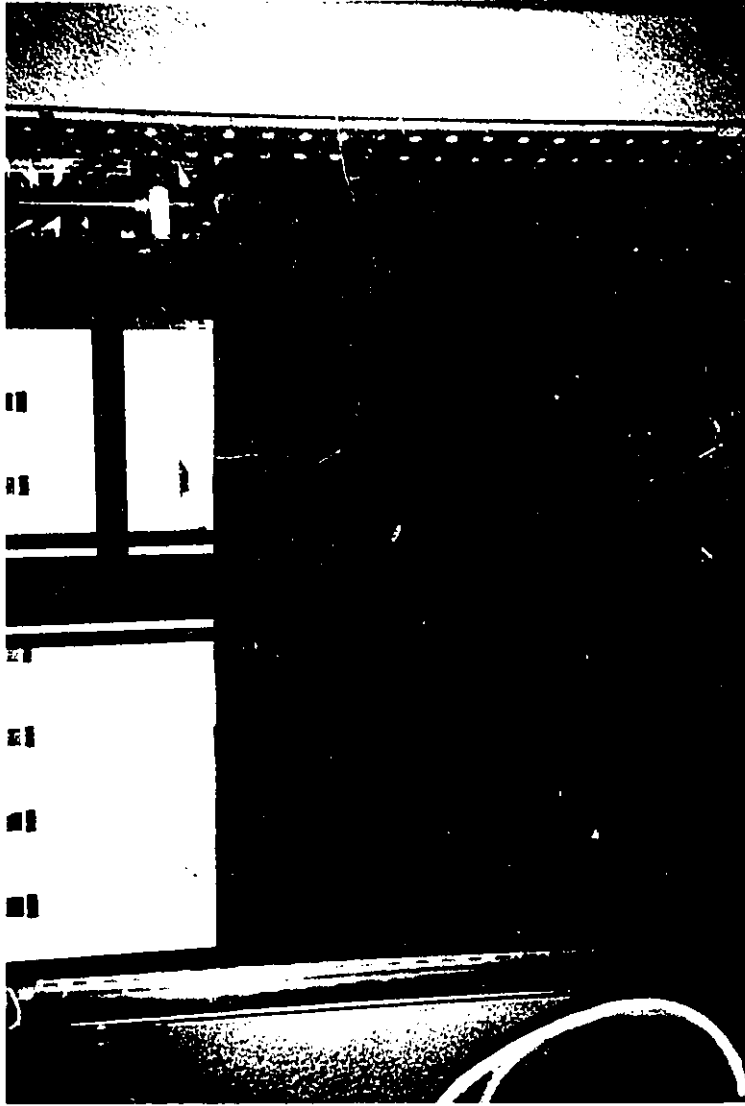


FIG. 5.186 a FAILURE MODE FOR BEAM BIIIb



FIG. 5.186 b FAILURE MODE FOR BEAM B11B

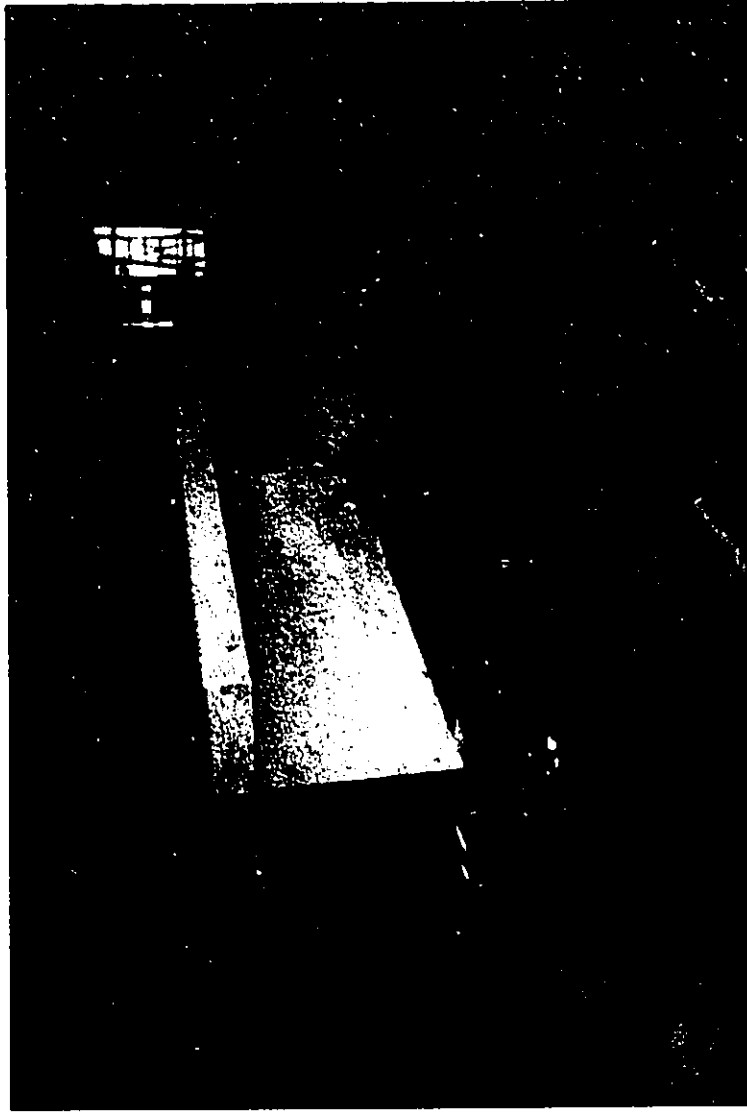


FIG. 5.186 c FAILURE MODE FOR BEAM BIIIIB



FIG. 5.186 d FAILURE MODE FOR BEAM BIIIb

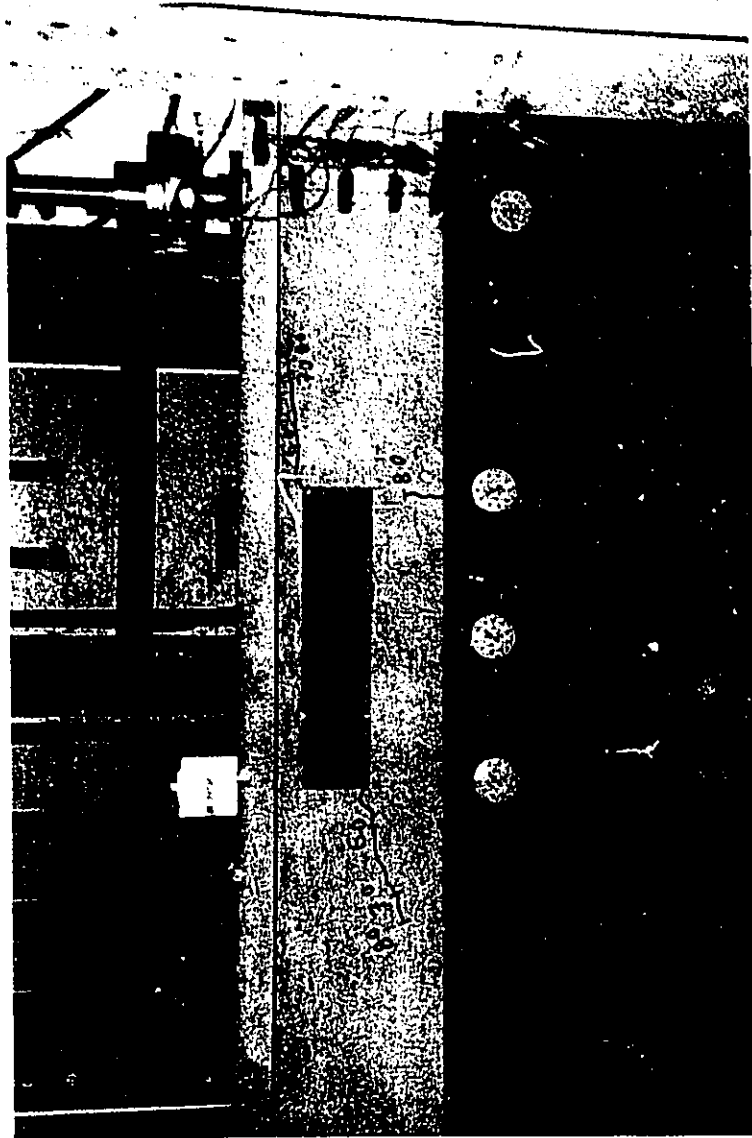


FIG. 5.187 a CRACK PATTERN FOR BEAM BIIC

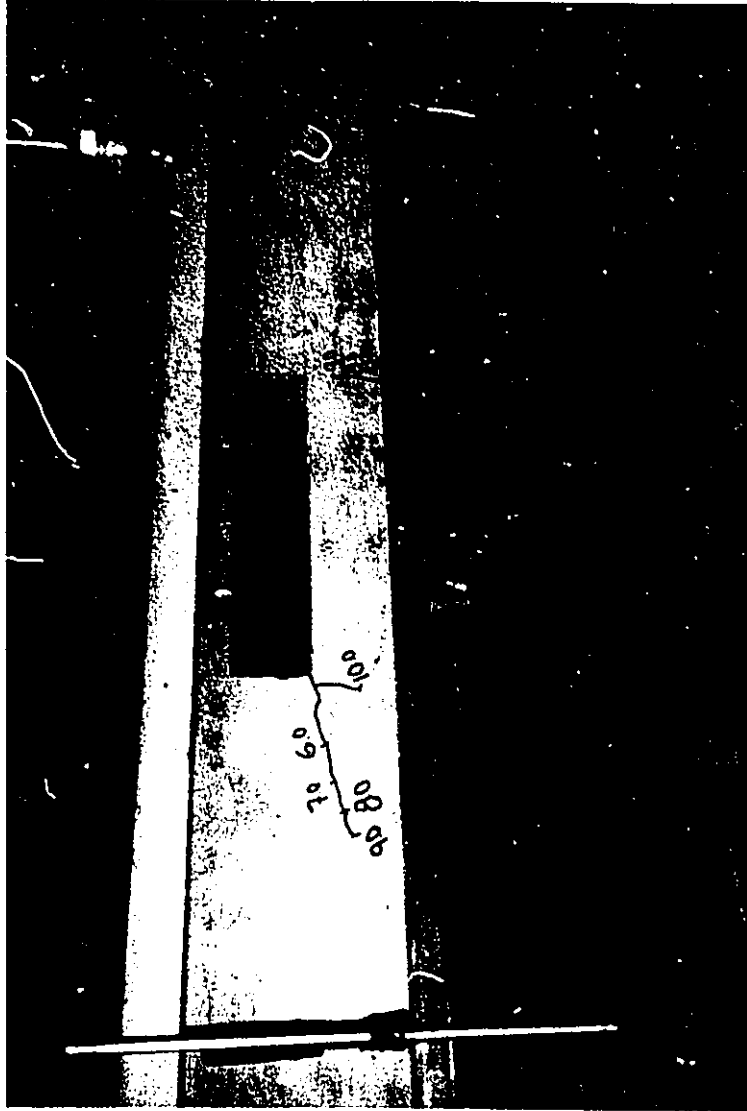


FIG. 5.187 b CRACK PATTERN FOR BEAM BIIC

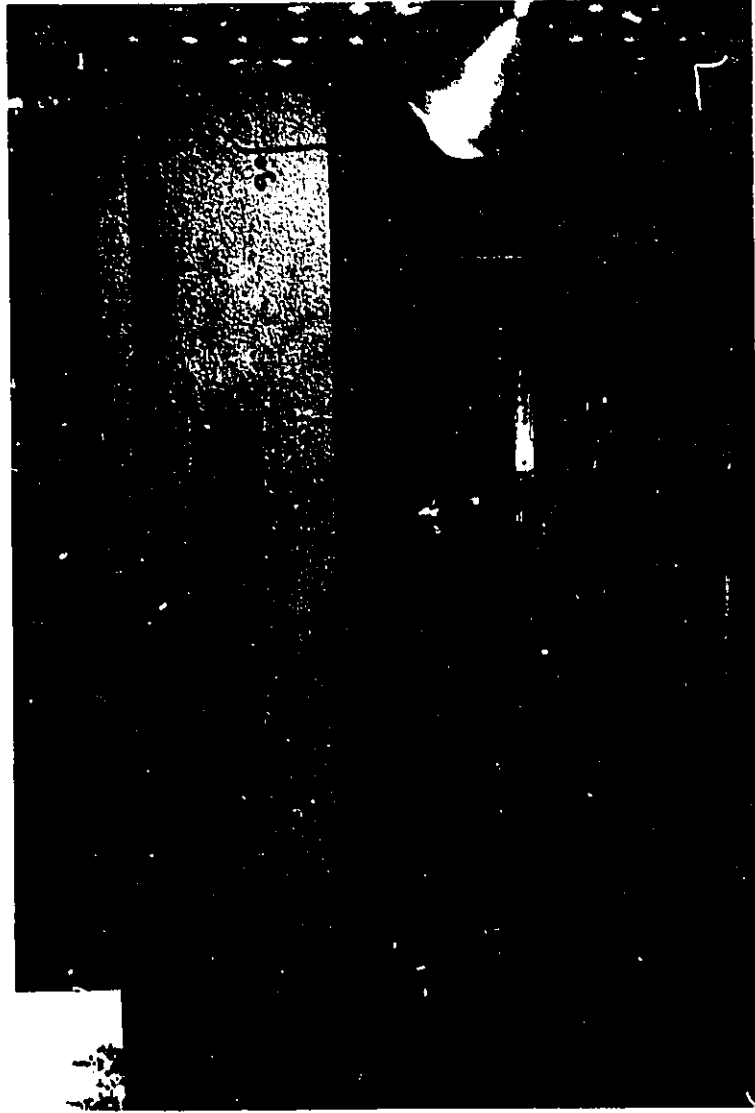


FIG. 5.188 a FAILURE MODE FOR BEAM BIIIIC

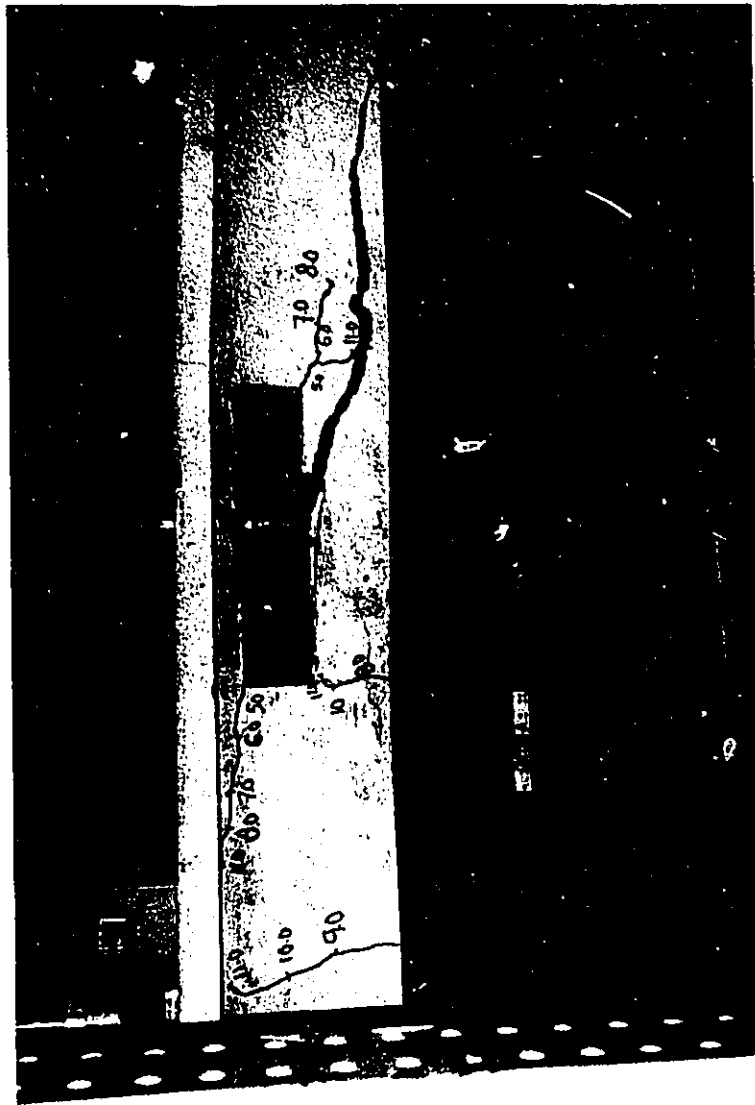


FIG. 5.188 b FAILURE MODE FOR BEAM BIIIc

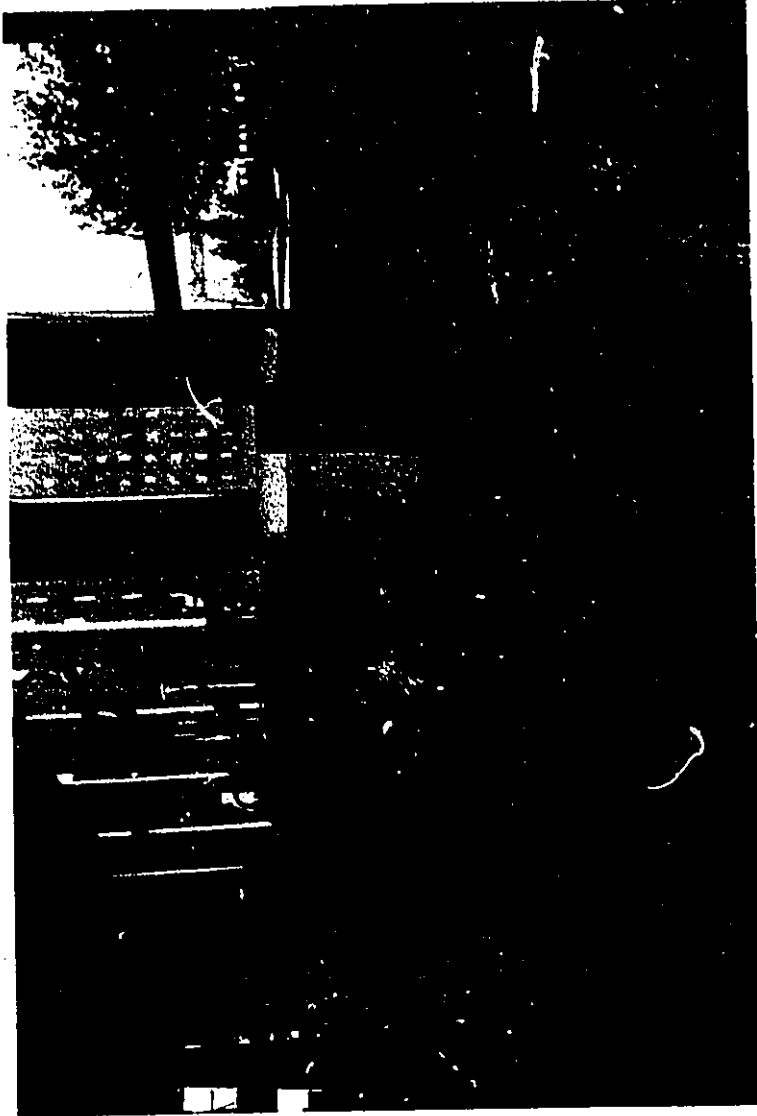


FIG. 5.188 c FAILURE MODE FOR BEAM BIIC

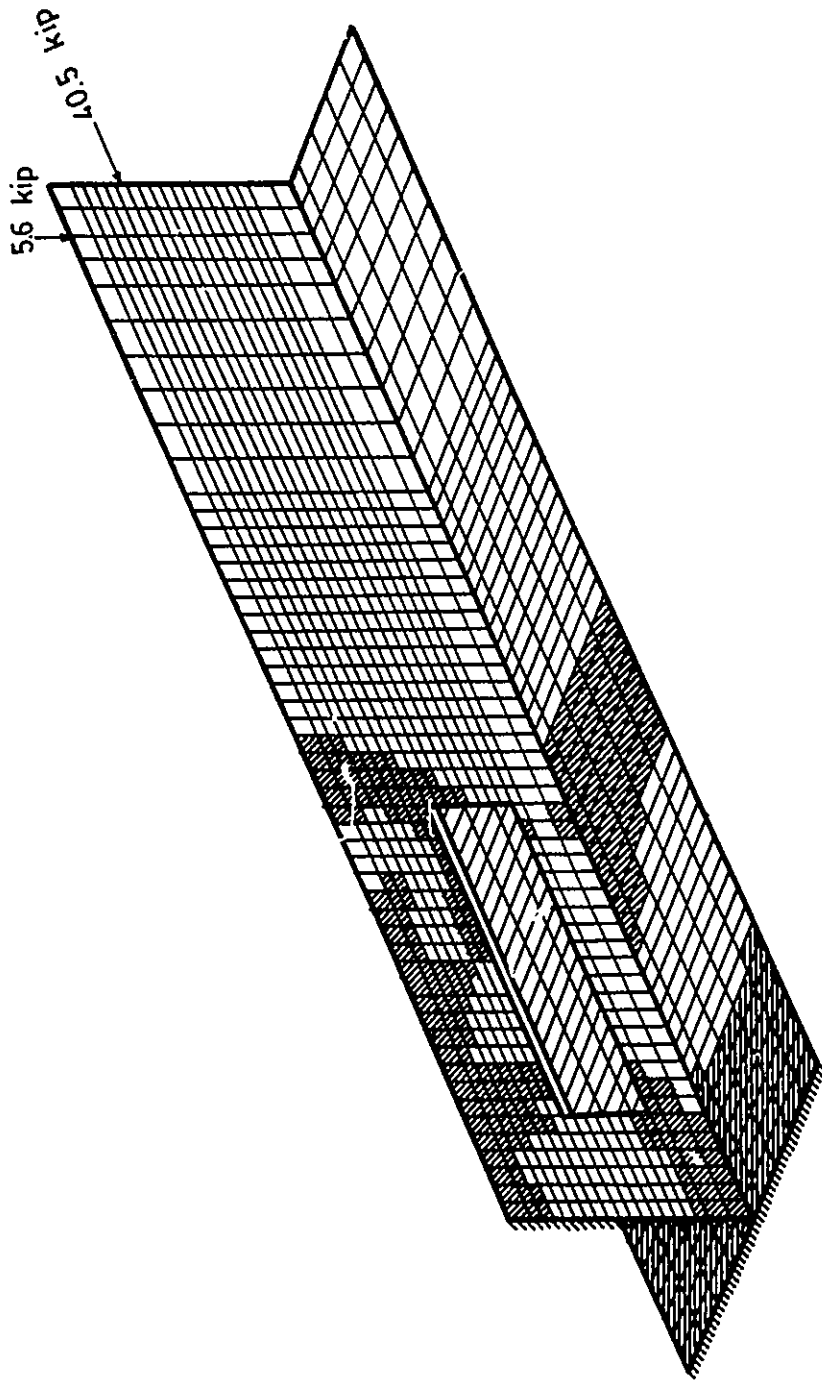


FIG. 5.189 THEORETICAL CRACK PATTERN FOR BEAM B111A

Note: cracked areas are hatched; 1 kip=4.45 kN

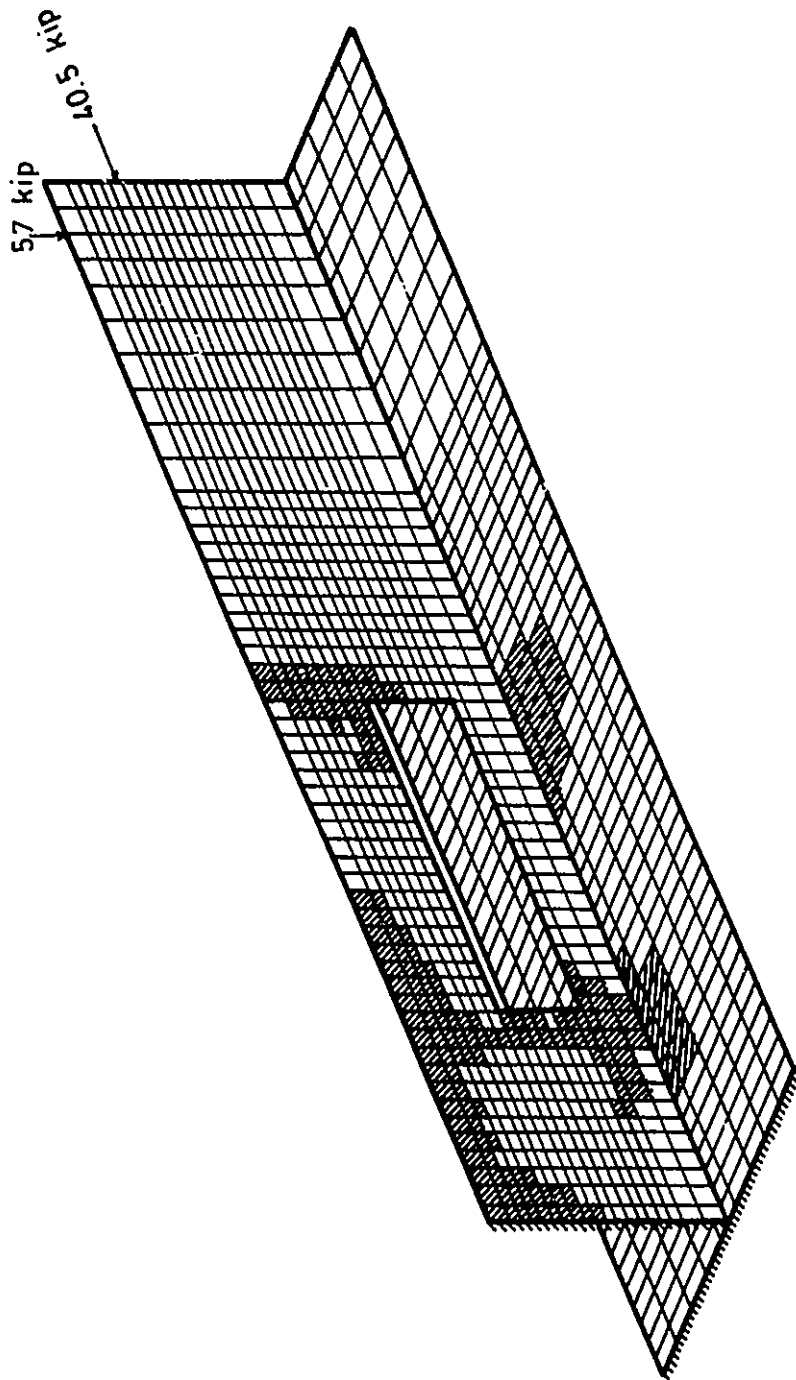


FIG. 5.190 THEORETICAL CRACK PATTERN FOR BEAM BU1B

Note: cracked areas are hatched; 1 kip=4.45 kN

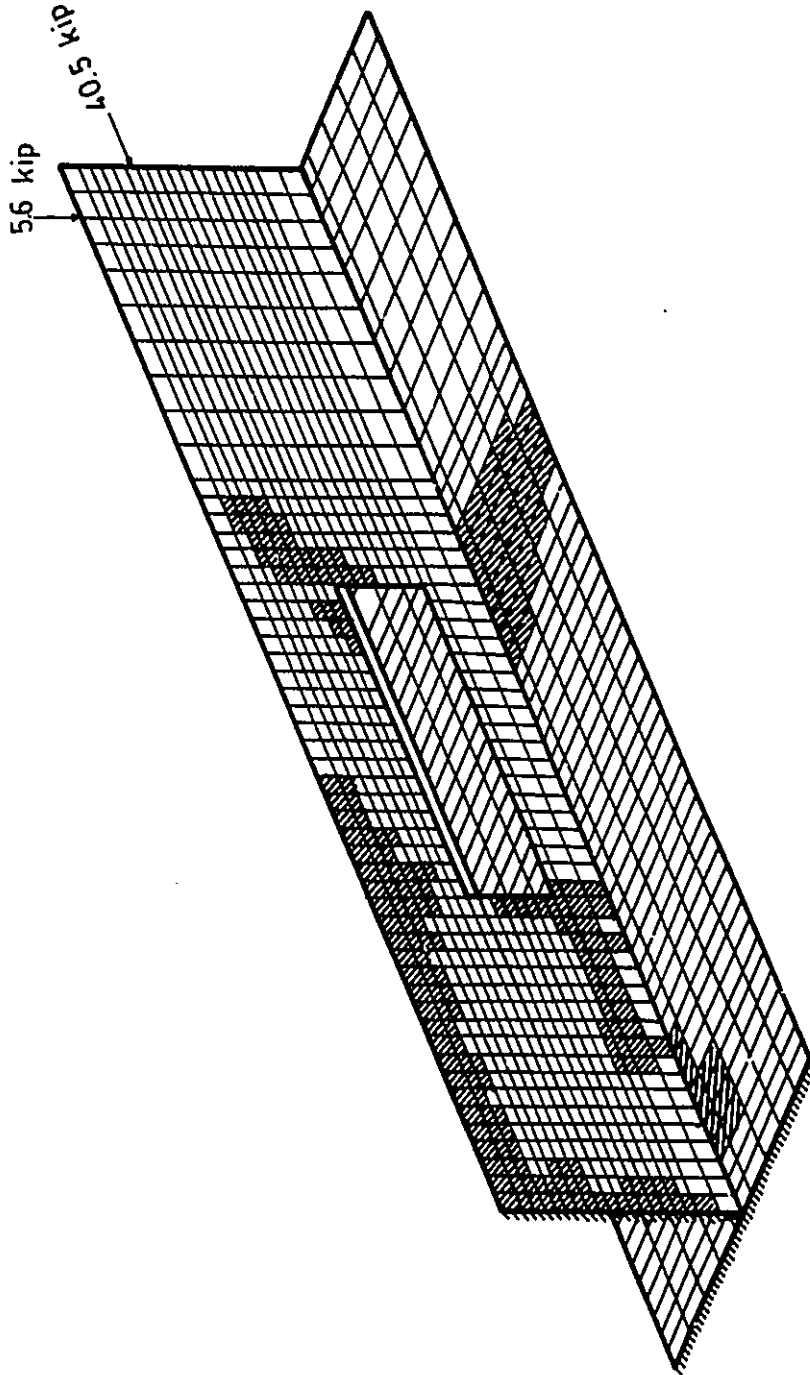


FIG. 5.191 THEORETICAL CRACK PATTERN FOR BEAM BUIC

Note: cracked areas are hatched; 1 kip=4.45 kN



FIG. 5.192 a CRACK PATTERN FOR BEAM BII2B

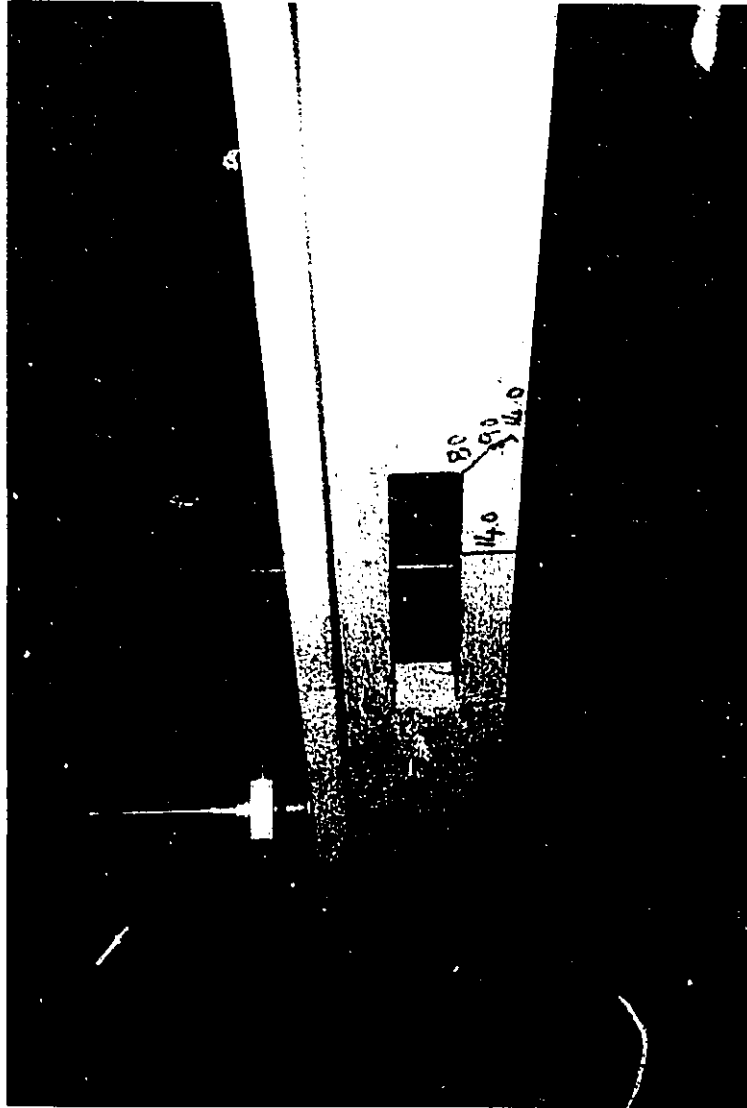


FIG. 5.192 b CRACK PATTERN FOR BEAM BI12B

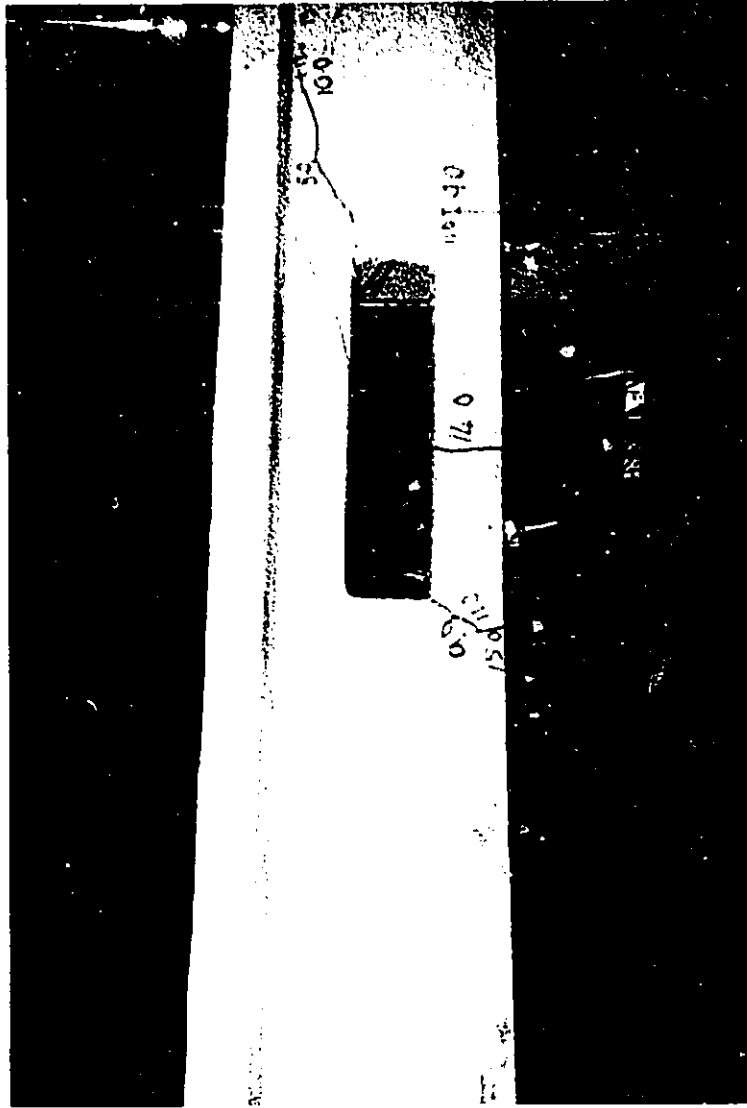


FIG. 5.192 c CRACK PATTERN FOR BEAM BII2B

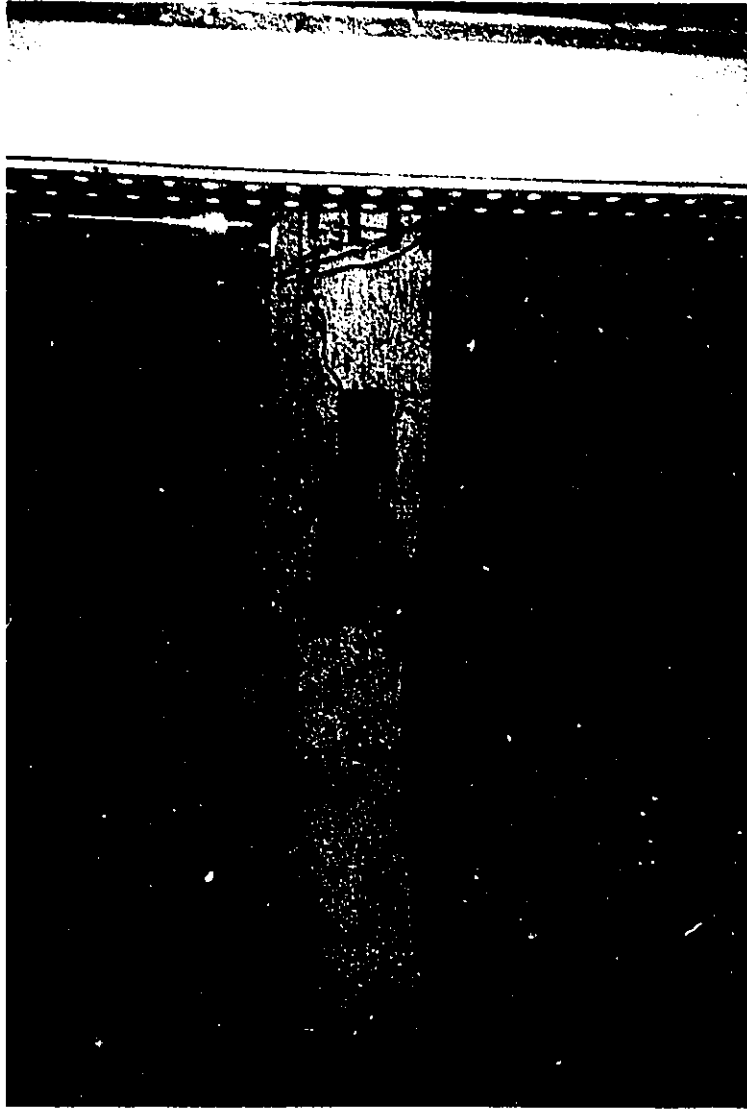


FIG. 5.193 FAILURE MODE FOR BEAM BI2B

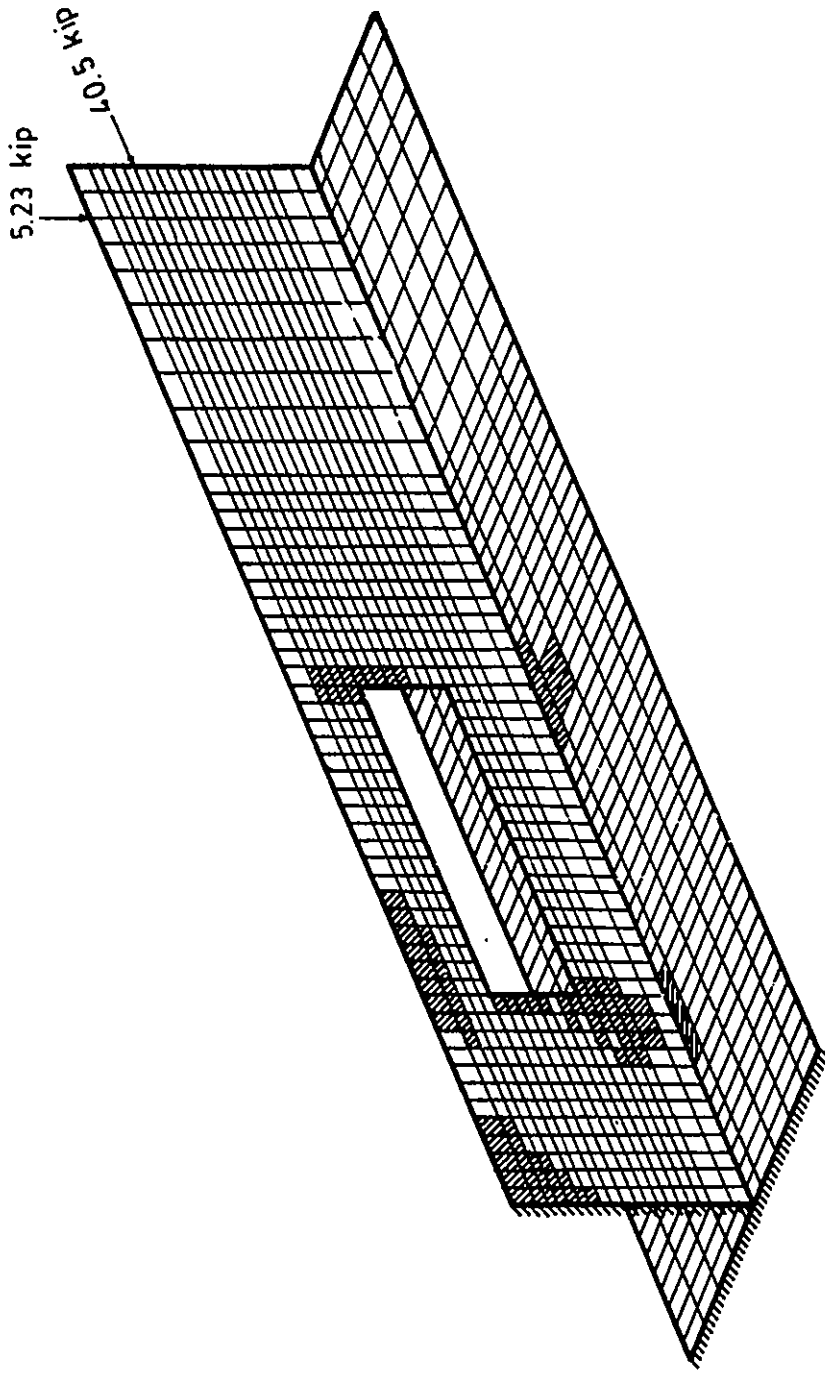


FIG. 5.194 THEORETICAL CRACK PATTERN FOR BEAM BU2B

Note: cracked areas are hatched; 1 kip=4.45 kN

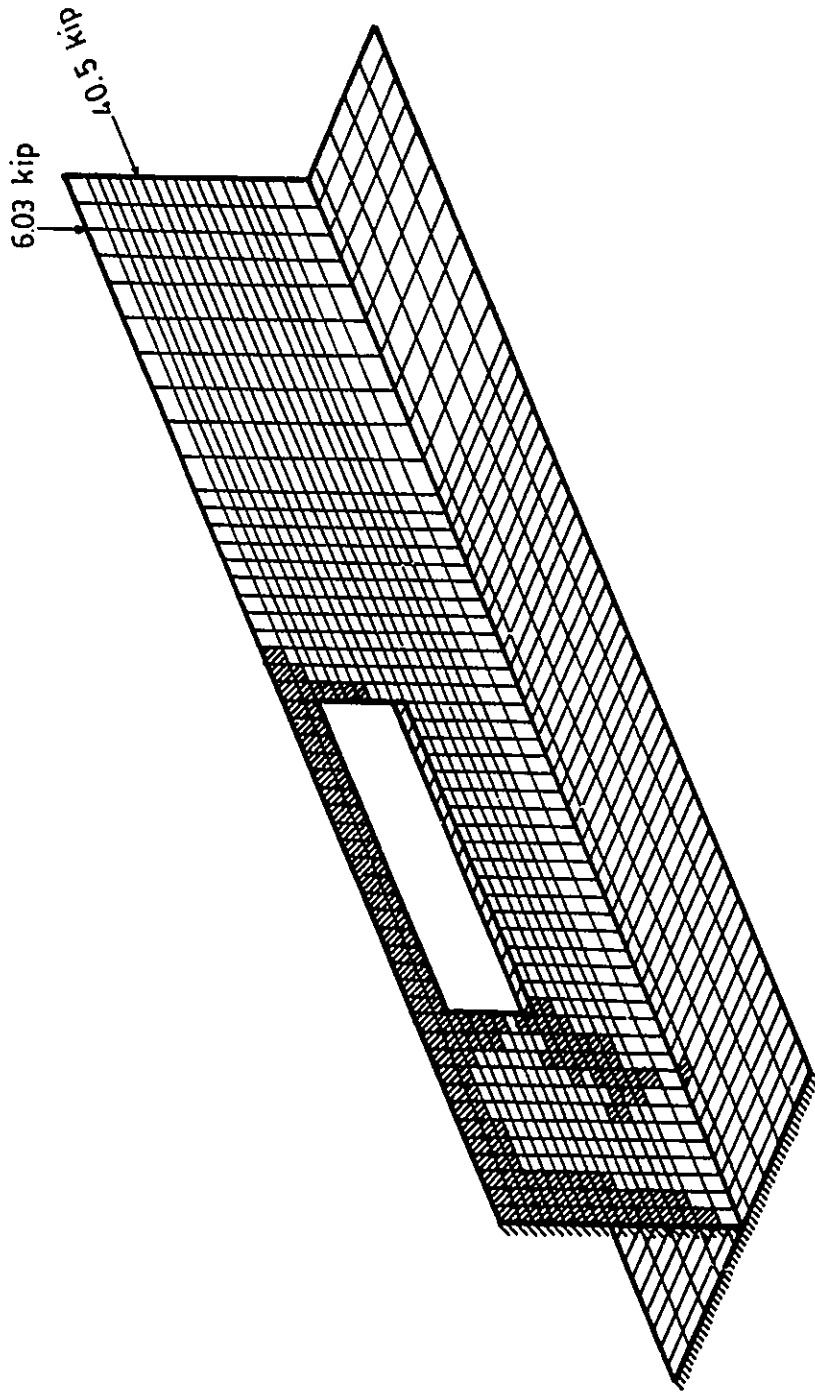


FIG. 5.195 THEORETICAL CRACK PATTERN FOR BEAM BII2C

Note: cracked areas are hatched; 1 kip=4.45 kN

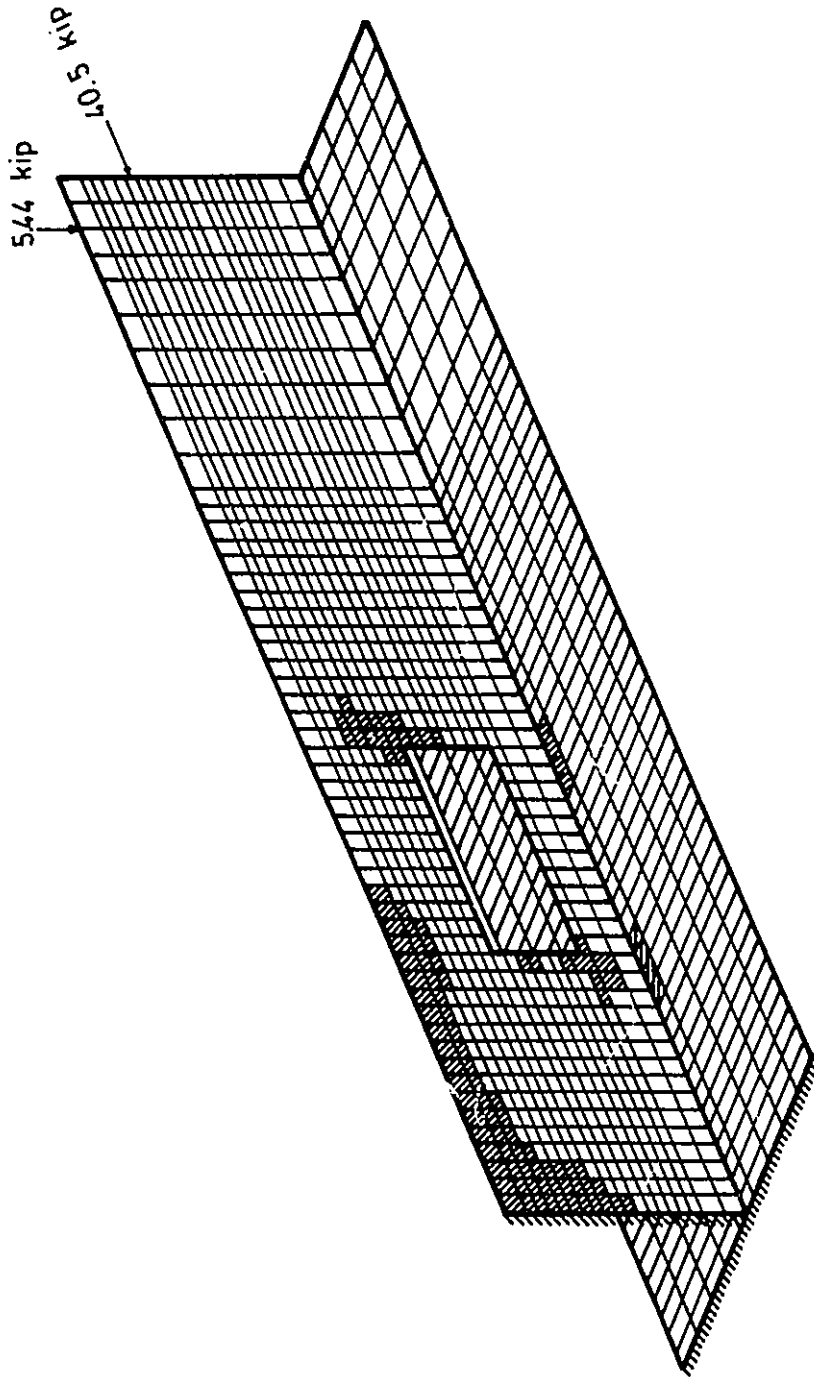


FIG. 5.196 THEORETICAL CRACK PATTERN FOR BEAM BII3A

Note: cracked areas are hatched; 1 kip=4.45 kN

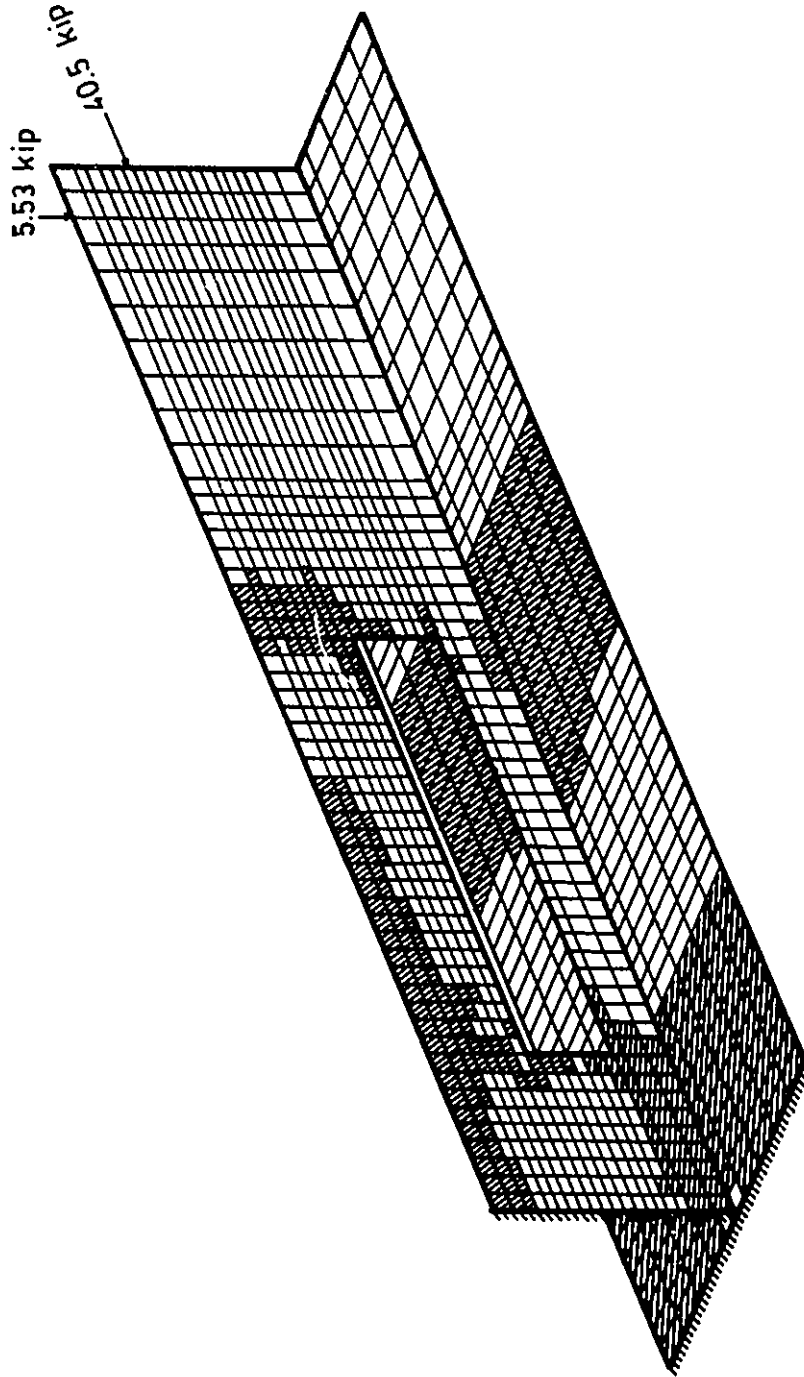


FIG. 5.197 THEORETICAL CRACK PATTERN FOR BEAM BI13C

Note: cracked areas are hatched; 1 kip=4.45 kN

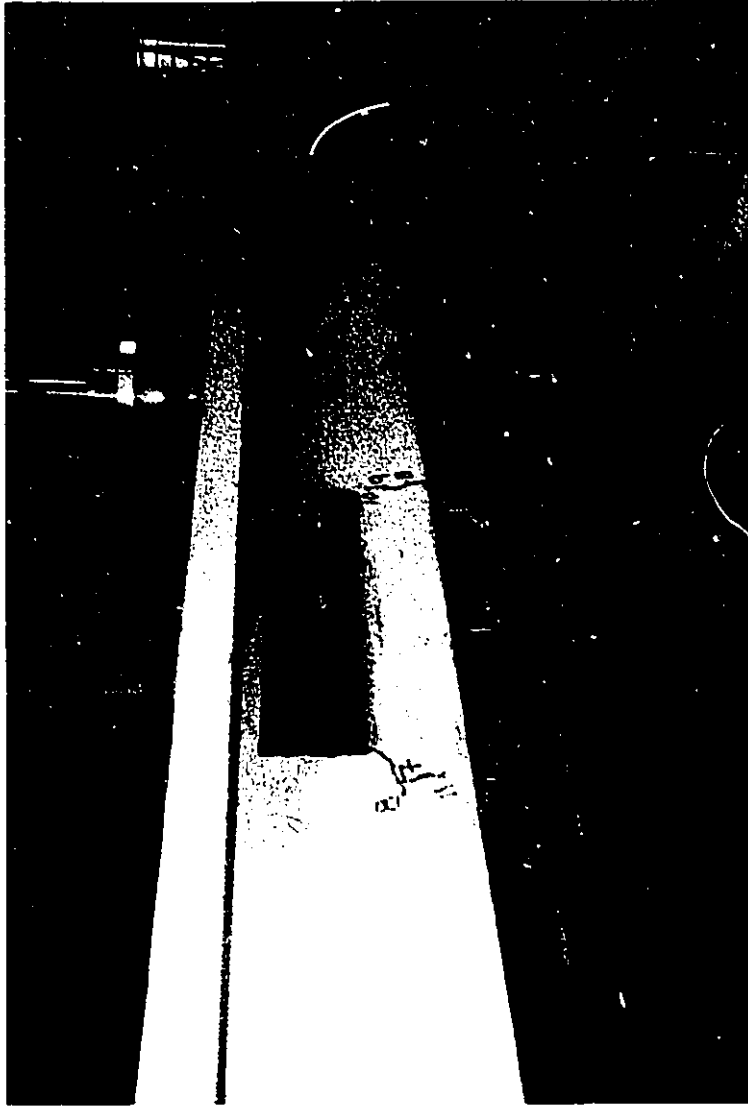


FIG. 5.198 a CRACK PATTERN FOR BEAM BIII4C

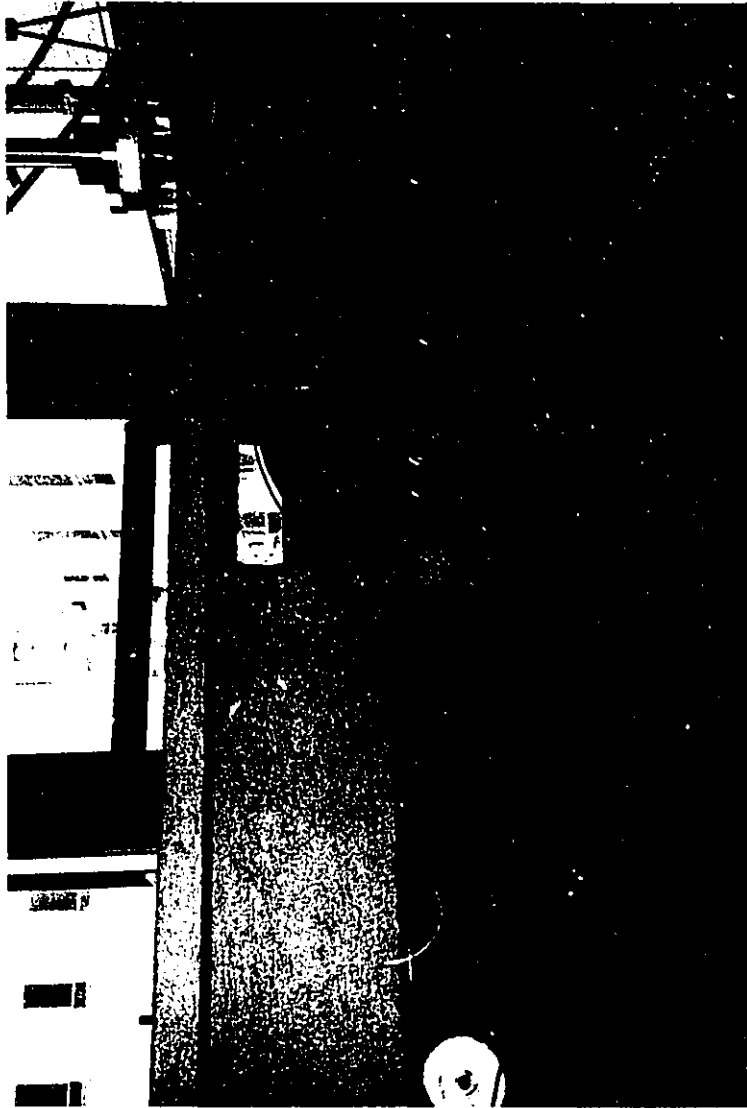


FIG. 5.198 b CRACK PATTERN FOR BEAM BII4C

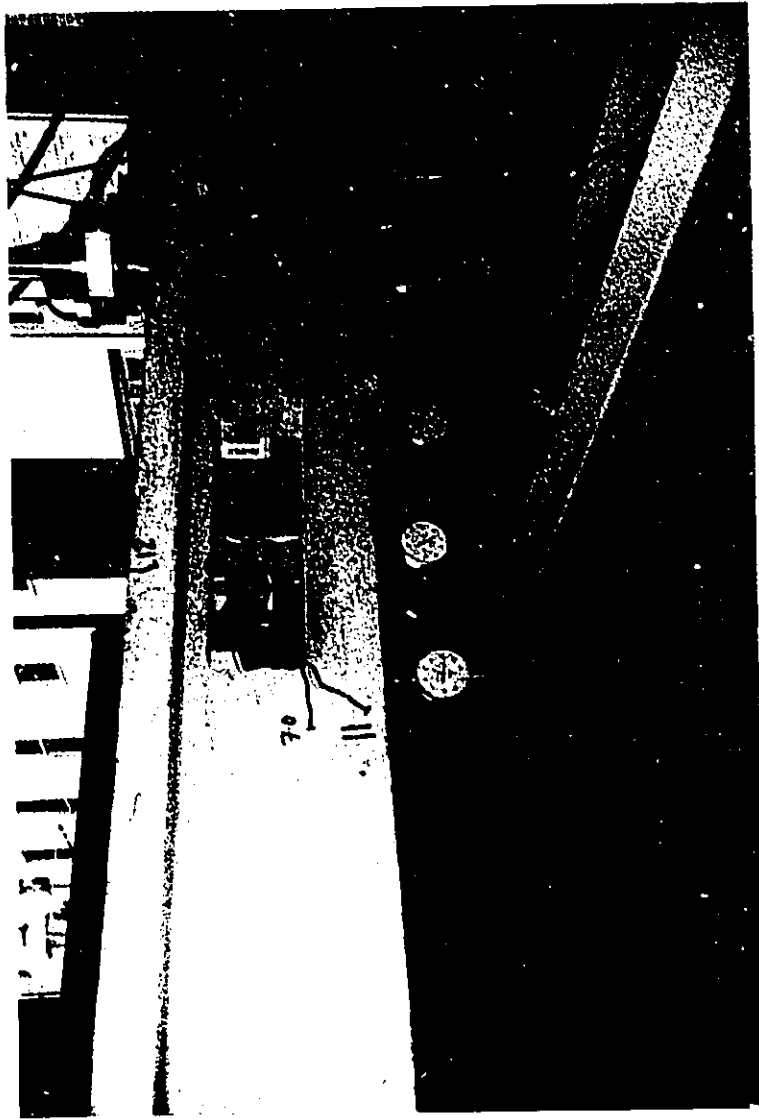


FIG. 5.198 c CRACK PATTERN FOR BEAM BII4C

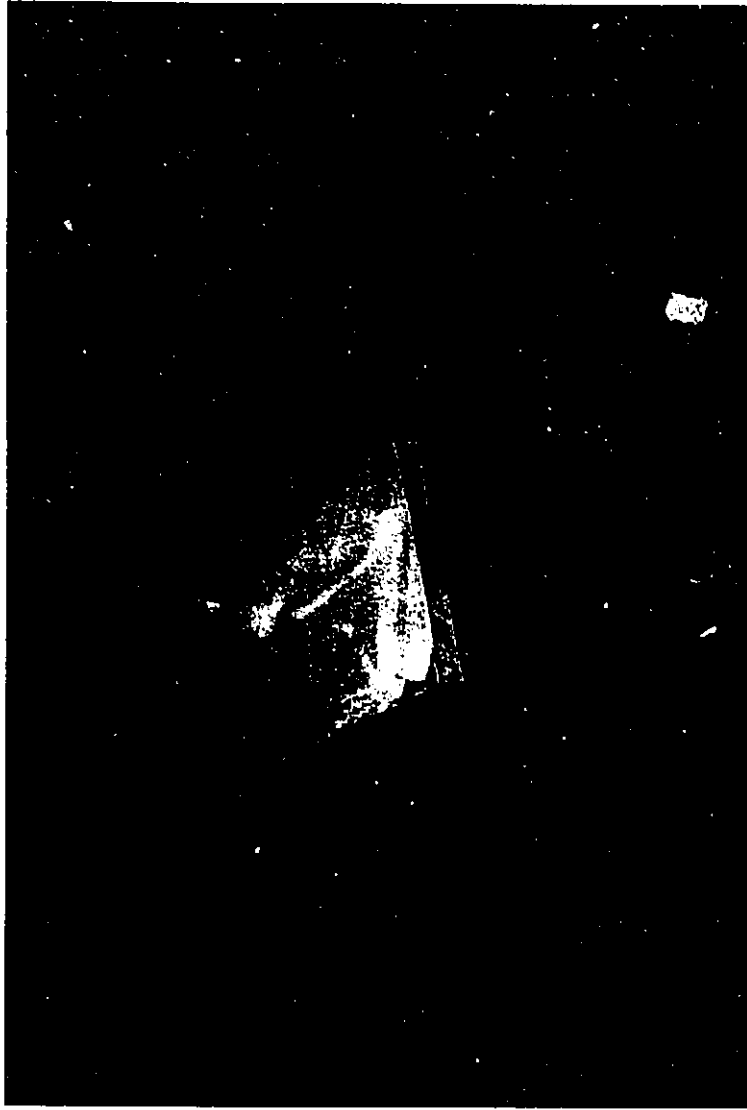


FIG. 5.198 d CRACK PATTERN FOR BEAM BII4C



FIG. 5.199 a FAILURE MODE FOR BEAM BIII4C



FIG. 5.199 b FAILURE MODE FOR BEAM BII4C

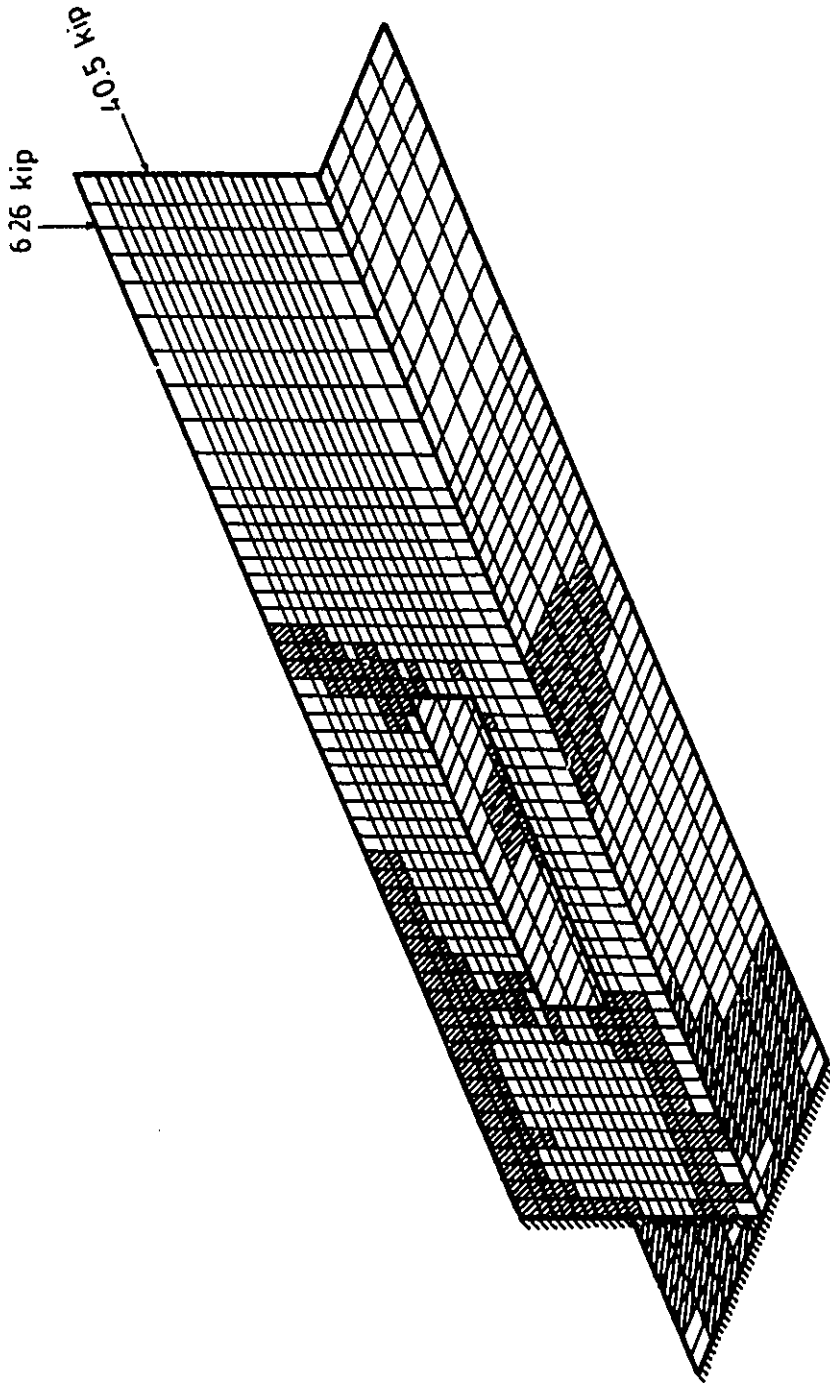


FIG. 5.200 THEORETICAL CRACK PATTERN FOR BEAM BII4A

Note: cracked areas are hatched; 1 kip=4.45 kN

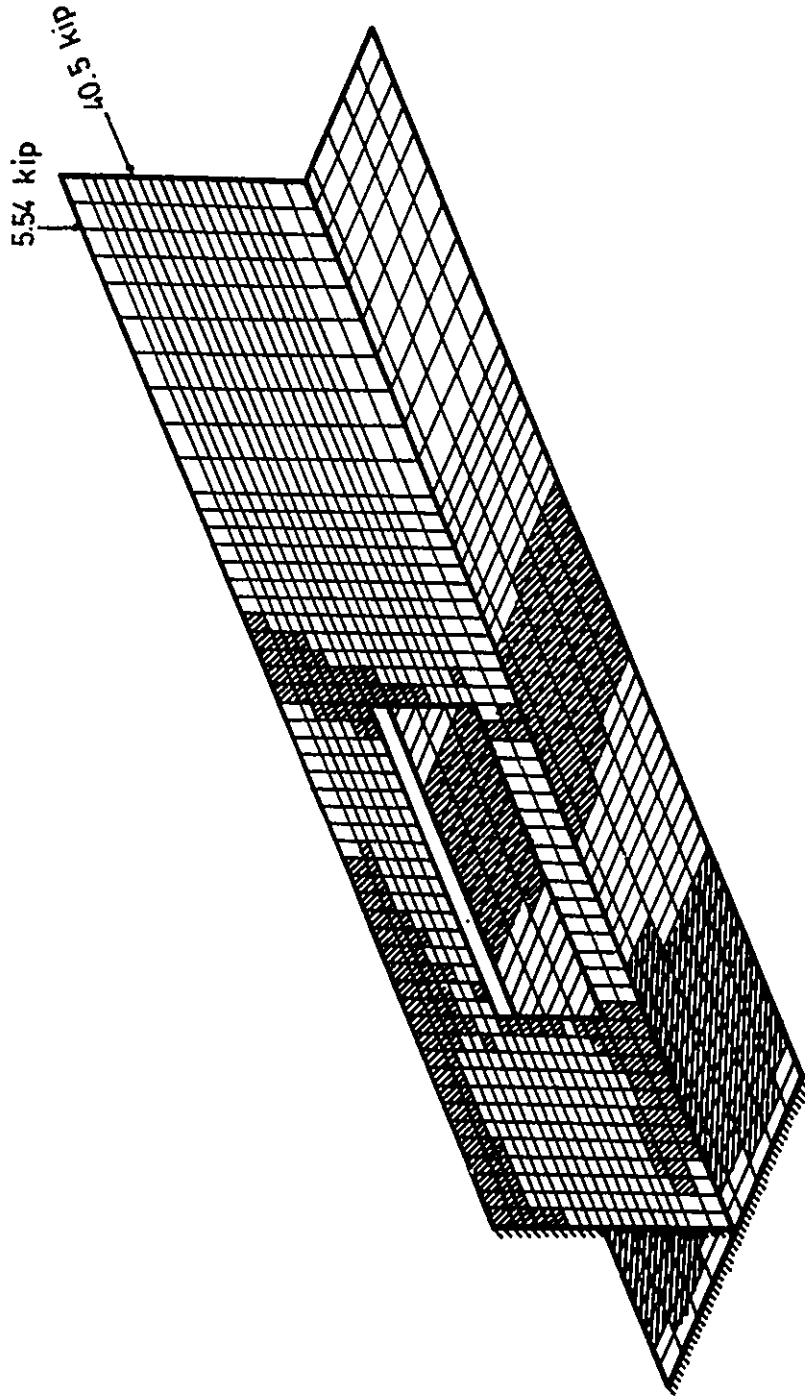


FIG. 5.201 THEORETICAL CRACK PATTERN FOR BEAM BIU4C

Note: cracked areas are hatched; 1 kip=4.45 kN

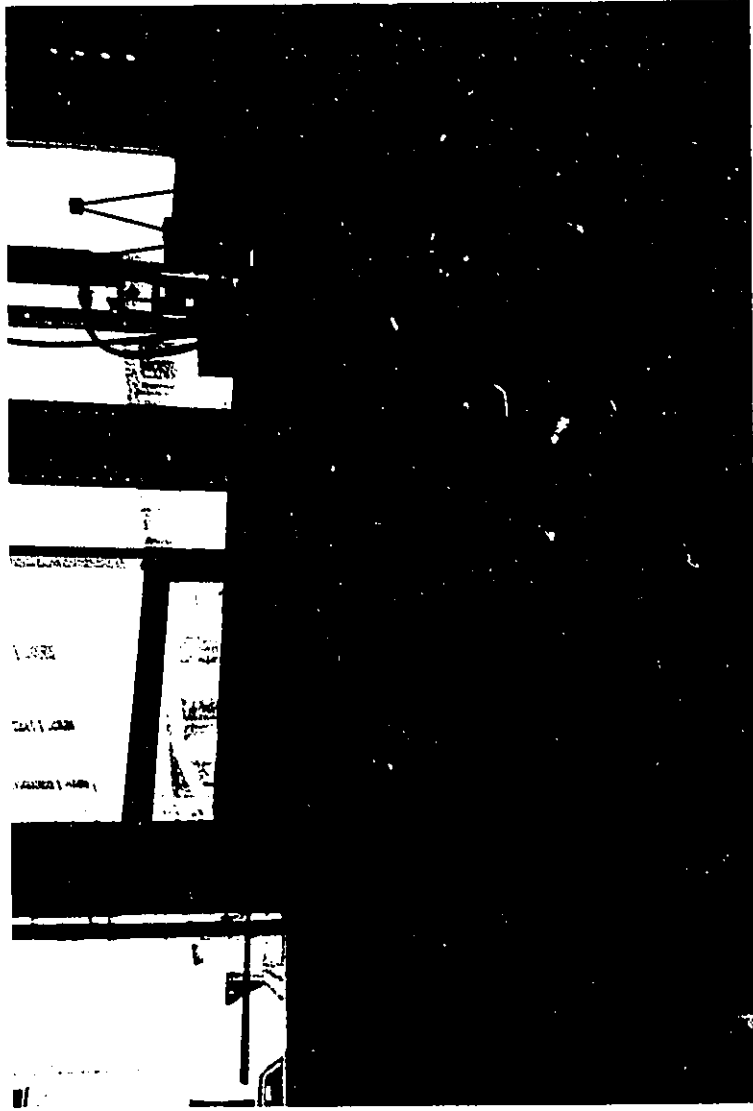


FIG. 5.202 a CRACK PATTERN FOR BEAM BIII1A



FIG. 5.202 b CRACK PATTERN FOR BEAM BIII1A

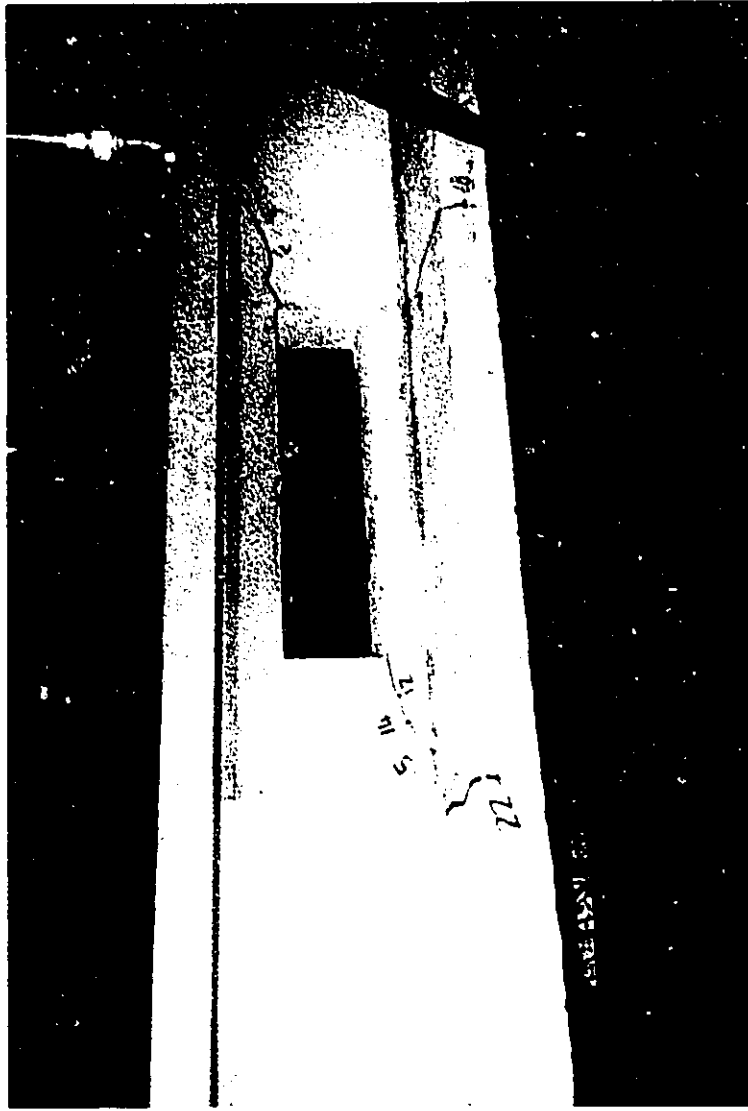


FIG. 5.202 c CRACK PATTERN FOR BEAM BIII A

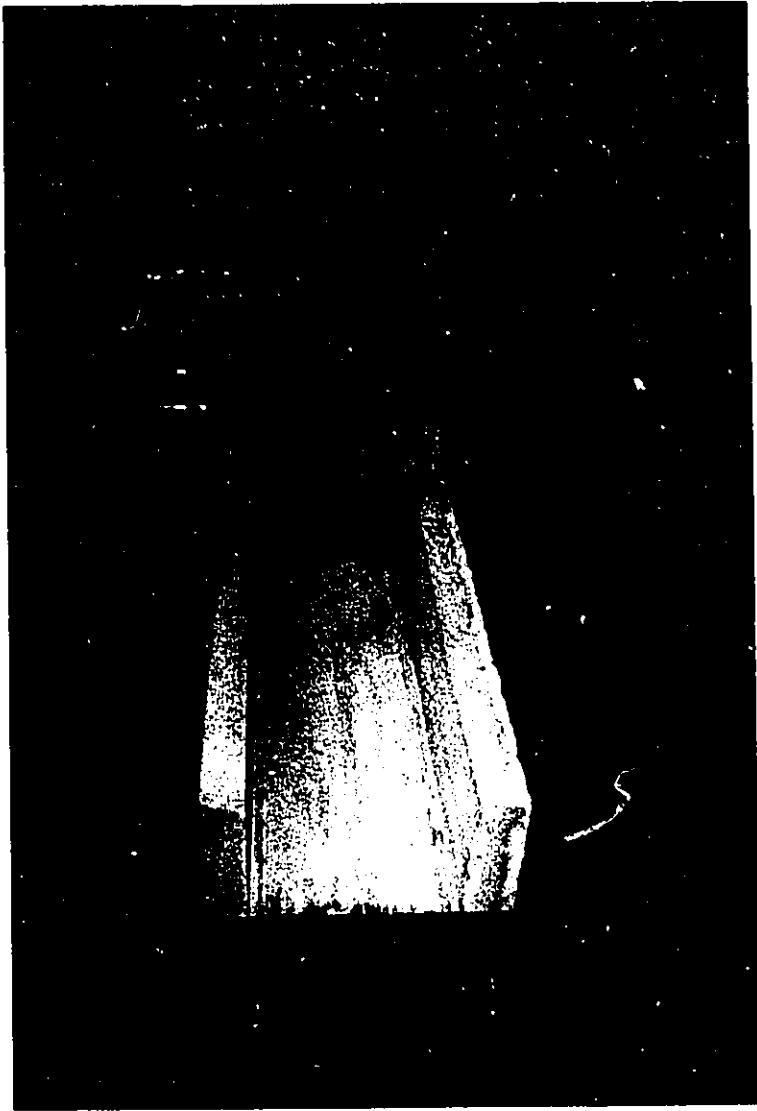


FIG. 5.203 a FAILURE MODE FOR BEAM B111A



FIG. 5.203 b FAILURE MODE FOR BEAM BIII1A



FIG. 5.203 c FAILURE MODE FOR BEAM BIII1A



FIG. 5.203 d FAILURE MODE FOR BEAM B1111A

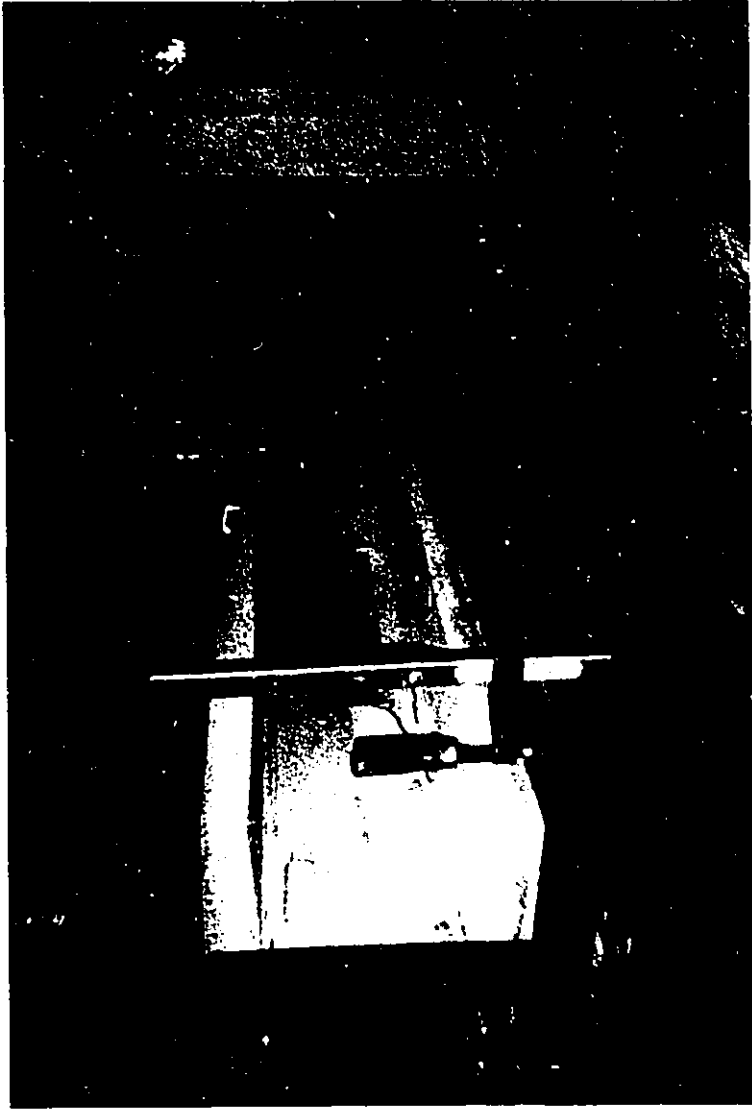


FIG. 5.204 a CRACK PATTERN FOR BEAM BIIIIC



FIG. 5.204 b CRACK PATTERN FOR BEAM BIIIIC



FIG. 5.205 FAILURE MODE FOR BEAM BIIIIC

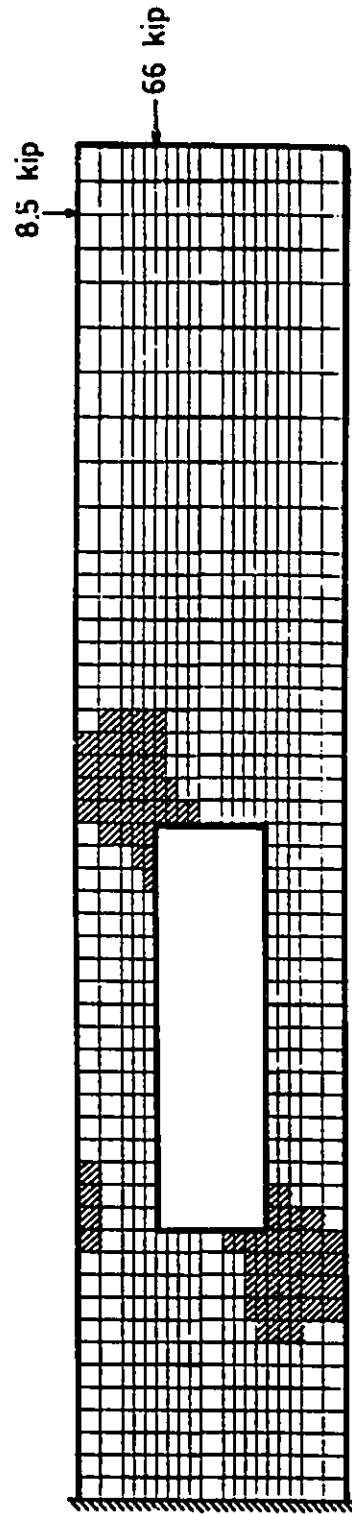


FIG. 5.206.a THEORETICAL CRACK PATTERN FOR BEAM BIII1A

Note: cracked areas are hatched; 1 kip=4.45 kN

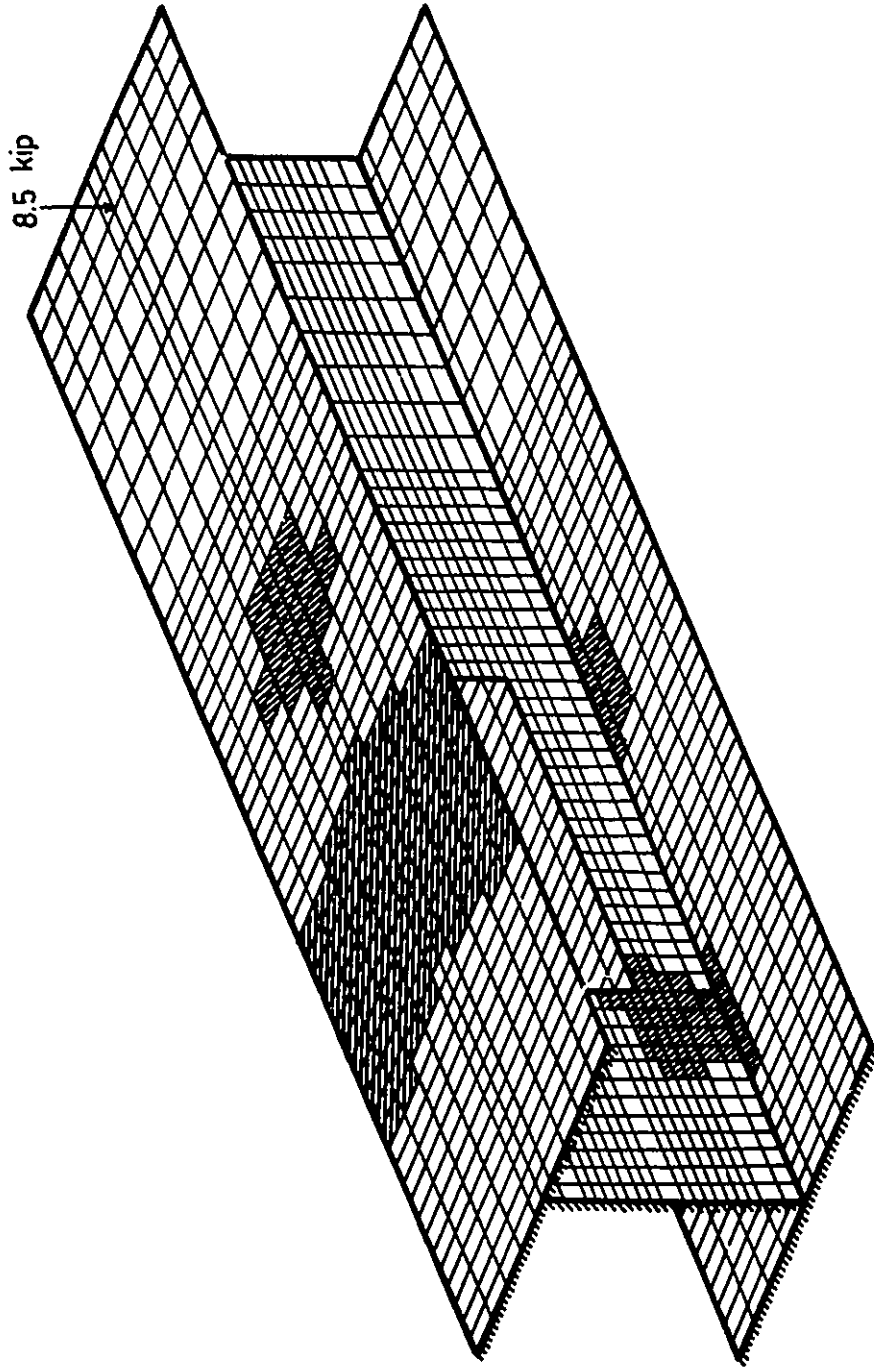


FIG. 5.206.b THEORETICAL CRACK PATTERN FOR BEAM BIII1A

Note: cracked areas are hatched; 1 kip=4.45 kN

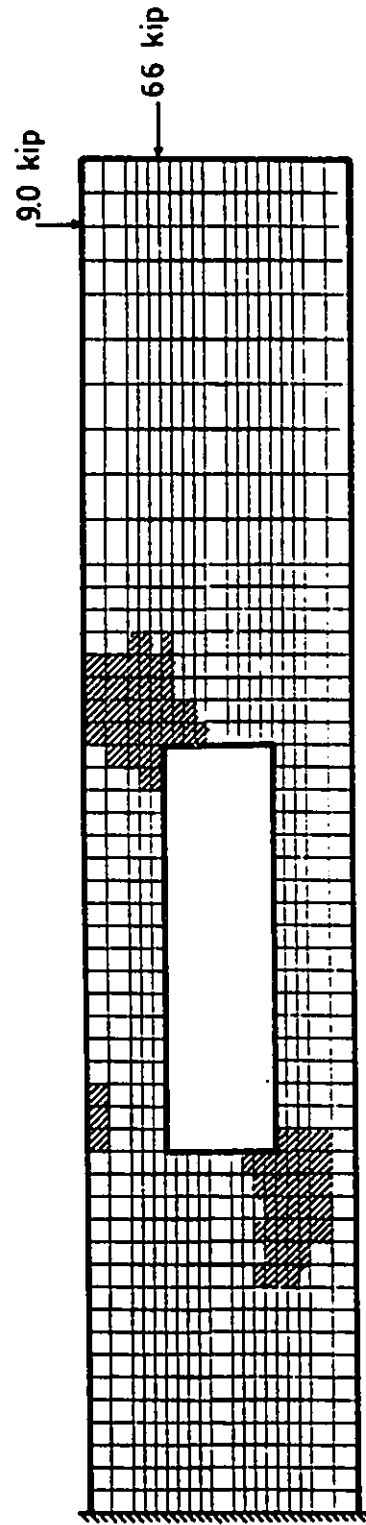


FIG. 5.207.a THEORETICAL CRACK PATTERN FOR BEAM BIIIIB

Note: cracked areas are hatched; 1 kip=4.45 kN

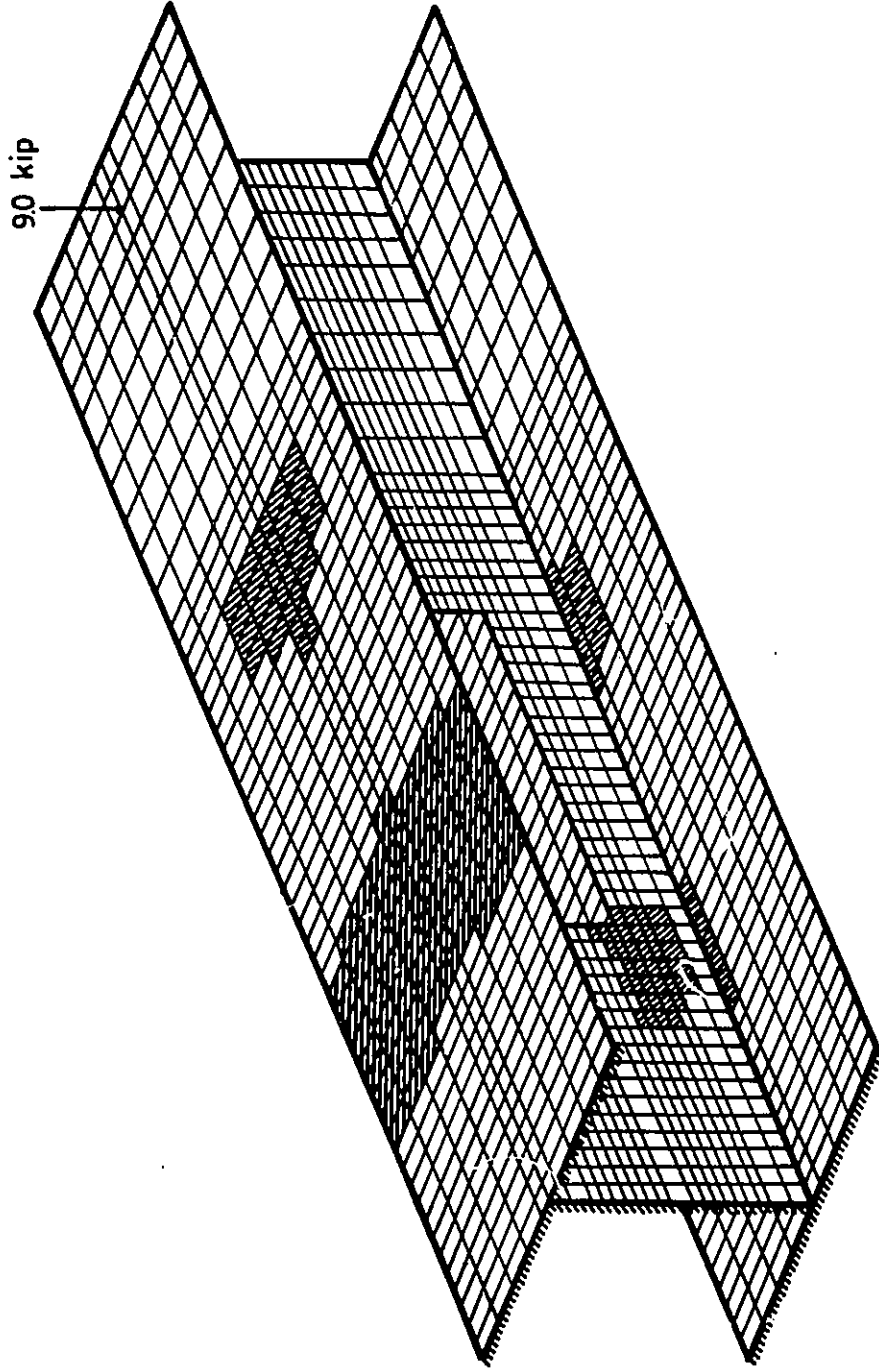


FIG. 5.207.b THEORETICAL CRACK PATTERN FOR BEAM BIIIB

Note: cracked areas are hatched; 1 kip=4.45 kN

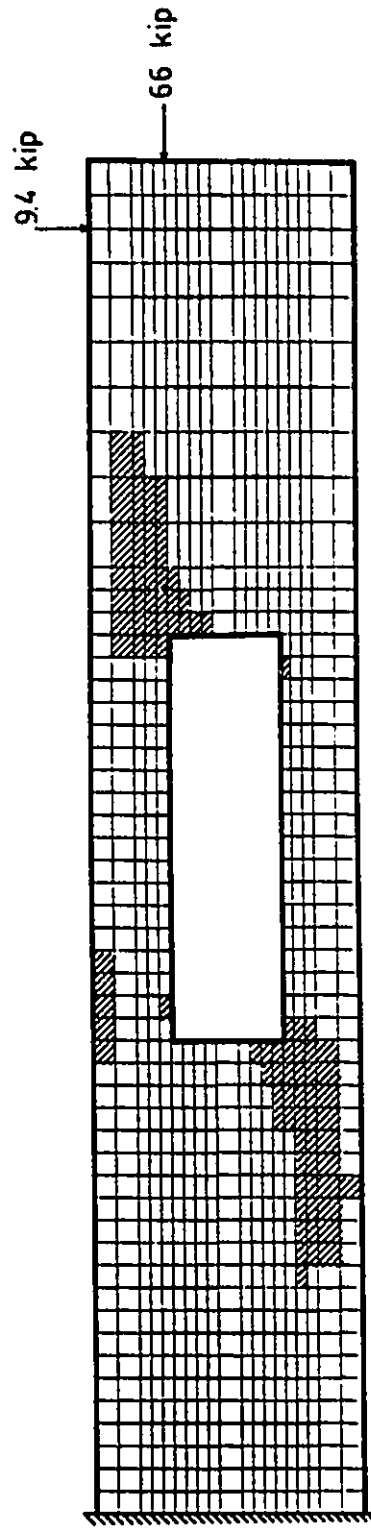


FIG. 5.208.a THEORETICAL CRACK PATTERN FOR BEAM BIHIC

Note: cracked areas are hatched; 1 kip=4.45 kN

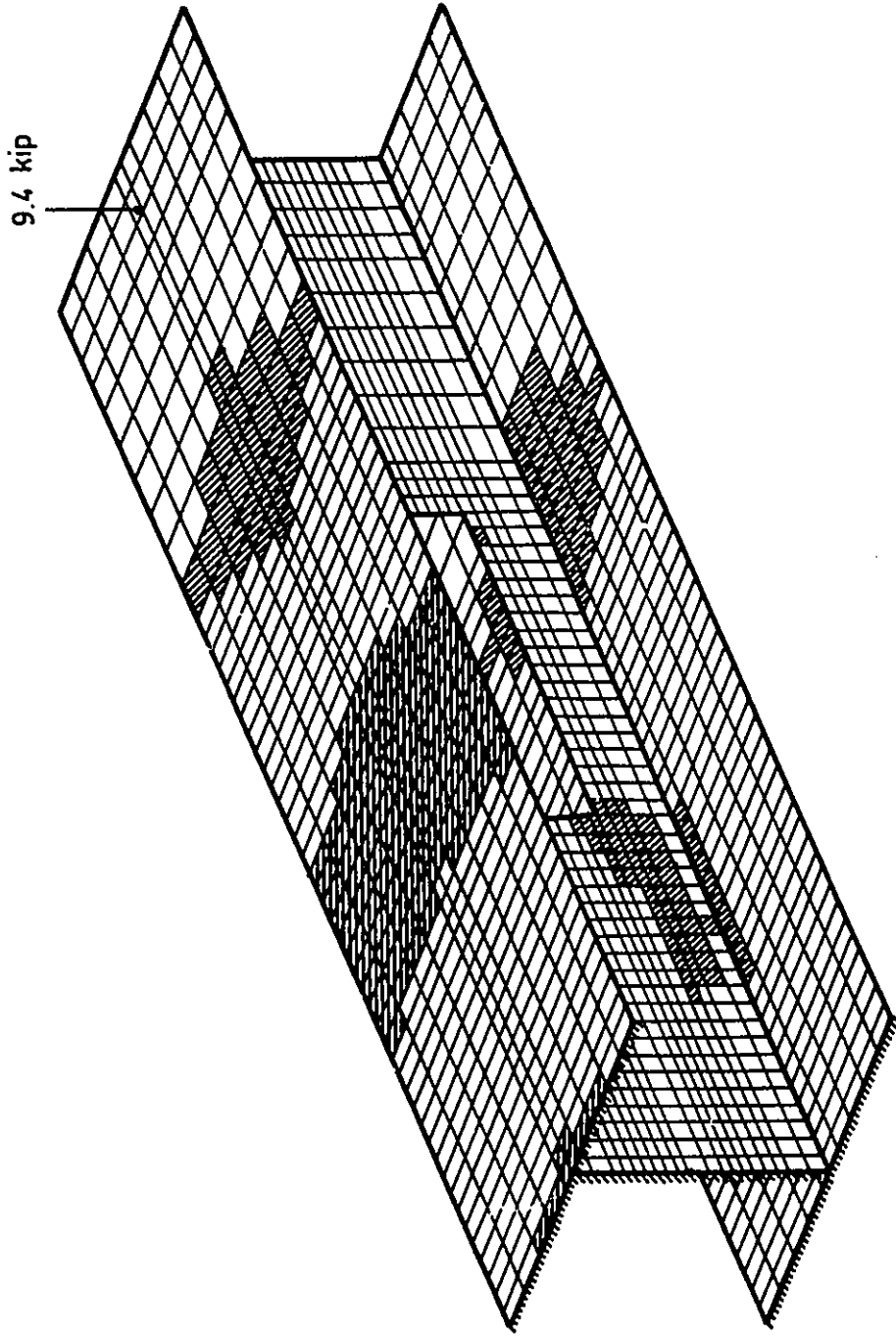


FIG. 5.208.b THEORETICAL CRACK PATTERN FOR BEAM BIIIIC

Note: cracked areas are hatched; 1 kip=4.45 kN

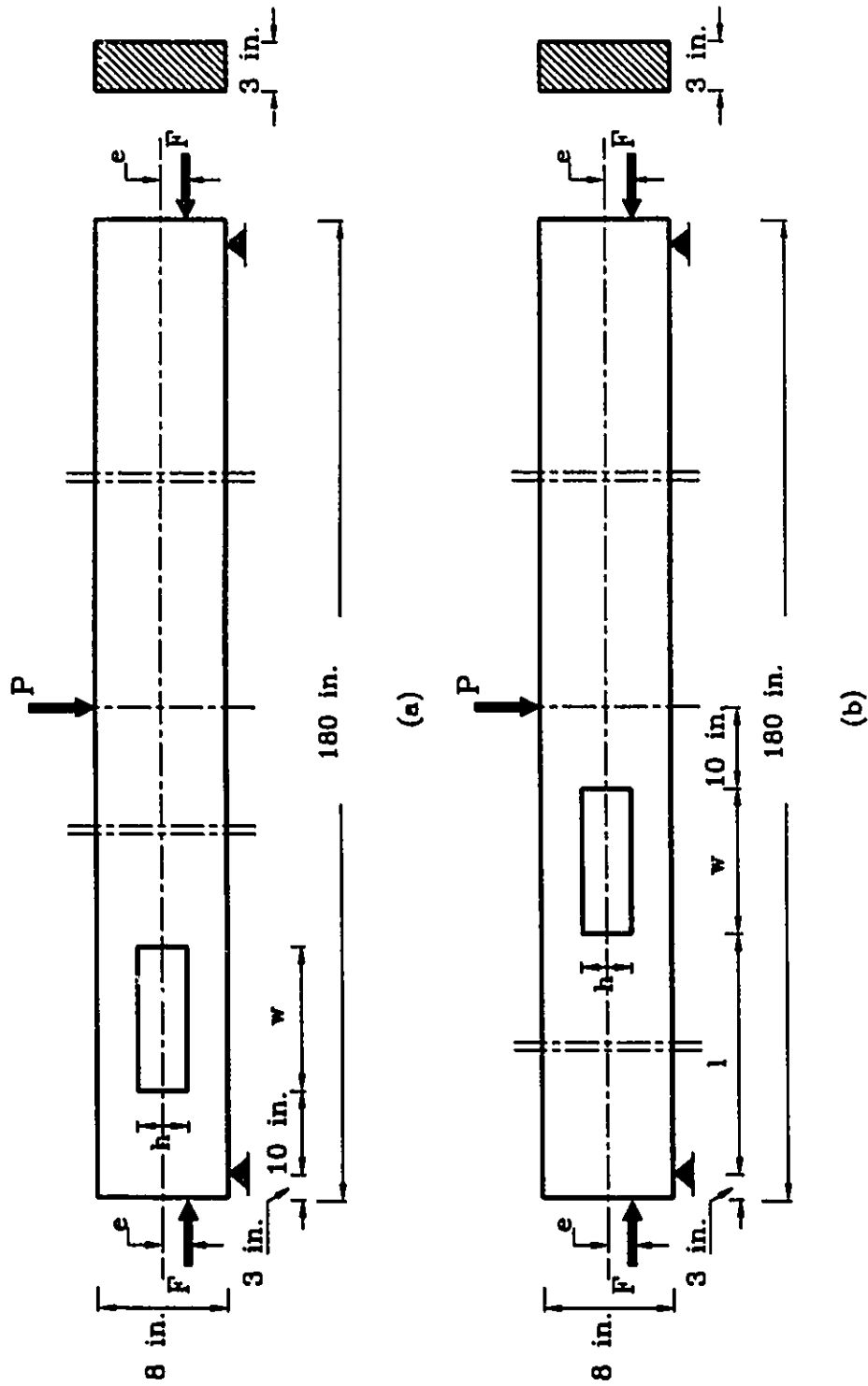
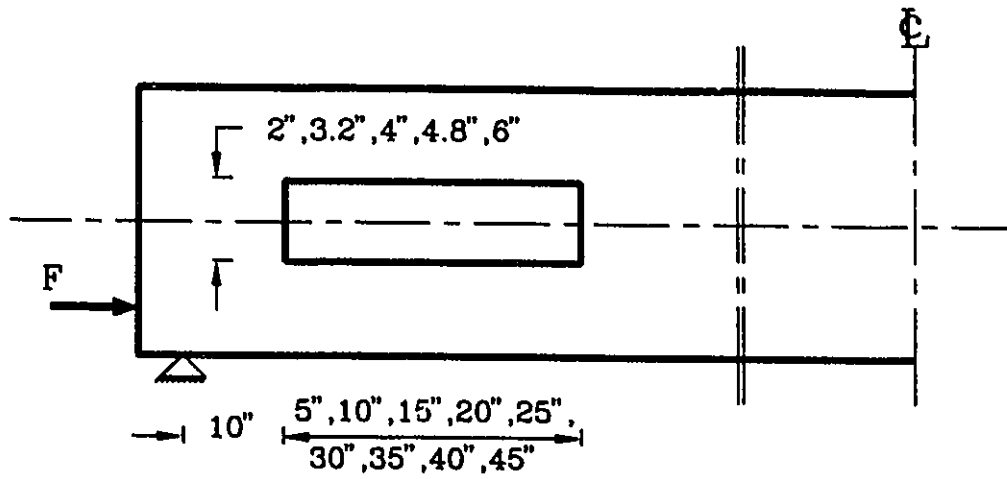
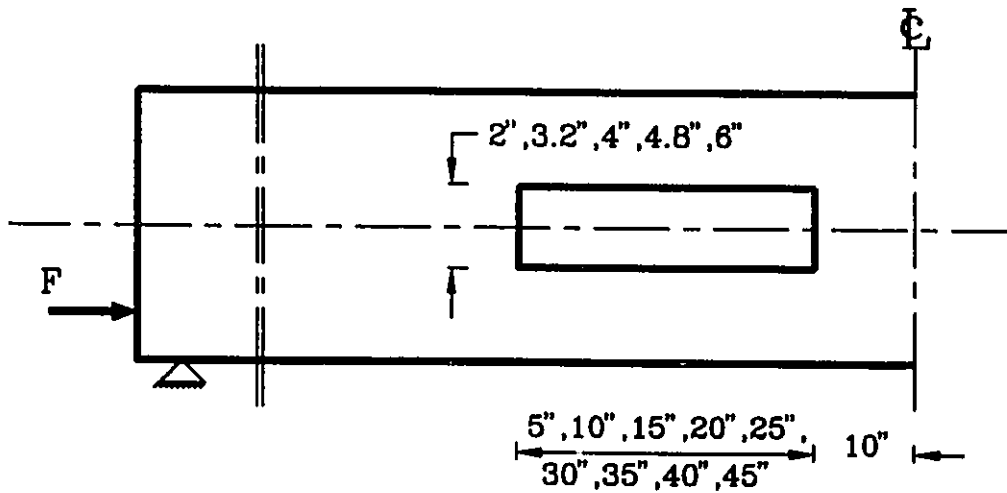


FIG. 6.1 SIMPLY SUPPORTED PRESTRESSED BEAMS CONSIDERED IN DYNAMIC ANALYSIS
 (a) OPENING IN HIGH SHEAR REGION; (b) OPENING IN HIGH MOMENT REGION

Note: 1 in. = 25.4 mm



(a) OPENING IN HIGH SHEAR REGION



(b) OPENING IN HIGH MOMENT REGION

FIG. 6.2 GEOMETRIES OF SIMPLY SUPPORTED BEAMS
CONSIDERED IN THE PARAMETRIC STUDY

Note: 1 in.=25.4 mm

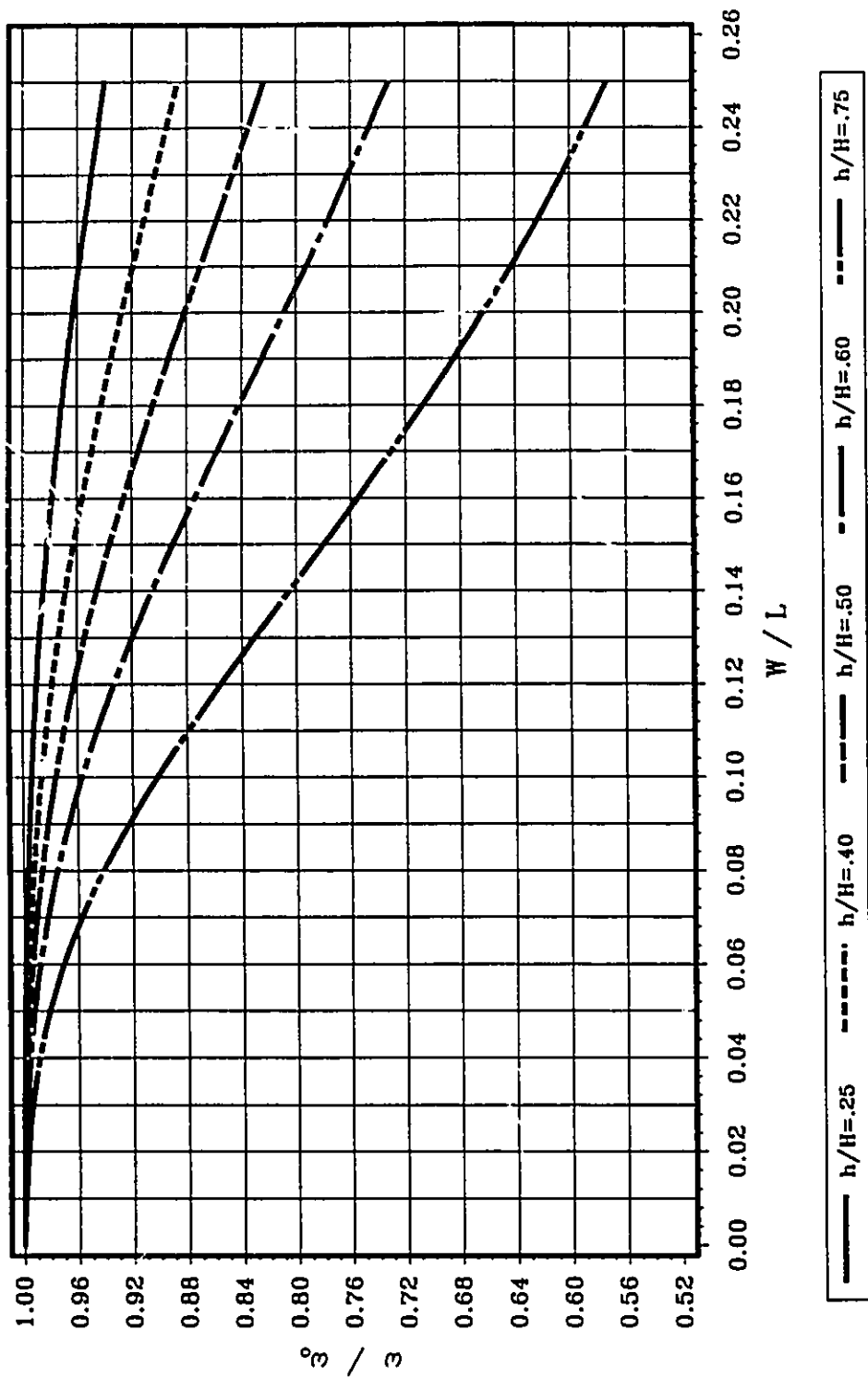


FIG. 6.3 FUNDAMENTAL FREQUENCY FOR BEAM WITH SHEAR OPENING

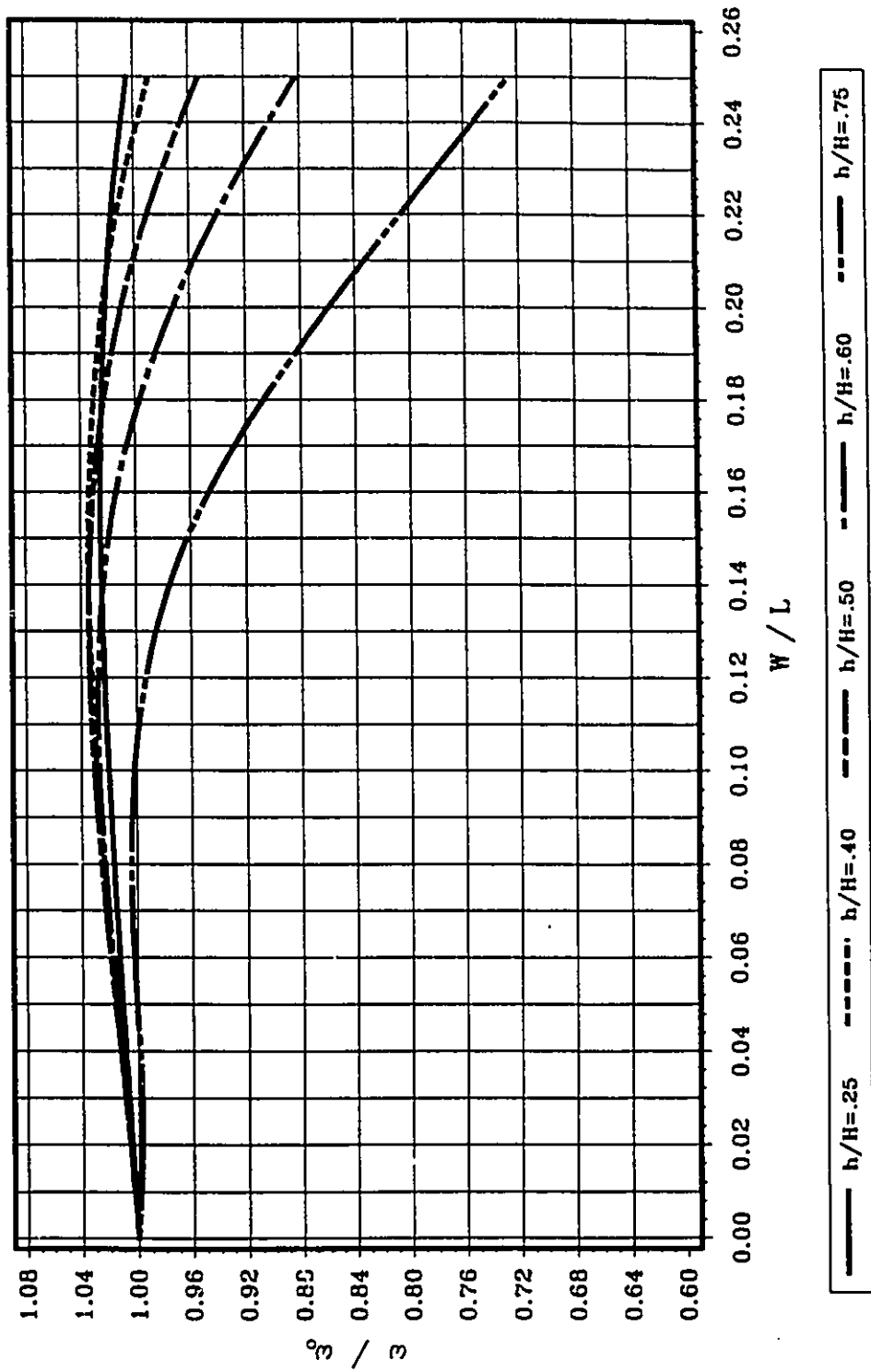


FIG. 6.4 FUNDAMENTAL FREQUENCY FOR BEAM WITH BENDING OPENING

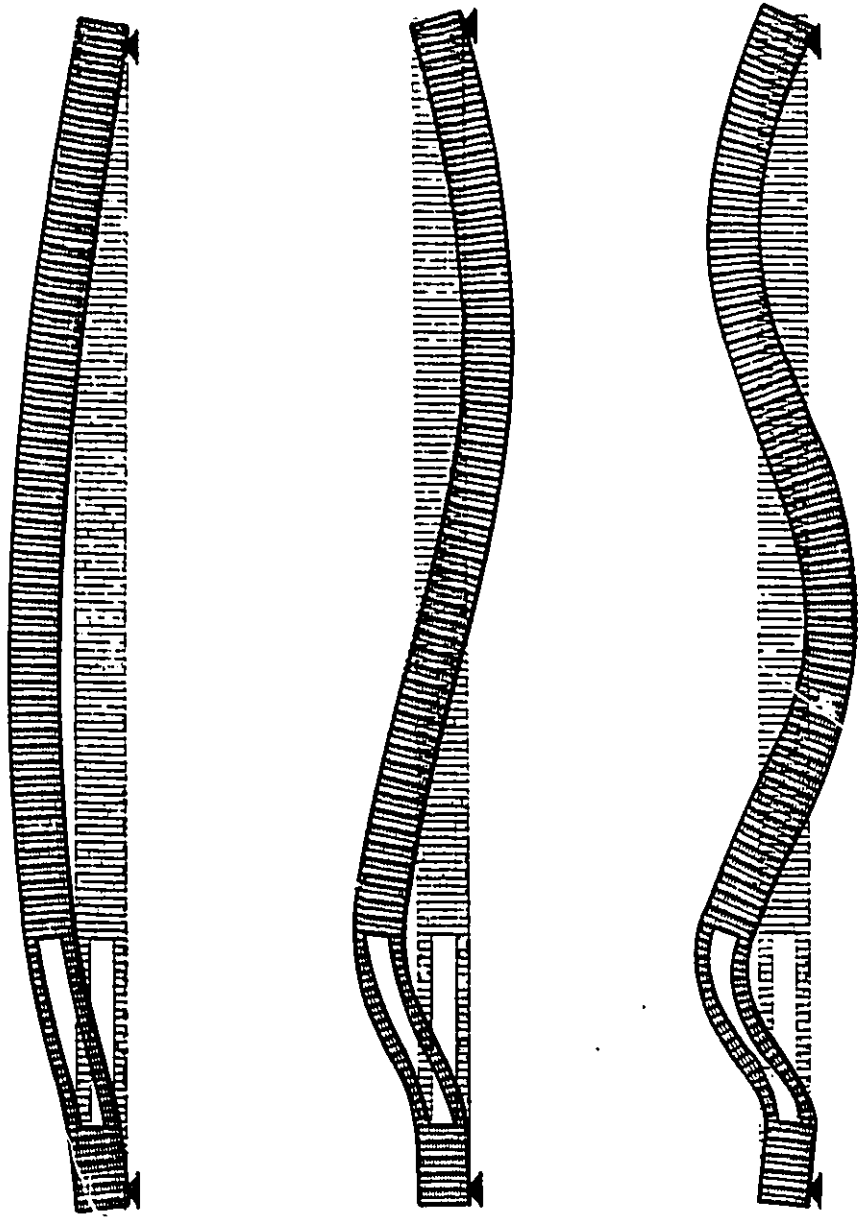


FIG. 6.5 FIRST THREE MODE SHAPES OF SIMPLY SUPPORTED BEAM
WITH SHEAR OPENING

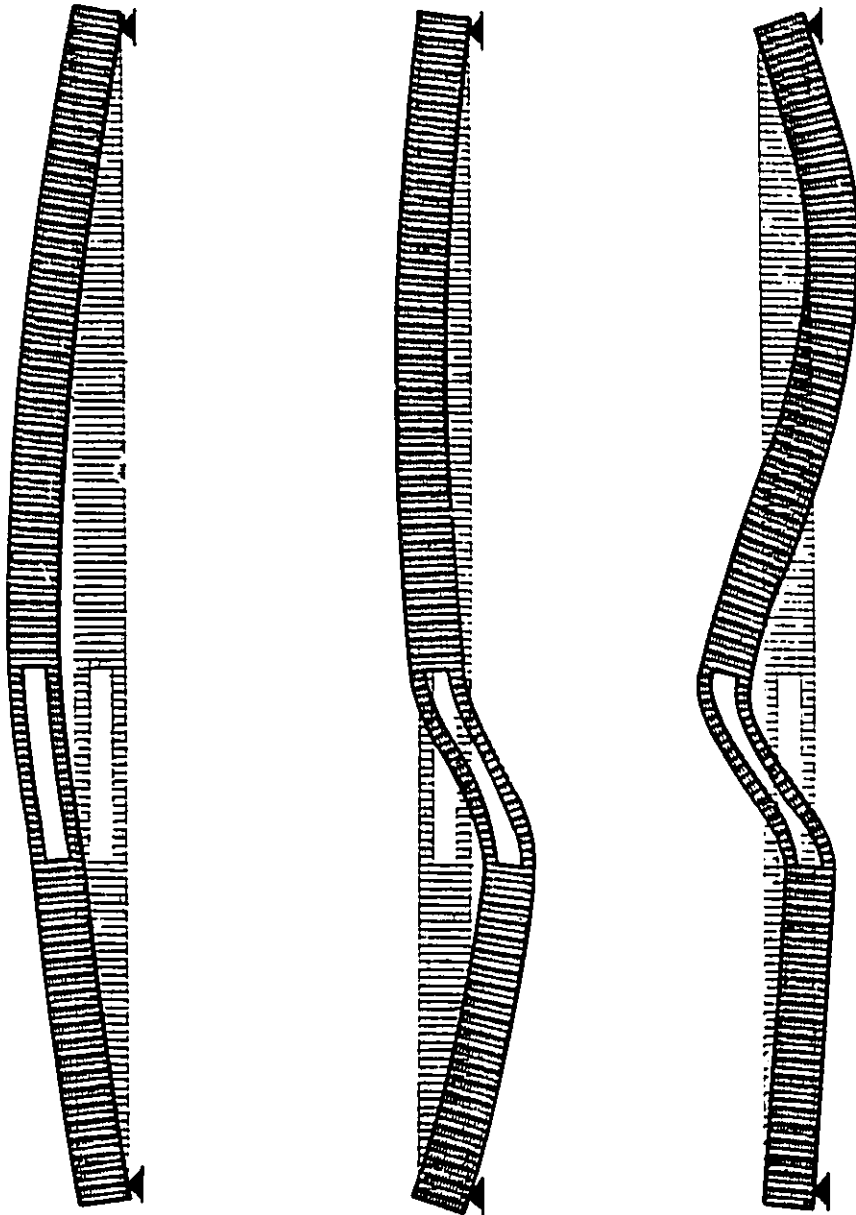


FIG. 6.6 FIRST THREE MODE SHAPES OF SIMPLY SUPPORTED BEAM
WITH BENDING OPENING



FIG. 6.7 NATURAL FREQUENCIES FOR SOLID BEAM, BEAM WITH SHEAR OPENING & BEAM WITH BENDING OPENING

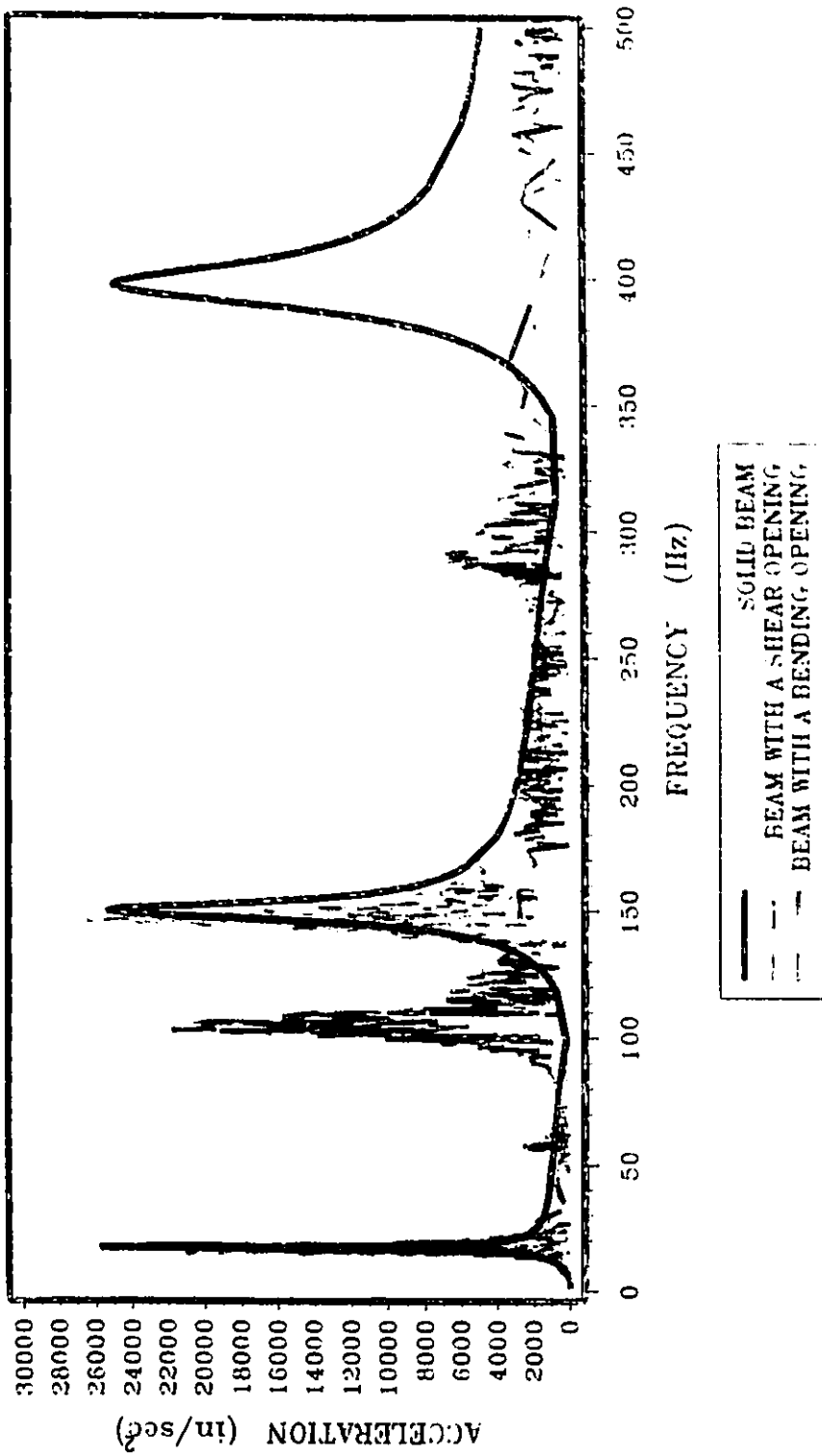


FIG. 6.8 FREQUENCY SPECTRUM RESPONSE
(STEADY STATE ANALYSIS)

Note. 1 in. = 25.4 mm

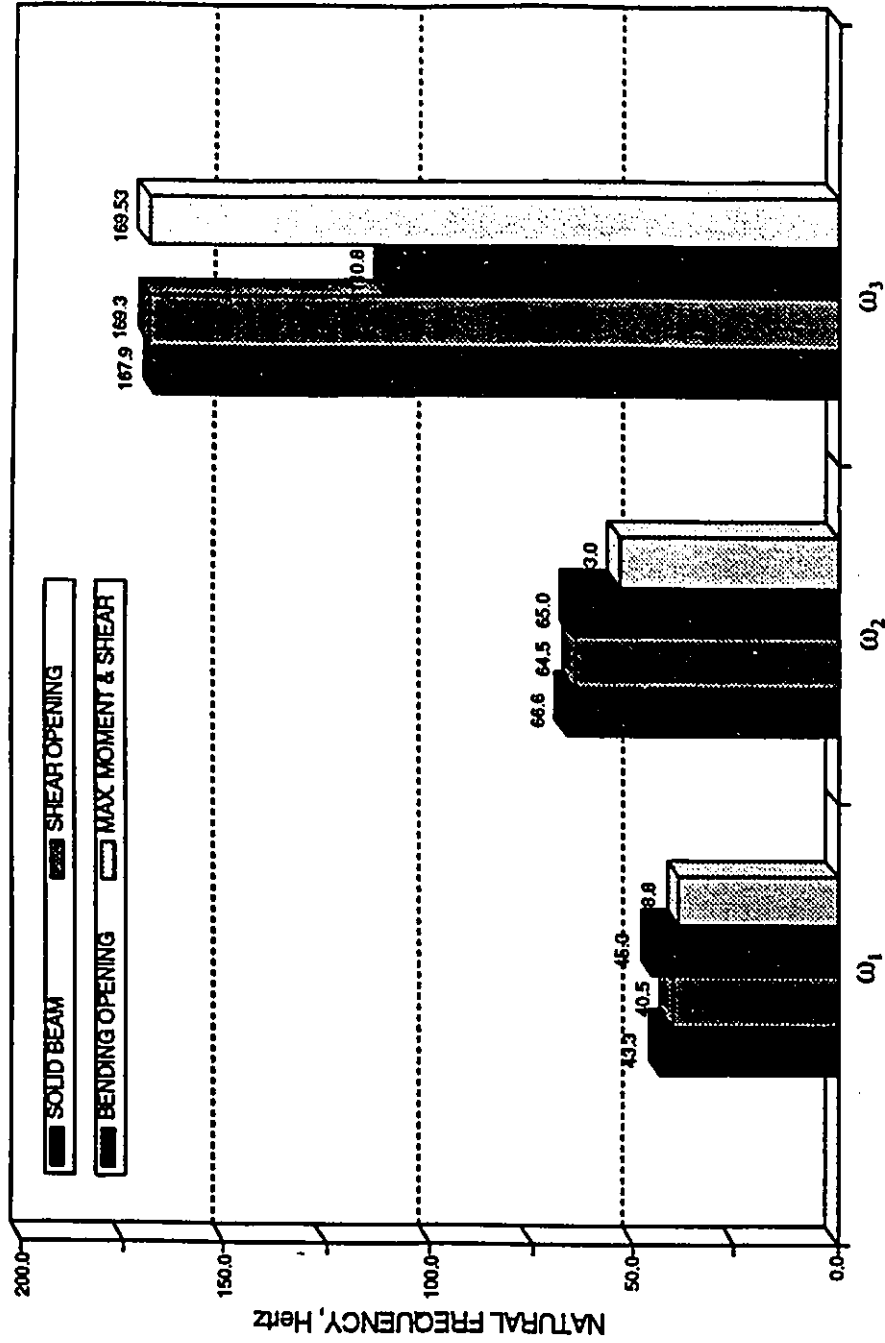


FIG. 6.9 NATURAL FREQUENCIES FOR CONTINUOUS BEAMS
WITH TWO EQUAL-SPANS

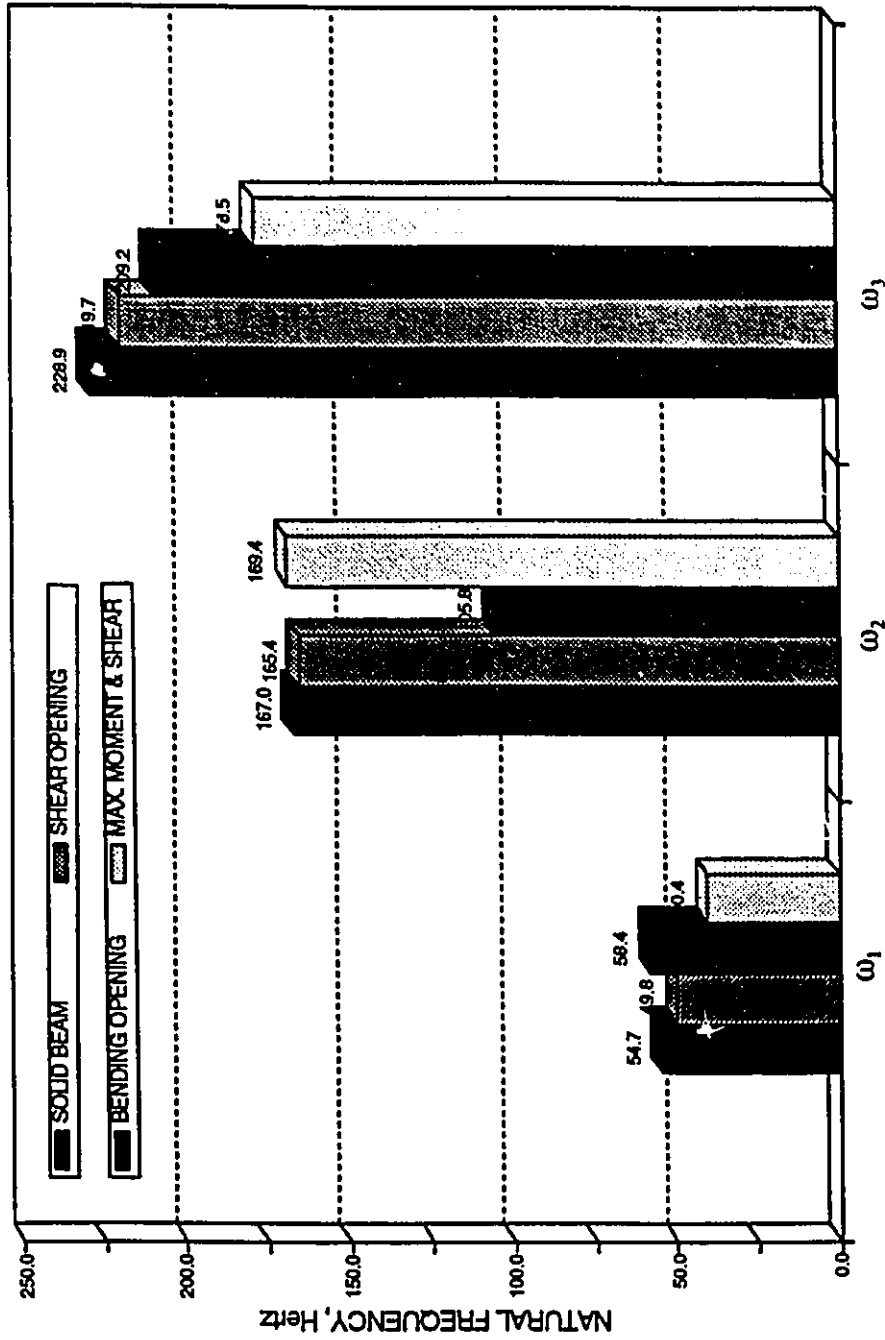


FIG. 6.10 NATURAL FREQUENCIES FOR CONTINUOUS BEAMS
WITH TWO UNEQUAL-SPANS

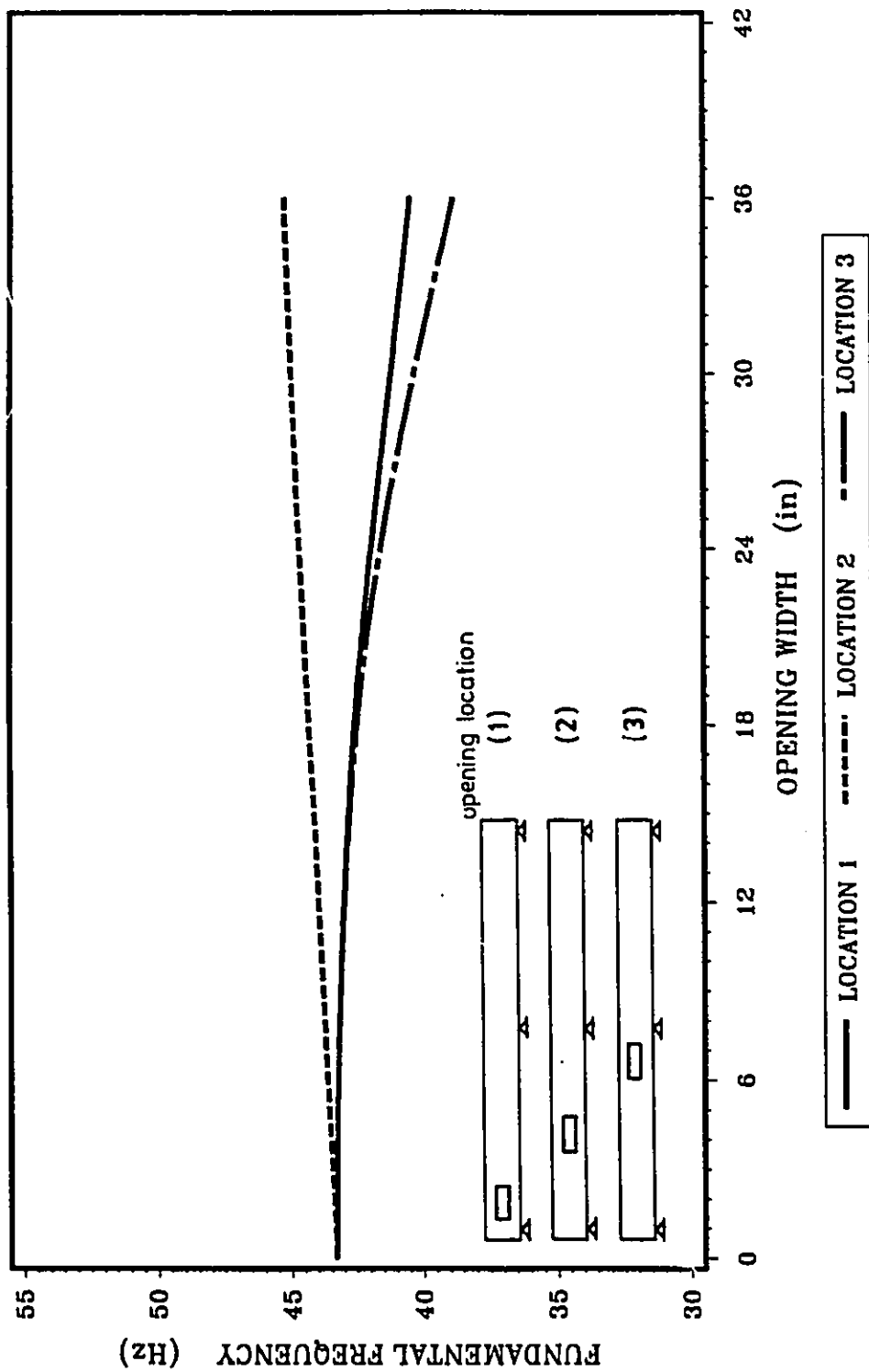


FIG. 6.11 RELATIONSHIP BETWEEN OPENING WIDTH AND FUNDAMENTAL FREQUENCY FOR CONTINUOUS BEAMS WITH TWO EQUAL SPANS

Note: 1 in.=25.4 mm

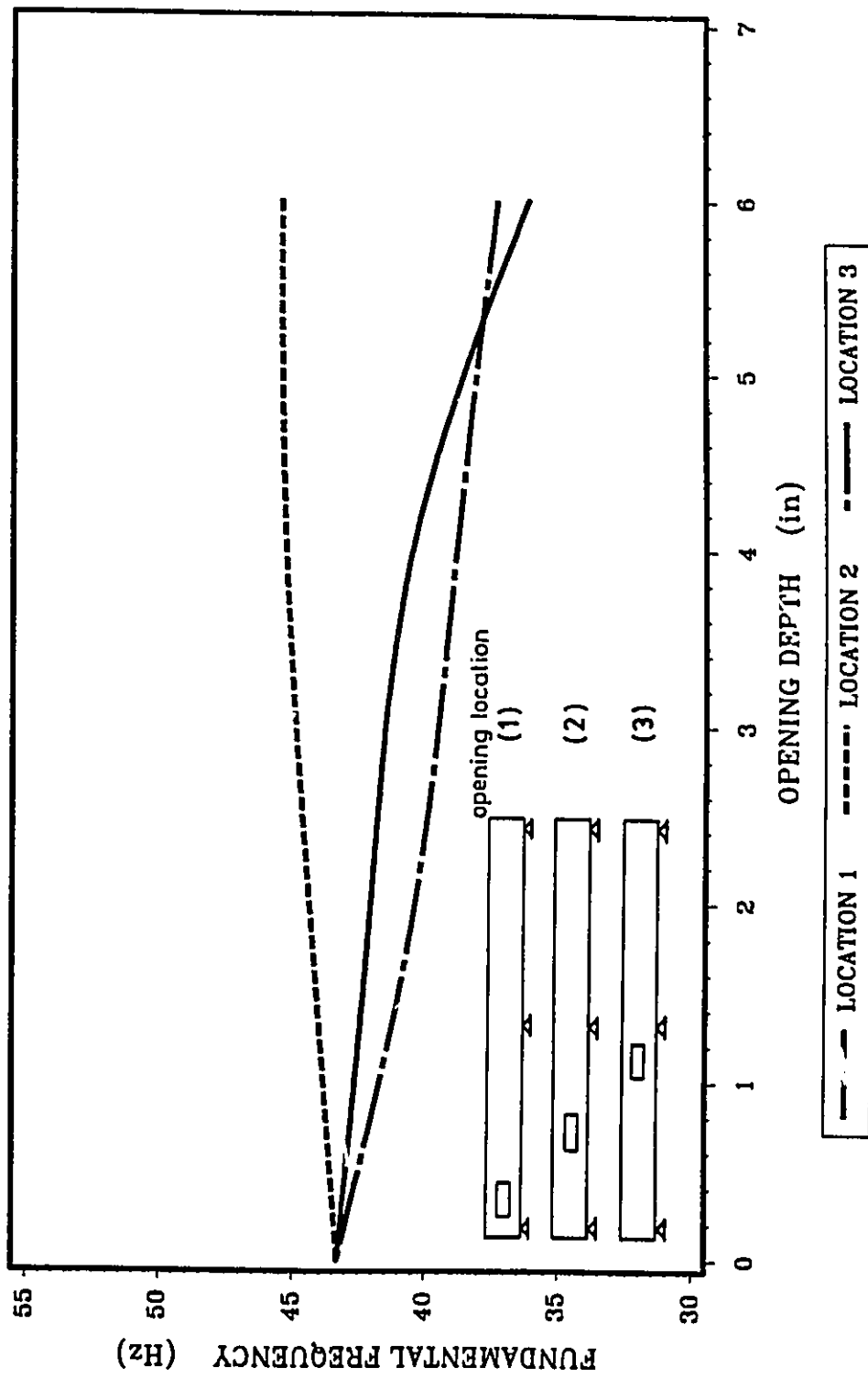


FIG. 6.12 RELATIONSHIP BETWEEN OPENING DEPTH AND FUNDAMENTAL FREQUENCY FOR CONTINUOUS BEAMS WITH TWO EQUAL SPANS

Note: 1 in.=25.4 mm

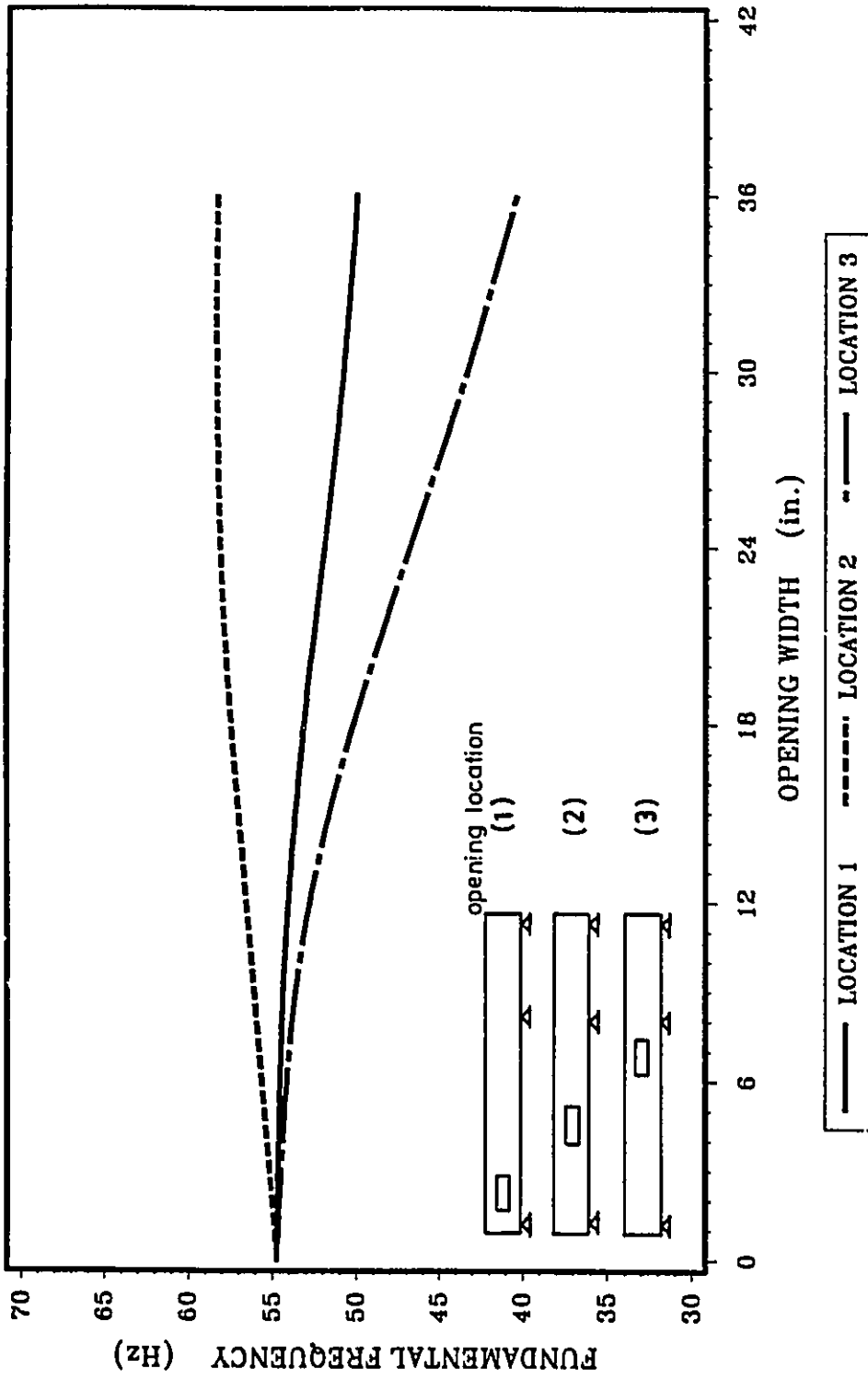


FIG. 6.13 RELATIONSHIP BETWEEN OPENING WIDTH AND FUNDAMENTAL FREQUENCY FOR CONTINUOUS BEAMS WITH TWO UNEQUAL SPANS

Note: 1 in.=25.4 mm

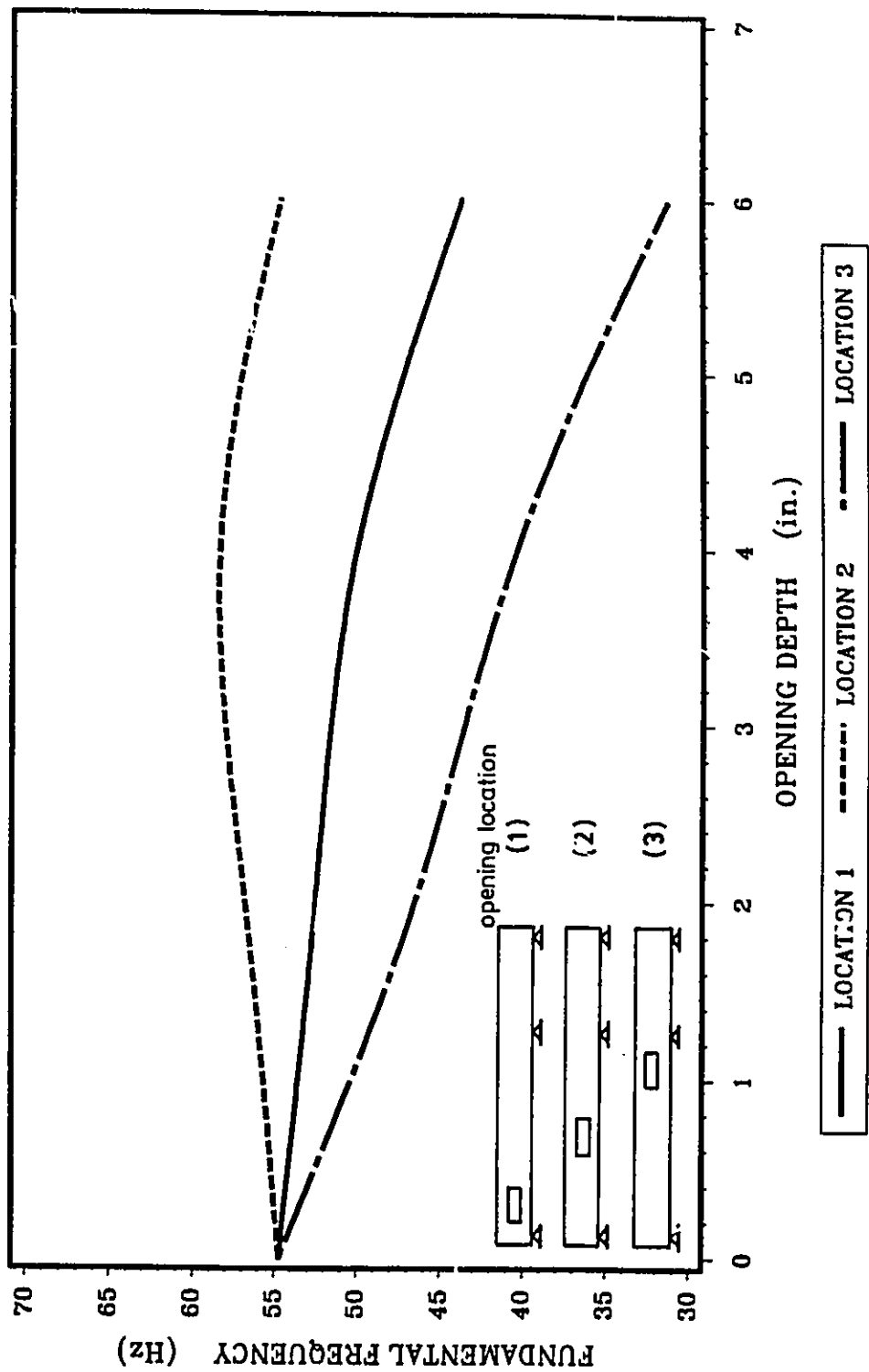


FIG. 6.14 RELATIONSHIP BETWEEN OPENING DEPTH AND FUNDAMENTAL FREQUENCY FOR CONTINUOUS BEAMS WITH TWO UNEQUAL SPANS

Note: 1 in. = 25.4 mm

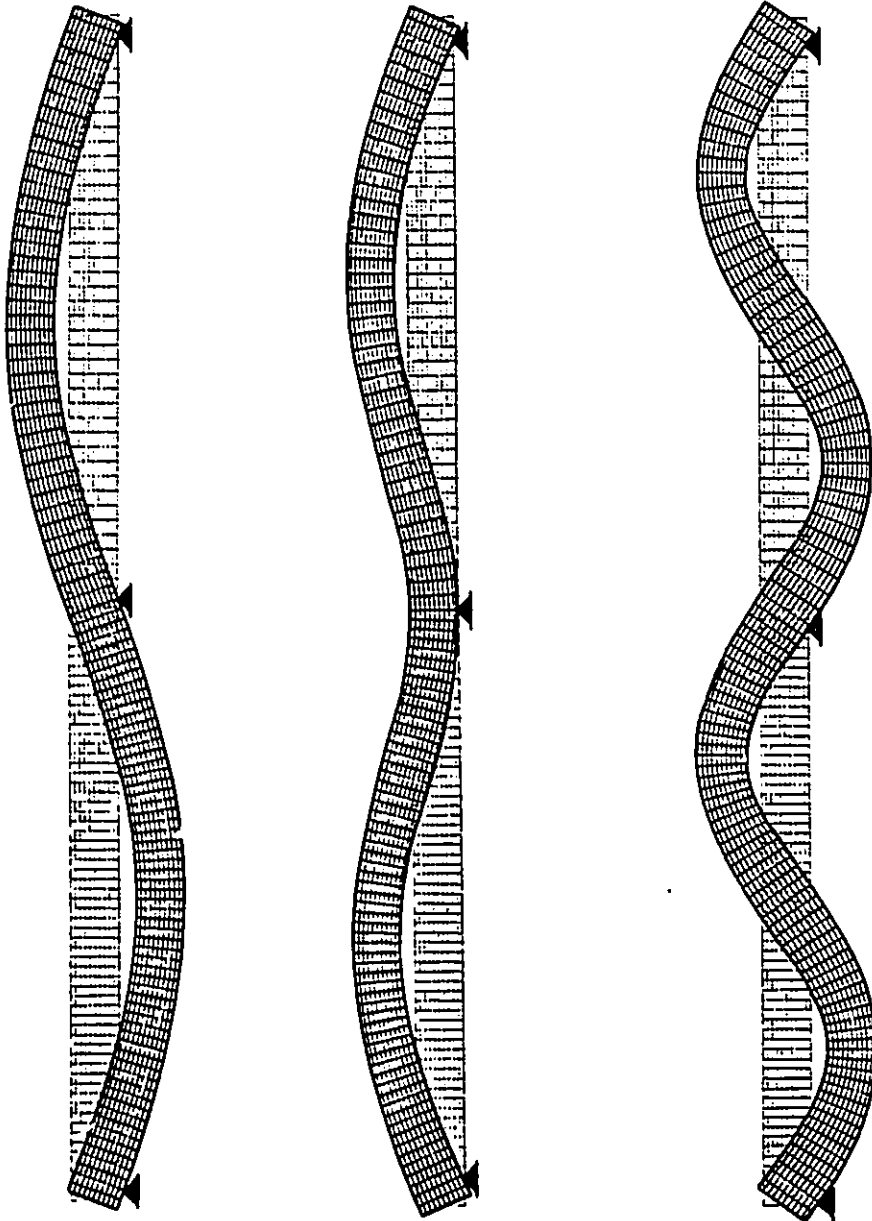


FIG. 6.15 FIRST THREE MODE SHAPES OF TWO EQUAL-SPANS CONTINUOUS BEAM
WITH NO OPENINGS

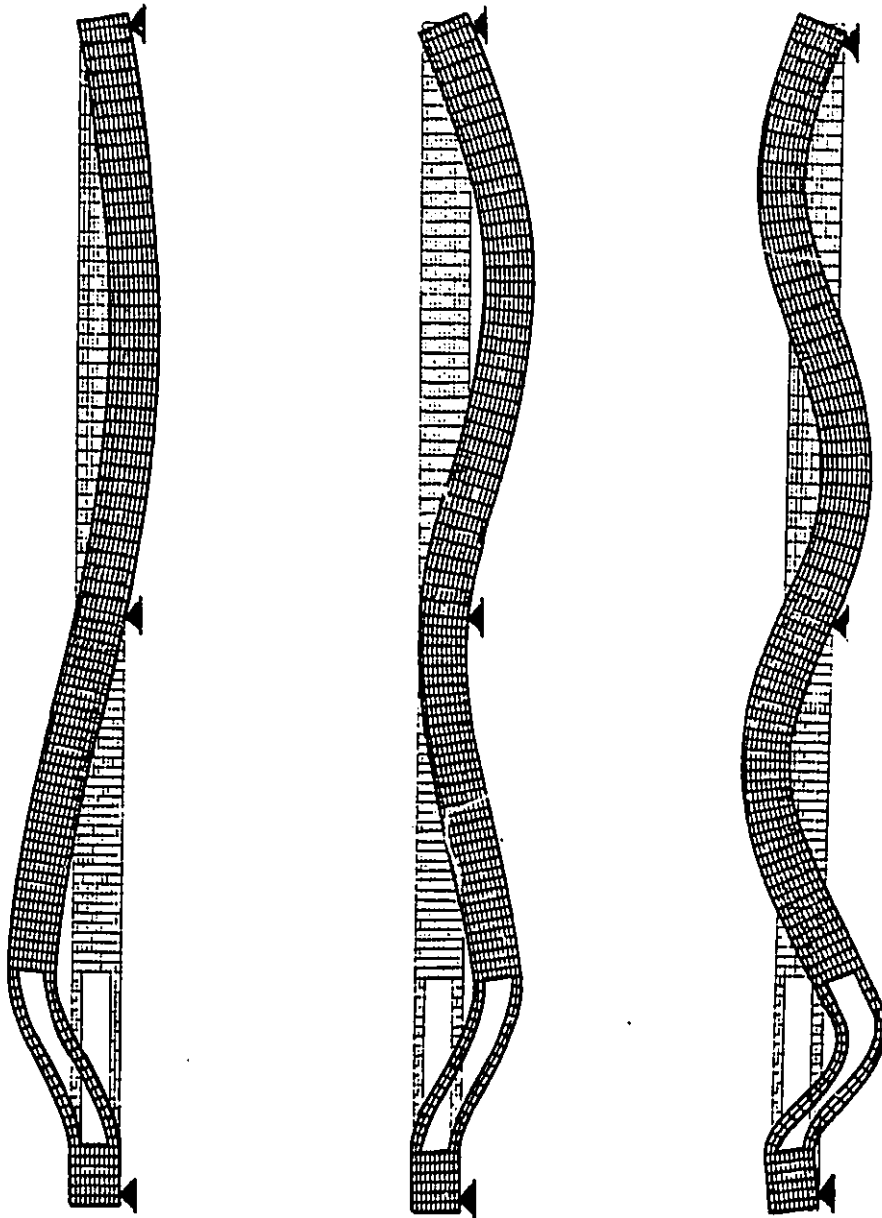


FIG. 6.16 FIRST THREE MODE SHAPES OF TWO EQUAL-SPANS CONTINUOUS BEAM
WITH OPENING CLOSE TO THE EXTERIOR SUPPORT

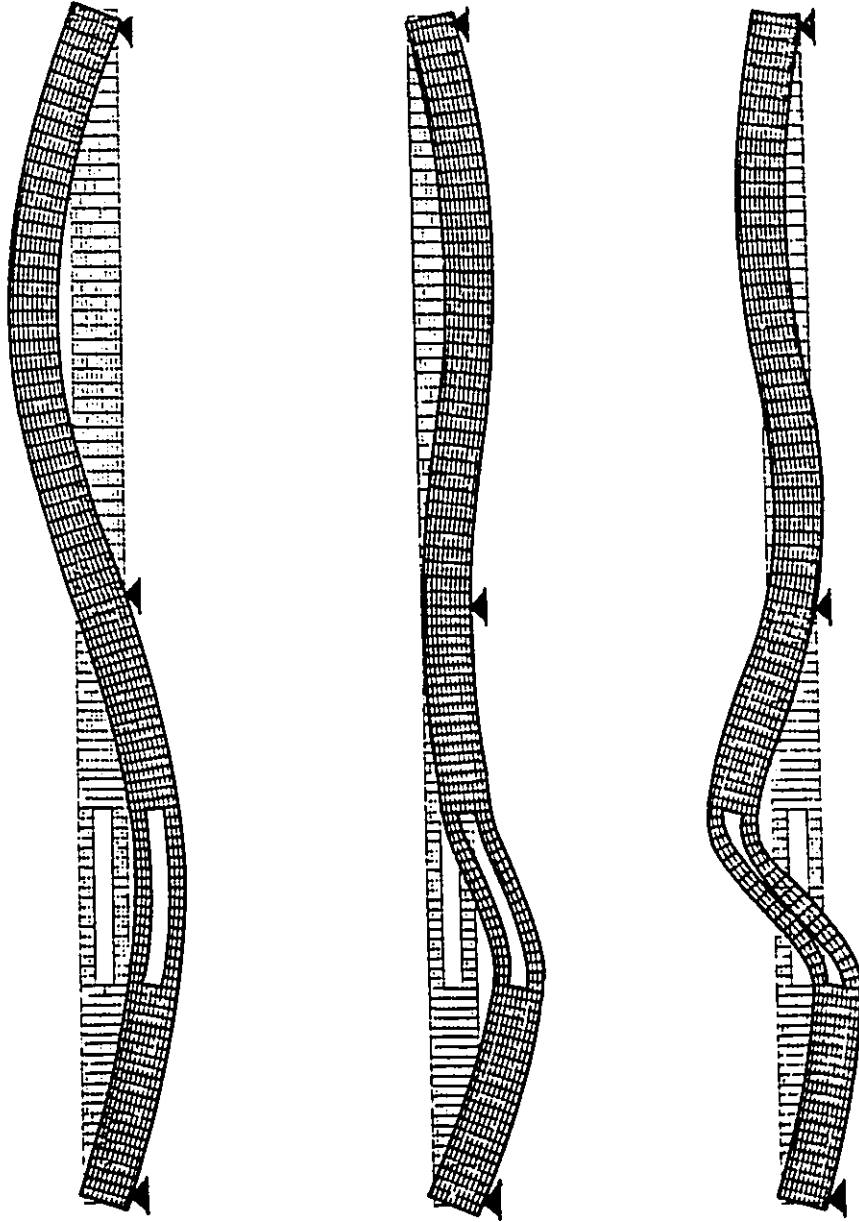


FIG. 6.17 FIRST THREE MODE SHAPES OF TWO EQUAL-SPANS CONTINUOUS BEAM
WITH OPENING AT MID-SPAN

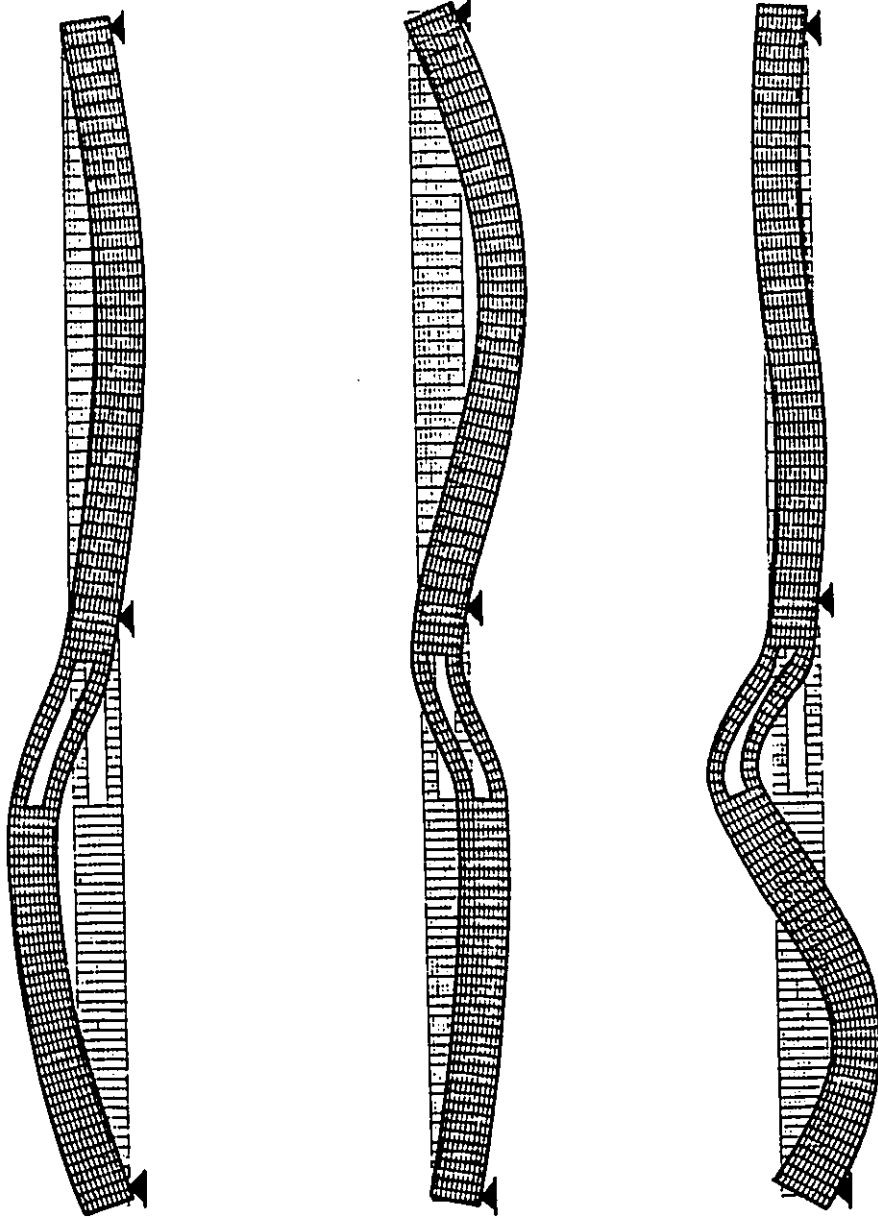


FIG. 6.18 FIRST THREE MODE SHAPES OF TWO EQUAL-SPANS CONTINUOUS BEAM
WITH OPENING CLOSE TO THE INTERIOR SUPPORT

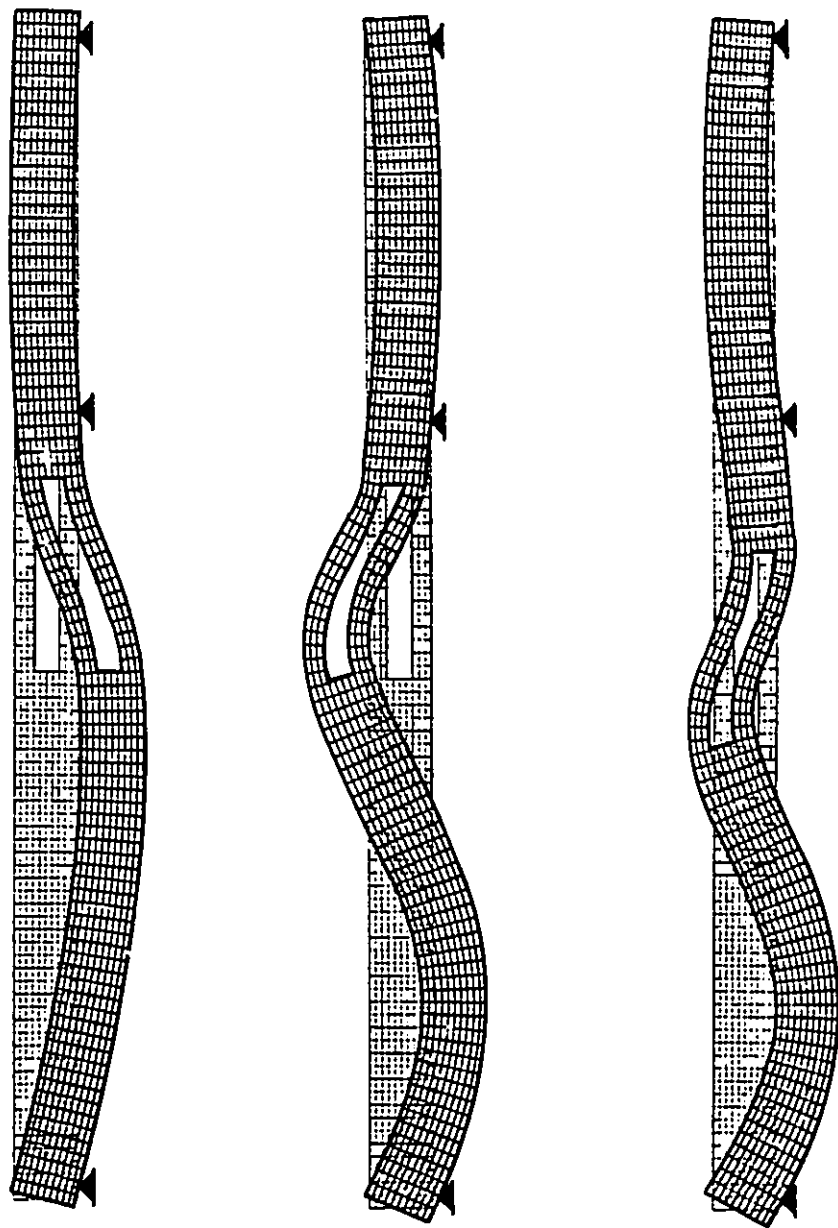


FIG. 6.19 FIRST THREE MODE SHAPES OF TWO UNEQUAL-SPANS CONTINUOUS BEAM
WITH OPENING CLOSE TO THE INTERIOR SUPPORT

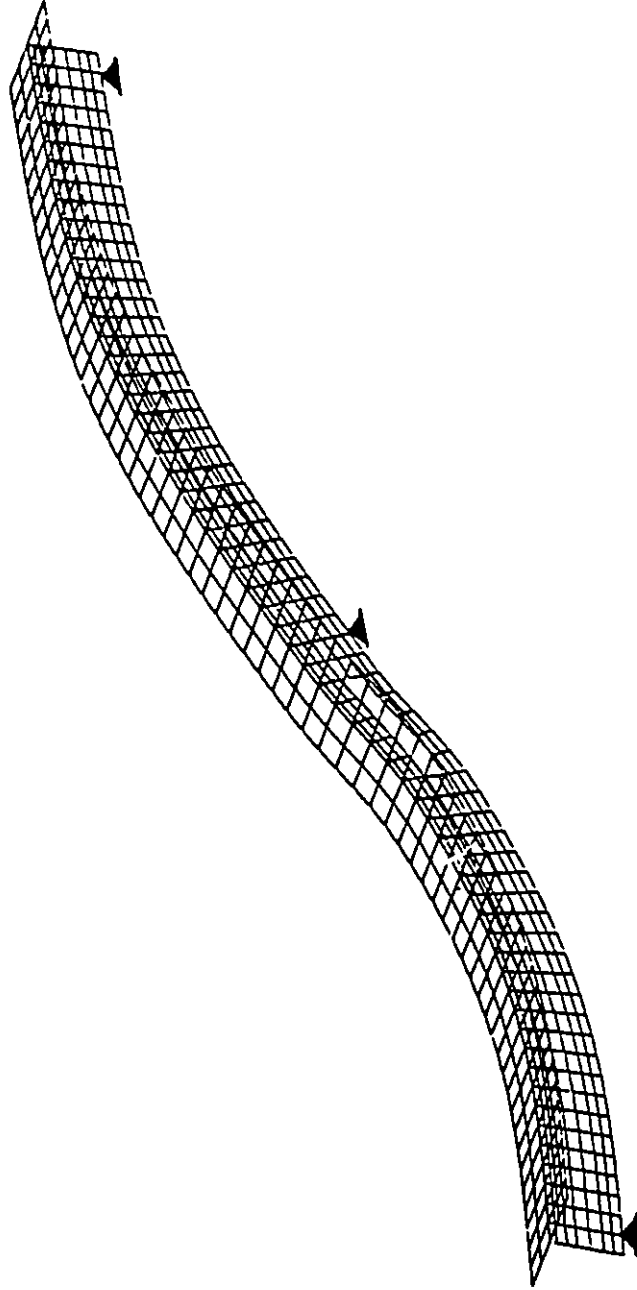


FIG. 6.20 a FIRST MODE SHAPE OF TWO EQUAL-SPANS CONTINUOUS T-BEAM
WITH OPENING

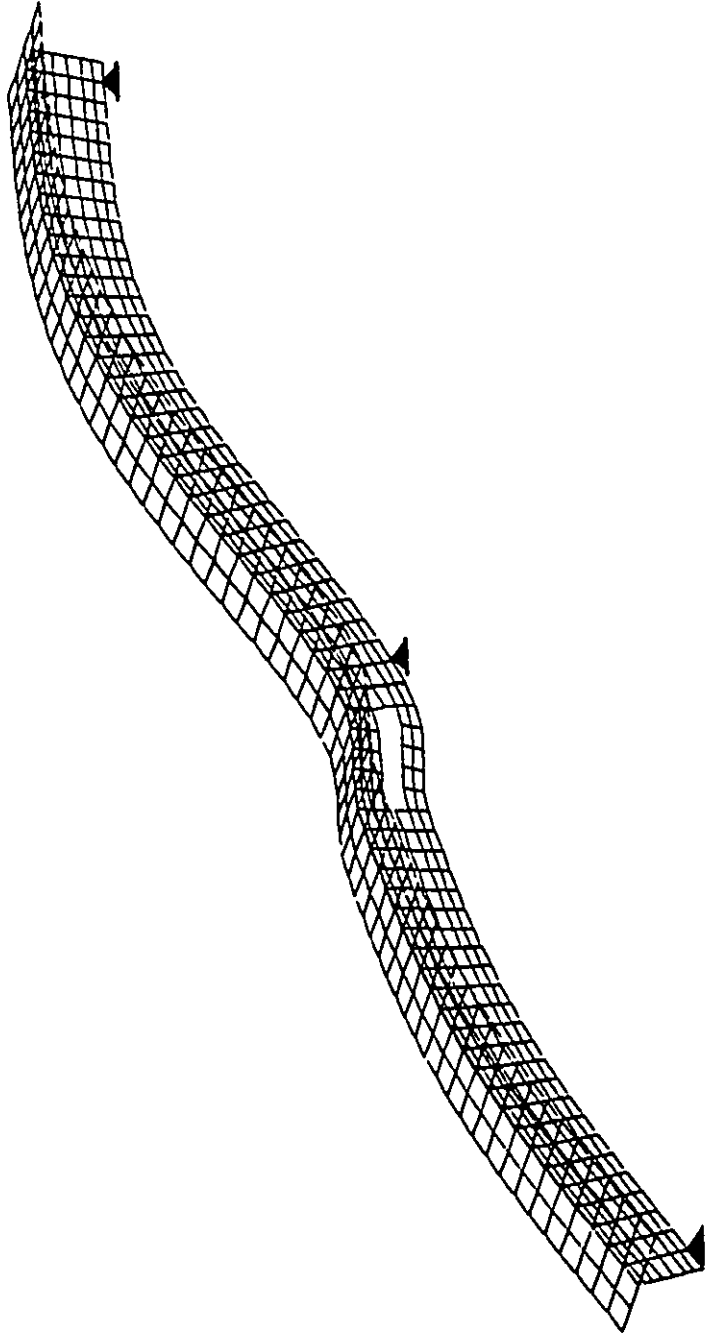


FIG. 6.20 b SECOND MODE SHAPE OF TWO EQUAL-SPANS CONTINUOUS T-BEAM
WITH OPENING

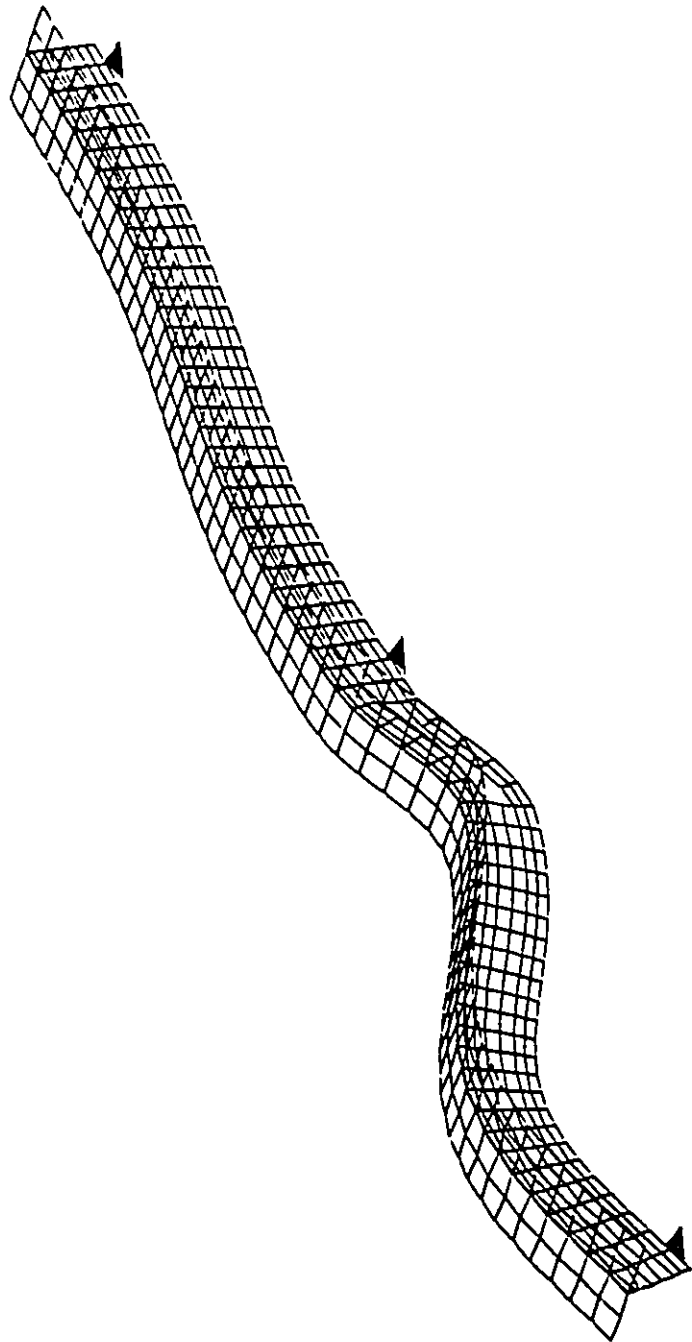


FIG. 6.20 c THIRD MODE SHAPE OF TWO EQUAL-SPANS CONTINUOUS T-BEAM

WITH OPENING

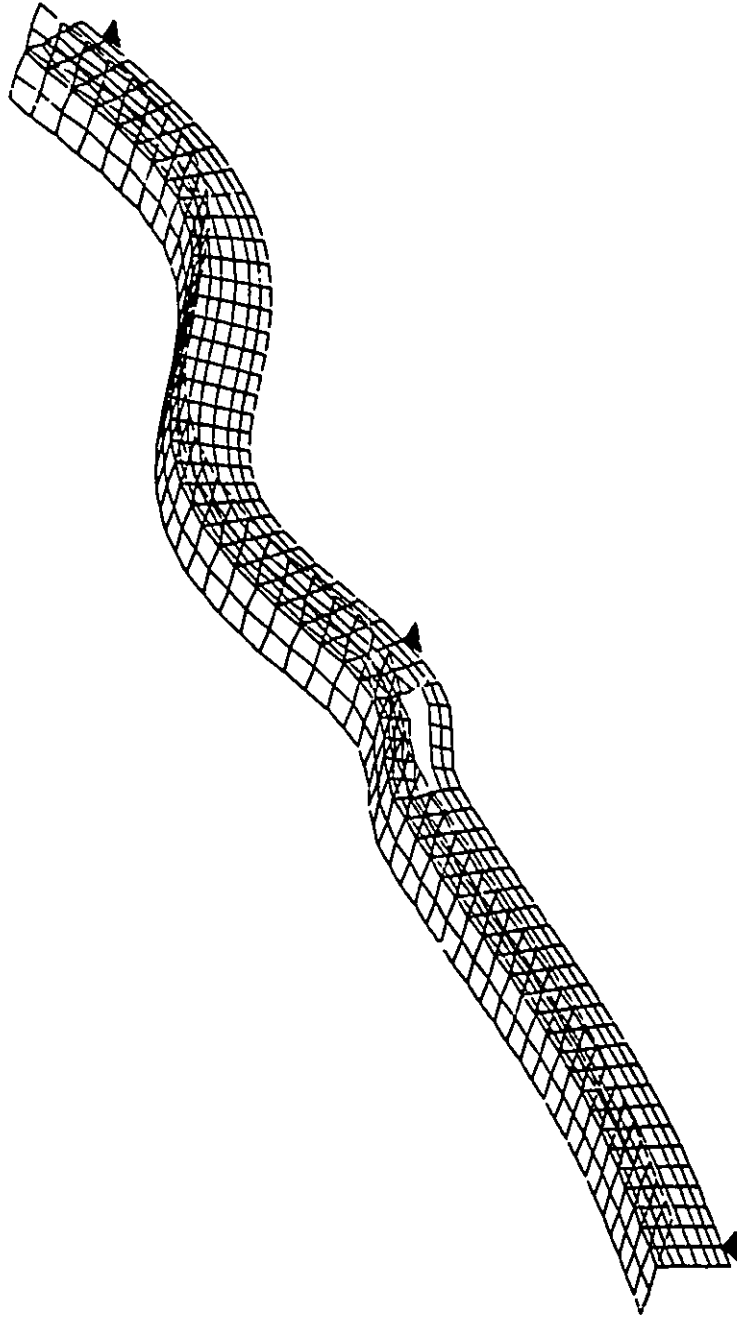


FIG. 6.20 d FOURTH MODE SHAPE OF TWO EQUAL-SPANS CONTINUOUS T-BEAM
WITH OPENING

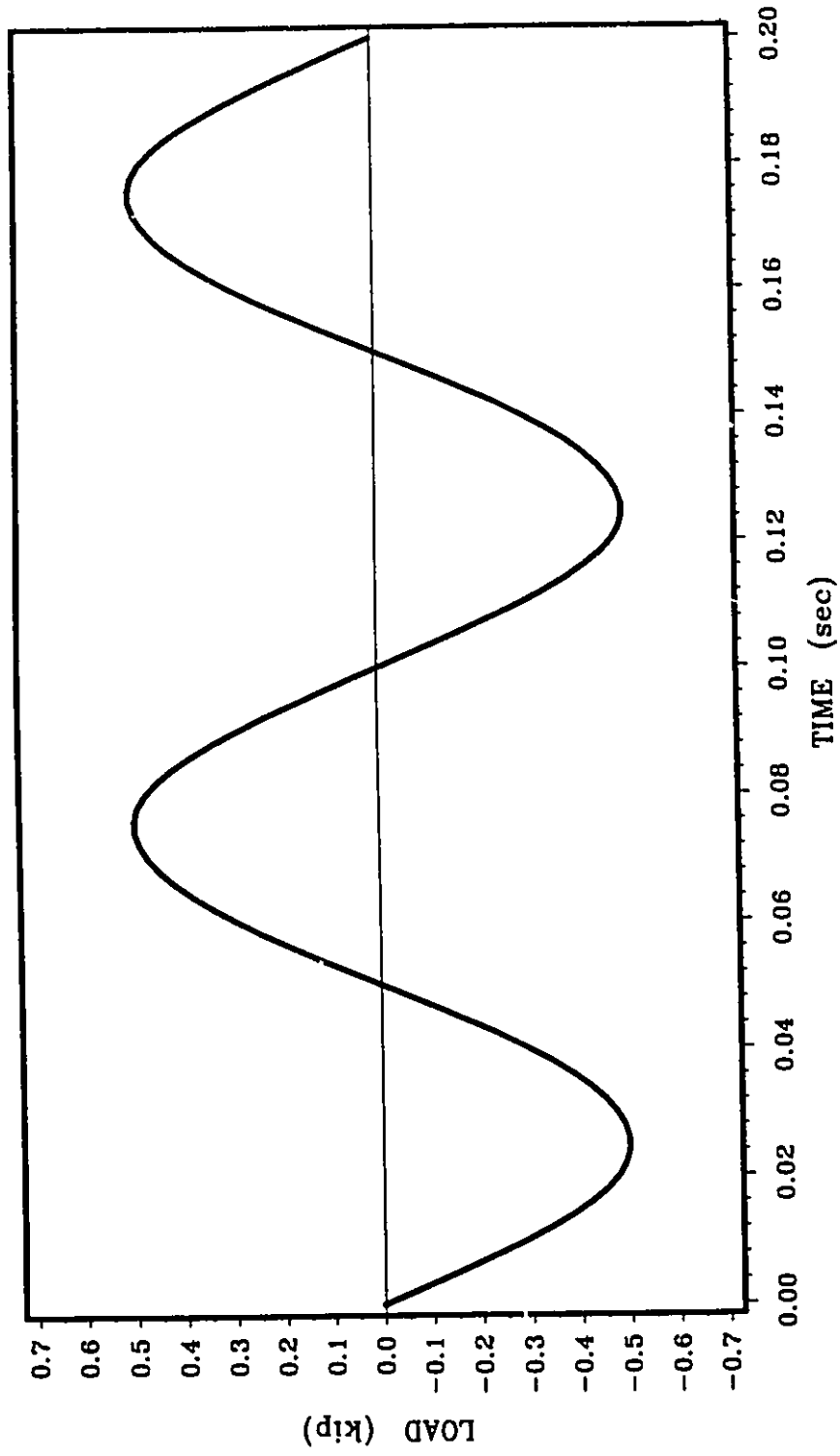


FIG. 6.21 a SINUSOIDAL FORCING FUNCTION FOR THE APPLIED LOAD
 ($\Omega=10$ Hz, $P_0=0.5$ kip)

Note: 1 kip=4.45 kN

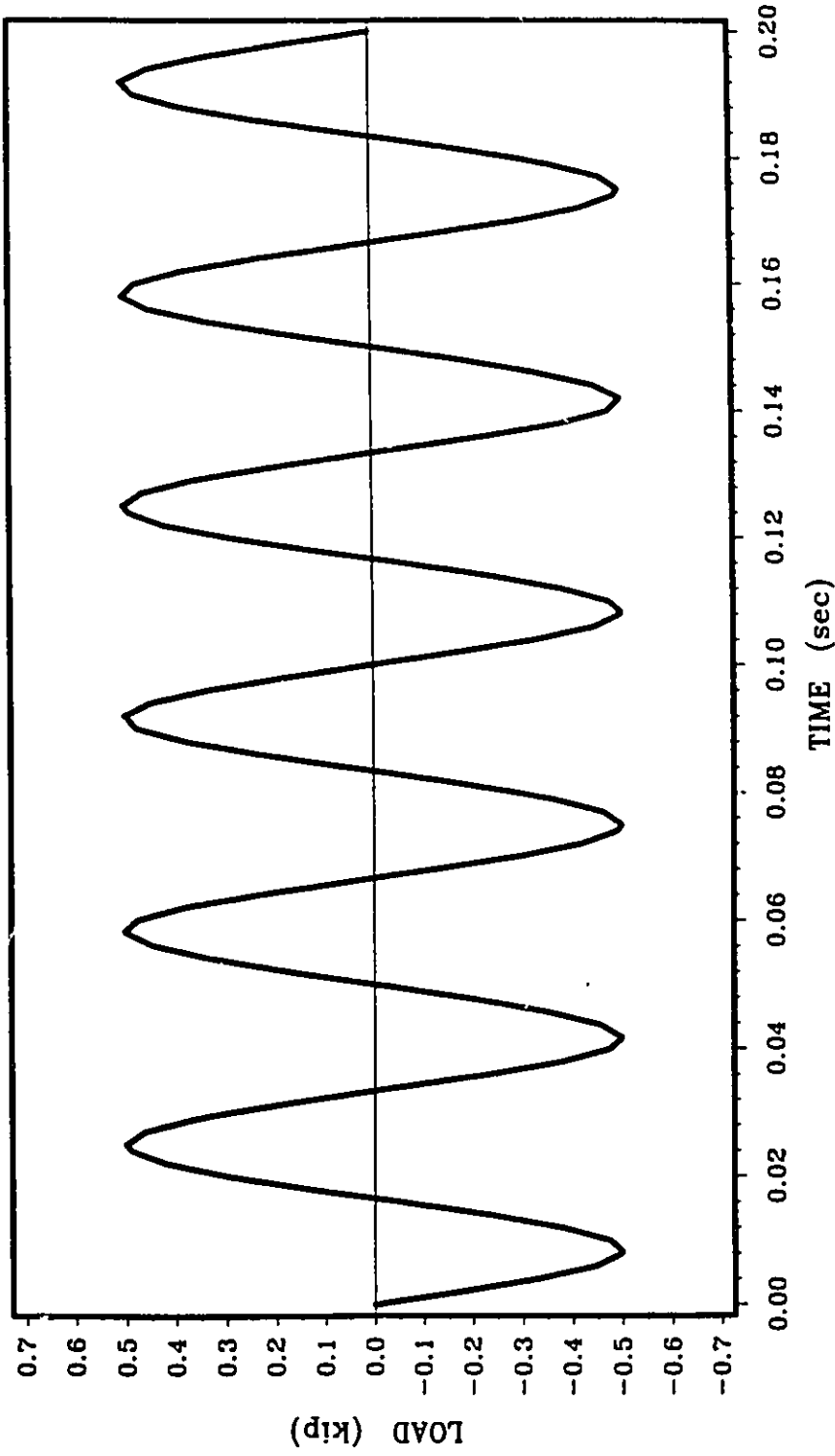


FIG. 6.21 b SINUSOIDAL FORCING FUNCTION FOR THE APPLIED LOAD
 ($\Omega=30$ Hz, $P_0=0.5$ kip)

Note: 1 kip=4.45 kN

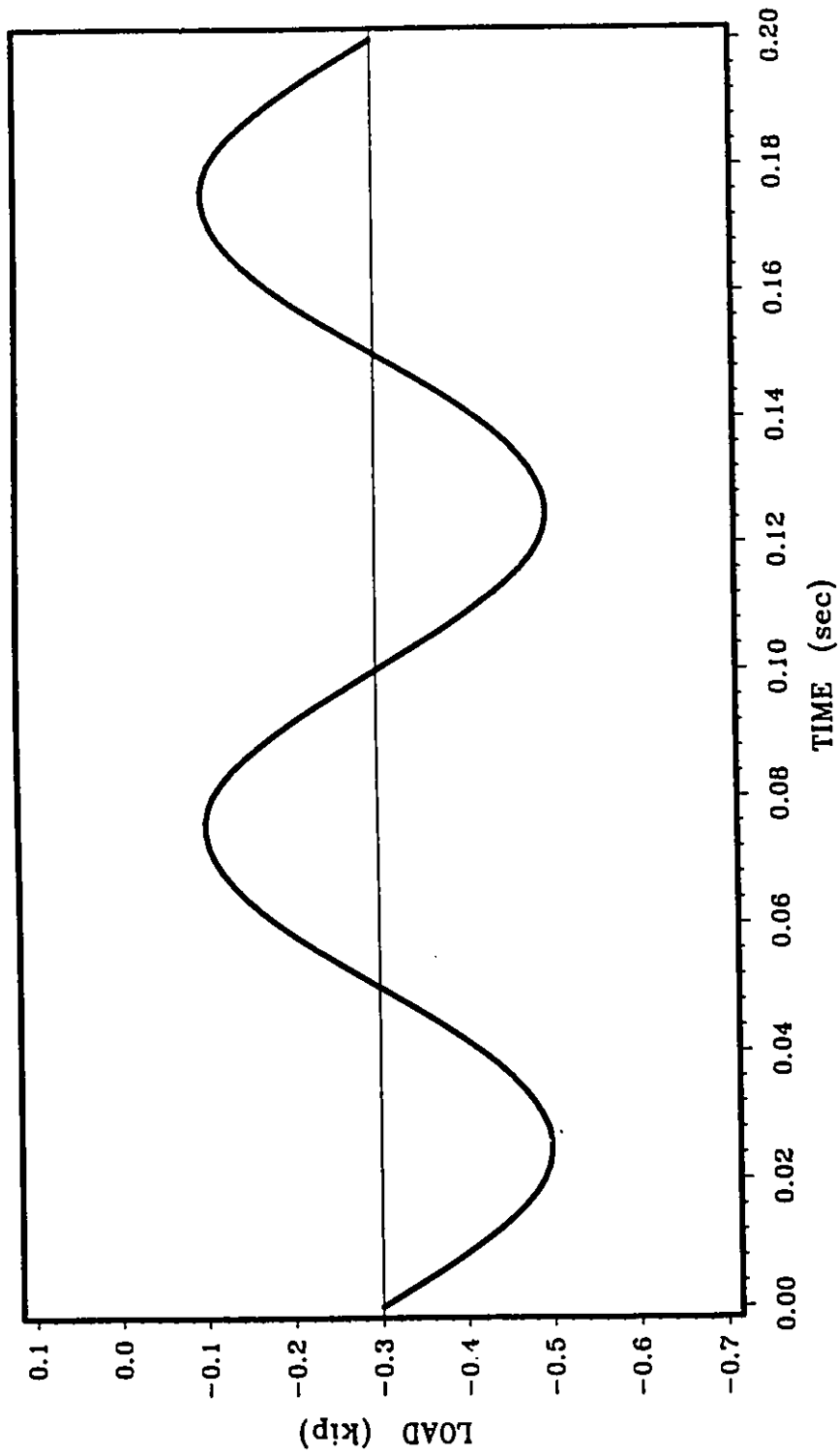


FIG. 6.22 SINUSOIDAL FORCING FUNCTION FOR THE APPLIED LOAD
 ($\Omega=10$ Hz, $P_0=0.2$ kip, $P_1=0.3$ kip)

Note: 1 kip=4.45 kN

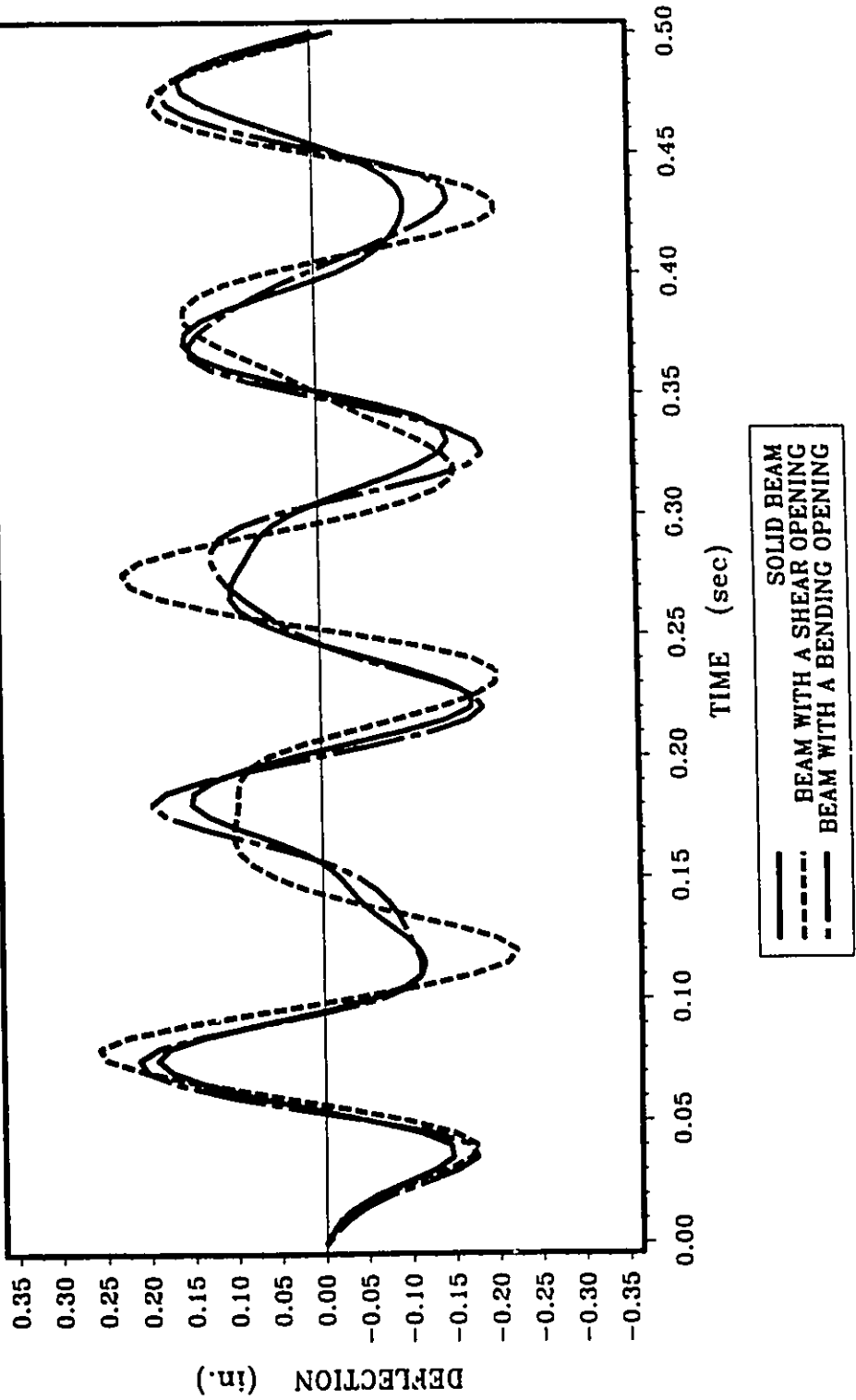


FIG. 6.23 a MID-SPAN DEFLECTION
 ($\Omega=10$ Hz, $P_0=0.5$ kip)

Note: 1 in.=25.4 mm, 1 kip=4.45 kN

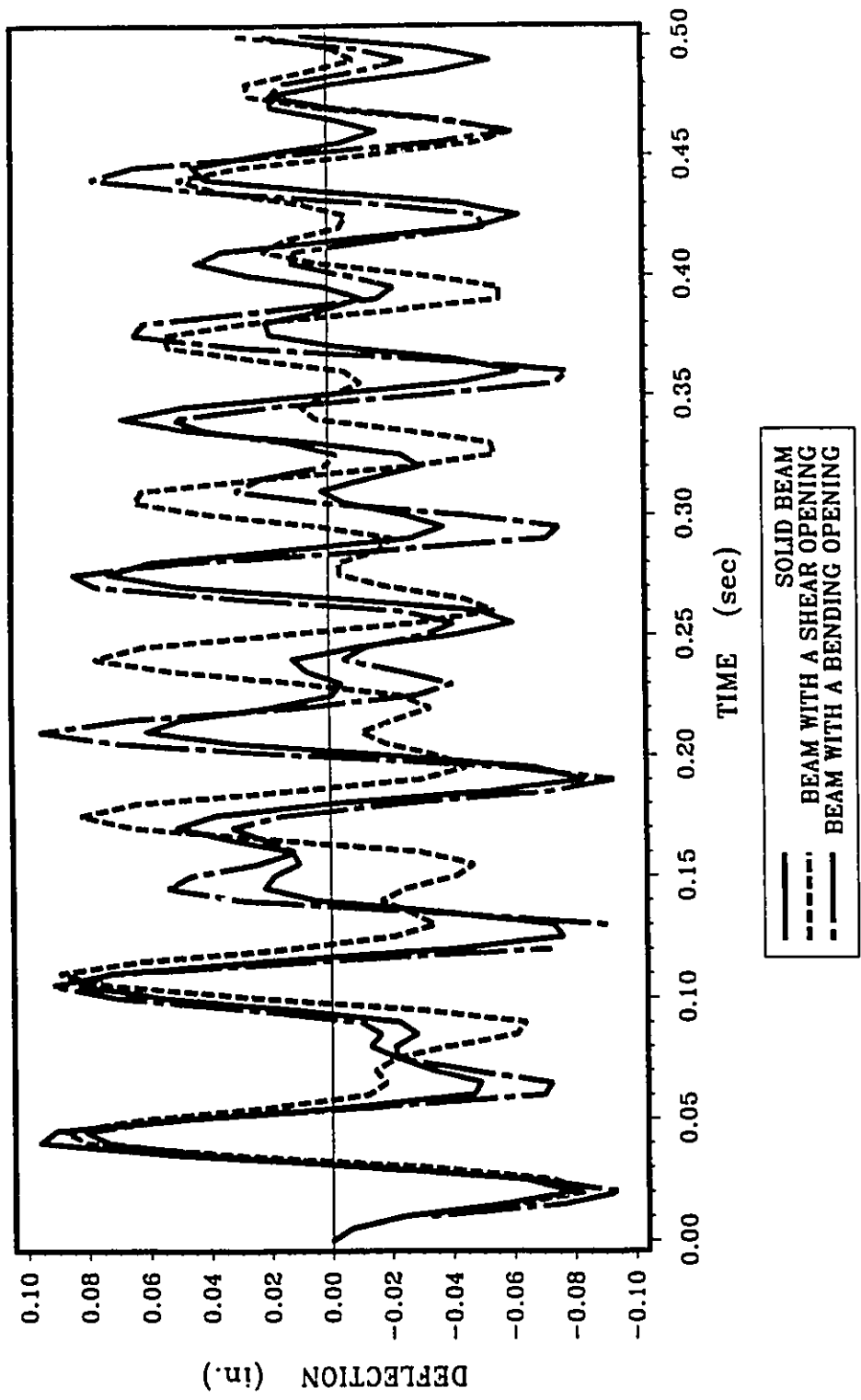


FIG. 6.23 b MID-SPAN DEFLECTION
 ($\Omega=30$ Hz, $P_0=0.5$ kip)

Note: 1 in.=25.4 mm, 1 kip=4.45 kN

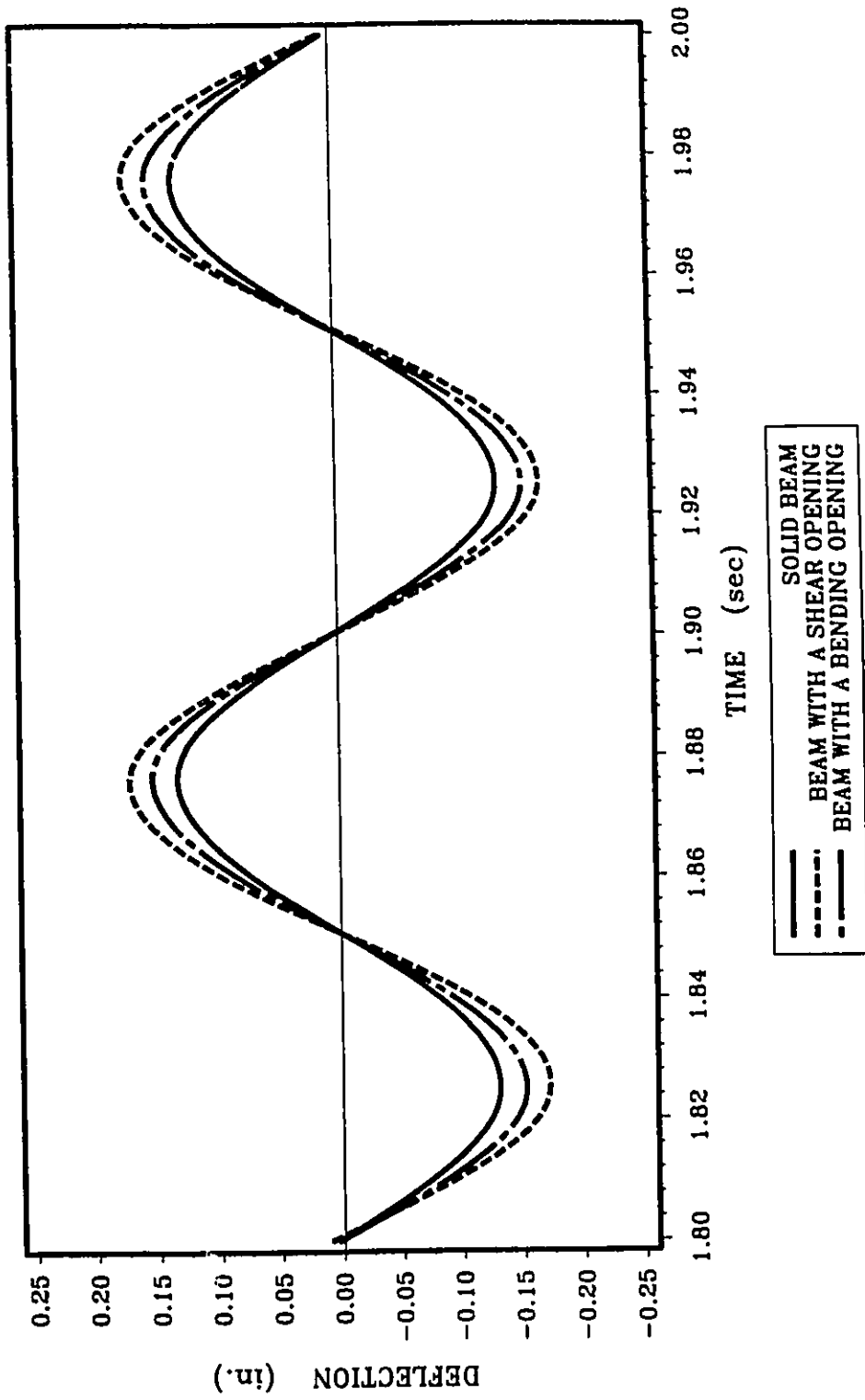


FIG. 6.24 a MID-SPAN DEFLECTION
 ($\Omega=10$ Hz, $P_0=0.5$ kip)

Note: 1 in.=25.4 mm, 1 kip=4.45 kN

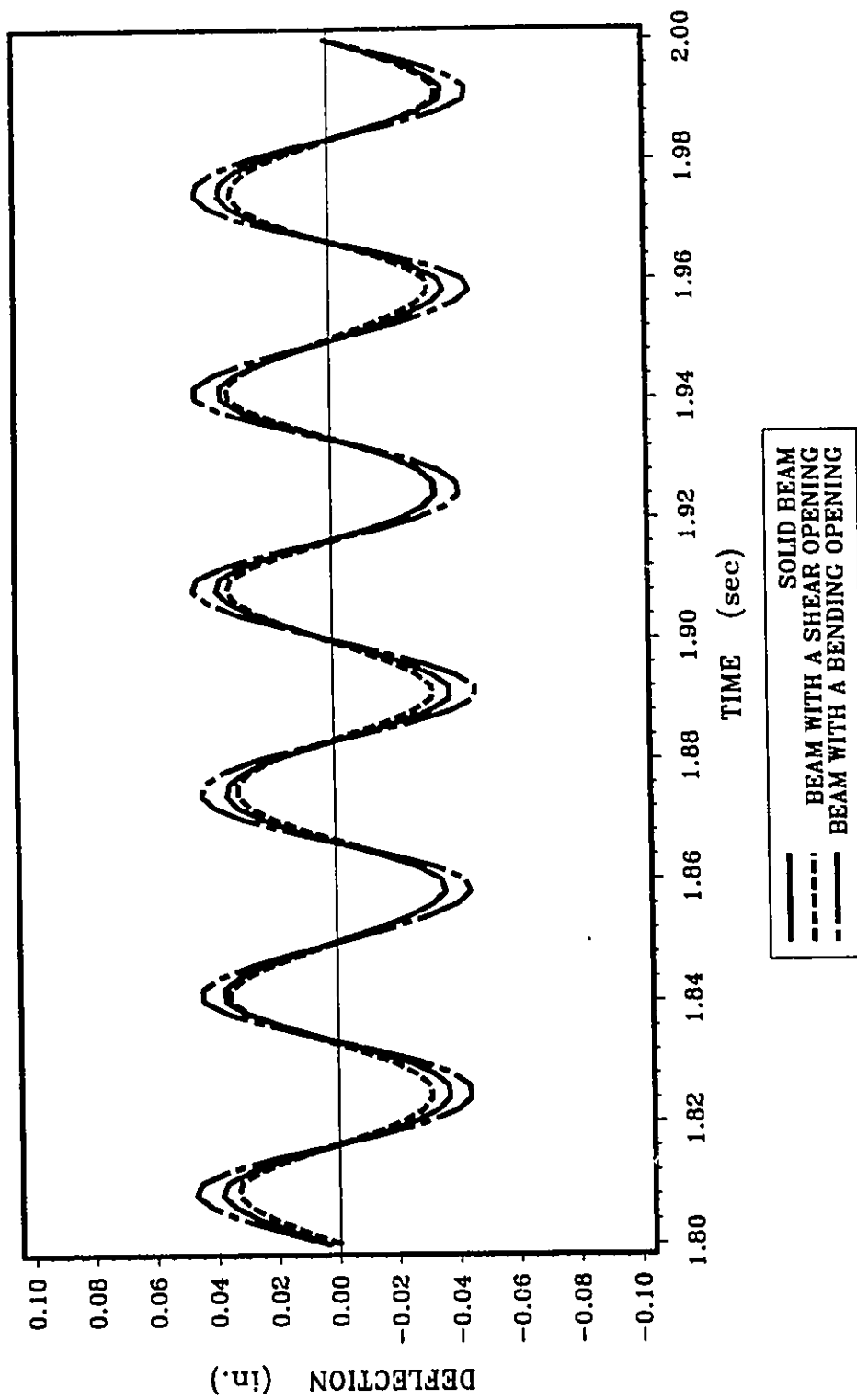


FIG. 6.24 b MID-SPAN DEFLECTION
 ($\Omega=30$ Hz, $P_0=0.5$ kip)

Note: 1 in.=25.4 mm, 1 kip=4.45 kN

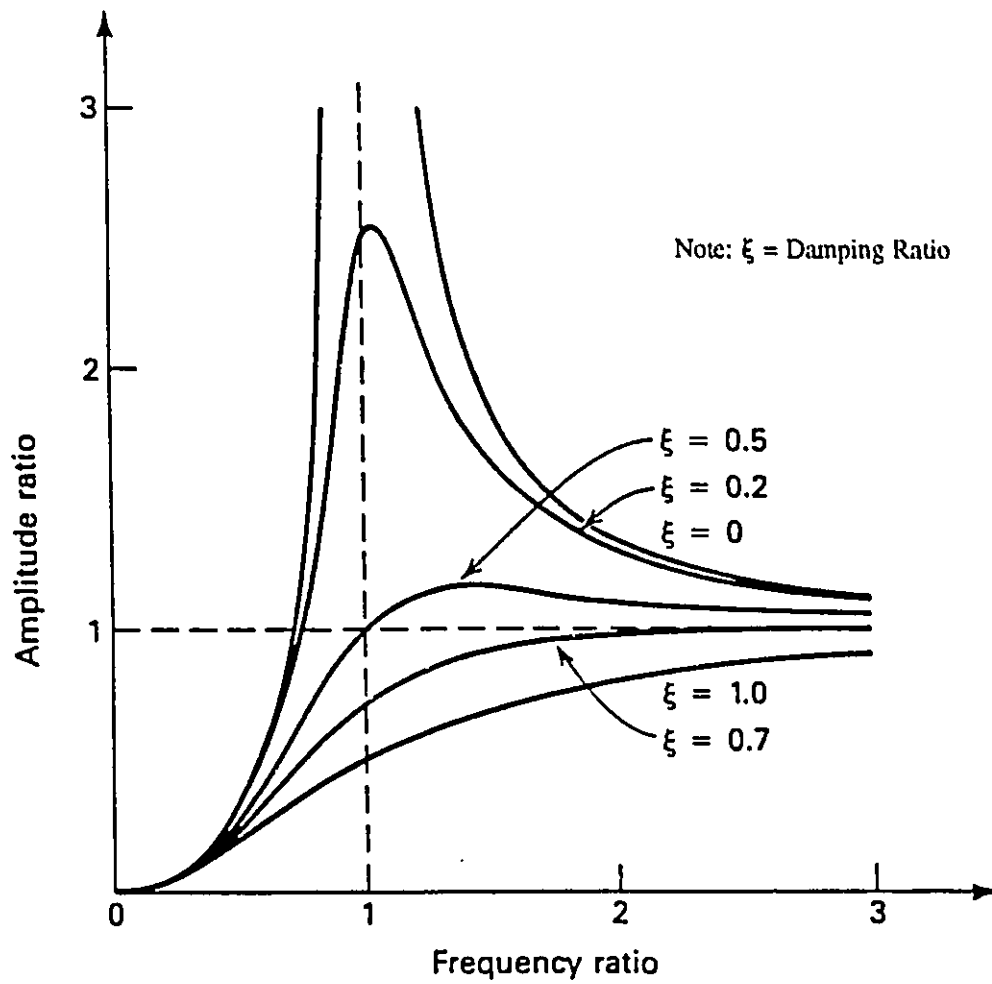


FIG. 6.25 VARIATION OF AMPLITUDE RATIO WITH FREQUENCY RATIO

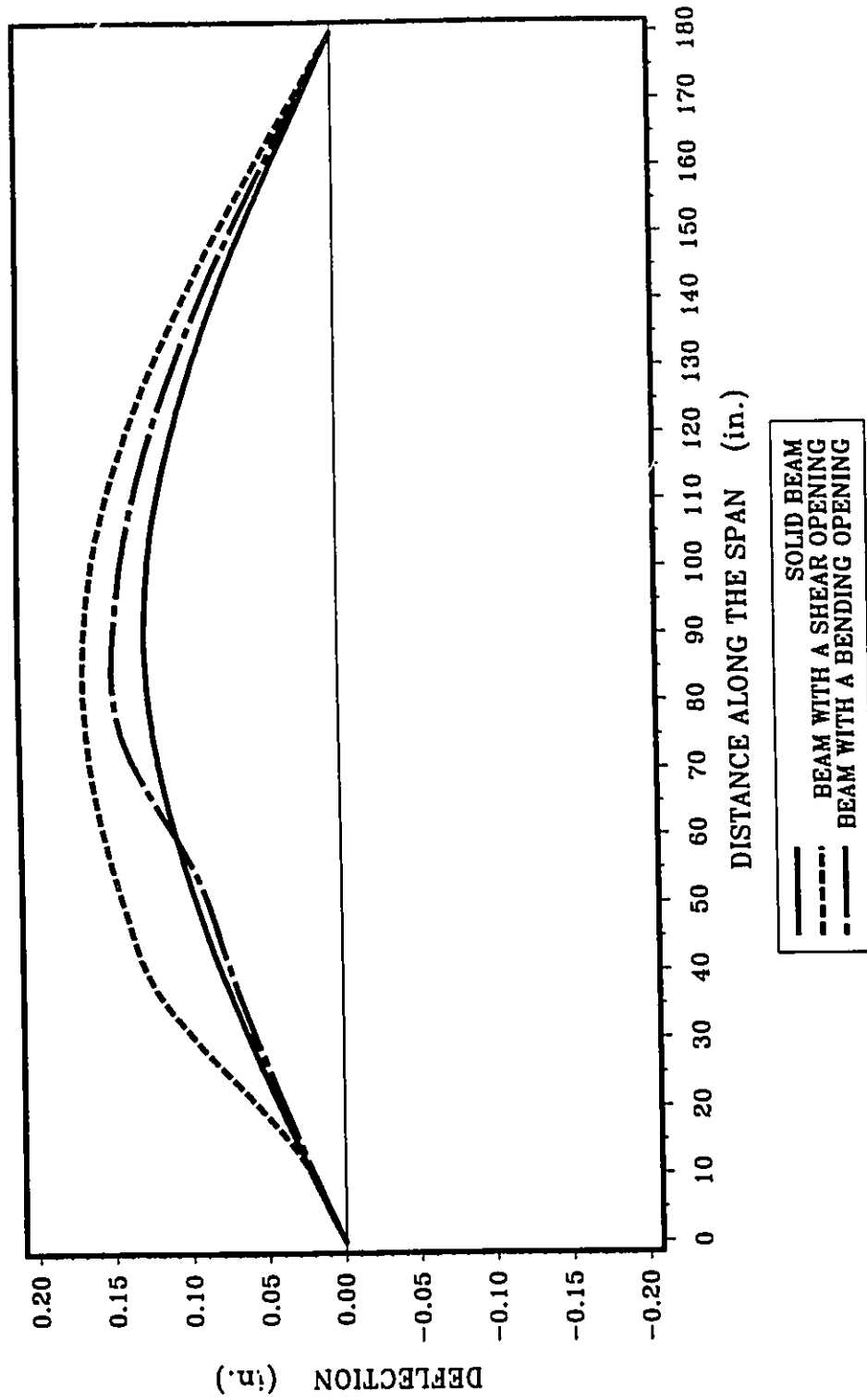


FIG. 6.26 a BEAM DEFLECTED SHAPE
 ($\Omega=10$ Hz, $P_0=0.5$ kip)

Note: 1 in.=25.4 mm, 1 kip=4.45 kN

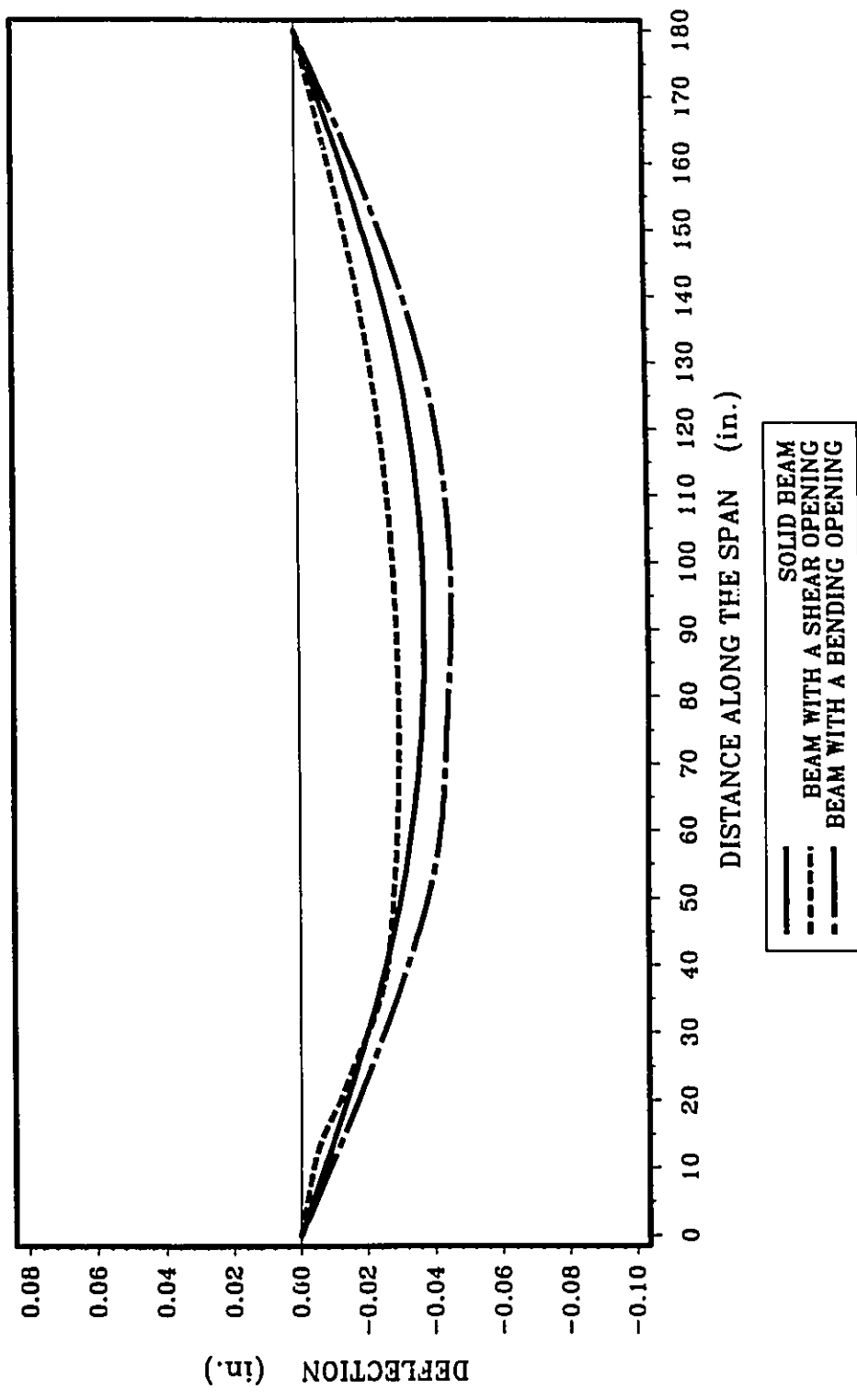


FIG. 6.26 b BEAM DEFLECTED SHAPE
 ($\Omega=30$ Hz, $P_0=0.5$ kip)

Note: 1 in.=25.4 mm, 1 kip=4.45 kN

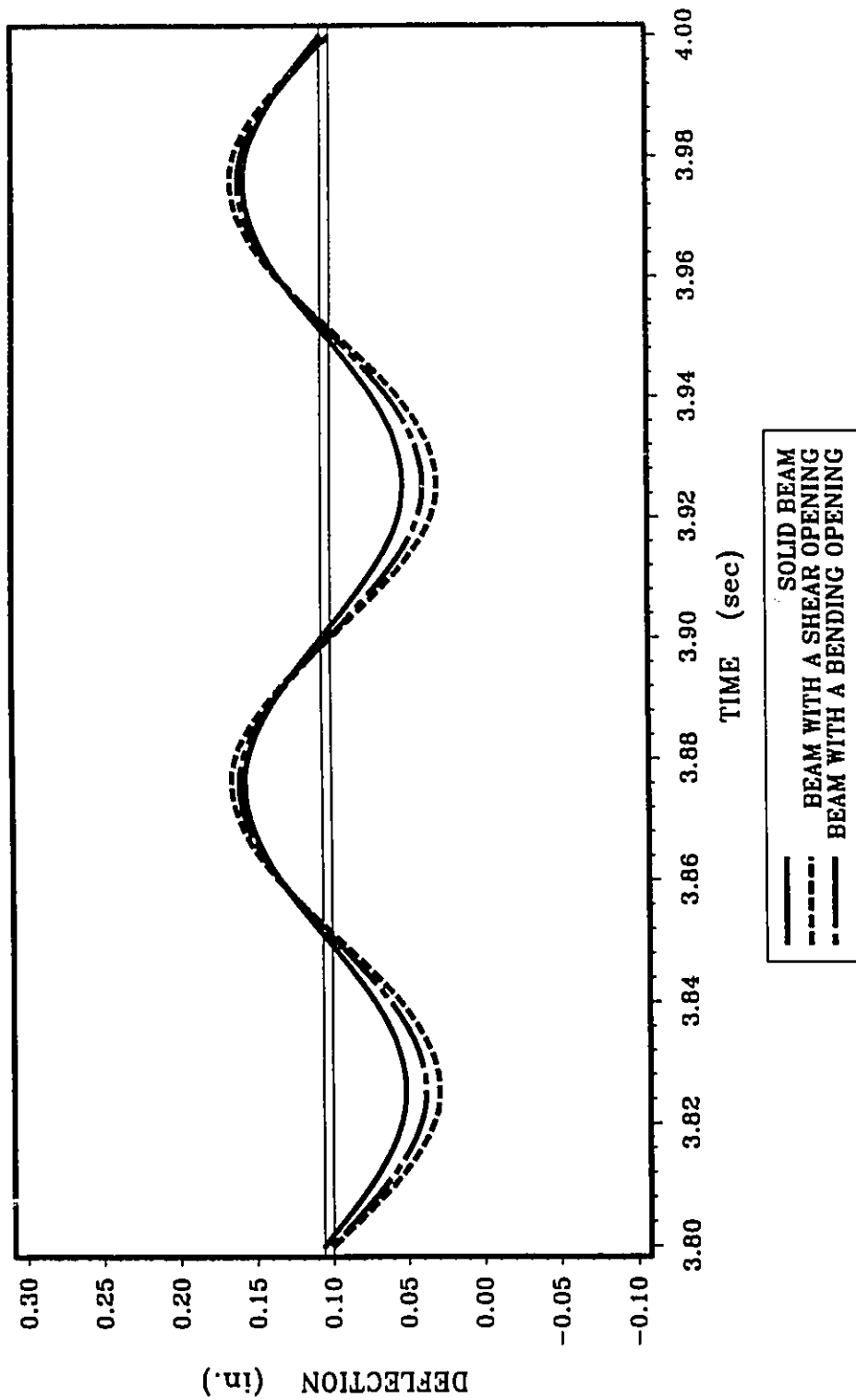


FIG. 6.27 MID-SPAN DEFLECTION
 ($\Omega=10$ Hz, $P_0=0.2$ kip, $P_1=0.3$ kip)

Note: 1 in.=25.4 mm, 1 kip=4.45 kN

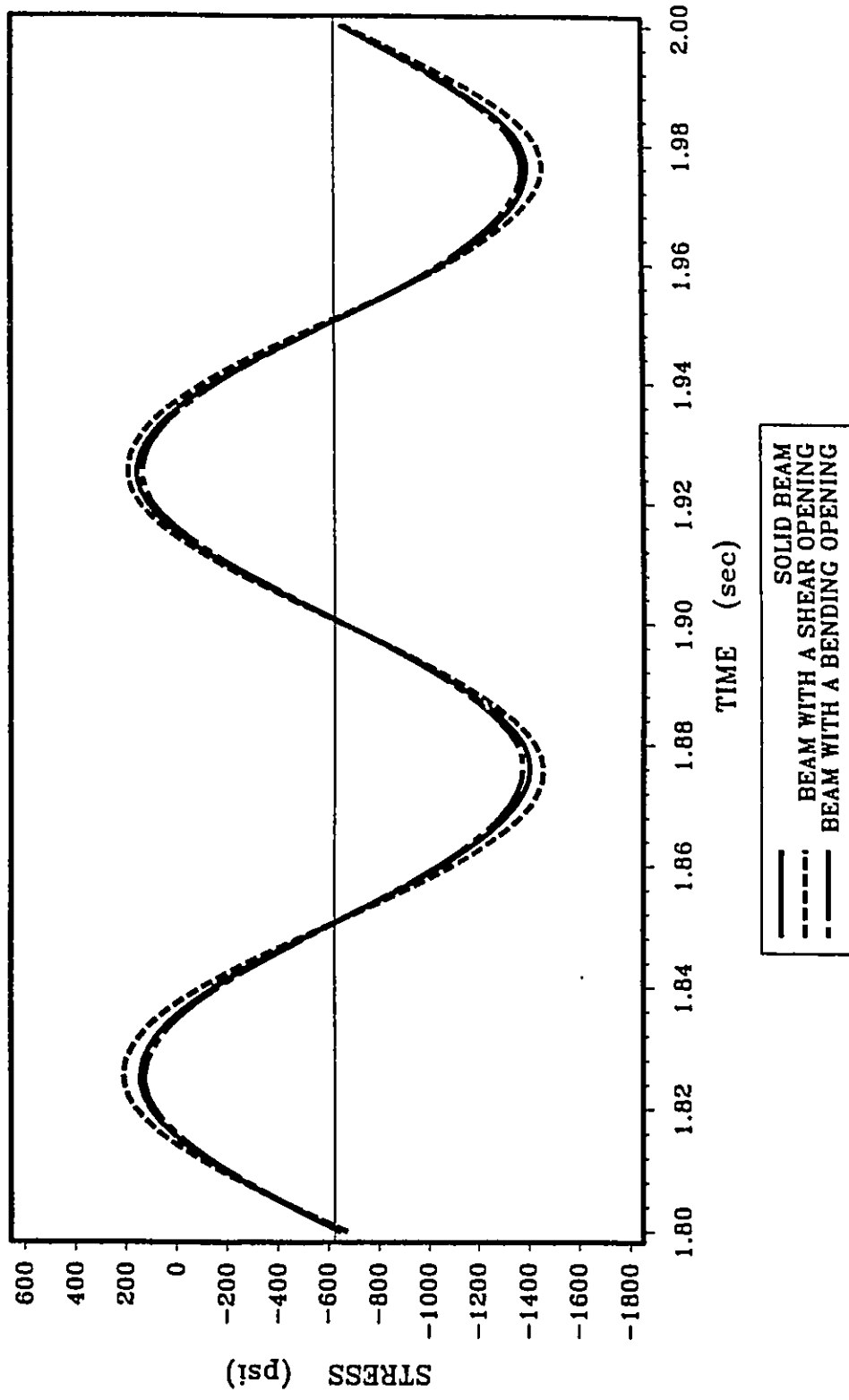


FIG. 6.28 a MAXIMUM HORIZONTAL STRESS AT MID-SPAN
 ($\Omega=10$ Hz, $P_0=0.5$ kip)

Note: 1 kip=4.45 kN, 1 psi=6.89 kPa

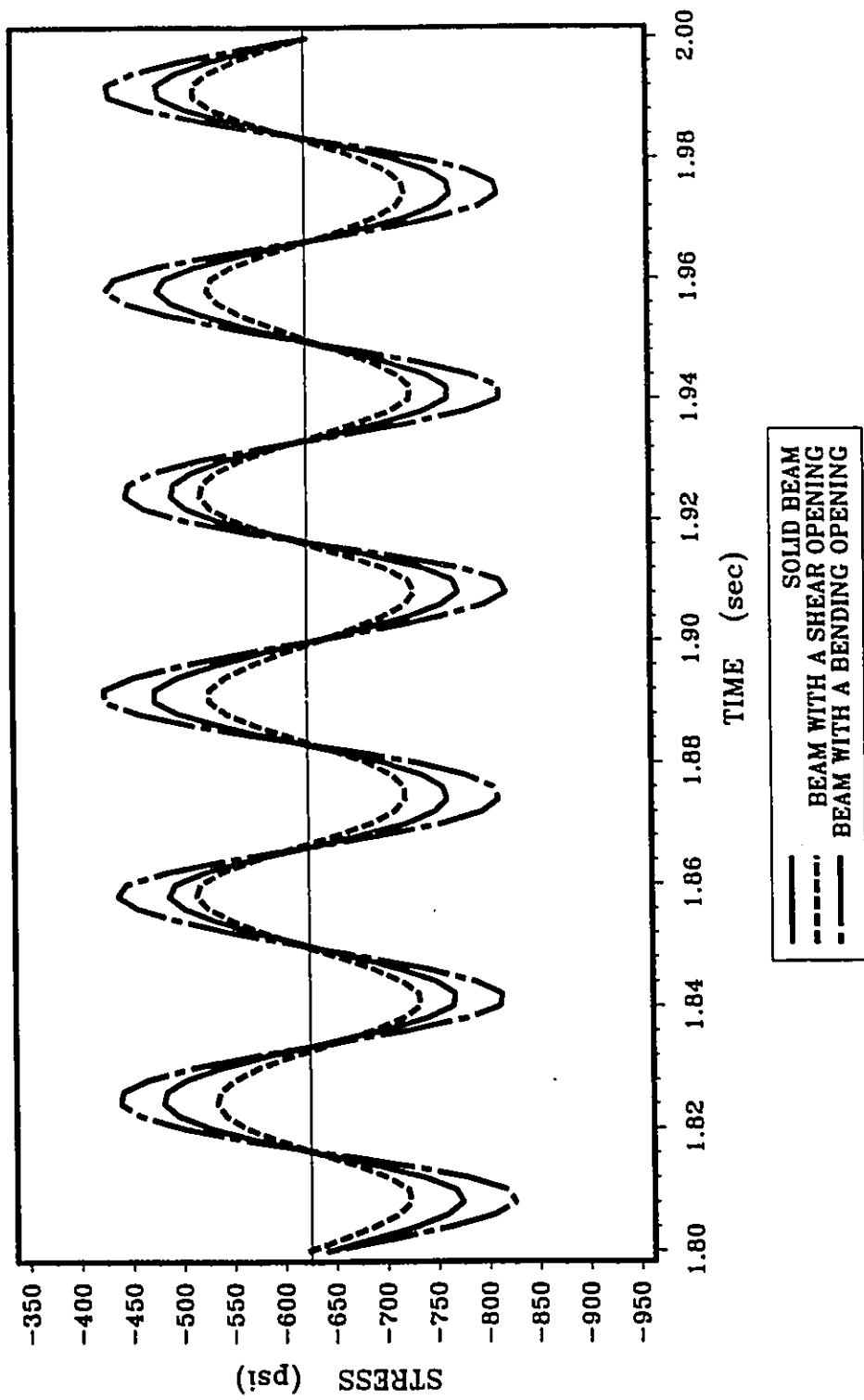


FIG. 6.28 b MAXIMUM HORIZONTAL STRESS AT MID-SPAN
 ($\Omega=30$ Hz, $P_0=0.5$ kip)

Note: 1 kip=4.45 kN, 1 psi=6.89 kPa

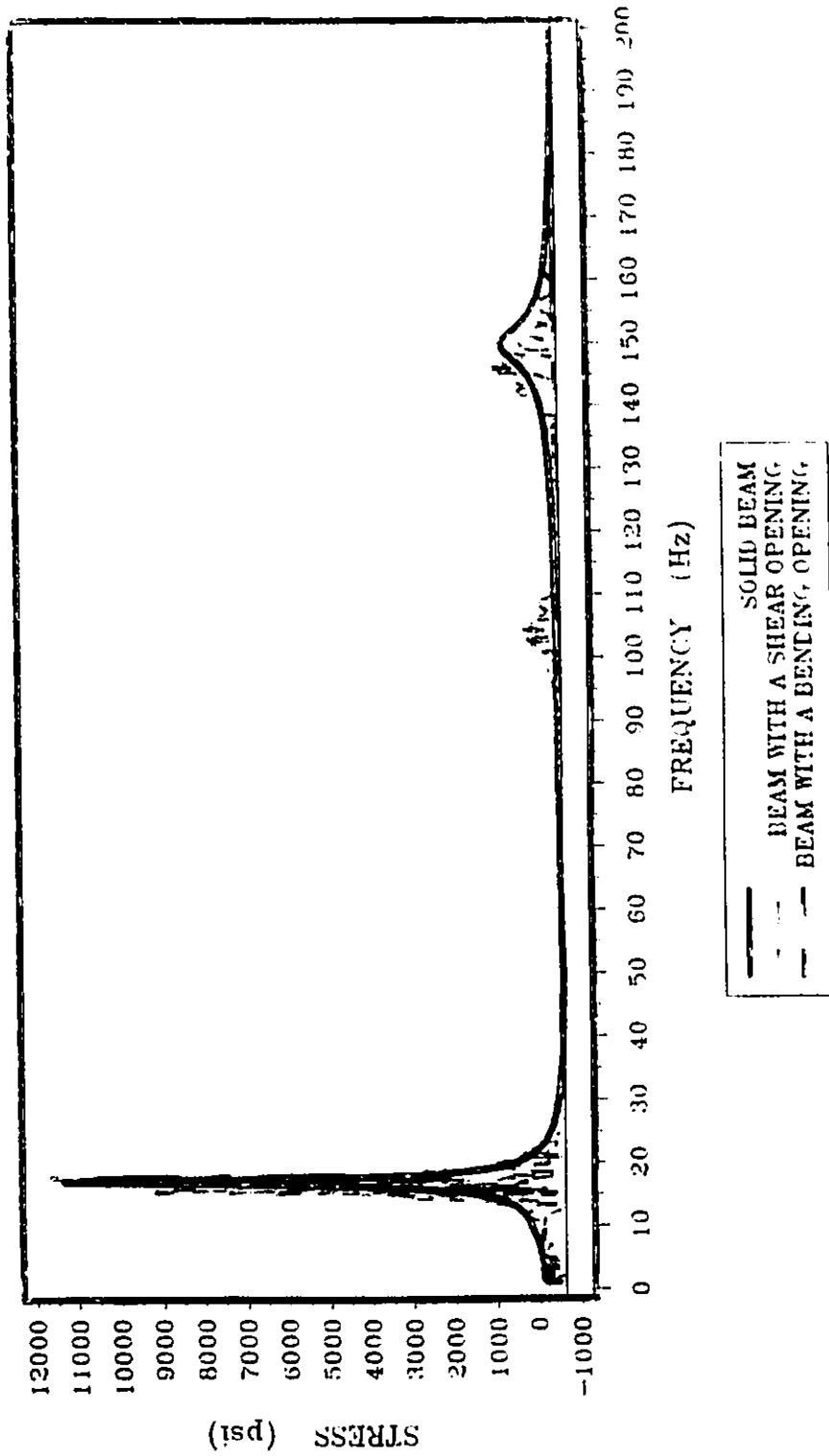


FIG. 6.29 MAXIMUM HORIZONTAL STRESS AT MID - SPAN
STEADY STATE ANALYSIS

Note: 1 psi = 6.89 kPa

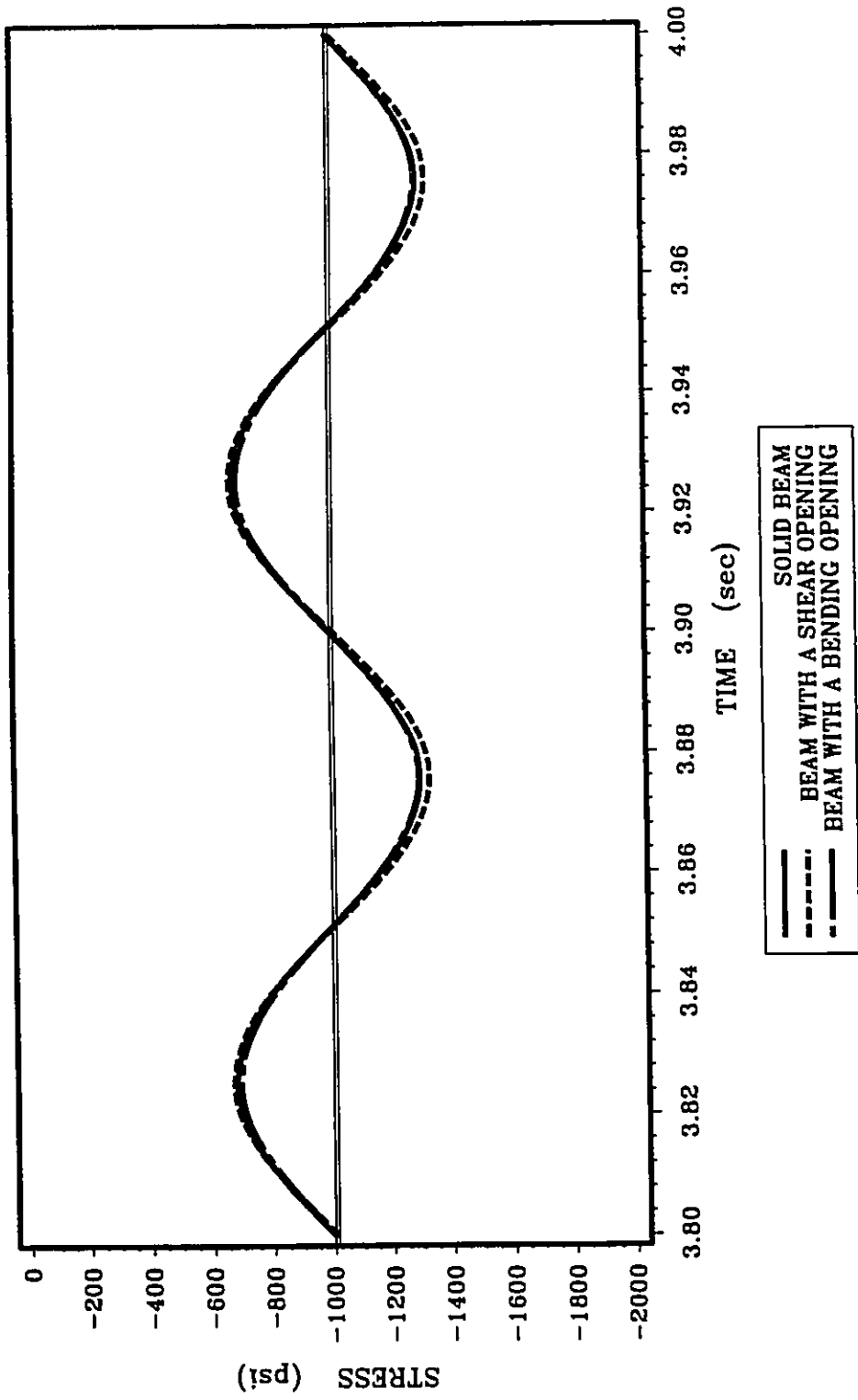


FIG. 6.30 MAXIMUM HORIZONTAL STRESS AT MID-SPAN
 ($\Omega=10$ Hz, $P_0=0.2$ kip, $P_1=0.3$ kip)

Note: 1 kip=4.45 kN, 1 psi=6.89 kPa

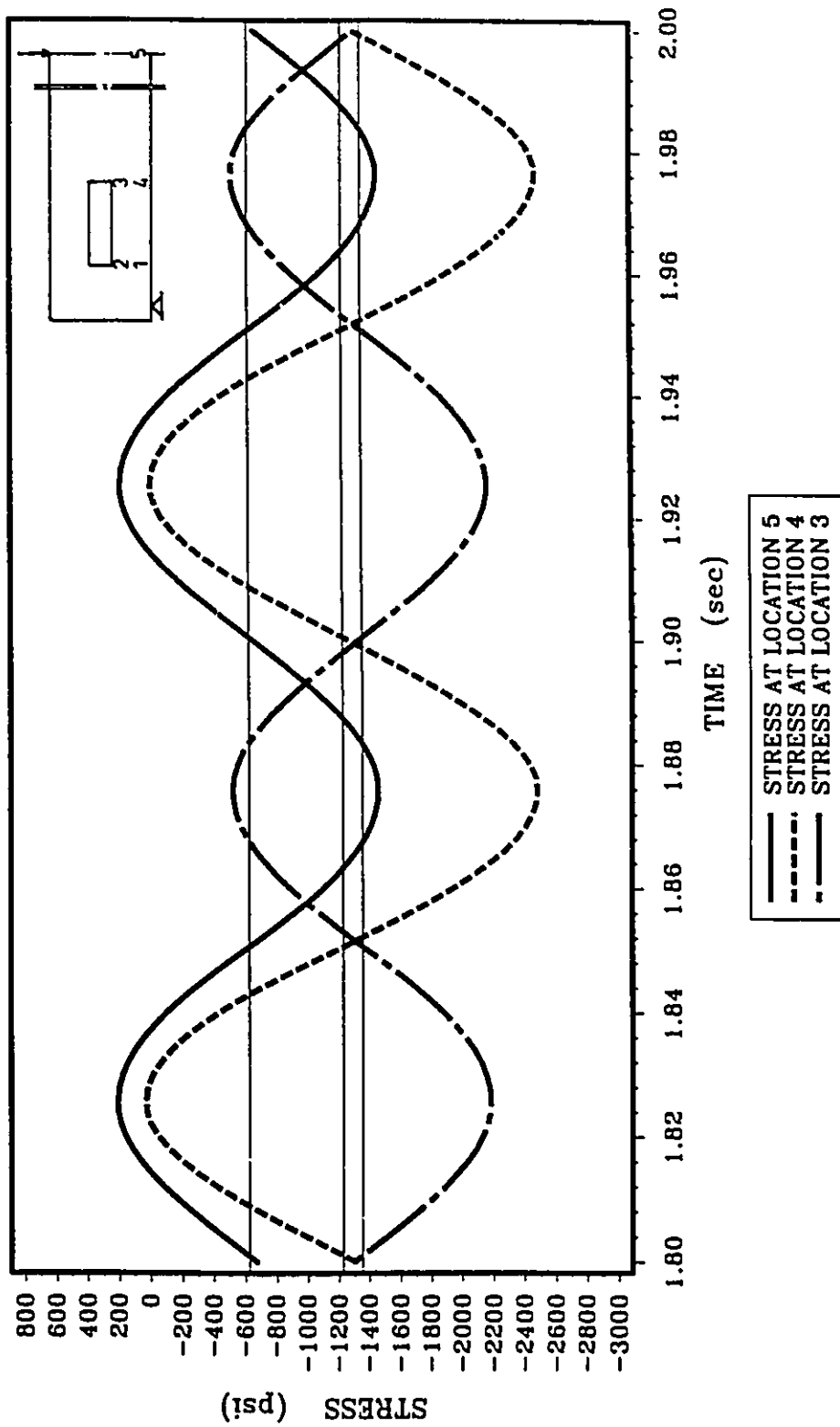


FIG. 6.31 a HORIZONTAL STRESS AT THE OPENING LOWER RIGHT CORNER
 ($\Omega=10$ Hz, $P_0=0.5$ kip)
 (SHEAR OPENING)

Note: 1 kip=4.45 kN, 1 psi=6.89 kPa

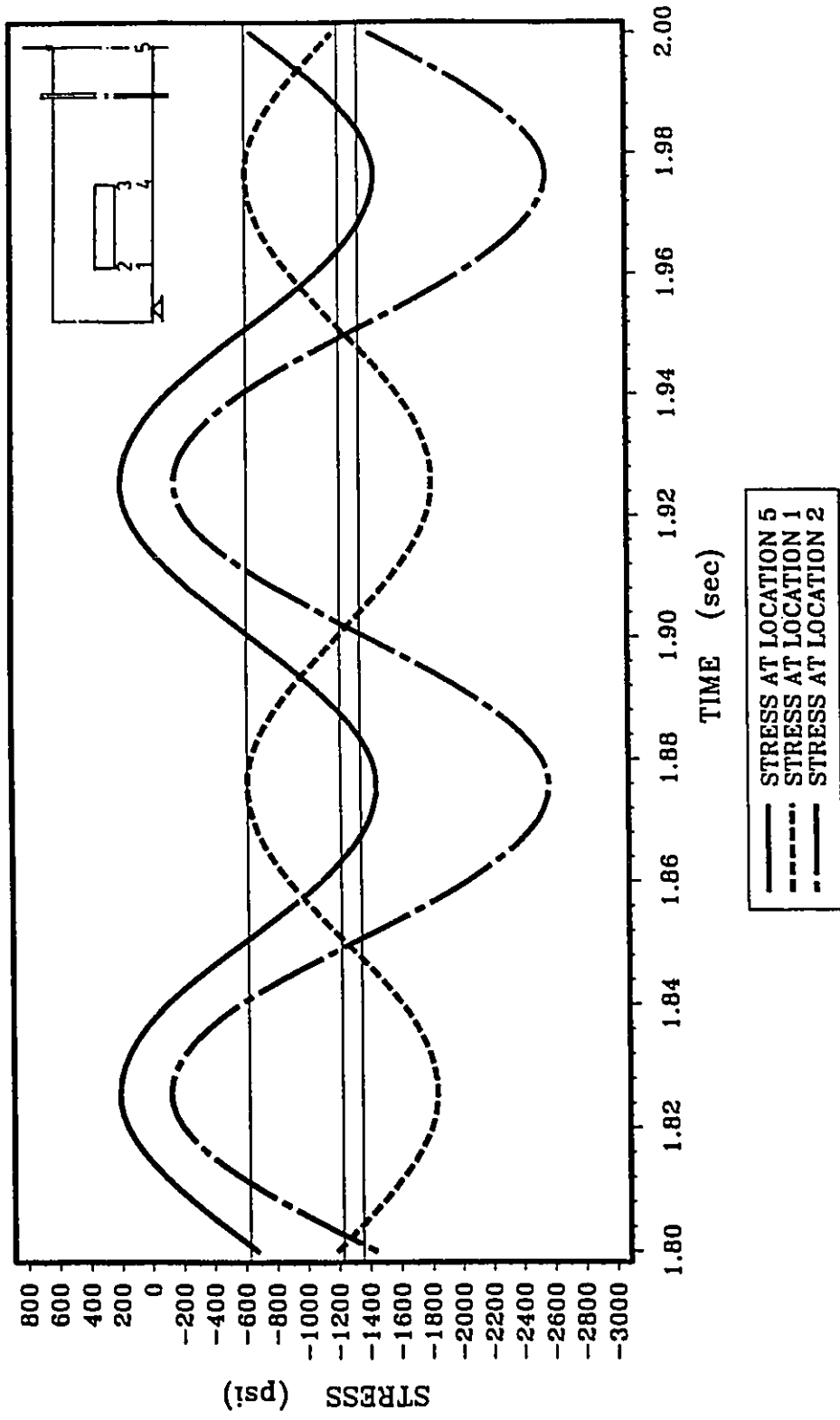


FIG. 6.31 b HORIZONTAL STRESS AT THE OPENING LOWER LEFT CORNER
 ($\Omega=10$ Hz, $P_0=0.5$ kip)
 (SHEAR OPENING)

Note: 1 kip=4.45 kN, 1 psi=6.89 kPa

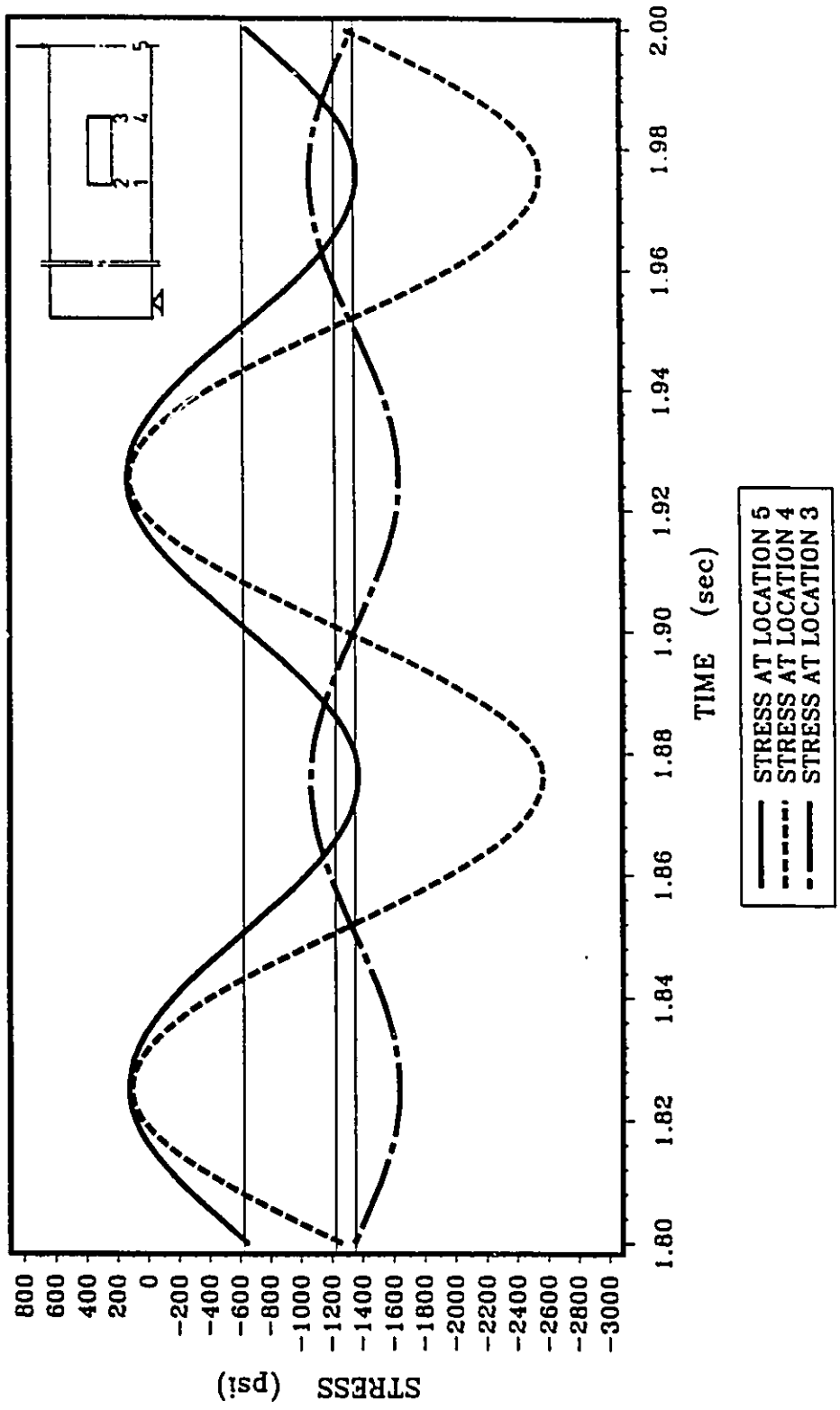


FIG. 6.32 a HORIZONTAL STRESS AT THE OPENING LOWER RIGHT CORNER
 ($\Omega=10$ Hz, $P_0=0.5$ kip)
 (BENDING OPENING)

Note: 1 kip=4.45 kN, 1 psi=6.89 kPa

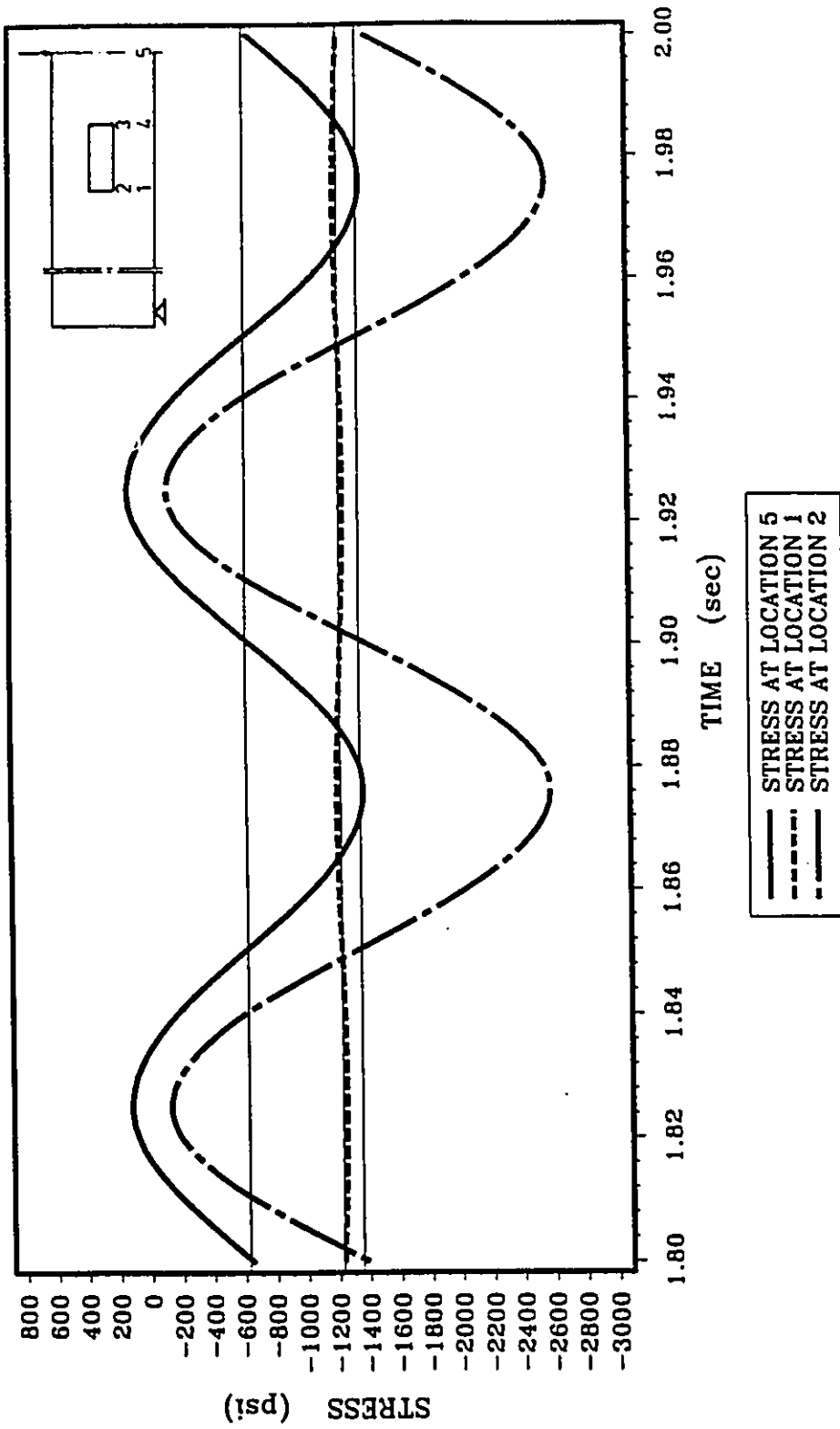


FIG. 6.32 b HORIZONTAL STRESS AT THE OPENING LOWER LEFT CORNER
 ($\Omega=10$ Hz, $P_0=0.5$ kip)
 (BENDING OPENING)

Note: 1 kip=4.45 kN, 1 psi=6.89 kPa

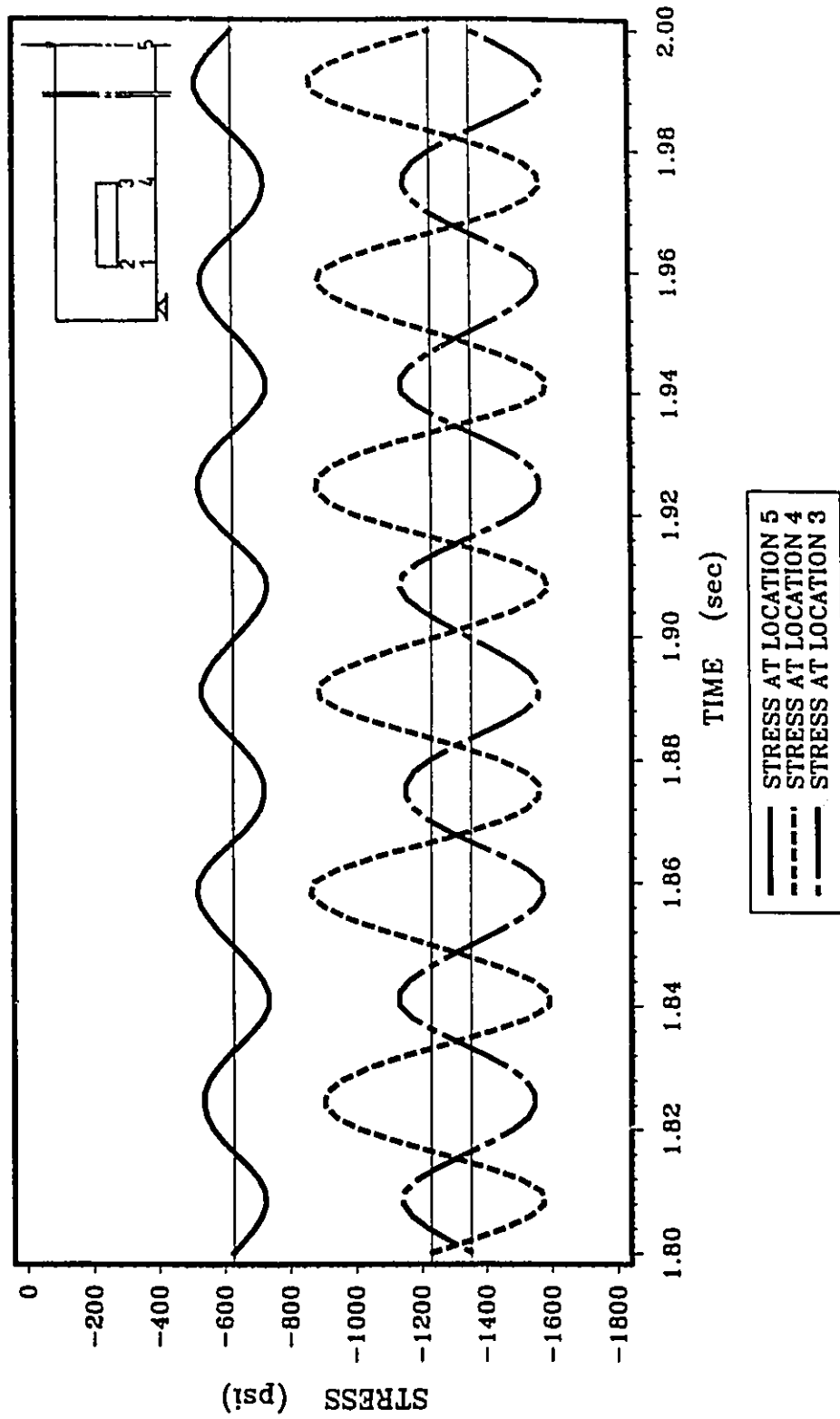


FIG. 6.33 a HORIZONTAL STRESS AT THE OPENING LOWER RIGHT CORNER
 ($\Omega=30$ Hz, $P_0=0.5$ kip)
 (SHEAR OPENING)

Note: 1 kip=4.45 kN, 1 psi=6.89 kPa

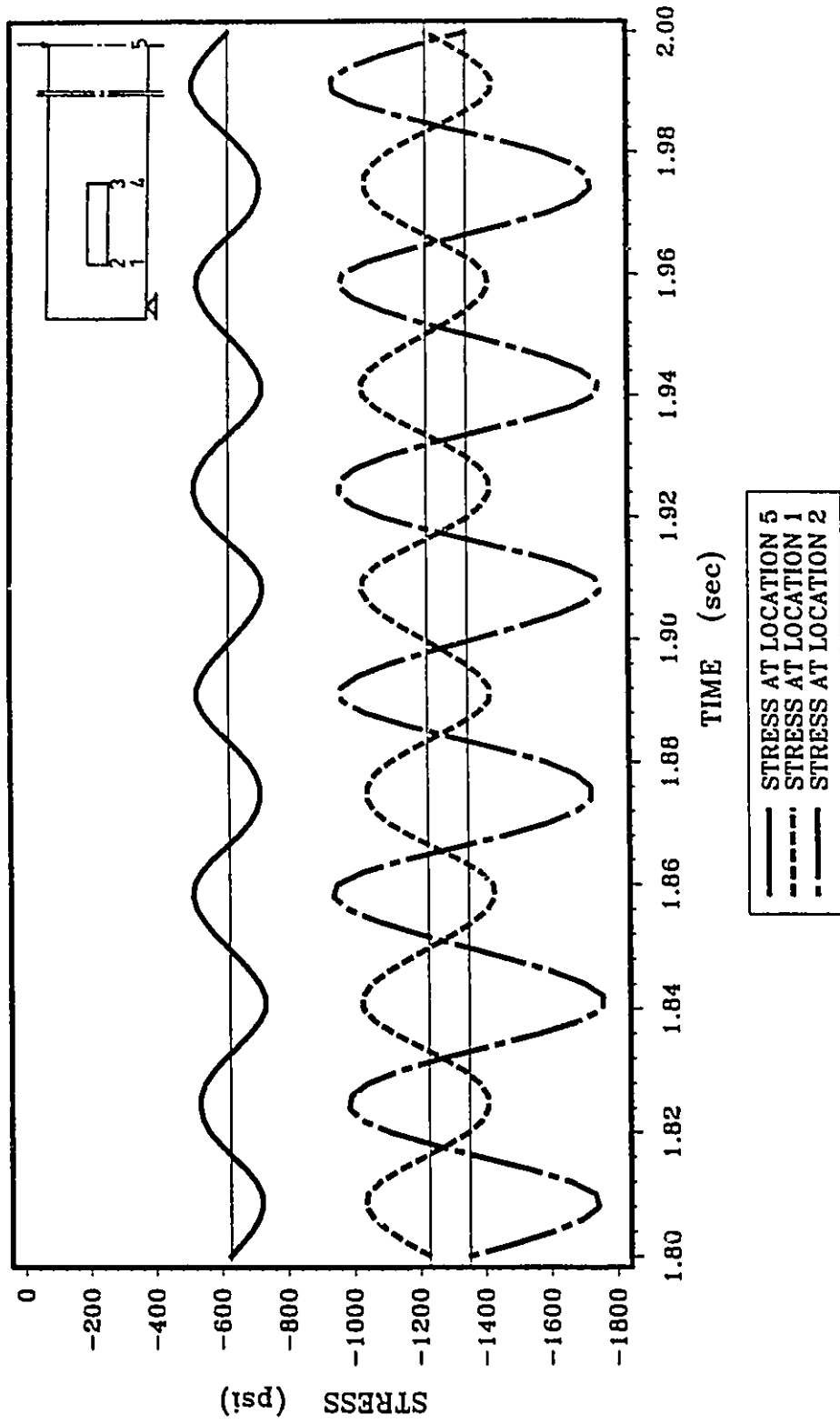


FIG. 6.33 b HORIZONTAL STRESS AT THE OPENING LOWER LEFT CORNER
 ($\Omega=30$ Hz, $P_0=0.5$ kip)
 (SHEAR OPENING)

Note: 1 kip=4.45 kN, 1 psi=6.89 kPa

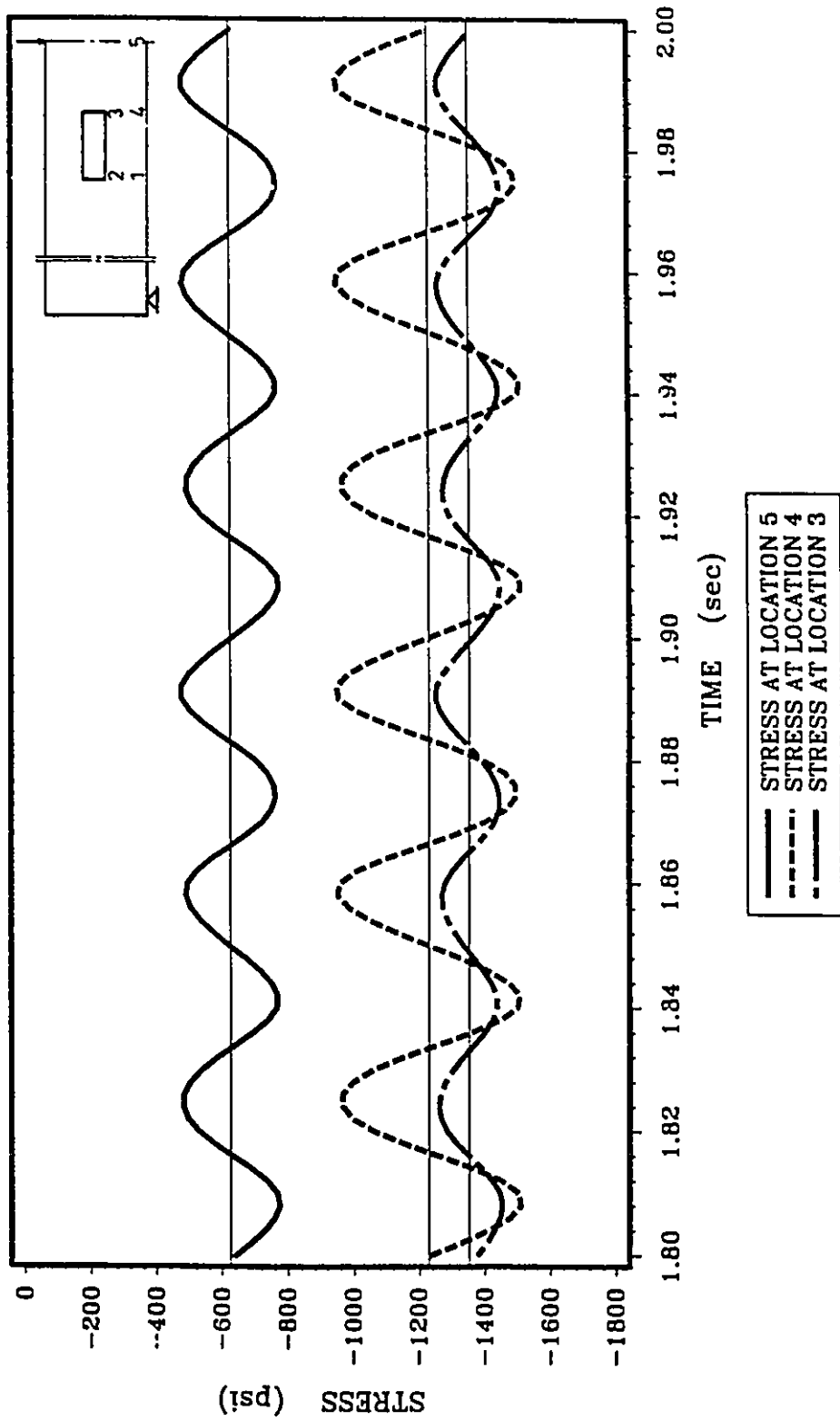


FIG. 6.34 a HORIZONTAL STRESS AT THE OPENING LOWER RIGHT CORNER
 ($\Omega=30$ Hz, $P_0=0.5$ kip)
 (BENDING OPENING)

Note: 1 kip=4.45 kN, 1 psi=6.89 kPa

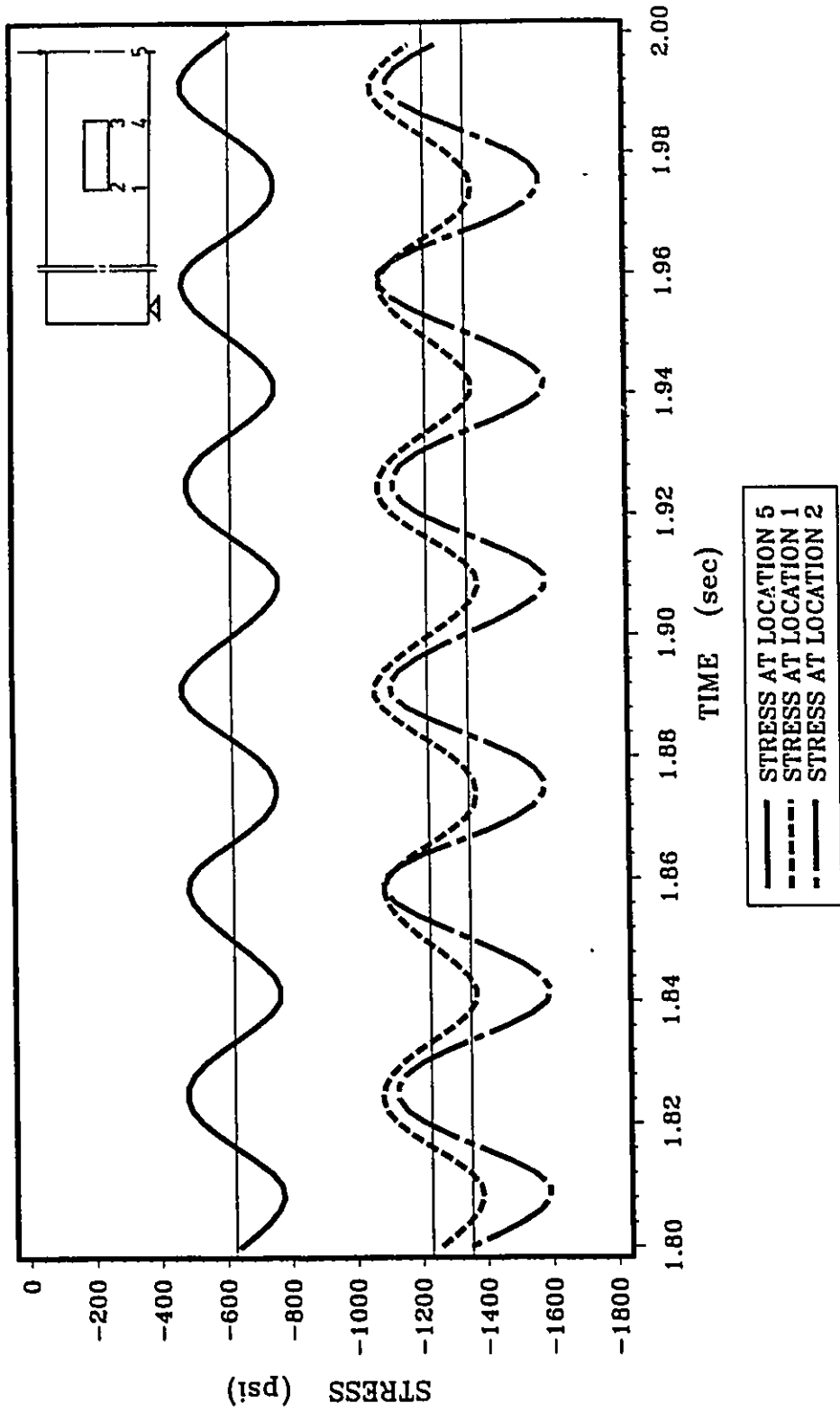


FIG. 6.34 b HORIZONTAL STRESS AT THE OPENING LOWER LEFT CORNER
 ($\Omega=30$ Hz, $P_0=0.5$ kip)
 (BENDING OPENING)

Note: 1 kip=4.45 kN, 1 psi=6.89 kPa

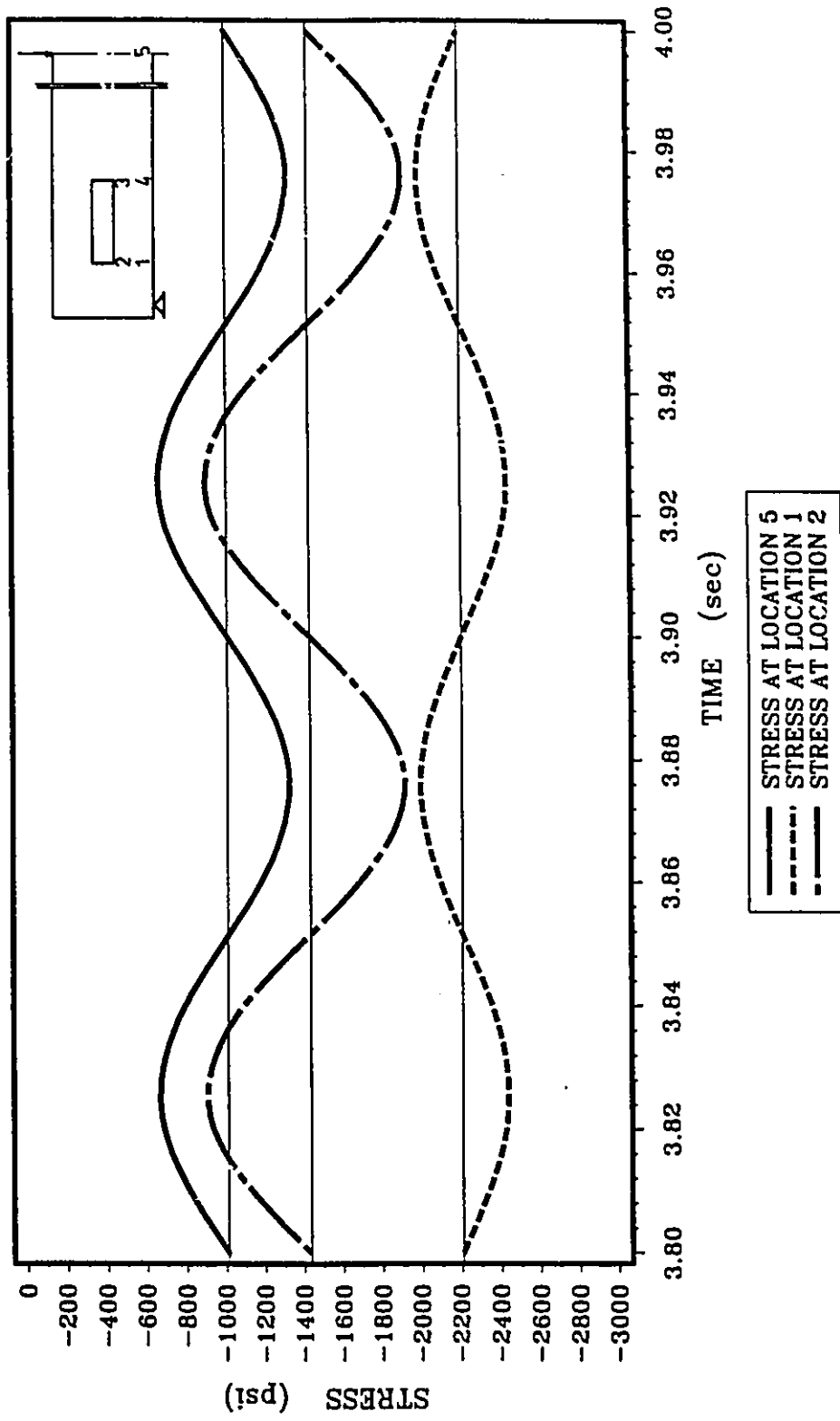


FIG. 6.35 a HORIZONTAL STRESS AT THE OPENING LOWER LEFT CORNER
 ($\Omega=10$ Hz, $P_0=0.2$ kip, $P_1=0.3$ kip)
 (SHEAR OPENING)

Note: 1 kip=4.45 kN, 1 psi=6.89 kPa

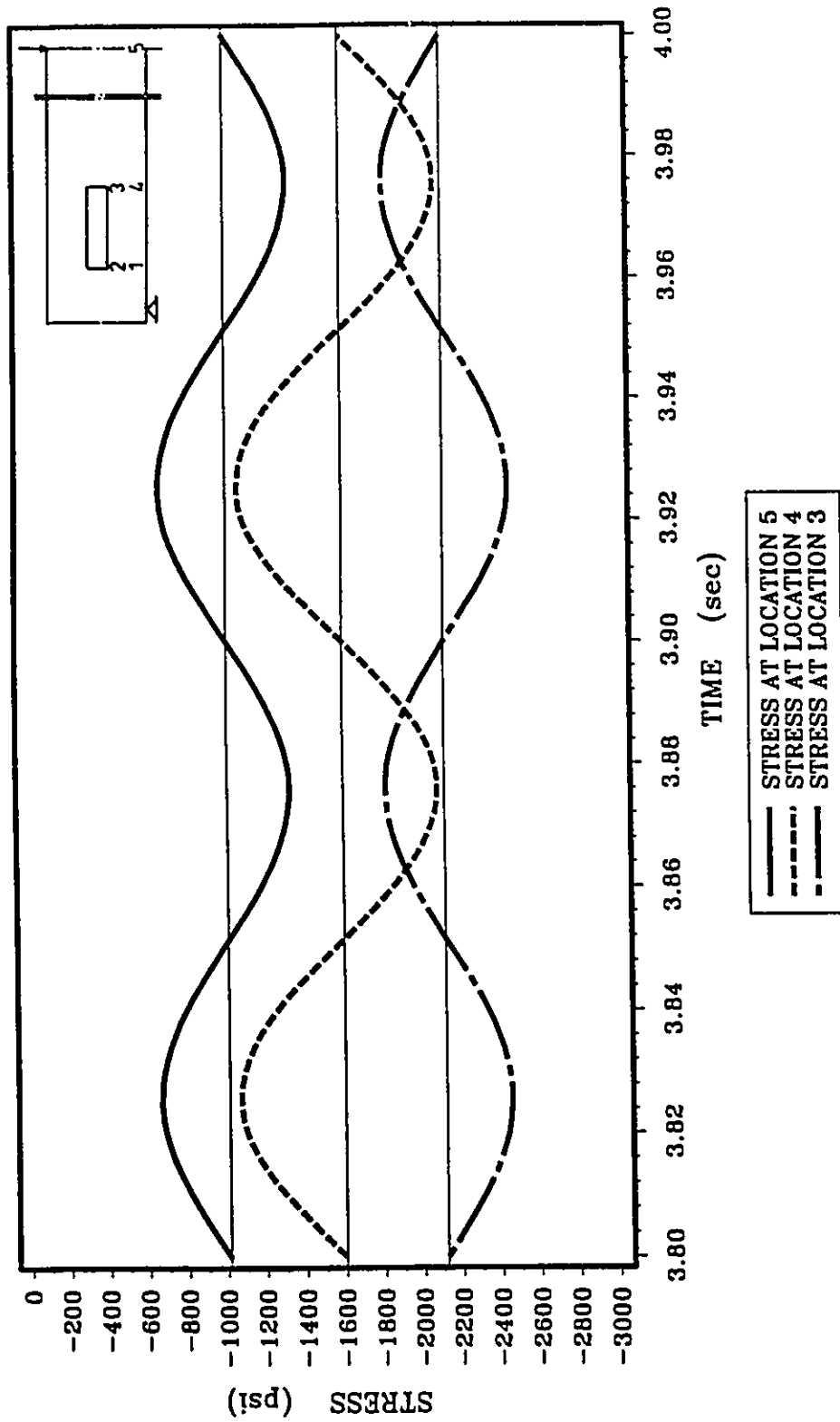


FIG. 6.35 b HORIZONTAL STRESS AT THE OPENING LOWER RIGHT CORNER
 ($\Omega=10$ Hz, $P_0=0.2$ kip, $P_1=0.3$ kip)
 (SHEAR OPENING)

Note: 1 kip=4.45 kN, 1 psi=6.89 kPa

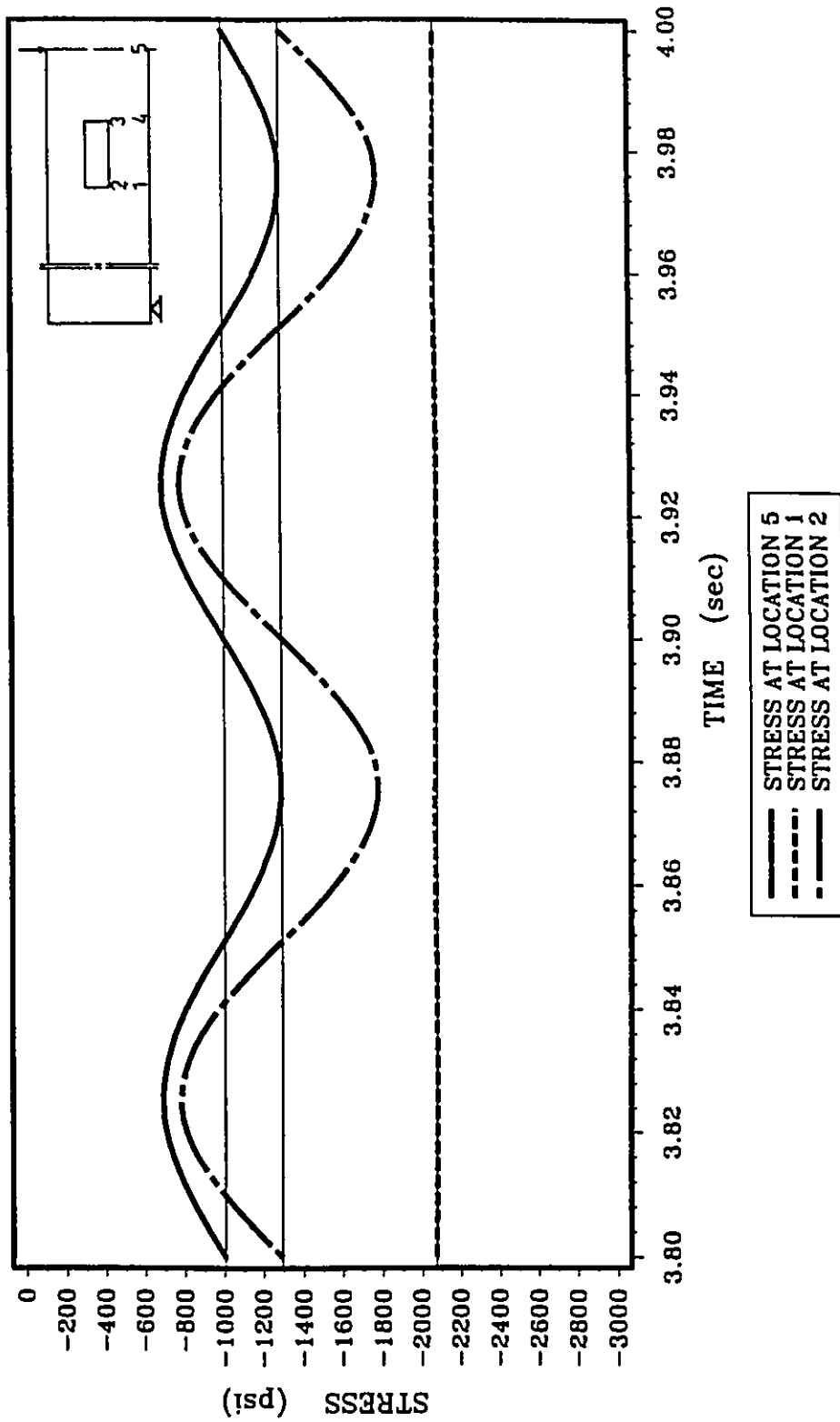


FIG. 6.36 a HORIZONTAL STRESS AT THE OPENING LOWER LEFT CORNER
 ($\Omega=10$ Hz, $P_0=0.2$ kip, $P_1=0.3$ kip)
 (BENDING OPENING)

Note: 1 kip=4.45 kN, 1 psi=6.89 kPa

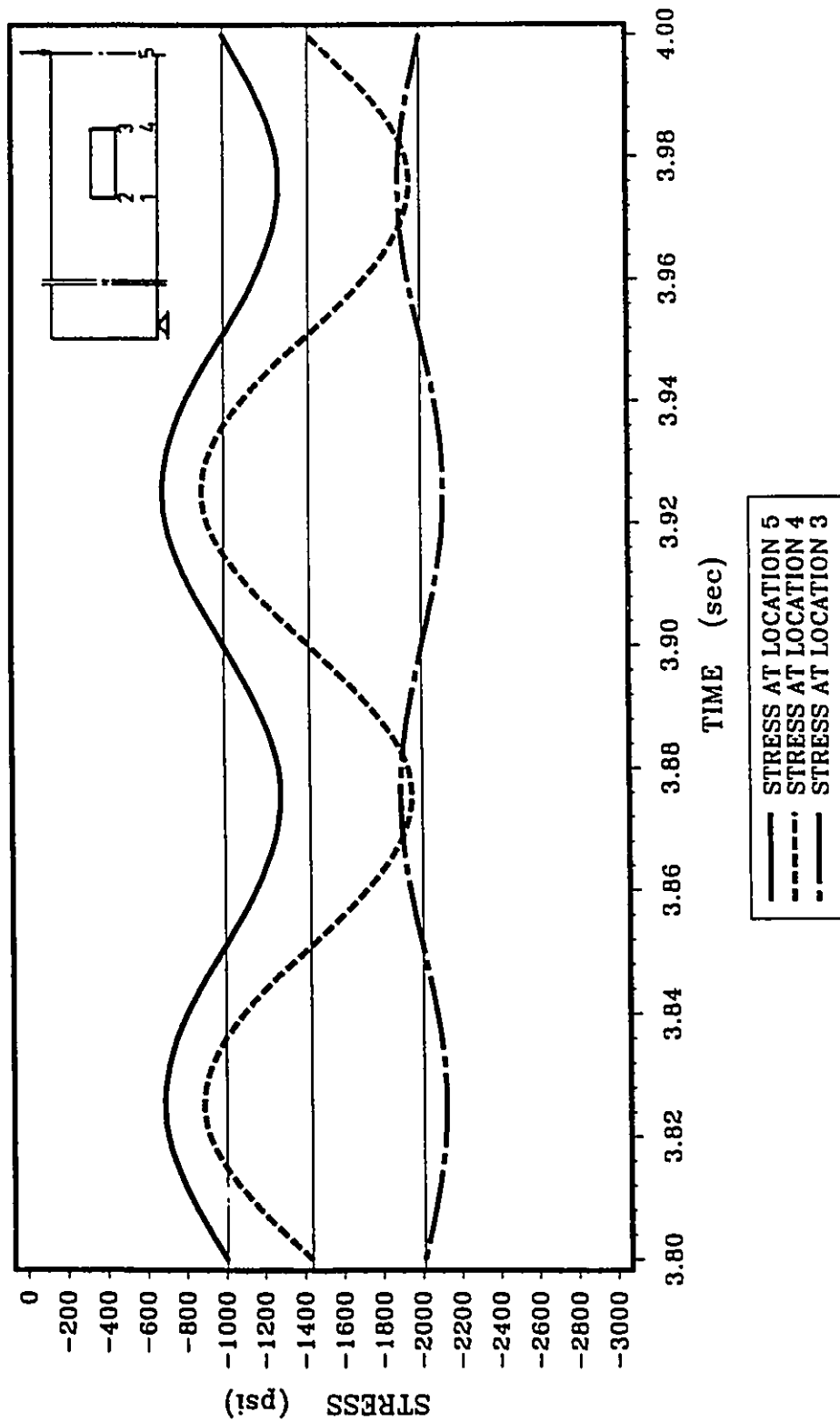


FIG. 6.36 b HORIZONTAL STRESS AT THE OPENING LOWER RIGHT CORNER
 ($\Omega=10$ Hz, $P_0=0.2$ kip, $P_1=0.3$ kip)
 (BENDING OPENING)

Note: 1 kip=4.45 kN, 1 psi=6.89 kPa

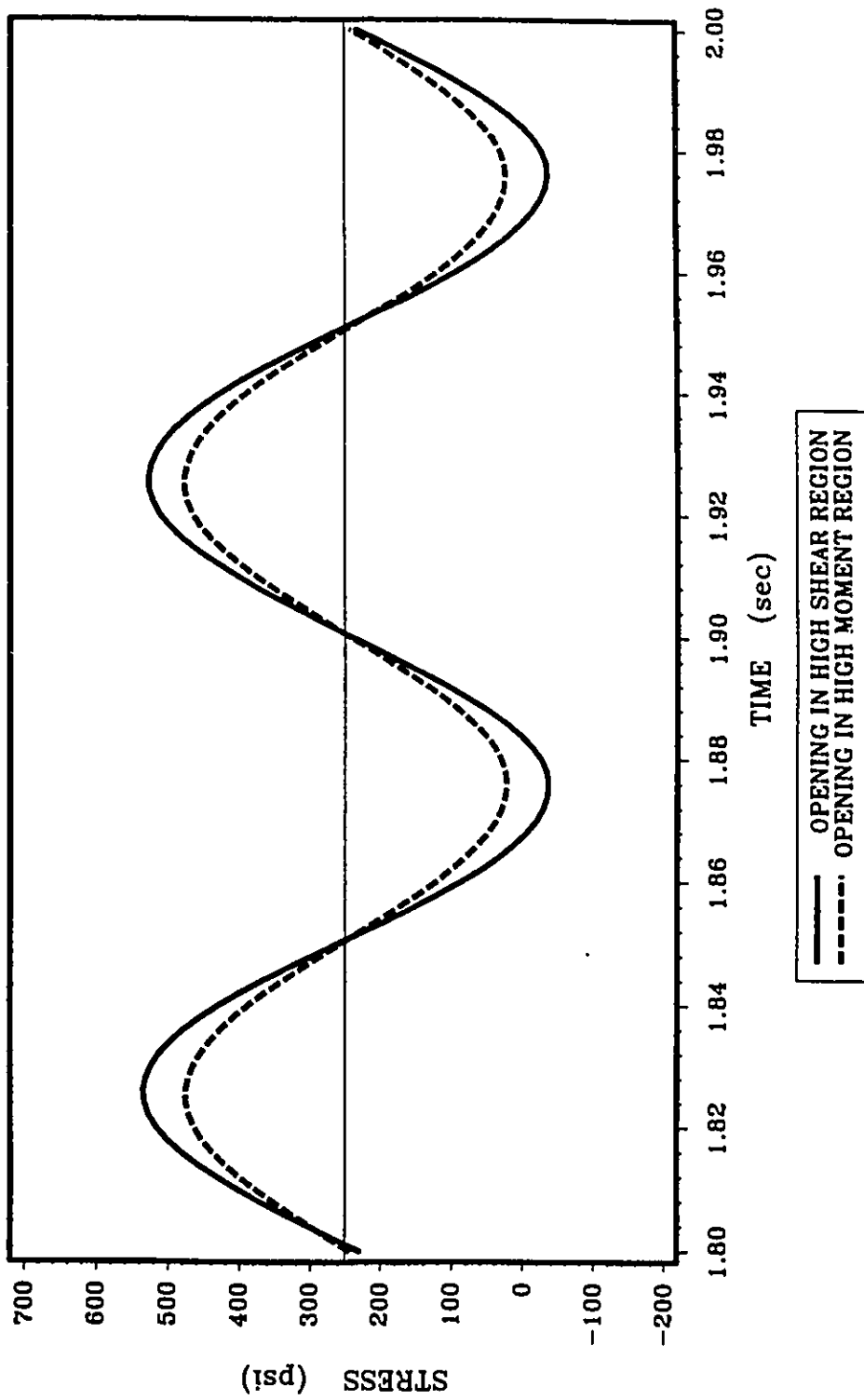


FIG. 6.37 SPLITTING STRESS AT THE CORNERS OF OPENING
 ($\Omega=10$ Hz, $P_0=0.5$ kip)

Note: 1 kip=4.45 kN, 1 psi=6.89 kPa

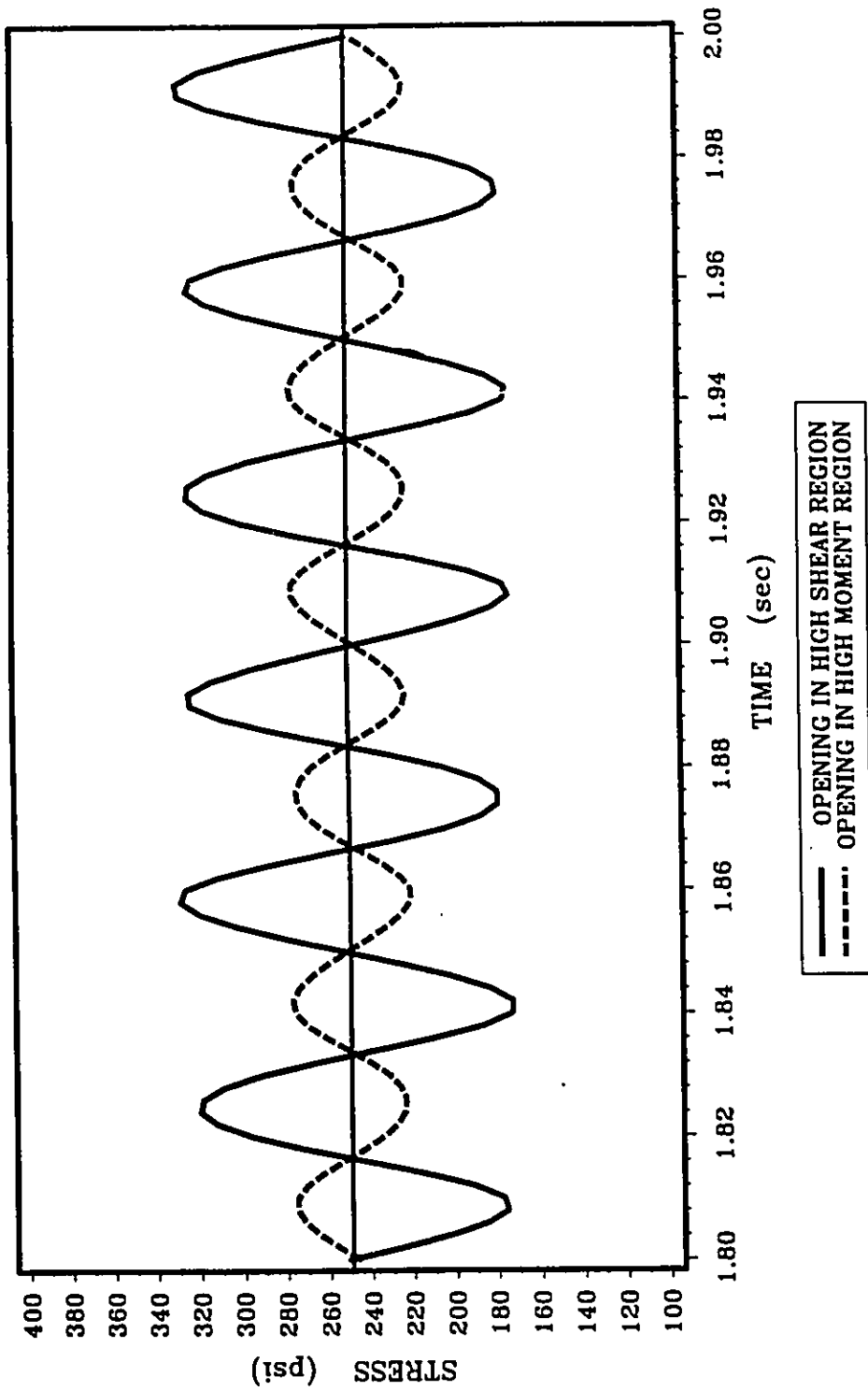


FIG. 6.38 SPLITTING STRESS AT THE CORNERS OF OPENING
($\Omega=30$ Hz, $P_0=0.5$ kip)

Note: 1 kip=4.45 kN, 1 psi=6.89 kPa

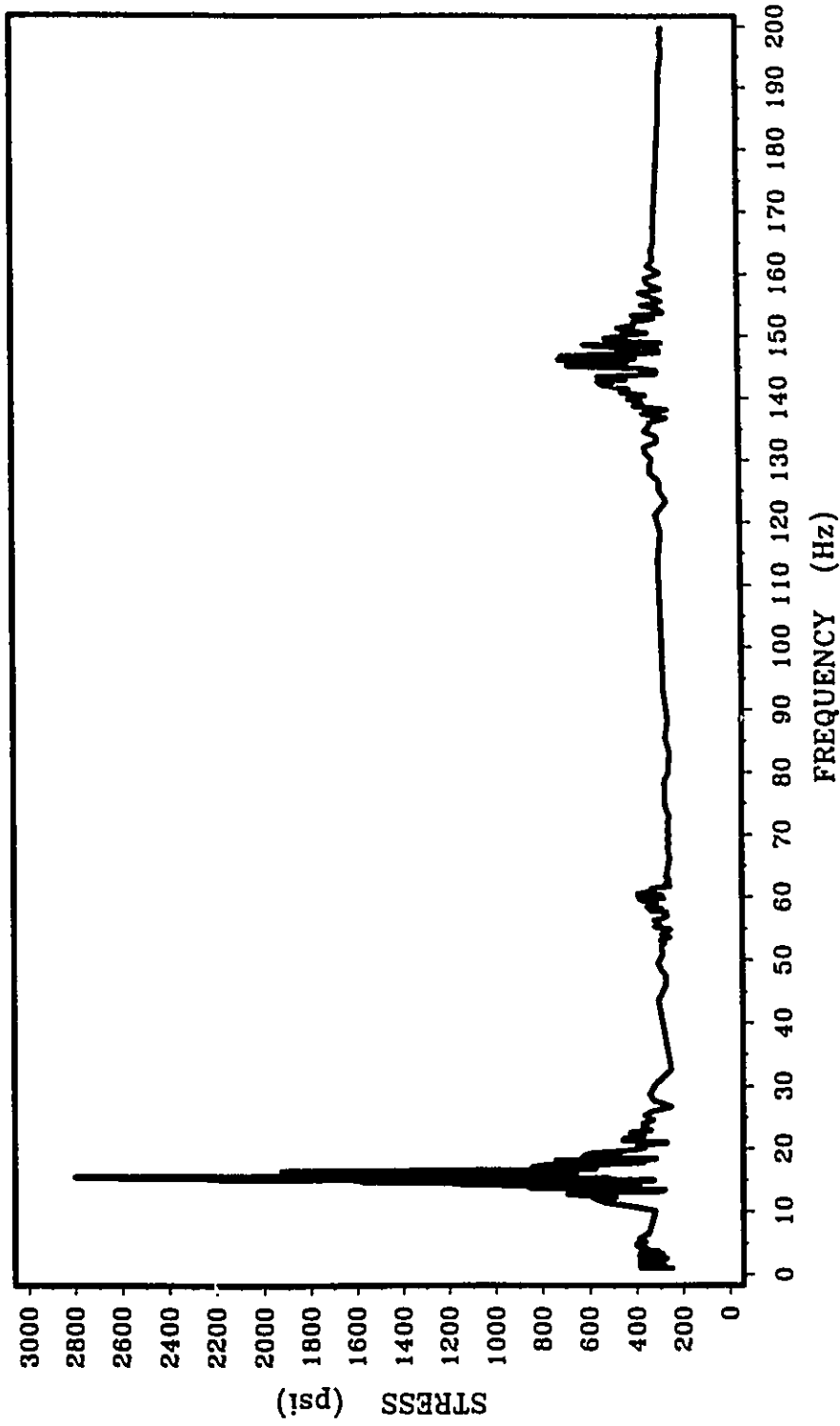


FIG. 6.39 a SPLITTING STRESS AT THE CORNER OF A SHEAR OPENING
(STEADY STATE ANALYSIS)

Note: 1 psi=6.89 kPa

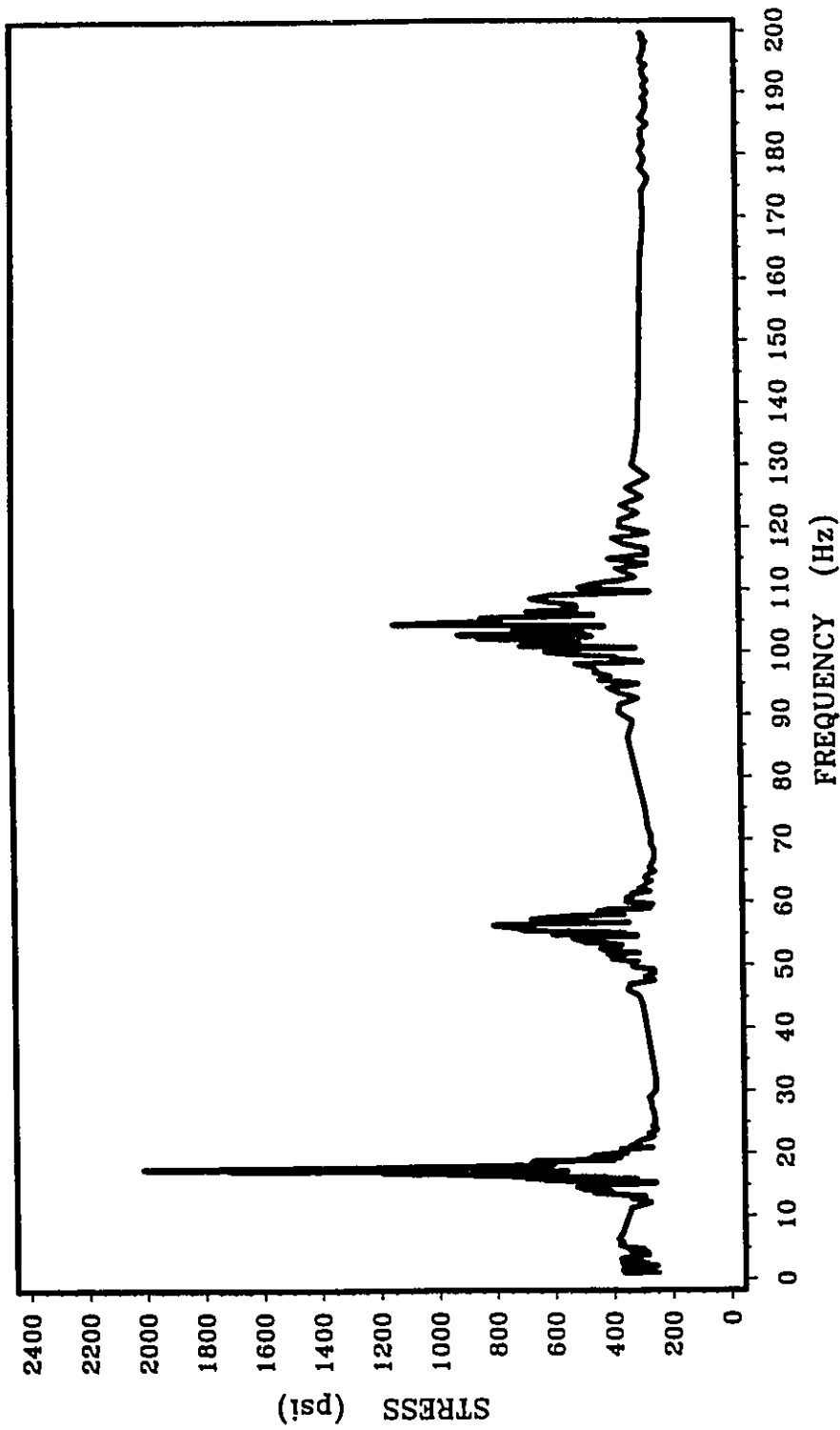


FIG. 6.39 b SPLITTING STRESS AT THE CORNER OF A BENDING OPENING
(STEADY STATE ANALYSIS)

Note: 1 psi=6.89 kPa

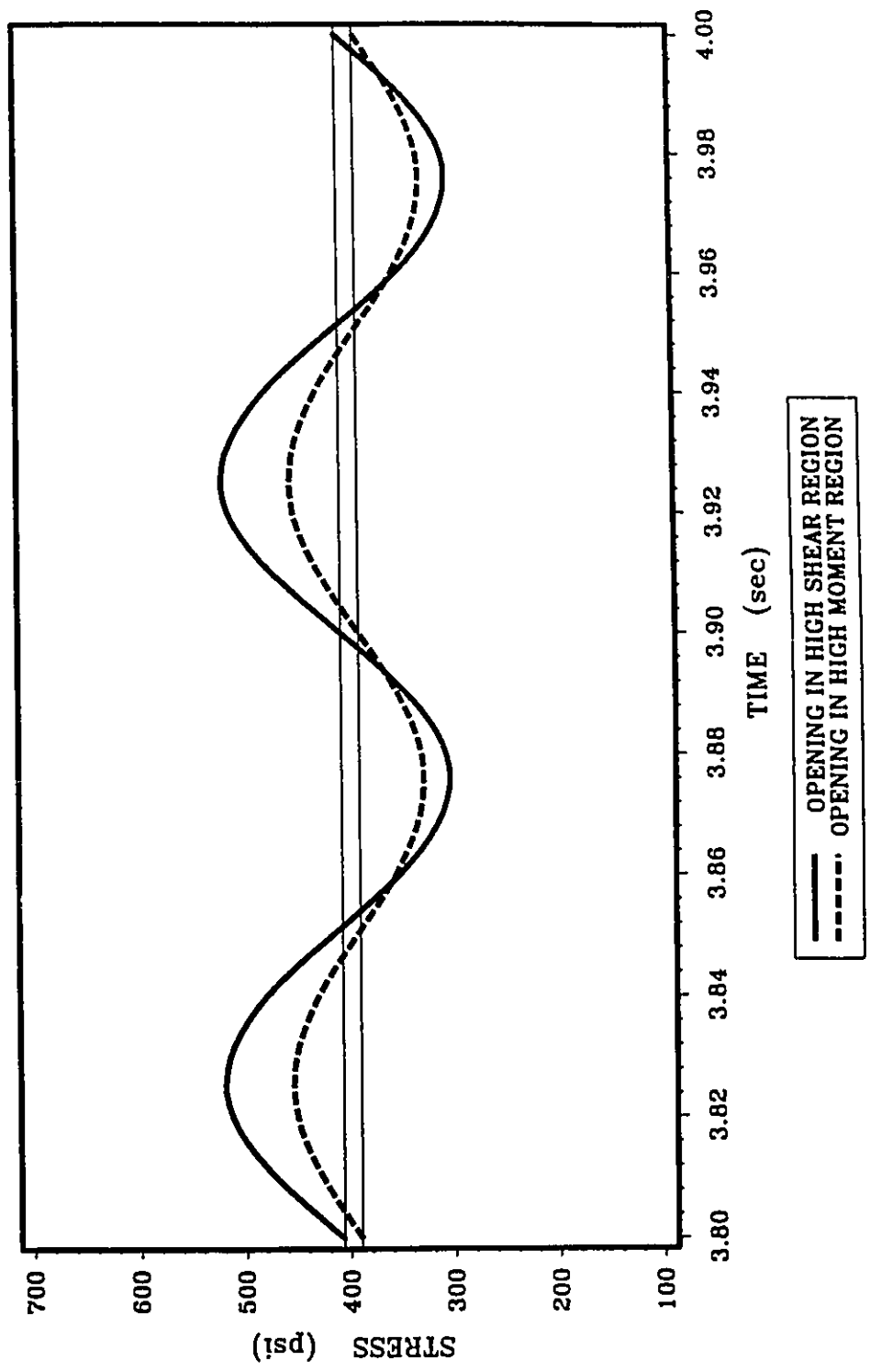


FIG. 6.40 SPLITTING STRESS AT THE CORNERS OF OPENING
 ($\Omega=10$ Hz, $P_0=0.2$ kip, $P_1=0.3$ kip)

Note: 1 kip=4.45 kN, 1 psi=6.89 kPa

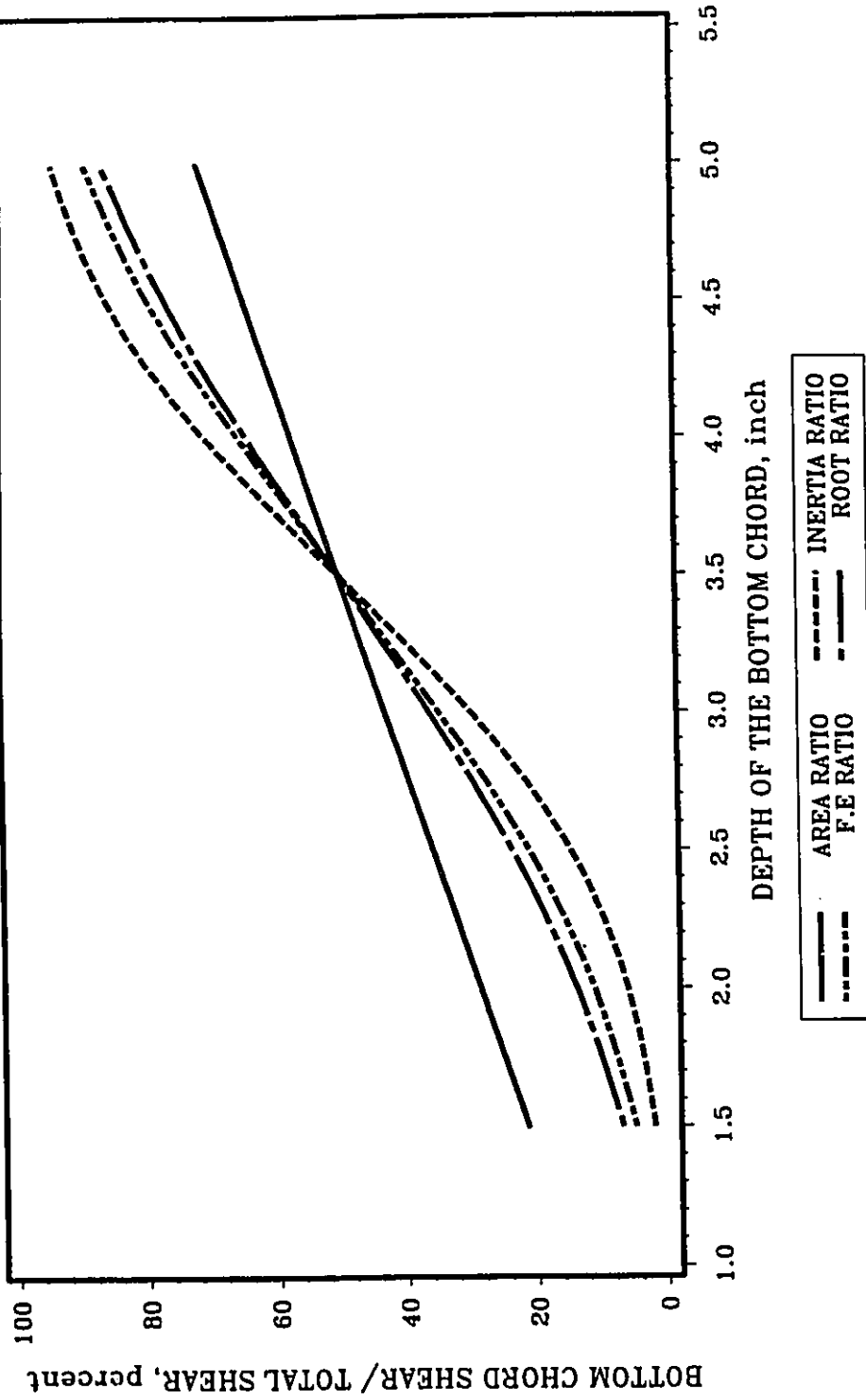


FIG. 7.1 SHEAR FORCE CARRIED BY THE BOTTOM CHORD
(RECTANGULAR SECTION)

Note: 1 in=25.4 mm

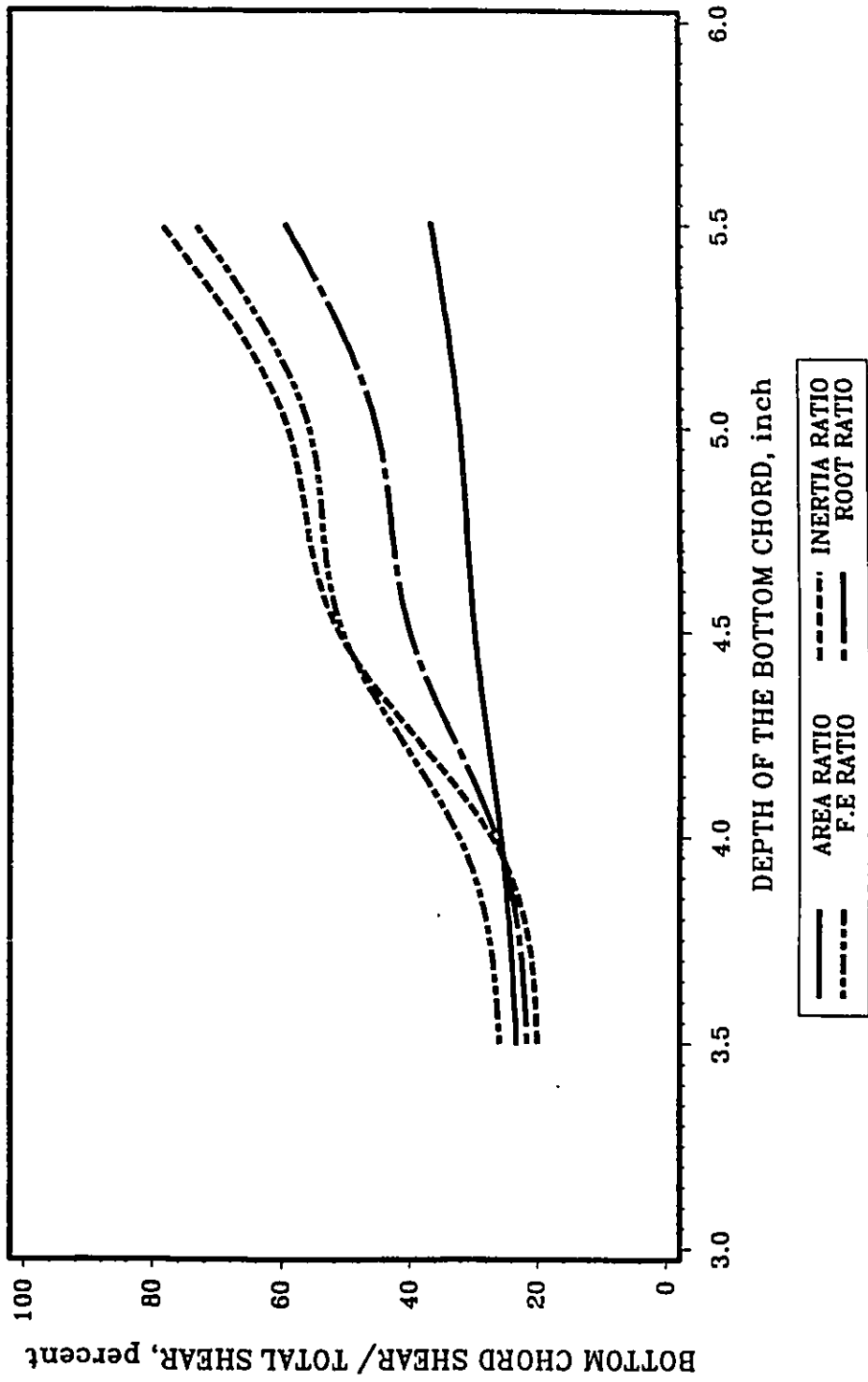


FIG. 7.2 SHEAR FORCE CARRIED BY THE BOTTOM CHORD
(T- SECTION)

Note: 1 in=25.4 mm

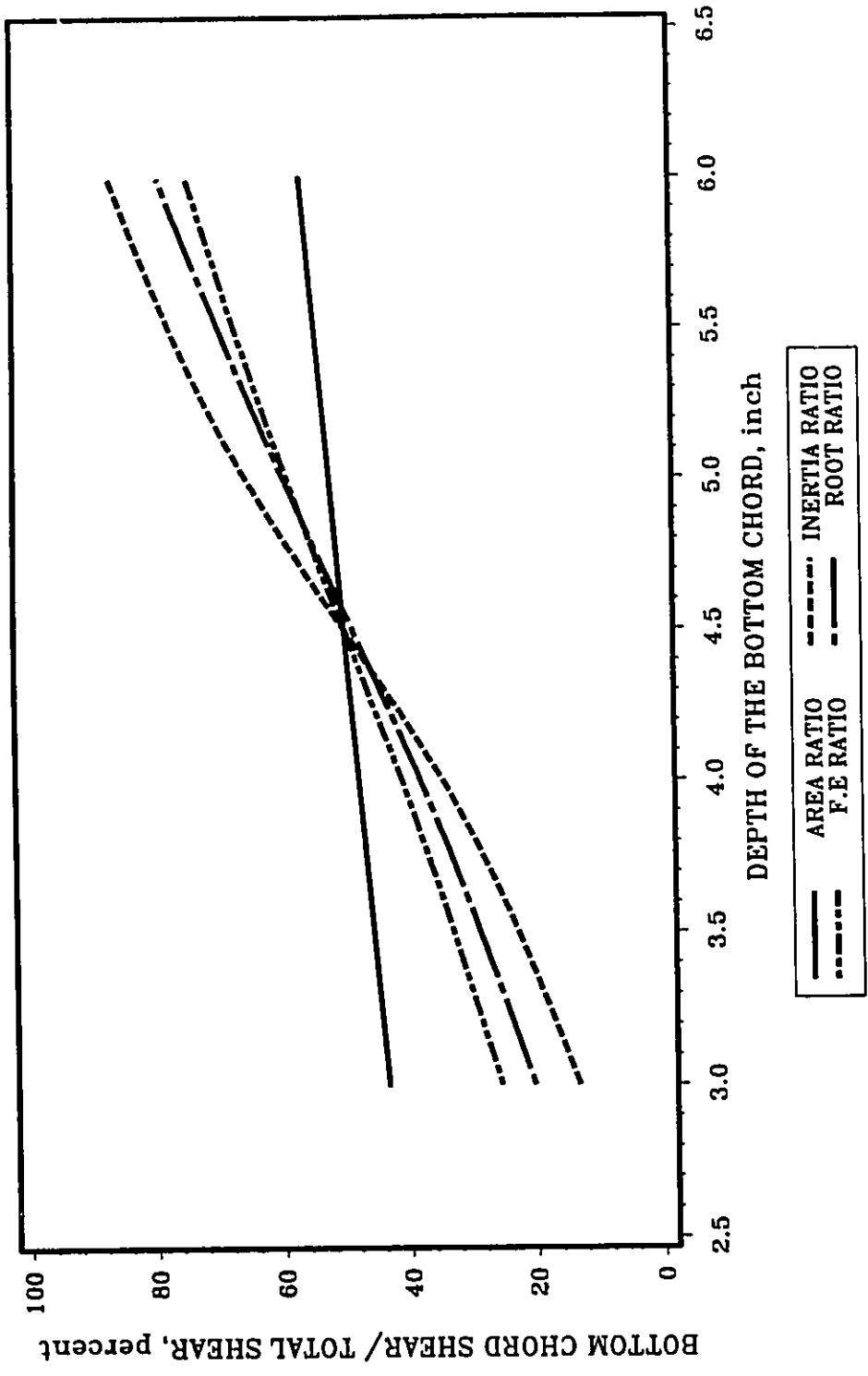


FIG. 7.3 SHEAR FORCE CARRIED BY THE BOTTOM CHORD (I-SECTION)

Note: 1 in=25.4 mm

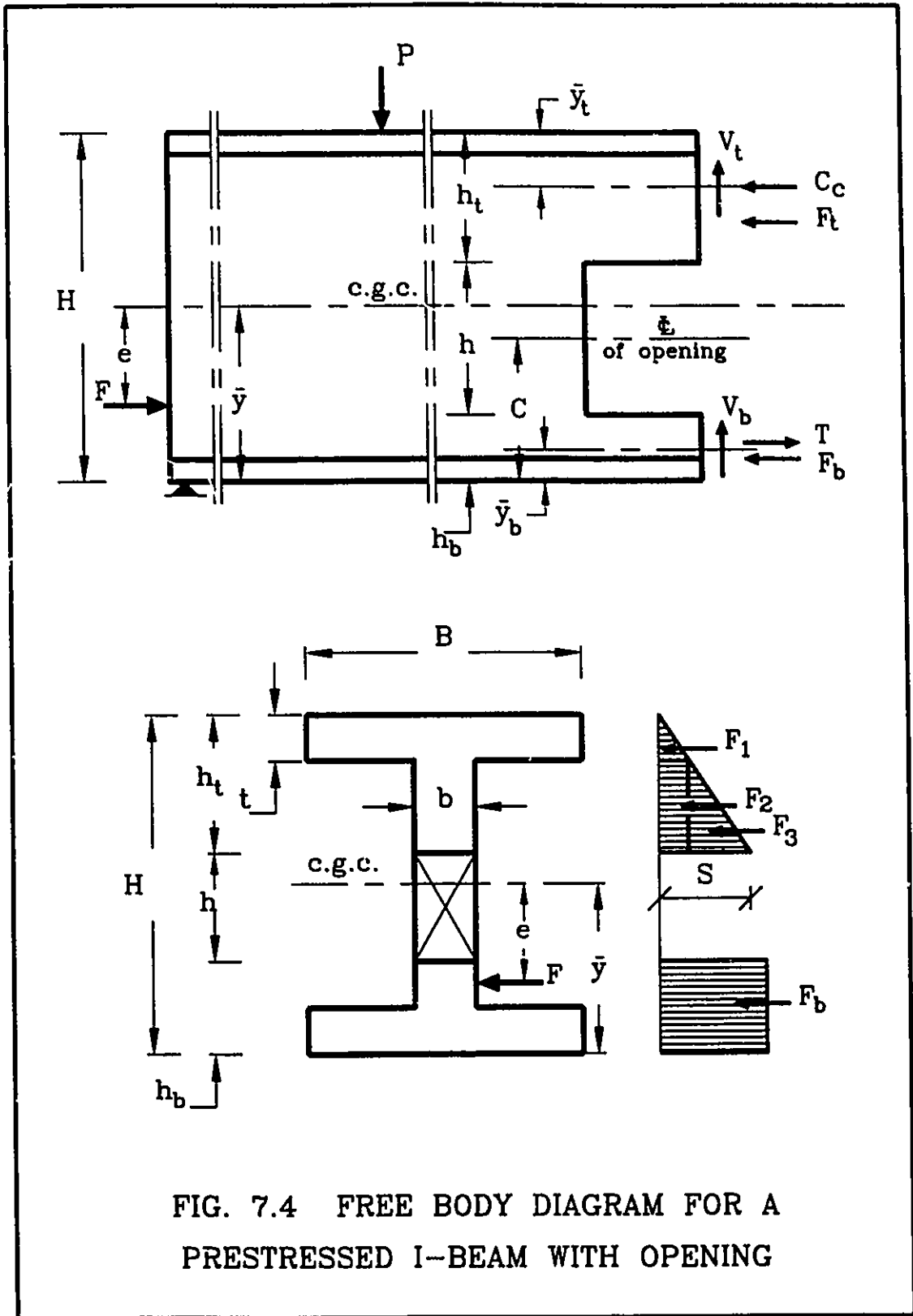


FIG. 7.4 FREE BODY DIAGRAM FOR A PRESTRESSED I-BEAM WITH OPENING

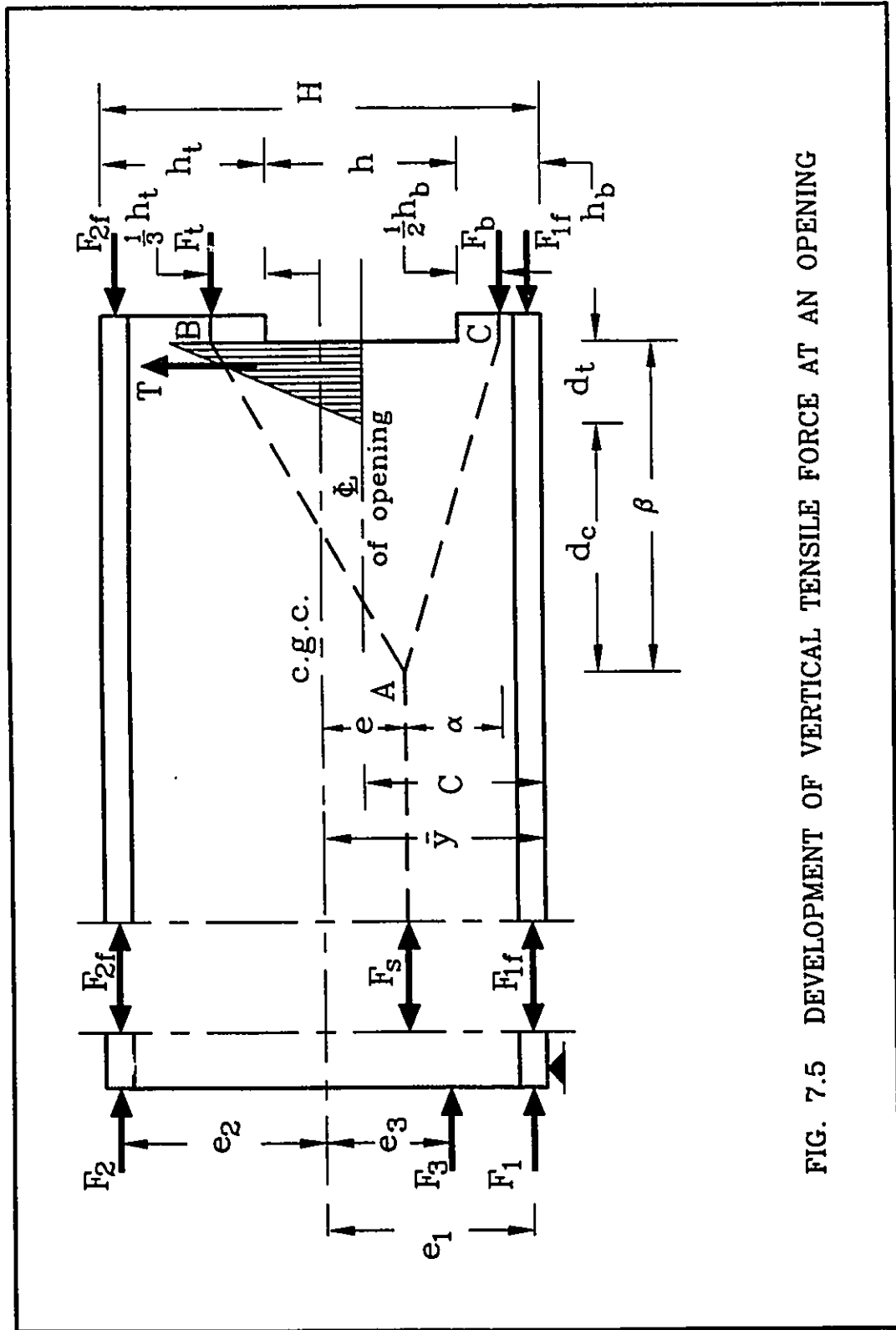


FIG. 7.5 DEVELOPMENT OF VERTICAL TENSILE FORCE AT AN OPENING

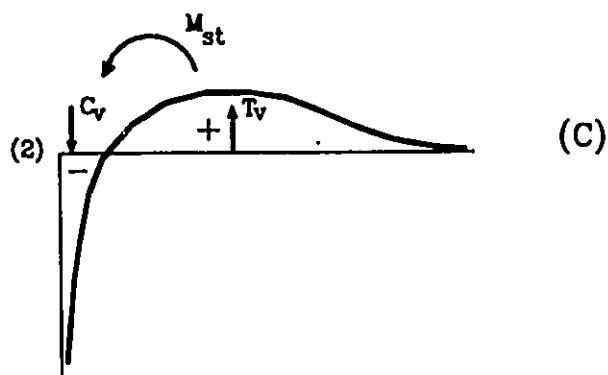
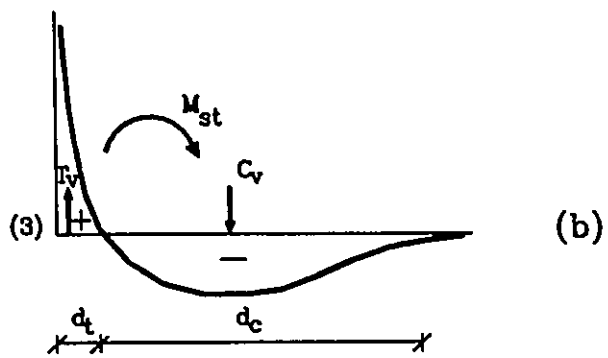
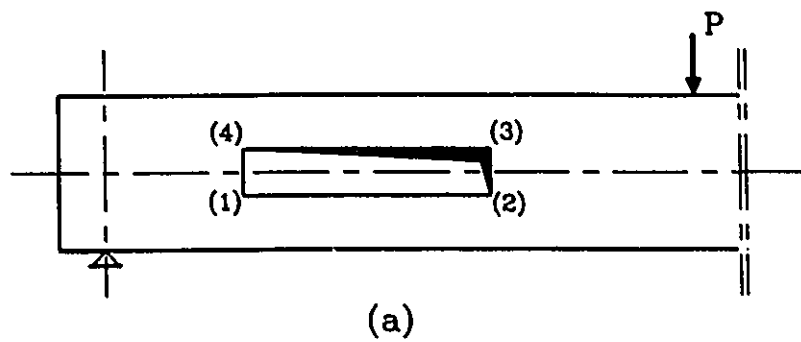
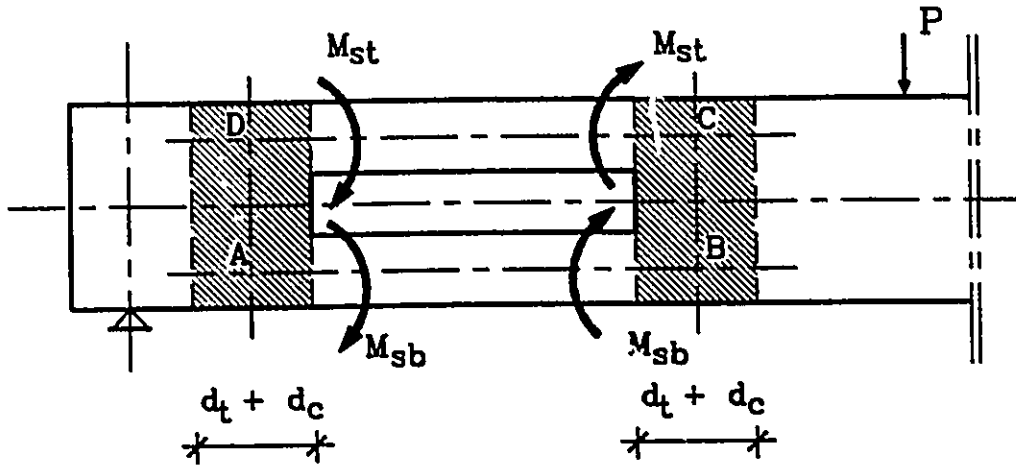
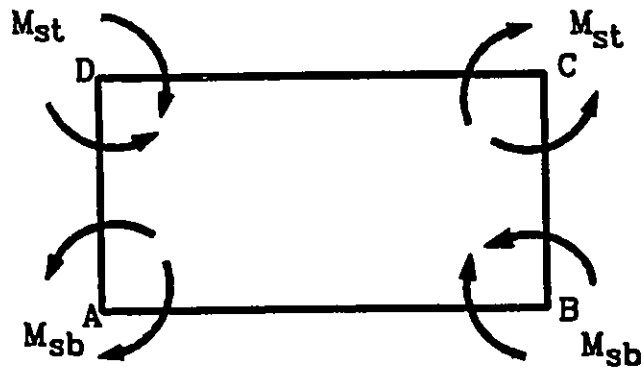


FIG. 7.6 VERTICAL TENSILE AND COMPRESSIVE STRESSES AT THE OPENING DUE TO VERTICAL LOAD ONLY

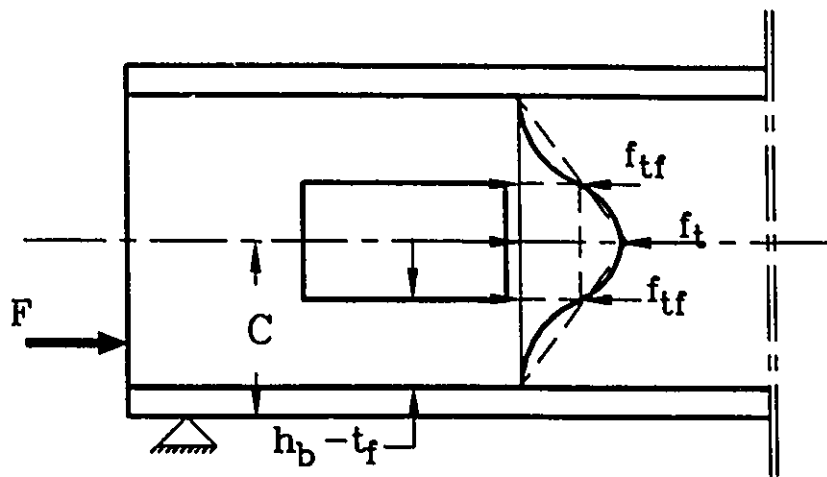


(a)

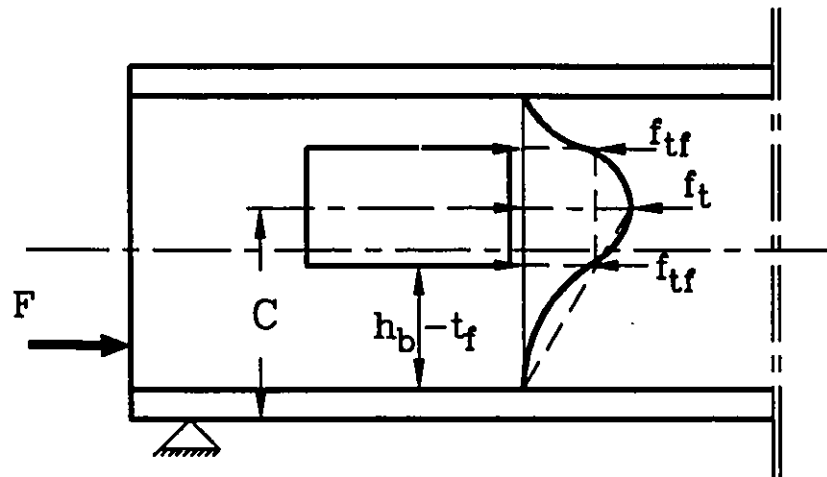


(b)

FIG. 7.7 FRAMING ACTION AROUND THE OPENING



(a) CENTRAL OPENING



(b) ECCENTRIC OPENING

FIG. 7.8 SPLITTING STRESS AT THE OPENING
DUE TO PRESTRESSING

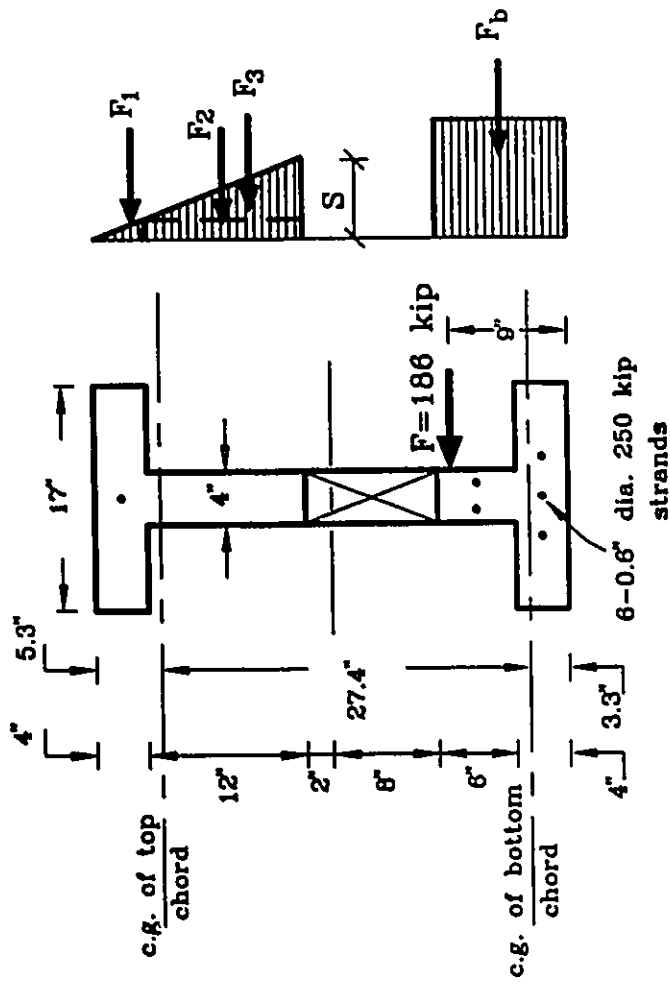
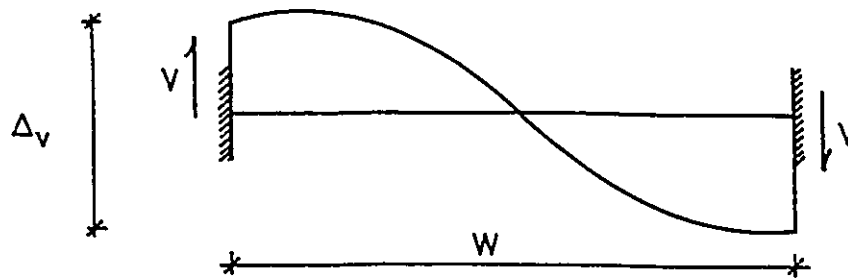
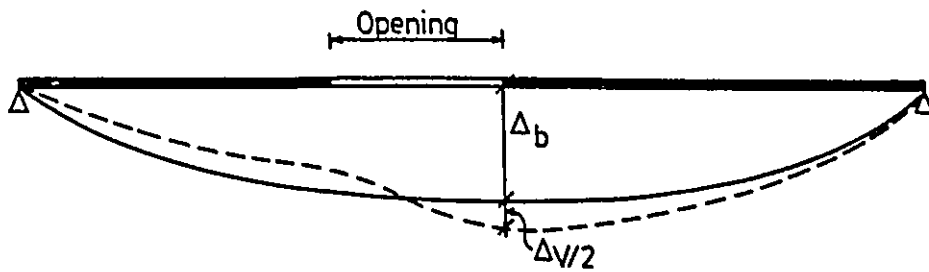


FIG. 7.9 CROSS-SECTION OF PRESTRESSED I-BEAM IN ILLUSTRATED DESIGN EXAMPLE

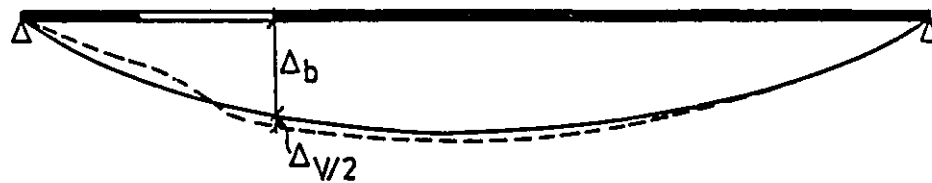
Note: 1 in.=25.4 mm, 1 kip=4.45 kN



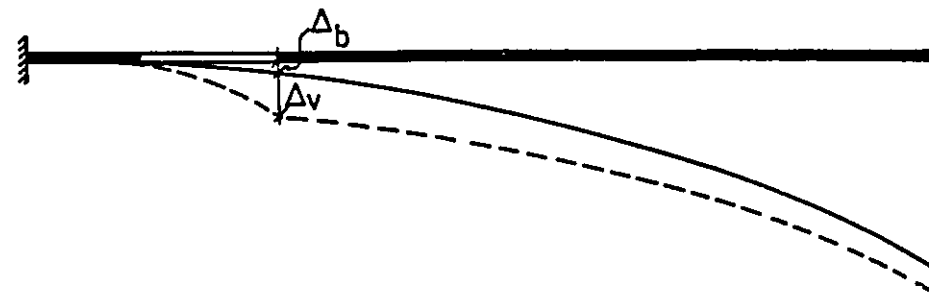
(a) OPENING WITH FIXED-FIXED ENDS



(b) BENDING OPENING



(c) SHEAR OPENING



(d) OPENING IN A CANTILEVER BEAM

FIG. 7.10 RELATIVE DISPLACEMENT BETWEEN THE ENDS OF OPENING DUE TO THE VIERENDEEL ACTION

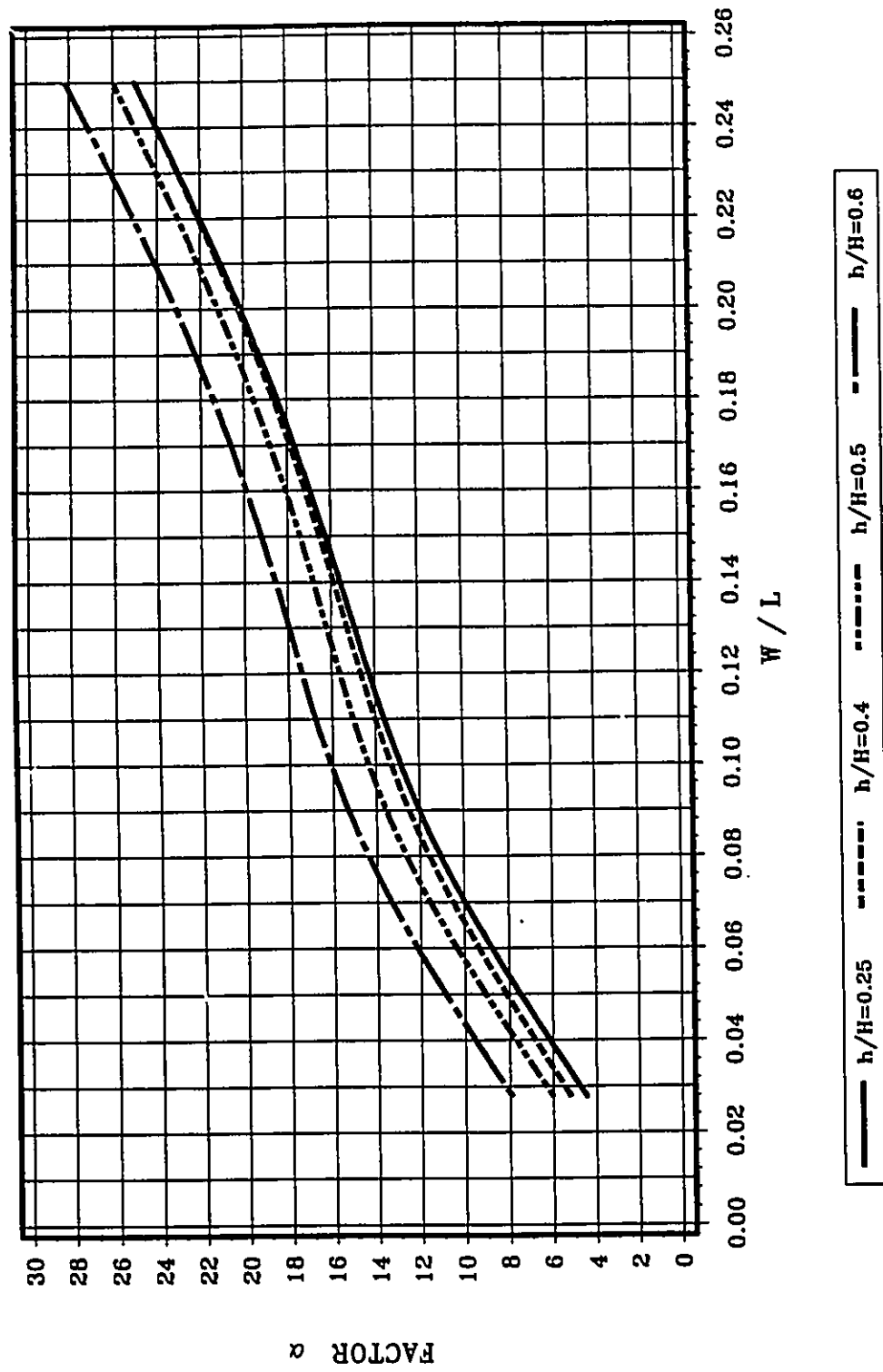


FIG. 7.11 FACTOR α FOR ESTIMATING THE LOCAL DEFLECTION AT THE OPENING

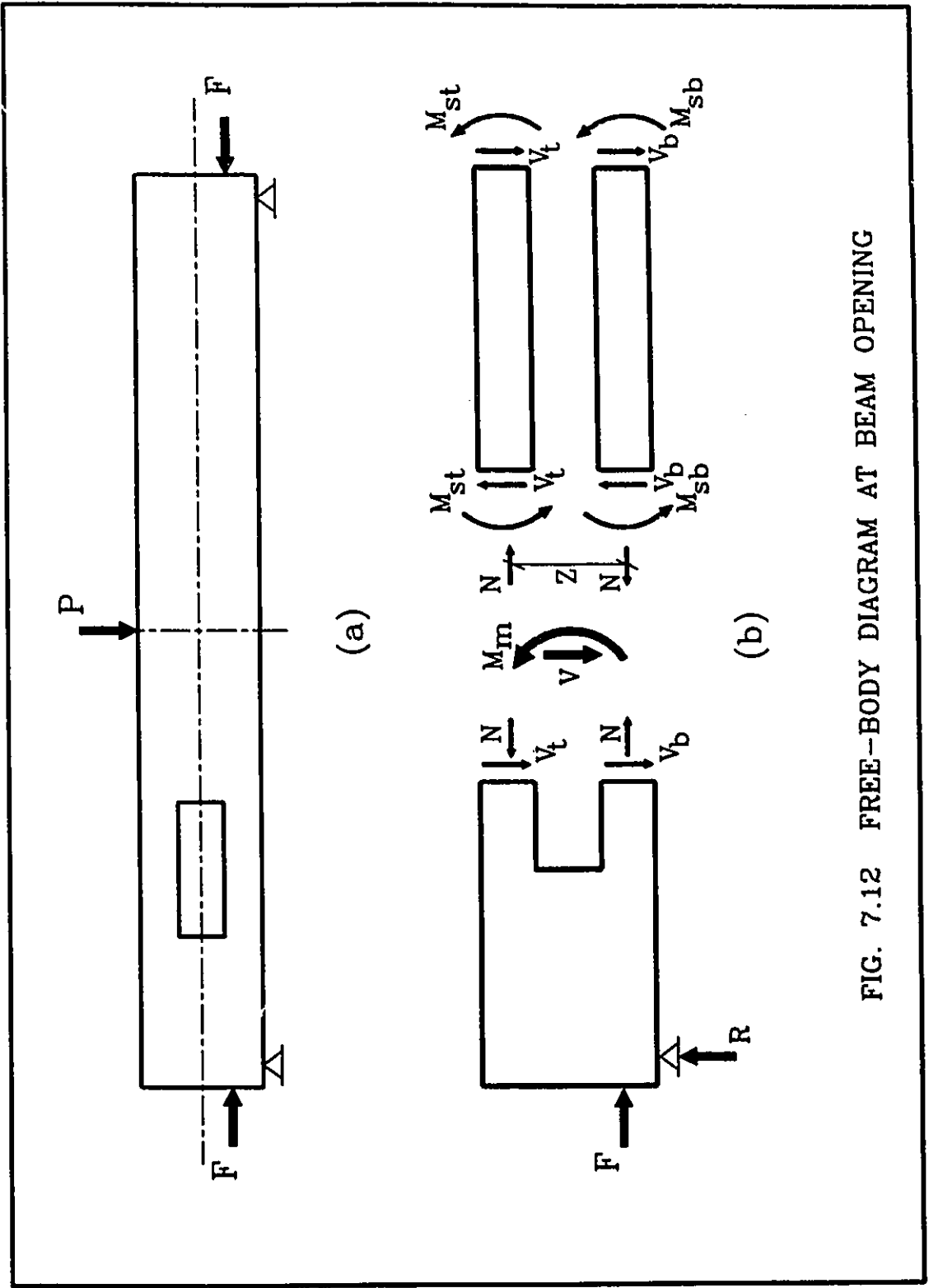
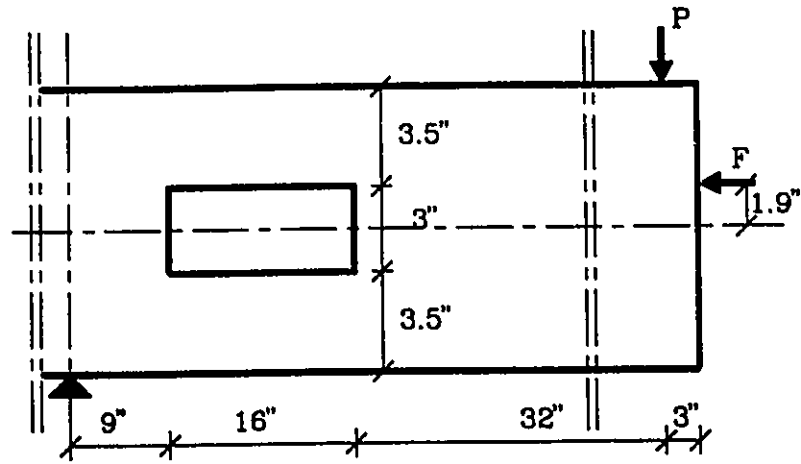
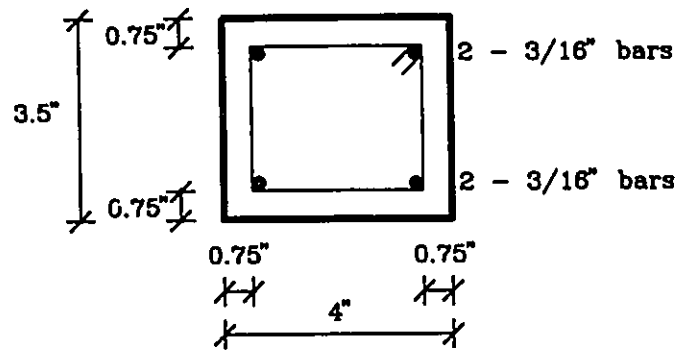


FIG. 7.12 FREE-BODY DIAGRAM AT BEAM OPENING



(a)

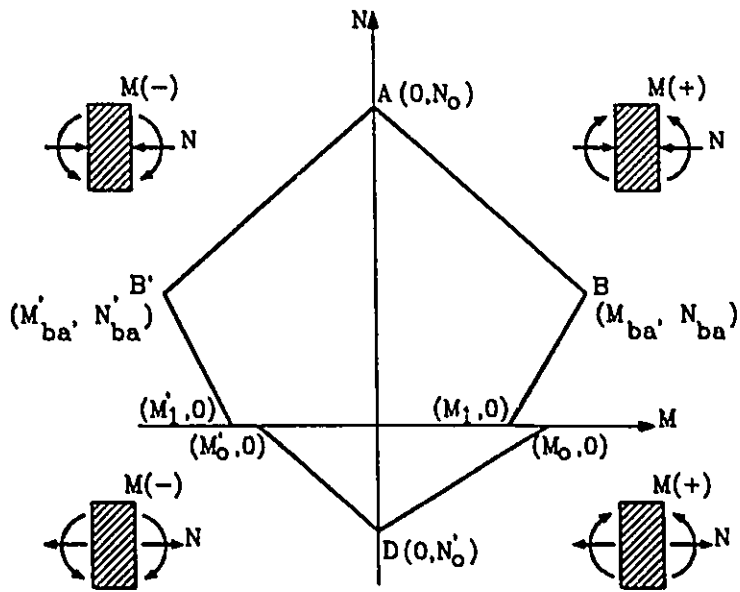


(b)

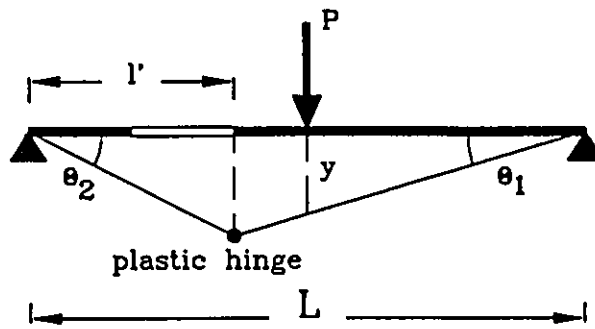
FIG. 7.13 PRESTRESSED BEAM IN ILLUSTRATED DESIGN EXAMPLE

(a) BEAM GEOMETRY; (b) DIMENSIONS OF BOTTOM CHORD

Note: 1 in.=25.4 mm

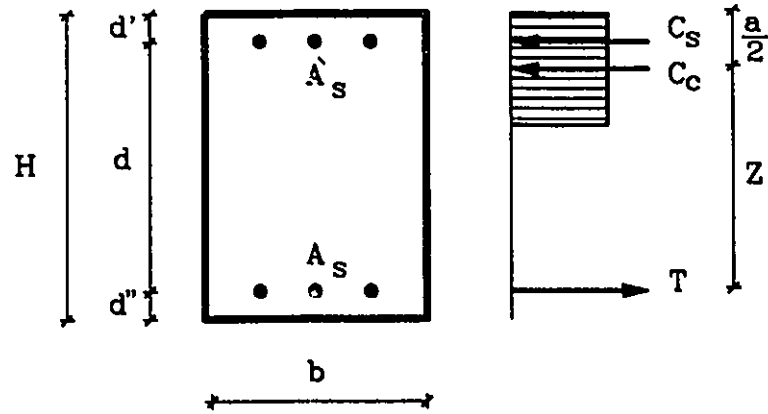


(a) INTERACTION DIAGRAM

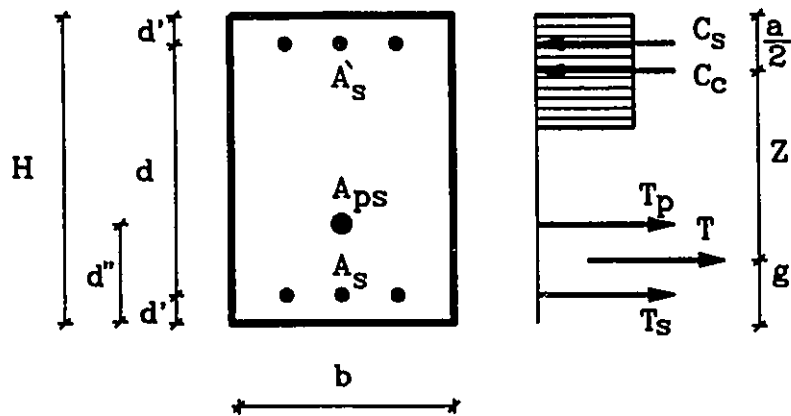


(b) MECHANISM OF FAILURE

FIG. 7.14 PLASTIC ANALYSIS OF
PRESTRESSED BEAMS WITH OPENINGS



(a) REINFORCED CONCRETE SECTION



(b) PRESTRESSED CONCRETE SECTION

FIG. 7.15 GEOMETRY OF REINFORCED AND PRESTRESSED CONCRETE SECTIONS

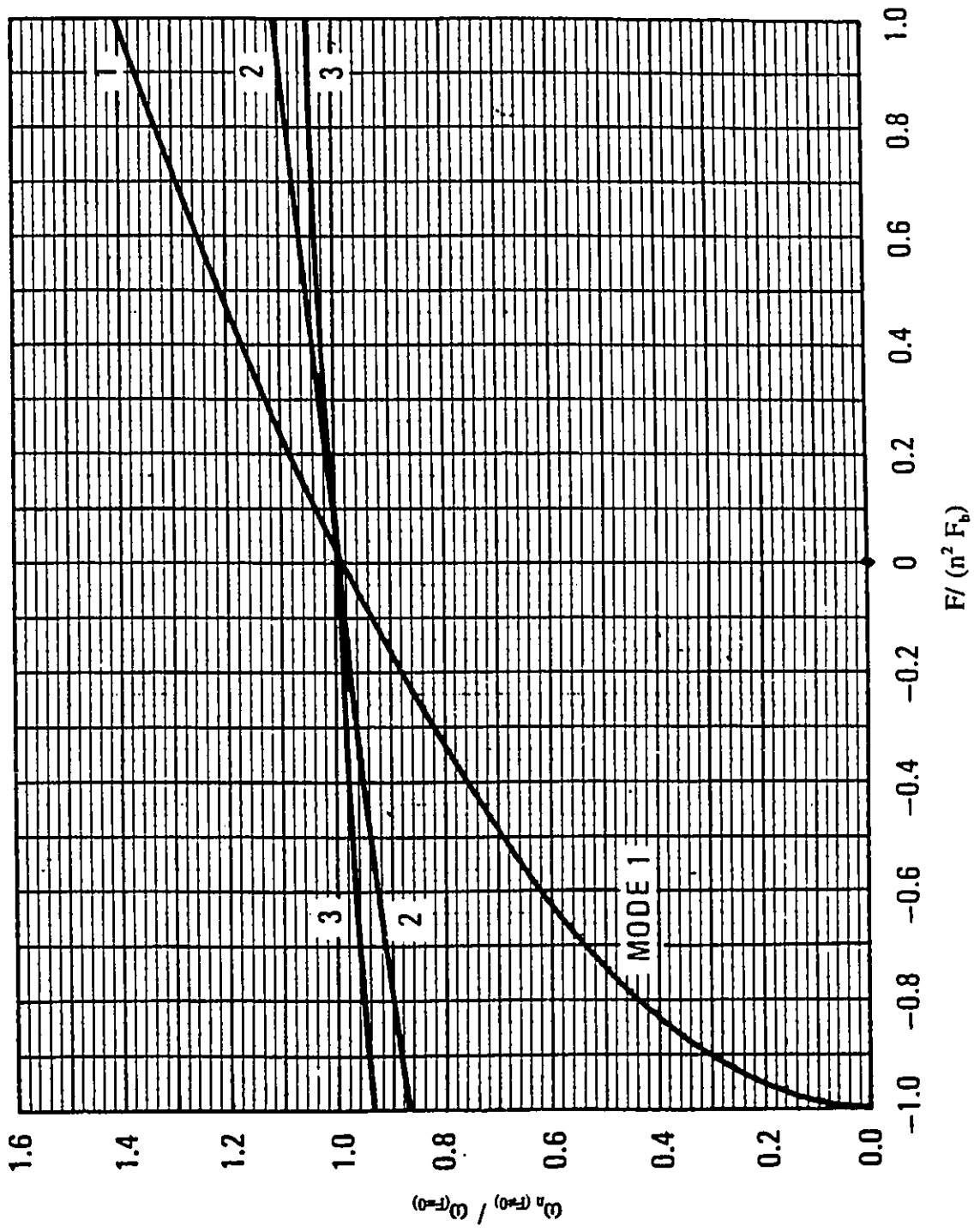


FIG. 7.16 EFFECT OF PRESTRESSING ON THE NATURAL FREQUENCIES

APPENDIX A.1

'ABAQUS' INPUT DATA

A.1.1 Non-Linear Static Analysis

```
*HEADING
*****
** BEAM BIII1A (OPENING 5X18 in., M/VH=2.57 & C=7 in.)
*****
**DATA CHECK
*PREPRINT,MODEL=NO,HISTORY=NO
***** COORDINATES OF WEB NODES
*NODE
1,0.,0.
2,0.,1.0
3,0.,2.0
4,0.,2.5
5,0.,3.0
6,0.,3.5
7,0.,4.0
8,0.,4.5
9,0.,5.0
10,0.,5.5
11,0.,6.5
12,0.,7.0
13,0.,7.5
14,0.,8.0
15,0.,8.5
16,0.,9.0
17,0.,9.5
18,0.,10.0
19,0.,11.0
20,0.,12.0
841,42.,0.
842,42.,1.0
843,42.,2.0
844,42.,2.5
845,42.,3.0
846,42.,3.5
847,42.,4.0
```

848,42.,4.5
849,42.,5.0
850,42.,5.5
851,42.,6.5
852,42.,7.0
853,42.,7.5
854,42.,8.0
855,42.,8.5
856,42.,9.0
857,42.,9.5
858,42.,10.0
859,42.,11.0
860,42.,12.0
961,54.,0.
962,54.,1.0
963,54.,2.0
964,54.,2.5
965,54.,3.0
966,54.,3.5
967,54.,4.0
968,54.,4.5
969,54.,5.0
970,54.,5.5
971,54.,6.5
972,54.,7.0
973,54.,7.5
974,54.,8.0
975,54.,8.5
976,54.,9.0
977,54.,9.5
978,54.,10.0
979,54.,11.0
980,54.,12.0
1041,60.,0.
1042,60.,1.0
1043,60.,2.0
1044,60.,2.5
1045,60.,3.0
1046,60.,3.5
1047,60.,4.0
1048,60.,4.5
1049,60.,5.0
1050,60.,5.5
1051,60.,6.5
1052,60.,7.0
1053,60.,7.5
1054,60.,8.0
1055,60.,8.5
1056,60.,9.0
1057,60.,9.5
1058,60.,10.0
1059,60.,11.0

```

1060,60.,12.0
***** END COORDINATES OF WEB NODES
***** WEB NODES GENERATION
*NSET,NSET=A,GENERATE
1,20
*NSET,NSET=B,GENERATE
841,860
*NSET,NSET=C,GENERATE
961,980
*NSET,NSET=D,GENERATE
1041,1060
*NFILL,NSET=AB
A,B,42,20
*NFILL,NSET=BC
B,C,6,20
*NFILL,NSET=CD
C,D,4,20
***** END OF WEB NODES GENERATION
***** COORDINATES OF FLANGE NODES
*NODE
2001,0.,0.,+9.0
2002,0.,0.,+7.0
2003,0.,0.,+5.0
2004,0.,0.,+3.0
2005,0.,0.,+1.0
2006,0.,0.,-1.0
2007,0.,0.,-3.0
2008,0.,0.,-5.0
2009,0.,0.,-7.0
2010,0.,0.,-9.0
2841,42.,0.,+9.0
2842,42.,0.,+7.0
2843,42.,0.,+5.0
2844,42.,0.,+3.0
2845,42.,0.,+1.0
2846,42.,0.,-1.0
2847,42.,0.,-3.0
2848,42.,0.,-5.0
2849,42.,0.,-7.0
2850,42.,0.,-9.0
2961,54.,0.,+9.0
2962,54.,0.,+7.0
2963,54.,0.,+5.0
2964,54.,0.,+3.0
2965,54.,0.,+1.0
2966,54.,0.,-1.0
2967,54.,0.,-3.0
2968,54.,0.,-5.0
2969,54.,0.,-7.0
2970,54.,0.,-9.0
3041,60.,0.,+9.0
3042,60.,0.,+7.0

```



```

3043,60.,0.,+5.0
3044,60.,0.,+3.0
3045,60.,0.,+1.0
3046,60.,0.,-1.0
3047,60.,0.,-3.0
3048,60.,0.,-5.0
3049,60.,0.,-7.0
3050,60.,0.,-9.0
4001,0.,12.,+9.0
4002,0.,12.,+7.0
4003,0.,12.,+5.0
4004,0.,12.,+3.0
4005,0.,12.,+1.0
4006,0.,12.,-1.0
4007,0.,12.,-3.0
4008,0.,12.,-5.0
4009,0.,12.,-7.0
4010,0.,12.,-9.0
4841,42.,12.,+9.0
4842,42.,12.,+7.0
4843,42.,12.,+5.0
4844,42.,12.,+3.0
4845,42.,12.,+1.0
4846,42.,12.,-1.0
4847,42.,12.,-3.0
4848,42.,12.,-5.0
4849,42.,12.,-7.0
4850,42.,12.,-9.0
4961,54.,12.,+9.0
4962,54.,12.,+7.0
4963,54.,12.,+5.0
4964,54.,12.,+3.0
4965,54.,12.,+1.0
4966,54.,12.,-1.0
4967,54.,12.,-3.0
4968,54.,12.,-5.0
4969,54.,12.,-7.0
4970,54.,12.,-9.0
5041,60.,12.,+9.0
5042,60.,12.,+7.0
5043,60.,12.,+5.0
5044,60.,12.,+3.0
5045,60.,12.,+1.0
5046,60.,12.,-1.0
5047,60.,12.,-3.0
5048,60.,12.,-5.0
5049,60.,12.,-7.0
5050,60.,12.,-9.0
***** END OF COORDINATES OF FLANGE NODES
***** FLANGES NODES GENERATION
*NSET,NSET=SA,GENERATE
2001,2010,1

```

```

*NSET,NSET=SB,GENERATE
2841,2850,1
*NSET,NSET=SC,GENERATE
2961,2970,1
*NSET,NSET=SD,GENERATE
3041,3050,1
*NFILL,NSET=SAB
SA,SB,42,20
*NFILL,NSET=SBC
SB,SC,6,20
*NFILL,NSET=SCD
SC,SD,4,20
*NSET,NSET=SAT,GENERATE
4001,4010,1
*NSET,NSET=SBT,GENERATE
4841,4850,1
*NSET,NSET=SCT,GENERATE
4961,4970,1
*NSET,NSET=SDT,GENERATE
5041,5050,1
*NFILL,NSET=SABT
SAT,SBT,42,20
*NFILL,NSET=SBCT
SBT,SCT,6,20
*NFILL,NSET=SCDT
SCT,SDT,4,20
***** END OF FLANGES NODES GENERATION
***** WEB ELEMENTS DEFINITION
*ELEMENT,TYPE=CPS4
1,1,21,22,2
241,241,261,262,242
255,255,275,276,256
601,601,621,622,602
841,841,861,862,842
961,961,981,982,962
***** END OF WEB ELEMENTS DEFENITION
***** WEB ELEMENTS GENERATION
*ELGEN,ELSET=EAA1
1,12,20,20,19,1,1
*ELGEN,ELSET=EA1A2B
241,18,20,20,5,1,1
*ELGEN,ELSET=EA1A2T
255,18,20,20,5,1,1
*ELGEN,ELSET=EA2B
601,12,20,20,19,1,1
*ELGEN,ELSET=EBC
841,6,20,20,19,1,1
*ELGEN,ELSET=ECD
961,4,20,20,19,1,1
***** END OF WEB ELEMENTS GENERATION
***** WEB SECTION DEFENITION
*ELSET,ELSET=BEAM

```

```

EAA1,EA1A2B,EA1A2T,EA2B,EBC
*SOLID SECTION,ELSET=BEAM,MATERIAL=A1
4.
*SOLID SECTION,ELSET=ECD,MATERIAL=A2
4.
***** END OF WEB SECTION DEFENITION
***** FLANGES ELEMENTS DEFENITION
*ELEMENT,TYPE=S4R
2001,2001,2021,2022,2002
2005,2005,2025,21,1
2006,1,21,2026,2006
2007,2006,2026,2027,2007
4001,4001,4021,4022,4002
4005,4005,4025,40,20
4006,20,40,4026,4006
4007,4006,4026,4027,4007
2961,2961,2981,2982,2962
2965,2965,2985,981,961
2966,961,981,2986,2966
2967,2966,2986,2987,2967
4961,4961,4981,4982,4962
4965,4965,4985,1000,980
4966,980,1000,4986,4966
4967,4966,4986,4987,4967
***** END OF FLANGES ELEMENTS DEFENITION
***** FLANGES ELEMENTS GENERATION
*ELGEN,ELSET=SLAB
2001,48,20,20,4,1,1
2005,48,20,20
2006,48,20,20
2007,48,20,20,4,1,1
4001,48,20,20,4,1,1
4005,48,20,20
4006,48,20,20
4007,48,20,20,4,1,1
*ELGEN,ELSET=SLABE
2961,4,20,20,4,1,1
2965,4,20,20
2966,4,20,20
2967,4,20,20,4,1,1
4961,4,20,20,4,1,1
4965,4,20,20
4966,4,20,20
4967,4,20,20,4,1,1
***** END OF FLANGES ELEMENTS GENERATION
***** FLANGES SECTION DEFENITION
*SHELL SECTION,ELSET=SLAB,MATERIAL=A1
2.
*SHELL SECTION,ELSET=SLABE,MATERIAL=A2
2.
***** END OF FLANGES SECTION DEFENITION
***** CONCRETE DEFENITION

```

```

*MATERIAL,NAME=A1
*ELASTIC
4.769E6,20
*CONCRETE
1500.,0.
6300.,.0015
*TENSION STIFFENING
0.,20.E-4
*MATERIAL,NAME=A2
*ELASTIC
4.769E6,20
***** END OF CONCRETE DEFENITION
***** REINFORCRD ELEMENTS DEFENITION
*ELSET,ELSET=RFT,GENERATE
19,1039,20
*ELSET,ELSET=RFB,GENERATE
1,1021,20
*ELSET,ELSET=RFT1,GENERATE
18,1038,20
*ELSET,ELSET=RFB1,GENERATE
2,1022,20
*ELSET,ELSET=RFBO,GENERATE
5,1025,20
*ELSET,ELSET=RFTO,GENERATE
15,1035,20
*ELSET,ELSET=RFS1,GEN
2004,3024,20
*ELSET,ELSET=RFS2,GEN
2003,3023,20
*ELSET,ELSET=RFS3,GEN
2002,3022,20
*ELSET,ELSET=RFS4,GEN
2001,3021,20
*ELSET,ELSET=RFS5,GEN
2007,3027,20
*ELSET,ELSET=RFS6,GEN
2008,3028,20
*ELSET,ELSET=RFS7,GEN
2009,3029,20
*ELSET,ELSET=RFS8,GEN
2010,3030,20
*ELSET,ELSET=RFS1T,GEN
4004,5024,20
*ELSET,ELSET=RFS2T,GEN
4003,5023,20
*ELSET,ELSET=RFS3T,GEN
4002,5022,20
*ELSET,ELSET=RFS4T,GEN
4001,5021,20
*ELSET,ELSET=RFS5T,GEN
4007,5027,20
*ELSET,ELSET=RFS6T,GEN

```

4008,5028,20
 *ELSET,ELSET=RFS7T,GEN
 4009,5029,20
 *ELSET,ELSET=RFS8T,GEN
 4010,5030,20
 *ELSET,ELSET=ST21,GENERATE
 21,39
 *ELSET,ELSET=ST221,GENERATE
 221,239
 *ELSET,ELSET=ST361B,GENERATE
 361,365
 *ELSET,ELSET=ST361T,GENERATE
 375,379
 *ELSET,ELSET=ST481B,GENERATE
 481,485
 *ELSET,ELSET=ST481T,GENERATE
 495,499
 *ELSET,ELSET=ST601,GENERATE
 601,619
 *ELSET,ELSET=ST681,GENERATE
 681,699
 *ELSET,ELSET=ST841,GENERATE
 841,859
 *ELSET,ELSET=ST961,GEN
 961,979
 *ELSET,ELSET=ST1021,GEN
 1021,1039
 ***** END OF REINFORCRD ELEMENTS DEFENITION
 ***** PRESTRESSING REINFORCEMENT
 *REBAR,ELEMENT=CONTINUUM,MATERIAL=PST,GEOMETRY=ISOPARAMETRIC,NAME=PHANY
 RFB1,.02991,1.,0.,.45,1
 *REBAR,ELEMENT=CONTINUUM,MATERIAL=PST,GEOMETRY=ISOPARAMETRIC,NAME=PEMAN
 RFT1,.02991,1.,0.,.4,1
 *REBAR,ELEMENT=CONTINUUM,MATERIAL=PST,GEOMETRY=ISOPARAMETRIC,NAME=PEMAN
 RFT,.04487,1.,0.,.65,1
 ***** END OF PRESTRESSING REINFORCEMENT
 ***** FLANGES REINFORCEMENT
 *REBAR,ELEMENT=SHELL,MATERIAL=ST,GEOMETRY=ISOPARAMETRIC,NAME=EMAN2
 RFS1,.0138,1.,0.,1
 *REBAR,ELEMENT=SHELL,MATERIAL=ST,GEOMETRY=ISOPARAMETRIC,NAME=EMAN3
 RFS2,.0138,1.,0.,1
 *REBAR,ELEMENT=SHELL,MATERIAL=ST,GEOMETRY=ISOPARAMETRIC,NAME=EMAN5
 RFS3,.0138,1.,0.,1
 *REBAR,ELEMENT=SHELL,MATERIAL=ST,GEOMETRY=ISOPARAMETRIC,NAME=EMAN6
 RFS4,.0138,1.,0.,1
 *REBAR,ELEMENT=SHELL,MATERIAL=ST,GEOMETRY=ISOPARAMETRIC,NAME=EMAN2
 RFS5,.0138,1.,0.,1
 *REBAR,ELEMENT=SHELL,MATERIAL=ST,GEOMETRY=ISOPARAMETRIC,NAME=EMAN3
 RFS6,.0138,1.,0.,1
 *REBAR,ELEMENT=SHELL,MATERIAL=ST,GEOMETRY=ISOPARAMETRIC,NAME=EMAN5
 RFS7,.0138,1.,0.,1
 *REBAR,ELEMENT=SHELL,MATERIAL=ST,GEOMETRY=ISOPARAMETRIC,NAME=EMAN6

```

RFS8,,0138,1,,0,,1
*REBAR,ELEMENT=SHELL,MATERIAL=ST,GEOMETRY=ISOPARAMETRIC,NAME=EMAN3
RFS2T,,0138,1,,0,,1
*REBAR,ELEMENT=SHELL,MATERIAL=ST,GEOMETRY=ISOPARAMETRIC,NAME=EMAN5
RFS3T,,0138,1,,0,,1
*REBAR,ELEMENT=SHELL,MATERIAL=ST,GEOMETRY=ISOPARAMETRIC,NAME=EMAN6
RFS4T,,0138,1,,0,,1
*REBAR,ELEMENT=SHELL,MATERIAL=ST,GEOMETRY=ISOPARAMETRIC,NAME=EMAN2
RFS5T,,0138,1,,0,,1
*REBAR,ELEMENT=SHELL,MATERIAL=ST,GEOMETRY=ISOPARAMETRIC,NAME=EMAN3
RFS6T,,0138,1,,0,,1
*REBAR,ELEMENT=SHELL,MATERIAL=ST,GEOMETRY=ISOPARAMETRIC,NAME=EMAN6
RFS8T,,0138,1,,0,,1
***** END OF FLANGES REINFORCEMENT
***** OPENING REINFORCEMENT
*REBAR,ELEMENT=CONTINUUM,MATERIAL=ST,GEOMETRY=ISOPARAMETRIC,NAME=HANY3
RFBO,,0138,1,,0,,0,,1
*REBAR,ELEMENT=CONTINUUM,MATERIAL=ST,GEOMETRY=ISOPARAMETRIC,NAME=HANY4
RFTO,,0138,1,,0,,1,,1
***** END OF OPENING REINFORCEMENT
***** STIRRUPS DEFENITION
*REBAR,ELEMENT=CONTINUUM,MATERIAL=ST,GEOMETRY=ISOPARAMETRIC,NAME=AHM
ED1
ST21,,0276,2,,0,,5,4
*REBAR,ELEMENT=CONTINUUM,MATERIAL=ST,GEOMETRY=ISOPARAMETRIC,NAME=AHM
ED2
ST221,,0276,2,,0,,5,4
*REBAR,ELEMENT=CONTINUUM,MATERIAL=ST,GEOMETRY=ISOPARAMETRIC,NAME=O1B
ST361B,,0276,2,,0,,1,,4
*REBAR,ELEMENT=CONTINUUM,MATERIAL=ST,GEOMETRY=ISOPARAMETRIC,NAME=O1T
ST361T,,0276,2,,0,,1,,4
*REBAR,ELEMENT=CONTINUUM,MATERIAL=ST,GEOMETRY=ISOPARAMETRIC,NAME=O2B
ST481B,,0276,2,,0,,1,,4
*REBAR,ELEMENT=CONTINUUM,MATERIAL=ST,GEOMETRY=ISOPARAMETRIC,NAME=O2T
ST481T,,0276,2,,0,,1,,4
*REBAR,ELEMENT=CONTINUUM,MATERIAL=ST,GEOMETRY=ISOPARAMETRIC,NAME=AHM
ED3
ST601,,0276,2,,0,,5,4
*REBAR,ELEMENT=CONTINUUM,MATERIAL=ST,GEOMETRY=ISOPARAMETRIC,NAME=AHM
ED4
ST681,,0276,2,,0,,5,4
*REBAR,ELEMENT=CONTINUUM,MATERIAL=ST,GEOMETRY=ISOPARAMETRIC,NAME=AHM
ED5
ST841,,0276,2,,0,,5,4
*REBAR,ELEMENT=CONTINUUM,MATERIAL=ST,GEOMETRY=ISOPARAMETRIC,NAME=AHM
ED6
ST961,,0276,2,,0,,5,4
*REBAR,ELEMENT=CONTINUUM,MATERIAL=ST,GEOMETRY=ISOPARAMETRIC,NAME=AHM
ED7
ST1021,,0276,2,,0,,5,4
***** END OF STIRRUPS DEFENITION
***** NON-PRESTRESSING STEEL DEFENITION

```

```

*MATERIAL,NAME=ST
*ELASTIC
29.E6
*PLASTIC
50.E3
***** END OF NON-PRESTRESSING STEEL DEFENITION
***** PRESTRESSING STEEL DEFENITION
*MATERIAL,NAME=PST
*ELASTIC
29.E6
*PLASTIC
210.E3
***** END OF PRESTRESSING STEEL DEFENITION
***** BOUNDARY DEFENITION
*BOUNDARY
A,1,3
SA,1,6
SAT,1,6
***** END OF BOUNDARY DEFENITION
***** MODEL PLOTTING
*PLOT
BEAM BIII1A (OPENING 5X18 in., M/VH=2.57 & C=7.0 in.)
10,10,7,7,3,2,3,1
.16,,,,.05
*DRAW
*VIEWPOINT
-5.,5.,-5.,0.,1.,0.
*DRAW,HIDE
*VIEWPOINT
-15.,10.,15.,0.,1.,0.
*DRAW,HIDE
*VIEWPOINT
***** END OF MODEL PLOTTING
***** BEAM PRESTRESSING
*INITIAL CONDITIONS,TYPE=STRESS(REBAR)
RFB1,PHANY,153397
RFT1,PEMAN,167228
RFT,PEMAN,154597
*STEP
*STATIC,PTOL=500
*PRESTRESS HOLD
RFB1,PHANY
RFT1,PEMAN
RFT,PEMAN
*EL PRINT,POSITION=CENTROIDAL
S11,S22,S12,E11,E22,E12
CONF
CRACK
*EL PRINT,REBAR
S11,E11,IE11
*NODE PRINT
U1,U2

```

```

CF
RF
*NODE FILE
U
*END STEP
***** END OF BEAM PRESTRESSING
***** NON-LINEAR STATIC LOADING
*STEP,INC=40,CYC=20,SUBMAX
*STATIC,PTOL=1600.,RIKS
.05,2.,1.E-4,,1.6
*CLOAD
1020,2,-10000.
*EL PRINT,POSITION=CENTROIDAL,FREQ=2
S,E
SF
CONF
CRACK
*EL PRINT,REBAR,FREQ=10
S11,E11,IE11
*EL FILE,POSITION=CENTROIDAL,FREQ=2
S
SF
*NODE PRINT,FREQ=2
CF
RF
U1,U2
*NODE FILE,FREQ=2
U
*END STEP
***** END OF NON-LINEAR STATIC LOADING

```


A.1.2 Dynamic Analysis

```
*HEADING
*****
** BEAM MDB1 - SHEAR OPENING - SINUSOIDAL LOAD - F=500 SIN(62.83 t)
*****
**DATA CHECK
*PREPRINT,MODEL=NO,HISTORY=NO
***** COORDINATES OF NODES
*NODE
1,0.,0.0
2,0.,0.5
3,0.,1.0
4,0.,1.5
5,0.,2.0
6,0.,2.5
7,0.,3.0
8,0.,3.5
9,0.,4.0
10,0.,4.5
11,0.,5.0
12,0.,5.5
13,0.,6.0
14,0.,6.5
15,0.,7.0
16,0.,7.5
17,0.,8.0
2961,185.,0.0
2962,185.,0.5
2963,185.,1.0
2964,185.,1.5
2965,185.,2.0
2966,185.,2.5
2967,185.,3.0
2968,185.,3.5
2969,185.,4.0
2970,185.,4.5
2971,185.,5.0
2972,185.,5.5
2973,185.,6.0
2974,185.,6.5
2975,185.,7.0
2976,185.,7.5
2977,185.,8.0
***** END COORDINATES OF NODES
***** NODES GENERATION
*NSET,NSET=A,GENERATE
1,17
*NSET,NSET=B,GENERATE
2961,2977
*NFILL,NSET=AB
```

```

A,B,148,20
*NSET,NSET=MID,GENERATE
9,2969,40
*NSET,NSET=CENTRAL,GENERATE
1461,1477
1481,1497
1501,1517
*NSET,NSET=NFILE
MID,CENTRAL
*NSET,NSET=NHALF1,GENERATE
61,77,2
81,97,2
181,197,2
201,217,2
241,257,2
281,297,2
321,337,2
361,377,2
401,417,2
441,457,2
481,497,2
521,537,2
561,577,2
601,617,2
641,657,2
681,697,2
701,717,2
1461,1477,2
1481,1497,2
1501,1517,2
*NSET,NSET=NHALF
NHALF1,MID
***** END OF NODES GENERATION
***** ELEMENTS DEFINITION
*ELEMENT,TYPE=CPS4
1,1,21,22,2
201,201,221,222,202
213,213,233,234,214
681,681,701,702,682
1481,1481,1501,1502,1482
***** END OF ELEMENTS DEFINITION
***** ELEMENTS GENERATION
*ELGEN,ELSET=EAB
1,10,20,20,16,1,1
*ELGEN,ELSET=EBCB
201,24,20,20,4,1,1
*ELGEN,ELSET=EBCT
213,24,20,20,4,1,1
*ELGEN,ELSET=ECD
681,40,20,20,16,1,1
*ELGEN,ELSET=EDE
1481,74,20,20,16,1,1

```

```

*ELSET,ELSET=IMP,GENERATE
681,696
701,716
721,736
741,756
1401,1416
1421,1436
1441,1456
1461,1476
1481,1496
*ELSET,ELSET=HALF
EAB,EBCB,EBCT,IMP
*ELSET,ELSET=BEAM
EAB,EBCB,EBCT,ECD,EDE
*ELSET,ELSET=EP,GENERATE
61,76
81,96
1461,1476
1481,1496
*ELSET,ELSET=EFILE
EP
***** END OF ELEMENTS GENERATION
***** REINFORCED ELEMENTS DEFENITION
*ELSET,ELSET=RFB,GENERATE
2,2942,20
*ELSET,ELSET=RFT,GENERATE
15,2955,20
***** END OF REINFORCED ELEMENTS DEFENITION
***** SECTION DEFENITION
*SOLID SECTION,ELSET=BEAM,MATERIAL=A1
3.
***** END OF SECTION DEFENITION
***** CONCRETE DEFENITION
*MATERIAL,NAME=A1
*DENSITY
2.2465E-4
*ELASTIC
4.729626E6,0.2
***** END OF CONCRETE DEFENITION
***** PRESTRESSING REINFORCEMENT
*REBAR,ELEMENT=CONTINUUM,MATERIAL=PST,GEOMETRY=ISOPARAMETRIC,NAME=HANY
RFB,.03988566,1.,0.,1.,1
*REBAR,ELEMENT=CONTINUUM,MATERIAL=PST,GEOMETRY=ISOPARAMETRIC,NAME=EMAN
RFT,.03988566,1.,0.,0.,1
***** END OF PRESTRESSING REINFORCEMENT
***** PRESTRESSING STEEL DEFINITION
*MATERIAL,NAME=PST
*ELASTIC
29.E6
*PLASTIC
210.E3
***** END OF PRESTRESSING STEEL DEFINITION

```

```

***** BOUNDARY DEFINITION
*BOUNDARY
49,2
2929,1,2
***** END OF BOUNDARY DEFINITION
***** PERIODIC LOAD DEFINITION
*AMPLITUDE,VALUE=R,TIME=D,NAME=SIN,DEFINITION=PERIODIC
1,62.83,0.,0.
0.,1.
***** END OF PERIODIC LOAD DEFINITION
***** MODEL PLOTTING
*PLOT
BEAM MDB1
10,10,7,7,3,2,3,1
.16,,,,,.05
*DRAW
***** END OF MODEL PLOTTING
***** BEAM PRESTRESSING
*INITIAL CONDITIONS,TYPE=STRESS(REBAR)
RFB,HANY,62679.16788
RFT,EMAN,62679.16788
*STEP,NLGEOM
*STATIC,PTOL=50
*PRESTRESS HOLD
RFB,HANY
RFT,EMAN
*EL PRINT,POSITION=CENTROIDAL,ELSET=HALF
S
*NODE PRINT,NSET=NHALF
U
CF,RF
*EL PRINT,REBAR
S,E
*ENERGY PRINT
*END STEP
***** END OF BEAM PRESTRESSING
***** NATURAL FREQUENCY EXTRACTION
*STEP
*FREQUENCY
6
*EL PRINT,MODE=10
S11,E11
*NODE PRINT,MODE=!0
U1,U2
**U
*END STEP
***** END OF NATURAL FREQUENCY EXTRACTION
***** MODAL DYNAMIC ANALYSIS
*STEP
MODAL DYNAMIC
*MODAL DYNAMIC
.01,4.

```

```
*MODAL DAMPING,MODAL=DIRECT
1,6,.02
*CLOAD,AMPLITUDE=SIN
1497,2,-500
*ENERGY PRINT,FREQ=2
*ENERGY FILE,FREQ=2
*EL PRINT,FREQ=3,POSITION=CENTROIDAL,ELSET=HALF
S
*EL FILE,POSITION=CENTROIDAL,ELSET=HALF,FREQ=2
S
*NODE PRINT,NSET=NHALF,FREQ=3
U,A
*NODE PRINT,FREQ=3
CF,RF
*NODE FILE,FREQ=2,NSET=NHALF
U
*NODE FILE,FREQ=2,NSET=NHALF
CF,RF
*END STEP
***** END OF MODAL DYNAMIC ANALYSIS
```

APPENDIX A.2

CONCRETE MIX DESIGN

A.2.1 General

The following design is based on the guide lines presented in the ACI manual of concrete practice (ACI, 1989).

A.2.2 Properties of the Materials

Water: tap water

Cement: high early strength (type III)

Coarse aggregate: dry rodded mass = 1600 kg/m³ (99.9 lb/ft³)

moisture content = 2%

maximum size = 3/8 in (9.5 mm)

Fine Aggregate: moisture content = 4%

fineness modulus (FM) = 2.56

A.2.3 Desired Characteristics:

Compressive strength $f'_c = 6000$ psi (41.3 MPa)

Slump = 3 inch (80 mm)

Air Content = 0%

A.2.4 Design Steps

Step (1) - Choice of Slump Value:

For beams, max. slump = 4 in. (102 mm), min. slump = 1 in. (25 mm)

Slump value = 3 in. (76 mm)

Step (2) - Max. Size of Aggregate:

* Max. size $\leq b/5 \leq 4/5 \leq 0.8$ in. (20 mm)

* Max. size $\leq 3/4$ spacing between bars

$\leq 3/4 (1 - 0.276) \leq 0.5$ in. (13 mm)

Take max. size = 3/8 in. (10 mm), to produce highest strength at a given water cement ratio.

Step (3) - Estimation of Mixing Water Content:

According to table 5.3.3, for slump = 3 - 4 in., nominal max. size of aggregate = 3/8 in;

$$W = 385 \text{ lb/yd}^3 = 228 \text{ kg/m}^3$$

Step (4) - Selection of Water-Cement Ratio:

According to table 5.3.4(a), W/C = 0.4

Step (5) - Calculation of Cement Content:

$$\text{Cement} = 228/0.4 = 570 \text{ kg/m}^3 (962.5 \text{ lb/yd}^3)$$

Step (6) - Estimation of Coarse Aggregate Content:

From table 5.3.6, for fineness modulus of 2.56 and max. size of 3/8 in. (10 mm), the coarse aggregate content = 0.484. As the rodded-weight of coarse aggregate = 1600 kg/m³ (2700 lb/yd³), the dry weight of coarse aggregate = 0.484 x 1600 = 775 kg/m³ (1308 lb/yd³).

Step (7) - Estimation of Fine Aggregate Content

From table 5.37.1, the estimated weight of fresh concrete = 3840 lb/yd³ (2278 kg/m³, hence:

$$\text{fine aggregate} = 2278 - (228 + 570 + 775) = 705 \text{ kg/m}^3$$

Step (8) - Adjustments for Aggregate Moisture:

The adjusted aggregate weights:

$$\text{Coarse aggregate (wet)} = 775 \times 1.02 = 791 \text{ kg/m}^3 (49.4 \text{ lb/ft}^3)$$

$$\text{Fine aggregate (wet)} = 705 \times 1.04 = 733 \text{ kg/m}^3 (45.8 \text{ lb/ft}^3)$$

Step (9) - Re-estimation of the Required Mixing Water:

Absorbed water does not become part of the mixing water, and must be excluded from the adjustment in added water. Thus, surface water contributed by the coarse aggregate amounts to $2 - 0.5 = 1.5$ percent; by the fine aggregate $4 - 0.7 = 3.3$ percent. The estimated requirement for added water, therefore, becomes: $228 - 775 \times 0.015 - 705 \times 0.033 = 193 \text{ kg/m}^3 (12.1 \text{ lb/ft}^3)$

Step (10) - The Final Estimated Batch:

$$\text{a) Water} = 193 \text{ kg/m}^3 (12.1 \text{ lb/ft}^3)$$

$$\text{b) Cement} = 570 \text{ kg/m}^3 (35.6 \text{ lb/ft}^3)$$

$$\text{c) Coarse aggregate} = 791 \text{ kg/m}^3 (49.4 \text{ lb/ft}^3)$$

$$\text{d) Fine aggregate} = 733 \text{ kg/m}^3 (45.8 \text{ lb/ft}^3)$$

Step (11) - Calculation of the Total Concrete Volume:

The total volume of concrete needed for a rectangular beam and three 6 in. (152 mm) by 12 in. (305 mm) test cylinders:

$$\text{Volume of the beam} = 4 \times 10 \times 120 / (12)^3 = 2.78 \text{ ft}^3 (0.08 \text{ m}^3)$$

$$\text{Volume of the cylinders} = 3 \times \Pi (6)^2 \times 12 / [4 \times (12)^3] = 0.59 \text{ ft}^3 (0.017 \text{ m}^3)$$

$$\text{Total volume} = 0.59 + 2.78 = 3.37 \text{ ft}^3 \approx 0.1 \text{ m}^3$$

Step (12) - Estimated Final Batch for the Needed Volume:

a) Water = $0.1 \times 193 \text{ kg} = 19.3 \text{ kg} (42.5 \text{ lb})$

b) Cement = $0.1 \times 570 \text{ kg} = 57 \text{ kg} (125.7 \text{ lb})$

c) Coarse aggregate = $0.1 \times 791 \text{ kg} = 79.1 \text{ kg} (174.4 \text{ lb})$

d) Small aggregate = $0.1 \times (0.4 \times 733) = 29.3 \text{ kg} (64.6 \text{ lb})$

e) Sand = $0.1 \times (0.6 \times 733) = 44 \text{ kg} (97 \text{ lb})$

Summary of Final Ratios:

Water / cement ratio = 0.35

Aggregate / cement ratio = 2.7

Fine aggregate / coarse aggregate ratio = 0.9

APPENDIX A.3

CALIBRATION OF LOAD CELLS AND STRAIN GAUGE ARRANGEMENT

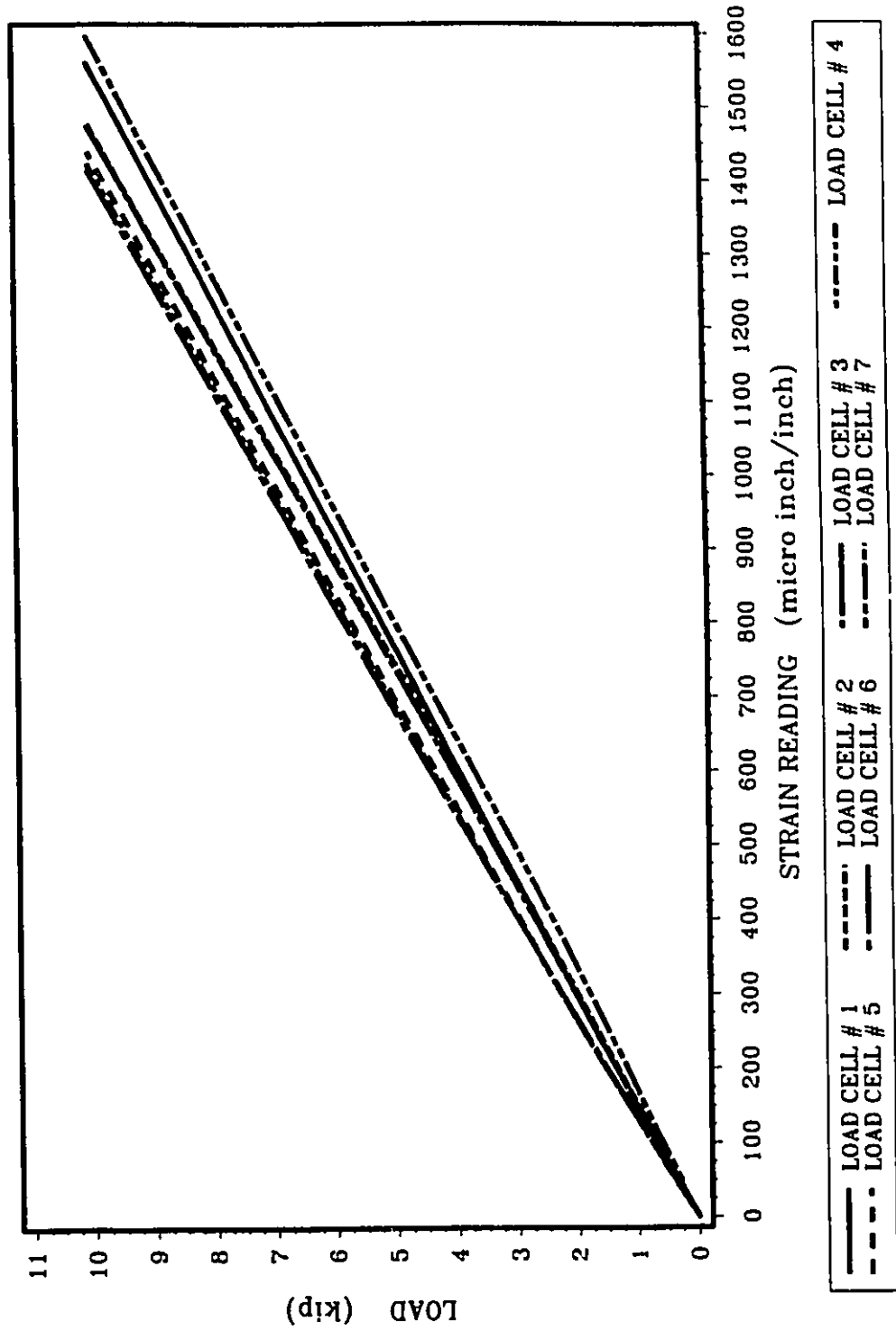


FIG. A.3.1 CALIBRATION OF PRESTRESSING LOAD CELLS

Note: 1 in.=25.4 mm, 1 kip= 4.45 kN

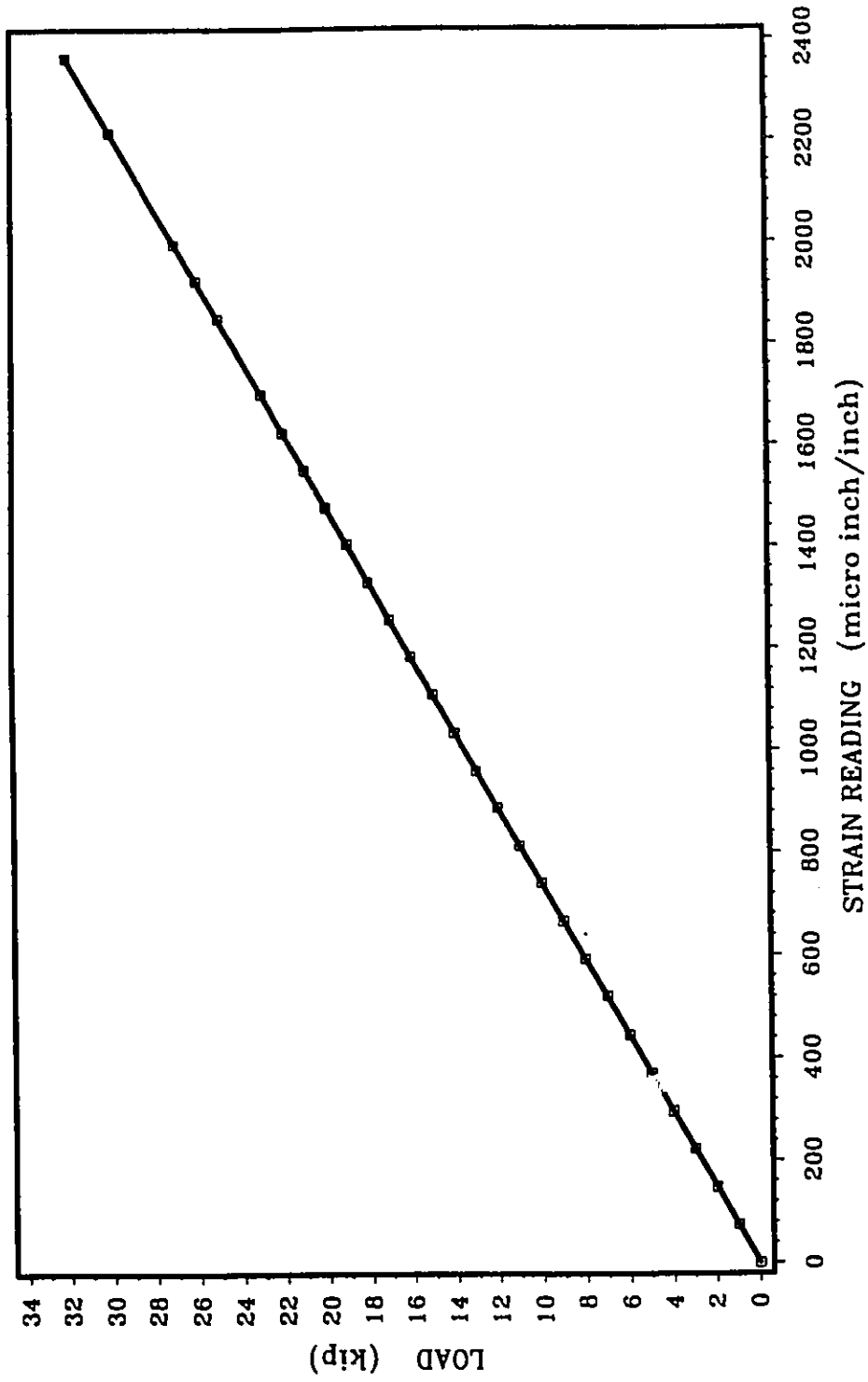


FIG. A.3.2 CALIBRATION OF VERTICAL LOAD CELL

Note: 1 in.=25.4 mm, 1 kip= 4.45 kN

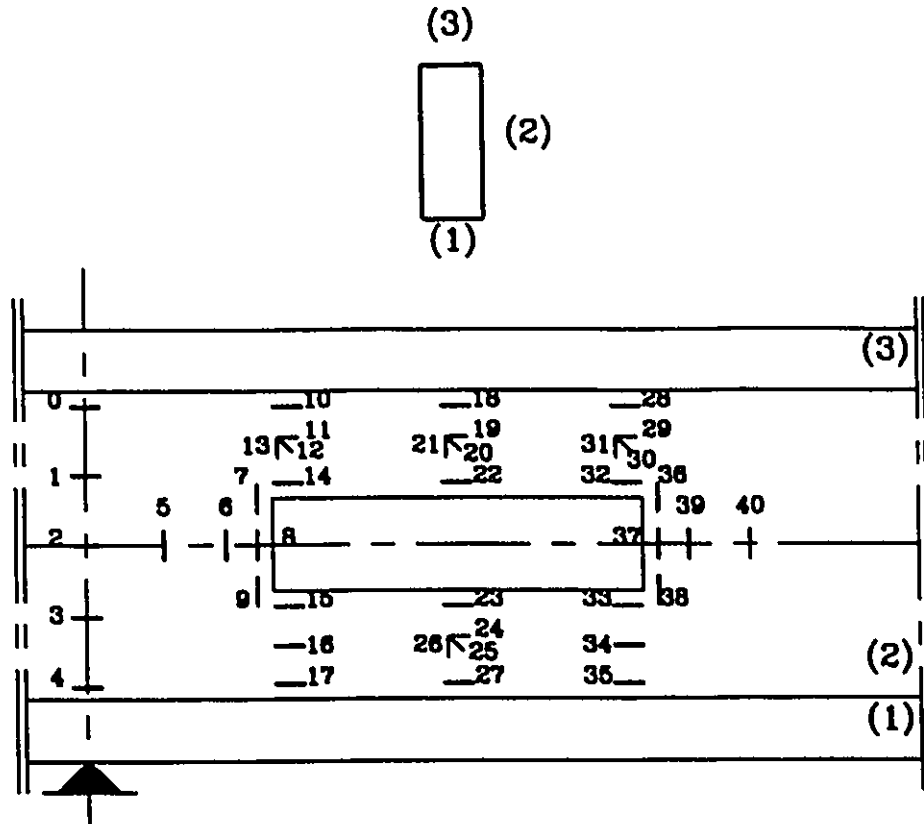


FIG. A.3.3.a STRAIN GAUGE ARRANGEMENT FOR BI1A

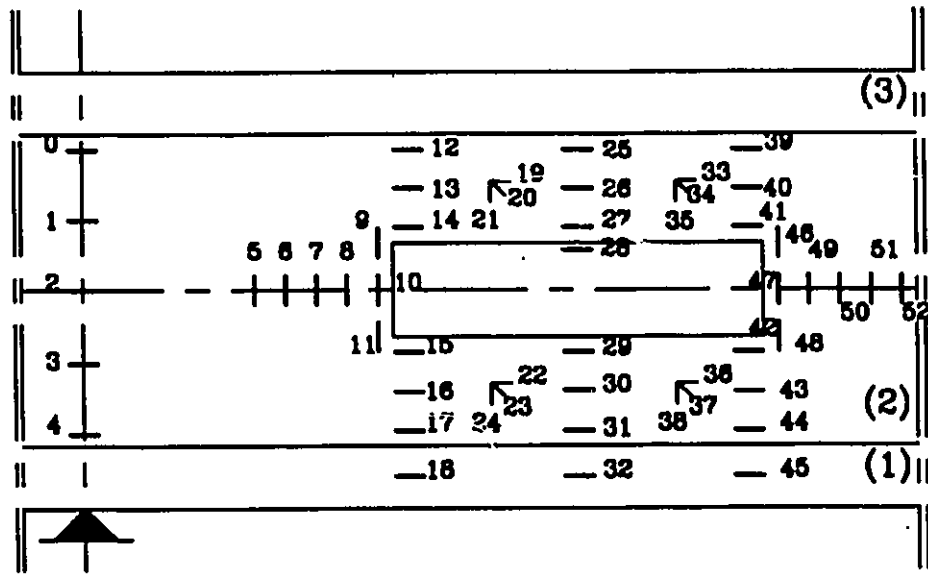


FIG. A.3.3.b STRAIN GAUGE ARRANGEMENT FOR BI1B

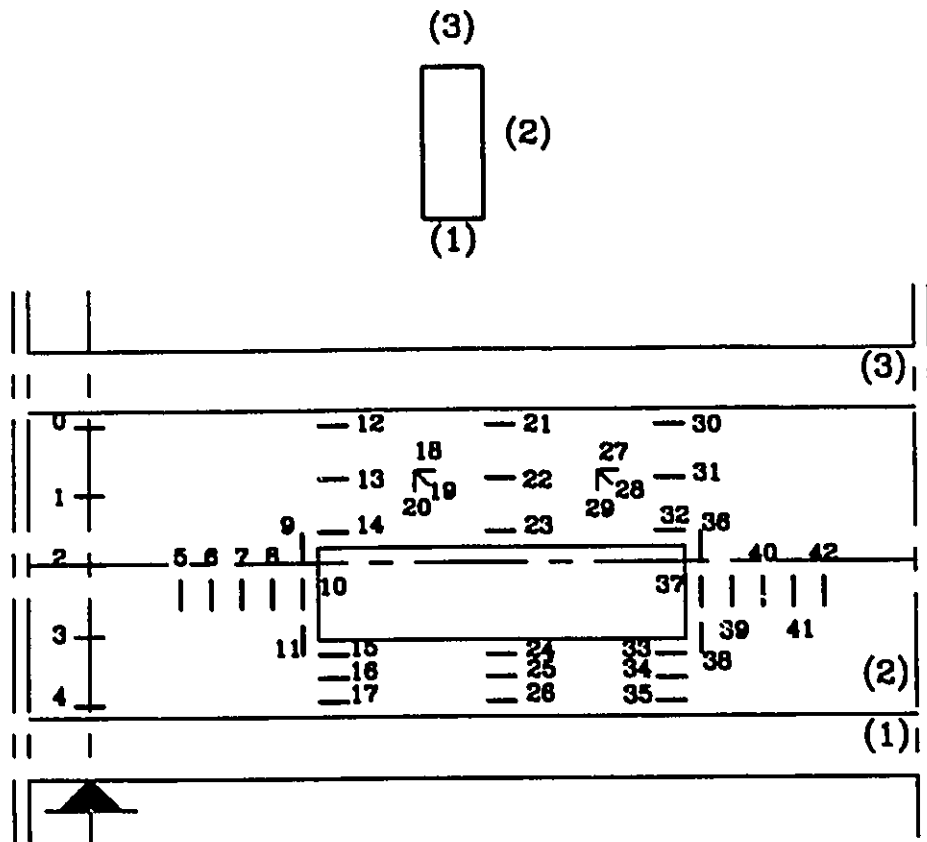


FIG. A.3.3.c STRAIN GAUGE ARRANGEMENT FOR BI2A

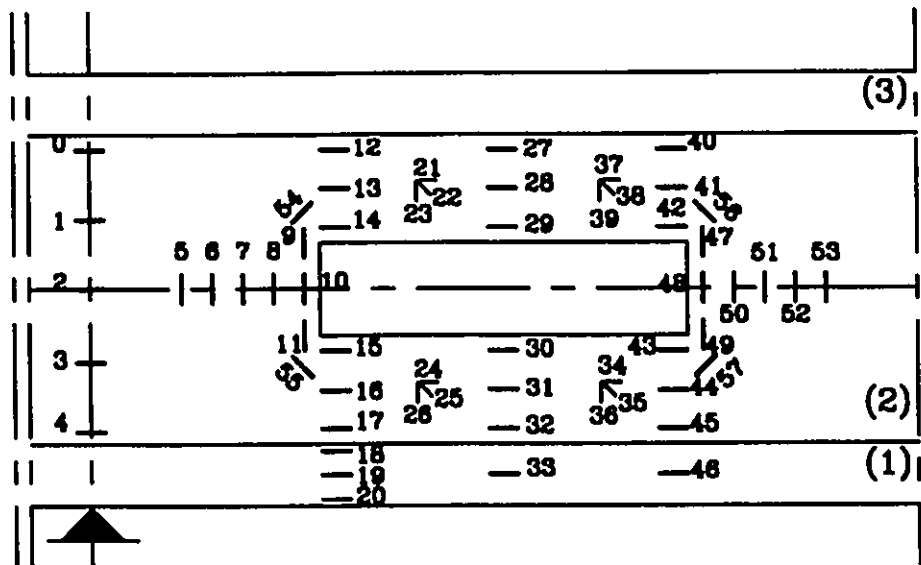


FIG. A.3.3.d STRAIN GAUGE ARRANGEMENT FOR BI2B

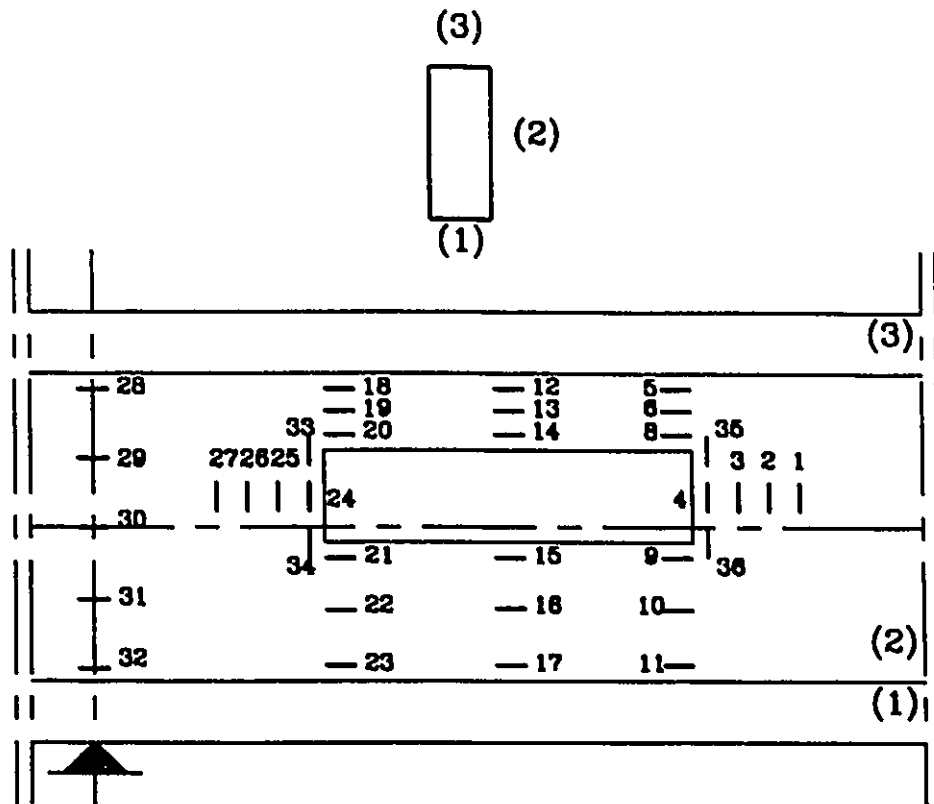


FIG. A.3.3.e STRAIN GAUGE ARRANGEMENT FOR BI2C

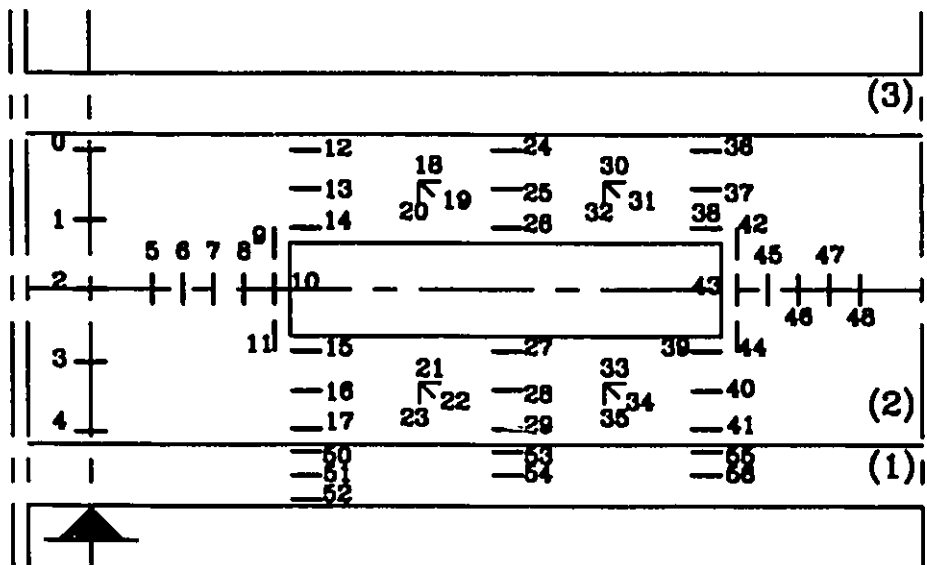


FIG. A.3.3.f STRAIN GAUGE ARRANGEMENT FOR BI3C

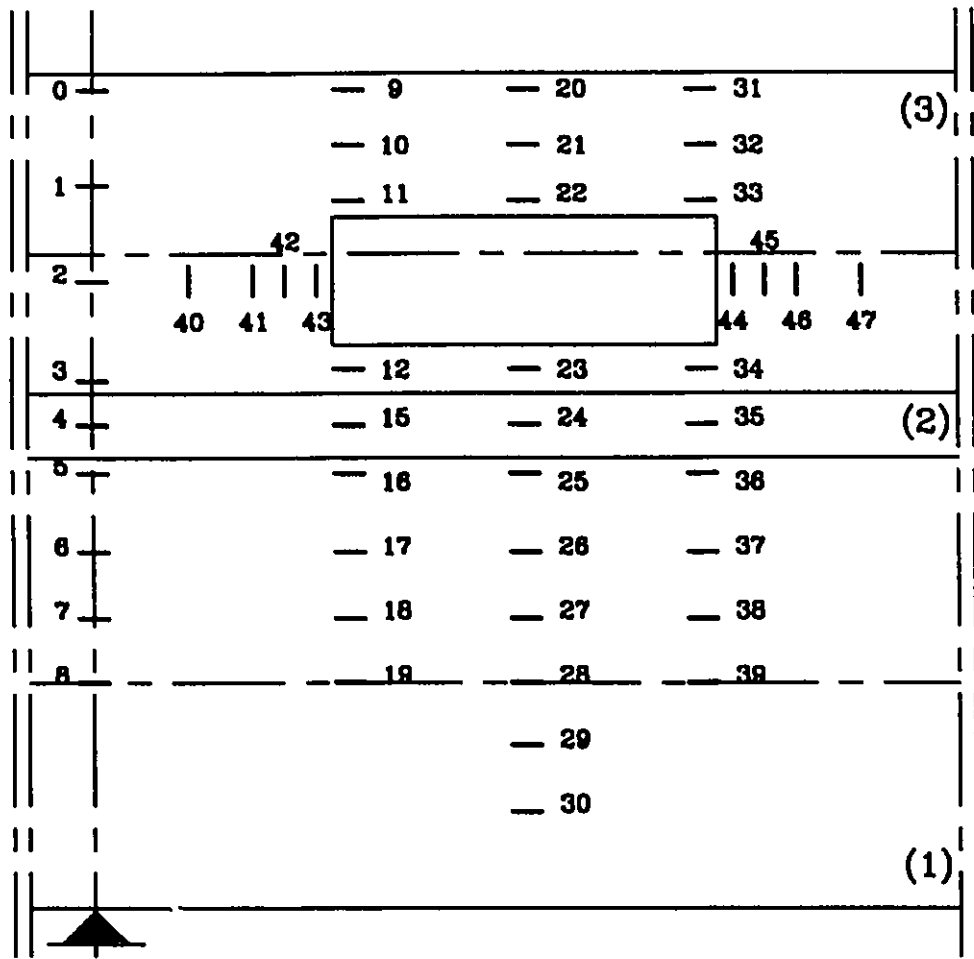
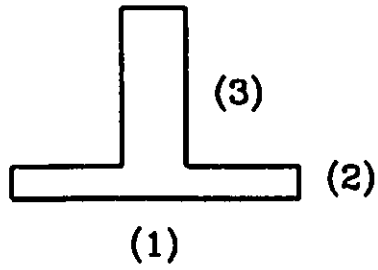


FIG. A.3.3.g STRAIN GAUGE ARRANGEMENT FOR BII1A

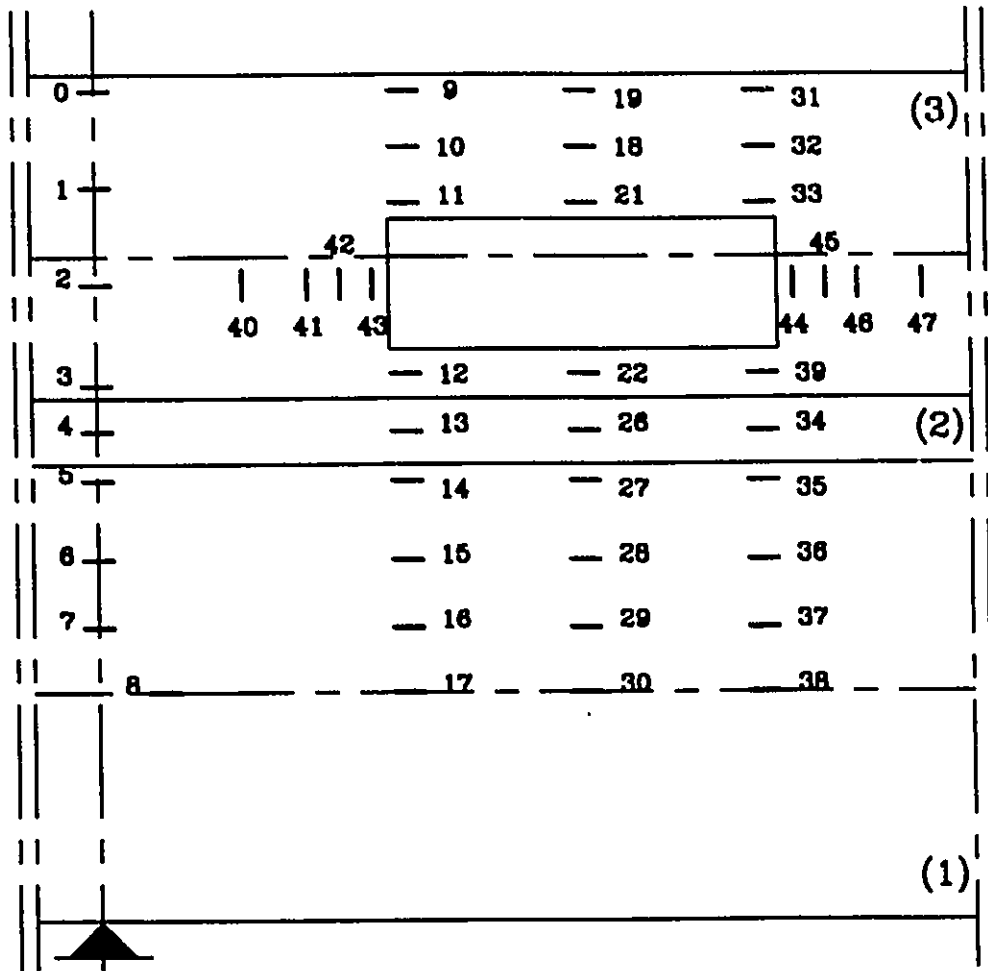
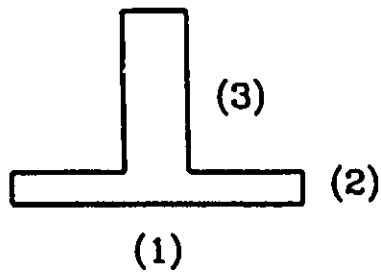


FIG. A.3.3.h STRAIN GAUGE ARRANGEMENT FOR BH1B

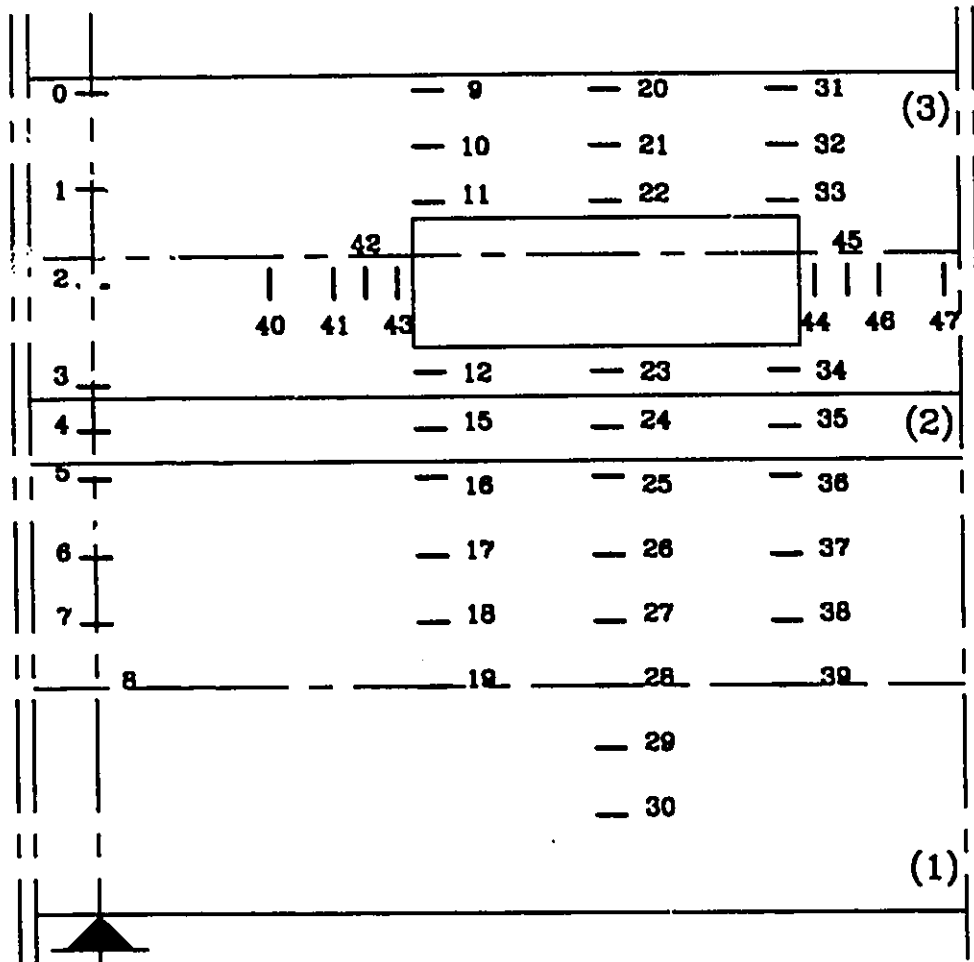
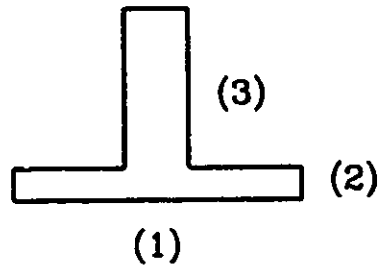


FIG. A.3.3.i STRAIN GAUGE ARRANGEMENT FOR BII1C

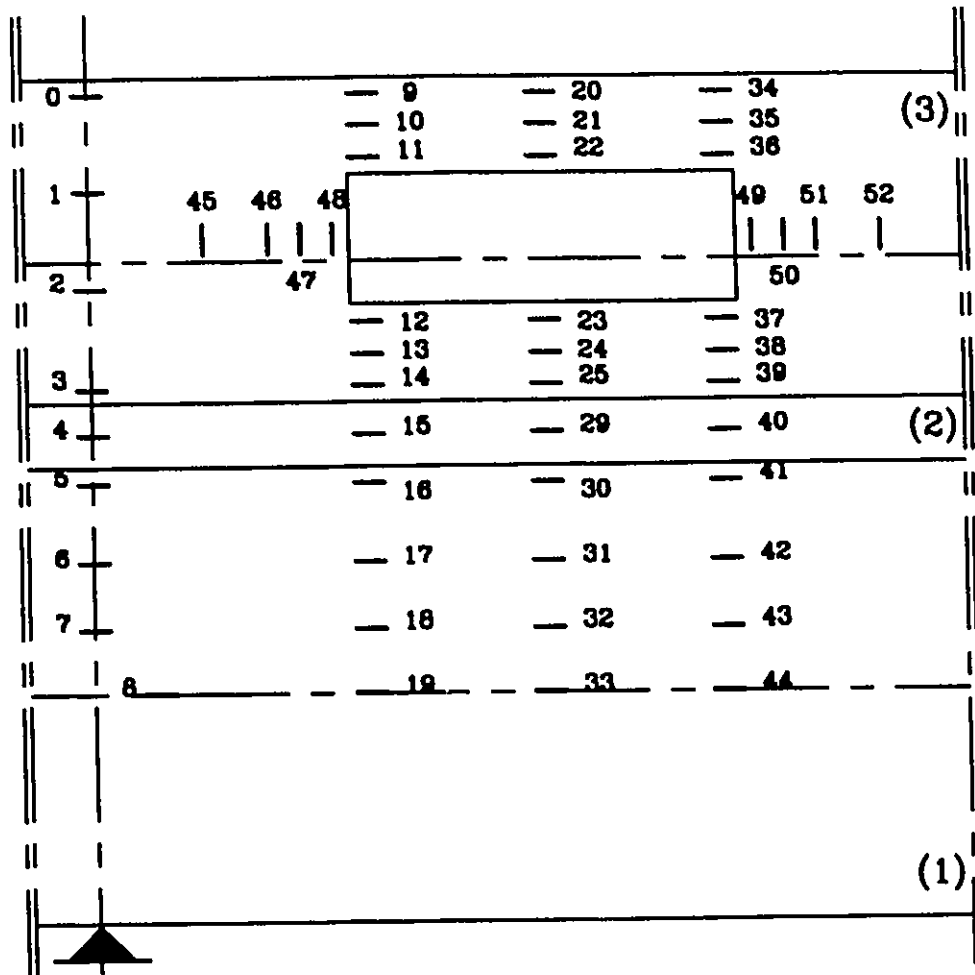
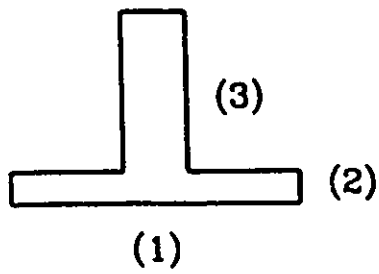


FIG. A.3.3.j STRAIN GAUGE ARRANGEMENT FOR BII2B

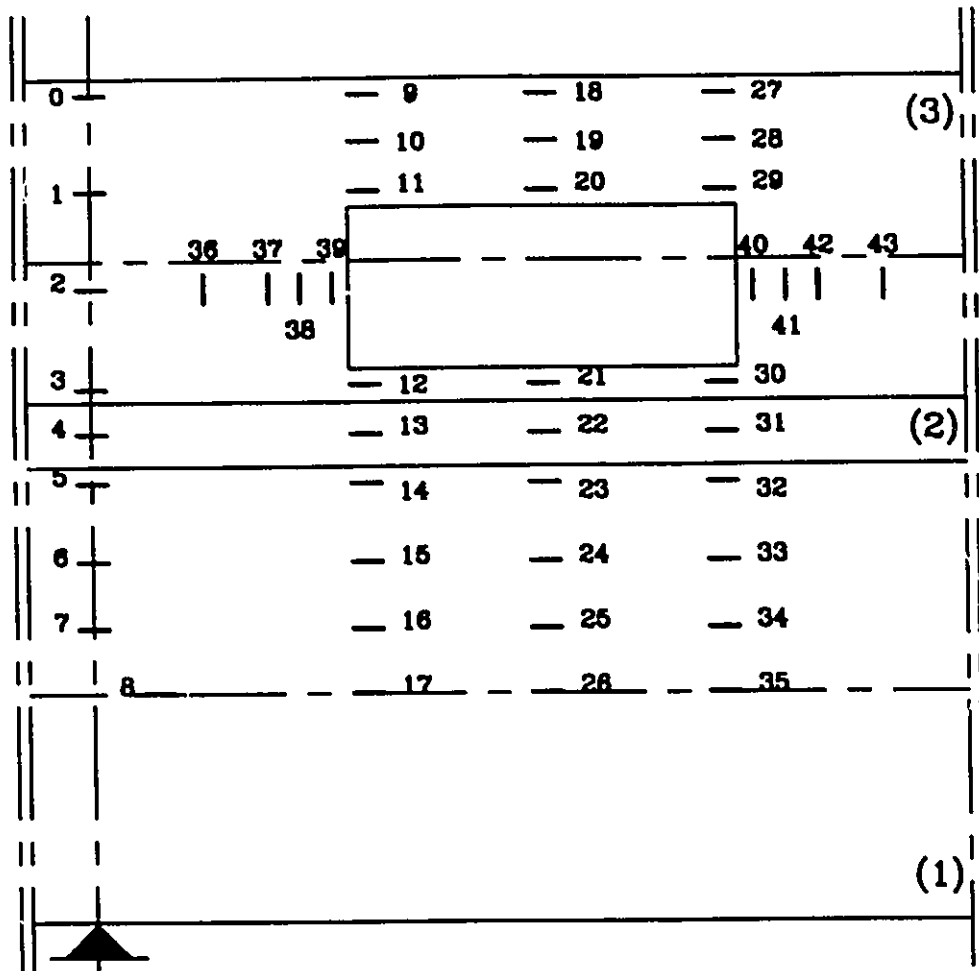
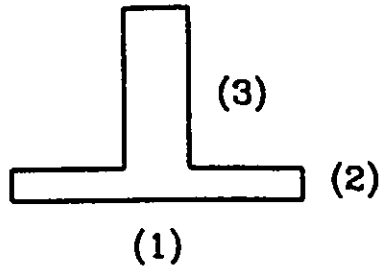


FIG. A.3.3.k STRAIN GAUGE ARRANGEMENT FOR BII4C

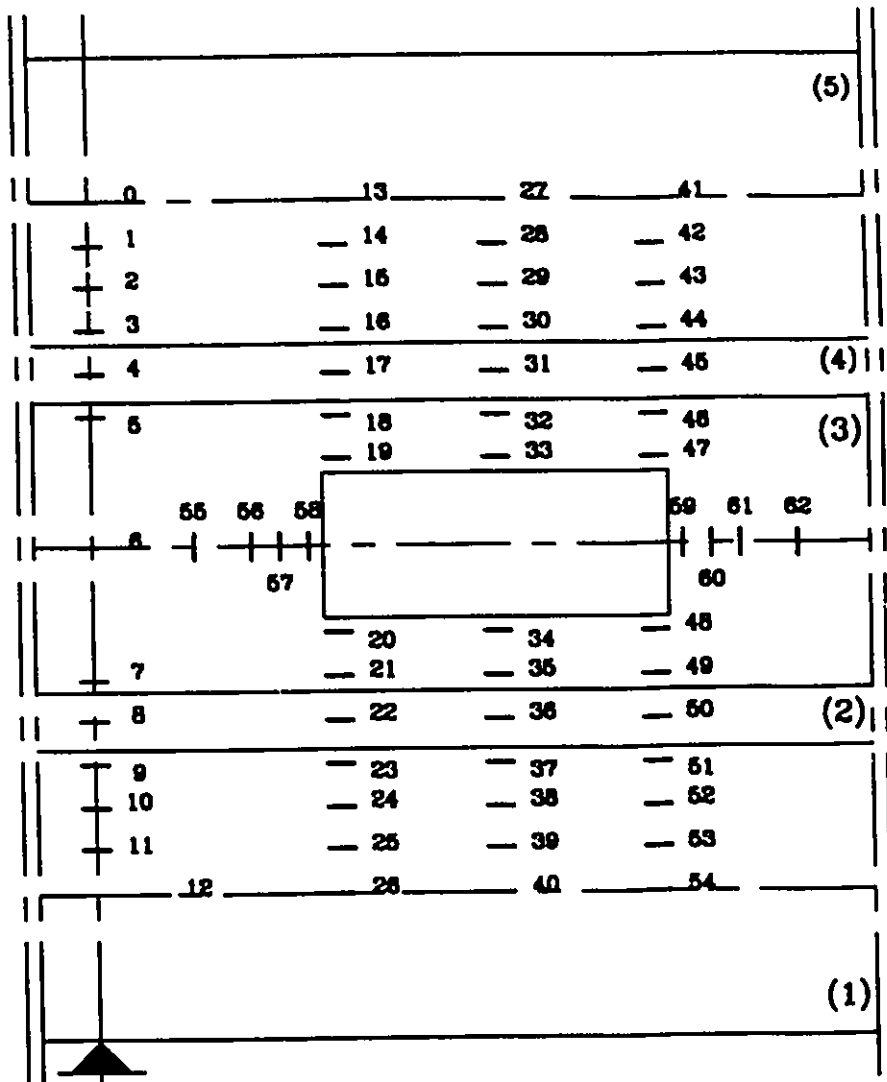
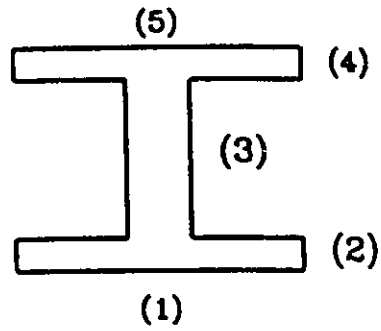


FIG. A.3.3.1 STRAIN GAUGE ARRANGEMENT FOR BIII1A

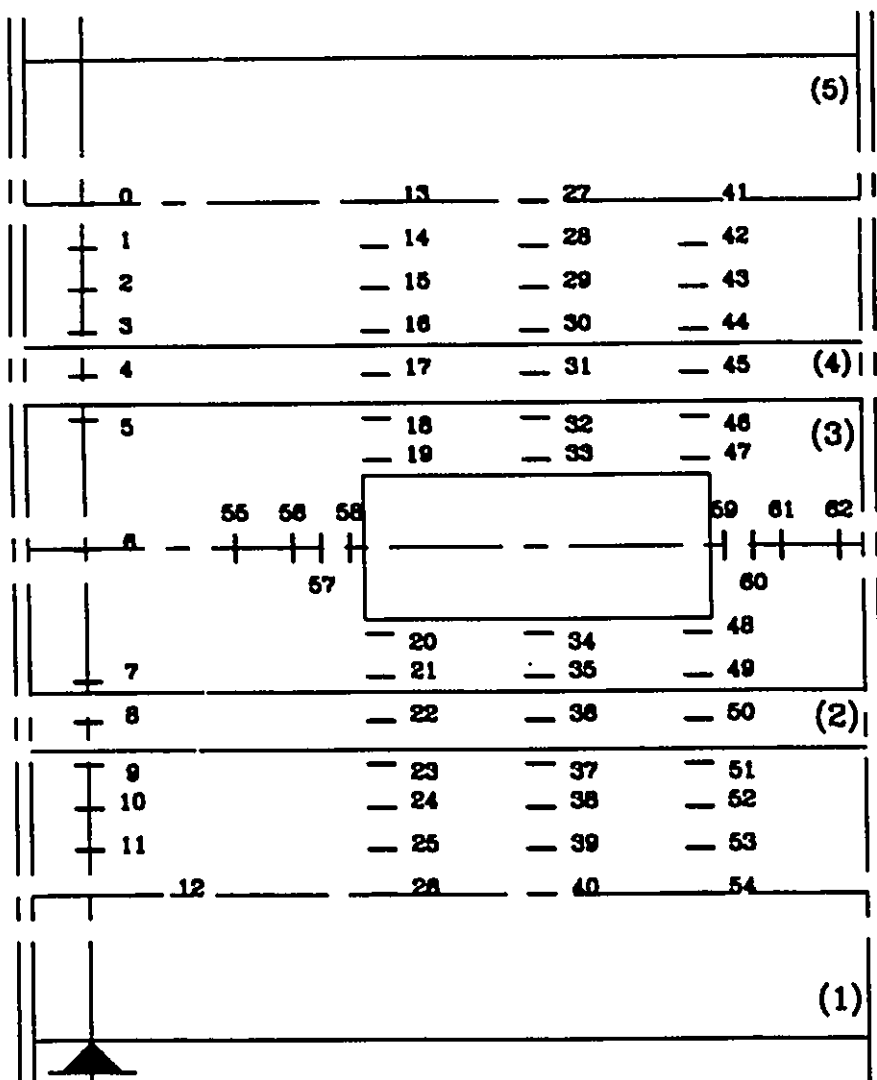
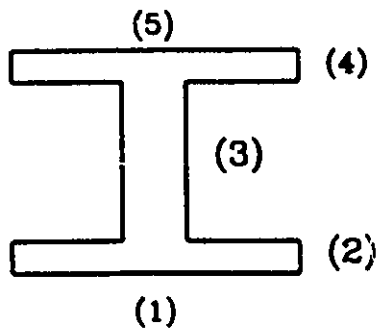


FIG. A.3.3.m STRAIN GAUGE ARRANGEMENT FOR BIII1C

REFERENCES

- 1- Abdalla, H.A., and Kennedy J.B., "*Analysis of Prestressed Girders with Openings*", accepted for publication in Computer & Structures Journal.
- 2- Abdus Salam, S., and Harop, J., "*Prestressed Concrete Beams with Transverse Circular Holes*", Journal of the Structural Division, ASCE, Vol. 105, No. ST3, pp. 635-652, 1979.
- 3- ACI Committee 318, "*Building Code Requirements for Reinforced Concrete (ACI 318-89) and Commentary- ACI 318 R-89*", American Concrete Institute, Detroit, 1989, 360 pp.
- 4- Aglan and Redwood, R.G., "*Elastic and Inelastic Instability of Webs between Holes*", McGill University Structural Mechanics Series, No. 73-5, Montreal, P.Q., 1973.
- 5- Alves, T.M.J., and Scanlon, A., "*Deflection of Prestressed Concrete Beams with Openings*", Symposium of Deflections of Structures, March 1984, Annual Convention of the American Concrete Institute, Phoenix, Ariz.
- 6- American Concrete Institute, "*ACI Manual of Concrete Practice, 1989*", Detroit, Michigan, 48219.
- 7- Balaguru, P.N., "*Analysis of Prestressed Concrete Beams for Fatigue Loading*", PCI Journal, May-June, 1981, pp. 70-94.
- 8- Barney, G.B., Corley, W.G., Hanson, J.M., and Parmelee, R.A., "*Behaviour and*

- Design of Prestressed Concrete Beams with Large Web Openings*", Journal of PCI, November-December 1977, pp. 32-61.
- 9- Biggs, John M., "*Introduction to Structural Dynamics*", McGraw-Hill, Inc., 1964.
- 10- Blevins, Robert D., "*Formulas for Natural Frequency and Mode Shape*". Van Nostrand and Reinhold Company, New York, NY 10020, 1979.
- 11- Bower, J.E., "*Elastic Stresses around Holes in Wide Flange Beams*", Journal of the Structural Division, ASCE, Vol. 92, No. ST3, April 1966.
- 12- Bower, J.E., et al., "*Suggested Guidelines for Beams with Web Holes*", Journal of the Structural Division, ASCE, Vol. 97, No. ST11, 1971, pp. 2707-2728.
- 13- Branson, D.E., and Trost, H., "*Unified Procedures for Predicting the Deflection and centroidal Axis Location of Partially Cracked Nonprestressed and Prestressed Concrete Members*", ACI Journal, March-April, 1982, pp. 119-130.
- 14- Bresler, B., and Pister, K.S., "*Strength of Concrete Under Combined Stresses*", ACI Journal, Vol. 30, No.3, Sept. 1958, pp. 321-345.
- 15- Buckland, P.G., and Barlett, F.M., "*Practical Design of Holes in Steel Webs*", Canadian Journal of Civil Engineering, Vol. 15, March. 1988, pp. 456-469.
- 16- Burton, K.T., "*Influence of Embedded Service Ducts on the Strength of Continuous Reinforced Tee-Beams*", ACI Journal, Vol. 62, No. 10, Oct. 1965.
- 17- Chami, S., "*Dynamic Characteristics of Post-tensioned Prestressed Concrete Beams with Openings*", M.A.Sc. thesis, University of Windsor, 1987.
- 18- Collins, M.P., and Mitchell, D., "*Prestressed Concrete Structures*", Prentice-Hall, Inc., Englewood Cliffs, New Jersey 07632, 1991.

- 19- Coles, B.C., and Hamilton, W.A., "*Repetitive Dynamic Loading on Pretensioned Prestressed Beams*", ACI Journal, Sept. 1969, pp. 745-747.
- 20- Congdon, J.E., and Redwood, R.G., "*Plastic Behaviour of Beams with Reinforced Holes*", Journal of the Structural Division, ASCE, Vol. 96, NO. ST9, Sept. 1970.
- 21- Cook, W.D., and Mitchell, D., "*Studies of Disturbed Regions near Discontinuities in Reinforced Concrete Members*", ACI Structural Journal, March-April 1988.
- 22- Darwin, D., and Donahey, R.C., "*LRFD for Composite Beams with Unreinforced Web Openings*", Journal of the Structural Division, ASCE, Vol. 114, No. 3, March 1988, pp. 535-552.
- 23- Dinakaran, V., and Sastry, M.K., "*Behaviour of Post-tensioned Prestressed Concrete T-Beams with Large Web Openings*". Indian Concrete Journal, Vol. 58, No. 2, 1984, pp. 34-38,55.
- 24- Donahey, R.C., and Darwin, D., "*Web Openings in Composite Beams with ribbed Slabs*", Journal of the Structural Division, ASCE, Vol. 114, No. 3, March 1988, pp. 518-534.
- 25- Douglas, T.R., and Gambrell, S.C., "*Design of Beams with Off-Center Web Openings*", Journal of the Structural Division, ASCE, Vol. 100, No. ST6, June 1974, pp. 1189-1203.
- 26- El-Laithy, A., "*Influence of Openings on the Behaviour of Rectangular Post-tensioned Prestressed Concrete Beams*", M.A.Sc. thesis, University of Windsor, 1978.
- 27- Fahmy, E.H., "*Strength of Composite Beams with Web Openings*", the Canadian Society for Civil Engineering, 1988 Annual Conference, May 1988, pp. 552-565.

- 28- Ferties, D.G., "*Dynamics and Vibration of Structures*", R.E. Krieger Publishing Company, Malabr, Florida, 1984.
- 29- Gorman, D.J., "*Free Lateral Vibration Analysis of Double-Span Uniform Beams*", Int. J. Mech. Sci., Vol. 16, 1974, pp. 345-351.
- 30- Hanson, J.M., "*Square Openings in Webs of Continuous Joists*", Research and Development Bulletin No. RD001.01D, Portland Cement Association, Skokie, IL., 1969.
- 31- Hanson, J.M., and MacGregor, J.G., "*Proposed Changes in Shear Provisions for Reinforced and Prestressed Concrete Beams*", ACI Journal, April 1969, pp. 276-288.
- 32- Hanson J.M., Hulsbos, C.L., and VanHorn, D.A., "*Fatigue Tests of Prestressed Concrete I-Beams*", Journal of the Structural Division, ASCE, Vol. 96, No. ST11, Nov. 1970, pp. 2443-2464.
- 33- Hibbitt, H.D., Karlsson, B.I., and Sorensen, E.P., "*ABAQUS Version 4-8, Finite Element Program*", Hibbitt, Karlsson, and Sorensen Inc., Providence, Rhode Island 02906-4402 (1989).
- 34- Hobbs, D.W., Pomeroy, C.d., and Newman, J.B., "*Design Stresses for Concrete Structures Subject to Multi-axial Stresses*", The Structural Engineer, Vol. 55, No. 4, April, 1977, pp. 151-164.
- 35- Humar, J.L., "*Dynamics of Structures*", Prentice-Hall Inc., 1990.
- 36- Inomate, Shunji, "*Comparative Study on Behaviour of Prestressed and Reinforced Concrete Beams Subject to Loading Reversals*", PCI Journal, Jan.-Feb. 1971, pp. 21-37.
- 37- Ito, M., Fujiwara, K., and Okazaki, K., "*Ultimate Strength of Beams with U-Shaped Holes in Top of Web*", Journal of Structural Engineering, ASCE, Vol. 117, No. 7, July

1991, pp. 1929-1945.

38- Johns, K.C., and Belanger, M.D., "*Dynamic Stiffness of Concrete Beams*", ACI Journal, May-June 1981, pp. 201-205.

39- Kennedy, J.B., and Abdalla, H.A., "*Static Response of Prestressed Girders with Openings*", Journal of Structural Engineering, ASCE, Vol. 118, No.2, February 1992.

40- Kennedy, J.B., Abdalla, H.A., and Grace, N.F., "*The Response of Prestressed Girders with Openings*", International Colloquium on Structural Engineering, ESE/CSCE, April 1992, Vol. 2, pp. 849-860, Cairo, Egypt.

41- Kennedy, J.B., Chami, S., and Grace, N.F., "*Dynamic and Fatigue Responses of Prestressed Concrete Girders with Openings*", Canadian Journal of Civil Engineering, Vol. 17, No. 3, 1990, pp. 460-470.

42- Kennedy, J.B., and El-Laithy, A., "*Cracking at Openings in Prestressed Beams at Transfer*", Journal of the Structural Division, ASCE, Vol. 108, No. ST6, 1982, pp. 1250-1265.

43- Knostman, H.D., Cooper, P.B., and Snell, R.R., "*Shear Force Distribution at Eccentric Web Openings*", Journal of the Structural Division, ASCE, Vol. 103, No. ST6, June 1977.

44- Kulkarni, G.G., and Ng, S.F., "*Behaviour of Limited Prestressed Beams Under Repeated Loads*", Canadian Journal of Civil Engineering, Vol. 6, 1979, pp. 544-556.

45- Lin, T.Y., "*Strength of Continuous Prestressed Concrete Beams under Static and Repeated Loads*", ACI Journal, V. 26, No. 10, June 1955, pp. 1037-1059.

46- Lin, T.Y., and Burns, N.H., "*Design of Prestressed Concrete Structures*", Third

Edition, John Wiley & Sons, Inc., 1981.

47- Lorentsen, Mogens, "*Holes in Reinforced Concrete Girders*", BYGGMÄSTAREN, Vol. 41, No. 7, July 1962, pp. 141-152, Translated from Swedish by Portland Cement Association, Chicago, Illinois, 60610.

48- Mansur, M., Tan, K., and Lee, S., "*Collapse Loads of R/C Beams with Large Openings*", Journal of the Structural Division, ASCE, Vol. 110, No. 11, Nov. 1984, pp. 2602-2618.

49- Mansur, M., Tan, K., and Lee, S., "*Design Methods for Reinforced Concrete Beams with Large Openings*", ACI Journal, Vol. 82, 1985, pp. 517-524.

50- Mansur, M.A., "*Ultimate Strength Design of Beams with Large Openings*", International Journal of Structures, Vol. 8, No. 2, December 1988, pp. 107-125.

51- Mansur, M.A., Lee, Y.F., Tan, K.H., and Lee, S.L., "*Tests on RC Continuous Beams with Openings*", Journal of Structural Engineering, ASCE, Vol. 117, No. 6, June 1991, pp. 1593-1606.

52- Mansur, M.A., Tan, K.H., Lee, Y.F., and Lee, S.L., "*Piecewise Linear Behaviour of Rc Beams with Openings*", Journal of Structural Engineering, ASCE, Vol. 117, No. 6, June 1991, pp. 1607-1621.

53- Mansur, M.A., Huang, L.M., Tan, K.H., and Lee, S.L., "*Deflections of Reinforced Concrete Beams with Web Openings*", ACI Journal, Vol. 89, 1992, pp. 391-397.

54- Marshall, P.W., and Ozell, A.M., "*Behaviour of Prestressed Concrete under Dynamic Loading*", PCI Journal, December 1960, pp. 74-84.

55- Nasr, M., Mostafa, M.T., and Torkey, A., "*Partially Prestressed Beams with*

- Openings in the Shear Span*", ESEC Proceedings, V. 2, Cairo University, Egypt, April 1985.
- 56- Nassef, M.A., Mostafa, M.T., and Kassem, M., "*Partially Prestressed Beams with Openings in the Pure Bending Zone*", ESEC Proceedings, V. 1, Cairo University, Egypt, April 1985.
- 57-Nasser, K.W., Acavalos, A., and Danile, H.R., "*Behaviour and Design of Large Openings in Reinforced Concrete Beams*", ACI Journal, Vol. 64, No. 1, Jan. 1967, pp. 25-33.
- 58- Pool, R.B., and Lopes, R., "*Cyclically Loaded Beams with Web Openings*", ACI Journal, September-October 1986, pp. 757-763.
- 59- Redwood, R.G., and McCutcheon, J.O., "*Beam Tests with Unreinforced Web Openings*", Journal of the Structural Division, ASCE, Vol. 94, No. ST1, Jan. 1968, pp. 1-17.
- 60- Redwood, R.G., and Uenoua, M., "*Critical Loads for Webs with Holes*", Journal of the Structural Division, ASCE, Vol. 105, No. ST10, 1979, pp. 2053-2067.
- 61- Redwood, R.G., and Shrivastava, S.C., "*Design Recommendations for Steel Beams with Web Holes*", Canadian Journal of Civil Engineering, Vol. 7, 1980, pp. 642-650.
- 62- Redwood, R.G., and Poubouras, "*Tests of Composite Beams with Web Holes*", Canadian Journal of Civil Engineering, Vol. 10, 1983, pp. 713-721.
- 63- Regan, H.S., and Warwaruk, J., "*Tee-Members with Large Web Openings*", PCI Journal, Vol. 12, No. 4, August 1967, pp. 52-65.
- 64- Sauve, J.S., "*Prestressed Concrete Tee-Beams with Large Web Openings*", M.Sc.

thesis, University of Alberta, Fall 1970.

65- Senger, E.P., "*Reinforcement Requirements for Girder Web Openings*", Journal of the Structural Division, ASCE, Vol. 90, No. ST3, June 1964, pp. 147-164.

66- Sokolovsky, A.M., Livolant, M., and Hoffmann, A., "*Study of Progressive Damage to Reinforced Concrete Structures Submitted to Dynamic Reversed Load*", Nuclear Technology, Vol. 49, June 1980, pp. 19-26.

67- Stanton, J.F., and McNiven, H.D., "*Towards an Optimum Model for the Response of Reinforced Concrete Beams to Cyclic Loads*", Earthquake Engineering and Structural Dynamics, Vol. 11, 1983, P. 299-312.

68- Subcommittee on Beams with Web Openings of the Task Committee on Flexural Members of the Structural Division, "*Suggested Guides for Beams with Web Holes*", Journal of the Structural Division, ASCE, Vol. 97, No. ST11, Nov. 1971.

69- Wang, C., and Salmon, C.G., "*Reinforced Concrete Design*", Fourth Edition, Harper and Row Publishers, New York, 1985.

70- Whitney, Charles S., "*Plastic Theory of Reinforced Concrete Design*", Journal of the Structural Division, ASCE, Vol. 107, 1942, pp. 251-326.

71- Zavriev, K.S., "*Research on Response of Prestressed Structures to Dynamic Loading*", PCI Journal, August 1964, pp. 27-32.

72- Zienkiewicz, O.C., "*The Finite Element Method*", 3rd edition, McGraw-Hill Book Company (UK) Limited, 1977.

VITA AUCTORIS

HANY AHMED ALY ABDALLA

The author was born on 21 June, 1962, in Cairo, Egypt. In 1979, he completed his high school education at "El-Maadi Secondary School", Cairo, Egypt. In September of 1979, he joined the faculty of Engineering at Cairo University. In 1984, he graduated from Cairo University with a degree of Bachelor of Civil Engineering (Distinction with honours). In October 1984, he was employed by Cairo University as a Demonstrator in the Structural Engineering Department. At the same time he joined, as a part time Designer Engineer, a structural engineering consulting firm in Cairo. In 1987, he graduated with Master of Applied Science from the Structural Engineering Department, Cairo University. In 1988, he joined the Department of Civil and Environmental Engineering at the University of Windsor, Windsor, Ontario, Canada, as a teaching and research assistant. He prepared this dissertation in partial fulfilment of the requirements for the degree of Doctor of Philosophy at the University of Windsor.